PROCEEDINGS

400-MeV Beam International Conference
Fermilab
October 24 - 27, 1993

Workshop to solicit design criteria, applications and experiments from physics and medical physics users of beams derived from Fermilab's 400 MeV Linac. The workshop sponsored and held by Fermilab.

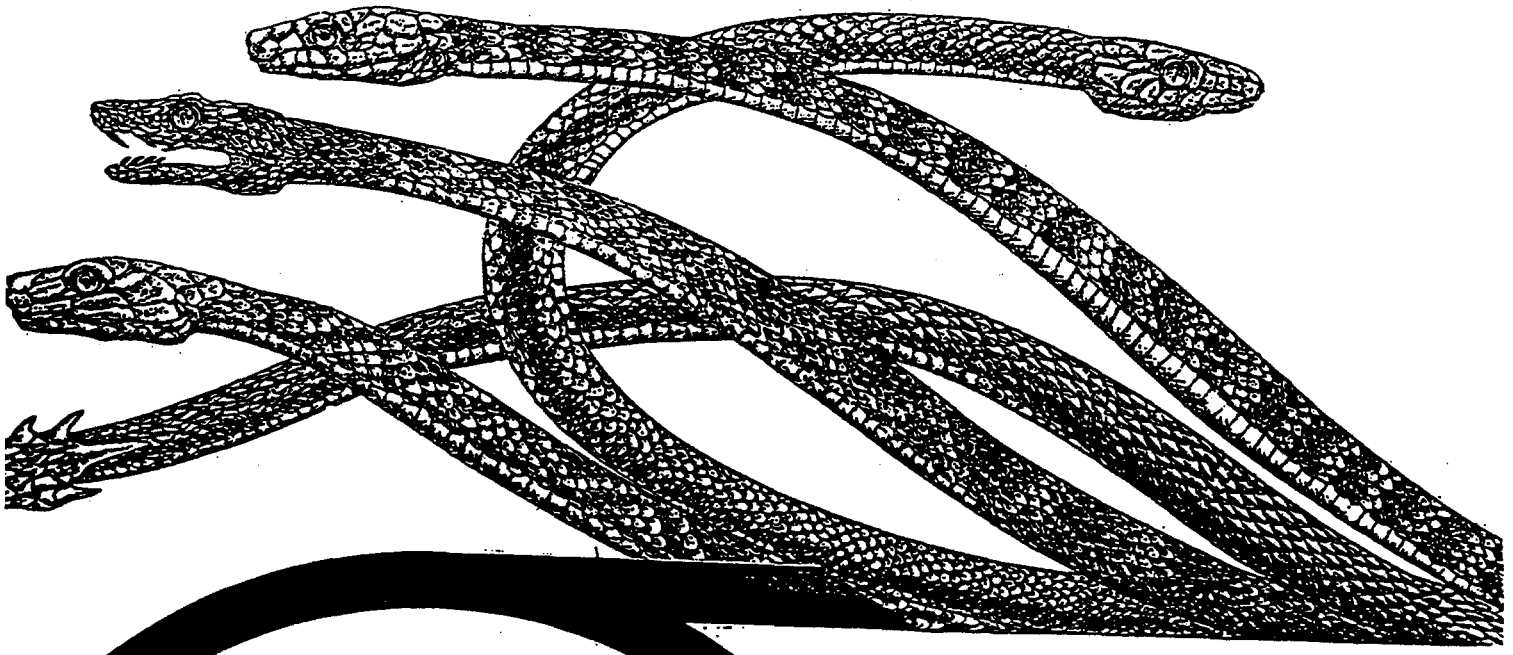

Organizing Committee:

Chuck Ankenbrandt (Fermilab)
Carol Johnstone (Fermilab)
Tom Kroc (Fermilab)
Arlene Lennox (Fermilab)
Howard Bryant (UNM
Stanley Cohen (LANL)
Dan Fitzgerald (LANL)
Eli Glatstein
(Southwest Medical Center)
Dan Miller
(Loma Linda Universtiy Medical Center)
Robert Wilson
(UT Medical Group)
Don Young
AC & Fermilab)

Operating Parameters of Proposed H^{-0+} Beams:

Energy:
min. 100 MeV
max. 400 MeV

Intensity:
min. few particles/pulse
max. 10^{13} particles/pulse

Pulse length:
min<1 μsec
max. 30 μsec

Transverse emittance
(unnormalized 90%):
min.<1 π mm-mrad
max. 7 π mm-mrad

Repetition rate:
15 Hz

Proceedings of the 400-MeV Beam International Workshop

Held at Fermilab October 24-27, 1993

Editor: Carol Johnstone

Fermi National Accelerator Laboratory
Batavia, Illinois

Operated by Univerisities Research Association, Inc.
Under Contract with the United States Department of Energy

The 400-MeV Beam International Workshop
Sponsored By:
Fermi National Accelerator Laboratory

Prepared By:
Diana DeLeon
Etta Johnson

INDEX

PROCEEDINGS

TRANSPARENCIES

PROTON THERAPY: ITS RATIONALE AND CLINICAL USE

James M. Slater, MD, FACR; John O. Archambeau, MD, FACR;
Jerry D. Slater, MD; Daniel W. Miller, PhD

Proton Treatment Center
Loma Linda University
Loma Linda, California, 92354

PROTON THERAPY: ITS RATIONALE AND CLINICAL USE

OVERVIEW

Cancer control occurs in about 50% of the more than one million new cancer patients seen in the United States each year. Of those uncontrolled, about 50% fail in the local region of origin. Morbidity and the cost of cancer treatment are unacceptable. Each of these issues should be addressed with developing new methods of cancer management.

Radiation therapy, appropriately used, addresses each of these issues favorably in selected clinical situations. Protons as a carrier of energy further enhance the favorability of radiation for each of these issues and broadens the range of selected clinical situations. Radiation therapy is the process of depositing excess energy into undesirable cells within a patient, to inactivate or destroy those cells. The major problem associated with clinical radiation therapy is the inability to avoid serious injury to normal cells. Minimizing normal tissue injury, therefore, is the primary concern and requires consideration of the energy-carrying particles' absorption characteristics as well as time, dose, and tissue-volume issues. Prior to the availability of hadrons for clinical use, the option of more-favorable absorption characteristics was a silent issue. The current availability of neutrons and protons in a hospital setting bring this consideration to the forefront.

Optimization of treatment planning, therefore, requires consideration of the type of radiation employed in each clinical situation. Each subatomic particle has a unique set of physical and electrical properties that influence its availability and desirability for therapeutic purposes. The variety of particles in clinical use today cause considerable confusion regarding their optimum role for treatment. Clarifying this confusion must begin with a clear understanding of the physical principles involved in the energy deposition of each particle on a subatomic and molecular basis, followed by understanding of biologic effects on molecular, cellular, tissue and organism levels. Table 1 provides data for some particles, including those in clinical use today.

Table 1: Subatomic particles

Category	Particle Name	Symbol	Anti-particle	Rest Mass (MeV/c^2)	Lifetime (s)	Principal Decay Modes*
Photon	Photon	γ	Self	0	Stable	
Leptons	Electron	e^-	e^+	0.511	Stable	
	Neutrino (e)	ν_e	$\bar{\nu}_e$	0(?)	Stable	
	Muon	μ^-	μ^+	105.7	2.20×10^{-6}	$e^-\bar{\nu}_e\nu_\mu$
	Neutrino (μ)	ν_μ	$\bar{\nu}_\mu$	0(?)	Stable	
	Tau	τ^-	τ^+	1784	$<4 \times 10^{-13}$	$\mu^-\bar{\nu}_\mu\nu_\tau$, $e^-\bar{\nu}_e\nu_\tau$, hadrons
	Neutrino (τ)	ν_τ	$\bar{\nu}_\tau$	0(?)	Stable	
Hadrons						
Mesons	Pion	π^+	π^-	139.6	2.60×10^{-8}	$\mu^+\nu_\mu$
		π^0	Self	135.0	0.83×10^{-16}	2γ
	Kaon	K^+	K^-	493.7	1.24×10^{-8}	$\mu^+\nu_\mu$, $\pi^+\pi^0$
		K^0_S	K^0_S	497.7	0.89×10^{-10}	$\pi^+\pi^-$, $2\pi^0$
		K^0_L	K^0_L	497.7	5.2×10^{-8}	$\pi^\pm e^\mp \bar{\nu}_e$ $\pi^\pm \mu^\mp \bar{\nu}_\mu$ $3\pi^0$
	Eta	η^0	Self	548.8	$<10^{-18}$	2γ, 3μ
Baryons	Proton	p	$\bar{p}$	938.3	Stable	
	Neutron	n	$\bar{n}$	939.6	920	$pe^-\bar{\nu}_e$
	Lambda	Λ^0	$\bar{\Lambda}^0$	1115.6	2.6×10^{-10}	$p\pi^-$, $n\pi^0$
	Sigma	Σ^+	$\bar{\Sigma}^-$	1189.4	0.80×10^{-10}	$p\pi^0$, $n\pi^+$
		Σ^0	$\bar{\Sigma}^0$	1192.5	6×10^{-20}	$\Lambda^0\gamma$
		Σ^-	$\bar{\Sigma}^+$	1197.3	1.5×10^{-10}	$n\pi^-$
	Xi	Ξ^0	$\bar{\Xi}^0$	1315	2.9×10^{-10}	$\Lambda^0\pi^0$
		Ξ^-	Ξ^+	1321	1.64×10^{-10}	$\Lambda^0\pi^-$
	Omega	Ω^-	Ω^+	1672	0.82×10^{-10}	$\Xi^0\pi^-$, Λ^0K^-

* Multiple notations, such as $p\pi^-, n\pi^0$ mean two possible decay modes. In this case, the two possible decays are $\Lambda^0 \rightarrow p+\pi^-$ or $\Lambda^0 \rightarrow n+\pi^0$. (Modified from Serway[1])

Basic factors to consider when selecting the most appropriate particle as a carrier of energy for therapeutic purposes include:

1) the macro pattern of energy distribution produced;

2) the micro pattern of energy distribution or the spatial structure of the particle track;

3) the cost associated with using the particle.

Generally, the fundamental or stable charged particles having a large mass relative to an electron provide the most desirable absorption characteristics for therapeutic purposes. The ideal depth-dose distribution is shown in Figure 1. Here the deposition of energy is maximum in the target volume for each single particle. This pattern, admittedly not realistic, serves as an objective for central axis depth dose intercomparisons.

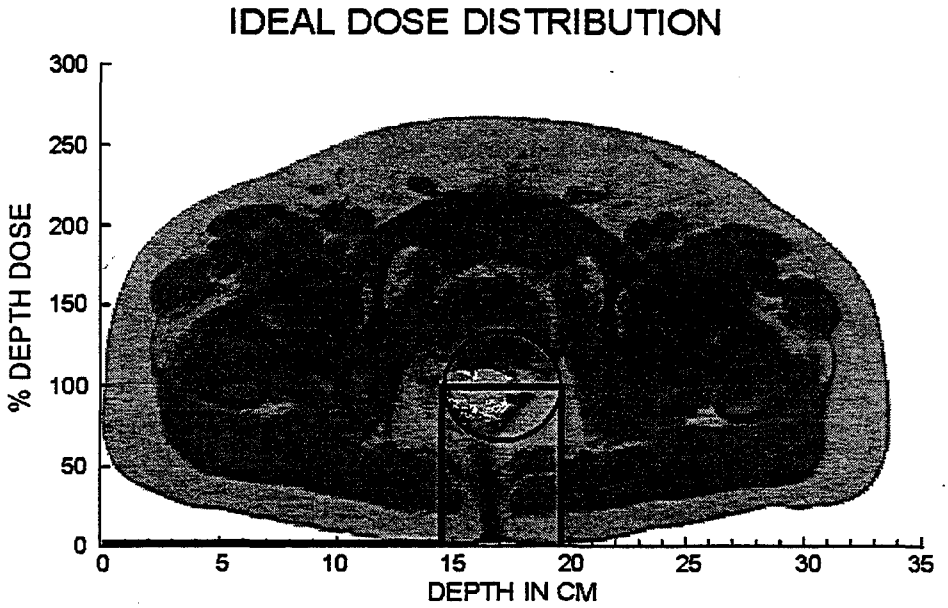

Figure 1: The ideal macro pattern of energy distribution along the central beam axis.

Heavy charged particles of the Hadron family most closely represent this ideal pattern. Figure 2 shows central axis depth dose plots for a variety of photon energies and protons.

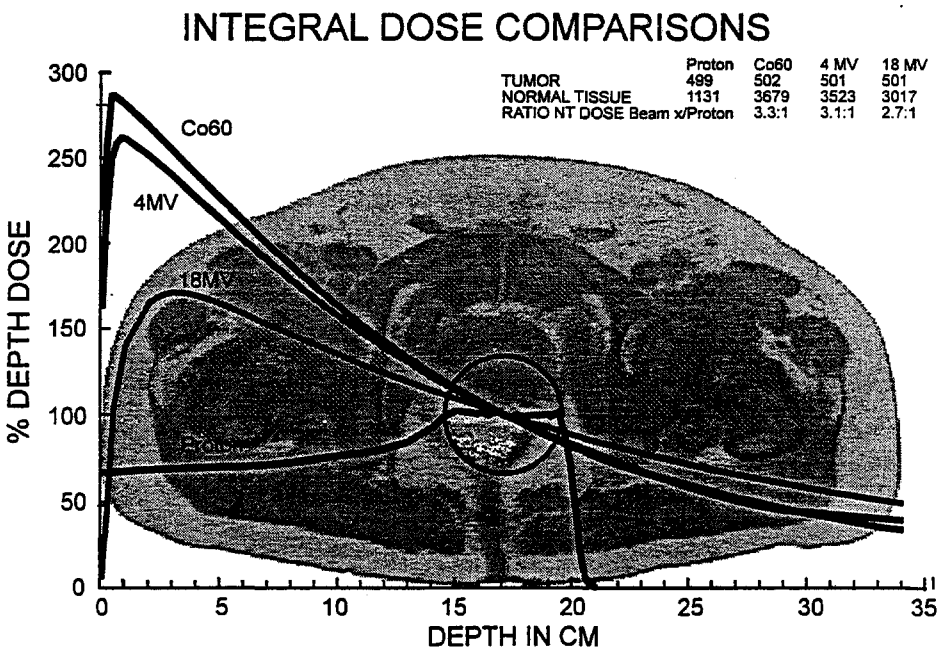

Figure 2: Central axis depth-dose distributions: photon and proton beams

The differences between the energy deposition of photons and protons result from the differences in their composition. Photons are fundamental particles having no mass and no charge, characteristics which produce inherent interactions with the target material. Photons deposit energy by ionization through the photoelectric, Compton and pair production mechanisms, resulting in an exponential energy loss with depth of penetration. Lateral scattering of the primary and secondary electrons is large with these mechanisms of interaction. Their absorption characteristics seriously limit their success in clinical therapy. Protons have a positive charge and about 1800 times the mass of an electron. Their energy is deposited primarily by charge interactions with orbiting electrons, resulting in ionization and excitation. This mechanism, plus the larger mass of a proton as compared to an electron, results in less lateral scatter for the primary proton beam. The secondary electrons are also primarily scattered in a forward direction. As the protons proceed forward, energy is transferred to the orbiting electrons along their path, depositing increasing energy as their velocity decreases. This characteristic provides a low deposition of energy at the point of entrance, in the patient, with increasing energy losses occurring until a critical velocity is reached, resulting in their remaining energy being deposited within a few millimeters of travel and forming the Bragg peak. The energy deposited varies only with the electron density of the tissue radiated and the velocity of the protons at any given point. Energy transferred is inversely related to the square of the proton velocity. The depth of the Bragg peak is directly related to the initial proton energy and the density of the tissue traversed. Less than two percent of the protons' interactions result in nuclear interactions which cause nuclear fragment recoils and lineal energy transfer ranging up to about 100 KeV per micron. The capability of minimizing the entrance dose and placing the Bragg peak at any desired depth in a patient, while producing a sharp stopping edge that conforms to the distal contour of the target tissue, makes the proton beam a superior instrument when compared to photons and electrons. Also, the biologic effect advantage resulting from ionization track structure places the higher biologic effectiveness in the target region, providing another advantage for protons.

To develop protons for routine clinical use, it was imperative that a hospital-based system be developed to demonstrate the feasibility of building and operating such a complex system in a health-care setting. To achieve this goal, scientists from many particle-physics laboratories,

universities and industries participated in developing a conceptual design of an entire clinical facility capable of accelerating protons from 70 to 250 MeV, and guiding them through a transport system into multiple treatment rooms. Design requirements for the clinical facility, largely developed at meetings hosted by Fermi National Accelerator Laboratory, were quite different from those of the physics laboratory, particularly with regard to patient treatment needs, safety, efficiency procedures and support facilities. Following completion of the facility conceptual design, Fermilab developed the engineering design of the proton accelerator and the system for transporting the beam to the treatment rooms. The beam delivery systems and treatment room facilities were designed by Loma Linda University staff with assistance from Lawrence Berkeley Laboratory (LBL), Harvard Cyclotron Laboratory (HCL) and the Paul Scherrer Institute, primarily. Three 360^0 rotating gantries were developed with additional design support from Science Applications International Corporation (SAIC). These, together with two fixed horizontal beam lines, provide delivery of proton beams from any angle. The gantries and the patient couch can be maneuvered for delivering beams at simple and compound angles to optimize beam entry, avoiding sensitive structures while the patient remains fixed in a comfortable position within a mould to assure precise positioning for treatment.

Patient treatments began in October, 1990, and by 1992, an average of 30 to 40 patients were being treated daily. Total facility uptime for patient use has exceeded 98%. To date, nearly 800 patients have been treated. The facility has clearly demonstrated the feasibility of bringing charged-particle hadron therapy into a hospital setting.

HISTORICAL MILIEU: DEVELOPMENT AT LOMA LINDA UNIVERSITY

Following Robert Wilson's lead in the 1940s and the early work done at Berkeley and Harvard in the United States, as well as international efforts in the 1960s, Loma Linda University investigators began to consider the possibility of hospital-based proton-beam therapy in the early 1970s. Promising early results reinforced that interest; it was clear that the absorption and distribution characteristics of protons resulted in the delivery of very precise treatments. Loma Linda investigators believed, however, that exploiting this precision in clinical radiotherapy required a medically-dedicated treatment and research accelerator. Initial feasibility studies

showed that even if such an accelerator were available, it could not be exploited to full advantage because of treatment planning limitations. Technology was needed which would enable clinicians to locate precisely each tumor volume within each patient, and precisely simulate treatment on each patient's anatomy.

In the early 1970s, Loma Linda laboratories developed a computer-assisted radiation treatment planning system which superimposed isodose contours on cross-sectional images. This planning system enabled radiation oncologists to design treatments, assess radiation effects before starting treatment, and modify a plan if necessary. Radiation oncologists and physicists at Loma Linda thus pioneered the union of precision tumor imaging with radiation therapy planning.[2,3] First using ultrasound images, then images from computed tomography, LLU investigators developed a treatment planning system that used digitized data from diagnostic images to plan radiation treatment fields. This system greatly improved the precision of conventional treatment planning; that precision was a step toward exploiting the precision inherent in proton beams.

By the mid-1980s, this improvement, together with improved computers and control systems, better knowledge of tumor biology and radiobiology, and advanced accelerator physics technology, made a medically dedicated proton-beam accelerator feasible.

During 1984-85, national and international interest in such an accelerator and a complete therapy system was growing. Ongoing discussions among a number of individuals and institutions interested in the therapeutic applications of protons led to the idea of a consortium to help with the planning process. A meeting of representatives from the high-energy physics laboratories, and other persons who had shown interest in heavy-charged-particle therapy, was held at Fermilab in January, 1985. That meeting led to the formation of a voluntary working group that would meet at regular intervals to define the design requirements for the accelerator, beam transport system, beam delivery system and the facility needed to house the hardware. The consortium became known as the Proton Therapy Cooperative Group (PTCOG).

Subsequently, the design requirements for the accelerator, beam transport system, treatment room delivery system, and facility layout, developed to a point where the feasibility of developing an engineering design became evident. In 1986, Loma Linda approached Fermilab with a proposal to develop the engineering design of the accelerator and its beam transport

system for Loma Linda University. Fermilab subsequently built the synchrotron and beam transport system, the latter with assistance from SAIC. The beam delivery system was developed by scientists at Loma Linda University Radiation Research Laboratories, in collaboration with scientists from LBL. In 1990, the Proton Treatment Center opened. A description of its components is presented elsewhere.[4]

The Center's accelerator is the world's smallest variable-energy synchrotron. It is designed to deliver a proton beam of energy sufficient to reach deep tumors in most patients. Partial funding was provided by appropriations from the United States Congress and implemented through grants from the U. S. Department of Energy.

ONGOING WORK AT LOMA LINDA UNIVERSITY

The first patient treated at the Loma Linda University Proton Treatment Center is a 35-year-old woman who had an ocular melanoma. She began treatment on October 23, 1990. Subsequently, many other patients with ocular melanoma were treated. Almost a year later, the first of three gantries became fully operational. This unique proton-beam delivery system made it possible for protons to be precisely directed toward any anatomic site within the body.

Basic science and applied research have been on-going. LLU investigators continued collaborative research with scientists from East Carolina University on the biological effectiveness of proton beams as compared to conventional forms of radiation. Collaboration also continued with Clarkson University investigators on proton-beam microdosimetry.[5] At LLU, proton-beam physics research is being performed on calibration dosimetry for proton beams using a water calorimeter. This work will result in the establishment of national and international standards for proton-beam dose calibration. LLU physicists are also developing new radiation detectors for proton dose dosimetry. Biological research on the effect of radiation on the microvasculature of the rat brain and sterological measurements of the late tissue effects therein, are also ongoing.[6-8]

In 1992, the Proton Radiation Oncology Group (PROG), in which Loma Linda participates in cooperation with LBL and HCL, secured funding from the National Cancer Institute to develop protocols for treating patients with protons and comparing the results with

other modes of therapy. Clinical research protocol development is an important step in establishing the place of protons in the cancer-treatment armamentarium. Collaborative clinical research continued at LLUMC through participation in NCI-supported national cooperative groups (RTOG, SWOB, CCG, NSABP) and with other proton therapy investigators of PROG.

The first gantry has been used for patient treatment 12-15 hours a day. The second and third gantries will become operational in the spring of 1994. The research beam room is being completed simultaneously and will also be available early in 1994. This room provides dedicated space for biological, physics and engineering research. Developmental work on the second and third gantries has improved the capabilities of the first gantry. The new gantries have a beam-spreading system which will make it possible to deliver protons to fields as large as 40 x 40 cm. All improvements on the new gantries will be retrofitted to the first. As the gantries are being prepared, work proceeds on a control system which will permit rapid and, eventually, continuously variable energy changes.

TREATMENT PROCEDURES

Of the nearly 800 patients treated at Loma Linda thus far, about 80% have come from California, 18% have come from other states in the Union, and 2% have come from other countries. Physicians or patients initiate the contact with the Proton Treatment Center by calling a referral representative who will connect the caller with appropriate personnel. If the patient's case appears to be appropriate for proton-beam therapy, the physician or patient is invited to send the patient's records to LLUMC for review in a new-patient conference. If the review process determines that the patient is indeed eligible, the patient is invited to come to Loma Linda. During the ensuing week, the patient is evaluated and prepared for treatment. Preparation procedures include detailed evaluations of the location and extent of disease; if these reveal the tumor to be appropriately localized, treatments proceed.

Patients are CT-scanned for treatment in the treatment position; that is, they are fitted in whole-body moulds or face masks which immobilize them during scanning in the same positions that they will assume during treatment. The objective of this is to ensure that the patient's anatomical landmarks during scanning are in positions identical to those they will assume during

treatment. The scans taken are then used to plan treatment portals; the digital information from which the images are derived are the same data employed to develop the treatment plans. The abnormal tissue is identified by digitizing the patient's volume of interest, then reconstructing images of the patient's anatomy in planes perpendicular to the beams' portal(s) of entry. The abnormal tissue is identified in terms of primary and secondary targets: the former is the tumor itself, which is targeted for destruction or sterilization by ionizing radiation; the latter includes the pathways of tumor spread, modulated by clinical prognostic indicators. Depending on the anatomical extent of the tissues at risk surrounding the primary target, they may or may not be included in proton-beam fields. If they are not, photon beams are used.

Treatment postioning is congruent with scanning positioning. This is accomplished by mounting devices which are identical on the scanning and treatment tables, and by the body or head moulds themselves. The process is repeated throughout every treatment. Anatomical verification x-rays are taken at each treatment to assure that precision is maintained.

Presently, patients are being treated for tumors in several anatomic sites. Protons are being delivered to patients having ocular melanomas and other eye and orbital malignancies; pituitary adenomas; acoustic neuromas, meningiomas, craniopharyngiomas, astrocytomas and other brain tumors[9]; base of brain and spinal cord chondrosarcomas and chordomas; cancers of the head and neck[10]; prostatic and other pelvic neoplasms; paraspinal tumors; and sarcomas of soft tissue. Over half the patients receiving protons are being treated for cancer of the prostate. Two protocols for the treatment of prostate cancer have been developed. For limited-stage, low-grade tumors, the proton beam is used as the only treatment modality. Protons are used in combination with high-energy photons for higher-stage, higher-grade tumors where the potential for spread outside of the prostate is greater. Although no patients treated with protons have yet been followed for the lengths of time traditionally required to assess disease-control results, observations concerning rates of side effects have been made and publications reporting these are in preparation at this time. Generally, side effects were expected to be reduced because of the macrodosimetric advantage afforded by proton beams, and this expectation is being met.

New proton-beam protocols are being developed, including those for lung cancer, esophageal carcinomas, primary tumors of the liver, and bladder cancer. Other anatomic sites which will be investigated in the near future include the uterine cervix[11], other cancers of the

urinary tract, neoplasms of the biliary tree, and cancer in the para-aortic lymph nodes. In the more-distant future, studies for treating patients with sarcomas of bone, breastcancer , mediastinaltumors, and hypopharyngeal, pancreatic, kidney and pediatric malignancies will be developed.

REFERENCES

1. Serway, JA. Physics for scientists and engineers. Philadelphia: Saunders College Publishing, 1990, p. 1422.

2. Slater, JM, Neilsen, IR, Chu, WT, Carlsen, EN, Chrispens, JE. Radiotherapy treatment planning ultrasound-sonic graph pen-computer system. Cancer 1974; 34:96-100.

3. Neilsen, IR, Slater, JM, Chu, WT. "An interactive system for radiation treatment planning utilizing computerized tomography data as input to the treatment planning process." Medinfo 77; Proceedings of the Second World Conference on Medical Information. 1977; North Holland Publishing Co., p. 1072.

4. Slater JM, Archambeau JO, Miller DW, Notarus MI, Preston W, Slater JD: The proton treatment center at Loma Linda University Medical Center: rationale for and description of its development. Int J Rad Onc Biol Phys 1992; 22(2):383-389.

5. Dicello JF, Archambeau JO, Slater JM, Coutrakon GB, Johanning J, Miller DW, Moyers JV, Siebers JV, Kim A, Zaider M, Robertson JB: Biological and clinical implications of microdosimetric distributions of high-energy protons. Radiation Protection and Dosimetry, in press.

6. Kennedy AS, Archambeau MH, Holshouser G, Thompson JR, Moyers MJ, Hinshaw DB Jr, Archambeau JO, McKiel L: MR imaging evaluation of rat brain parenchymal changes produced by high-dose proton irradiations. Radiology (Supplement) 1991; 181:183.

7. McMillan PJ, Archambeau JO, Gokhale A, Archambeau MH, Oey CM: Morphometric and stereologic analysis of cerebral cortical microvessels using optical sections and thin slices. Acta Stereologica, in press.

8. Archambeau MH, Kennedy AS, Holshouser B, Thompson JR, Moyers M, Hinshaw D, Archambeau JO, McKiel L: Hemibrain irradiation of rats with 25-50 Gy dose fractions of 100 MeV protons. Radiology (Supplement) 1991; 181:183 (Abstract).

9. Archambeau JO, Slater JD, Slater JM, Tangeman R: Role of proton beam irradiation in treatment of pediatric CNS malignancies. Int J Rad Onc Biol Phys 1992; 22(2):287-294.

10. Slater JM, Slater JD, Archambeau JO: Carcinoma of the tonsillar region: potential for use of proton beam therapy. Int J Rad Onc Biol Phys 1992; 22(2):311-319.

11. Slater JD, Slater JM, Wahlen S: The potential for proton beam therapy in locally advanced carcinoma of the cervix. Int J Rad Onc Biol Phys 1992; 22(2):343-347.

Biomedical User Facility at the 400-MeV Linac at Fermilab

William T. Chu

Lawrence Berkeley Laboratory, Berkeley, CA 94720

In this paper, general requirements are discussed on a biomedical user facility at the Fermilab's 400-MeV Linac, which meets the needs of biology and biophysics experiments, and a conceptual design and typical operations requirements of the facility is presented. It is assumed that no human patient treatment will take place in this facility. If human patients were treated, much greater attention would have to be paid to safeguarding the patients.

General requirements for biology user facility

First, let's consider the differences between biomedical experiments and physics experiments that are conducted at an accelerator facility. Physics experiments generally take a long time to set up, and take an extended period, over days, weeks, and even years at a stretch, to accumulate data. During an experiment, changes in beam characteristics, such as the particle energy or beam intensity, are requested only occasionally, unless these variables are specifically designed parameters of the experiment. On the other hand, biology experiments have to be set up quickly, in minutes to hours at most, and the irradiations of biological samples are accomplished quickly, again in minutes or hours. Therefore, in a typical biology running time of an 8-hour shift, several biology experiments are scheduled requiring frequent switching of beam parameters, such as the beam energies impinging upon the biological samples, dose rates, beam sizes, and extents of modulation of stopping range within the samples. This implies that a biomedical facility must be designed to accommodate varied requirements of biology experiments quickly and reproducibly. As the same irradiation room as well as the preparation rooms will be successively used by several different experimenters, they must be designed as a <u>multi-user facility</u>.

Next, the extracted beam characteristics are discussed to meet varied biomedical experimental requirements. Many cell experiments need uniform radiation fields of moderate size, e.g., 10 cm diameter with a dose uniformity within ±2.5% of the norm. Then, there are experiments in which large mammals or groups of animals are

irradiated, requiring 30 cm x 30 cm fields, and sometimes even up to 1 m x 1m radiation field. The biology experiments also use varied thicknesses of the targets in which the protons are brought to rest; therefore, requiring different widths of the spread-out Bragg peak. Typical cell colonies grown on the flat surfaces of incubation flasks measure less than 100 μm, and usually pristine (*i.e.*, unmodified) Bragg peaks are used to irradiate them. When tumors or organs in animals, or entire animals are irradiated, the width of the spread-out Bragg peaks must be enough to cover the thick targets, up to the entire range of the beam in the target (≈30 cm or more). Certain experiments, such as for irradiating yeast or spores, call for high dose, e.g., $>10^6$ cGy, in ≈1 minute of irradiation time. There are occasions when the experimenters vary dose rates, in which very high dose rate may be requested, *e.g.*, an instantaneous rate of $>10^6$ cGy/sec. On the other hand, in a low-dose chronic irradiation experiment, such as simulating the galactic cosmic-ray environment, experimenters may request the beam of 10^4 protons/cm^2/sec administered in 1-second exposure per animal per day, 5-7 days per week, for 6 months. All these varied experiments must be accommodated in a sequence in quick succession; the Linac must provide extracted beams of varied beam characteristics, with their change-over accomplished quickly and reliably.

Next, general requirements are considered of accelerator and the beam delivery reliabilities. Most experiments with living organisms are time-sensitive, in the sense that delays in irradiation schedule due to breakdowns in accelerator operation, beam delivery, or dosimetric system painfully, and sometimes irrevocably, affect the biology experiments. In the case when the sensitive time-window of the living organisms is missed, the experiment must be postponed as the biological samples must discarded and new samples re-prepared. Such preparation may take weeks for cells and months for animals. Another important aspect of biology runs is delivering repeated irradiations on schedule. In most biology experiments, many samples are irradiated to account for variations in biological systems (statistics), or samples are sometimes irradiated many times (fractionation). Some samples are irradiated over extended periods, weeks, months, and even years. It implies that the accelerator performance, dosimetry, beam quality, and experimental setups must be accurately and reliably reproducible. In a certain fractionation experiment using cells, for example, 12 samples are to be irradiated 10 times in succession, every 4 hours, with allowed 10 minutes of slips in irradiation schedule. Such an experiment requires that the 120 irradiations must be delivered in approximately 40 hours without missing a single irradiation schedule by more than 10 minutes. Otherwise the whole experiment must be repeated from scratch. In simulating radiation treatments, two-dozen animals may be irradiated three times

per week (Mondays, Wednesdays, and Fridays) for four weeks. Any miss in the irradiation schedules will result in obtaining new (non-irradiated) animals and start the experiment all over — an expensive affair for the experimenters. If the miss occurs at the latter stage of the experiment, it is more costly as the loss of the experimenters' labor must be accounted for. Typically a biology research group consists of a scientist (the principal investigator), a post-doc, and a technician. The group's annual budget for experiments may include two trips to the accelerator facility. It is easy to appreciate the devastation the group suffers of an accelerator failure that ruins one of their experimental runs. (Because of the accelerator failure, an assistant professor may lose the chance of obtaining her tenure.) Physics experiments can be usually repeated at a later time; biology experiments often do not have the luxury of next time or later time. Because any unrecoverable malfunctioning during the irradiation process can ruin biological samples, it is important that the irradiation procedure must be reliable. The facility, including the accelerator, beam delivery, and dosimetry systems, should be, within reason, ready when needed by the experimenters. The availability of the proton beams with appropriate beam parameters must be better than 99.9% within minutes of demands. The beam delivery and dosimetry system should be designed "fail-safe"; and when the malfunctions do occur, the irradiation data must be recoverable so that the interrupted irradiation procedure can be resumed without wasting the biological samples.

Typical biomedical facility

A typical biomedical irradiation facility may consist of a shielded irradiation room, two experimental preparation rooms, a biomedical control room, and an irradiation control station.

The irradiation room should be able to bring protons of all interested energies into the shielded irradiation room. The beam line should probably be split into two independent and fully-equipped beam lines to facilitate setting up two different experiments at the same time, because the beam-line setups are different for different experiments. As soon as one experiment is over, the beam can be switched to the other beam line, possibly at a different beam energy, to start the second experiment.

The experimental preparation rooms should be located in an immediate vicinity of the irradiation room. It is necessary to protect the biological samples from natural elements during transportation from the preparation room to the irradiation area. One of the experimental preparation rooms is for cell experiments and the other for animal

experiments. The former is equipped with laminar air flow hoods to prevent contamination of an experiments, and one experiment contaminating the other. The latter has two segregated areas to store two kinds of animals at the same time. (For details, see below.)

The beam delivery and dosimetry are controlled from the biomedical control room, which should be distinguished from the main Linac control room, which controls the accelerator and the beam transport up to the irradiation room. An irradiation control station is located immediately outside of the irradiation room to facilitate biology experiments. Many biology experiments irradiate multiple samples requiring many sample changes and short exposures (opening the radiation door breaking the radiation chain, entering the irradiation room by experimenters for sample exchanges, exiting the room, resetting the radiation chain, and resuming irradiations). For these experimenters, controlling the exposure procedures from the irradiation control station greatly facilitate the running of the experiments. Availability of robotic sample changers will greatly facilitate the multi-sample biology runs.

Dosimetry control system

The protons are accelerated in the Linac, extracted at a certain specified energy, and transported into the irradiation room by a series of bending and focusing magnets. As the proton beam enters the irradiation room, it is modified according to the requirements of the biology experiments. Various beam parameters are manipulated and monitored by the dosimetry control system to ensure the delivery of the desired radiation.

Here, the impact on biology experiments is discussed of the emittance of the proton beam from the Fermilab Linac, which is taken to be: the transverse emittance (unnormalized 90%) of $<1\pi$ mm-mrad (minimum) and 7π mm-mrad (maximum). When a proton beam impinges a biological sample, taken to be of uniform water density, the multiple scattering broadens the beam. An order-of-magnitude analysis will be performed to see whether the Linac emittance will be the limiting factor in the biomedical beam delivery. The first analysis is for a proton beam irradiating a field of r = 10-cm radius into z = 20-cm range. For such protons the multiple scattering will produce a Gaussian-like spread with $\sigma_y \approx 0.43$ cm. A comparable divergence is given by: $\varepsilon \approx r \cdot \theta \approx r\frac{\sigma_y}{z} \approx 10^{cm}\frac{0.43^{cm}}{20^{cm}} \approx 2.2 \times 10^3$ mm − mrad, which is two orders of magnitude larger than the Linac emittance. The second analysis is for a proton beam irradiating a field of r = 0.5-cm radius into z = 10-cm range. For such protons the

multiple scattering $\sigma_y \approx 0.23$ cm. A comparable divergence is given by: $\varepsilon \approx r \cdot \theta \approx r\frac{\sigma_y}{z} \approx 0.5^{cm}\frac{0.23^{cm}}{10^{cm}} \approx 1.2 \times 10^2$ mm − mrad, which is again much larger than the Linac emittance. In either case, the Linac emittance is not the limiting factor for biomedical beam delivery. Practical limitations originate from not only the multiple scattering in the target, but also in beam path, as well as the angular confusion and effective "source-to-target" distance. All these considerations strengthen the above conclusion: the Linac emittance is quite acceptable for most of contemplated biomedical experiments.

A beam line may be built over optical rails, which facilitate the alignment and positioning of various monitors and beam modifying devices. Since the beam transported into the irradiation room has a small spot size, <1 cm in diameter, and since the desired target size is larger than the beam spot, the beam is scattered and/or defocused to broaden its profile laterally. The profile of the scattered beam is approximately Gaussian, and, for radiation fields of <5 cm diameter, the scattered beam is collimated to utilize the portion of the beam around the central ray before it irradiates the biological sample. The attainable field size depends on the proton beam energy, and the required field uniformity within the useful field (usually biologists insist on getting better than ±2.5%). The lateral beam broadening is determined by the beam energy, the beam emittance, the scattering material and its thickness, and the drift space between the scatterer and the target. Larger fields necessitate thicker scatterers, which produce more fragmentations of the target nuclei and much background neutrons, and consequently compromise the beam quality of the radiation received by the biological samples. For larger radiation fields up to ≈20 cm diameter can be produced either using double scattering system with occluding post-and-ring assembly[1, 2] or the contoured scatterer.[3] Even larger fields may be obtained using a beam scanning system.[4-6]

The sample is positioned at the end of the beam line, usually at the distal location on the optical rail. For multiple sample experiments, the samples are mounted on a sample translator which sequentially place the samples in the beam line for irradiation. The sample translator eliminates the tedious sample exchange by the experimenters that necessarily break the radiation chain, entering and exiting the irradiation room by the human experimenters, and resetting the radiation chain. In irradiating large animals, a computer-controllable precision target alignment table, with 6 degrees of freedom (3 space and 3 angles) will be very useful. The alignment of a sample on the beam line is facilitated by laser localizers, and verified by two orthogonally-positioned x rays.

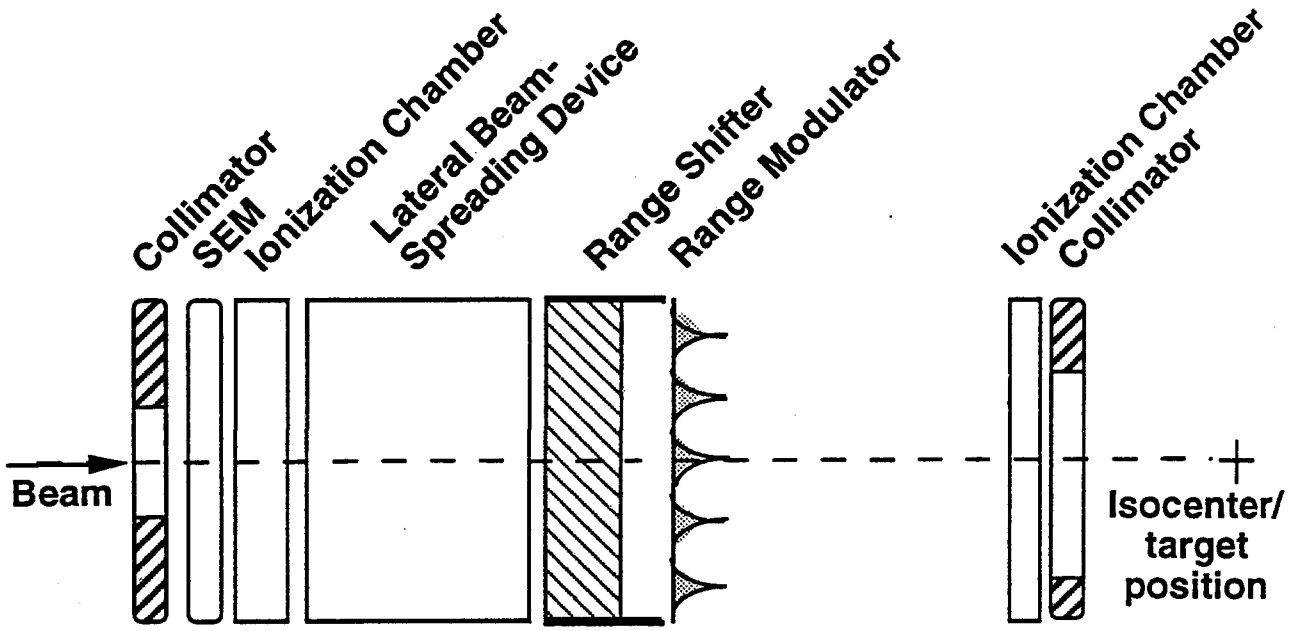

Fig. 1. A typical beam line for biology experiments.

A typical beam-line set up for a biology experiment is shown in Fig. 1. The proton beams are tuned using wire chambers, which measure x and y positions and dimensions of the beam spot. (Here, the beam axis is taken as +z direction, and the lateral directions x and y.) Most of the instruments discussed below are described in a recent review article,[7] and their descriptions are kept to minimum here. Parallel-plane, segmented-element ionization chambers are used as dose detectors. Each ionization chamber has two charge collecting planes, one of them is divided in four quadrants to detect the position of the center of the beam, and the other is divided into several concentric circles which measure the size of the beam spot if the Gaussian distribution of the beam profile is assumed and the beam is centered accurately.[8] In each biology experiment, the ionization chambers are calibrated against a standard thimble ionization chamber, which is positioned at the center of the target, and whose calibration is traceable to a National Institute of Standards and Technology (NIST, formerly the NBS) source. A secondary emission monitor (SEM) is used as a backup to the ionization chambers. It has a lower dose sensitivity than the ionization chambers, but it serves well when the ionization chambers saturate because of a high dose rate.

The beam range is varied using a variable water column, which automatically places specified thickness of water in the beam path. A Bragg curve of a proton beam may be

measured by placing one ionization chamber upstream of the water column, and the second ionization chamber downstream of it and immediately upstream of the target. If a series of measurements at various water thickness settings is made, the dose measured by the second chamber (relative ionization at a given depth of water) normalized to the readings of the first chamber (the total number of the incident protons) produces the Bragg curve of the ion beam inside a water absorber. Either plastic or metal range shifters (called "binary filters") may be used in place of the variable water column.

The width of the Bragg peak can be spread out by modulating the range using a ridge filter. The profiles of the plastic or metallic ridge absorbers are machined in such a way that a constant biological dose is imparted across the entire width of the spread-out Bragg peak. A monoenergetic beam so modulated would have particles of different energies with different divergences. The shorter-range particles would suffered higher scattering by going through the thicker material, and consequently larger divergence. Therefore, a ridge filter must be designed for each energy of the incident beam, and for a given drift space. Low-Z materials, such as plastic or aluminum, are preferred for making ridge filters as they scatter the beam particles less than the higher-Z materials, such as copper or steel. As mentioned above, thin samples, such as cells grown on flat plates, do not need range modulation and are irradiated using pristine Bragg peaks.

The dosimetry control system performs irradiation procedures according to the parameters specified by the experimenters. It should also perform various irradiation procedures, such as beam monitoring, Bragg curve taking, calibration of the dosimetry system, irradiation procedures for single sample and multiple samples, and data collection and bookkeeping of all the irradiation procedures performed by the system. It also controls the position of the beam plug, the thickness of the variable water column, the placement of the target by the sample translator, etc. Recently a very extensive dose delivery control system, that was developed for human treatments at LBL, was described,[9] and specifications of a patient treatment control system were published.[10]

Description of a biomedical irradiation facility

A sketch is made to equip a biomedical user facility as described above. The items are grouped in the following categories:

- Biomedical control room : The operator must have visual access to all computer functions and monitors, and immediate access to the controls of critical devices to terminate irradiations in case of malfunctions. It includes a control room structure, electronics racks, CCTV systems to monitor the experiments, and an

operator's console. Dosimetry control computer system — Computers, peripheral devices, graphics display terminals, as well as the software implementation and documentation.

- Irradiation room equipment includes the beam-line modifiers and monitors for two beam lines, laser localizers, x-ray units to align animals, automatic sample positioner for multi-sample experiments, overhead hoist, CCTV, and intercom system. The beam-line monitors include optical rails, wire chamber for beam tuning, ionization chambers for dose measurements, secondary emission monitor, associated power supplies, dosimetry control electronics, including VME or CAMAC and appropriate electronic crates and patch panels, and fast beam chop system to terminate the irradiation. Also included is testing equipment such as a standard current source for calibrating charge integrators for ionization chambers, an electrometer for calibration verification, an oscilloscope, and a Geiger counter for monitoring items removed from radiation area. Beam-modifying devices include degrader foil system to scatter the beam for broadening of the beam profile, set of ridge filters to modulate the proton ranges, and a variable water column to modulate the range of the beam. Also, collimators to define the port shape or to protect the detectors must be provided. If on-line imaging system is not available, and films are used for alignment aids, x-ray film developer should be provided.
- Biology experimental preparation rooms: To perform biology experiments, experimental preparation facilities must be located in the immediate vicinity of this irradiation room. A sketch of a biomedical experiment preparation room is shown in Fig. 2. Constructing a cell preparation room equipped with cell handling equipment, and a animal holding room which has two segregated areas to hold two different experiments are proposed. To perform biology experiments using large uniform-dose fields to irradiate large animals, such as monkeys and dogs, a large radiation field must be prepared without resorting to the scattering method which provides a limited field size while degrading the beam quality of proton beams. A large uniform-dose field of radiation may be provided by using a wobbler[4] or a raster scanner.[5] It is also highly advisable to provide an alignment couch if large animals experiments are planned. It will provide an efficient way to align the target accurately to the beam. Such a setup may include: alignment couch and its control electronics (required for accurate alignment in 3-dimension

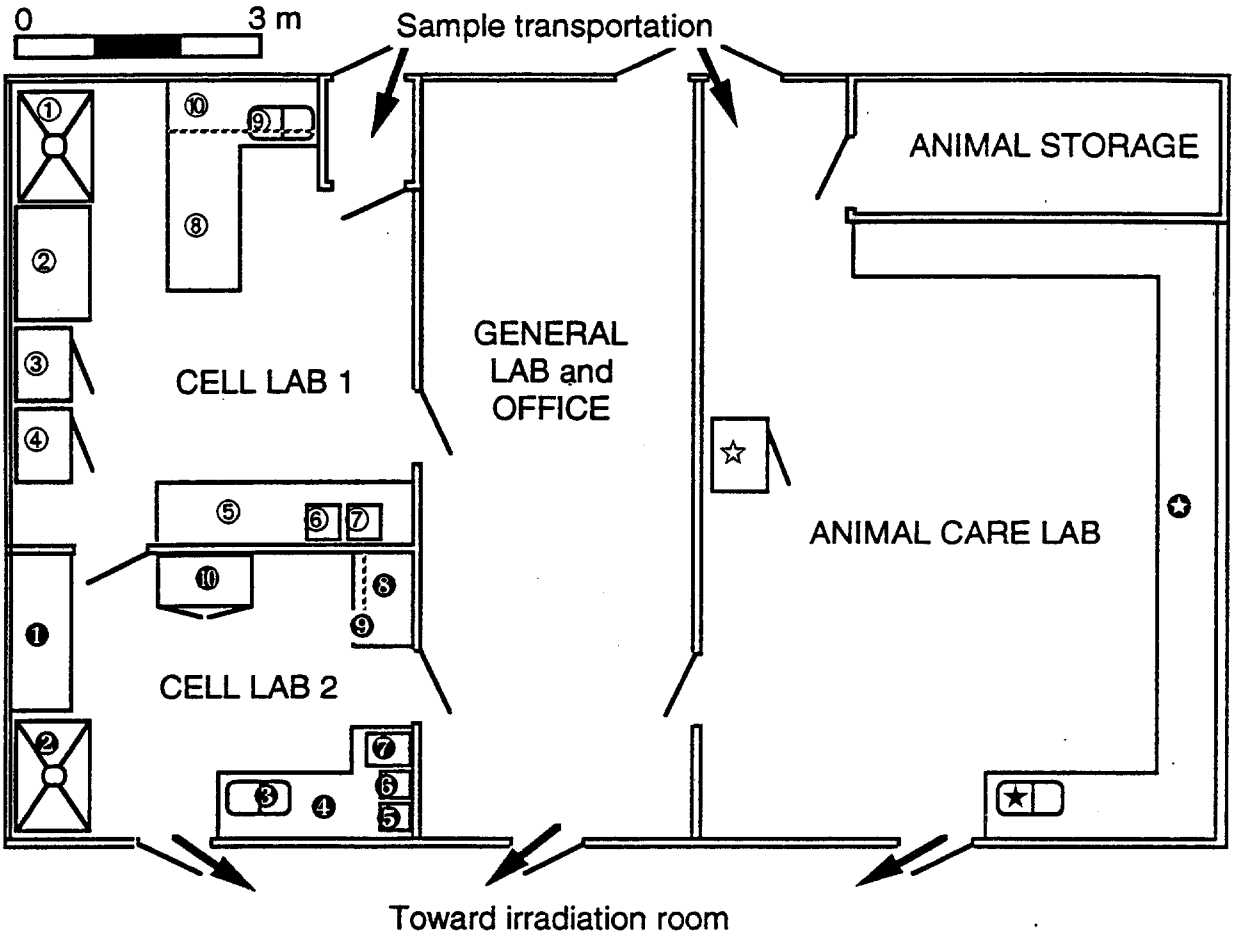

① Laminar flow hood, vented
② Laminar flow hood
③ CO_2 incubator
④ Flammable material storage refrigerator
⑤ Workbench, with drawers under
⑥ Coulter Counter
⑦ Coulter Channelyzer
⑧ Workbench, with drawers under
⑨ Double sink
⑩ Wall-hung storage cabinet

❶ Workbench, with drawers under
❷ Chemical fume hood, vented
❸ Double sink
❹ Workbench, with drawers under
❺ Milli-Pore Purifier
❻ Milli-Que Purifier
❼ Sterilematic Autoclave
❽ Wall-hung storage cabinet
❾ Workbench, with drawers under
❿ Flammable material storage cabinet

☆ Flammable material storage refrigerator
★ Double sink
✪ Workbench

Fig. 2. A sketch of a biomedical experimental preparation room

with respect to the beam), a raster scanner (2 magnets, their power supplies, and the scan control system), and a large-area (30 cm x 30 cm), high resolution (3600 elements) ionization chamber and associated electronics.

Operating a biomedical facility

For physics experiments, the accelerator operations group produces a desired beam, transports it to the experimental area, and tune it into a desired target. The experimenters set the experiment up, check the workings of detectors, calibrate them, and finally take data. What you do with the beam is almost entirely left to the experimenters. On the contrary, the biologists walk in the accelerator facility with biological samples, and expect the accelerator operations group provide not only the beam with appropriate parameters, but also the controls and monitoring of the beam so that the biological samples would obtain right doses on planned schedules. One may consider automating the beam-line setup procedures, beam calibration procedures, and irradiation procedures, so that the biology experimenters go about their ways by themselves with little help from the accelerator operations group. Such a process is hard to implement for various reasons: computer illiteracy of experimenters (even they are dying breeds) and physics inexperience of experimenters (biologists do not feel comfortable unless a physicist tell them what dose their samples got).

To make the biomedical experiments work well at the planned Linac facility, an biomedical operator must be present whenever there is a biology user group performing an accelerator experiment. The operator must be knowledgeable to change the beam-line setups, calibrate the beams, and perform reliable dosimetry for the experimenters. Once the beam and the beam line are set up, the experimenters can run the experiment by turning the beam on and off from the irradiation control station with little supervision by the operator. During the irradiation time, however, the operator must be on call to resolve problems or uncertainties the experimenters may experience.

The accelerator operations group should also provide sufficient physics support. Whenever a new biology experiment is planned, the biology users must confer with the physicists to discuss for any peculiar requirements of the planned experiments, so that the solutions may be proposed and implemented. The physics staff should be responsible for setting up the beam line, and accurate execution of the experiment. The physicists will be responsible for running the biomedical facility and training the operators.

Acknowledgments

I would like to Bernhard Ludewigt, Mark Nyman, Tim Renner, R. P. Singh, and Ron Stradtner of LBL, who designed operated the LBL Bevatron Biomedical Facility, on which this paper is heavily based. This work is supported by the Director, Office of Energy Research, Office of High Energy and Nuclear Physics, of the U.S. Department of Energy under Contract No. DE-AC03-76SF00098 and in part by the National Institutes of Health, National Institute of Cancer under Grant No. CA56932-01.

References

1. K. Crowe, L. Kanstein, J. T. Lyman and F. Yeater, "A large field medical beam at the 184-inch synchrocyclotron," Lawrence Berkeley Laboratory Report, LBL-4235 (1975).

2. A. M. Koehler, R. J. Schneider and J. M. Sisterson, "Flattening of proton dose distributions for large-field radiotherapy," **Med. Phys. 4**, 297-301 (1977).

3. B. Gottschalk and M. S. Wagner, "Contoured scatterer for proton dose flattening," Harvard Cyclotron Laboratory, a preliminary report 3/29/89 (1989).

4. T. R. Renner and W. T. Chu, "Wobbler Facility for Biomedical Experiments," **Med. Phys. 14**, 825-834 (1987).

5. W. T. Chu, T. R. Renner and B. A. Ludewigt, "Dynamic Beam Delivery for Three-Dimensional Conformal Therapy," *Proc. of the EULIMA Workshop on the Potential Value of Light Ion Beam Therapy, November 3-5, 1988 , Nice, France*, 295-328 (1988).

6. E. Pedroni, H. Blattmann, T. Böhringer, A. Coray, S. Lin, S. Scheib and U. Schneider, "Voxel Scanning for Proton Therapy," *Proc. of the NIRS International Workshop on Heavy Charged Particle Therapy and Related Subjects , July 1991, Chiba, Japan,* 94-109 (1991).

7. W. T. Chu, B. A. Ludewigt and T. R. Renner, "Instrumentation for Treatment of Cancer Using Proton and Light-Ion Beams," **Reviews of Scientific Instrument, 64,** 2055-2122 (1993).

8. T. R. Renner, W. T. Chu, B. A. Ludewigt, M. A. Nyman and R. Stradtner, "Multisegmented Ionization Chamber Dosimetry System for Light Ion Beams," **Nucl. Instrum. Methods in Phys. Res. A281**, 640-648 (1989).

9. R. P. Singh, W. T. Chu, B. A. Ludewigt, K. M. Marks, M. A. Nyman, T. R. Renner and R. Stradtner, "Software Quality Assurance and Software in the Biomed Control System," Lawrence Berkeley Laboratory Report LBL-27948 (1989).

10. W. T. Chu, J. W. Staples, B. A. Ludewigt, T. R. Renner, R. P. Singh, M. A. Nyman, J. M. Collier, I. K. Daftari, H. Kubo, P. L. Petti, L. J. Verhey, J. R. Castro and J. R. Alonso, "Performance Specifications for Proton Medical Facility," Lawrence Berkeley Laboratory Report LBL-33749 (1993).

APPLIED BEAM PROGRAMS AT TRIUMF

Summary of Talk to Fermilab 400 MeV Beam Workshop

E. W. Blackmore
TRIUMF, 4004 Wesbrook Mall, Vancouver, B.C., Canada, V6T2A3

Introduction

The TRIUMF cyclotron has been delivering intense proton beams with energies in the region of interest for this workshop for over 15 years, primarily for research in particle and nuclear physics. However over the years of operation the user community has shifted to include more applications research in chemistry, material sciences and the life sciences. TRIUMF's location near the University of British Columbia in Vancouver has been an important reason for the applications research programs. The presence of the University Departments of Medicine, Chemistry, Plant Sciences, Engineering, and Physics provides research groups interested in making use of the beams. For about 10 years there has been a PET imaging group at the University Hospital, and a 2 km pipeline has been used for many years for transferring short-lived positron emitting radiopharmaceuticals from one of the TRIUMF cyclotrons to the hospital.

Fig. 1 lists some of the parameters of the cyclotrons at TRIUMF – which now amount to four, as the large 500 MeV cyclotron has spawned three smaller ones. Variable energy beams up to 520 MeV and cw currents of 225 μA are available from the large machine. Some early research and demonstration programs in isotope production for nuclear medicine resulted in attracting the interest of a Canadian company, now called Nordion International, which purchased a 42 MeV cyclotron for location at TRIUMF and proceeded to market radioisotopes commercially. This proved so successful that Nordion were unable to meet the demand for isotopes and ordered a second machine. This time, as a technology transfer activity, TRIUMF, together with a local manufacturing company, designed and built a 30 MeV cyclotron, the TR30, which is probably the most reliable, high intensity accelerator in isotope production today. The success of the PET program and the demand for positron emitting radioisotopes has led to the recent design and installation of a 13 MeV cyclotron. This machine is just being commissioned for use as a research tool, not for commercial production.

All cyclotrons at TRIUMF make use of H^- ions for acceleration so that efficient extraction by stripping can provide high intensity variable energy beams. Typically three beams are extracted simultaneously on the large cyclotron — a high current beam for meson production, a low energy beam for isotope production and studies of reaction mechanism, and a lower intensity beam for nuclear physics research. The cw proton beam from cyclotrons has advantages over a pulsed beam from a linac in the design of high power targets, in diagnostic instrumentation and in therapy where uniform beam delivery is helpful.

Fig. 2 is the layout of the full facility and the three isotope-producing cyclotrons and indicates (i) where isotopes are also produced at 500 MeV and 70–100 MeV, (ii) the pion cancer therapy beam line, using negative pions, and (iii) the proton therapy beam which is presently being installed. The high intensity 500 MeV beam is used to produce beams of pions and muons for the research programs. The largest number of users of muons at TRIUMF are involved in μSR or muon spin resonance/relaxation/rotation, which is a technique for studies of the structure of materials and can be applied to magnetic materials such as high-temperature superconductors or buckeyballs etc. More than 100 users are involved in this program, many from the U.S. and Japan. TRIUMF has excellent high luminosity polarized muon beams for this purpose produced by the intensity 500 MeV proton beam. The Fermilab linac energy of 400 MeV is probably too low for efficient pion or muon production.

This talk will concentrate on three areas involving applications of proton beams.

Radioisotope Production

The commercial use of cyclotrons for the production of radioisotopes for the biosciences is rapidly expanding. Fig. 3 shows that the largest use is for Mo/Tc generators, but the use of ^{123}I and ^{201}Tl, which are produced by cyclotrons, is rapidly increasing. Although ^{122}Xe has better decay properties for diagnostic procedures, it requires a 100 MeV beam and as yet is not widely used. The main isotopes produced commercially at TRIUMF are listed in Fig. 4.

About 50 professionals are involved with the PET program connected with TRIUMF, using this technique to study movement disorders such as Parkinson's Disease with ^{18}F-fluorodopa, as well as the development of new tomographic techniques and new radiopharmaceuticals. Typically the positron emitters have half lives of several minutes and therefore the cyclotron must be close to the end-user. A program is under way to develop other isotopes, studying reaction mechanisms mainly using (p, xn) reactions to look for maximum purity of the desired isotope. As mentioned earlier the PET program has become so demanding for radioisotopes that a grant was awarded to build a dedicated cyclotron for this purpose, with a self-shielded, compact design for the hospital environment as shown in Fig. 5. The 70–120 MeV beam line is used to study radioisotope production as well as for some commercial production.

Radiation Damage/Detector R&D

Particle beams at TRIUMF are in heavy demand for detector R&D and radiation damage studies. Typical applications are particle identification tests as pure or tagged pion, muon, proton and electron beams are available and high rate studies. The energies available for

protons and pions are in the range of interest for space applications and for damage tests of detector components for the TeV colliders.

Radiation damage tests (see summary Fig. 6) have been carried out at very high doses, 10^9–10^{10} rads, for tests of components to be used in the TRIUMF target areas, to 10^3–10^6 rads for tests of electronics and detector components. A typical requirement for some of the detector tests for the SSC is a flux 10^{14} protons/cm^2 over a 10 cm $\times$ 10 cm area.

The solar proton flux in a polar orbit has energies from tens to a few hundreds of MeV. Fig. 7 shows a proton energy spectrum behind two thicknesses of aluminum absorber. The average yearly dose to a satellite is in the order of a few krad. Testing of microelectronics and development of radiation hard electronics requires proton beams in this energy range.

As yet there is no dedicated irradiation beam line at TRIUMF and ad hoc solutions are found to provide the proton fluxes and beam spots required using one of the existing beam lines. Typical of a high dose study was a test of the radiation hardness of permanent magnet materials. TRIUMF was planning to install quadrupoles made of samarium cobalt near the meson production target and was interested in finding out how long their magnetic properties would be retained. Fig. 8 shows the result of this work. It was found that radiation hardness was better with a 2:17 composition of SmCo, but it depended on the manufacturing process. Magnets with this material are expected to last >10 years in the required location.

Radiation Therapy at TRIUMF

The medical program in cancer therapy is a collaboration between the B.C. Cancer Agency, the U.B.C. Faculty of Medicine and TRIUMF. Pion therapy has been carried over 10 years with more than 300 patients having been treated. Fig. 9 shows a summary of the pion treatment sites. At the present time a randomized trial is underway for two sites, glioblastomas and cancer of the prostate. This treatment makes use of negative pions, a flux of 10^8/second at 80 MeV produced by 150 μA of 500 MeV protons.

A more recent development involves the construction of a proton beam treatment facility for tumours of the eye or orbit. This facility will use the existing 70–120 MeV beam which can treat to a depth of about 10 cm. The layout of the beam delivery system is shown in Fig. 10 and first patient treatments are expected to begin by summer 1994. The use of proton beams up to 250 MeV for the treatment of AVM's and deeper tumours is also planned but not funded as yet. The proposed layout of the proton therapy facility is shown in Fig. 11.

The higher proton energies available from the TRIUMF cyclotron offer the possibility of proton radiography as well. Some tests of the sensitivity of protons to detect small density

variations in materials were carried out in the late 1970s at TRIUMF using a scanned 1 mm diameter proton beam. Fig. 12 shows a schematic of the arrangement used and Fig. 13 shows a contour plot of a small mouse in a 25 cm thick water box as measured using 200 MeV protons.

Conclusion

There is a very active applications research program at TRIUMF using the proton beams from the four cyclotrons. Although TRIUMF was initially conceived as a laboratory for the study of nuclear and particle physics using beams of pions, muons, protons and neutrons, TRIUMF management has always encouraged collaborations with other disciplines and industry. The resulting benefits include not only royalty funds which are used to further technology transfer programs but also the cross fertilization of expertise from different fields which has led to the successful programs in PET tomography, radiopharmaceutical production, microelectronics and material sciences.

TRIUMF H^- Cyclotron

- Operating since 1975
- Extracted energy: 65-120 MeV, 180-520 MeV protons
- Extracted current: 225 μA CW, 10μA polarized
- 3 simultaneous beams: variable energy and intensity

CP42 H^- Cyclotron

- Operating since 1979 (Nordion)
- Extracted energy: 11-42 MeV protons
- Extracted current: 200 μA CW
- Single beam with 7 target stations

TR30 H^- Cyclotron

- Operating since 1990 (Nordion)
- Extracted energy: 15-30 MeV protons
- Extracted current: 420 μA CW
- 2 simultaneous beams with 3 target stations

TR13 H^- Cyclotron

- Operating since 1993
- Extracted energy: 5-18 MeV protons
- Extracted current: 100μA CW
- 2 simultaneous beams and target stations

Fig. 1. Parameters of the cyclotrons at TRIUMF

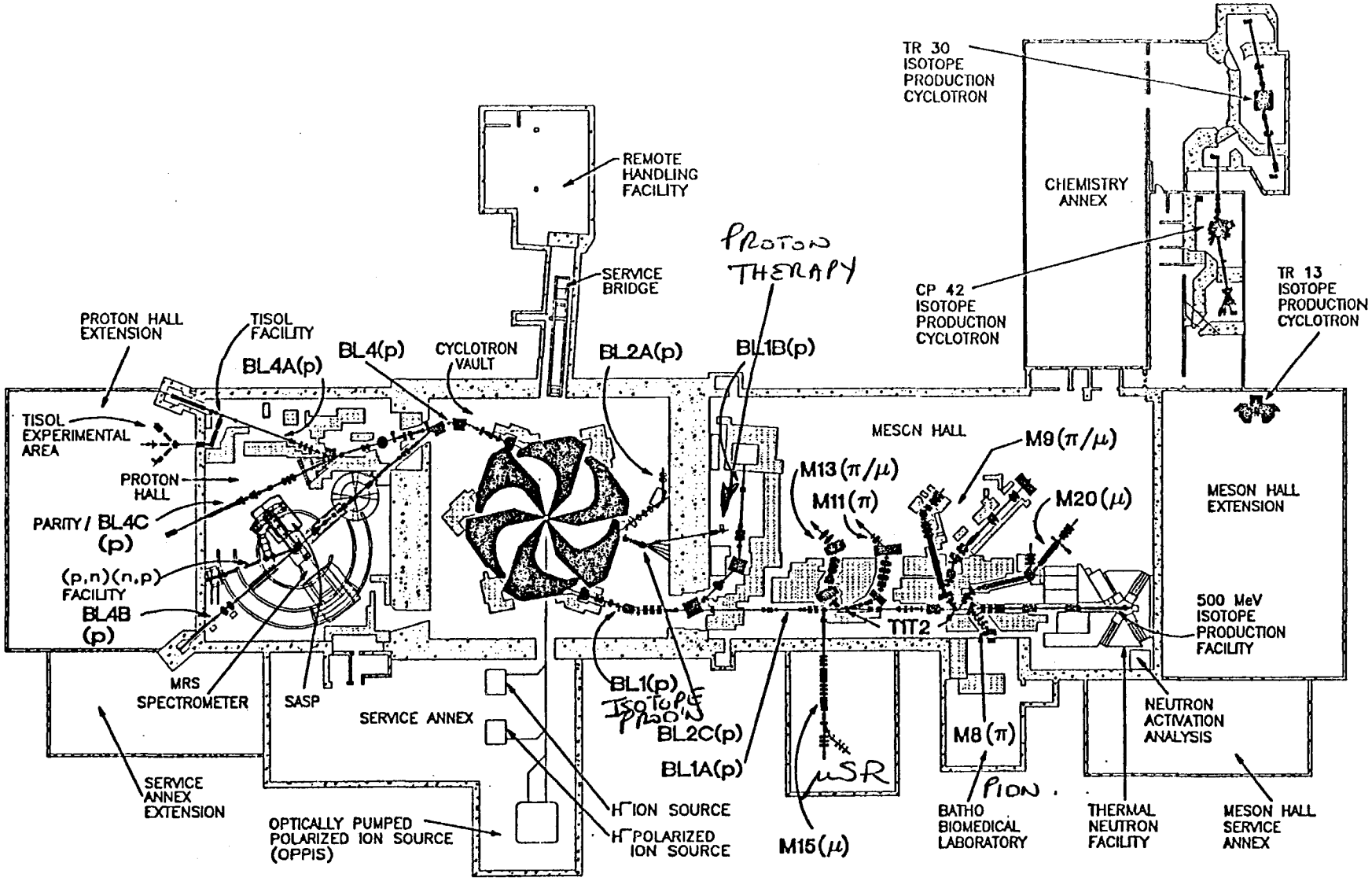

Fig. 2. Layout of the TRIUMF cylotron(s) and beam lines

ESTIMATED USAGE OF SELECTED RADIOISOTOPES BY YEAR
(Curies)

Nuclide	$t_{\frac{1}{2}}$	Retail Consumption 1982	Retail Consumption 1987	Retail Consumption 1990
$^{99}Mo/^{99m}Tc$	66 h/6 h	100,000 (^{99}Mo)	120,000	150,000
^{111}In	68 h	150	160	185
^{123}I	13.2 h	75	1,250	3,100
^{127}Xe	36.4 d	100	100	100
^{133}Xe	5.2 d	25,000	25,000	45,000
^{201}Tl	73 h	500	2,500	6,000

Fig. 3. Useage of radioisotopes

Radioisotopes at TRIUMF

Commercial: Nordion International

^{201}Tl, ^{123}I, ^{67}Ga, ^{111}In, ^{57}Co

$^{82}Sr/^{82}Ru$ generator

PET: Neurodegenerative Disease Program

^{18}F (FDG, FDOPA), ^{11}C (Raclopride), ^{15}O, ^{13}N

Radioisotope/Radiopharmaceutical Development

^{188}Pt, ^{178}W, ^{97}Ru, ^{67}Cu, ^{127}Xe, $^{122}Xe/^{122}I$ generator

Target Preparation

^{22}Na, ^{44}Ti

Fig. 4. Radioisotopes produced at TRIUMF

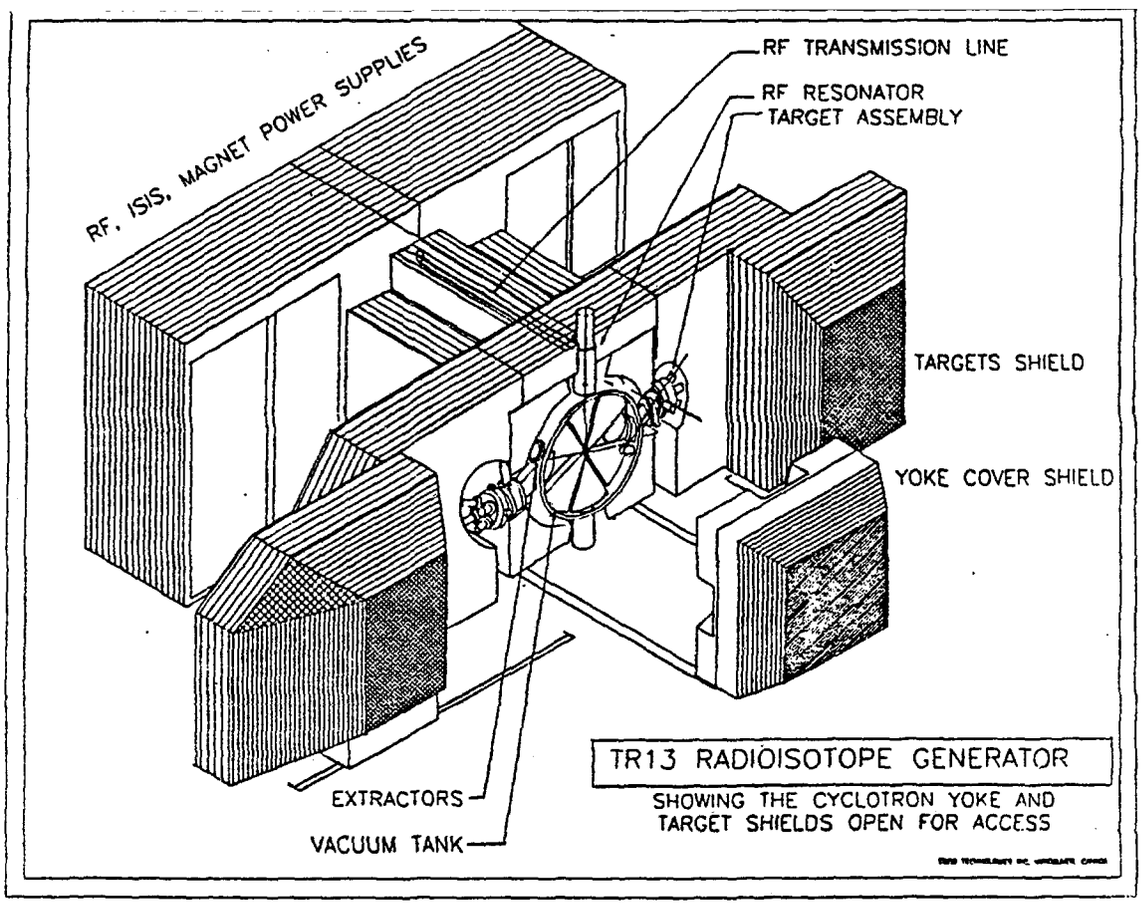

Fig. 5. Design of the TR13 - 13 MeV Cyclotron

TEST BEAMS at TRIUMF

Calibration, efficiencies, particle ID, high rate studies

- protons, neutrons to 500 MeV (1.10 GeV/c)
- pions, muons, electrons to 0.4 GeV/c (tagged)
- energy resolutions $\approx$ 1% or better
- secondary beam rates 10^2 to 10^8 particles/sec

Radiation Damage Studies

- protons to 10^9 rads/cm^2 per week
- proton fluxes between 10^5 to 10^{10} p/cm^2/sec
- uniform proton irradiations over areas of 10x10 cm^2
- some neutron irradiation capability
- proton and neutron energies in range of interest for space applications and TeV collider radiation damage

SOME APPLICATIONS USING TRIUMF BEAMS

Radiation Damage/Detector Studies

- TRIUMF - study of radiation damage to permanent magnet materials
- TRIUMF - study of radiation damage to magnet coil insulation
- Sandia - radiation hardened electronics
- Boeing - single upset rates in I.C.s
- U of Sask.- Calibration of SALAD detector with protons
- BNL/RHIC - CsI, PbF, BaF_2 crystals with 300 MeV/c e, π beams
- Tau/charm - CsI crystal tests
- BNL E787 - lead glass radiation damage
- SSC - diamond detector studies
- SDC/Santa Cruz - radiation damage in silicon microstrip detectors

Fig. 6. Radiation damage and detector R&D applications

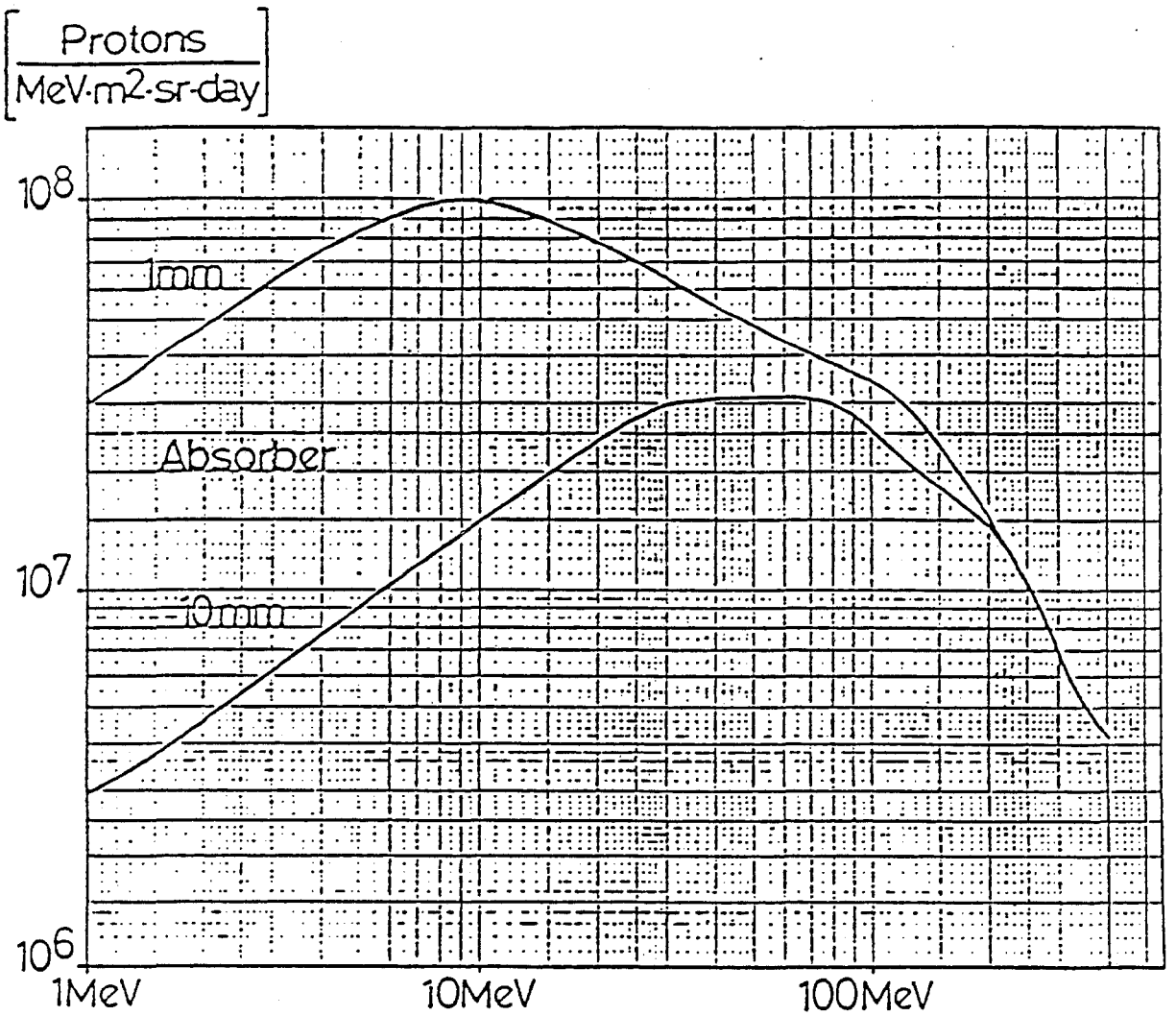

Fig. 7. Differential energy spectrum of trapped protons for 850 km 88.8° inclination.

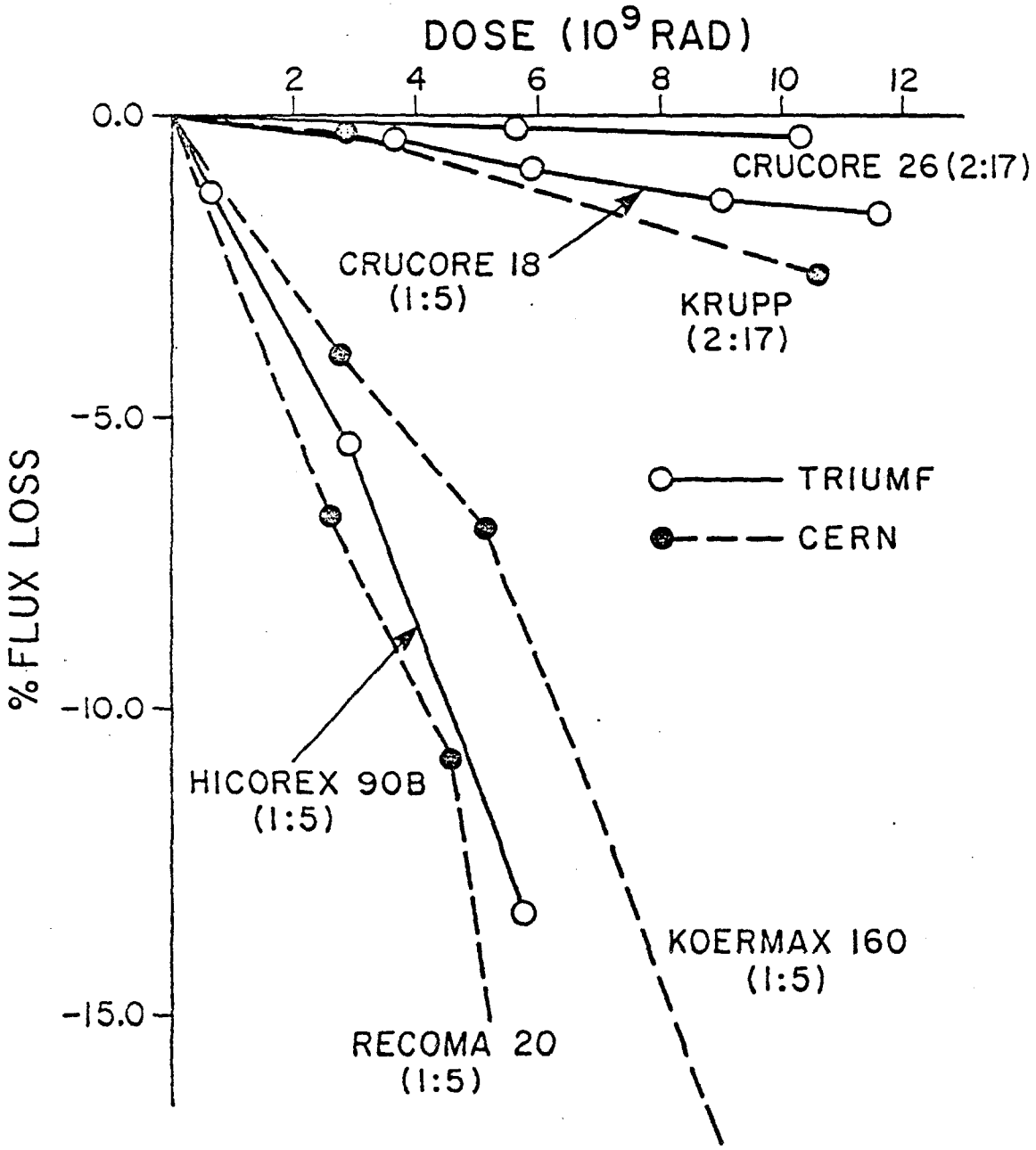

Fig. 8. Radiation damage of samarium-cobalt permanent magnet samples

Pion Therapy

Since 1982

$2 \times 10^8 \pi^-$/sec @ 180 MeV/c.

	1992
Total number of patients	306
no. of sites treated:	
Brain (Glioblastoma)	137
Pelvis (Prostate)	147
Leg	5
Groinskin	1
Nasopharynx	3
Chordoma	1
Schwanoma	1
Parotid	3
Meningioma	2
Temperal Bone Adeno CA	1
Melanoma Rt. Antrum	2
Adenoca L Middle Ear	1
Skin Nodule Trials	11
Total number of sites	315
Phase three - randomized trial patients	
Brain	
- Photons	32
- Pions	31
Total	63
Total no. required for trials	82
Prostate	
- Photons	54
- Pions	69
Total	123
Total no. required for trials	200

Fig. 9. Number of patients treated using pions at TRIUMF

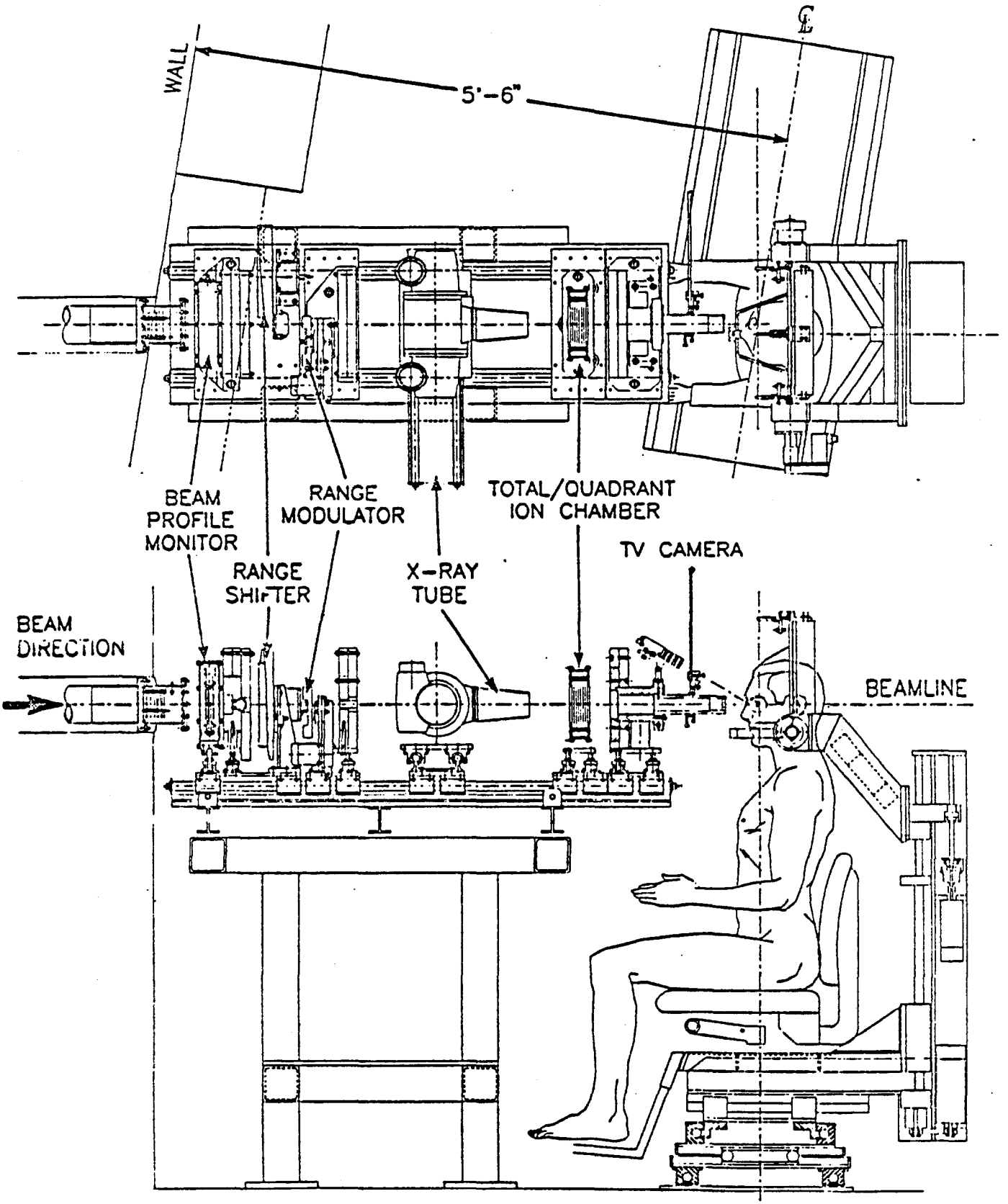

Fig. 10. Arrangement of eye therapy proton beam delivery system

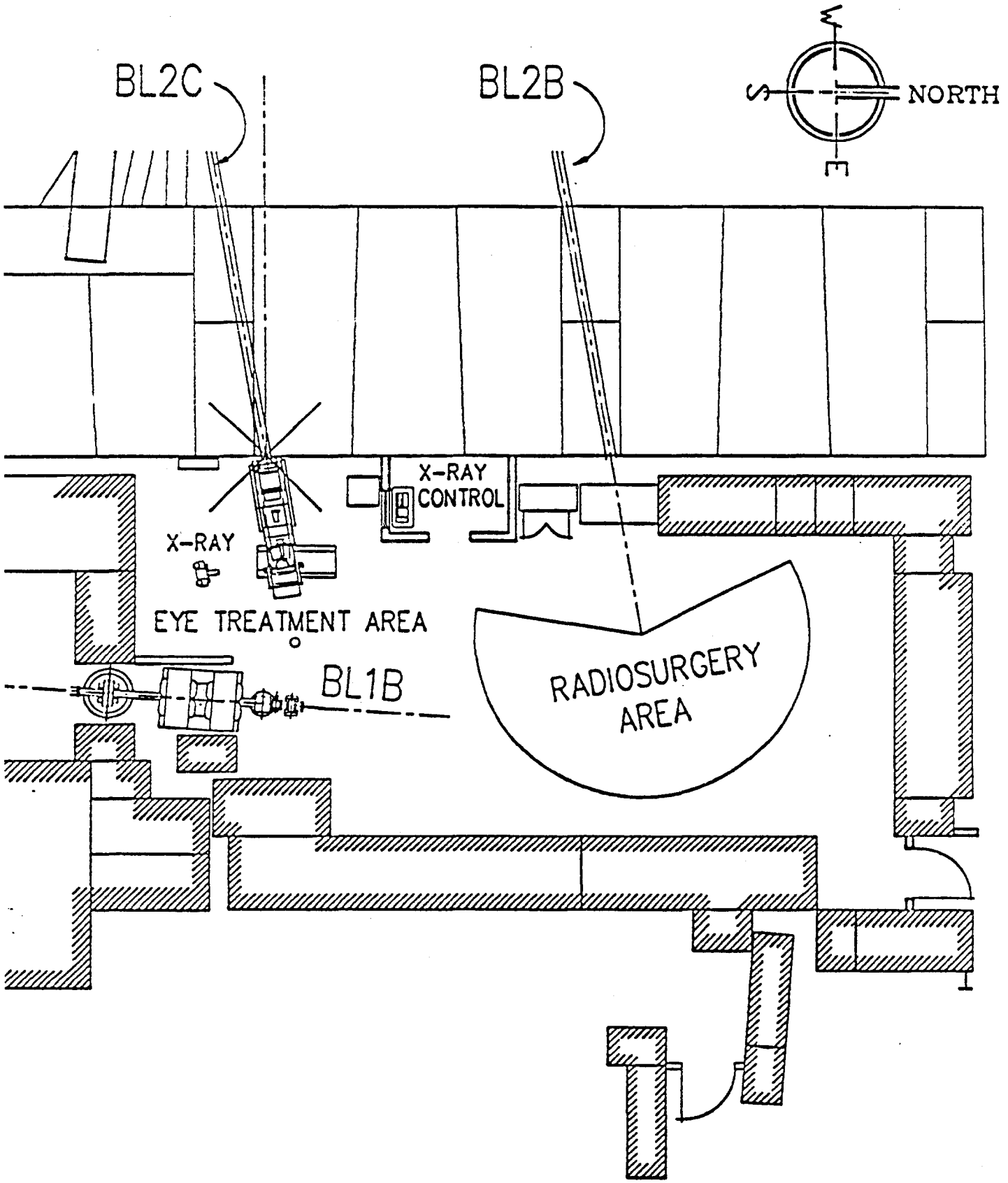

Fig. 11. Layout of the combined eye treatment and radiosurgery area.

PROTON RADIOGRAPHY

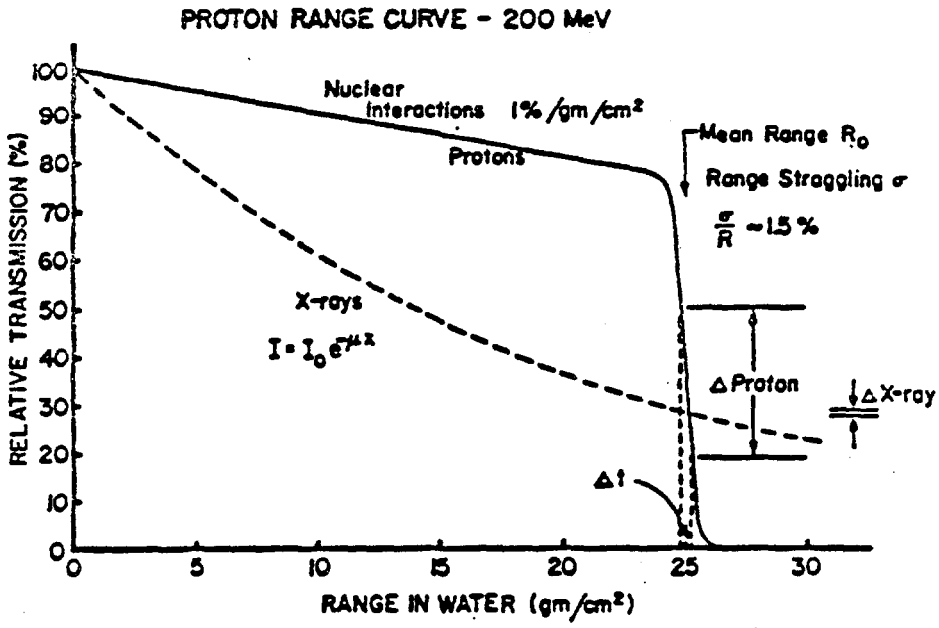

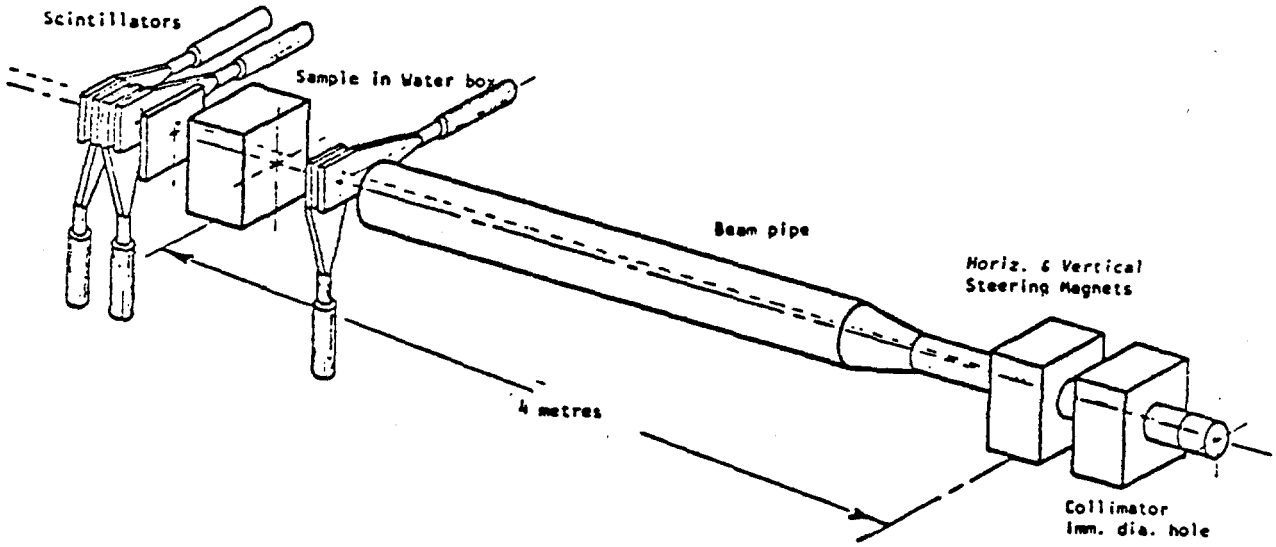

Fig. 12. Schematic arrangement for scanned beam proton radiography

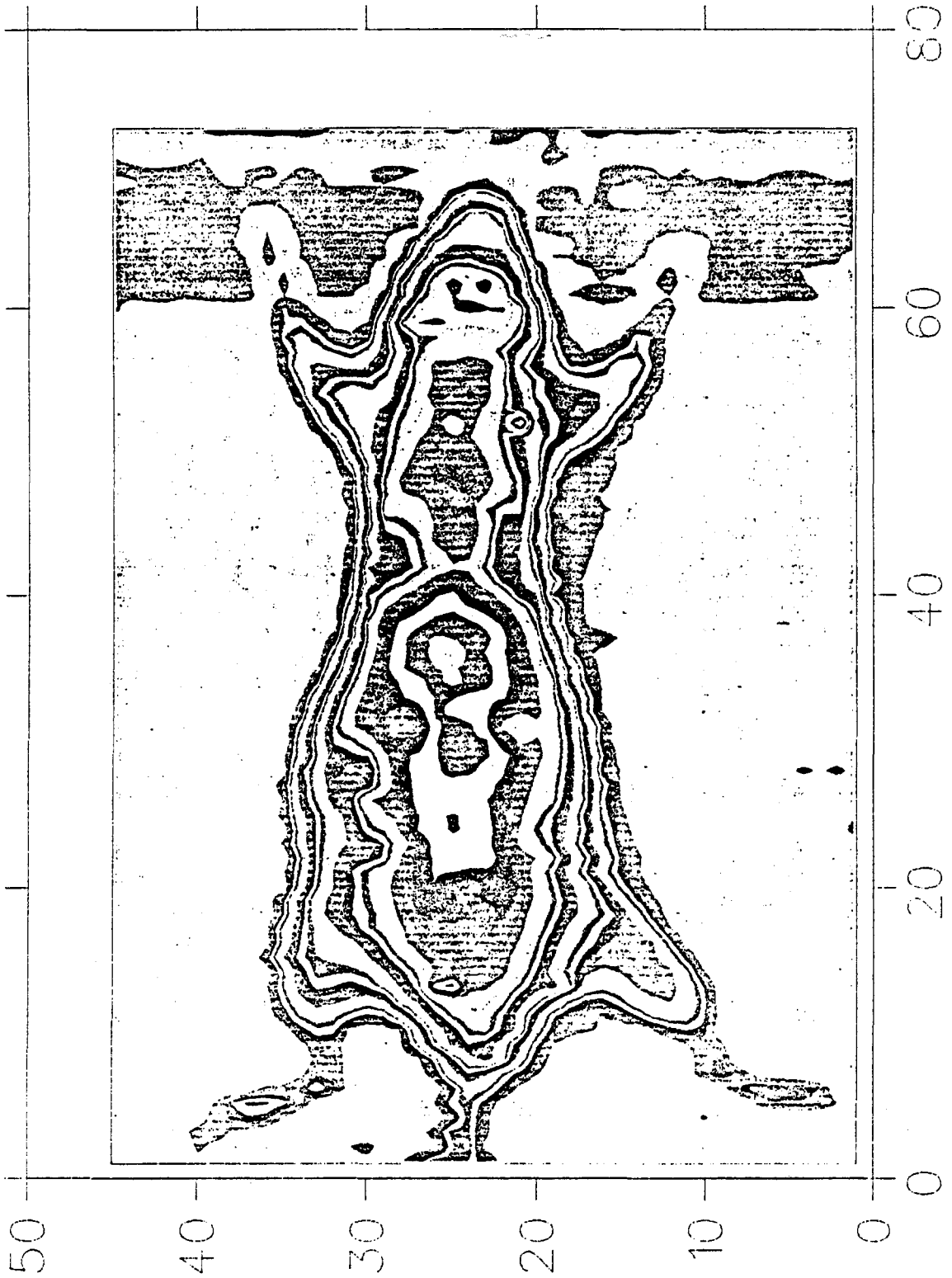

Fig. 13. Contour plot of mouse taken with 200 MeV protons.

Present Status and Future Plans for Proton Beam Therapy at Tsukuba

Sadayoshi Fukumoto
National Laboratory for High Energy Physics
Oho 1-1, Tsukuba-shi, Ibaraki-ken, 305, Japan

400-MeV Beam Workshop at Fermilab
October 25,1993

Abstract

Cancer therapy is ongoing with KEK 500-MeV protons. They are decelerated to 250 MeV with a graphite degrader and irradiated to patients with a passive delivery system. Liver cancer and others have been successfully treated. Hospital-based dedicated facilities based on a synchrotron and a cyclotron are designed.

1. Introduction

When the proton accelerator complex was being built at National Laboratory for High Energy Physics, KEK, in 1970's, medical use of high energy protons was proposed. Because of energy and intensity of the available protons, proton beam therapy was chosen referring the clinical results of Massachusetts General Hospital with protons of Harvard Cyclotron Laboratory.

2. Present Facility

In 1980, a medical organization, Particle Radiation Medical Science Center (PARMS), University of Tsukuba, was founded and its facility construction started at KEK. It aimed at clinical trial of cancer therapy with fast neutrons and proton beams, and development of radiography using KEK protons. The KEK proton accelerator complex consists of 750-kV Cockcroft preaccelerator, 20-MeV injector linac, 500-MeV Booster Synchrotron and 12-GeV Main Ring. During acceleration, extraction and return phase of the Main Ring magnets, 500-MeV protons are transferred to Booster Synchrotron Facility, which includes PARMS, materials science with neutron diffraction and meson physics groups as shown in Fig. 1.

Thus, only 9 pulses are injected into the Main Ring out of 80 pulses in one Main Ring cycle of 4 seconds.

The PARMS had three rooms of high energy beams. The first one was a treatment room equipped with a vertical beam for proton beam therapy (Fig. 2). This is the first vertical beam for proton beam therapy in the world. The second one was a treatment room with fast neutrons that were supplied from the spallation source. Neutrons were used for biology but no patient has been treated with them. When PARMS was reorganized to Proton Medical Research Center (PMRC) in 1990, the neutron treatment room was closed. The third room was a room for radiography. However, it was modified to a treatment room with a horizontal beam (Fig. 3). There were three reasons for the modification as follows. (1) Since the Booster beam was a several ten nano-second pulse every 50 milli-second, it took too long time to take CT pictures. (2) X-ray CT and MRI became popular very quickly. (3) Skin reaction of proton beams was bigger than supposed, so that two-portal irradiation was preferred.

Protons of 500 MeV pass through a human body. They can be used for therapy just like cross-fire, but their energy is too high to use Bragg peak advantage. Therefore, they are degraded with a 53-cm graphite degrader to 250 MeV with a 1-m long, 24-mm diameter iron collimator (range in water 32.7 cm). The degraded beams are analyzed by a spectrometer. To get 10 nA, a large emittance of 183 π mm.mrad and a momentum width of 1.35 % are tolerated[1]. The beams are expanded laterally by multiple Coulomb scattering of 6-mm thick lead plate (Fig. 4). Since the repetition rate of the Booster Synchrotron is 20 Hz, the spot scanning would take too long time for patient irradiation. A uniform field of 16 cm $\times$ 16 cm is obtained at the patient position, 5 m apart from the scatterer. Two other degraders were installed to get different energies, but they have never been used for patient treatment.

Momentum spread for spread-out Bragg peak corresponding a tumor is produced with a ridge filter (Fig. 5). Two collimators are in the delivery system. One defines roughly the field with a square opening. The other is a block collimator, which is a stack of metal plate 5-mm thick and high enough to stop protons completely (Fig. 6). It is placed just upon the patient and defines the field shape

finally. The bolus is a kind of energy absorber and designed by treatment planning to make maximum energy distribution corresponding to distal shape of the cancer. It is made of wax-like material, Mix-DP, with an NC milling machine, and put on the block collimator.

The scattering system has merits of simplicity and dependability, which are important for safety and efficient treatment. It can accept any beam time structure too. On the other hand, beam utilization efficiency is higher in a scanning system. This, in turn, a scanning system can decrease unwanted neutron dose to a patient. Even for the scattering system, however, estimated neutron dose equivalent is at the most one thousandth of proton irradiation dose equivalent and no effect has been detected clinically so far.

3. Clinical results

Because of high energy advantage at Tsukuba, and because of less frequent eye melanoma in Japan, mostly deep-seated tumor has been treated[2]. Patients treated so far is not so many, but more than ones treated with pions at Los Alamos. Liver cancer is not rare in Japan as in the U.S., and its overall 5-year survival is only 3 %. The results of liver cancer treated at PMRC are shown in Table 1 with results of other cancers. Although figures shown are 3-year survival, they seem quite promising and much different from conventional radiotherapy experience. The total dose amounts to 80 Gy typically. The liver moves with respiration, so that the proton acceleration is synchronized with its movement (Figs. 7,8). This method is effective for reduction of normal tissue irradiation (Figs. 9,10).

When the accelerator is running, machine time of three hours is assigned to patient treatment everyday afternoon except weekend. Because of competition among Booster Synchrotron Facility users, the PMRC machine time is limited to four hours a day including three hours above mentioned. Other clinical results including esophagus, lung and bladder cancer also seem to demonstrate merits of the proton beam (Figs. 11,12).

Irradiation time is about 2-3 minutes without respiration synchronization, whereas 5-10 minutes with it. The time for patient

setting is typically 10 minutes. During patient setting, proton beams are switched to another user.

4. Future plans

Patients treated with proton beams in the world is more than ten thousands and increasing rapidly. Eye melanoma is treated with an accelerator of around 70 MeV, whereas deep-seated tumor treatment needs about 250 MeV. The maximum energy at the patient so far is a little bit lower than 200 MeV at Tsukuba, therefore, a design goal of 230 MeV is chosen for the dedicated facility plan. Since eye melanoma is rare in Japan, its treatment is not included in the future plans.

4.1 Synchrotron version

A few years ago, we hoped approval of a dedicated proton beam therapy facility would be soon, and supposed no enough time for R & D of the new accelerator and equipments. At that time the Fermilab design for Loma Linda University Medical Center was already disclosed. We preferred a well-established, strong focusing, separated-function synchrotron instead of an edge focusing machine[3]. The 3-m long straight sections can accept the injection and extraction apparatus of the KEK Booster Synchrotron. Medical doctors always want a smaller accelerator. This type of lattice can shorten the straight sections with minor parameter modification (Fig. 13).

The injector is a commercially available 10-MeV linear accelerator. The simplest injection system is one-turn injection that was adopted by Fermilab design and needs a high current proton beam. The next simplest is charge-exchange injection, which is used routinely now. According to the 20-MeV H^- injection experiment at KEK, we estimated the system works down to 8 MeV. Thus a potential drawback of a high energy injection was removed. An H^- ion source is not so simple in operation as a duoplasmatron, but it is sill developing.

An appropriate untuned RF cavity was proposed by Fermilab. RF acceleration might be a "bottle neck" of a medical machine that requires simple structure and easy operation. A model cavity was

made and tested at KEK. It was confirmed that the cavity works well.

Requirement for beam time structure depends on the beam delivery system. To irradiate a tumor uniformly, the beam must be expanded spatially with a scatterer or scanned magnetically. No restriction is for a scattering system, but uniform beam spill of slow extraction is required for a scanning system. We assumed a scattering system at the phase one and later a scanning system in the future plan, because the scattering system is working satisfactorily now.

The planned facility has two treatment rooms. Room No.1 is equipped with a horizontal beam and two vertical beams, one from the upper direction and the other from the lower direction. Room No.2 is equipped with two vertical beams as Room No.1, but no horizontal beam.

4.2 Cyclotron version

In fall of 1991, Sumitomo Heavy Industry Co., in Japan and Ion Beam Applications in Belgium jointly proposed a compact cyclotron for proton beam therapy[4]. Its energy is fixed to 230 MeV. Its weight is about 200 tons, one fifth of conventional cyclotron of this energy, but it is not a superconducting one. We called for cyclotron experts to a meeting on this cyclotron. The conclusion is "in principle, it is possible" (Fig. 14).

On the contrary to the early expectations, the dedicated facility will be approved not so soon. Then a plan was made based on the cyclotron[5]. Fixed 230-MeV energy is acceptable because eye melanoma treatment is not included in the plan as mentioned above, and because other energies than 250 MeV were not used till now although the present PMRC facility has capability of selecting three steps of energy.

If the cyclotron is equipped with an external ion source, it is very easy to turn on and off the beam quickly. This might be a favorable feature for scanning system with CW beam characteristics. This is one reason why we are interested in the cyclotron. Since the needed beam intensity is one thousandth of conventional cyclotrons, the external source might be effective to prevent over dose in case of ion source failure.

Even for proton beams, a rotating gantry is favorable. According to experiences at PMRC, it is not only useful to decrease skin effect, as mentioned earlier, but for treatment where a head is irradiate from several directions. In the stage of the synchrotron version design, few patients of this type of disease, AVM, were treated, but later, the number of patients increased. Therefore, in the cyclotron version, one treatment room is equipped with a rotating gantry. The design goal of uniform field is 15 cm × 15 cm. The drift space from the first scatterer to the patient is 3 m. The other room is equipped with a vertical and a horizontal fixed beams. Much bigger field can be produced in this room.

The facility will be built next to the conventional radiotherapy facility in the University Hospital of Tsukuba.

5. Conclusion

A fixed-energy beam of 500 MeV is decelerated to 250 MeV and used for cancer therapy with a passive delivery system. This enables us to treat patients reliably, safely and quickly. The needed beam intensity is at the most 10 nA even for a single scatterer beam-delivery system, while any beam time structure can be accepted by the passive system. Drawback of the system in dose distribution is greatly reduced by multi-portal irradiation that is common in conventional radiotherapy. Two dedicated facilities are designed. Either a synchrotron or a cyclotron can deliver proton beams for therapy. The former has an advantage of variable energy, whereas the latter with an external ion source is more suitable for a scanning system.

References

1) D. Kurihara et al., A 300-MeV proton beam line with energy degrader for medical science, Japanese Journal of Applied Physics, Vol. 22, 1599-1605, 1983.
2) H. Tsujii et al., Clinical results of fractionated proton therapy, Int. J. Radiation Oncology Biol. Phys., Vol. 25, 49-60, 1993.
3) K. Endo et al., Medical synchrotron for cancer therapy, Proc. European Particle Accelerator Conf., 1459-1561, 1988.
   S. Fukumoto et al., A dedicated proton accelerator for cancer therapy, Particle Accelerators, Vol. 33, 153-158, 1990.

S. Fukumoto et al., Tsukuba medical proton synchrotron, Proc. Int. Heavy Particle Workshop, PSI, 70-74, 1990.
4) Y. Jongen et al., Progress report on the IBA-SHI proton therapy system, Proc. 13th Int. Conf. on Cyclotrons and Their Applications, 244-247, 1993.
5) S. Fukumoto et al., A proton therapy facility plan, ibid., 258-261.

Table caption

Table 1. Results of proton beam clinical trial at Proton Medical Research Center, University of Tsukuba.

Figure caption

Fig. 1. Bird's eye view of Proton Medical Research Center, University of Tsukuba. Proton beams come from upper right and go to one of three facilities, PMRC(left), spallation neutron target(center) and Meson Physics Facility(right).

Fig. 2. Treatment room with a fixed vertical beam.

Fig. 3. Treatment room with a fixed horizontal beam.

Fig. 4. Beam delivery system of the vertical beam. The proton beam is expanded laterally with a scatterer.

Fig. 5. Ridge filters. They produce momentum spreads of protons and spread-out Bragg peaks corresponding to the sizes of tumors.

Fig. 6. Block collimator(left) and bolus(right). The block collimator is a stack of metal plate 5 mm thick with an opening of the cancer shape. It is high enough to stop the protons outside the cancer. The bolus is an energy absorber to make the maximum energy distribution corresponding to distal shape of the cancer.

Fig. 7. A strain gauge sensor is attached to a patient to detect movement of the body caused by respiration.

Fig. 8. Signal from the respiration sensor with level setting pulses (upper trace) to produce gate pulses for accelerator beams (lower trace). Delivered proton beams are shown in the middle trace.

Fig. 9. Treatment planning of two-portal irradiation for liver cancer. A cross section of the bolus is determined from the distal tumor configuration of the CT slice.

Fig. 10. Recurrent liver cancer. Black area in the left before treatment(left) almost disappeared 2 years after the treatment(right).

Fig. 11. Esophagus cancer. Before treatment(left), and 26 months after treatment(right).

Fig. 12. Arterio-venous malformation(AVM). Before treatment (left), and 15 months after treatment(right).

Fig. 13. Synchrotron-based dedicated proton beam therapy facility plan. Two treatment rooms are equipped with fixed beams.

Fig. 14. Commercially available cyclotron-based dedicated proton beam therapy facility. One treatment room has a rotating gantry, and the other has horizontal and vertical fixed beams.

Table 1. Results of proton beam clinical trial at Proton Medical Research Center, University of Tsukuba

July 1993

Site	No. of patients	Local control (%)	3-year survival	Morbidity
Skin	8	7 (87.5)	87.5	0
Brain Glioma	17	5 (29.4)	18.5	3
Menineioma	14	12 (85.7)	75.0	0
Head and neck	21	14 (66.7)	73.3	0
Lung	21	15 (71.4)	45.0	1
Esophagus	28	22 (78.6)	53.8	4
Liver	70	59 (84.3)	41.4*	3
Stomach	5	3 (60.0)	61.0	0
Kidney	5	2 (40.0)	60.0	0
Uterus	26	21 (80.8)	80.0	3
Bladder	19	14 (73.7)	86.0	2
Prostate	8	8 (100.0)	86.0	0
Pediatric tumors	6	5 (83.3)	75.0	0
Others	4	3 (75.0)	100.0	1
Total	252	190 (75.4)		17(6.7%)

* 75.0 % for good liver function

A1: Energy degrader & collimator
A2: Medical proton beam line
A3: Vertical beam delivery system
A4: Horizontal beam delivery system
A5: Treatment room
A6: Dose monitoring system
A7: Treatment planning room
A8: Alignment device
A9: Proton CT apparatus

B1: Neutron irradiation apparatus
(not used at present)
C1: Radiation safety control system
C2: Data processing and beam control

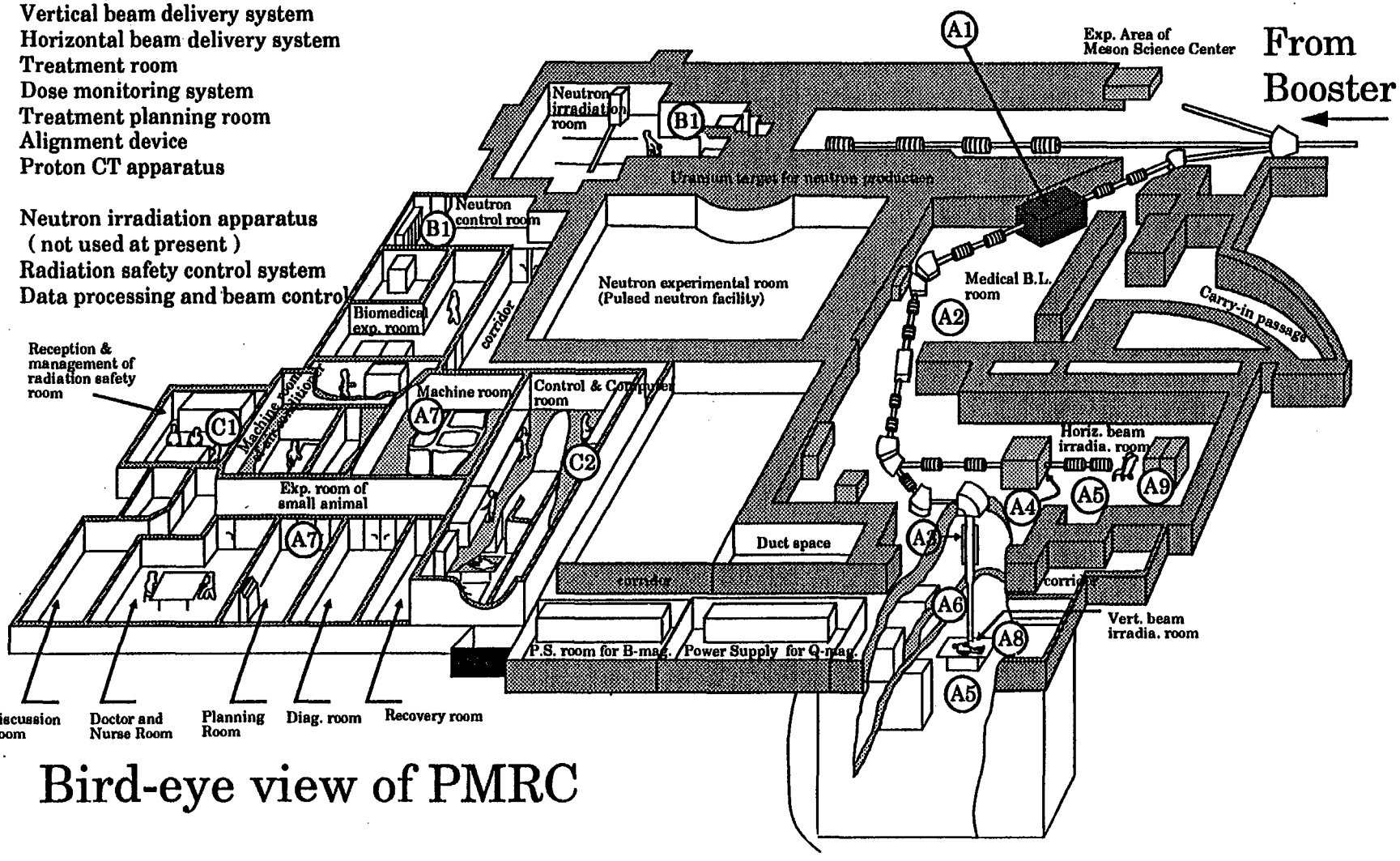

Bird-eye view of PMRC

Two beam ports (Vertical & Horizontal) available

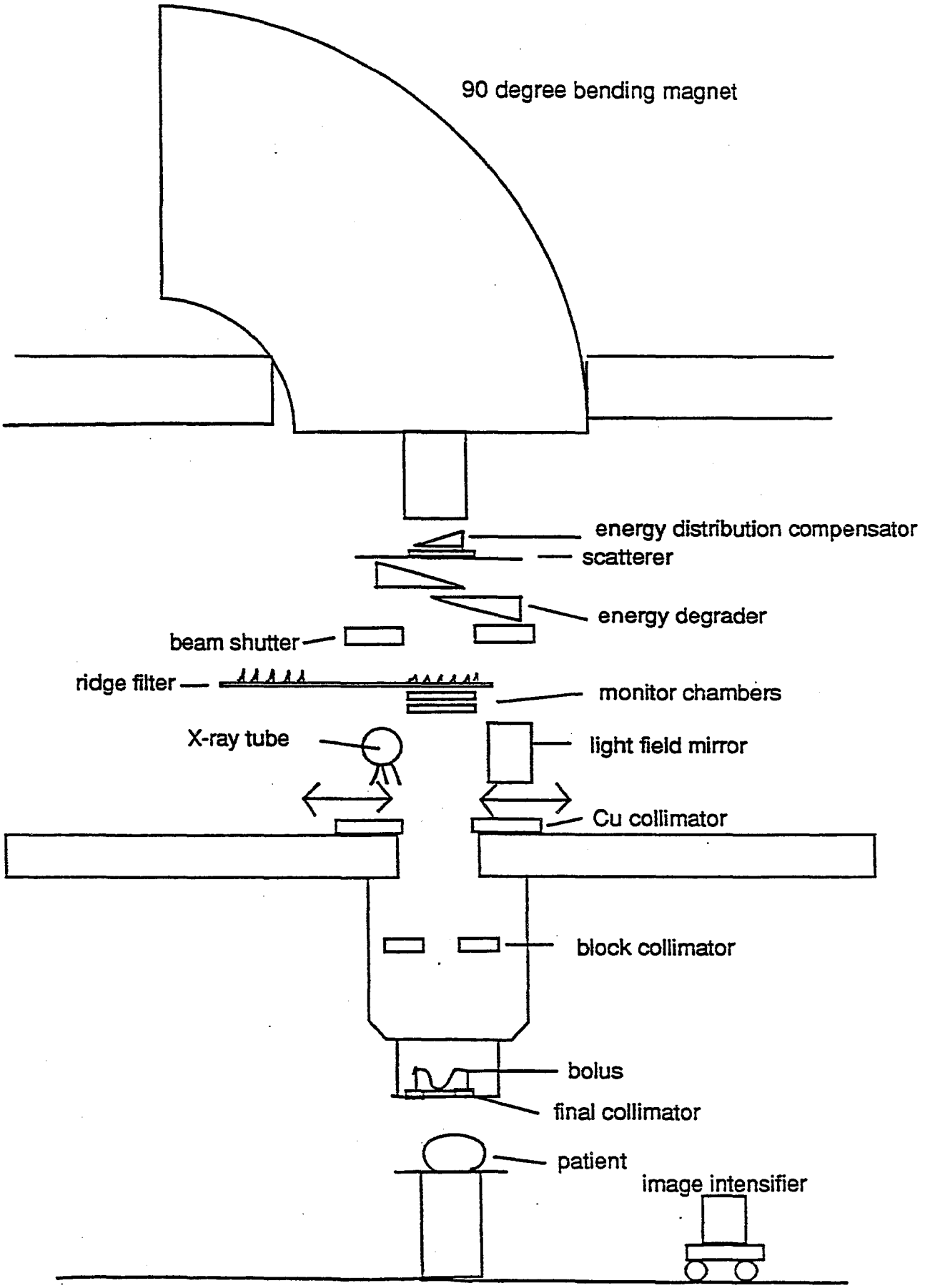
90 degree bending magnet
energy distribution compensator
scatterer
energy degrader
beam shutter
ridge filter
monitor chambers
X-ray tube
light field mirror
Cu collimator
block collimator
bolus
final collimator
patient
image intensifier

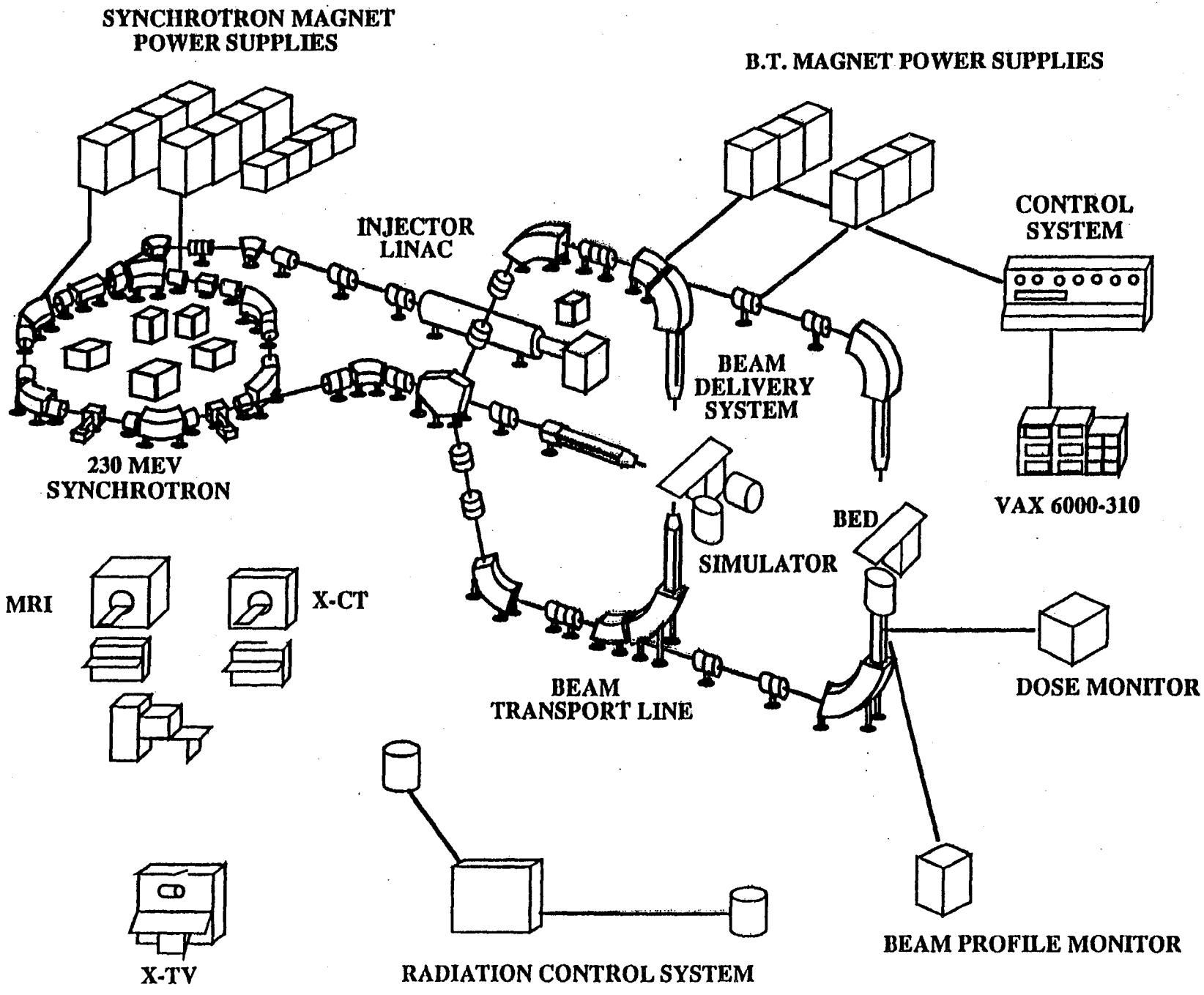
SYNCHROTRON MAGNET POWER SUPPLIES
B.T. MAGNET POWER SUPPLIES
CONTROL SYSTEM
INJECTOR LINAC
BEAM DELIVERY SYSTEM
230 MEV SYNCHROTRON
VAX 6000-310
BED
SIMULATOR
MRI
X-CT
DOSE MONITOR
BEAM TRANSPORT LINE
BEAM PROFILE MONITOR
X-TV
RADIATION CONTROL SYSTEM

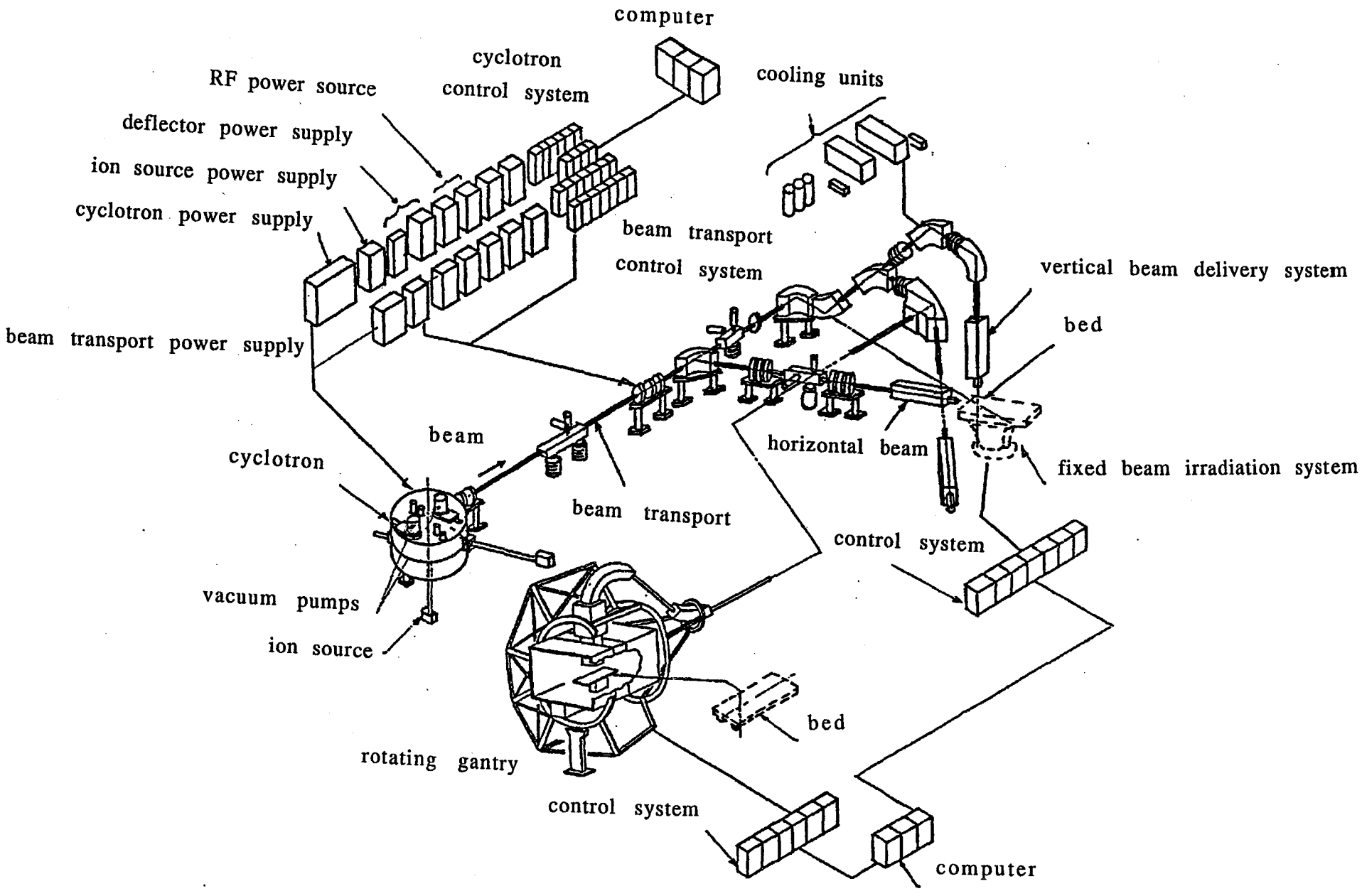
computer
cyclotron
control system
RF power source
deflector power supply
ion source power supply
cyclotron power supply
cooling units
beam transport
control system
vertical beam delivery system
bed
beam transport power supply
beam
cyclotron
horizontal beam
fixed beam irradiation system
beam transport
control system
vacuum pumps
ion source
bed
rotating gantry
control system
computer

Practical Implementation of a Proton Radiation Therapy Facility

Donald Rosselot
Project Engineer
Proton Radiation Therapy Research Project
Department of Radiation Oncology
Indiana University School of Medicine
Indianapolis IN

Abstract:
A proton therapy facility is in operation at the Indiana University Cyclotron Facility [1] for cancer study and treatment. The cost of implementing the proton therapy facility was less than $500,000 and took 1.9 years to complete after receiving funding. The average staff at the site was only 2.5 (Ph.D. Physics, M.Sc Physics. and/or B.S.E.E., typical). Virtually all of the specific design work and fabrication required for the treatment room, control system and control room was accomplished in the last year and a half and culminated in our first patient treatment, September of 1993. The project was accomplished by multitasking personnel and by using (where possible) existing accelerator lab resources, existing software, used hardware, and using personnel and techniques from the I.U. Department of Radiation Oncology. Systems were designed for simple manufacturing techniques and all beam-line components requiring vacuum (i.e. the SEM's) were designed to fit in our standard beam pipe (four inch i.d. Dependex). Many of our practical solutions and techniques in implementing a proton radiation therapy facility can be applied elsewhere.

Important note: This document is not intended to be a general description of the Indiana University proton radiation therapy project. For this description please refer to [1]. Nor is this document intended to be a text on proton therapy concepts in general. For an excellent introduction to proton therapy and other heavy particle therapy, please refer to the book by M. Raju, *Heavy Particle Radiotherapy*, 1980 [7].

LIST OF FIGURES:

LIST OF ABBREVIATIONS

CSF: Contour Scattering Foils. CT: Computer Tomography. CTF and CTF2: Current To Frequency converters/electrometers. DADDIO: Digital Input/Output board. GUI: Graphical User Interface. HLBCS: High Level Beam Current Sensor. IUCF: Indiana University Cyclotron Facility. MWIC: Multi Wire Ion Chamber. NEU: beam spreading Nozzle with Everything Upstream. NIM: Nuclear Instrument Module (or corresponding electronics standard). RF S/D Xmitter: Radio Frequency Shut Down Transmitter. SEM: Secondary electron emission monitor. WP: Water Phantom.

1) SAFETY

We have tried to design and build a proton therapy facility as safe as practically possible. A procedural check list is run through and filled out for each patient treatment. The control computer and electronic systems are backed by an un-interruptable power supply. Virtually all electronic and control systems which affect patient safety at the I.U. Proton Therapy Facility feature fail safe logic. Any wire disconnection, any sensor failure or any power failure to all systems that could present a safety risk to the patient will cause an immediate stop to the treatment. There are several shutdown modes (3 fully independent shutdown modes) to stop a patient treatment. Normal shutdown mode, which occurs at the end of the treatment and is automatically initiated by the control computer. Emergency # 3 shutdown mode (# 3 halt), which stops the beam functionally the same as the normal mode, except that it may be initiated by the control computer, a dedicated hardware device or the operator via the X-terminal control console (see description below), and occurs before the end of the treatment. Emergency # 2 shutdown mode (# 2 halt), which is hard wired to the interlock circuit (see description below), functions independent of all computers and effects only the proton therapy beam. Emergency # 1 shutdown mode (# 1 halt), which is hard wired to the RF shutdown circuits (see description below), functions independent of all computers, and quickly stops all beam in the cyclotron. There is a "panic button" key switch located next to the control terminal and a panic button at the treatment room door for stopping the beam.

2) HUMAN RESOURCES

To design, build and operate a proton therapy facility, expertise in the following fields will probably be required.

a. Physics

Accelerator physicist
Cyclotron operator

b. Engineering and technical

Electrical engineer
Controls engineer
Electronic engineer
Electronic assembly, repair and test technician
Mechanical engineer
Mechanical systems assembly, repair and test technician
Computer programmer
Machinist
Detector and dosimetry system specialist

c. Medical

Radiation Oncologist
Medical Physicist
Radiologist
Dosimetrist
Radiation therapist
Radiation therapy nurse

d. Administrative and Financial

Our solution:
During the construction phase of the project at the accelerator lab, we were able to minimize human resource requirements by multitasking and paralleling job duties of the I.U. medical group personnel at the accelerator lab and thus i.) virtually eliminated multiple personnel requirements ii.) greatly reduced the use outside contractors iii.) minimized the use of the general IUCF labor pool and iv.) minimized the use of human resources from the I.U. Medical Center at Indianapolis.

a. Physics and

b. Engineering

A staff scientist at IUCF (Vladimir Derenchuk, M.Sc.) did the initial investigations, feasibility and requirements work. A nuclear physicist (Chuck Bloch, Ph.D.) at IUCF was hired to manage the project at the Lab. Dr. Bloch's roles included accelerator physicist, computer control system programmer, laboratory liaison, personnel director, major systems specifier, and writer/researcher. Engineering and technical support were provided by Donald Rosselot, E.E. (electrical, controls, electronic, dosimetry hardware, mechanical systems design, programming, specifications, purchasing, fabrication, electronic assembly, machining, systems installation, writing and experimental setup) and Matt Fasano (beam shaping system design, mechanical system design, machining, fabrication and installation, electronic assembly, experimental setup, detector hardware fabrication, programming, purchasing and writing).

c. Medical

Personnel costs were minimized during the six days of the (first and only to this date) patient treatment phase of the project by utilizing existing employees at the I.U. School of Medicine. The necessary staff traveled 1.3 hours from the I.U. Medical Center in Indianapolis to the IUCF lab in Bloomington IN. This staff included:
George Sandison, Ph.D., Medical Physicist; Jim Morphis, M.D and Radiation Oncologist; Moses Spray, Radiation Therapist; Rose Powers, Radiation Dosimetrist; Donna Cocks, Radiation Therapy Nurse; Jane Berby, Chief Radiation Therapist.

d. Administration and Financial

Administration and Financial matters were handled through the Department of Radiation oncology at the I.U. Medical Center.

3) PROTONS AT 200 MeV OR GREATER ENERGY

To obtain protons of this energy with today's technology requires an expensive ($50 million +) accelerator.

Our Solution:
George Sandison, Ph.D. (Chief Medical Physicist, Department of Radiation Oncology, I.U. Medical Center) initiated the project. He reached an agreement with the I.U. Cyclotron Facility (IUCF) to begin a proton therapy project and use (where possible) existing lab systems. A small experimental area capable of receiving up to 200 MeV proton beam at variable current [1] was designated the proton therapy room. To minimize the impact on the nuclear physics research work at the lab, the beam is "split" (using an existing fast switching magnet/lambertson septum magnet system) to another user any time the proton therapy group is using the beam [2].
The IUCF staff and administration have been very supportive of the proton therapy project and deserves a special thanks. Proton therapy research at a physics proton accelerator laboratory benefits the lab by creating general public interest and easily recognizable public benefits in a world of vague understanding of basic physics research.

4) DOSE SHAPING SYSTEMS

The proton beam must, in general, be spread out with an even energy distribution across the field (flattening) and the depth of the field must be varied within the tumor site to obtain the full benefits of the properties of proton radiation [4]. The two basic methods for beam flattening systems are active and passive. Depth spreading of the dose must be accomplished by modulating the energy of the beam.

Our solution:

4) a. Beam area spreading

Passive spreading of the proton beam is based on designs created with the NEU (Nozzle with Everything Upstream) program (copyright 1990, President and Fellows of Harvard College, file NEUDOC.TEX) by Dr. B. Gottschalk [3]. The NEU design program is extremely versatile and we found good agreement between predicted and experimental results. NEU allows for several user input variables including beam energy, divergence, materials for the first scattering foil, materials for the contoured scattering foils (CSF) and distances between the first foil, CSF and the patient. An annular scattering system is also permitted (and easier to machine) but our best results were obtained with the CSF using lucite and lead for the contour materials and lead only for the first target foil. Our first foil is mounted on a target ladder in vacuum and is simply a square piece of lead of the appropriate thickness. The CSF was machined in the IUCF machine shop with a computer controlled milling machine. The lucite was machined first and the lead was glued with epoxy to the lucite. A good quality machineable epoxy should be used (i.e. Eccobond 45 clear epoxy with catalyst 15 clear resin hardener, Emerson & Cumming Canton, MA). The lead was then machined.

4) b. Beam depth spreading (Range Modulation)

The proton depth dose distribution has a sharp peak, known as the Bragg peak. The distal edge of this peak falls off very rapidly to zero. To obtain a uniform dose over a typical tumor, the peak is spread out into a plateau. Beam depth spreading is accomplished by dynamically varying the energy of the beam. This is done with an acrylic energy degrader (fan) of varying widths [10] [see Fig. 7]. A two blade fan design was used and constructed out of 6 mm lucite sheets. This was very easy to manufacture, and can be made very rigid by gluing the individual sheets with clear acrylic cement. The specifications were calculated by "fan_design" program, written in Fortran by C. Bloch, Ph.D, Indiana University School of Medicine. The fan is driven by a 1/4 Hp, 10 amp dc motor at a constant speed, usually between 11 and 17 rev/sec. Poor dosimetry profile measurements occurred with the water phantom (see description below) at frequencies near multiples of the beam split frequency due to beating.

4) c. Range shifting

The beam energy, if higher than needed for experiments or treatment, may be "range shifted" to a lower energy. This may be accomplished by placing energy absorbers of the appropriate thickness of acrylic or other low Z material to obtain the desired range for the beam. This is particularly convenient when the beam energy is fixed during an experimental run or a treatment requiring multiple ports and multiple energies. Energy shifting by this method causes the mono-energetic beam to become energy straggled. A poorly defined range and diffuse bragg peak is expected for a high energy beams (i.e., 800 MeV) when compared to a beam of 100-200 MeV [7] [9]. The range shift can be accurately measured in a Water Phantom dosimetry system (WP), calculated with the range_shift program (Fortran), or found in data tables (e.g. Janni [11]).

5) DOSIMETRY AND DETECTOR SYSTEMS

Detectors of various types are required to setup and monitor the dose and beam properties. One quality commercial ion chamber for monitoring dose can easily cost $10,000. Most accelerator labs have detector design and assembly capabilities and manufacture their own. IMPORTANT NOTE: The dosimeters commonly used (i.e. TLD's and ion chambers) may not give linear and/or comparable results in all range of beam currents, between types of dosimeters and between types of radiation [8].

Our Solution:

There are five independent detectors (two SEM's, two split ion chambers and a multi-wire ion chamber, see descriptions below) in the proton therapy beam line to monitor beam properties and/or dose. All of our detectors produce a current output which is processed by several electronic devices (see descriptions below). First they are converted to a frequency pulse train (whose frequency is proportional to the incoming current) by a current to frequency converter (either a CTF or CTF2, which differ in sensitivity). These output pulses are counted by LeCroy 1151 scalers, which are read through the VME bus by the rt300 computer. Signals are processed by the rt300 control computer and compared with acceptable operating parameters that are established during the setup and calibration procedures to confirm the correct operation of each detector. Signal analysis consists of comparing the ratio of several signal pair subsets from all detectors and the level of each detector signal. For example, the output current ratio between the split ion chamber #1 and SEM #1 are dynamically compared during treatment for ratios outside of the limit setpoints. Failure of a detector or signal to remain within it limits will cause a termination of treatment. This signal analysis is protection against signal loss in either of the

SEM's, loss of vacuum that could effect SEM calibration, loss of gas flow to the MWIC which would affect calibration, loss of bias voltage to the ion chambers which would effect calibration, against intentional or unintentional modification of beam-line components, or against calibration changes occurring in any detector or electrometer circuit for whatever reason.

5) a. SEMs

The SEMs (Secondary Electron Emission Monitors [5]) are the primary dose monitor detectors at the IUCF proton therapy facility. They also provide signals for the HLBCS system (see below). There are two independent SEMs in the proton therapy beam line which are used to redundantly monitor the dose. SEMs are very linear over a wide range of beam intensities and energies, and unlike ion chambers, they are not susceptible to saturation at high beam intensities. The SEMs, which must be operated in vacuum, are relatively insensitive to changes in bias voltage. Each SEM is constructed of eleven, .0003 inch-thick aluminum foils (Alufoil Products Co, Hauppauge NY) and bonded with high vacuum epoxy (Varian, Lexington MA.) and conductive adhesive to aluminum rings (Fig. 6). Aluminized mylar is not recommended in place of aluminum foils because radiation damage to the mylar will necessitate periodic replacement. Beam energy loss caused by these foils is negligible. They are held together with three steel rods and spaced with ceramic beads (Omega Inc, Stamford CT.) to minimize the leakage current. Every other foil is biased at -100 volts and electrons are knocked off the foil surface by the high energy protons. The electrons are collected by the unbiased foils (which are connected electrically), and their summed current is processed by the CTF2 (see description below). The gain of this SEM is approximately 0.8 of the beam current, i.e 10 nA of beam produces 8 nA output current. The total number of pulses from the CTF2 is directly related to the total integrated dose and the pulse rate is directly related to the dose rate. These pulses are counted by independent LeCroy 1151N scalers (see description below) which monitor the dose and will terminate treatment independent of all computers in the event the control computer does not. The SEM's are calibrated against both a Farady Cup and a Markus ion chamber, whose calibration is traceable to a national standard. Hence the SEM's provide both a measure of beam current (in nA) and dose (in cGy). SEM bias is monitored by SEM bias detectors (described in the electronic section below) and deviation of bias voltage will initiate treatment halt.

5) b. Split ion chambers

The two split ion chambers are refurbished CGR Sagitaire (commercial electron-photon radiation

therapy machine) monitor chambers. Each chamber has two planes and each plane is split, two vertically and two horizontally. These ion chambers redundantly monitor the symmetry of the beam. The gain of our ion chambers is approximately 50, i.e. 1 nA of beam produces a 50 nA output current. There are a total of eight current signals (4 signals from each ion chamber: up, down, left, right) and they are initially processed by the CTF. Beam position and trajectory at the entrance of the scattering system affects the beam symmetry, which in turn determines the lateral dose distribution. Beam asymmetry will cause a relative signal imbalance between the split ion chamber halves. By relating these signals to lateral dose profiles taken with the water phantom (see description below), the lateral dose distribution can be determined.

5) c. Multi Wire Ion Chamber (MWIC)

The MWIC [6] consists of two wire planes (vertical and horizontal), each with ten wires spaced at 2 mm, and two foil anode planes. The MWIC measures the incident beam position, profile and intensity.
Typical operation parameters are:

a) Gain --> Approximately 50, i.e. 1 nA of beam produces 50 nA output current summed from all wires (with bias voltage equal to -100 Vdc).
b) Bias Voltage --> -100 to -300 Vdc.
c) Beam Spot Size --> 3.5 mm (Full Width Half Maximum).
d) Gas type and flow rate --> Argon at 25 cc/min.

The MWIC is located upstream of the treatment room in the Beam Line 4 area (see figure 2) and is used to verify that the beam properties have not changed between calibration and patient treatment. The 20 channels from the MWIC are processed by the CTF and LeCroy Scalers for analysis by the local control computer (rt300) and for graphical display on the computer X-terminal.

5) d. Water Phantom (WP)

To map a simulated patient radiation dose, a detector (thimble ion chamber or diode) is placed in water on a three axis (x,y,z) computer controlled motion setup. (Water is used since it is a close approximation to human tissue as far as stopping power and electron density are concerned). A reference detector of the same type is placed on the front of the WP. The

radiation field is scanned in one or two dimensions and the signals from the scanning probe and the reference probe are integrated simultaneously, and their ratios are plotted as a function of position. The signals are normalized in this manner so that variations in beam current do not cause variations in the WP profile scans. Commercial WP systems are available to perform this task and plot the results on a computer. Beam profiles and depth-dose curves (Bragg peaks, lateral dose distributions, etc. for protons) can be obtained with the same systems commonly used in hospitals. Typical cost is $50,000 for a complete system including the water phantom, computer, computer controlled ion chamber, reference ion chamber, and software. Our WP (real time dosimetry system) was surplus from the I.U. Medical Center and is manufactured by Multidata Systems. Good results were obtained with this system for use in protons [Figure 9 a. and b.]. Because of the slow speed that a WP acquires the data, the iteration process of tuning the proton beam using only a WP is tedious. Therefore, several detectors (i.e. SEMS, MWIC, split ion chambers, viewing scintillators) are used in conjunction with the WP to speed beam tuning.

6) TREATMENT PLANNING SOFTWARE

To deliver the correct dose to the correct anatomical site, treatment planning software is required. Most treatment planning software on the market today has been designed for photons and electrons. For proton therapy application, the software must be capable of handling the special case of proton radiation.

Our solution:

Conventional treatment planning software was obtained from Dean Renner, University of Maryland (Renner Plan). This a UNIX, X-window based commercial software package and the cost is in the neighborhood of $25,000 (contact D. Renner for actual price). The Renner Plan will read in, graphically display, and manipulate Computer Tomography (CT) scans in color formats. The treatment can be simulated, including multiple port treatment plans, integrated with isodose curves onto the CT scans, and plotted out. We have installed it on an HP workstation running under Unix, and on Sun workstations at I.U. Medical Center. Dean Renner has provided us with access to the source code for the development of proton capabilities. Cris Lee (M.Sc.) and Xiao-Yi Lu (M.Sc.), working at the I.U. Medical Center have modified (and added approximately 1000 lines of Fortran code for the dose calculations and approximately 10,000 lines of 'C' code for the display and plotting routines) to incorporate proton beam characteristics into the package. We have used this system in a limited scope [Fig. 4] for protons and hope the

completed package will become available in the very near future. Contact G. Sandison for additional information.

7) PATIENT POSITIONING, ALIGNMENT AND PORT VERIFICATION SYSTEMS

POSITIONING:

We are using a fixed horizonal beam line 196.5 cm in height and we will restrict our initial treatments to head, neck and brain tumors. The patient is positioned by means of a hospital grade examination chair (Ritter Manufacturing, Model F, surplus from I.U. medical center) which features power driven 42 cm of motion in the vertical axis, +140/-180 degrees of manual rotation and +30/-15 degrees of power tilt. This chair is mounted on a custom built base (designed and built at IUCF by Donald Rosselot) which features power movement 19 cm laterally and 19 cm longitudinally, casters for expediting large movements/rotations, position lock brakes and quick brake release. The chair and base are controlled by a remote hand-held control which features digital position(angle) readout in tenths of a millimeter(degree). Due to the large amount of the flexibility in the treatment chair, reproducibility under load is no better than 2 mm. Therefore, lasers (accurate to .5 mm) are used for final positioning verification (see below).

ALIGNMENT:

Patient diagnostics, treatment planning, treatment simulation and head restraint custom fitting are performed at I.U. Medical Center using local staff and traditional methods and materials. After simulation at the I.U. Medical Center, alignment of the patient is repeated at the proton therapy facility with two opposing, laterally mounted, cross-hair lasers, one overhead-mounted, line-beam sagittal laser and one proton-beam-coincident rear-mounted point laser. This configuration is typical in conventional radiation therapy. The rear mounted point laser also serves to align beam line components and alignment-critical structures. It is easily removable to prevent bombardment by the proton beam during experiments. A point laser can easily be converted to a line or cross-hair laser by installing a 3/8 inch diameter glass rod in the laser beam near the laser output. A smaller diameter rod will create a larger length line (but less intense) for a given distance. By using surplus lasers (typical source, MWK Industries, Corona, CA) and glass rods (optical quality is best) we were able to assemble a complete alignment laser for $200 instead of (typically) $2000 from commercial vendors.

PORT VERIFICATION:

Port verification is done with a surplus portable X-Ray machine from the I.U. Medical Center. An overhead structure (rails) parallel to the beam-line (to better than .5 mm along the 7 foot span) supports linear bearings and (see Fig. 8) was designed, built, installed and aligned at IUCF by Donald Rosselot and Matt Fasano. The X-Ray head was mounted on the rails with an additional axis of linear motion perpendicular to the beam to permit the X-Ray head to be removed from the path of the proton beam. The X-Ray film cassette and the patient specific collimator are also mounted on the rail bearings.

8) ELECTRONICS AND CONTROL SYSTEM

Much has been written about computer control systems in general and several very good and economical commercial systems are available. There are a few special devices in a proton therapy control system that require design and construction of special circuits before integration into a commercially available computer control system.

Our solution: [See block diagram, Fig. 5 a. & 5 b.]

8) a. Electronics

i. CTF and ii. CTF2 Introduction

The CTF and CTF2 are NIM module current to frequency converters that utilize the charge pump current neutralization method. They are basically a LM331 IC chip (See National Semiconductor application note # 240 by R. Pease) with an op-amp at the input and a Motorola TTL to ECL (MC10124) on the output. ECL to NIM conversion is performed by a Motorola ECL driver chip (MC10192) and a 680 ohm resistor to ground on the driver output. Three layer (including ground plane) custom printed circuit boards were designed using the software package OrCad to mount the components to. CTF and CTF2 designer, Donald Rosselot (D.R.@IUCF).

8) a. [i] Indiana University Current-to-Frequency converter (CTF)

The CTF gain is optimized (.1 na to 200 uA, 100 Khz full scale) for use with our ion chambers and is used with the MWIC and the split ion chambers. The inputs (eight each) are currents (collected charge) and the outputs (eight each) are NIM pulses in a train whose frequency is

proportional to the input current. Alternatively, the output can be considered as one NIM pulse for every 100 pC of charge collected by the CTF. Those pulses are sent to the LeCroy 1151 scaler modules for processing and readout/display by the control computer.

8) a. [ii] Indiana University Current-To-Frequency converter model #2 (CTF2)

The CTF2 is our primary dose electrometer and is used in conjunction with the LeCroy 1151N scaler to integrate the dose. The CTF2 also provides a pulse train to the digital High Level Beam Current Sensor (HLBCS) circuit. The CTF2 gain is optimized for use with the SEMs (10 pA to 1 uA, 100 Khz full scale) and has four independent channels. The inputs (four each) is a current (collected charge). The outputs (twelve each, consisting of 2 NIM and one TTL per channel) is a NIM digital pulse train frequency that is sent to the LeCroy 1151N scaler module and a TTL digital pulse train that is sent to the HLBCS circuit. Two independent CTF2 modules are used to integrate the dose (leaving 3 spare channels in each module).

8) a. [iii] LeCroy 1151N

The LeCroy 1151N is a scaler module for the VME bus. A primary function of the 1151N is it is used in conjunction with the SEMs, the CTF2 and control computer to monitor dose. The control computer normally halts treatment within 1% of the prescribed dose by reading the 1151N count over the VME bus and initiating a normal treatment halt. For added safety, each 1151N module counts NIM standard pulses from the independent SEM's and is preset to count down and deliver an output pulse to halt treatment (via halt #1, #2 & 3) when the dose plus 5% is reached, independent of the VME bus and control computer. This high tolerance is allowed since this is the last level of redundant treatment halt mechanisms excluding operator intervention. Protection against failure of an 1151N is provided by the dual redundant independent 1151N modules and dose monitoring systems. Other uses of the 1151 are 1) integration of CTF processed wire chamber and ion chamber signals, 2) input for an external clock signal 3) as a general input for any pulse signal and 4) communication of count information of these signals to the VME bus for computer processing.

8) a. [iv] Matrix DAADIO input/output board

The DAADIO is an input/output module for the VME bus, manufactured by Matrix corporation. (DAADIO stands for Digital-to-Analog, Analog-to-Digital, digital-Input, digital-Output). The

DAADIO card is used for input or output of various signals (e.g. input: range modulator rotating OK, no high beam current detected; output: beam stop control) related to dose delivery and communicates with the control computer for appropriate action. Failure of this device would cause several fail-safe logic levels to change state, initiating a # 3 halt. Critical functions related to patient safety are backed by independent hardware devices, which initiate appropriate treatment halts independent of the DADDIO board. Normal treatment termination proceeds through the DADDIO board.

8) a. [v] High Level Beam Current Sensor (HLBCS) circuit

Our standard operating mode makes an excessive dose rate very unlikely. Although the IUCF cyclotron is capable of producing maximum beam currents of several uA, it is difficult to produce large currents, and a rapid increase of an order of magnitude is rare. However, the dual redundant HLBCS system was designed with rigid timing specifications and a dynamic range of 5 orders of magnitude to stop the beam before an overdose can occur under worst case conditions. The HLBCS is basically a specialized frequency counter. The HLBCS receives input from the CTF2 in the form of a TTL pulse train whose frequency is proportional to the beam current (the number of pulses is proportional to the delivered dose).. A higher frequency corresponds to a higher beam current or dose rate. A frequency set-point is established to correspond to a maximum allowable beam current which is found to cause ten times the expected (normal) dose rate. The HLBCS consists of two independent circuits and the setpoint is assigned with dip switches on one circuit and with software via the DADDIO board on the other. The outputs are digital signals to the RF shutdown Xmitter circuit and the interlock circuit (see descriptions below). The HLBCS monitors the signals from the CTF2's and are # 1 halt, # 2 and # 3 halt devices. The computer control system will initiate an independent # 3 halt if the dose rate is high by a factor of two more acts as a first level of dose rate control. Although the computer cannot respond fast enough to prevent an overdose in a worst case scenarios as does the HLBCS (i.e. massive beam current increase with fast beam current rise time near end of treatment), it acts as a triple-redundant level of protection for dose rate control. Beam overcurrent will cause a # 1, #2 and # 3 halt, an error message at the control console, a green LED to go off and a red LED to come on, and an audible alarm. Designer, D.R.@IUCF.

8) a. [vi] Range modulator fault circuit

The range modulator has a hardware dedicated circuit which monitors the rotational velocity. This circuit is basically a specialized frequency counter. The input is a CMOS level signal from

a metal proximity sensor mounted near a bolt on the coupler that attaches the range modulator fan to the motor shaft. Pulses are produced as the fan turns and the frequency of these pulses is the rotational speed of the range modulator in hertz. The output is a TTL signal which is sent to the DAADIO board and the interlock circuit. Failure of the range modulator to maintain velocity above a set-point causes a # 2 and # 3 halt, an error message at the control console, a green LED to go off and a red LED to come on, and an audible alarm. Designer, D.R.@IUCF.

8) a. [vii] SEM bias monitor

The bias voltage on each SEM is monitored by independent hardware circuits. This circuit is basically a low current offset (to prevent exceeding bias power supply output) voltage comparator circuit. The input to the SEM bias monitor is the SEM bias voltage and features a cable (independent of the bias voltage cable) which is attached directly to the SEM. The output is a TTL signal to the DAADIO board and the interlock circuit. Failure of the SEM to maintain bias voltage causes a # 2 and # 3 halt, an error message at the control console, a green LED to go off, a red LED to come on, and an audible alarm. Designer, D.R.@IUCF.

8) a. [viii] Interlock circuit

The interlock circuit is a dual-redundant dedicated hardware circuit that accepts TTL inputs from all safety critical systems (i.e. dose monitoring system, range modulator fault circuit, etc). The TTL outputs are to two independent cyclotron stops that defines the # 2 halt and acts independently of all computers. This circuit will also initiate a # 2 halt if an input wire is disconnected or an input circuit is turned off. Designer, D.R.@IUCF.

8) a. [ix] RF (Radio Frequency) shutdown transmitter circuit (RF S/D Xmitter)

The RF S/D Xmitter is dual redundant and hard-wired to the RF shutdown circuit in the injector cyclotron. Its purpose is to transmit a beam stop request at high speed to the RF shutdown circuit (see below). The inputs are 1) digital NIM from the LeCroy scaler and 2) TTL from the HLBCS. The outputs are to 1) independent differential digital signals that are sent direct to the RF shutdown circuit via independent cables for initiation of a # 1 halt, 2) the DADDIO board

for computer initiation of a # 3 halt and logging of the fault and 3) the interlock circuit for initiation of a # 2 halt. Designer, D.R.@IUCF.

8) a. [x] RF shutdown circuit

The RF shutdown circuit is dual redundant circuit designed to rapidly halt the beam by killing the injector cyclotron RF. Injector RF kill was chosen for fast beam-off response time and to minimize the effort required to restore beam after clearing the fault. This shutdown mode is used only when a rapid response time is required (i.e. a rapid transition to a high beam current level and/or the prescribed dose is exceeded by 5% due to the failure of several other beam halts) and halts treatment by terminating all beam acceleration independent of all computers. The inputs are 1) differential digital signals from the RF S/D xmitter circuit and 2) TTL level from the Proton Therapy RF control enable (RF enable) key switch. The output are 1) TTL signals to enable the independent North and South RF drivers in the injector cyclotron, 2) TTL signals to the DADDIO board for verification of the RF enable switch position, and 3) a relay contact closure for enabling an audible alarm in the cyclotron control room. Designers, David Jenner and D.R.@IUCF.

8) a. [xi] Audible alarm

The Proton Therapy audible alarm will sound in the event of any malfunction to warn the staff of a problem. The alarm is part of the interlock circuit. The alarm can be silenced (acknowledged) without clearing the fault to eliminate the annoyance of an alarm while locating/correcting a fault. The interlock circuit will not reset until the fault is cleared. Safety critical hardware devices activate the alarm independent of all computers. The alarm sounds whenever there ia a # 1, 2, or 3 halt issued, but not under normal treatment completion.

8) b. Computers and peripherals

Note: The failure modes of the computers and peripherals are made fail safe through the use of independent hardware devices for all critical functions (see hardware and electronics section), which initiate the appropriate halt, activate the audible alarm and LED display warnings independent of the computers and peripherals.

[i] rt300 (Clotho)

Clotho is the main control computer for the proton therapy treatment system. Clotho is a Digital Equipment Corporation (DEC) computer on a VME card, installed in the VME crate, and it runs under the ELN real time operating system. Clotho monitors the proton therapy system status, automatically maintains the treatment sequence, and initiates the appropriate shutdown modes independent of the X-terminal display console, the display computer (OCNUS), and the ethernet connection. Clotho maintains a database that defines the proton therapy control system status. This data base is accessed by the Vaxstation 3100 for graphical display on the X-terminal. Failure of the rt300 initiates a # 2 halt. In the event of failure of this device and/or the # 2 halt, dose is monitored and terminated by the two independent LeCroy 1151N modules using # 1 halt, and treatment can be terminated by the proton therapy operator using the "panic button" key switch.

8) b. [ii] Vaxstation 3100 (Ocnus)

Ocnus is a Vax workstation computer that runs under the VMS operating system. Ocnus accesses the rt300 database via DECNET and uses Vista control system software to create a graphical user interface (GUI). Ocnus is responsible for displaying the proton therapy control system status graphically on the X-terminal and transferring commands and data between the proton therapy operator and the rt300, for program development, and loading programs to Clotho. Failure of this device will initiate a # 3 halt.

8) b. [iii] Ethernet network

The ethernet network handles the communications between the rt300 control computer, the Vaxstation 3100 and the X-terminal. Ethernet serves to communicate information between the control computer (Clotho), the X-terminal and Ocnus. Ethernet failures results in a # 3 halt.

8) b. [iv] X-terminal

The X-terminal is used to download information to the rt300 control computer before treatment, start treatment, display graphically the status of the proton therapy device during treatment, and

panel and status of critical systems during treatment, and can be used to halt treatment by the operator. The graphical display of the beam profile and position, beam symmetry and other relevant information can be displayed at any time, and software calibrations made during setup, by opening a window. This is especially useful for rapid beam tuning. Failure of this device causes no problem with the treatment sequence. The operational procedure for loss of graphical display is the manual termination of treatment with the "panic button" key switch.

8) c. Control computer software

The control system software for the proton therapy control system is based on the commercial software "Vsystem" from Vista Control Systems, Inc., and is running under the real time operating system VAX ELN on a VME based DEC rt300 real-time control computer. This system is dedicated to Proton Therapy data acquisition and control functions only. Vsystem, as configured for Proton Therapy, maintains a database and provides a user configurable graphical interface and several functions for communicating with the database. Device drivers for the VME bus provided by most hardware vendors would not work with the VAX rt300 (VME modules are typically designed with 68000 based microprocessors in mind) and were written by John Collins, Ph.D., division head of computer and electronics at IUCF. IUCF uses this configuration (rt300 in the VME crate, Vsystem software, etc.) for their control system and it simplifies support and integration for the Proton Therapy group to follow the local standards. Several custom programs were written in "C" or Fortran to run on the rt300 including:

8) c. [i] DOSE

The basic function of Dose is to monitor the dose, write the dose to a file every second to maintain the dose record, and halt treatment when the dose is reached.

8) c. [ii] PSTART

Pstart is used to start or stop treatments from the computer terminal.

8) c. [iii] SCAL_PRESET

Scal_preset downloads prescribed dose information to the LeCroy scalers.

8) c. [iv] WC_PROFILE

WC_profile calculates the beam centroid and width for the horizontal and vertical planes based on information from the MWIC. The results are compared to optimum beam profile parameters established during calibration to verify that the beam properties have not changed. Information from the MWIC, split ion chambers and SEMs are crossed checked during patient treatment to verify correct operation of all detectors.

8) c. [v] SYMMETRY

Symmetry monitors the data from the split ion chambers for symmetry and calculates Left/Right and Up/Down symmetry values which can be displayed graphically. The program indicates when these variables are out of established limits.

8) c. [vi] INTERLOCK

Interlock monitors all of the conditions for correct operation of the proton therapy system. Interlock will indicate whether conditions are satisfied to begin or continue treatment, as appropriate, based on all hardware and software interlocks (i.e. SEM bias ok, beam symmetry ok, etc.).

8) c. [vii] BEAM_OFF

Beam_off is activated if either Dose indicates the treatment is complete or if Interlock indicates the treatment should be halted for other reasons. Beam_off then initiates the appropriate halt sequence.

9) REGULATORY APPROVAL

Several agencies may specify requirements before a proton therapy facility can be used with a human patient. Our work has been monitored by the Indiana State Department of Health, U.S. Food and Drug Administration (FDA), Indiana University Institutional Review Board, Indiana University Machine-produced Radiation Safety committee, and the IUCF Safety committee. Proper and accepted documentation techniques should be followed in all areas of a proton therapy project to expedite the approval process. A document filing and revision procedure should be adopted and adhered to. Standard drafting procedures should be followed on all drawings. Formal techniques should be followed while developing, testing and documenting software [see the book "Verification and Validation of Real-Time Software, W.J. Quirk for an introduction]. Most important, quality and safety should be designed into the system and the approval process will go smoother.

ACKNOWLEDGEMENTS

We wish to thank The Lions Cancer Control Fund of Indiana, Inc., and the Lions International for their generous financial support. Special thanks should be made to Ira Barker, Indiana Lions Liaison for his personal commitment to the Proton Therapy Project.

REFERENCES

[1] C. Bloch, V. Derenchuk, J. Cameron, M.Fasano, J. Gilmore, R. Hashermian, N. Hornback, D. Low, J Morphis, C. Peterson, D. Rosselot, G. Sandison, R-N Shen, and H. Shidnia. The Indiana University Proton Radiation Therapy Project, Nuclear Instruments and Methods in Physics Research B79 (1993) 890-894

[2] D.L. Friesel, T. Ellison and T. Sloan, IUCF Scientific and Technical Report, 919860 142.

[3] B. Gottschalk, Harvard Cyclotron Lab internal report, HCL 3/23/90 (1990)

[4] Koehler, A.M., Schneider, R.J. and Sisterson, J.M.: (1977) Flattening of proton dose distributions for large-field radiotherapy. Med. Phys. 4, 297-301.

[5] G.W. Tautfest and N.R. Fechter, Rev. Sci. Instr. 26 (1955) 229

[6] F. Sauli, Principles and operation of multiwire proportional and drift chambers, CERN 77-09, 3 May 1977, lectures given in the Academic Training Programme of CERN, 1975-1976

[7] M. Raju, *Heavy Particle Radiotherapy*, 1980, page 235, New York Acedemic Press.

[8] Ibid, pages 197 to 201

[9] V. Khoroshkov, ITEP, Moscow, Russia. Private conversation.

[10] Koehler, A.M., Schneider, R.J. and Sisterson, S.M. Range Modulators for protons and Heavy Ions, Nucl. Inst. and Meth. 131 (1975) 437-440.

[11] J.F. Janni, Calculations of Energy Loss, Range, Pathlength, Stragglling, Multiple Scattering and the Probability of Inelasic Nuclear Collisions for 0.1 to 1000 MeV Protons, Air Force Weapons Laboratory Technical Report no. AFWL-TR-65-150.

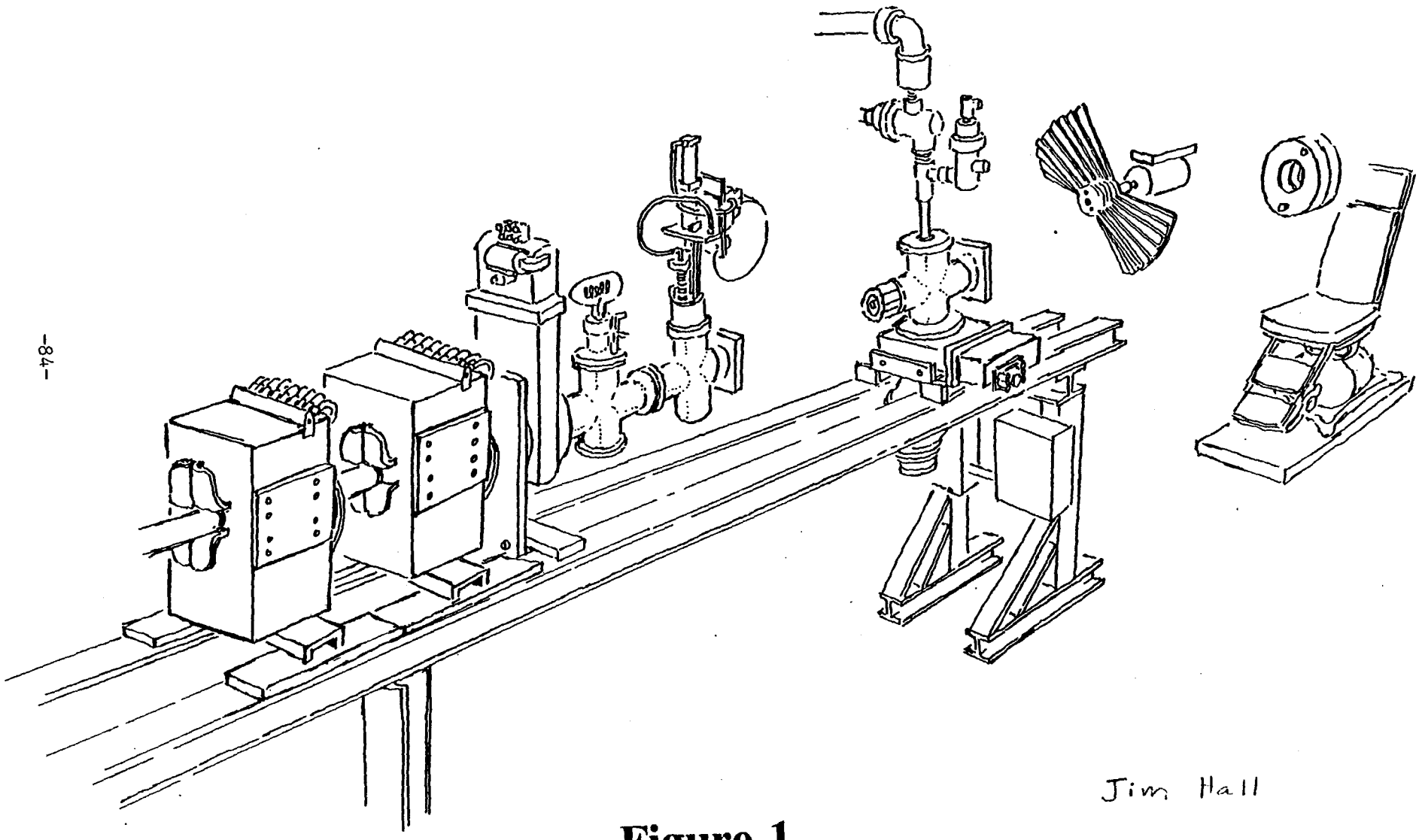

Figure 1

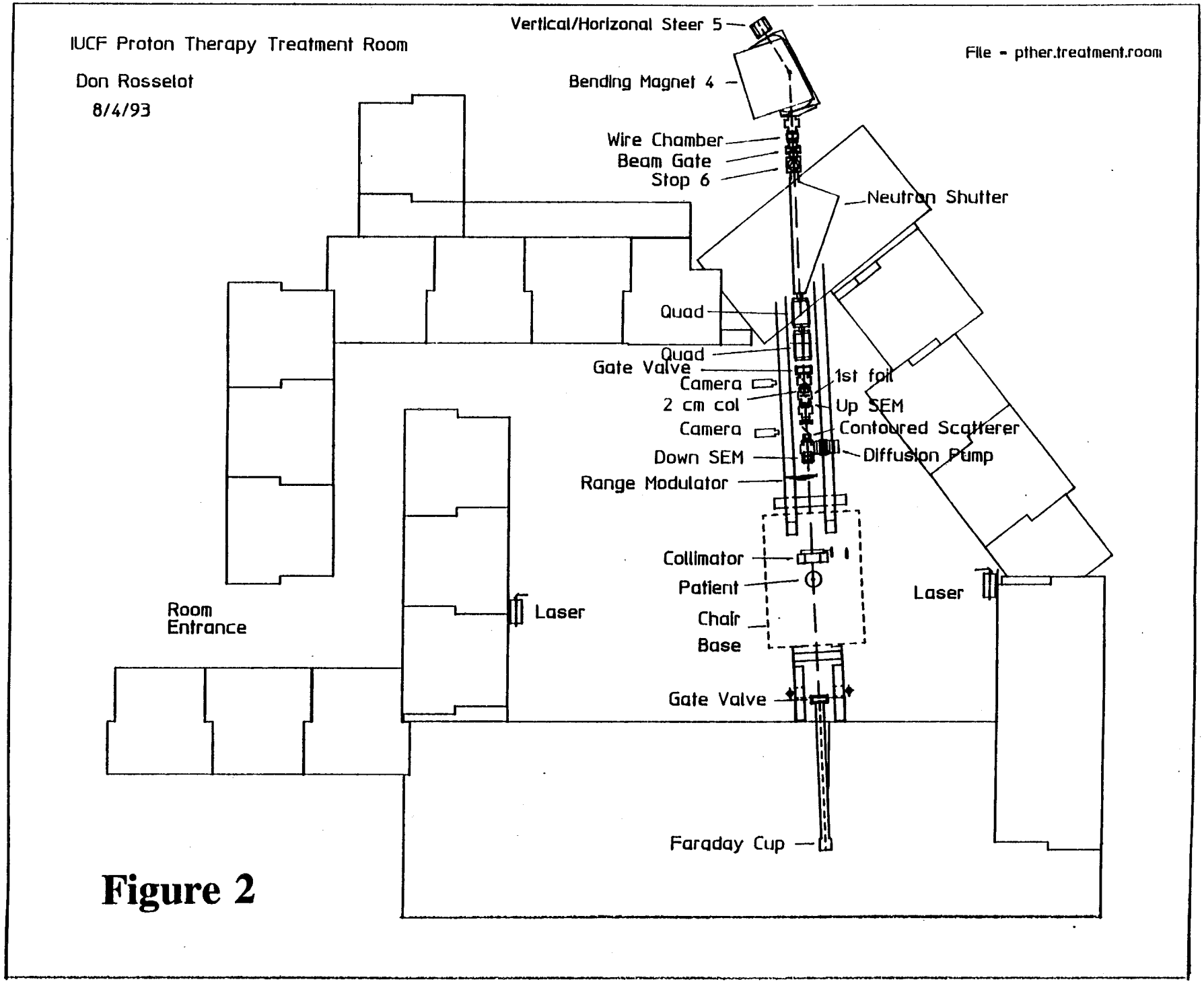
IUCF Proton Therapy Treatment Room
Don Rosselot
8/4/93
File = pther.treatment.room
Vertical/Horizonal Steer 5
Bending Magnet 4
Wire Chamber
Beam Gate
Stop 6
Neutron Shutter
Quad
Quad
Gate Valve
Camera
2 cm col
Camera
Down SEM
Range Modulator
1st foil
Up SEM
Contoured Scatterer
Diffusion Pump
Collimator
Patient
Chair
Base
Gate Valve
Faraday Cup
Laser
Laser
Room
Entrance

Figure 2

Figure 3

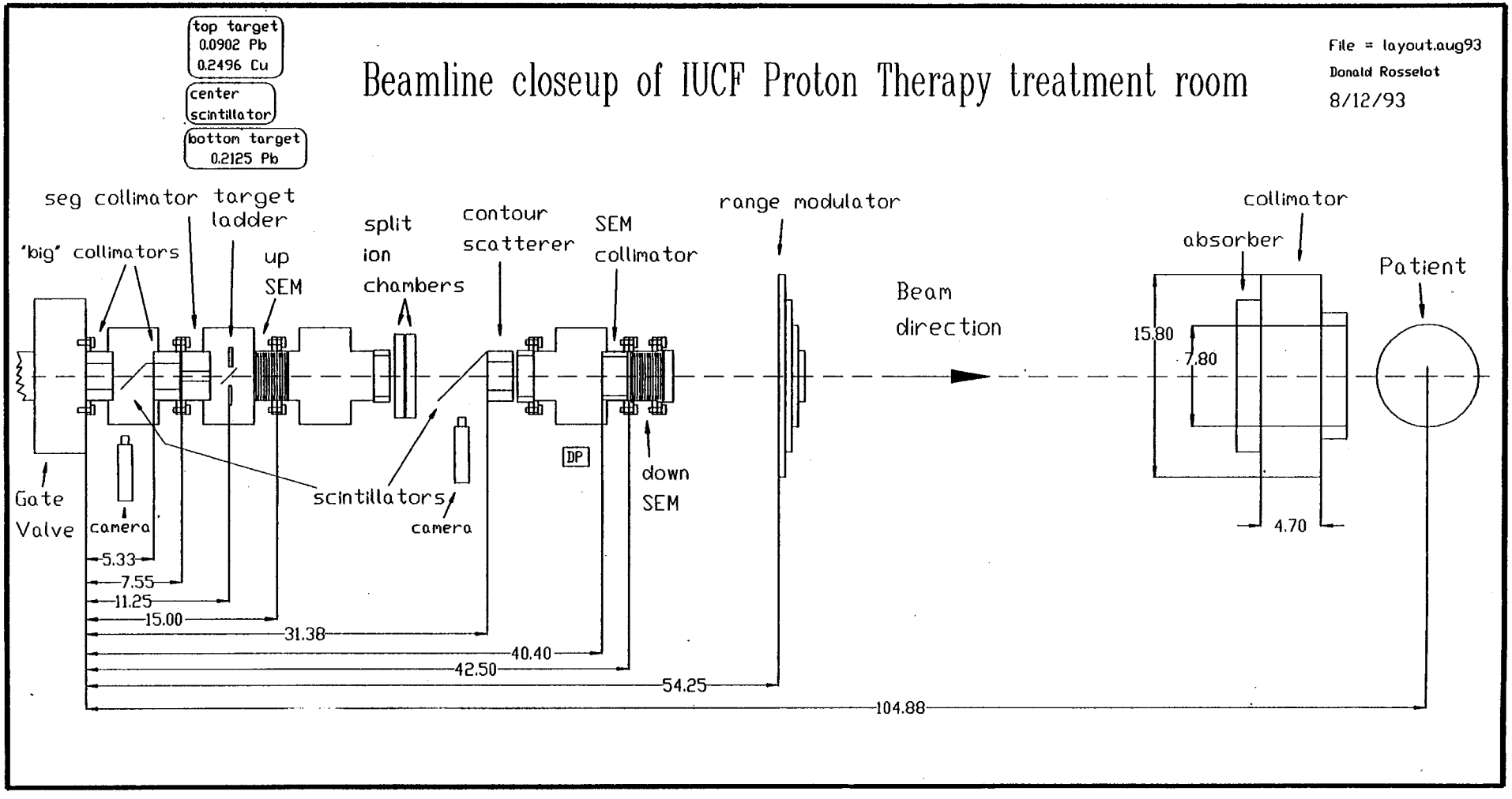
Beamline closeup of IUCF Proton Therapy treatment room
File = layout.aug93
Donald Rosselot
8/12/93
top target
0.0902 Pb
0.2496 Cu
center
scintillator
bottom target
0.2125 Pb
seg collimator
target
ladder
'big' collimators
up
SEM
split
ion
chambers
contour
scatterer
SEM
collimator
range modulator
Beam
direction
collimator
absorber
Patient
15.80
7.80
4.70
Gate
Valve
camera
scintillators
camera
DP
down
SEM
5.33
7.55
11.25
15.00
31.38
40.40
42.50
54.25
104.88

Transverse plane. Plot magnification= 1.00 Frame number 1

Center at X= 0.0 Y= -0.2 Z= 0.2 cm

20-OCT-1993 14:53:59

Signature _____

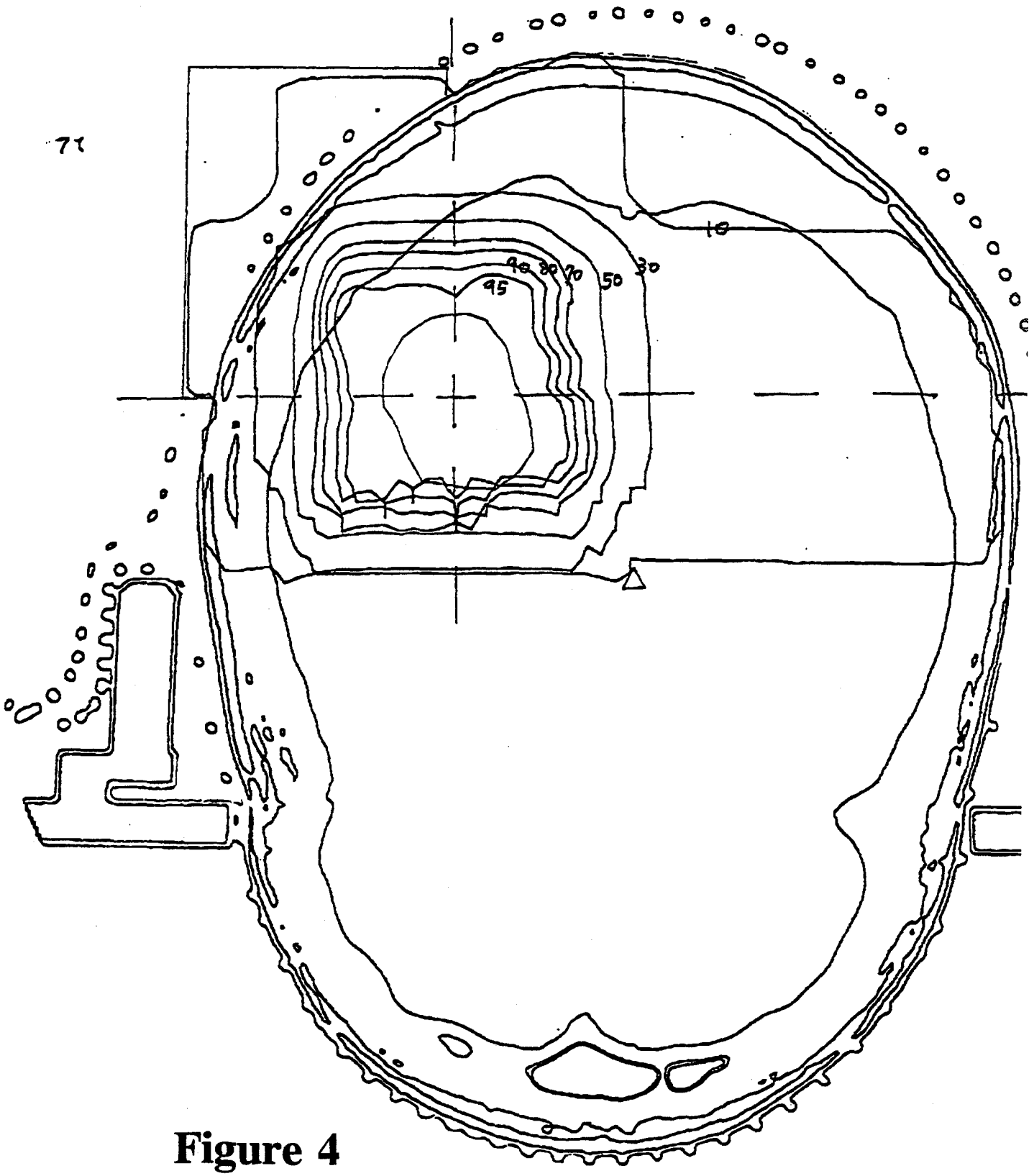

Figure 4

Figure 5 a

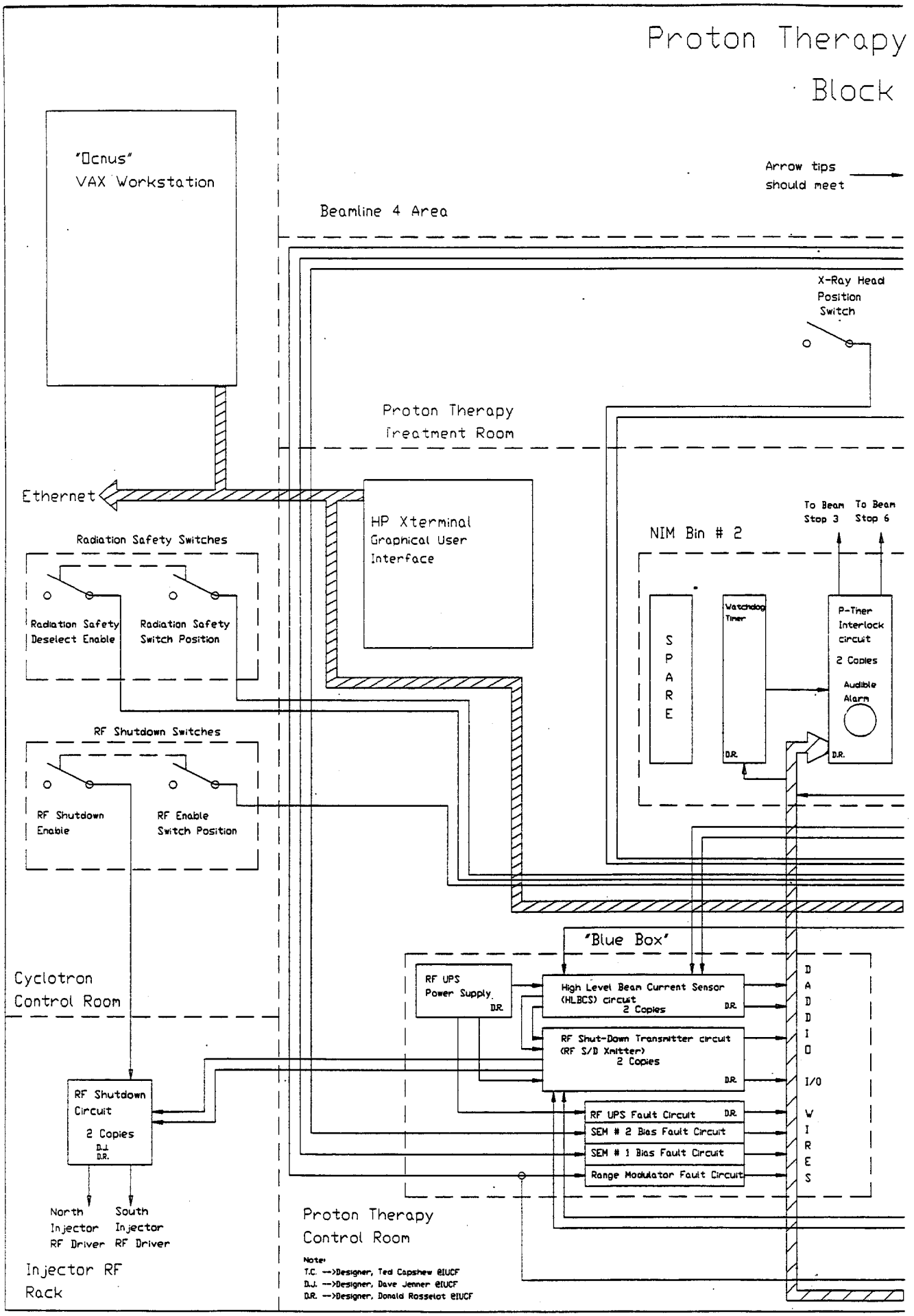
Proton Therapy Block
"Ocnus" VAX Workstation
Arrow tips should meet
Beamline 4 Area
X-Ray Head Position Switch
Proton Therapy Treatment Room
Ethernet
HP Xterminal Graphical User Interface
To Beam Stop 3
To Beam Stop 6
NIM Bin # 2
Radiation Safety Switches
Radiation Safety Deselect Enable
Radiation Safety Switch Position
SPARE
Watchdog Timer
D.R.
P-Tiner Interlock circuit
2 Copies
Audible Alarm
D.R.
RF Shutdown Switches
RF Shutdown Enable
RF Enable Switch Position
"Blue Box"
Cyclotron Control Room
RF UPS Power Supply
D.R.
High Level Beam Current Sensor (HLBCS) circuit
2 Copies
D.R.
RF Shut-Down Transmitter circuit (RF S/D Xmitter)
2 Copies
D.R.
RF UPS Fault Circuit
D.R.
SEM # 2 Bias Fault Circuit
SEM # 1 Bias Fault Circuit
Range Modulator Fault Circuit
DADDIO I/O WIRES
RF Shutdown Circuit
2 Copies
D.J.
D.R.
North Injector RF Driver
South Injector RF Driver
Injector RF Rack
Proton Therapy Control Room
Note:
T.C. -->Designer, Ted Capshew @IUCF
D.J. -->Designer, Dave Jenner @IUCF
D.R. -->Designer, Donald Rosselot @IUCF

Figure 5 b

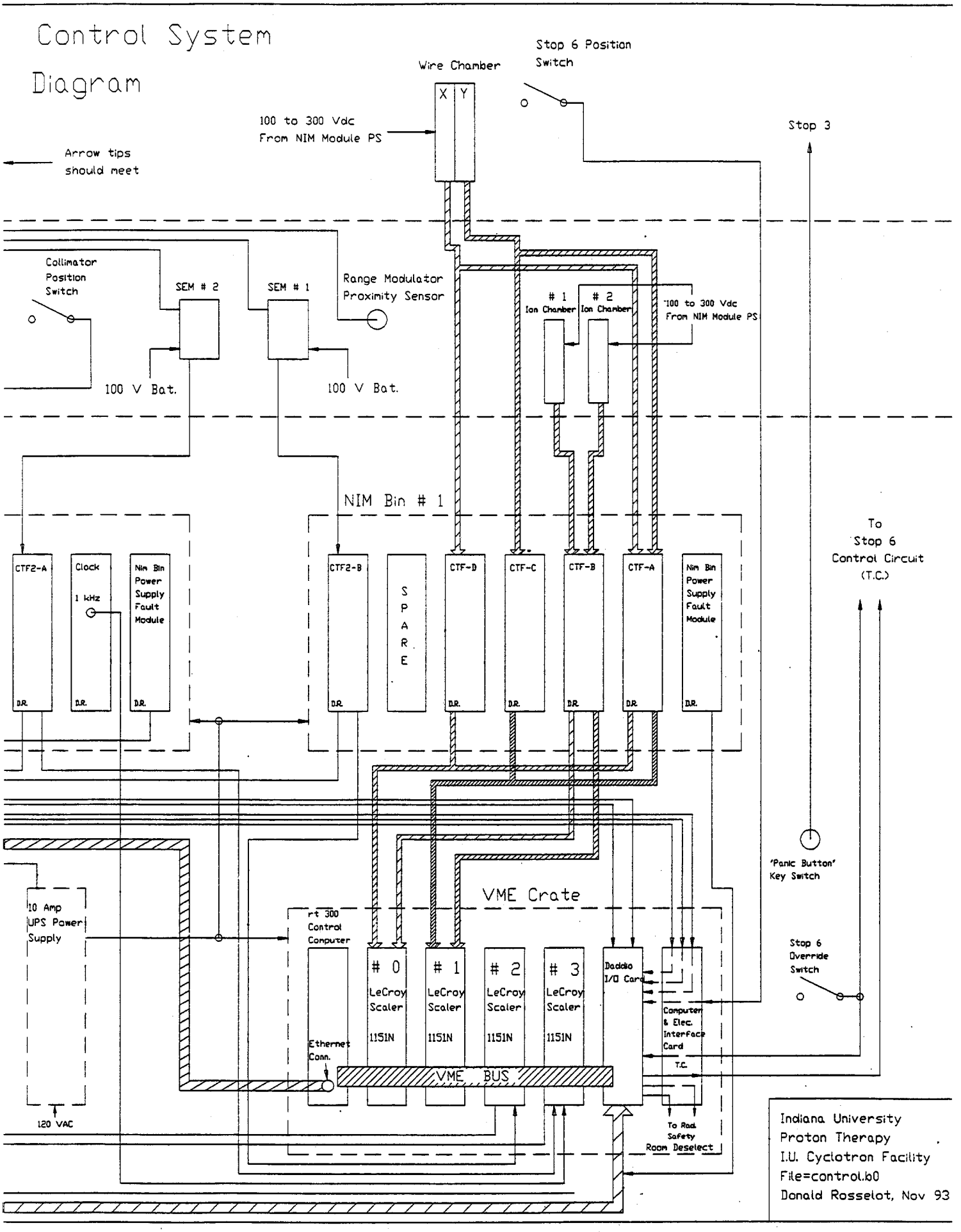
Control System Diagram
Wire Chamber
X
Y
Stop 6 Position Switch
100 to 300 Vdc From NIM Module PS
Stop 3
Arrow tips should meet
Collimator Position Switch
SEM # 2
SEM # 1
Range Modulator Proximity Sensor
1 Ion Chamber
2 Ion Chamber
100 to 300 Vdc From NIM Module PS
100 V Bat.
100 V Bat.
NIM Bin # 1
CTF2-A
Clock
1 kHz
Nim Bin Power Supply Fault Module
CTF2-B
SPARE
CTF-D
CTF-C
CTF-B
CTF-A
Nim Bin Power Supply Fault Module
D.R.
To Stop 6 Control Circuit (T.C.)
'Panic Button' Key Switch
VME Crate
10 Amp UPS Power Supply
rt 300 Control Computer
Ethernet Conn.
0 LeCroy Scaler 1151N
1 LeCroy Scaler 1151N
2 LeCroy Scaler 1151N
3 LeCroy Scaler 1151N
Daddio I/O Card
Computer & Elec. Interface Card
T.C.
Stop 6 Override Switch
VME BUS
120 VAC
To Rad. Safety Room Deselect
Indiana University
Proton Therapy
I.U. Cyclotron Facility
File=control.b0
Donald Rosselot, Nov 93

SEM Assembly

Secondary Electron Emission Monitor

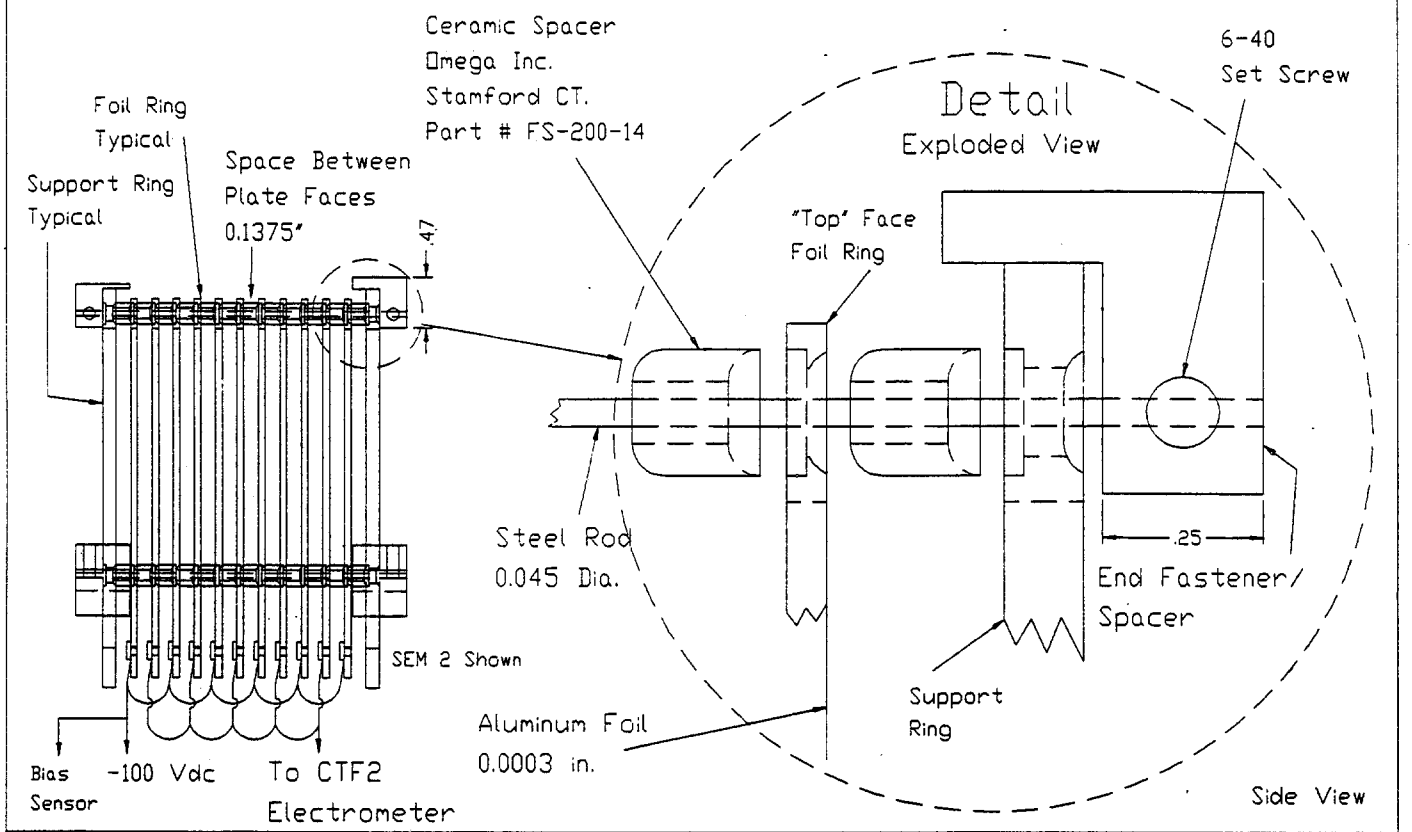

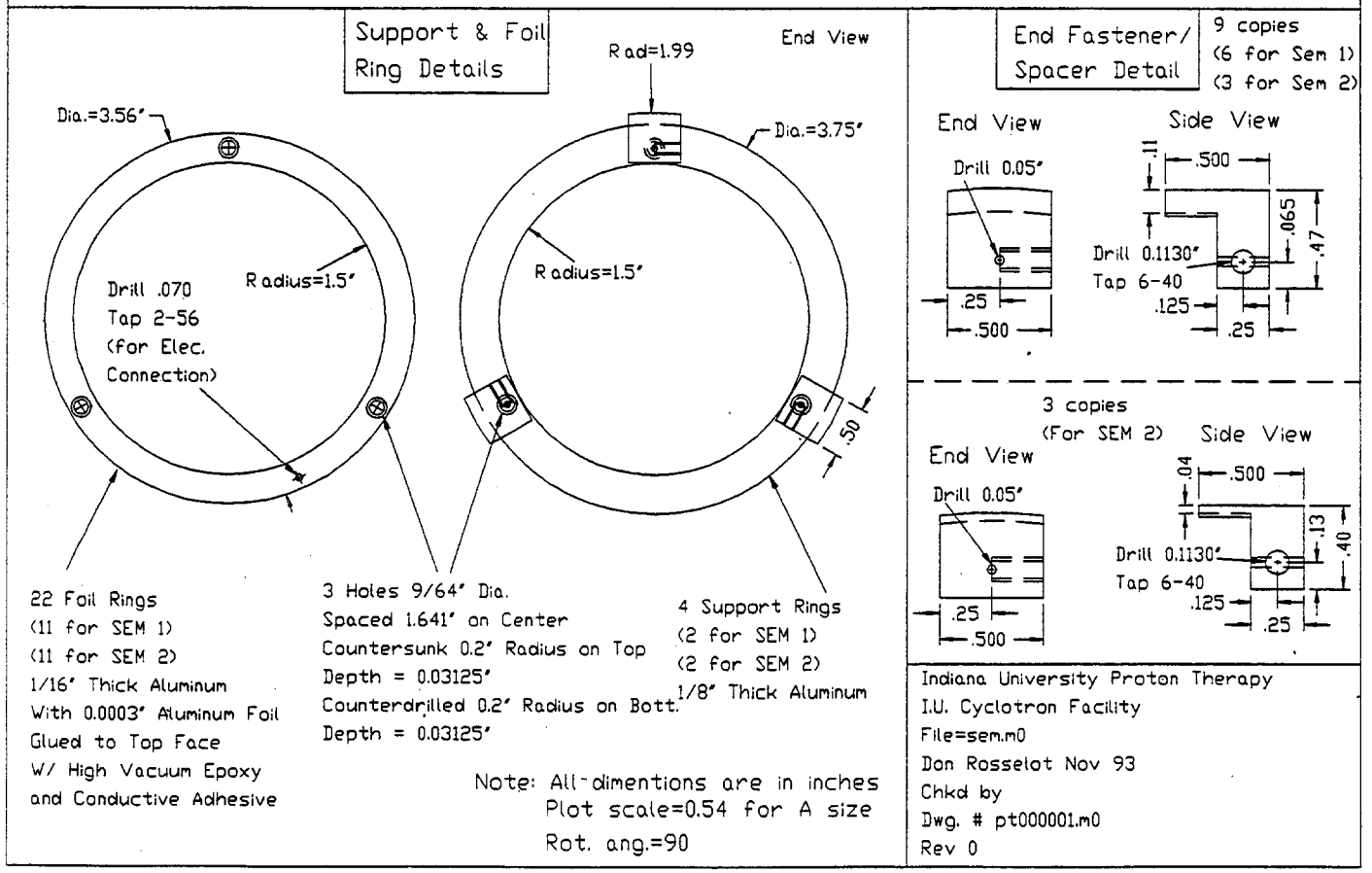

Figure 6

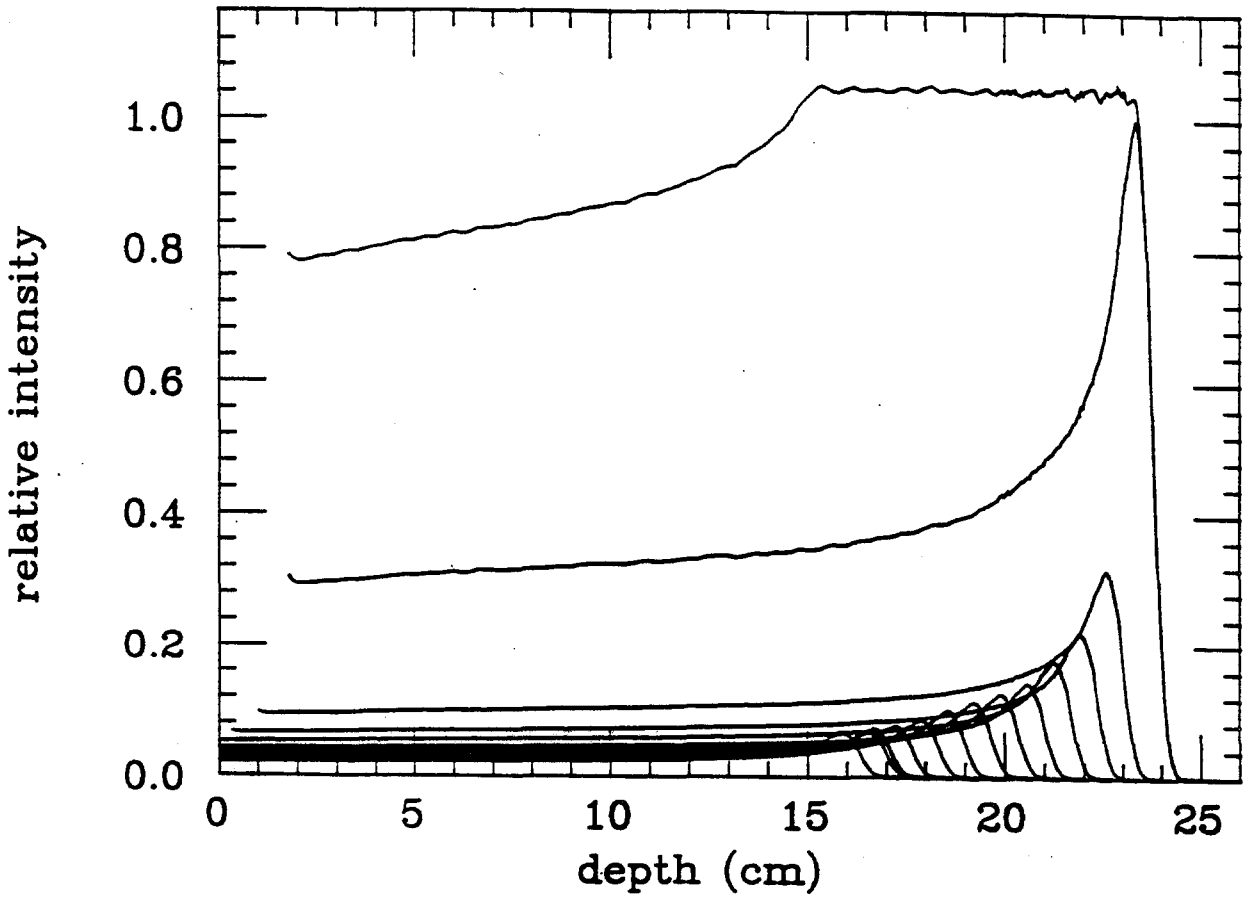

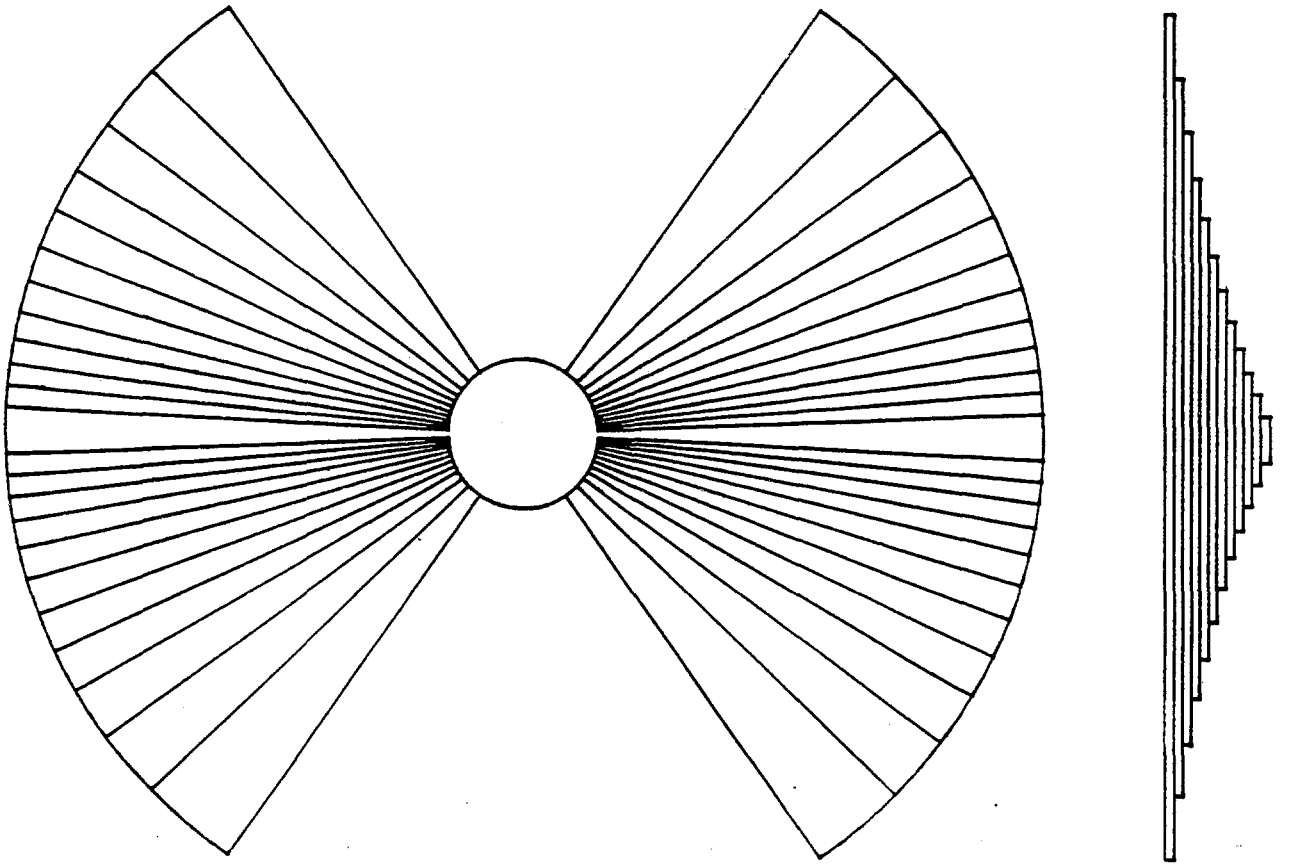

Figure 7

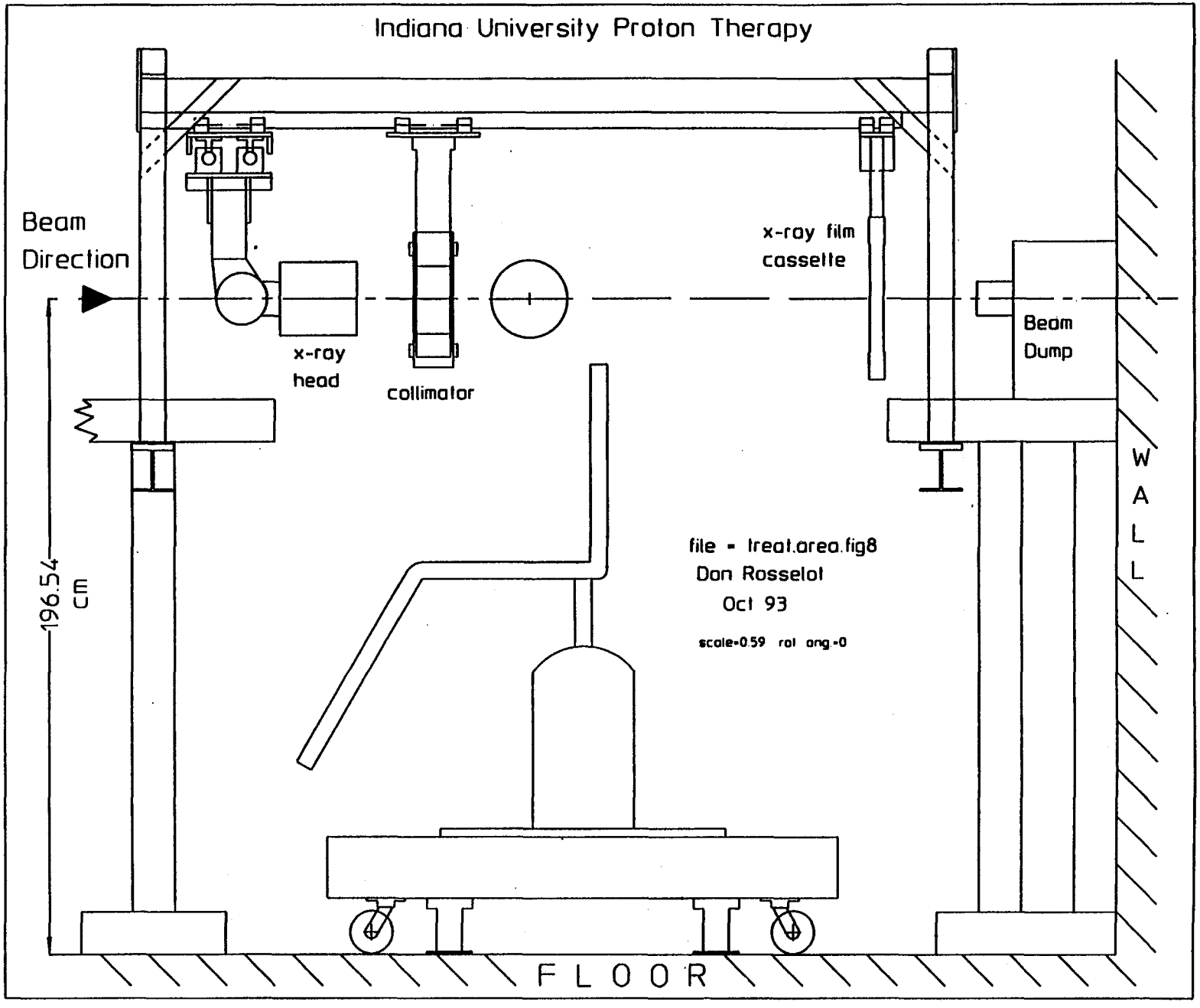
Indiana University Proton Therapy
Beam
Direction
x-ray
head
collimator
x-ray film
cassette
Beam
Dump
W
A
L
L
196.54
cm
file = treat.area.fig8
Don Rosselot
Oct 93
scale=0.59 rot ang.=0
F L O O R

Figure 8

Figure 9

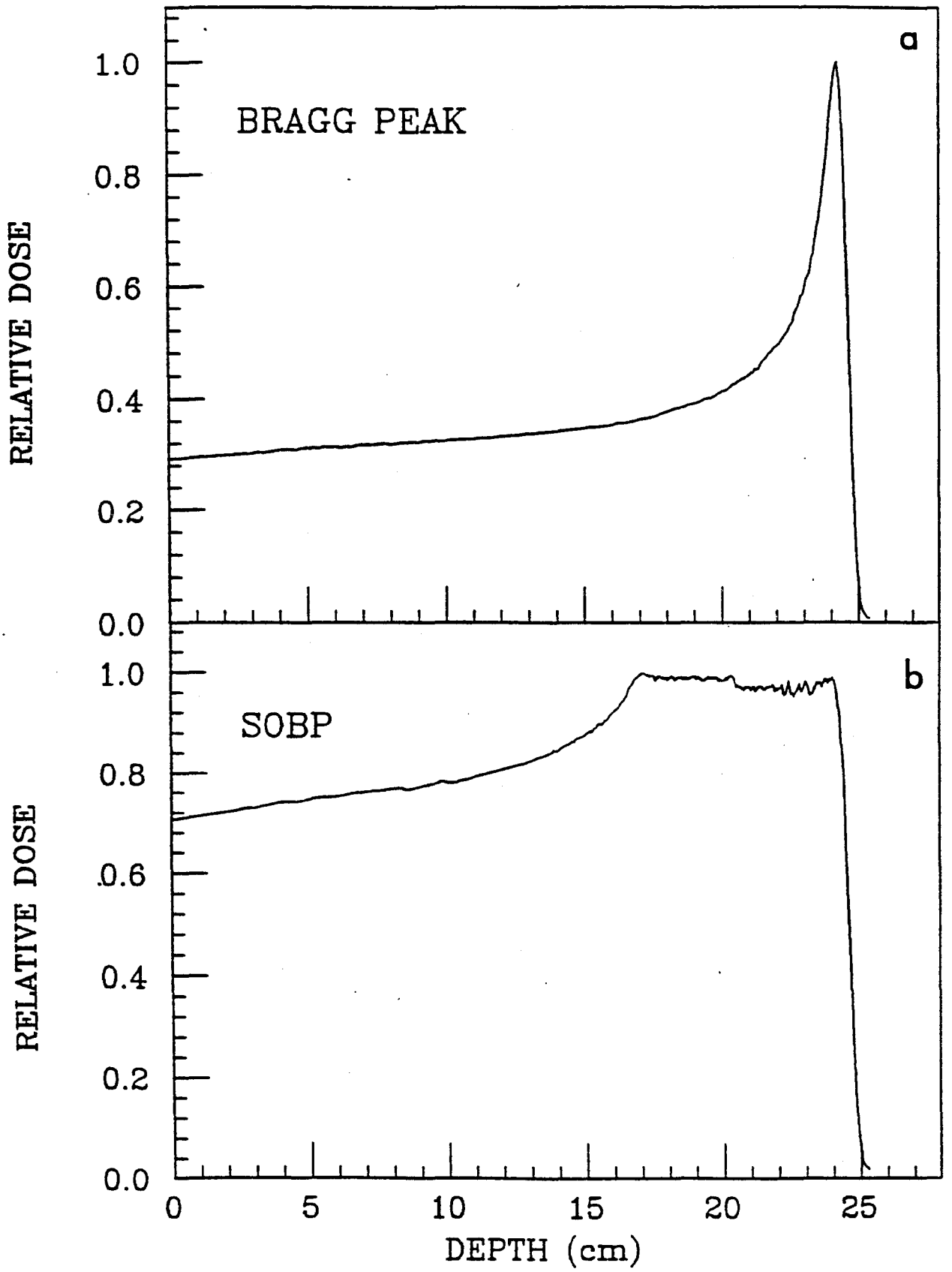
a
BRAGG PEAK
b
SOBP
RELATIVE DOSE
RELATIVE DOSE
1.0
0.8
0.6
0.4
0.2
0.0
1.0
0.8
0.6
0.4
0.2
0.0
0
5
10
15
20
25
DEPTH (cm)

Use of Short-pulse Beams in Proton Therapy
(ITEP experience and FNAL linac possibilities)

V.S.Khoroshkov, K.K.Onosovsky

Institute for Theoretical and Experimental Physics (ITEP)

Today, it has been fairly convincingly demonstrated [1, 2, 3, 4] that beams with long pulse duration (hundreds milliseconds up to a second) or continuous ones, are most suitable for proton therapy (PT). In this sense, the situation and beam parameters are not the best ones in ITEP synchrotron and FNAL linac. Nevertheless, the situation in FNAL is better and with a right approach, certain shortcomings of short-pulse beams could be avoided.

Analyzing ITEP experience in proton therapy, we are going to consider only three fields, namely:

1. Dosimetry and monitoring.
2. Dose compliance, choosing the intensity limit, and method of intensity reduction.
3. Dose delivery system.

These items are the ones in which difficulties of short-pulse beams in proton therapy manifest themselves most clearly.

First of all, there is a need to agree on terminology. We are going to use

- number of particles per pulse (N_p, part./pulse)
- pulse flux (F_p, part./s)
- pulse intensity (I_p, part./cm^{2}s).

All the data is related to the situation inside the pulse. Only this is interesting from the viewpoint of the three chosen fields

above. Of course, time-average parameters are also interesting, but only from the viewpoint of irradiation time and they will be considered separately.

Fig. 1 presents ITEP proton therapy facility in a very simple way. The medical proton beam is ejected from the synchrotron by a kicker and is delivered into one of the three treatment rooms.

Below, ITEP synchrotron and FNAL linac internal beam main parameters are presented which are of special interest for the subject:

	ITEP	FNAL
Energy, MeV	70 - 200	100 - 400
N_p, part./pulse	$10^9 - 5 \cdot 10^{10}$	10^{13}
Pulse length	100 ns	30 μs
Repetition rate	15 p/min	15 p/s

For the FNAL linac, the maximum number of particles per pulse is given here. The real limit for this number and the correct way to reduce it, will be considered below.

The last two parameters of ITEP synchrotron namely a very short pulse duration and its low repetition rate, are the main source of troubles. Note straight away that in FNAL, the pulse duration and the 15-Hz repetition rate, are much more suitable. This fact gives hope for lifting a number of problems, speaking in terms of proton therapy.

1. Monitoring and Dosimetry

Fig. 2 demonstrates the means used in ITEP for absolute dosimetry, phantom dosimetry and monitoring. Let us consider each of these instruments in a little more detail.

Absolute dosimetry. Measurements of activity (β-γ coincidences) induced in polystyrene in $^{12}C(p,pn)^{11}C$-reaction, are used in ITEP for this purpose. Closer definition made lately for the reaction cross-section, gives hope for the accuracy of the method to be within ± 5% [5]. It was ± 7% before [6].

Phantom dosimetry.

a. Photographic technique. We consider it one of the best methods of measuring the distribution of particles (dose) across the beam. Presently available photographic materials provide for measurements in all pulse intensity ranges possible both in ITEP and in FNAL. The presently existing microdosimetry devices provide the space resolution level of a few μm. Unfortunately, the response of the photographic material depends on the energy of the particles, and in any case, preliminary study of the particle spectrum (Bragg curve) is required, e.g. by means of an ionization chamber.

b. Semiconductor dosimetry. Standard dosimeters give linear response up to the level of 0.4 Gy/pulse (in ITEP conditions, $t_{pulse} \sim 100$ ns). Special dosimeters (special additives, technology, selection) upgrade this level up to 2 Gy/pulse.

c. Thermoluminescent dosimetry was used by us in comparative dosimetry research between PTF in Russia and abroad [6].

d. Ionization chamber (ICh). We believe, ICh is the most important and absolutely necessary dosimetry device. Exact knowledge of the ICh working volume gives directly the value of the absorbed dose. Unfortunately, the use of ICh in pulsed beams is always limited by some pulse intensity value I_p or other depending on the chamber design. When a certain I_p value is exceeded, initial recombination process (recombination in one track) in the chamber changes into general recombination process (recombination of particles in neighboring tracks). The response of the ICh ceases being proportional to the dose. The work in this zone is practically impossible (Fig. 3). Two ways exist for widening the working range of linear response, namely the decrease of the gap and the increase of electric field tension. Consider just two examples of ICh in operation.

ICh of JINR PTF (ordinary ICh):

Gap - 7 mm, voltage - 2 kV (300 V/mm), $I_p \leqslant 10^9 - 10^{10}$ p/cm^{2}s.

ICh of ITEP PTF (non-ordinary ICh):

Gap - 1 mm voltage - 1.5 kV (1.5 kV/mm), $I_p \leqslant 10^{15}$ p/cm^{2}s.

It should be noted that the technology for the second ICh is complicated; high manufacturing precision is required. It is especially difficult to make and operate a large-size chamber for monitoring - the operation goes on the margin of electrical breakdown. Years were spent in ITEP to make the chamber 80 mm in diameter. It is easy to show that even the second type of the chamber does not cover the maximum pulse intensities in ITEP ($I_p^{max} = 10^{16}$ p/cm^{2}s) and in FNAL ($I_p^{max} = 3 \cdot 10^{16}$ p/cm^{2}s for 10^{13} p/pulse, target diameter $\sim$ 4 cm). Our experience shows that it is not too difficult to build ICh with transverse dimensions of 25 - 30 cm for $I_p^{max} \leqslant 10^{13}$ p/cm^{2}s. In this

case, the gap and the voltage between electrodes remain reasonable.

Beam monitoring.

Up to now, a current transformer was used as beam monitor in ITEP. It is not the best instrument for dose counting, but the high pulse intensity of the beam did not allow to use an ionization chamber for it, which would be a better instrument from our point of view.

Fig. 4 illustrates two methods of measuring the number of particles by the current transformer.

The signal from the current transformer (CT) is proportional to the number of beam particles crossing its aperture. Unfortunately, the length of the CT together with the steel shielding against electromagnetic noise, is big. We can't place it in front of a patient. We are forced to place it in front of the last collimator through which not all the particles pass that passed through the CT. The ratio of the particles passing through the collimator and those passing through the CT, depends on the distribution of particles in the initial beam. Unfortunately, this distribution is not stable. Frequent CT calibration is required. It is not the best way to work. Another way of CT connection has been suggested which is in use now. The collimator is insulated and its ground contour is passed through the CT aperture. It is easy to understand that in this configuration, the particles perishing in the collimator will be subtracted from the CT signal, so the CT measures only those particles passing through the collimator.

But in any case, the CT measures the number of particles and not the energy (that is, the dose). For dose determination, the knowledge of the energy spectrum of particles is required. Thus, in any case

preliminary Bragg curve measurements are required by means of an ionization chamber (at decreased pulse intensity) or a semiconductor detector.

Fig. 5 presents three examples of using dosimetry means in ITEP in pre-clinical investigations.

Conclusions

1. It is possible to build a dosimetry system without an ionization chamber for all intensity ranges, but it is not the best solution.

2. Even high-voltage strength ionization chambers don't cover all ranges of ITEP and FNAL pulse intensities and they can't be used as monitors at full intensity.

3. In order to use an ionization chamber, it is desirable to have the pulse intensity upper limit of 10^{13} part/cm^{2}s.

2. Dose Compliance, Choosing the Pulse Intensity Limit and Method of Pulse Intensity Reduction

Evidently, the smaller number of particles in a pulse, the more exact compliance of delivered dose and prescribed dose, can be provided. But the number of pulses must be greater, as well.

This requirement (reducing the number of particles in a pulse) comes to contradiction with the work conditions in ITEP. Treatment is conducted simultaneously with physical research. One bunch out of the four accelerated, is taken off the accelerator

orbit. The remaining three are accelerated on, and used by physicists who need high beam intensity, as a rule. Often, we have to use only 5 - 6 pulses for dose delivery in a fraction; that's what determines the dose non-compliance. Naturally, it is corrected in irradiation from a different port, or in the next fraction, but this is not the best way to work.

Presently, we are changing the work conditions, which will enable us to reduce the pulse intensity, improve dose compliance, and - which is no less important - use the ionization chamber for all modes of operation. We believe that in order to avoid our mistakes and difficulties, this approach (correct reduction of the number of particles in a pulse) should and can be chosen from the beginning for medical work in FNAL.

First of all, consider an example of a large-target irradiation under FNAL linac conditions:

Target volume	15 liters (25 x 25 x 25 cm^3)
Dose	2 Gy
Total number of particles	$\sim 5 \cdot 10^{12}$
Irradiation time	100 s
Repetition rate	15 Hz
Reserve	2
Number of particles per pulse	$N_p = \frac{5 \cdot 10^{12} \cdot 2}{100 \cdot 15} \simeq 7 \cdot 10^9$ p/pulse

Generally speaking, we obtained the result that is usual for the majority of modern PTF projects: time average intensity of 10^{11} part/s

This simple result leads to a number of successive and very important conclusions:

1. Probably, there are no clinical cases requiring more than $7 \cdot 10^9$ part/pulse at 15 Hz.

2. For all clinical and pre-clinical work, it is necessary to put this limit ($7 \cdot 10^9$) to the number of particles in a pulse, the full pulse duration remaining 30 μs (for example, by decreasing the pulse flux of the source).

3. Pulse intensity of the beam incident to the large target or to the beam monitor, becomes $I_p \leqslant 4 \cdot 10^{11}$ part/cm^{2}s.

4. Further decrease of the number of particles per pulse (down to 10^8 - 10^7 part/pulse) for irradiation of smaller targets, may be done in two ways (first, by 10-fold decrease of the source pulse flux and then by shortening the pulse length).

5. The limit $I_p \leqslant 10^{13}$ part/cm^{2}s must always be maintained.

As the result:

- It becomes possible to use an ordinary large-aperture ionization chamber in all ranges of operation (of pulse intensity) for both purposes - as the research instrument in pre-clinical studies and as the dose monitor for treatment.

- It becomes possible in all cases, to provide good compliance of the real and prescribed doses since not less than a few hundred pulses are required for the dose delivery.

3. Dose Delivery Systems

In principle, there are two types of dose delivery systems, namely passive and active ones. The active method implies scanning of a narrow pencil beam in two or three directions: along the target, across the target and in depth (change of energy).

ITEP is absolutely short of time (in terms of pulse duration and repetition rate) for this method of work. The pulse duration and repetition rate of FNAL linac are not sufficient as well, and it is not too simple to use active systems at FNAL linac beam. At the same time, at least two serious problems exist if passive dose delivery systems are used:

1. If the target is to be irradiated fairly precisely, with the use of conformal (or close to conformal) dose fields, individual boluses, ridge filters and collimators are to be manufactured practically for each clinical case. At best, the latter two devices can be selected from those accumulated previously.

All this is not too convenient. The PTF has to include a workshop for prompt manufacture of these irradiation means. Nevertheless, this difficulty can be overcome.

2. Unfortunately, the second difficulty cannot be overcome in principle. At least we don't know the technique and methods for passive dose delivery to overcome it.

Fig. 6a illustrates this shortcoming in a very simple way. For irradiation of a complex-shape target, a ridge filter is used in order to form a spread Bragg peak. The length of the spread peak is to be equal to the biggest depth of the target. And for layer "b", the shape

of Bragg curve is ideal. For layers "a" and "c", the whole curve is shifted closer to the surface by a bolus (compensator), but the extension of the spread Bragg peak remains the same and the shaded healthy tissues in front of the target become irradiated with a greater dose than possible. The proton radiation potentials are not used to full extent [7].

For the correct irradiation (Fig.6b), it is necessary to have the possibility to adjust both parameters - the total length of the curve and the length of the spread Bragg peak. In reality, it is this what is done by all the dynamic dose delivery systems, in one way or other.

While for 30 years we have been developing proton therapy, the conventional methods of therapy also were not standing still. These methods (electron beams, Bremsstrahlung) combined with good computer support, have got excellent technology for conformal irradiation, and good results these days. Today, any new PTF will be able to compete with conventional radiation therapy methods only if active dose delivery systems are used.

It is extremely desirable to look for the way to create dynamic dose delivery systems for the FNAL linac. 15 Hz repetition rate, 30 μs pulse duration and, especially, the H^- beam available, open certain possibilities for it [8].

The authors express their gratitude to Drs. V.Kostjuchenko, V.Lukjashin, D.Nichiporov and I.Zubarev, for useful discussions and assistance in work.

References

1. H.Blattmann, E.Pedroni, T.Boehringer, et al. Proton Therapy at PSI, Status and Plans. Proceedings of the Proton Therapy Workshop at PSI. Villigen, Switzerland, 1991, 25-8.

2. U.Amaldi, G.Tosi. The Hadron Therapy Project Two Years Later. TERA 93/2 GEN 5.

3. W.T.Chu, J.W.Staples, B.A.Ludewgt et al. Performance Specifications for Proton Medical Facility. Preprint LBL-33403, US-406, Feb. 1993.

4. V.S.Khoroshkov, K.K.Onosovsky, H^- Synchrotron for Proton Therapy Facility. In: A.Itano, T.Kanai eds. Proceedings of the NIRS International Workshop on Heavy Charged Particle Therapy and Related Subjects. Chiba, Japan: National Institute of Radiological Sciences, 1991, 204-12.

5. V.Kostjuchenko and D.Nichiporov. Measurement of the $^{12}C(p,pn)^{11}C$ Reaction from 95 to 200 MeV. Appl.Radiat. Isot., Vol.44, No9, 1993, pp 1173 - 5. .

6. V.Kostjuchenko and D.Nichiporov. Clinical Dosimetry at ITEP. A Review of Instruments and Methods. Preprint ITEP, 1993-21.

7. M.M.Urie and M.Goitein. Variable versus Fixed Modulation of Proton Beams for Treatments in the Cranium. Med. Phys., 16, 1898, pp 593 - 601.

8. K.K.Onosovsky and V.S.Khoroshkov. Medical Accelerators for Conformal Proton Irradiation and H^- Linac Possibilities. Proceedings of 400-MeV Beam Workshop. Fermilab, Oct. 24 - 27, 1993.

Figure Captions

Fig. 1. ITEP proton therapy facility.
M - distributor magnets; Ia,b,c - treatment rooms; IIa,b - contr rooms; III - patient preparation rooms.

Fig. 2. Main dosimetry means of ITEP PTF and fields of ths application.

Fig. 3. Working and non-working areas of the ionization chamber

Fig. 4. Two ways of monitoring by current transformer. See t text for explanations.

Fig. 5. Top - Bragg curve study by a semiconductor detector. Bottom left - Calibration of ionization chamber and semiconducto detector using induced activity in polystyrene: 1 - curre transformer; 2 - ionization chamber, 3 - polystyrene pellet (induc activity), 4 - semiconductor dosimeter (top - in water phantom).

Fig. 6a. Irradiation with the use of a passive dose delive system. Dose-volume histogram confirms incorrect irradiation.

Fig. 6b. Irradiation with the use of an active dose delive system (ADDS). It is possible to reduce considerably the volume healthy tissues in front of the target which are exposed to hi dose.

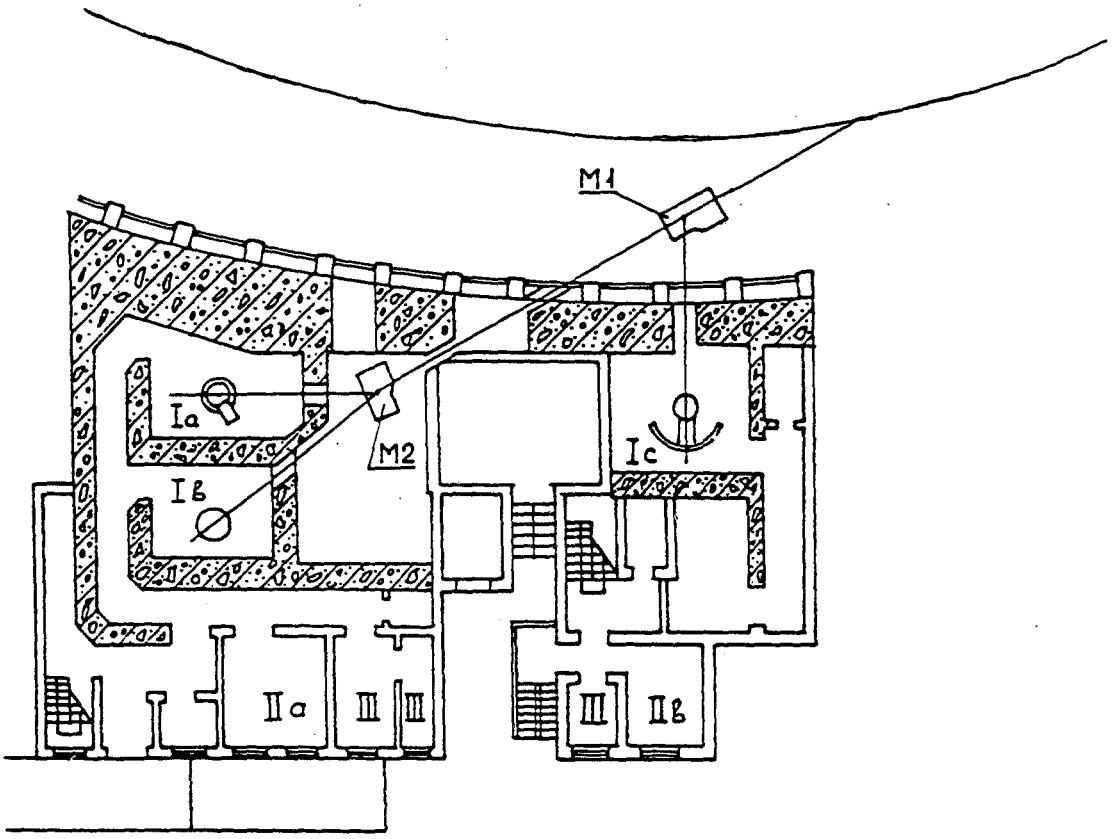

Fig. 1.

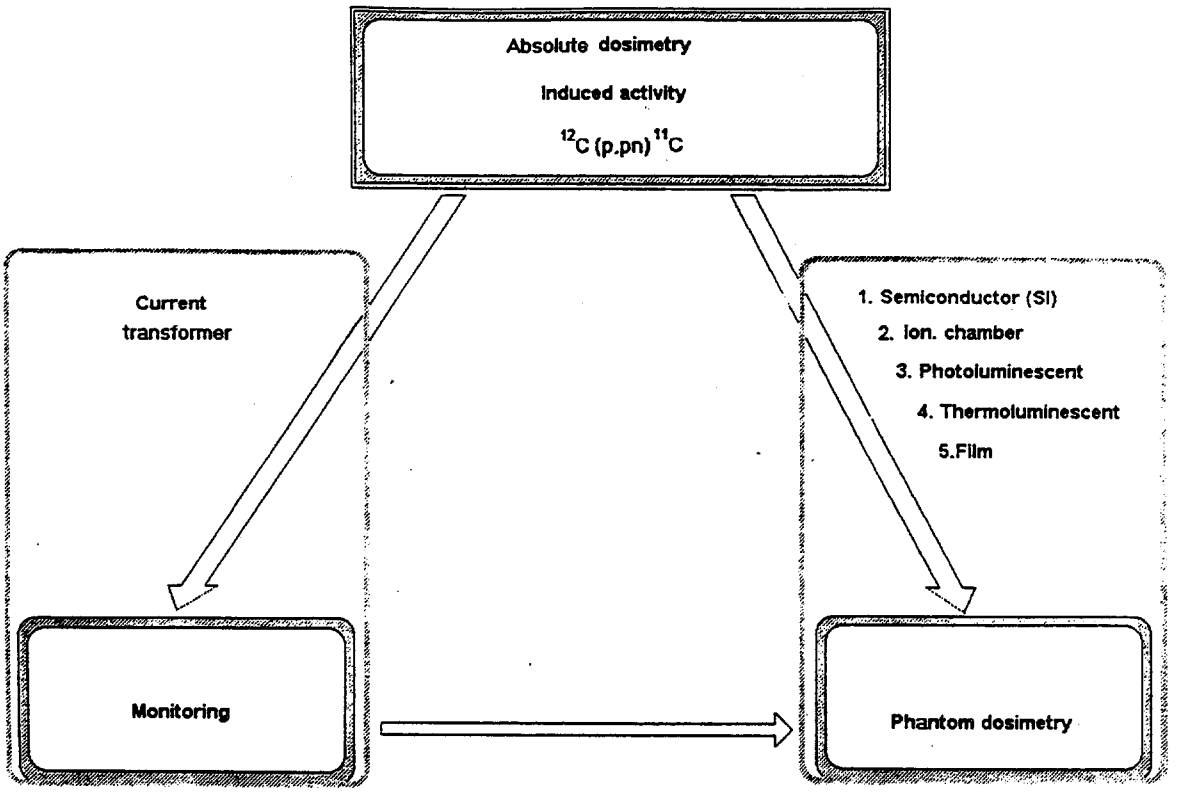
Absolute dosimetry
Induced activity
^{12}C (p.pn) ^{11}C
Current transformer
1. Semiconductor (SI)
2. Ion. chamber
3. Photoluminescent
4. Thermoluminescent
5.Film
Monitoring
Phantom dosimetry

(c) Luck.V.

Fig 2

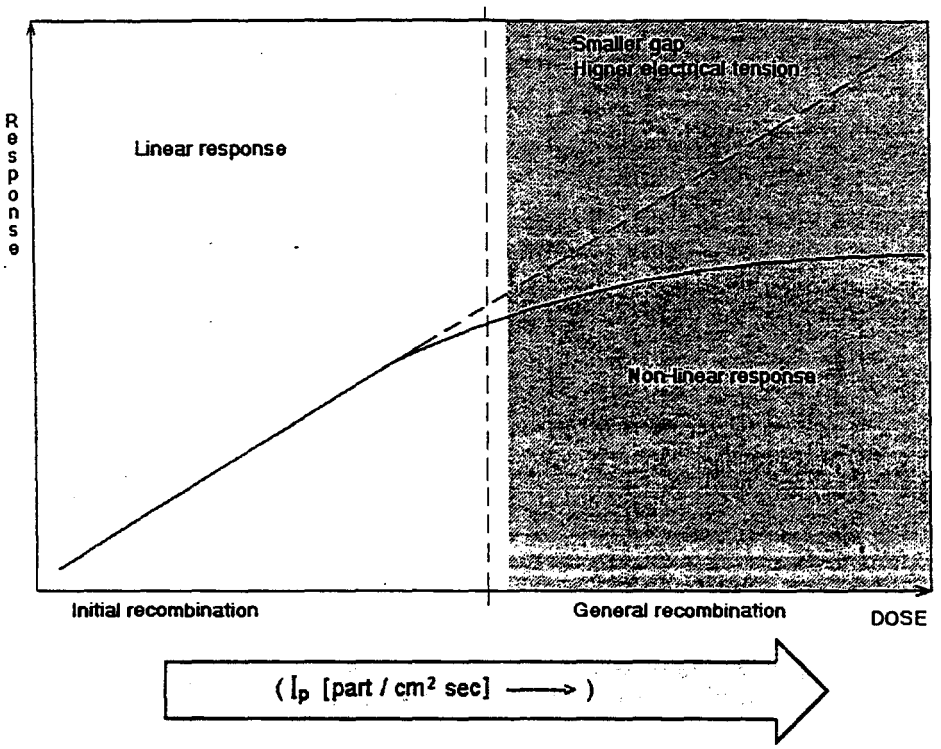
Smaller gap
Higher electrical tension
Linear response
Response
Non-linear response
Initial recombination
General recombination
DOSE
(I_p [part / cm² sec] ⟶)

(c) Luck.

Fig. 3.

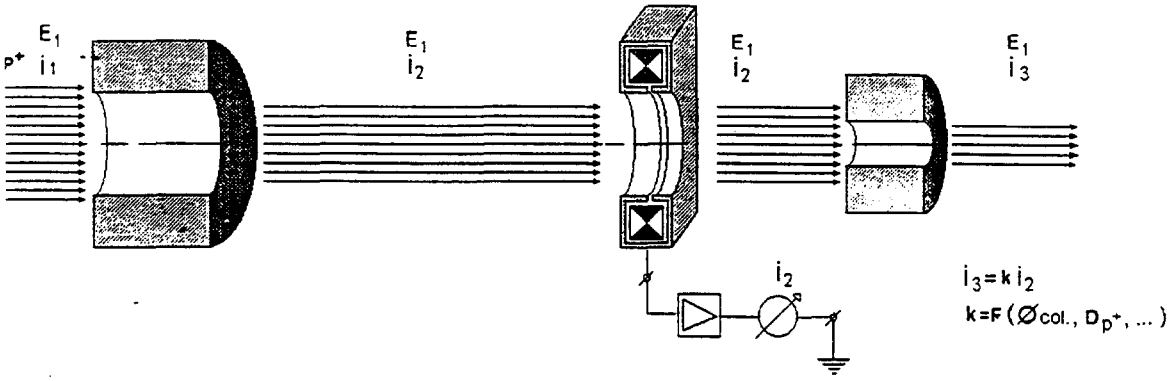
E1
p+ i1
E1
i2
E1
i2
E1
i3
i2
i3=k i2
k=F(Ø col., Dp+, ...)

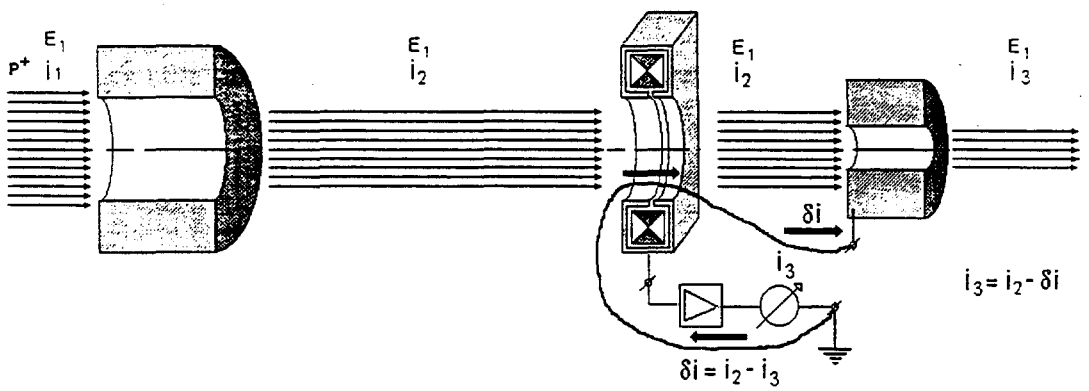
E1
p+ i1
E1
i2
E1
i2
E1
i3
δi
i3
i3= i2- δi
δi = i2 - i3

Fig 6

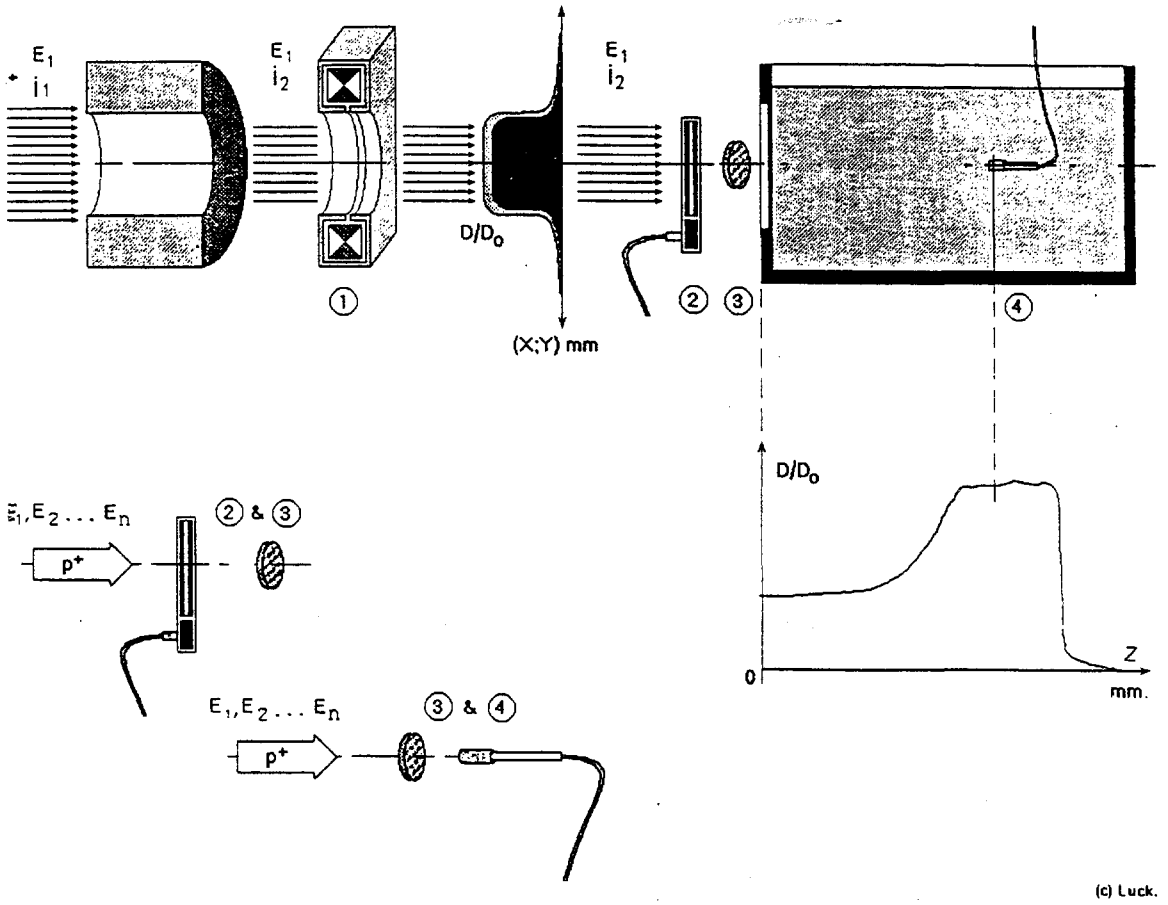

(c) Luck.

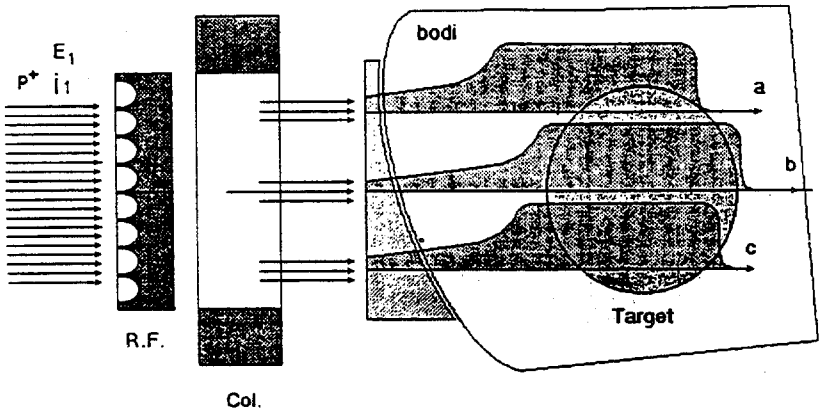
E1
p+ i1
R.F.
Col.
bodi
a
b
c
Target

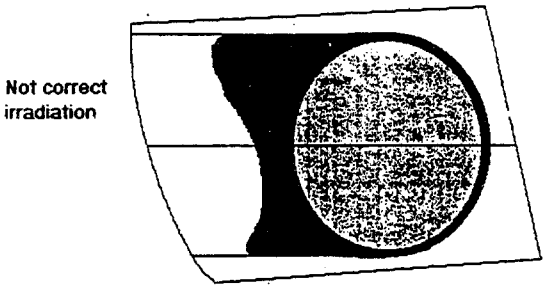
Not correct
irradiation

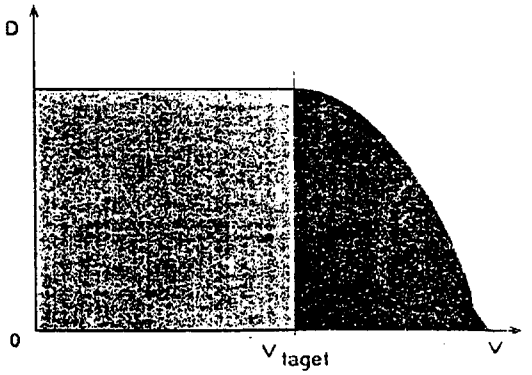
D
0
V taget
V

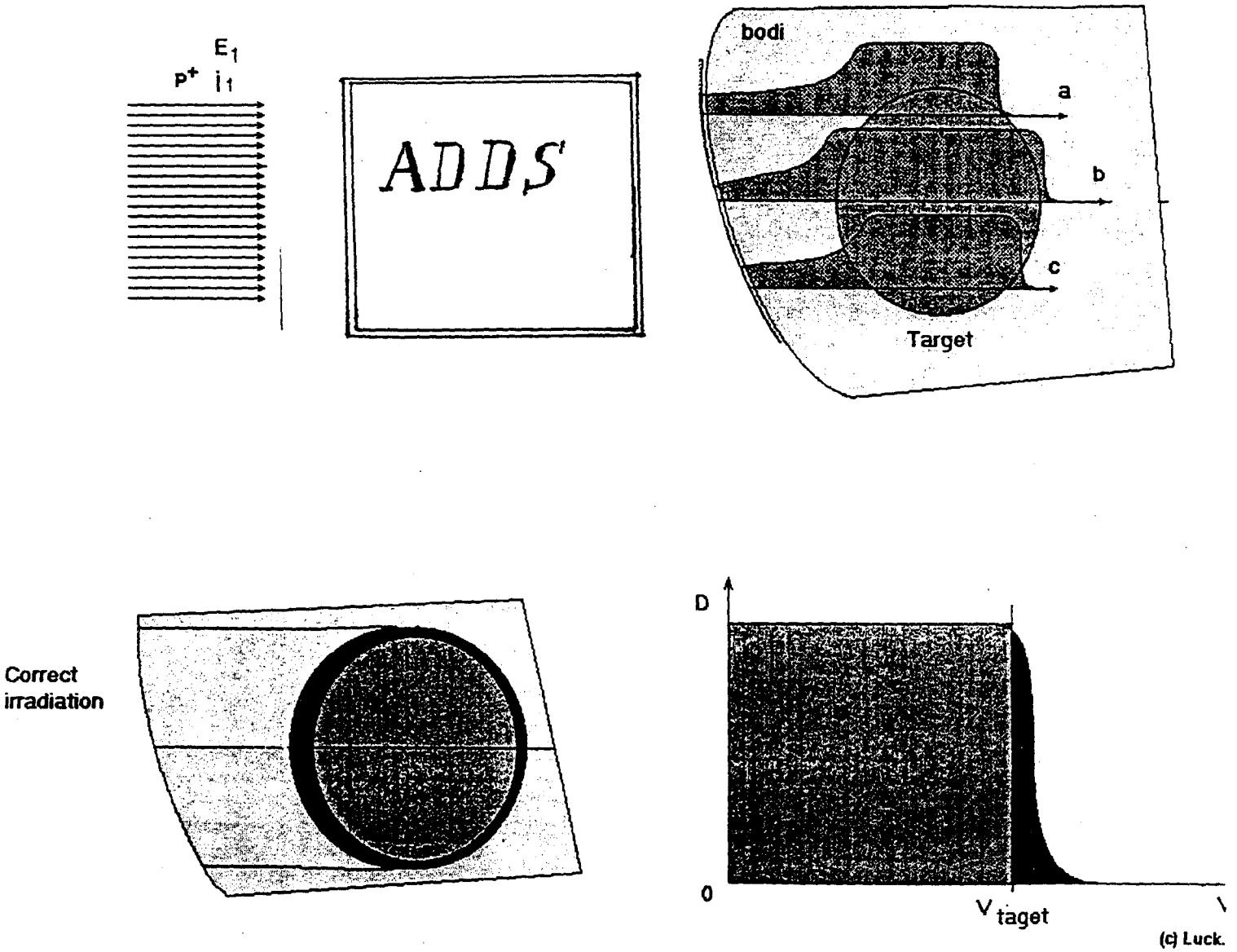
E1
p+ i1
ADDS
bodi
a
b
c
Target
Correct irradiation
D
0
V taget
(c) Luck.

Fig 66

Medical Accelerators for Conformal Proton Irradiation and H^- Linac Possibilities

K.K.Onosovsky, V.S.Khoroshkov
Institute for Theoretical and Experimental Physics (ITEP)

The experience of using proton beams in medicine, has been acquired for almost 40 years. During this period, the advantage of protons has been demonstrated for the treatment of a number of pathologies. At the same time, the technique of using electron beams and hard γ-radiation, has also not been at standstill. Presently, it provides in essence, for the use to the utmost of these types of radiation for conformal irradiation of most of the targets. As new means of computer topometry, X-ray and NMR tomography appeared, it became possible to use the advantages of a proton beam to the same extent. However, physical accelerators designed not for medical purposes, do not provide for these aims.

Unfortunately, in designing proton accelerators specifically for medical purposes, basic attention is often paid as well to the construction parameters of the proton accelerators. If we wish to win the competition with conventional methods of irradiation, we should not pay the basic attention to the simplicity and structural merits of proton accelerators. First of all, it is necessary to provide for the maximum use of the proton beam. Unfortunately, today we are far from realizing this possibility. Moreover, not always we lay this in the concepts of future medical accelerators.

As Russians we would like to make a rough comparison. Market economics are evidently more efficient than planned ones. But to prove this, it is necessary to create the proper conditions. Today, there is no such conditions in Russia, and so far it has been impossible to prove the statement above. Accordingly, if we wish to prove and use the advantages of a proton beam it is necessary to build a proton accelerator with such beam ejection and dose delivery systems that would provide for conformal irradiation of any target, and exact fitting to the plan, safety and reasonable irradiation time without additional mechanical devices. Of course, besides fitting these requirements, it is necessary to account for the parameters which determine the accelerator reliability and those affecting its cost and the cost of the PTF as a whole.

Below, the table is presented in which the accelerators have been placed as to the priority of certain parameters, and corresponding comments are made.

	CHARACTERISTICS	PRIORITY			
1.	SIZE	cyclotron	synch. H^+	synch. H^-	linac.
2.	WEIGHT	synch. H^-	synch. H^+	linac.	cyclotron
3.	OPERATION COSTS	synch. H^-	synch. H^+	cyclotron	linac.
4.	COST	synch. H^+	synch. H^-	linac.	cyclotron
5.	RELIABILITY	linac.	cyclotron	synch. H^+	synch. H^-
6.	RADIATION LEVEL	synch. H^-	synch. H^+	linac.	cyclotron
7.	PHASE SPACE OF EXTRACTED BEAM	synch. H^-	linac.	synch. H^+ linac.	cyclotron
8.	ENERGY SPREAD	synch. H^-	synch. H^+	linac.	cyclotron
9.	EXTRASTION ENERGY CHANGING	synch. H^-	synch. H^+	linac.	cyclotron
10.	BEAM INTENSITY CHANGING	synch. H^-	synch. H^+	linac.	cyclotron
11.	EXTRACTION DEVICE	linac.	synch. H^-	synch. H^+	cyclotron
12.	POSSIBILITY TO ACCELERATE LIGHT IONS WIHT SMALL CHANGE OF INSTALLATION	synch. H^-	-	-	-

Infortunately, the table is of a subjective character since in certain cases the parameters are almost identical. We will try to comment this table. For demensions, we would put a cyclotron the first place (a synchrotron for 5 T is smaller in size, but it does not fit all the specifications for a medical accelerator). An H^- accelerator has the smallest weight since the magnetic field is 0.6 T for 250 MeV and despite of the longer magnetic path compared to that of a proton accelerator, the weight of the magnetic system is less. Running expenses are lower for the same reason. Here we are using estimations made with regard to the cost of electric power and salary in Russia. Electric power consumption is lowest in the H^- accelerator. The costs of the H^- sygchrotron and proton synchrotron H^- are approximately the same. Vacuum and pumping systems of an H^- accelerator are more expensive than of proton synchrotron. But magnetic, power and ejection systems are more expensive in proton accelerators.

Reliability seems to be higher in the linear accelerator. We made estimation of the idle time of the ITEP injector, 25-MeV linear accelerator, and 10-GeV ITEP synchrotron for 10 years from 1977 to 1986. The average idle time was 1.9% for the linac, 4.2% for the proton synchrotron. The idle time of the Harvard cyclotron was 2.3%. These accelerators are close in age and time of operation and I think they can be compared.

The smallest phase volume of the ejected beam is in the H^- synchrotron. The energy spread in the H^- and proton synchrotron, are practically the same.

As for the possibility to change the ejected beam energy in the process of ejection or from cycle to cycle, the H^- synchrotron has definitely to be in first place.

The radiation level is lower in the H^- accelerator since due to smaller phase volume it is possible io form the dose field by superposition of beams instead of cutting out a collimator after double scattering.

Beam intensity variation is possible in an H^- accelerator in the process of ejection. Improvement of the resonant slow ejection by means of RF transverse stirring of the beam also makes it possible to change the intensity in the process of ejection but not to such extent. If an external injection system is

used in cyclotron it is possible to control its intensity.

Definitely, a linear accelerator has the simplest ejection system. As for a synchrotron, we are sure the recharge system is more simple than the resonant system both in manufacturing and in routine operation.

An H^- accelerator has another advantage in comparison with a proton synchrotron, that is, a light-ion accelerator can be built on its base. This is a perspective for the future develorment of therapy with light ions.

And in conclusion, one more possibility that is given by the H^- accelerator which may be used in future. CERN scientists have studied the behavior of H^- ions in the antiproton storage ring, and studied the process of the H^- beam neutralization by light. They have carried out an interesting experiment on H^0 beam ejection from the accelerator by a laser [2].

This opens unique possibilities to build the ejection system where in the process of ejection within one cycle, the intensity can be varied within wide limits and the energy can be changed; thus the advantages of a synchrotron are used to the utmost. A 3D scanning system will make it possible to give up completely all additional devices, collimators, boluses, filters, etc.

The main advatage is that only required part of the beam is used, and simultaneous ejection from several places of the accelerator for different treatment rooms, is possible. The particles remaining in the ring can be slowed down to ejection energy, and therefore the radiation background can be reduced to minimum.

If CERN scheme is used, a light source of about 100 W will be required for the ejection of particles from the accelerator within 1 second. However, various methods and constructions which would provide for many-times power decrease are possible, thus making it technically reasonable. We are deeply convinced that only construction of a perfect ejection system capable of irradiating the target based on topometry results and treatment planning without individual mechanical devices, will make protons to win the competition with conventional types of irradiation.

Returning to FNAL linac problems, consider a few possible variants of organizing the external proton medical beam.

In order to fit the requirements of the active dose delivery system (ADDS), it is desirable to stretch the external beam pulse considerably (up to hundreds milliseconds). The most evident solution to this problem would be to construct a stretcher capable of energy variation within 250 - 70 MeV interval, or to vary linac ejection energy, or to install an additional accelerating-decelerating system for the beam with the appropriate power system for the magnet. Since the linac in this case works as a sufficiently intensive and high-energy injector, the design of the stretcher is relatively simple and its cost is not high. The aperture of magnets may be made smaller, the specifications to vacuum and to the accelerating system may be degraded. The problems in connection with the injection device, do not seem too serious. If negative hydrogen ions H^- are injected into the stretcher, an ejection system may be used with recharge of H^- ions on a small recharge target or with a laser [1, 2].

In this case, we obtain reasonable pulse length, good operation, small phase volume, and the possibility to measure the ejected beam intensity by the current of electrons procuced in beam recharge on the target.

Consider the possibility to build a 3D spot scanning system without the stretcher, i.e. the one where the H^- beam from the linear accelerator is used, with 200 MeV energy, 30 μs pulse length, and 15 Hz frequency.

The patient irradiation time is usually assumed to be 120 s. In this case, the number of pulses accessible for dose field formation (1800), is probably insufficient. For instance, in the 3D spot scanning system designed by Pedroni [4] the need has been demonstrated to use 10000 pulses and there is the possibility to adjust the number of particles per each pulse (each spot).

Consider one of the possible systems of raster irradiation. It has been demonstrated in Ref. 5 that for organizing a raster scanning system, the following conditions are required:

- Time of irradiation should not exeed 120 s;

- the frequency of fast sawtooth scanning magnet should not exeed 1 kHz (higher frequency of the sawtooth scan is hardly to be realized);

- for averaging the dose distribution and/or its correction at the expence of multiple cross of each voxel, the summary number of crosses should not be less than 100 -200.

Depending on accelerator time parameters (pulse lehgth, repetition rate), different modes of irradiation may be chousen. During one pulse, different parts of the whole target volume may be irradiated: one layer in depth, part of the depth layer, one line of voxels of one of the layer, etc.

In any case,it is easy to show that for fitting the above three conditions, the accelerator duty factor (especially if the accelerator is used for treatment in several treatment rooms), should be within 0.5.

Thus non of the raster systems considered in [5], can't be organized with FNAL linac parameters, where the duty factor is 0.5*10^-3, and for organizing the raster scanning of the beam at FNAL linac, there is 10^3 times less real beam time than required.

Nevertheless, the existence of the H^-, makes it possible to organize the beam scan and the required dose distribution even with such time deficit. If the variable density recharge target (position 2 Fig. 1) is used on the path of the H beam, scanned by an electrostatic inflector (position 1 Fig. 1) or in some other way, it becomes possible to adjust the number of protons falling to each voxel of the irradiated target.

On the path of the H beam scanned in one plane by an electrostatic device (position 1), a recharge target (position 2) of variable density is placed (meaning the existence or absence of material in one point of the recharge target or other). After magnetic separation (position 3) of the H ions and protons, the latter are decelerated in the degrader (position 5). The energy of protons after deceleration provides their stop in a line of Voxels (line "a" shaded in Fig. 1). The 1 MHz frequency of the electrostatic device provides the 60-fold pass of this line of Voxels during one pulse.

Multiple pass of each Voxel by the beam, overages the dose

distribution in the line despite the time instability of the initial beam during the pulse. The sinusoidal character of the beam scan (different time of its stay in the middle of the line and in its periphery), may be compensated by changing the density of the recharge target in accordance with the same law. The same variable parameter (recharge target density in different points) may, generally speaking, be used for creating any prescribed dose distribution in the line of Voxels.

After change of the recharge target and degrader during the 65 ms pause between the pulses, the next line of Voxels is irradiated (line "b" in Fig.1). In the similar way, all lines a, b, c, d, e of the layer are irradiated. The layers that follow (a_1 - e_1; a_2 - e_2; .....a_n - e_n), are irradiated in the same way with successive change of the field in the slow magnet (position 4) scanning the beam in perpendicular direction.

Assume the volume of one line of Voxels be 1/400 ÷ 1/500 of the total target volume. The repetition rate being 15 Hz, the whole target can be once irradiated in 40 seconds. The typical 2 minute irradiation time provides for triple irradiation of the whole volume. Repeated irradiations are used for the correction of the dose distribution, and for better compliance of prescribed and real dose distribution. The information for repeated (correction) irradiations may be obtained in the case considered, both from a multi-electrode ionization chamber and by collecting the extra-electrons on special electrodes after the recharge target.

Fig. 1 demonstrates the target of simple (cubic) shape; naturally, for a complicated-shape target, an individual recharge target is required for each pulse (each line of Voxels), with its own density distribution law from point to point. Here, a number of solutions is possible: mechanical devices with movable toothed foils [Fig.2. left] or a film perforated by cutter or laser. (Fig.2, right] This solution is possible if the film perforation is done directly during the irradiation in the real time mode, and the cutter is controlled by an on-line computer.

Generally speaking, a combination of a quadrupole, octupole, and dodecapole lenses may be used instead of the scanning device in order to transform the beam into a line with maximum possible density

uniformity. All depends on stability of particle density distribution in the primary beam although complete uniformity is not required in the primary beam, since correction may be introduced by the recharge target density. In case of excess linac intensity, a beam with rectangular density distribution and low dispersion, can be obtained by means of an extra recharge target and magnetic system. In this case, a quadrupole lens would be enough for scanning. To provide safety, it is necessary to have a device which would pass the beam through only in case of the scanning mechanism in operation or with the beam stretcher lenses working.

A similar scanning system may be used in a gantry. Fig. 3 presents the schematic of the gantry designed in ITEP [3].

The small phase volume of extracted proton beam from H^- synchrotron allows to build the gantry system of relatively small size and weight. In our case, the system diameter is 6.5 m, and weight is 5 - 6 ton. The magnets have 11-mm gaps, the field is about 1.5 T. The only sweep magnet is placed before the last 90 bending magnet about 4 m from the patient. The sweep magnet is scanning a single beam into a line up to 30 cm long on a skin along the patient sagital axis. If the line length is up to 120 mm the single beams are parallel, for bigger line length, the divergency of single beams does not exceed .06 radian (Fig. 4 left).Depth scanning (transition of lines in depth) is achieved by changing beam energy from pulse to pulse. Scanning the beam in the direction perpendicular to the sagital one is done by parallel transition of lines in simultannneous turns of the gantry system and the last 90 magnet (Fig. 4 right). Thus, the dose fieldmay be formed with 300*300 mm*mm transverse dimensions and minimum divergency of particles. The effect of dose increase on the surface noticed by Goitein, is either absent (for fields below 12 cm) or brought to minimum.

In a case of extraction from the linear accelerator H^- beam instead of a sweep magnet an electrostatic scanning device is installed. Before the last 90 magnet, the recharge target is placed (Fig.5). The layers obtained are summed not by means of a slow sweep magnet as in the previous case, but by simultaneous turn of the gantry system and the last 90 in respect to the beam entrance axis. For the

dose field formation with required accuracy, a number of gantry turns in forward and backward directions, is also required. The stop-time o the gantry before the reversal is 3 - 4 seconds. This idle time may b used for results calculating and for preparing of irradiation program for the next passage.

The authors are grateful to Drs. V.M.Lukjashin and E.I.Potryasova for discussion and preparation of illustrations, and to Dr. I.L.Zubarev f assistance in translation the text into English.

REFERENCES

[1] V.S.Choroschkov,K.K.Chossovsky,H^- synchrotron for proton therapy facility.
Proc.of NIRS International workshop on heavy Charged Part.therapy and Related subjets,(jule 4-5 1991)p213-220.

[2] M.Chanel, EPLUCHAGE DES H^- DANS LEAR PAR LE GAS RESIDUEL LA LUMIERE DES JAUGES PAR UN FAISCEAU LASER. OU UNE LAMPE SPOT.
PS/LEA/Note 87-2,Fevrier (1987).

[3] V.S.Khoromchkov at all, H-synchrotron for proton therapy Facility. Proc.of the NIRS int. works on Heavy Charged Particle therapy and Related subjects (1991) p204-213.

[4] E.Pedrony, Cancer therapy with 200 MeV protons at PSI development of a Fast Beam scanning method and Future plans for a hospital based Facility.
Proc.of the 2nd European particle acc.conf. V1, p222.

[5] W.Chu at all,Performance specification for proton Medical Facility.
LBL-33749. Lawrence Berkeley Laboratory (march1993).

Figure cuptions

Fig.1. Schematic of the active dose dilivery system with electrostatic scanning and recharge device.
1. electrostatic sweep; 2. recharge device; 3. divider magnet; 4. slow sweep magnet; 5. rotating degrader; 6. irradiated targe

Fig.2. Schematic of recharge devices.
left: 1. H- beam; 2. set of toothedfoils; 3. individual gears for eac piece of foil; 4. picture of H- , p distribution.
right: 1. H- beam; 3. gear; 5. perforated film.

Fig.3. Schematic of ITEP gantry.
1. electrostatic chopper; 2. magnet trap for deflected beam; 3. shielding; 4. last quadrupole; 5. measuring device; 6. sweep magnet; 7. magnets; 8. quadrupole lenses.

Fig.4. Schematic of irradiation along sagittal axes.
left: 1. sweep magnet; 2. bending magnet; 3. last quadrupole; a) quadrupole switched off; b) beam diverged by lens; c) parallel beam; d) coverged beam.
right: 2. magnet turning around the entrance axes; 4. irradiated targ

Fig.5. Schematic of gantry for H- beam from linac.
1. electrostatic scanning device; 2. recharged device; 3. rotati degrader; 4. irradiated target.

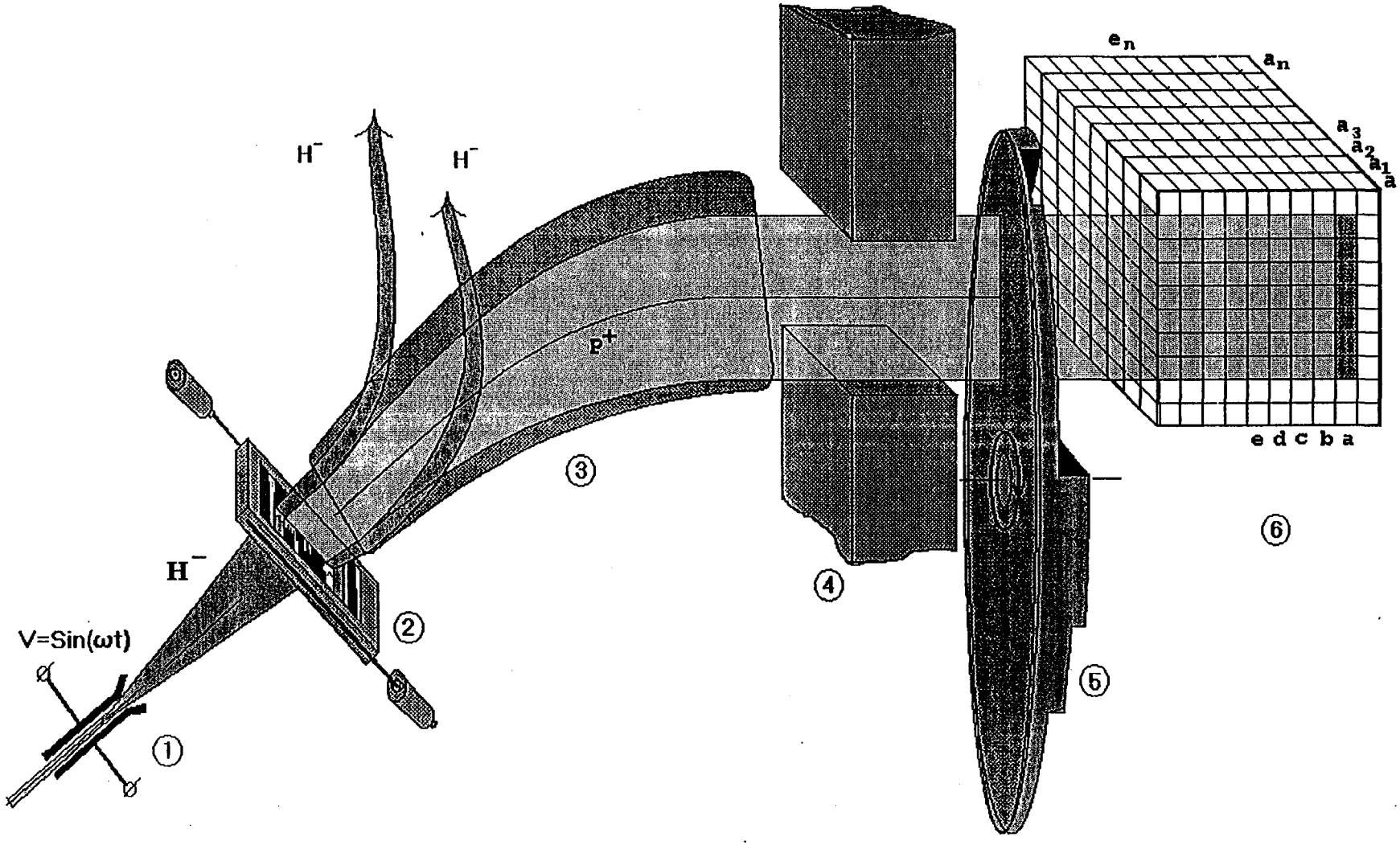

Fig.1.

© Luck.

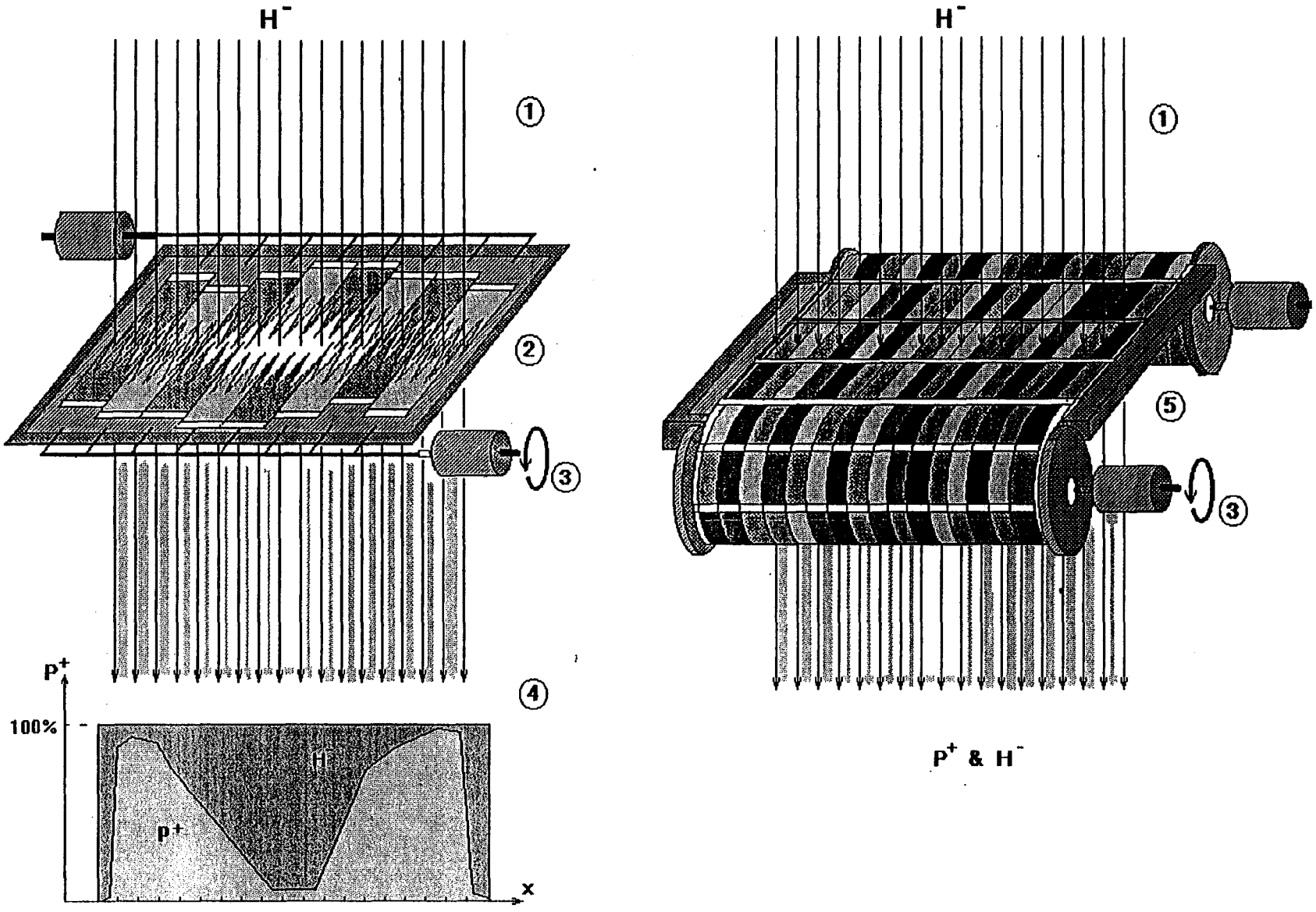

Fig.2.

Gantry magnet channal shceme.

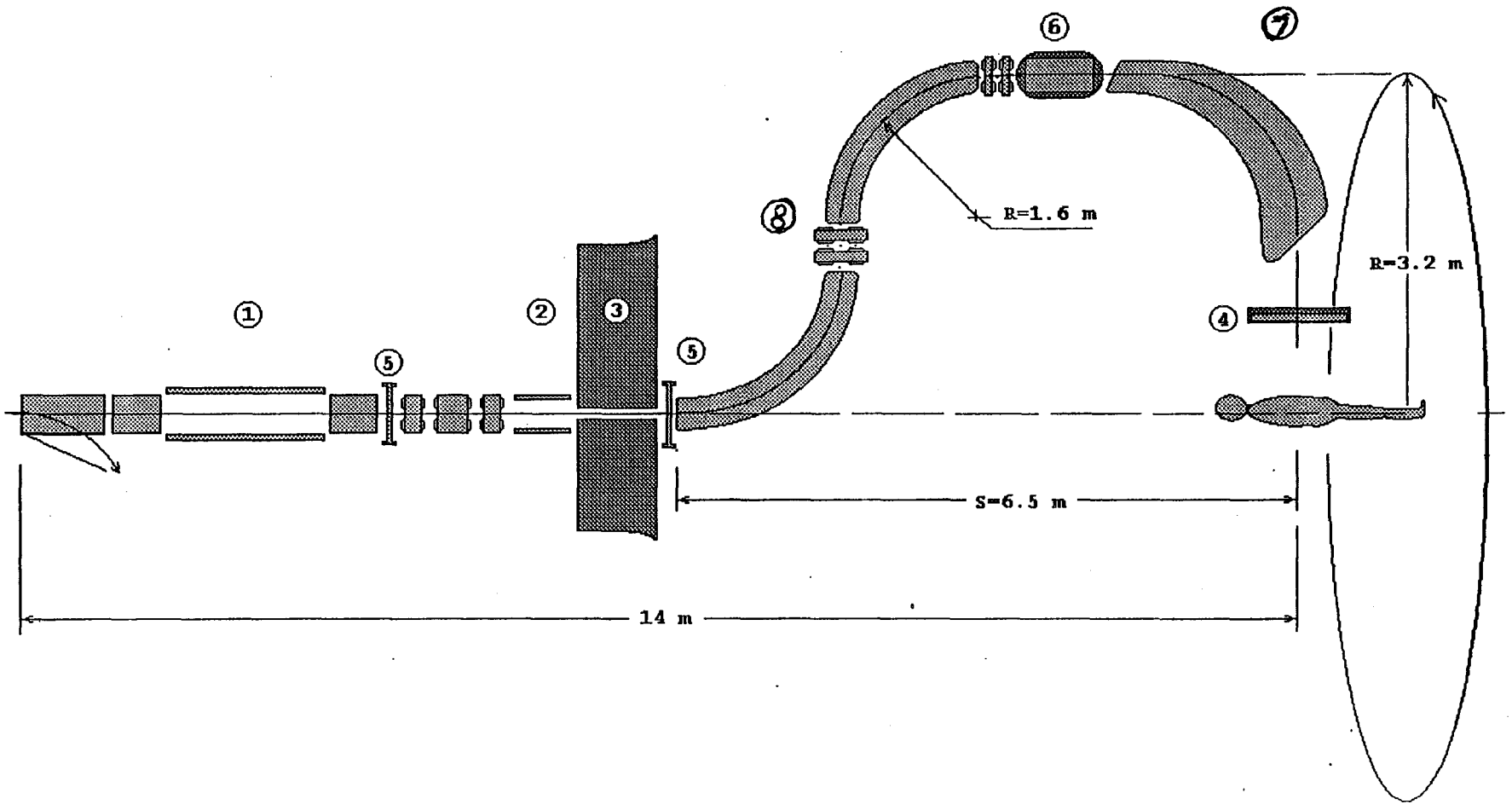

Fig.3.

Scheme of irradiation along sagital axe.

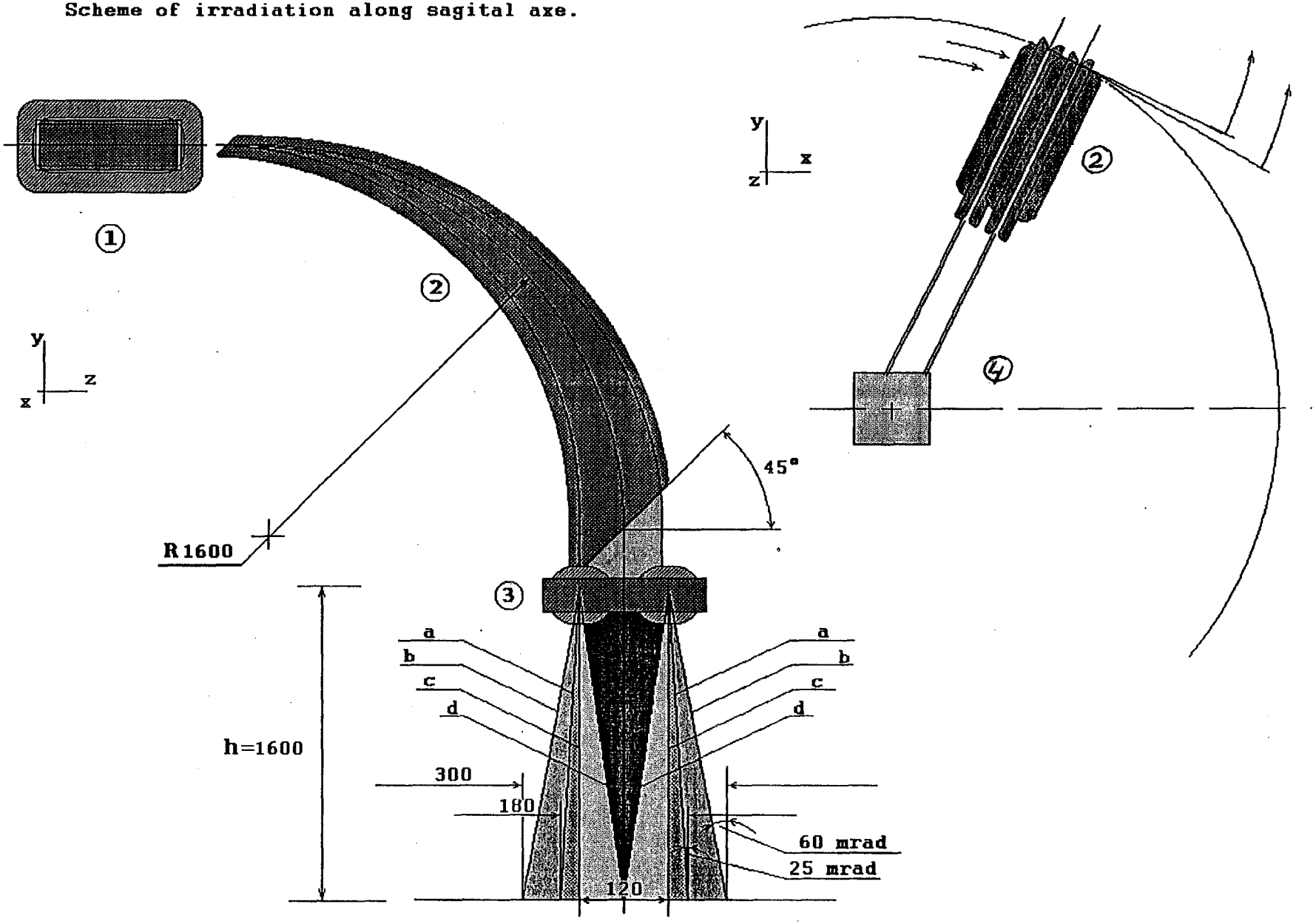

Fig 4

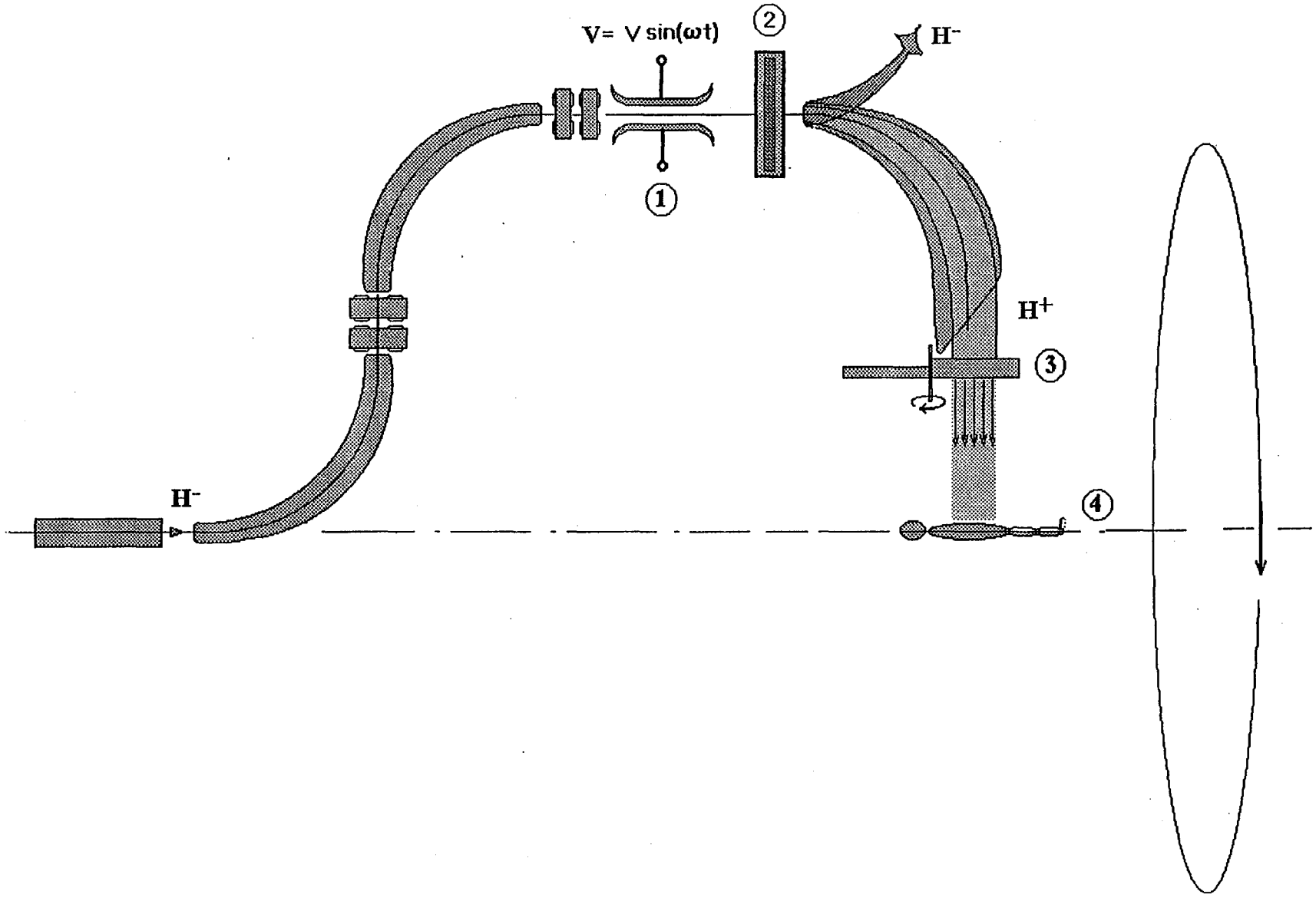

Fig.5.

A 400 MeV $H^{-,0,+}$ Beamline

T. Kroc, Fermilab

A proposed 400 MeV beamline was made possible by the construction of an equipment access for the installation of the components for the 400 MeV Linac Upgrade. This access starts outside in an equipment drop pit, penetrates the shielding berm, and merges into the existing linac enclosure. The beamline itself would be produced by putting a fast pulsed magnet about 10 feet downstream of the end of the linac. This could divert the beam on a pulse-by-pulse basis to a beamline constructed in the accessway.

Figure 1 shows the layout of the area in question with a very simple beam line drawn in. It shows the pulsed magnet, two additional bending magnets, and two beam dumps. The first dump would be a high intensity dump capable of collimating the beam to low intensity for use in the pit area. Figure 2 shows the area more closely where the proposed beamline meets the linac. Figure 3 shows the contour of the berm and the gravel hardstand area surrounding the access pit.

The linac RF pulses at 15 Hz. However, beam is only accelerated when there is a need for it. During p-bar production at Fermilab, a pulse of beam is needed every 2.4 seconds. (P-bar production is presently the largest user of protons, but in addition the Booster has a physical limitation of one pulse per second on average.) This leaves 35 of every 36 potential beam pulses for other uses There is a medical treatment facility in the upstream half of the linac that uses less than three hours of beamtime per day three days a week. This leaves a large amount of available beam time for the proposed 400 MeV beamline.

A 400 MeV H^- beam can withstand 7.5 KG of magnetic field without stripping. A five foot long magnet, such as some surplus one that may be available at Fermilab, could provide up to a 20° bend. As can be seen on figure 1, the access pit is at a 45° angle with respect to the linac. This would require three bending magnets to get the beam to the access area, including the pulsed one (the pulsed magnet however would probably have to be specially constructed) . It is anticipated that surplus quads removed from

the 200 MeV transfer line between the linac and booster would be available for this new line.

The linac tunnel ceiling is 13 feet above the floor. The ceiling of the covered ramp in 10 feet high. The linear accelerator is four feet above the floor and presumably the 400 MeV line would be also. However, the floor of the covered ramp and the access pit slopes up at approximately 1.6° moving away from the linac. The covered part of the access is 9' 6" wide while the pit is 10' 9" wide. The pit is 80 feet long, the covered access is 60 feet, long and the area where it joins the linac enclosure is approximately 25 feet long.

Any equipment in the linac enclosure including the covered part of the access (upstream of the first dump) would only be available during scheduled down periods for the linac. Intervals between these down periods can be weeks or months and tend to last for only a few hours. Any components in this area would have to be remotely controlled with high reliability. The beam delivery system to the open pit (which would have some type of environmental enclosure built to suit the apparatus inside) will be designed to allow access to equipment once proper safeguards are in place to ensure beam is not delivered during the access. In the example beam line in figure 1, the first beam dump would be designed to allow only low intensity beam into the less well shielded access pit.

The energy can be varied by delaying the RF pulse of linac cavities above the desired energy with beam drifting through the delayed cavities to the pulsed magnet and the new line. The energies possible in this manner are 166, 152, 190, 230, 271, 314, 357, 401 MeV. It may also be possible to further vary the energy within these increments by changing the phase of the last active cavity. The extent to which this would be compatible with other desired beam parameters would require more study.

Transverse beam characteristics and beam intensity will be controlled mostly by collimation after the pulsed magnet.

This description gives the very basics of how the line would be implemented. More elaborate designs are possible and would almost certainly evolve in any case. Beam requirements not addressed here will can be evaluated to determine the feasibility of meeting them.

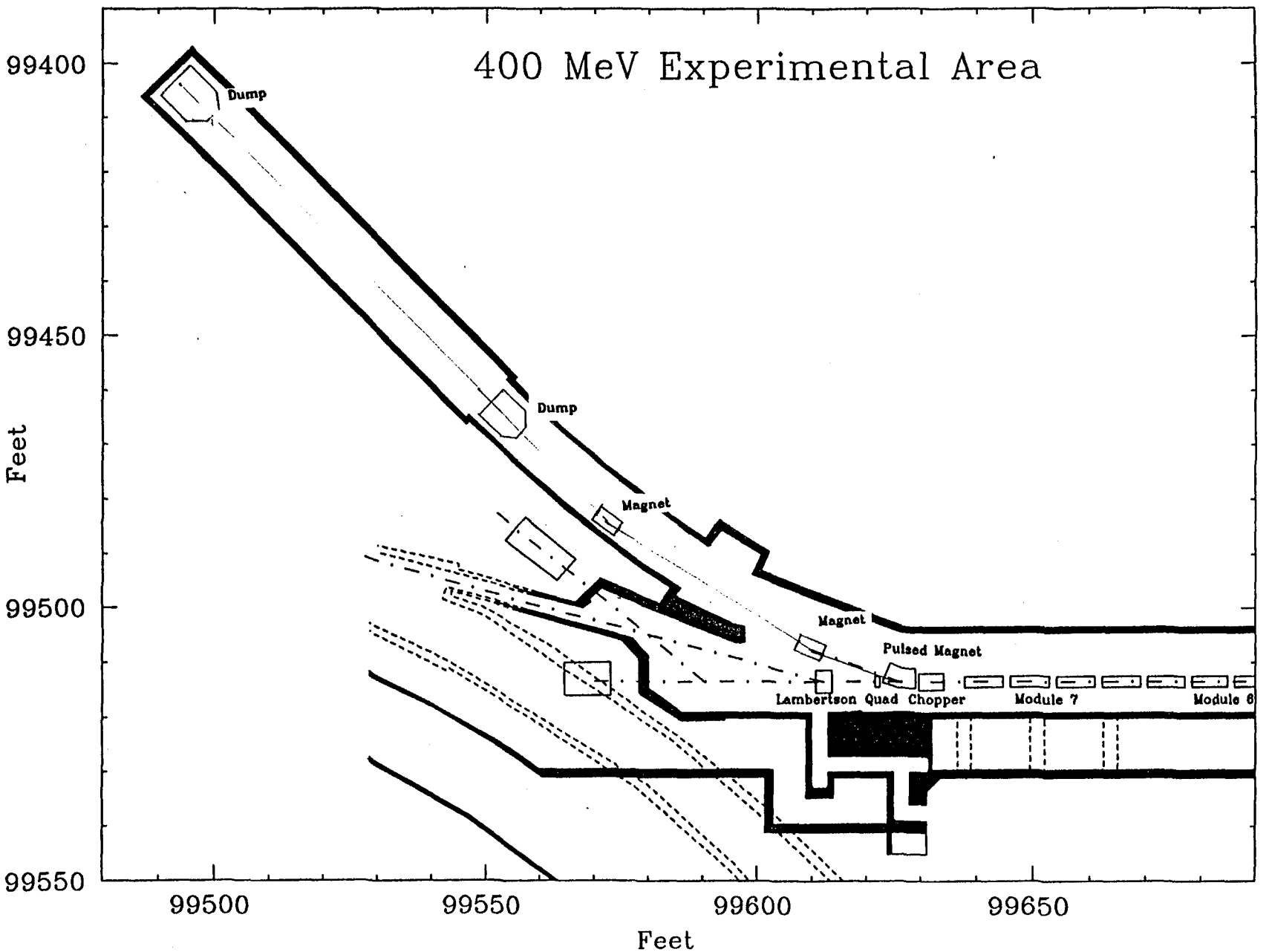
400 MeV Experimental Area
Dump
Dump
Magnet
Magnet
Pulsed Magnet
Lambertson
Quad
Chopper
Module 7
Module 6
99400
99450
99500
99550
Feet
99500
99550
99600
99650
Feet

Figure 1

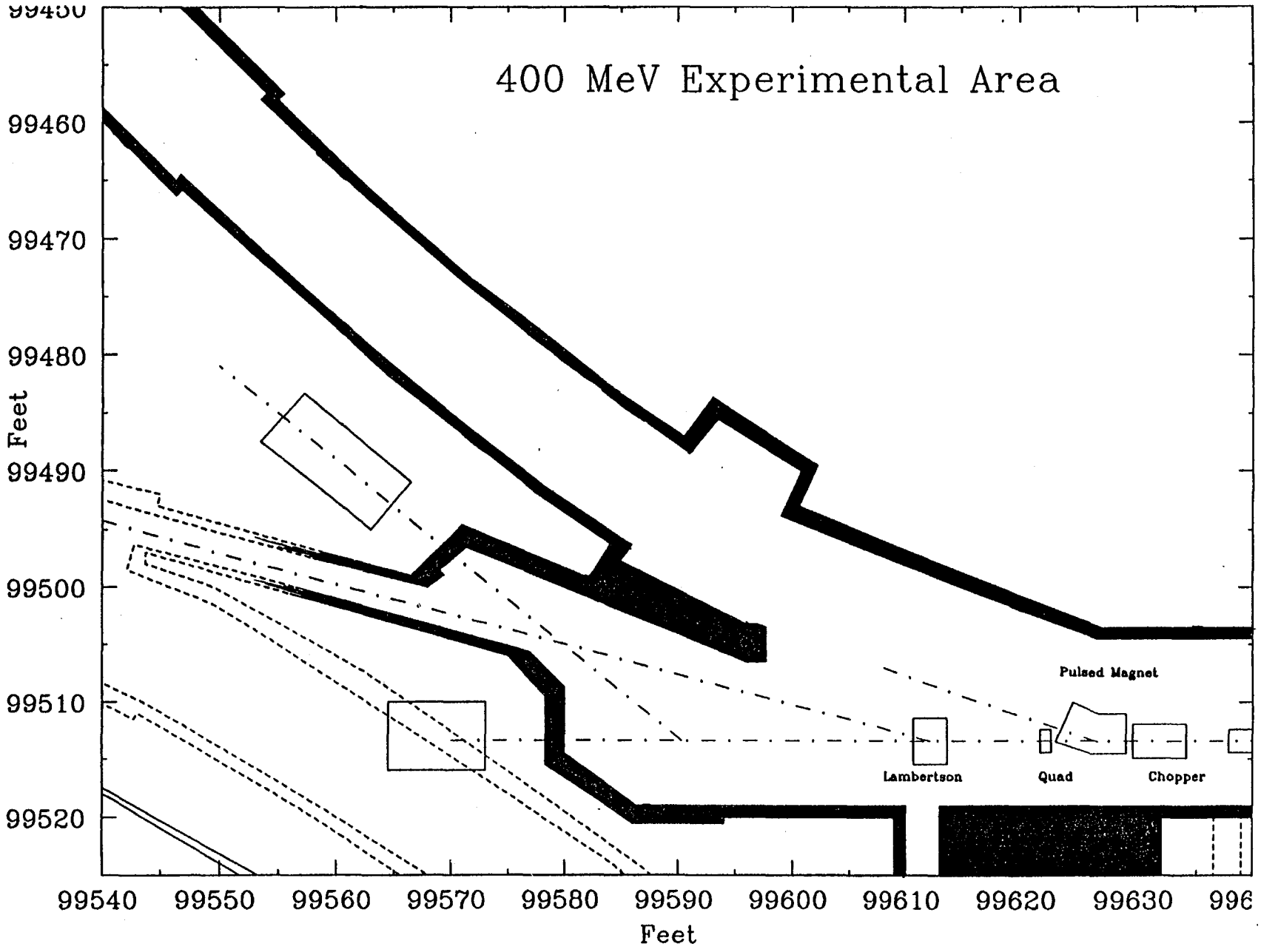
400 MeV Experimental Area
Pulsed Magnet
Lambertson
Quad
Chopper
Feet
99450
99460
99470
99480
99490
99500
99510
99520
99540
99550
99560
99570
99580
99590
99600
99610
99620
99630
Feet

Figure 2

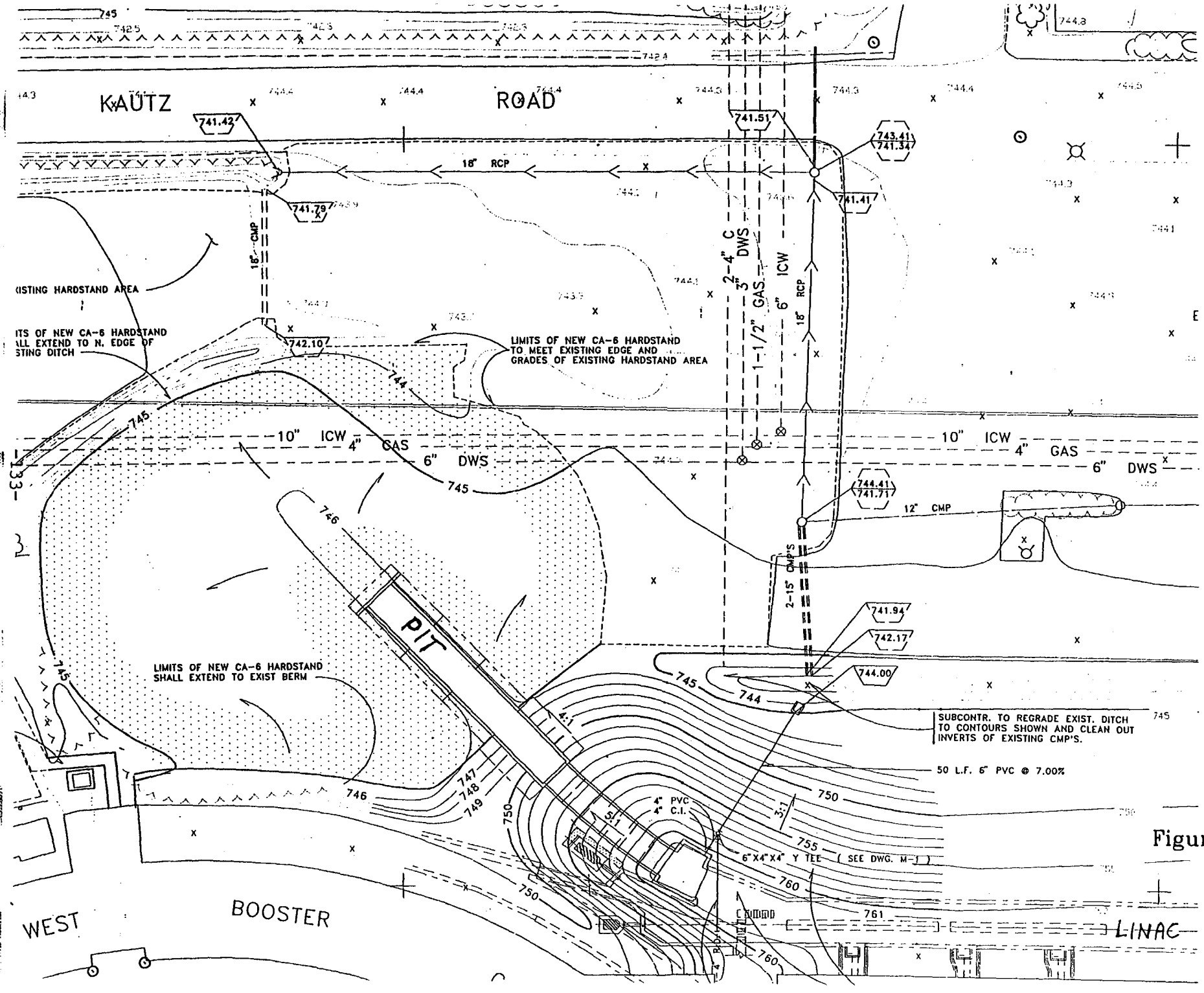
KAUTZ ROAD
741.42
741.51
743.41
741.34
741.41
741.79
18" RCP
18" CMP
742.10
ISTING HARDSTAND AREA
ITS OF NEW CA-6 HARDSTAND
ALL EXTEND TO N. EDGE OF
STING DITCH
LIMITS OF NEW CA-6 HARDSTAND
TO MEET EXISTING EDGE AND
GRADES OF EXISTING HARDSTAND AREA
2-4" C
3" DWS
1-1/2" GAS
6" ICW
18" RCP
10" ICW
4" GAS
6" DWS
744.41
741.71
12" CMP
2-15" CMP'S
741.94
742.17
744.00
PIT
LIMITS OF NEW CA-6 HARDSTAND
SHALL EXTEND TO EXIST BERM
SUBCONTR. TO REGRADE EXIST. DITCH
TO CONTOURS SHOWN AND CLEAN OUT
INVERTS OF EXISTING CMP'S.
50 L.F. 6" PVC @ 7.00%
4" PVC
4" C.I.
6"X4"X4" Y TEE (SEE DWG. M-1)
4:1
5:1
3:1
745
744
746
747
748
749
750
755
760
761
WEST BOOSTER
LINAC

Figure 3

Accelerator Physics and Technology Applications of the Fermilab Linac Beams

Gerald P. Jackson
Fermi National Accelerator Laboratory
MS 341
P.O. Box 500
Batavia IL, 60510 USA

gpj@fnal.fnal.gov

Relativity and the Beam Energy

The specifications for the expected beam kinetic energy are:

Condition	Kinetic Energy
minimum	100 MeV
maximum	400 MeV

The total energy and kinetic energy T of a particle are related by the relationship

$$E_t = T + m_o c^2$$

The total energy of a particle is related to the momentum and its rest mass by the equation

$$E_t^2 = P^2 c^2 + \left(m_o c^2\right)^2$$

where m_o is the rest mass of the particle (proton = 938 MeV, electron = 0.511 MeV). Another way of stating the total energy of a particle is a unitless parameter, sometimes called the time dilation factor, which has the value

$$\gamma_r = \frac{E_t}{m_o c^2}$$

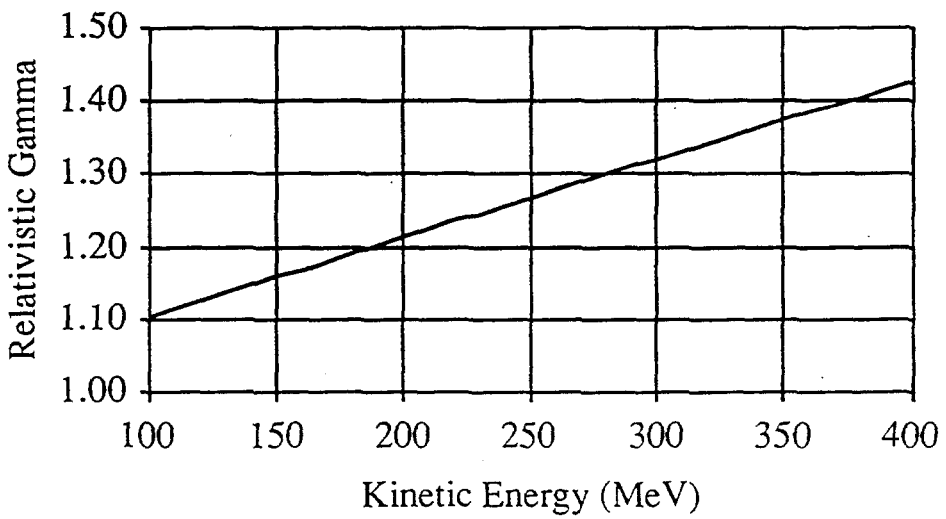

Beam Size vs Beam Energy

The specifications for the expected transverse beam emittance are:

Condition	Emittance
minimum	1π mmmr
maximum	7π mmmr

where the emittance ε_N is a 90% unnormalized value at 400 MeV. Assuming a transverse beta-function of 100 meters, the rms beam size can be calculated using the equation

$$\sigma_{x,y} = \sqrt{\beta_{x,y} \frac{\varepsilon_N[\pi\ 90\%\ \text{normalized}]}{6\,\beta_r\gamma_r}}$$

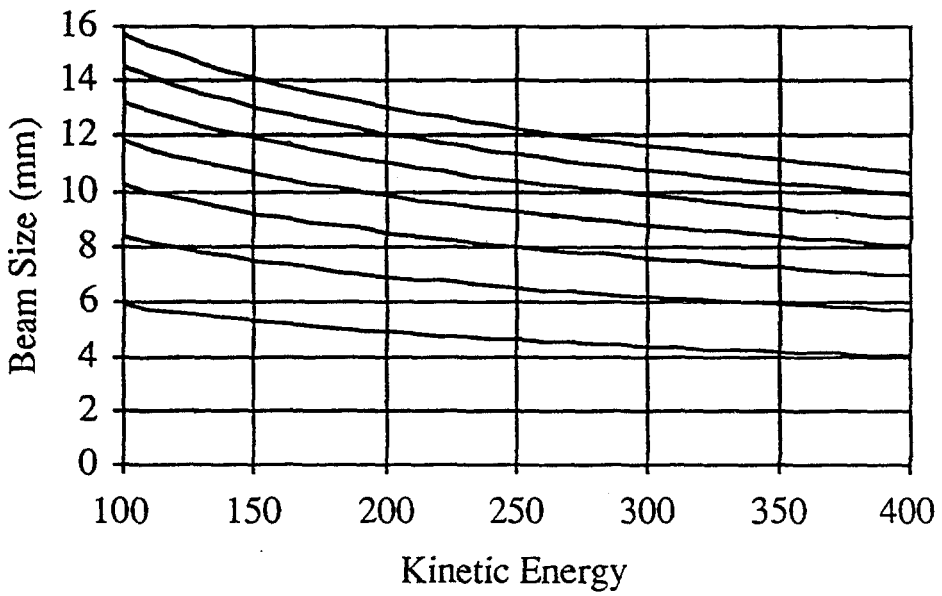

If the required beam pipe radius is 3 times the rms beam size, then the beam pipe and any fixed beam instrumentation must have a radius of 50 mm (2") in order to transmit any of the beam sizes pictured above.

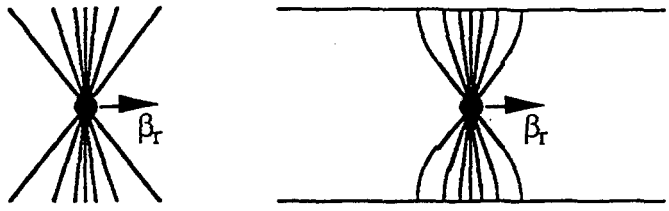

On the left is a sketch of the electric field density for a particle with a time dilation factor of γ_r=3 residing in a vacuum. On the right is the same fields, but for a particle inside a perfectly conducting, round beam pipe.

An equal but opposite image charge distribution flows along the inside pipe surface with the particle. The electric field lines flowing from the charge are terminated by this image current distribution which has an rms length described by the approximate relationship

$$\sigma_t \approx \frac{b}{c\beta_r\gamma_r}$$

for a particle traveling down the center of a round beam pipe of radius b.

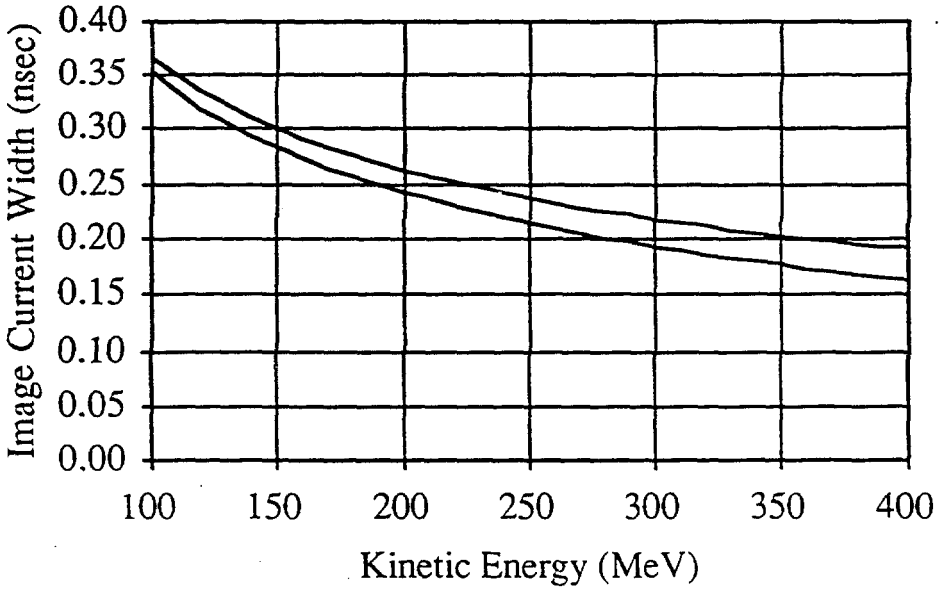

The upper curve is the expected distribution width of the image currents from a 0.1 nsec long bunch. The lower curve is the width from a single particle.

The shape of the frequency spectrum depends strongly on whether a *single* bunch or a train of bunches are being used.

In the case of a 400 MeV 0.1 nsec bunches (σ_t=0.16 nsec), the single and multibunch spectra are shown below.

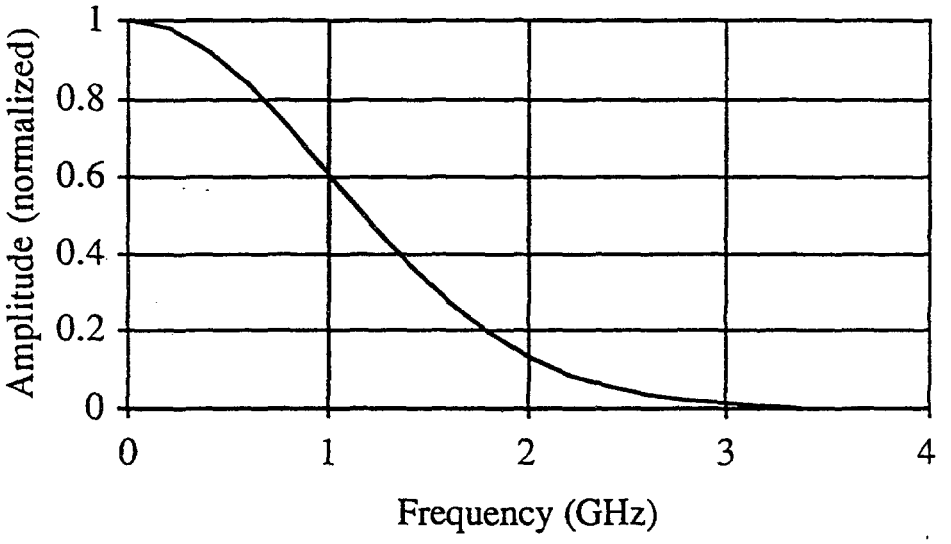

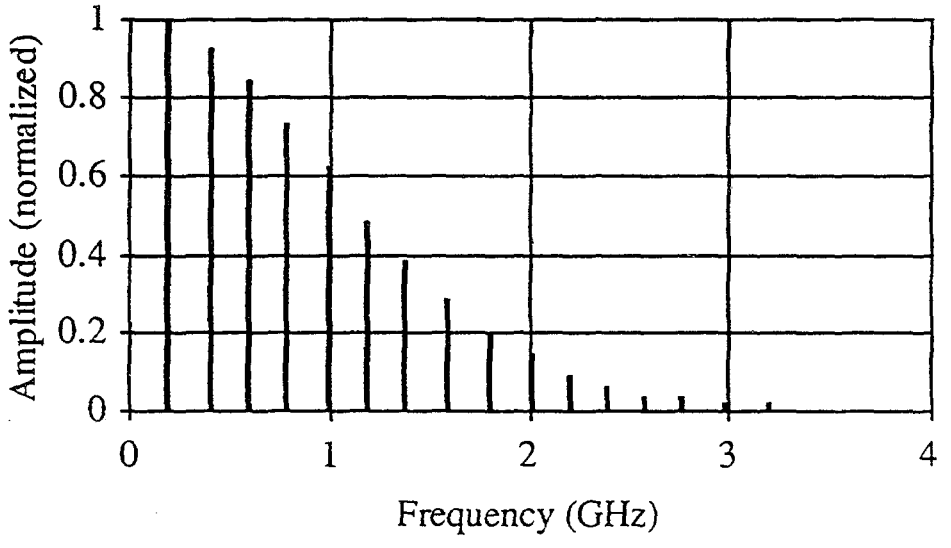

In the case of a train of bunches (lower plot), all of the spectral energy is concentrated into very narrow bands around harmonics of the bunch repetition frequency.

Electromagnetic Beam Detector R&D

When discussing the development of beam detectors, it is important to understand how the charge profile is measured electromagnetically.

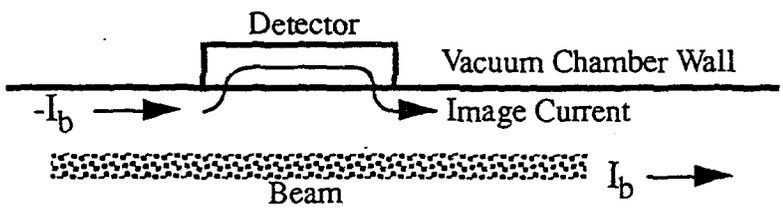

In general, the response of a beam detector can be analyzed using the equivalent circuit

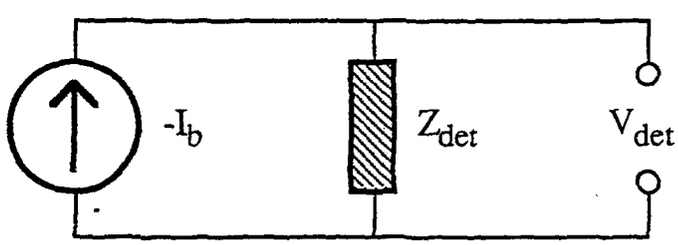

The voltage developed in the detector is proportional to the longitudinal charge density (i.e. current) with a spectrum which may look like the one below.

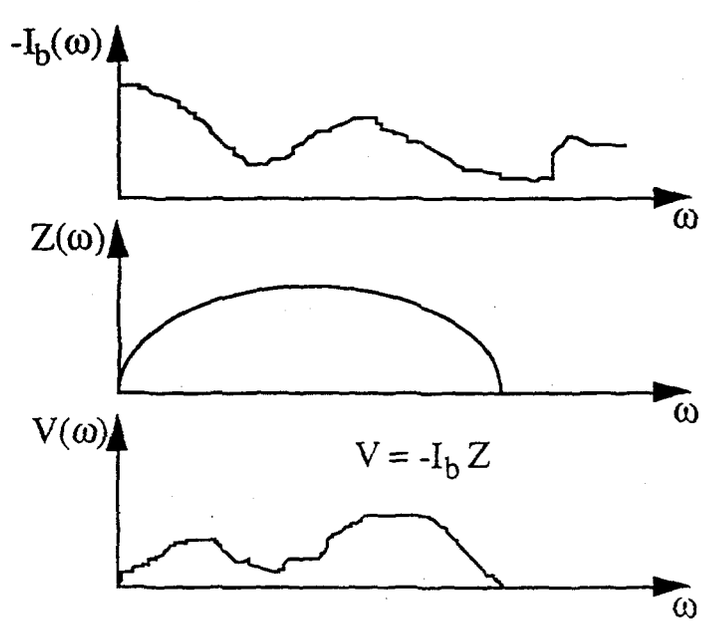

Some of the detector types which may be studied are beam position monitors (BPMs), current monitors (Torroids, resistive wall monitors), etc ...

Ion Dynamics Experiments

In the Fermilab Accumulator and a variety of light sources, ion formation, trapping, and beam-ion interaction dynamics are significant problems. In the Accumulator, Pat Colestock, Ping Zhou, and others have tried to perform measurements of the ion distribution. In light sources, gaps in the bunch distribution around the ring are used to defocus and eliminate the ions.

The 400 MeV H^- beam may be a perfect laboratory for measuring the transient response of ion formation and defocusing.

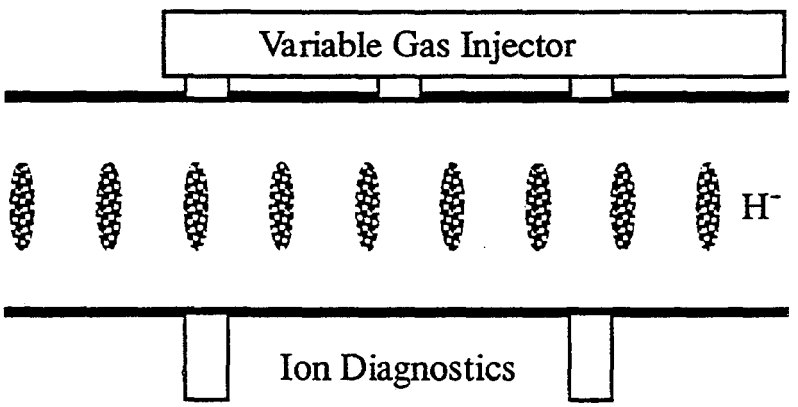

The spatial and momentum distribution of the ions can be measured as a function of gas type, gas density, and time within the pulse without compromising operation time on accelerators dedicated to their physics program.

Intercepting Beam Diagnostic R&D

There are a large number of types of intercepting beam detectors which are used in various beam transfer lines to measure the intensity, position, and size of the beam. Some of these detector types would be of tremendous value for measuring and tuning beam quality into and out of the Main Injector.

Having a readily accessible beamline for tests of these detectors would be tremendously useful.

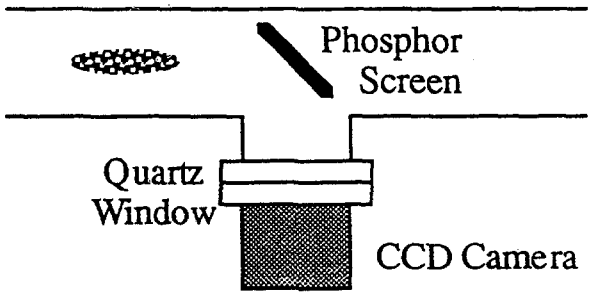

For instance, as shown in the above figure, phosphor type screens coupled with CCD cameras are now becoming quite popular again. The chemical coatings are now very advanced, with very high sensitivity and very high saturation characteristics. CCD cameras coupled with framegrabbers, video switchers, and laser spot analysis software provide cheap but powerful beam position and p0rofile information with very high fidelity.

Kicker R&D

The measurement of kicker waveforms is devilishly difficult. It would be very useful if one had a beam to act as a probe of the kicker waveform as a function of time. All that would be needed 90° of betatron phase downstream of the kicker is a fast beam position monitor.

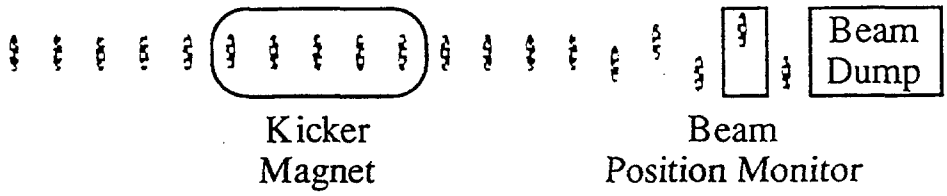

As shown in the figure above, the 400 MeV beam would be a sensitive monitor for kicker ripple. One could fire the main pulse before the beam arrived and then look at the remnant ripple with the beam after the pulse.

Advanced Acceleration Research

There is a great deal of interest in the invention of advanced methods of beam acceleration. In most cases beams with some initial kinetic energy are required. Even though most of these methods have been aimed at electron beams, proton beams are sometimes the more obvious particle to work with. For example, crystal acceleration where a crystal lattice is resonantly excited will only accelerate protons.

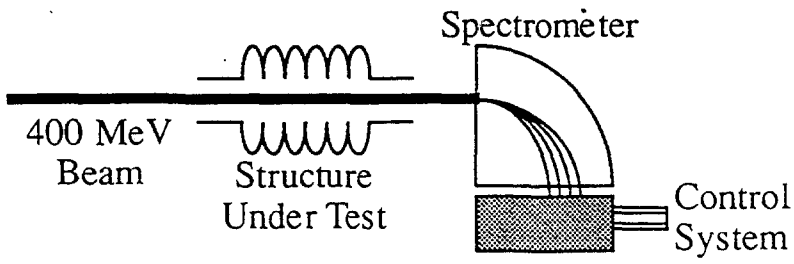

A 400 MeV Ion Beam Research Facility at Fermilab

M.B. Popovic, T.L. Owens and T. Bynum

22 February, 1994

1 Introduction

With completion of the Linac Upgrade, a rare opportunity exists to create a research facility which uses a portion of the high-energy ion beam produced by the new linac. A number of people have recently expressed an interest in a project of this type. The intent of this paper is to present a few of our own thoughts on the subject and stimulate more widespread discussion among diverse groups at Fermilab and elsewhere.

We propose a baseline facility that would divert only the portion of the ion beam which is normally sent to the straight-ahead beam dump during routine operations. The baseline program would not perturb the high-quality part of the pulse train that is gated out of the total Linac beam pulse and transferred to the Booster. The full ion beam pulse fron Linac could also be diverted to the new research facility during Booster and NTF dead times, as opportunities allow.

2 Beam Line

A convenient place to divert the beam for the new research facility would be the Linac enclosure access area at the high-energy end of the Linac enclosure. A diagrams of access area, showing its relation to the Linac and existing beam lines, are presented in figure 1 and 2.

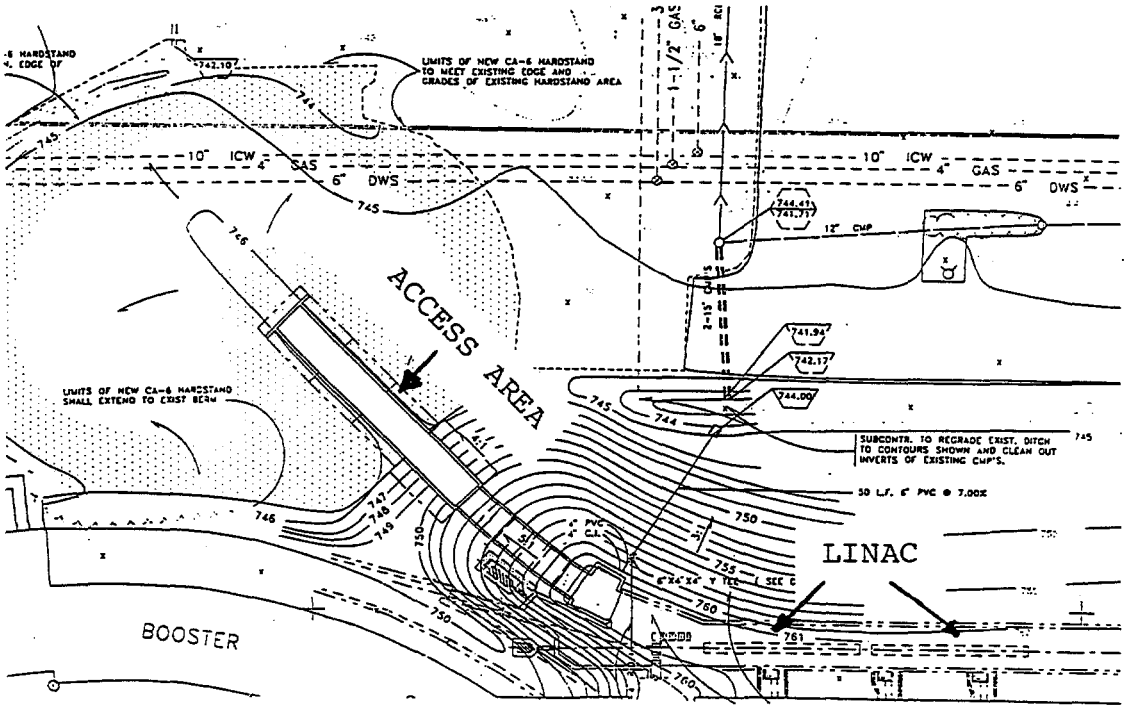

Figure 1.

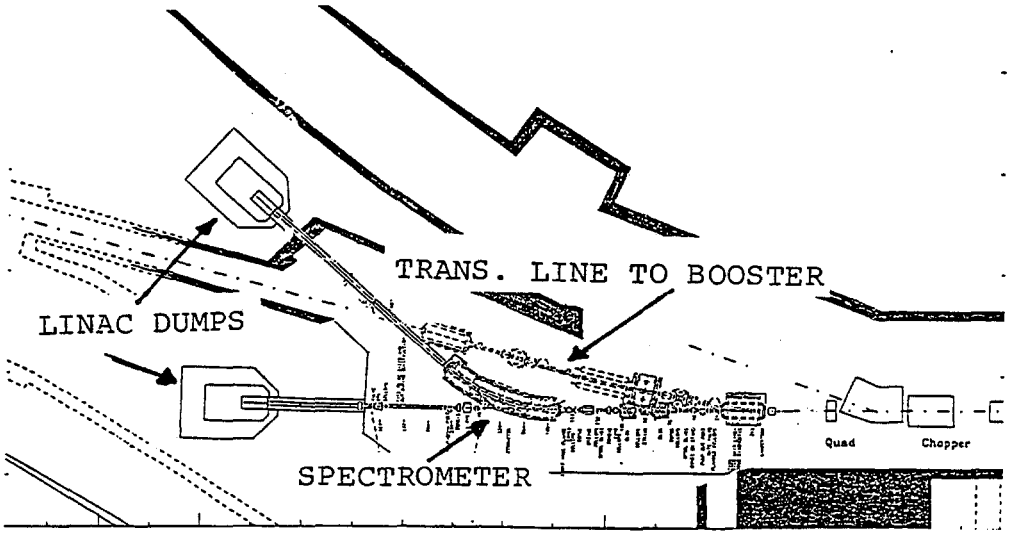

Figure 2.

The access area has been lined with concrete and is below ground level. The concrete lining provides a place to mount hardware and stage experi-

ments. Because the access area is below ground level, most of the radiation created by the beam can be shielded by the ground. Twelve meters of the access area is part of the linac encloser and is already shielded. The space above the open part of the access area would have to be shielded and/or a building would have to be erected to house the experimental area. The size and design of the experimental building will depend upon the types of experiments that will be conducted.

A relatively simple transfer line could be used to direct the beam to the access area. The principal elements of the transfer line would be a pair of dipole magnets and a series of the quadruplole and trim magnets arranged as shown in Figure 3.

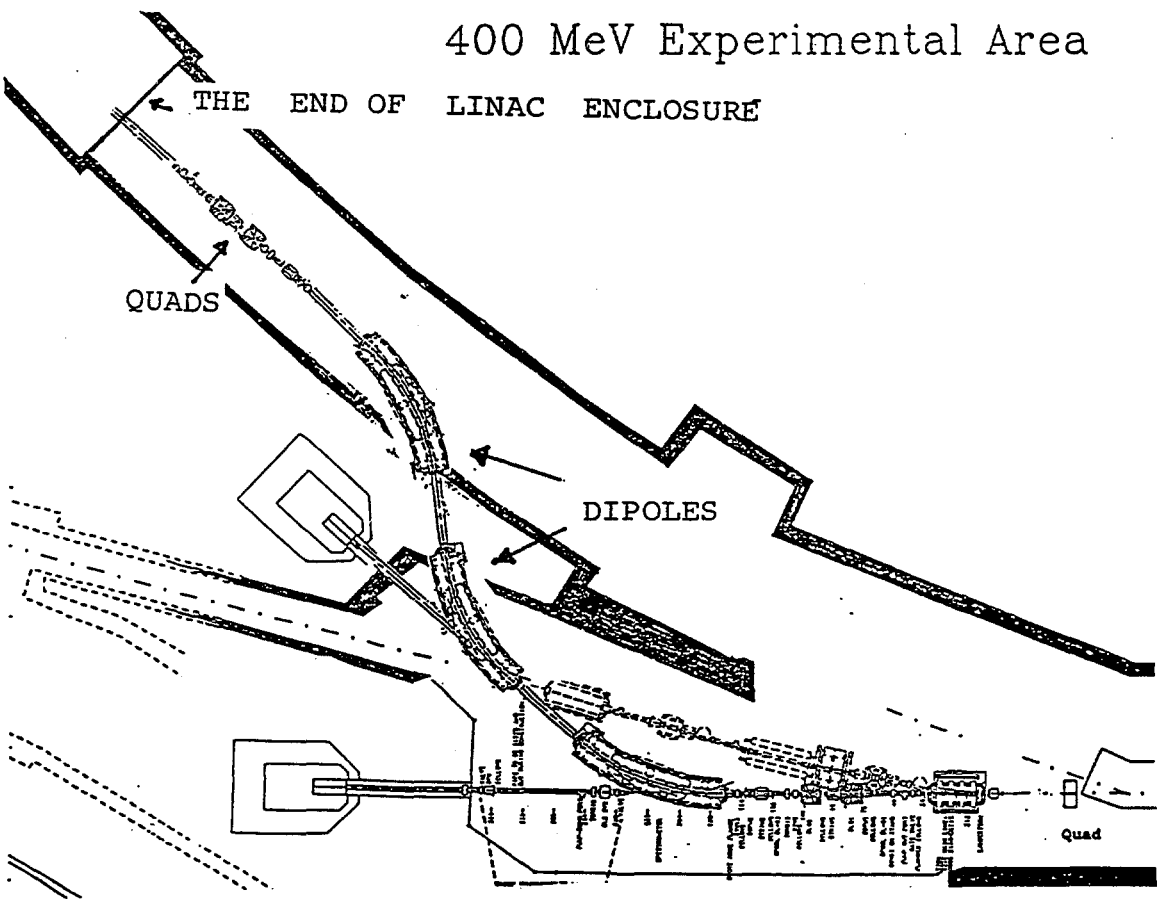

Figure 3.

The dipole magnets would be indentical to the spectrometer magnet that has already been fabricated for the Linac Upgrade. No engineering cost would be incurred for dipole magnets. Fabrication cost of the Linac Upgrade spectrometer was approximatly $60,000. The cost of the quadrupoles would be approximatly $11,000, if new quadrupoles are used. This estimate is based upon the cost of similar quadrupoles built for Upgrade. There are numerous spare quadrupoles that could also be used for this line, instead of purchasing new quadrupoles.

Initial engineering layouts indicate that the first downstream dipole magnet can bend the beam up to 42.5 degrees and the second dipole can bend the beam 37.5 degrees to impart the proper angular trajectory to direct the beam down the access hall. The spectrometer magnet was designed to bend a 400 MeV beam by 40 degrees and the design beam trajectory coincides with the curved axis ot the dipole. For the bending angles required to divert the beam into the access hall, the beam trajectories, in this extreme case, will have slightly different curvatures, but the trajectories will remain well inside the bore of the magnets.

A beam dump must be located outside of the experimental area of the access hall. It should be possible to locate it at the end of the access area where it can be left permanently without obstructing access to the linac enclosure. It is important that the dump be located in a place where it does not need to be moved because of the hazards of handling the dump as it becomes activated.

3 Conclusion

In summary, we believe that it will be possible to divert the linac beam to an experimental area in the linac enclosure access hall inexpensively, using transfer line components that have already been designed. The transfer line can be build downstream of the chopper. In this position, the unchopped portion of the beam can be diverted to an experimental area without disturbing the beam going to the booster. The impact on operations and demands upon the linac are minimal. In addition, in a position past the chopper, DC magnets can be used, which do not require complex pulse, timing, and control circuits. By diverting the beam to the access area, ample space is avaible for an experimental building.

LASER DIAGNOSTICS FOR H^- BEAM MOMENTUM AND MOMENTUM SPREAD

E.P. MacKerrow, S. Cohen, J.B. Donahue, D.R. Swenson.
Los Alamos National Laboratory, Mail Stop H840, Los Alamos, NM 87545

H.C. Bryant*
University of New Mexico, Dept. of Physics and Astronomy, 800 Yale NE, Albuquerque, NM 87131

ABSTRACT

Non-invasive laser diagnostics are capable of measuring p absolutely and $\delta p/p$ of high-energy H^- ion beams. A Q-switched Nd:YAG laser, operating at 0.266 μm, can excite narrow auto-ionizing resonances in the H^- ion. The measured width of the resonances is sensitive to $\delta p/p$ of the ion beam. Doppler tuning of the laser photon energy, by angle tuning, allows the absolute beam energy to be measured. The principle of these diagnostics was tested at LAMPF during a series of atomic physics experiments. It was found[1] that the absolute energy of the H^- beam could be measured to an accuracy of 10^{-4} and the momentum spread to an accuracy of 10^{-5}. The diagnostic was sensitive to dephasing of a single Rf module on the LAMPF linac. The applicability of this type of diagnostic for H^- beams of different phase space and energy than LAMPF will be presented.

INTRODUCTION

The negative hydrogen ion consists of a "core" hydrogen atom, which becomes polarized in the presence of a second electron, allowing that electron to be bound. This outer electron is bound only by 0.7542 eV, and there are no excited states below the continuum (i.e. there are no states with just one electron excited, known as *singly-excited* states[2]). The H^- photodetachment spectrum does however have structure at higher photon energies due to *doubly-excited* states. These doubly-excited states, also known as resonances[3], are all auto-detaching, with the exception of a predicted $^3P^e$ state, investigated by Drake[4]. The excitation energies of these doubly excited states lie between 10.2 eV and 14.35 eV above the ground state. Only $^1P^o$ states are accessible by single-photon absorption from the $^1S^e$ H^- ground state. Two very prominent resonances have been observed in the H^- photodetachment spectrum just below 11 eV. The lower energy resonance, at 10.9264 eV, can be thought of as a bound state formed by the attachment of an electron to the first excited state of hydrogen. It is known as a Feshbach[5] resonance. Its has a narrow width predicted to be only 30 μeV wide[6]. The higher energy state, known as the "shape resonance", lies at 10.9724 eV in energy[7] (just above the $H^0(n=2)$ threshold) and is much stronger and wider (21.2 ± 1.1 meV)[7] than the Feshbach resonance below it.

*Work supported by the U.S. Dept. of Energy, and the Div. of Chemical Sciences, Office of Basic Energy Sciences, Office of Energy Research.

Numerous experimental measurements[7] have been made on the H^- photodetachment spectrum at the Los Alamos Meson Physics Facility (LAMPF). At the High Resolution Atomic Beam Facility (HIRAB), located at LAMPF, laser beams are intersected with a H^- beam whose energy ranges from 100 MeV to 800 MeV. The relativistic Doppler shift is used to angle tune the laser photon energy in the laboratory frame into the H^- rest frame. Information on the H^- beam momentum and momentum spread can be found by measuring the location and width of H^- resonances.

RELATIVISTIC DOPPLER SHIFT

The laser photon energy, as seen in the H^- rest frame, is a function of the laser photon energy in the laboratory frame, E_L, and the relative velocity, $\vec{v} = c\beta$, between the two frames[8]

$$E'(E_L, \beta, \theta) = E_L \gamma (1 - \beta \cos\theta). \tag{1}$$

This relation can also be written in terms of the beam momentum as

$$E'(E_L, |\vec{p}|, \theta) = \frac{E_L}{E_0}\left\{\sqrt{p^2c^2 + E_0^{\,2}} - pc\cos\theta\right\}, \tag{2}$$

where E_0 is the H^- rest mass energy (939.294 MeV/c^2) and the intersection angle, θ, between the photon wavevector, $\vec{k}$, and the ion beam is defined as

$$\vec{k} \bullet \vec{\beta} = k\beta\cos\theta. \tag{3}$$

The doubly-excited resonances in the H^- ion appear in the vacuum-ultraviolet and cannot be excited by available lasers. The Doppler shift method allows ultraviolet lasers to be blue-shifted up to the vacuum-ultraviolet. By merely changing the intersection angle one can tune the laser photon energy seen in the ion's frame. The angle at which the Feshbach resonance will be found at different beam energies and laser wavelengths is shown in Figure 1.

The uncertainty in the variables E_L, p, or θ determines the resolution of the Doppler technique. The rms energy resolution can be found by expanding Eq. 2 in a Taylor series, to first order, about the central value of each of the three variables (neglecting any correlated errors between angle and momentum)

$$\delta E' = \left\{\left(\frac{(1-\beta\cos\theta)}{\beta}\right)^2\left(\frac{\delta E_L}{E_L}\right)^2 + (\sin\theta\delta\theta)^2 + (\beta - \cos\theta)^2\left(\frac{\delta p}{p}\right)^2\right\}^{1/2} \tag{4}$$

This relation is nothing more than the experimental resolution using the Doppler shift method. In the LAMPF experiments the resolution is typically 7 meV for a 800 MeV H^- beam ($\delta p/p = 5.0 \times 10^{-4}$ and $\delta\theta = 0.5$ mrad). The resolution function is shown in Figure 2.

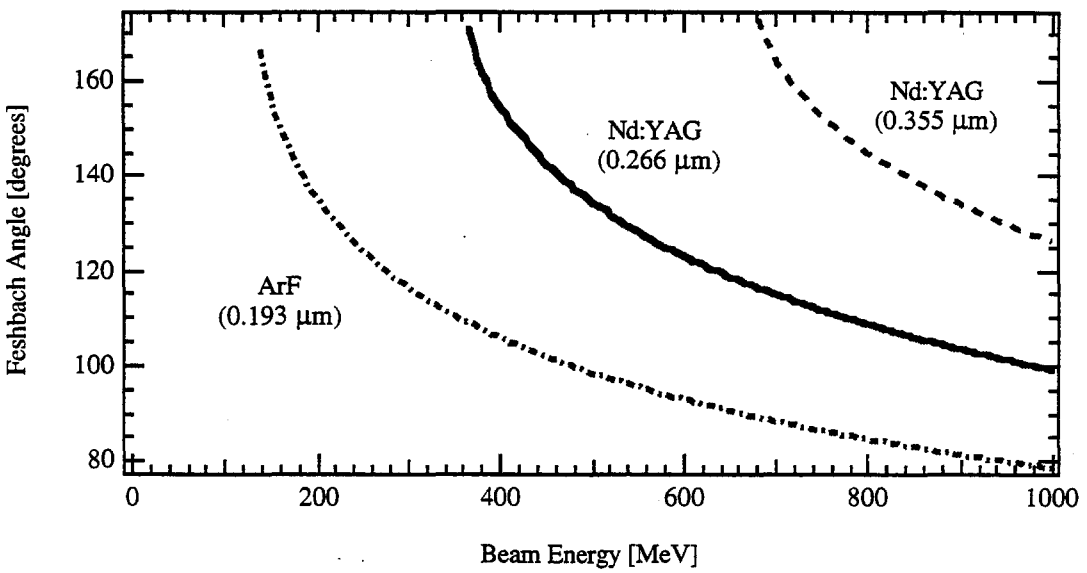

Figure 1. The angle of intersection needed to blue-shift fixed frequency lasers for excitation of the H^- Feshbach resonance (10.9264 eV). As the beam energy gets smaller, shorter wavelength lasers are needed to excite the doubly-excited resonances in the H^- ion.

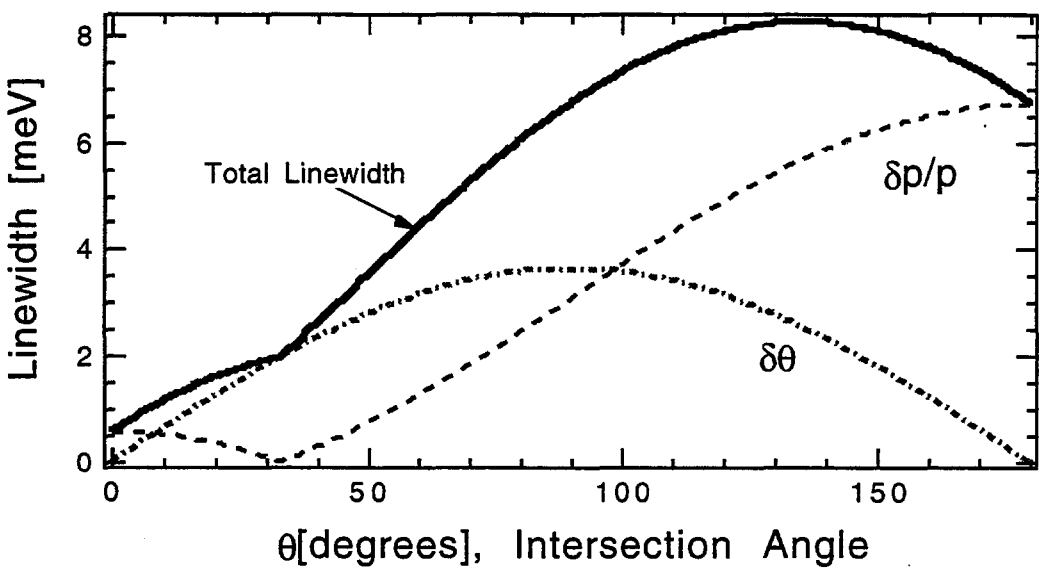

Figure 2. Resolution function for the Doppler shifted photon energy at 800 MeV. The above figure assumes a Nd:YAG 4th harmonic (λ=0.266 μm) laser beam with $\delta\lambda$=0.1 cm^{-1} and a divergence of $\delta\theta$=0.5 mrad. The H^- beam momentum spread was $\delta p/p$=0.05%. The Feshbach resonance is found at a angle of 108 degrees.

EXPERIMENTAL APPARATUS

The photodetachment of a doubly-excited state in H^- can be represented as

$$\hbar\omega + H^- \rightarrow H^{-**} \rightarrow H^0(n) + e^- . \tag{5}$$

Experimentally the photon energy is scanned, by changing the intersection angle, and the photodetached electron signal is recorded as a function of intersection angle. The signature of a photodetachment event is the detection of the free electron (in coincidence with the laser pulse) in a electron spectrometer. A schematic of the typical experimental setup is shown in Figure 3.

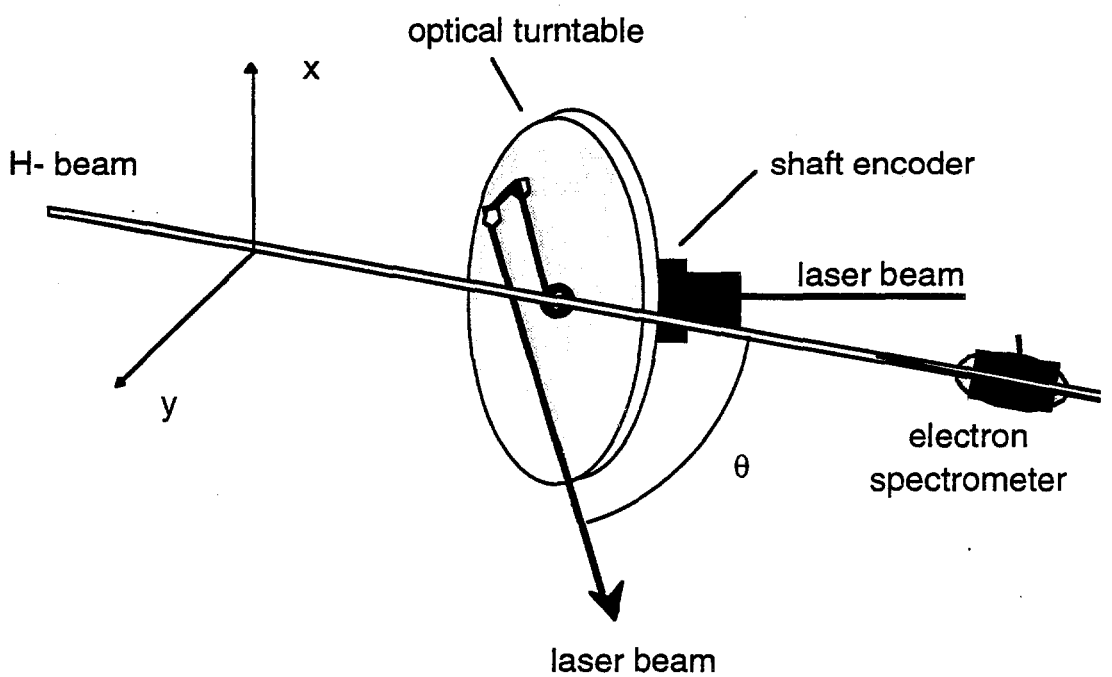

Figure 3. Schematic of the photodetachment apparatus used in the LAMPF experiments. The laser beam is directed onto the ion beam by a mirror system and the relative angle between the laser beam and ion beam is measured by a shaft encoder. The photodetached electrons are collected by the electron spectrometer and directed into a scintillation counter.

A Q-switched Nd:YAG laser operating at 0.266 μm is used to excite the doubly excited resonances. The laser has a repetition rate of 10 Hz and delivers of train of 5 ns (FWHM) laser pulses. Typical pulse energies are 50 mJ. At LAMPF the beam structure consists of 250 ps long micropulses separated by 5 ns and gated into macropulses varying from 100 ns to 750 μs long. The firing of the laser flashlamps is delayed relative to a precursor signal for the macropulse. The laser Q-switch trigger is delayed relative to the lamp firing and synchronized with a micropulse signal, which can be derived from any beam pick-off device, such as a beam position monitor. The electron signal is averaged over many laser shots to account for time jitter. The typical time jitter of the laser pulse is 0.10 ns rms.

The electron spectrometer[9] bends the photodetached electrons out of the beam and into a scintillation detector. The spectrometer is a sector magnet with a trajectory curvature of 20 cm and a path length of 34 cm through a field of 135 gauss.

The intersection angle between the laser beam and the ion beam is measured using a 14 bit shaft encoder. The encoder is coupled to a turntable-mirror system that delivers the laser beam onto the ion beam. A schematic view of the turntable is shown in Figure 4.

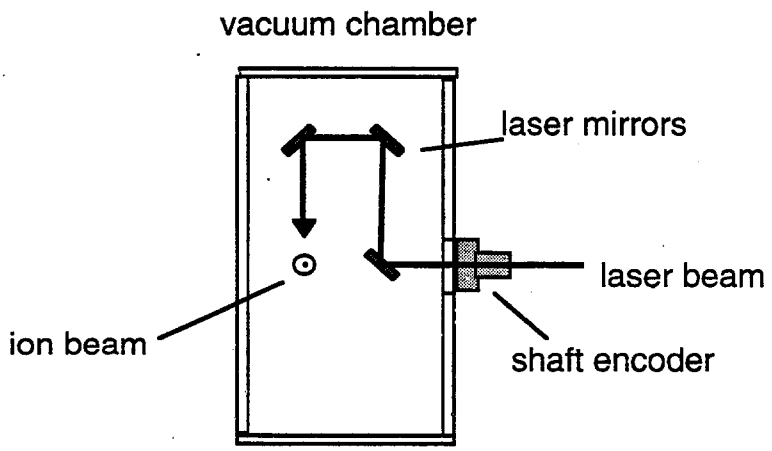

Figure 4. Laser interaction chamber. The H^- beam is coming out of the page in this picture. The laser beam enters through a vacuum window (AR coated) and is then folded by a three 45 degree mirrors. The turntable rotates about the laser beam axis.

For good statistics the intersection angle is held fixed for a certain integrated beam current, from a Faraday cup, and then stepped with a stepper motor to the next angle. Usually 100 laser shots are taken per angle.

MEASUREMENT OF THE CENTRAL BEAM MOMENTUM

Using a known laser wavelength to excite a known H^- resonance, one can find the beam momentum by measuring the Doppler angle where the resonance takes place. In this case there are two unknowns in Eq. 2; the "encoder zero" and the beam momentum. The encoder zero, N_0, is the encoder reading when the laser beam is parallel to the ion beam. It is needed to give an absolute angle measurement. The intersection angle, θ, is given by

$$\theta = \frac{N - N_0}{K}, \tag{6}$$

where K is the number of encoder counts per degree. For the 14 bit encoder $K = 45.5$ counts per degree (0.38 mrad per count).

To determine the two parameters, N_0 and p, at least two measurements must be made. Many different methods are available to complete these measurements. Usually the Feshbach resonance is measured on both sides of the ion beam; Eq. 2 is then fit to the two data points to determine N_0 and p. This method requires that the mirror system pass through the ion beam. Another less invasive method is to use two different laser wavelengths from the Nd:YAG laser (0.355 μm and 0.266 μm) and measure the resonance angle for each wavelength staying on one side of the ion beam only. This method requires optics specially coated for two wavelengths.

Measuring the position of more than one spectroscopic feature, such as the shape and Feshbach resonances, without letting the mirror system cross the ion beam, is another method that can be used for determining the two unknown parameters.

If a thin foil can be temporally inserted into the beam, then things are much easier. The foil interaction will populate many different hydrogenic states. The laser can then be used to promote hydrogenic transitions to states above $H^0(n=11)$, where there are easily field ionized in the electron spectrometer. This allows many angles to be measured for a better curve fit for N_0 and p. This method has been used at LAMPF where the beam energy was measured to be 797.26 ± 0.12 MeV[10] (β = 0.84109 ± 0.00012).

MEASUREMENT OF THE BEAM MOMENTUM SPREAD

Since the Feshbach resonance has a narrow spectral width, the measured width will be the experimental resolution and therefore the momentum spread.. The dependence of the experimental resolution on $\delta p/p$ is seen in Figure 2.

The H^- photodetachment spectrum has been measured at 800 MeV and parameterized[11]. The parameterization of the shape and Feshbach resonances, at different momentum spreads, is shown in Figures 5a-5b for an 800 MeV H^- beam and a 400 MeV H^- beam.

As can be seen from Figure 5 the momentum spread of the beam can be monitored by measuring the width of a resonance using the Doppler shift technique. Note that if the momentum spread is too large the Feshbach resonance will be washed out. At this point the width of the shape resonance starts to broaden with increased momentum spread and can then be used to monitor the momentum spread of the beam.

The LAMPF group has used the Feshbach resonance to monitor changes in the momentum spread resulting from detuning of a single Rf module on the LINAC[11].

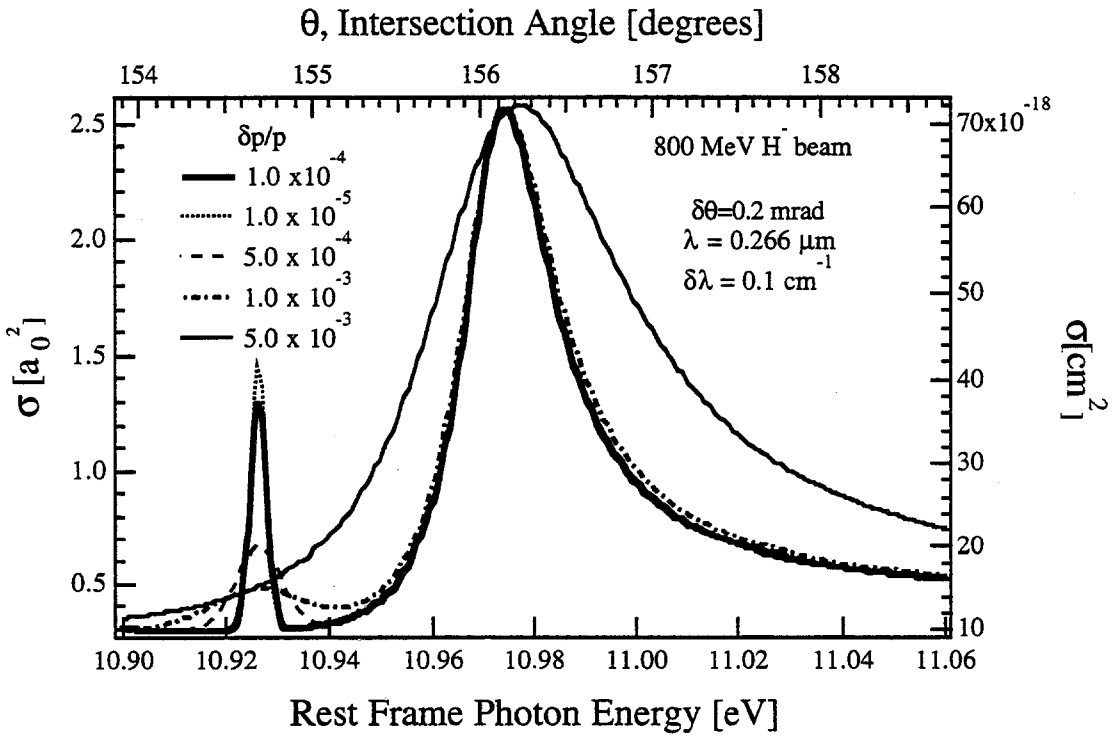

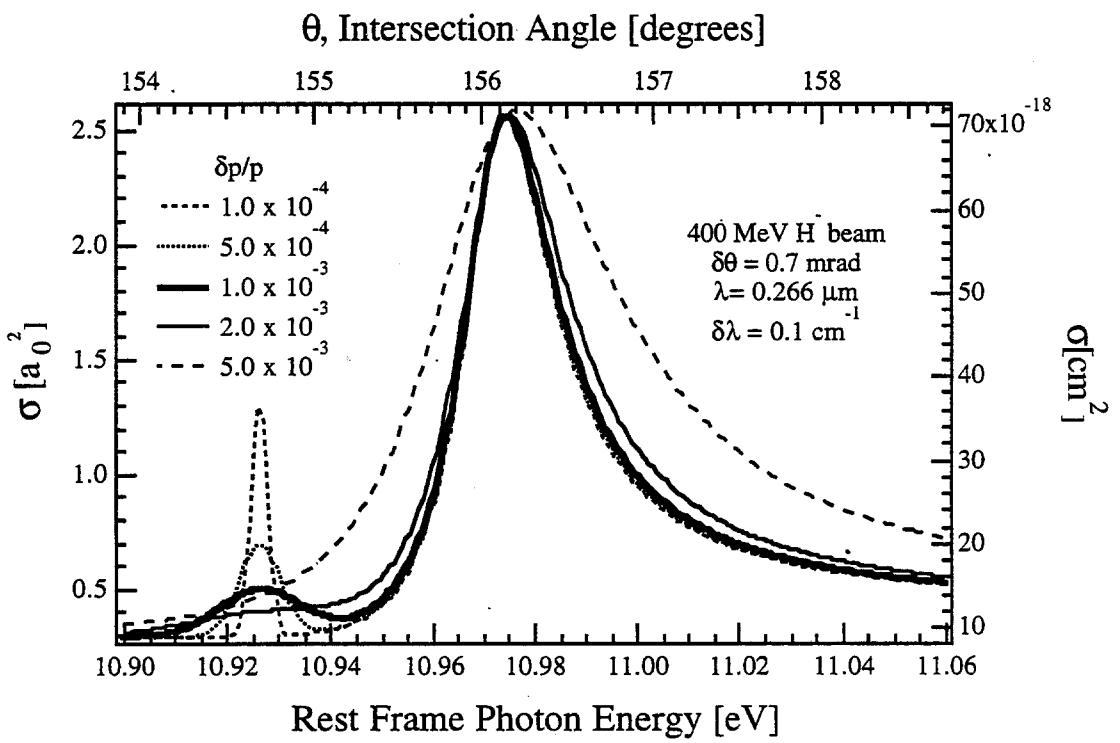

Figure 5. The H^- photodetachment spectrum at (a) 800 MeV and (b) at 400 MeV. Note that the Feshbach resonance is spread out into the continuum for $\delta p/p>0.1\%$. The shape resonance is sensitive to momentum spread for $\delta p/p>0.1\%$.

A similar method of monitoring the Feshbach resonance as a momentum spread diagnostic has been presented by Holtkamp and Quick[12]. They proposed sending a tunable laser beam onto the H^- beam in a head on fashion (θ=180 °) and detecting H^0 atoms resulting from the decay of the Feshbach resonance. Working at θ=180° is advantageous since the linewidth of the Feshbach resonance is most sensitive to $\delta p/p$ at this angle. However, this technique requires special beam line geometry, is extremely sensitive to any movement of the beam, and may have a high H^0 background due to gas stripping. The method also requires tuning, and measuring, the laser wavelength continuously.

CONCLUSION

We have discussed the use of the H^- photodetachment spectrum for a beam momentum diagnostic. The range of applicability of this technique has been discussed along with some of the expected problems in determining the absolute intersection angle.

The H^- spectroscopy experiments at LAMPF have shown that the Doppler tuning method is capable of measuring the momentum and momentum spread of a 800 MeV H^- beam (see Figure 6).

This method looks hopeful for developing diagnostics for other H^- accelerators. The Feshbach resonance is washed out for beams with $\delta p/p > 0.10$ % and would not be a useful measure for beams with this momentum spread. For beams of this momentum spread the width of the shape resonance could be monitored as a momentum diagnostic.

Development is being carried out at Los Alamos National Laboratory to try and improve these techniques so that an automated diagnostic system can be realized. The problem of having to measure spectroscopic features on both sides of the ion beam, to find the angle between the ion beam and laser beam, is being studied and several designs now exist that need testing.

REFERENCES

[1] D.W. MacArthur et al., Phys. Rev. A 32, 1921 (1985), Phys. Rev. Lett. **56,** 282 (1986).

[2] R.N. Hill, Phys. Rev. Lett. 38, 643 (1977); J. Math. Phys. 18, 2316 (1977).

[3] G. J. Schulz, Rev. Mod. Phys. 45, 378 (1973).

[4] G. W. Drake, Phys. Rev. Lett. 24, 126 (1970).

[5] H. Feshbach, Ann. Phys. ((N.Y.) 5, 357 (1958); 19, 287 (1962).

[6] J.T. Broad and W. P. Reinhardt, Phys. Rev. A 14, 2159-2173 (1976). See also L. Lipsky and M.J. Connely, Phys. Rev. A 14, 2193 (1976).

[7] H.C. Bryant et al., Phys. Rev. A 27, 2889 (1983).

[8] J.D. Jackson, Classical Electrodynamics, 2nd ed. John Wiley & Sons, New York, (1975), p. 522.

[9] J.E. Stewart, Los Alamos National Laboratory Thesis, LA-11152-T (1987).

[10] A.H. Mohagheghi, Los Alamos National Laboratory Thesis, LA-11925-T (1990).

[11] P.G. Harris, H.C. Bryant, A.H. Mohagheghi, R.A. Reeder, C.Y. Tang, J.B. Donahue, C.R. Quick, D.C. Rislove, H. Sharifian, H.Tootoonchi, T.C. Altman, Nucl. Instr. and Meth. A292 (1990) 254-258.

[12] D.B. Holtkamp and C.R. Quick, Nucl. Instr. and Meth. A287 (1990) 348-352.

Health Physics Applications for a 400 MeV Proton Beamline

David Boehnlein

October 26, 1993

Introduction

The field of accelerator health physics is one in which a great deal of research remains to be done. The radiation fields which are present at accelerator facilities differ greatly in their nature and their energies from those of nuclear facilities, where most of the health physics work is done. Research in a variety of areas, from dosimetry to development of instrumentation, is typically performed using radiation from encapsulated radioactive materials or from nuclear reactors. The results found in such radiation fields do not necessarily reflect those that would be found in the fields produced by an accelerator used for research in high energy physics.

The Radiation Physics Group at Fermilab, as at most other high energy physics facilities, is primarily a support group. Their foremost task is to ensure radiological safety for the workers at the facility and for the public. A thorough understanding of accelerator health physics is often taken for granted by other experimenters. Therefore, when the health physicists talk of using an experimental resource such as the proposed 400 MeV beamline, some might wonder if they are not a bit like a dog chasing a car: After all, what would he do with the thing if he actually got it? This talk is intended to address that question. It will encompass work in several areas which describes the lines along which future research may be done.

The potential applications of a proton beamline to health physics research include work in dosimetry, materials activation, shielding studies, software benchmarking and development of instrumentation.

Dosimetry Applications

High Energy Neutron Dosimetry This is the area of dosimetry in which further work is needed most. It might surprise many high energy physicists, who are used to dealing with energies of hundreds of GeV, to learn that in the context of neutron dosimetry, 20 MeV is "high energy." The radiation sources which are used in the development and testing of dosimetric devices do not produce energies much higher than this. Indeed, the Department Of Energy Laboratory Accreditation Program (DOELAP) only specifies performance criteria in the energy range from 1 keV to 2 MeV, using spectra from moderated and unmoderated ^{252}Cf, even though many DOE facilities produce neutrons of substantially higher energies.

A set of studies have been performed at Fermilab[1] using a standard multisphere ("Bonner sphere") technique[2] which illustrates this problem with measured accelerator neutron spectra. Polyethelene spheres of seven different sizes were used to moderate neutrons in radiation fields at various locations around Fermilab. The neutron spectra were studied by placing a detector at the center of each sphere as well as using a bare detector to measure the unmoderated neutron field. The detectors used were either a LiI(Eu) "phoswich" scintillator, using a fast pulse to distinguish muons from

neutrons, or a LiF thermoluminescent dosimeter (TLD). Both of these are sensitive to thermal neutrons which are detected through a capture reaction. By varying the size of the moderator, a different portion of the energy spectrum is observed with each successive sphere. Measurements were made at 14 sites outside of shielding at Fermilab. Although the neutron spectrum may vary considerably from one place to another at Fermilab, the overall results are shown in Table 1.

Table 1. Neutrons at Fermilab

Neutron Energy	% of Fluence	% of Dose Equivalent
< 0.1 MeV	77	23
> 0.1 MeV	23	77
> 2 MeV	13	50

Table 1 shows that although neutrons of energy greater than 2 MeV comprise only 13% of the neutron fluence, they are responsible for 50% of the dose equivalent due to neutrons because of the higher quality factor of high energy neutrons. Clearly, the need for accurate high energy neutron dosimetry exists.

In November of 1992, the U. S. Department of Energy sponsored a workshop in Gaithersburg, MD to address the problems in the current state of high energy neutron dosimetry. The above results and others were presented there. Some of the conclusions reached at the workshop included:[3]

- Neutron dosimetry at energies above 2 MeV are imprecise and inaccurate. Since the uncertainty in measurements is often on the order of 300%, neutron dosimeters are little more than neutron indicators in high energy neutron fields.

- Better dosimeters and area monitors are needed, especially at high energy research facilities.

- The response of dosimeters as a function of energy is poorly known.

- There are no calibration standards for high energy neutron detectors.

- There is no serious research and development effort underway at this time to improve the state of high energy neutron dosimetry.

One of the recommendations to come out of this workshop was for a committed and available neutron source for the near- and long-term improvement of high energy neutron dosimetry. The WNR facility at Los Alamos was suggested as a candidate for such a source, however, the prospects for a committed neutron source at WNR or elsewhere look bleak as of this writing due to severe funding problems. Although a 400 MeV beamline at Fermilab could not be committed solely to dosimetric research, it could be used to at least partially address some of the concerns cited above.

Muon Dosimetry

A muon source with energies of 100-300 MeV is also under consideration. Should such a source become available, there are potential health physics applications for it as well.

Some studies in muon dosimetry have been conducted at CERN. Calculations of dose and dose equivalent due to muons of energies up to 1000 GeV have been compiled by Stevenson.[4] These studies indicated that the rate of energy loss of muons of energy < 1 GeV changes considerably as the muons pass through tissue. This is due to a "ranging out" effect at low energies. A study of the variability of the energy loss (dose) in phantoms would be interesting from the standpoint of health physics. Furthermore, according to Stevenson, "although the energy deposition along the track of a muon can be calculated with some certainty, its conversion into dose equivalent depends on a number of philosophical considerations." Such considerations seem to merit further study as well.

In addition to calculations, some dosimeter intercomparisons were performed at CERN.[5] A variety of detectors and muon telescopes were placed in protected areas where high energy muons were virtually the only source of radiation. The dosimeter readings were compared to each other and to calculated values. Similar studies could be performed with a low energy muon source such as the one under consideration.

The response of personal dosimeters to a mixed field of neutrons and muons has been studied at Fermilab.[6] The neutron spectrum was measured using the Bonner Sphere technique described in the previous section. A recombination chamber was used to measure the overall quality factor of the field, but a quality factor of 1 was assumed for the muons based on ref. 4. The results of the field characterization are shown in Table 2.

Table 2. Results of muon and neutron measurements using plastic scintillators and multisphere technique normalized to 10^{12} protons on target. Data are taken from ref. 6.

Particle Type	Neutrons	Muons
Fluence ($m^{-2}x10^7$)	9.12 ± 0.38	5.62
% Fluence	62	38
Absorbed Dose (mGy)	0.19 ± 0.06	2.25
% Absorbed Dose	8 ± 3	92
Dose Equivalent (mSv)	1.16 ± 0.31	2.25
% Dose Equivalent	34 ± 26	66
Quality Factor	6.24 ± 0.18	1

Roughly 2/3 of the dose equivalent in the fields studied were due to muons. The personal dosimeters used in this study were film badges and pocket ion chambers. Film is no longer used for dosimetry at Fermilab. Given the clear need for muon dosimetry at Fermilab, it would be of interest to conduct studies involving TLDs, bubble dosimeters and electronic dosimeters as well.

Dosimetry Intercomparisons

Radiation dosimetry intercomparison studies are an important method for determining the state of the art. They provide indications of how various types of dosimetry perform under defined conditions. Regular intercomparison studies have been conducted at Oak Ridge National Laboratory for a number of years.[7] Personnel Dosimetry Intercomparison Studies (PDIS) 1-12 were performed using the Health Physics Research Reactor at Oak Ridge. These studies, however, would not necessarily indicate how personnel dosimeters might respond in the radiation environments at an accelerator. Accelerators of energies up to 15 MeV were used for PDIS 13-16. The doses administered in the accelerator studies ranged from 0.6 to 10 mSv. The conclusion reached in ref. 7 on the basis of these studies is that, under ideal conditions, 51% of the measurements of neutron dose equivalent from accelerators were within 50% of the reference value. This is compared with 60% of measurements within 50% of the reference for the HPRR studies. These results make clear one reason why there is no DOELAP requirement for high energy neutron dosimetry: There are no dosimeters currently in service which could consistently meet such a requirement.

Fermilab is currently taking part in another intercomparison study which is being conducted at Battelle Pacific Northwest Laboratory. Dosimeters were irradiated with neutrons produced from protons incident on a Be target at 28 and 50 MeV. The final results of this study are not available as of this writing. No studies at higher energies are contemplated at this time.

Beam-On Exposure

The worst-case accident at an accelerator facility such as Fermilab is the direct exposure of personnel to the beam or beam spray. However, estimates of the dose involved in such an incident are based largely on guesswork. An experiment of interest would be to study the dose deposition in a phantom. The phantom could be layered and TLDs or activation foils could be implanted within it. An available beamline would make it possible to study the dose dependence on the radiation field composition, energy and geometry. An experiment of related interest would be to study the activation of tissue-equivalent material. Current procedures for dose assessment following a beam-on exposure call for the measurement of radioactivity induced in the exposed individual. The accuracy of this process might be improved with such data.

Materials Activation

When the particle beams at Fermilab interact with matter, they induce radioactivity in it. Most of the dose accumulated at Fermilab is due to employees working with or around activated materials. Radioactivation of matter provides a potential pathway for radioactivity to enter the environment. Furthermore, if radioactive material is to be disposed of as waste, state and federal regulations require that it be characterized as to its content of radionuclides. Studies of material activation are thus of interest from the standpoint of radiation safety, environmental regulation and waste disposal.

Isotopic Content

Some studies have been conducted at Fermilab to examine the isotopic content of a variety of activated materials.[8] In these studies, activated items were collected from a temporary storage area on site. Their γ-ray spectrum was then analyzed using a high purity germanium detector and multi-channel analyzer. These studies gave a rough indication of the types and relative amounts of radionuclides to be found in a random sampling of materials activated by particle beams at Fermilab. However, these studies were not comprehensive and not well-controlled, since the history of the activated items was not entirely known. Since many activated materials contain several radioisotopes with various half-lives, the relative abundance of the isotopes is a function of the time elapsed since irradiation. A comprehensive study of the relative abundance of accelerator-induced isotopes should include measured doses of radiation at a known energy for a known irradiation time. The time between irradiation and characterization should also be known. An available beamline would make such studies possible.

The data from such studies would be useful in characterizing low level radioactive waste. Current methods of characterization involve considerable approximation.[9]

Environmental Studies

Two sources of environmental concern at a high energy accelerator are the activation of soil and the activation of ground water. Soil and water samples could be exposed to measured doses under well-controlled conditions and the subsequent activity measured. This would remove much of the uncertainty from estimations of soil and water activation and provide confirmatory measurements for calculations.

Radiation Damage Studies

Studies of radiation damage to materials and equipment could also be conducted with an available beamline. The effect of radiation on materials, such as scintillators, could be measured as a function of dose. Studies are currently carried out by the CDF experiment at Fermilab to determine the degradation of its silicon vertex detector due to radiation damage. The dose is measured using TLDs. It is highly unlikely that a major experiment like CDF would invest the time and take the risks necessary to develop a complete understanding of the radiation damage mechanisms and correlation with absorbed dose. The ability to perform such studies under conditions with better experimental controls could enhance the choice of materials for detectors for high energy physics experiments.

Shielding Studies

Another area of health physics which could be studied is shielding. Shielding assessments at Fermilab are conducted by computer modelling combined with the measurement of dose rates outside of existing shielding. Controlled studies of shielding effectiveness for a well-determined radiation field are rare. Experiments could be devised to expose shields of various types to such fields. Dose rates could be measured in front of and behind the shield to determine the effectiveness of different materials or geometries.

A diagram of a conceptual setup to measure the shape of radiation cone from a beam incident on a shield is shown in Figure 2. A shield is subdivided into slabs which can be interspersed with detectors to measure dose rates at points within the shield. Alternatively, slabs could be analyzed for induced radioactivity as an indication of "star density." This term, carried over from Monte Carlo simulations, indicates the number of nuclear interactions per unit volume.

Software Benchmarking

Radiation shielding is typically designed using Monte Carlo computer programs, such as CASIM, FLUKA, or HETC. Such programs are generally used to simulate high energy particles and have a low energy cutoff around 50 MeV.

Some of these codes have been modified to follow particles to thermal energies through the inclusion of cross section libraries. FLUKA, for example, has been so modified,[10] and the LAHET program has been developed at Los Alamos. The benchmarking study for LAHET[11] is a good example of the type of work that could be done. Such work would be especially important in incorporating improved production models into these programs, since it would be crucial to compare the predictions of such models with controlled experiments.

Instrumentation

Radiation detection instruments in common use at high energy accelerators, for example the Chipmunk ion chambers used at Brookhaven and Fermilab, are not calibrated in high energy radiation fields. Calibration is performed with radioactive sources such as AmBe or PuBe. Consequently, the response of these instruments is not well known for neutron energies above a few MeV. Measurements of the neutron response of the Chipmunks have been performed by Krueger.[12] Figure 3, taken from Krueger, shows neutron response curves of the Chipmunk as a function of average neutron energy. In each of the three curves shown, the γ response has been subtracted using the method indicated. The γ-ray detectors used were an Al-Ar ion chamber and a Geiger-Muller counter. The GM counter was used both with and without a Pb shield over the sources. The responses are normalized to that from ^{60}Co. The main point to be taken from this figure here is that the measurements do not extend to average energies above a few MeV. Since these instruments are used in areas where neutron energies are likely to be considerably higher, it would be of interest to have measurements of their response at higher energies.

Conclusion

This paper has attempted to cover a very broad range of possible projects which could be carried out if a beamline, such as the proposed 400 MeV proton beamline at Fermilab, were available for health physics studies. Areas for study include dosimetry, activation of materials for waste characterization and environmental studies, studies for shielding design and benchmarking of shielding software, and instrument response studies. This list is not comprehensive, but is simply intended to provide examples of areas of accelerator health physics where further research is needed. Brief summaries of some previous work in each of these areas has been presented to illustrate the extent and limitations of present knowledge and to provide a foundation for future work. The author is indebted to Don Cossairt, Vernon

Cupps, Alex Elwyn, Kathy Graden, Fred Krueger and Kamran Vaziri for their suggestions and helpful discussions in the preparation of this paper.

References

[1] J. D. Cossairt, A. J. Elwyn, W. S. Freeman, W. C. Salsbury, and P. M. Yurista, *Measurements of Neutrons in Enclosures and Outside of Shielding at the TEVATRON*, Fermilab-Conf-88/106, published in Proceedings of the 22nd Midyear Topical Meeting of the Health Physics Society, San Antonio, TX, Dec. 4-8, 1988.

[2] R. L. Bramblett, R. I. Ewing, and T. W. Bonner, *A New Type of Neutron Spectrometer*, Nucl. Instr. and Meth. 9, pp. 1-12, 1960.

[3] K. R. Alvar and A. Gavron, *Report on High Energy Neutron Dosimetry Workshop; November 19, 1992 at Gaithersburg, MD*, Los Alamos National Laboratory publication LA-UR 93-747.

[4] G. R. Stevenson, *Dose and Dose Equivalent From Muons*, CERN TIS Divisional Report TIS-RP/099, March 1, 1983.

[5] M. Höfert, *Dosemeter Response to Muons*, CERN report TIS-RP/197/PP, September 7, 1987.

[6] J. D. Cossairt and A. J. Elwyn, "Personal Dosimetry In A Mixed Field Of High-Energy Muons And Neutrons," *Health Physics*, 52, 813, June, 1987.

[7] C. S. Sims and W.H. Casson, *Overview of Neutron Radiation Dosimetry*, course notes, Oct. 27-29, 1992, Oak Ridge, TN.

[8] K. Vaziri, V. Cupps and A. Elwyn, *Isotopic Analysis Of Accelerator Induced Radioactivity In Material*, Fermilab Radiation Physics Note 98, September 1992.

[9] G. Bonano, *A Method For Estimating The Activity Of Packaged Accelerator-Induced Low-Level Radioactive Waste*, Master's Thesis, Northwestern University, May 1993.

[10] J. M. Zazula, *Implementation of a Low Energy Neutron Transport Module into a Monte Carlo Hadronic Shower Code and Its Applications for Accelerator Shielding Problems*, DESY Internal Report D3-69, 1990.

[11] R. E. Prael, *LAHET Benchmark Calculations of Differential Neutron Production Cross Sections for 113 MeV and 256 MeV Protons*, Los Alamos report LA-UR-89-3347, September 1989.

[12] F. Krueger, *Determining the Fast Neutron Energy Response Characteristics of Fermilab Instrumentation*, Fermilab Radiation Physics Note 86, June 1990.

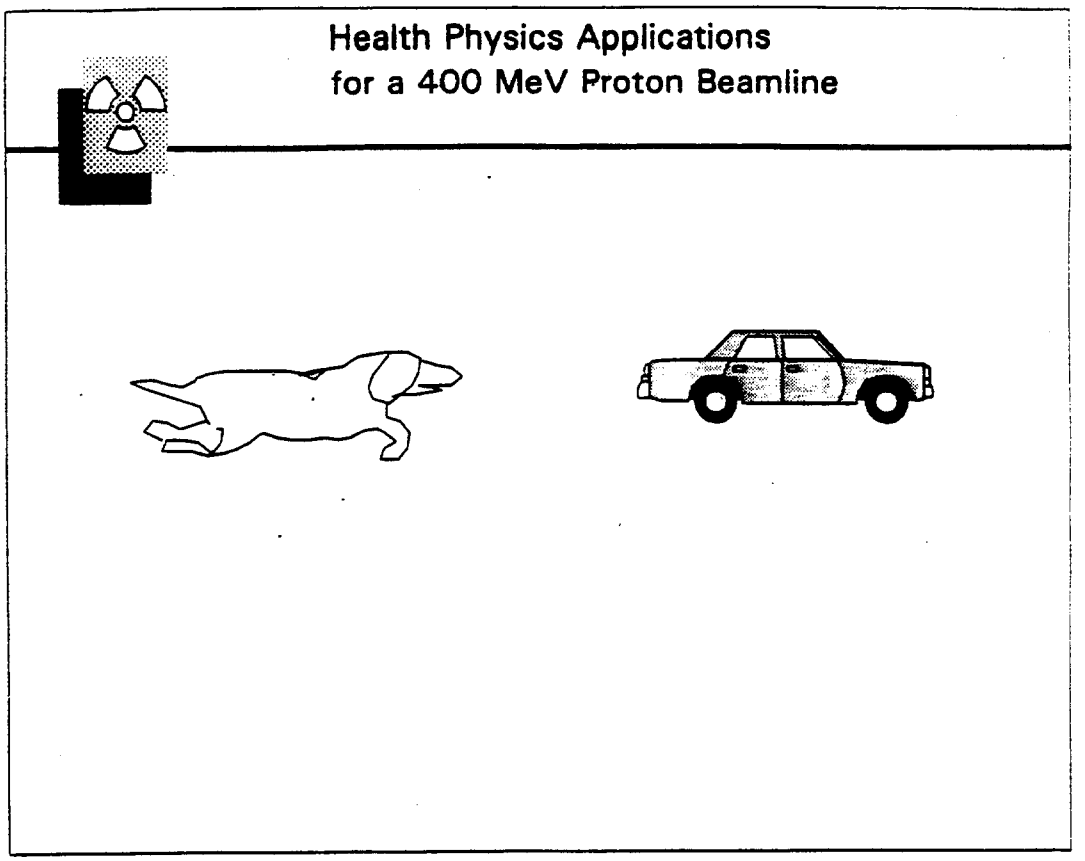

Figure 1. Health Physics personnel seeking experimental resources.

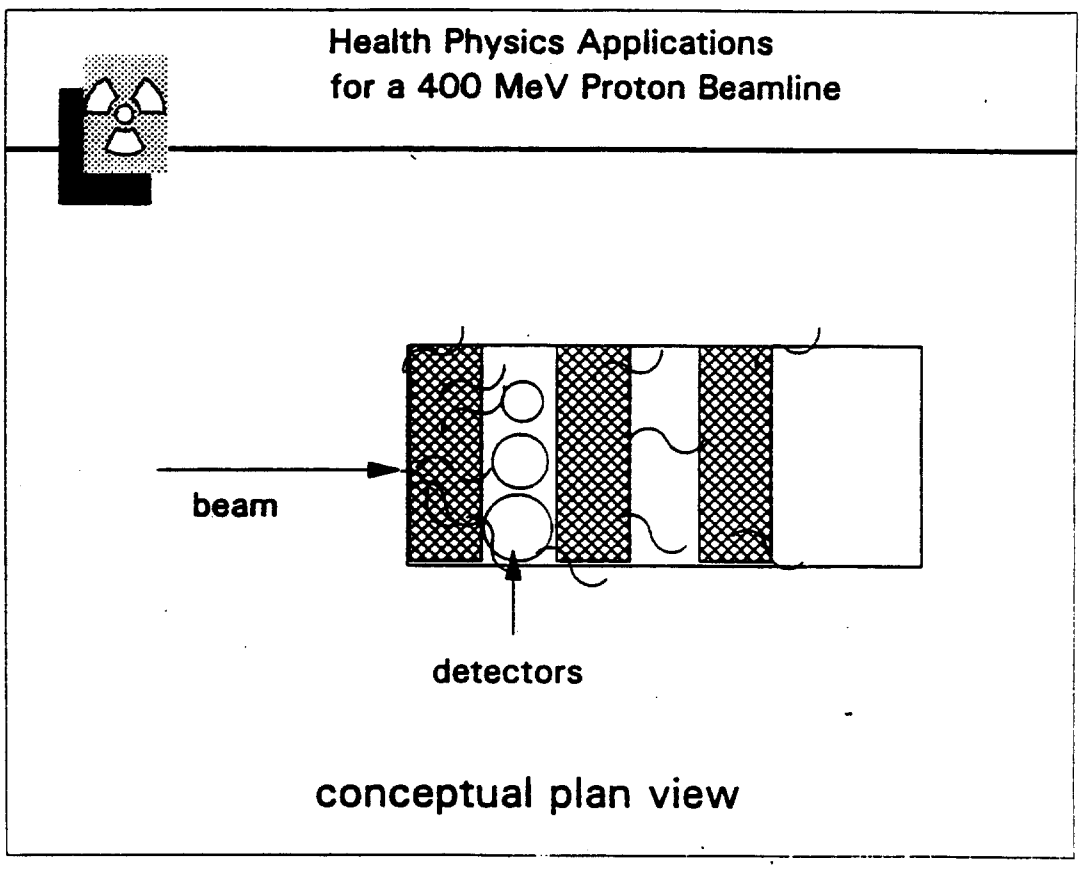

Figure 2. Schematic diagram of hypothetical shielding experiment.

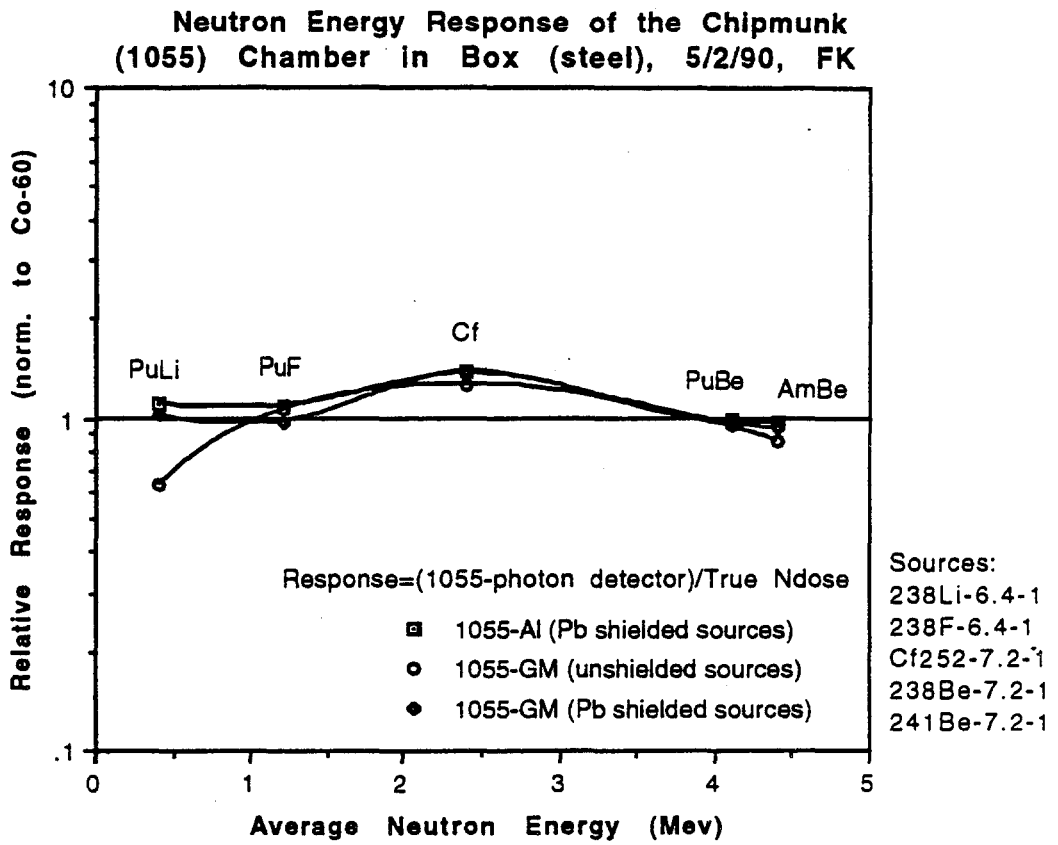

Figure 3. Chipmunk response curves from three sets of measurements.

ATOMIC PHYSICS AT FERMILAB

H.C. Bryant
Department of Physics and Astronomy
The University of New Mexico
Albuquerque, NM 87131 USA

ABSTRACT

In its own way, a high quality, intense, beam of H^- ions with energies of 400 MeV is just as unique in the physical world as is the beam of ultra high energy protons being produced in a big ring. Both beams allow us to make observations at the frontiers; in the linac case, the unique probes available would allow us to open a new window on the one- and two-electron atom. Moreover, the use of laser detachment techniques could have useful applications to accelerator physics.

1. Introduction

The advent of the SSC machine was widely expected to give a strong impetus to high energy particle physics in the U.S. What may not, however, have been recognized is that the H^- linac injector at the new facility would have also meant a major advance for an emerging branch of atomic physics involving the study of atoms and ions moving at near luminal velocities: relativistic atomic physics. With the cancellation of the SSC and the looming demise of an accessible H^- beam at LAMPF, the new linac at Fermilab appears to be unique.

Table I presents the Fermilab linac requirements and parameters.[1]

Table I Fermilab Linac Parameters

Beam Energy	400 MeV
Peak Current	35 mA
Pulse Duration	$\leq 30\ \mu s$
Pulse Repetition Rate	15 Hz
Microstructure	200 MHz
Emittance	7πmmmr normalized
$\delta p/p$	$\lesssim 2.5 \times 10^{-4}$

[1]Carol Johnstone, private communication.

Since the late seventies,[2] following proof of principle at a 4 MeV Van de Graaff,[3] work has been going on at the 800 MeV linear accelerator (LAMPF) at Los Alamos using laser beams and other probes, such as strong fields and thin foils, to study the structure and electromagnetic interactions of the simplest of atomic systems H^0 and H^-. The basic idea is to take advantage of the relativistic kinematics of an atom moving with a large β (at 800 MeV, $\beta = 0.84$) to Doppler-shift beams from ordinary pulsed lasers into the vacuum ultraviolet, corresponding to excitation energies of the neutral hydrogen atom and its negative ion. Enormous electric fields can be induced in the atom's frame using modest laboratory magnets. Recently, continuously tunable, intense beams from the CO_2 laser have been used to study for the first time multiphoton processes in the H^- ion.

To give a clearer idea of the power of relativistic kinematics in laser-ion beam studies, consider the relativistic Doppler formula,

$$E=\gamma E_L(1+\beta \cos \alpha). \tag{1}$$

Here the center-of-mass photon energy, E, is given in terms of its laboratory energy, E_L, with α being the angle between the laser beam and the particle beam, such that for head-on collisions $\alpha=0$. At 400 MeV, since $\gamma=1.426$ and $\beta=.713$, one can <u>continuously</u> tune a fixed-frequency laser through the range,

$$0.41\ E_L \le E \le 2.4\ E_L\ .$$

Furthermore the laser intensity, I, in the center of mass (Watts/cm^2) is related to the lab intensity, I_L, by the <u>square</u> of the Doppler factor. That is,

$$I = \gamma^2(1 + \beta \cos \alpha)^2\ I_L\ , \tag{2}$$

so that one can get an intensity gain at $\alpha=0$ of nearly 6.

Finally, the barycentric electric field F produced by a transverse laboratory magnetic field B is given, in S.I. units, by

$$F = \gamma\beta c\ B\ , \tag{3}$$

so that a 1 Tesla lab field can result in a center of mass electric field of 3.1 MV/cm.

Before the development of relativistic beam techniques, the resonance structure of the H^- ion in the vacuum ultraviolet was essentially unobserved except for a few electron-hydrogen scattering measurements. With the new methods we were able to demonstrate a rich structure of doubly-excited resonances in H^- and to study their

---

[2]H.C. Bryant et al., Phys. Rev. Letters <u>38</u>, 228 (1977).

[3]H.C. Bryant, P.A. Lovoi and G.G. Ohlsen, Phys. Rev. Letters, <u>27</u>, 1628 (1971).

behavior in electric and magnetic fields.[4] We were also able to do similar studies on the low-lying states of H^0. Precision checks on the isotropy of space-time are also possible by looking for discrepancies in the relativistic Doppler shift and the electromagnetic field transformations.

The work already done at LAMPF may be regarded as prelude to the eventual flowering of these endeavors at Fermilab.

2. Diagnostics, Monitoring and Tailoring for the H^- Linac at Fermilab

The use of lasers to probe relativistic atomic beams, developed at LAMPF over the past years, can be applied to the diagnosis, monitoring, and tailoring of the H^- linac beam at Fermilab. The basic idea is to direct a laser beam at the H^- beam so that its Doppler-shifted frequency is centered on a well-defined feature in the absorption spectrum. This feature could be the well-known Feshbach resonance (see Figure 1) in H^-, for example, at an excitation energy of 10.9264(6) eV, whose intrinsic width is some 30 microvolts, or it could be a hydrogen resonance line excited by a 2-step process in which the H^- is first photodetached using a precursor infrared beam and the ground-state H^0 is then excited. Even a three-step process might be contemplated, in which the complication of 3 separate laser beams might be exchanged for higher resolution and more convenient laboratory wave lengths as well as a higher signal-to-noise ratio. By selective photodetachment or excitation, small regions of the overall phase space could be studied.

The energy resolution in the center of mass of a system moving at βc in a beam whose momentum dispersion is $\delta p/p$, and where the rms angular uncertainty is $\delta\alpha$, is given by

$$\frac{\delta E}{E} = \left\{ \left(\frac{\delta E_L}{E_L}\right)^2 + \left(\frac{\beta \sin\alpha}{1+\beta\cos\alpha}\right)^2 (\delta\alpha)^2 + \left(\frac{\beta^2+\beta\cos\alpha}{1+\beta\cos\alpha}\right)^2 \left(\frac{\delta p}{p}\right) \right\}^{\frac{1}{2}} . \tag{4}$$

Let us assume now for example that the laboratory energy resolution of the laser line is negligibly narrow, so that $\delta E_L/E_L \sim 0$, and that we are exciting the ^1P Feshbach resonance at 10.926 eV just below the threshold for $\gamma + H^- \rightarrow H^0(2) + e$. By using a fixed-frequency laser, the observed angular width of the resonance would reflect both the angular uncertainty $\delta\alpha$ and the momentum spread $\delta p/p$ of the beam. At LAMPF $\delta\alpha$ can be as low as 10 microradians and $\delta p/p$ about 10^{-4}.

---

[4] P.G. Harris, H.C. Bryant, A.H. Mohagheghi, R.A. Reeder, H. Sharifian, C.Y. Tang, J.B. Donahue, C.R. Quick, D.C. Rislove, W.W. Smith, J.E. Stewart, Phys. Rev. Letters 65, 309-312 (1990).

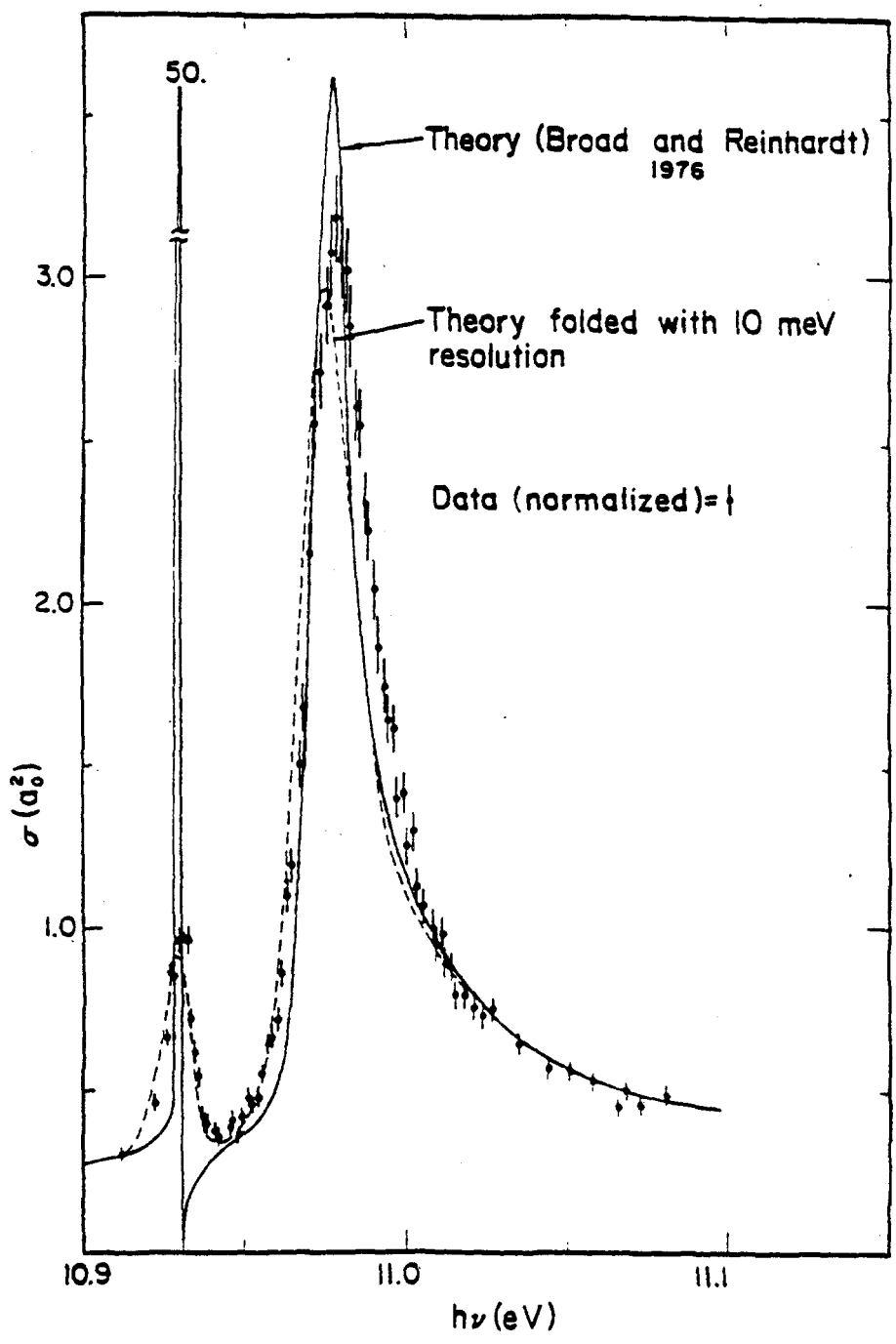

Fig. 1. The ^1P doubly excited resonances in H^-. The resonance on the left is known as the Feshbach resonance and the one on the right as the "shape resonance." See reference 2.

If it were possible to operate near $\cos \alpha = -\beta$ (the "Doppler free" angle),[5] sensitivity to $\delta p/p$ would disappear.

If it were possible to operate near $\alpha = 0$, sensitivity to $\delta\alpha$ would disappear.[6]

If we wished to monitor both variables at once we would have to use one of the hydrogen lines, by first photodetaching (to either the ground state or an excited state) and then exciting the line. Such a technique has been used to observe the narrowing of the momentum spread at LAMPF.[7]

In Figure 2 we show as an example the laboratory intersection angle α required to excite the Feshbach resonance below n=2 in H^- using garden-variety pulsed lasers. The use of pulsed lasers gives a large signal to noise ratio. It is worth pointing out that the availability of a tunable laser in the lab with sufficient intensity would be a great boon for this work because it would allow for continuous monitoring.[8]

Table II presents the center of mass range of photon energies corresponding to three readily available pulsed lasers.

Table II Some Representative C of M Photon Energies and Tuning Ranges for 400 MeV H^- Beam

Laser Line	Center of Mass Photon Tuning Range
Quadrupled YAG (4.66 eV)	1.91 — 11.38 eV
Argon Fluoride (6.42 eV)	2.63 — 15.68 eV
Carbon Dioxide (0.117 eV)	0.48 — 0.286 eV

In order to permit flexibility in monitoring the linac beam, space should be provided to insert laser beams with precision optics so that the angle α may be altered at will with high resolution. The resulting electrons could be bent out of the beam at any point into a detector with a weak magnetic field. By operating near 90° and focusing the laser beam with a cylindrical lens in the transverse direction, one could examine separately small

[5] H.C. Bryant, Electronic and Atomic Collision, N. Oda and K. Takayanagi, eds., North Holland Pub. Co. 1980, pp. 145-160.

[6] D.B. Holtkamp and C.R. Quick, Nuclear Instruments and Methods in Physics Research, A287, 348 (1990).

[7] P.G. Harris et al., Nuclear Instruments and Methods...A292, 254 (1990).

[8] A UV laser that could operate essentially CW while the H^- beam were present, for example, is a hollow cathode Cu^+ laser which would offer unique possibilities: 1) Several UV lines together very near to the 4th YAG line (259.06, 259.90 and 260.03 nm) would allow step-wise tuning. 2) Single mode operation with 10-15 MHz FWHM. 3) A long laser pulse that overlaps the beam pulse. 4) The excellent beam quality of the CW gas laser.

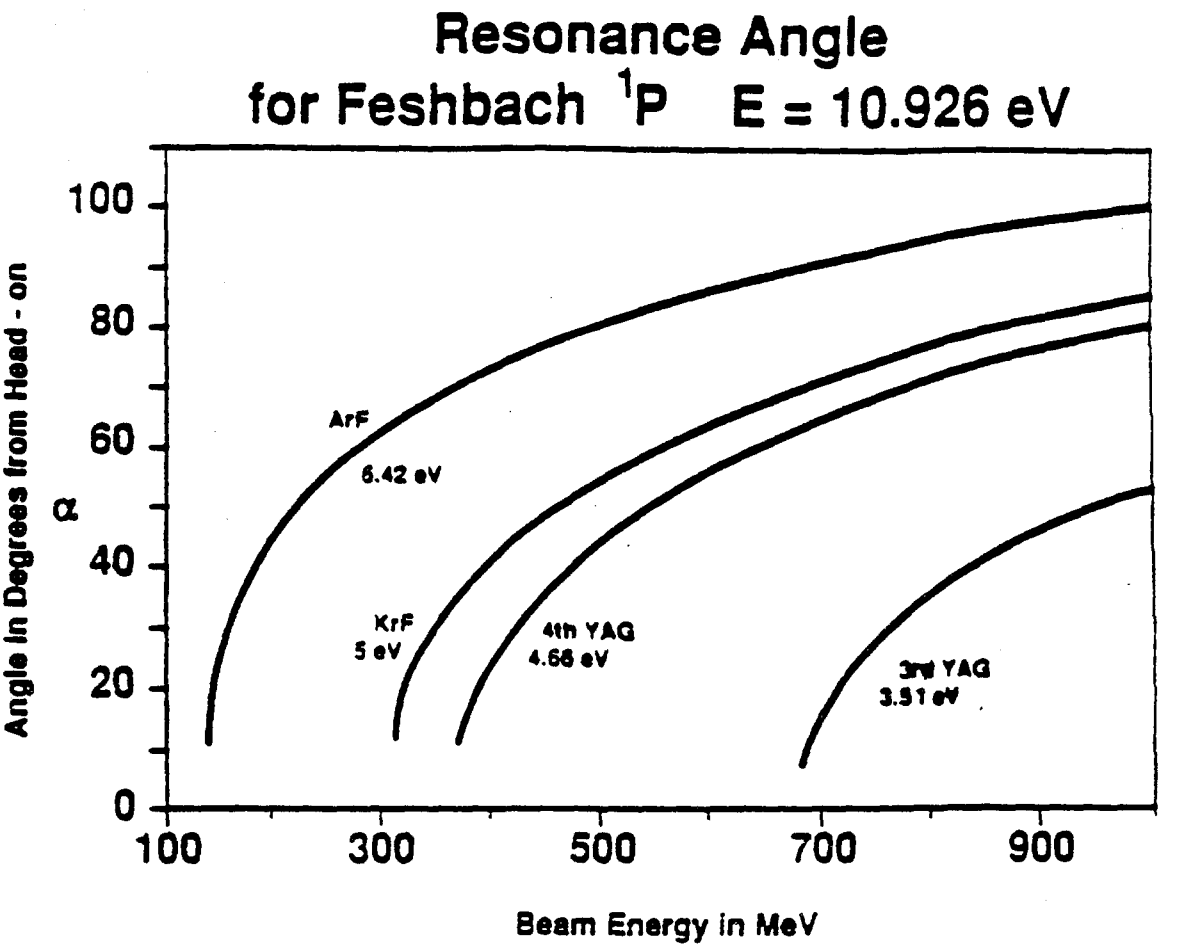

Fig. 2. Angle of excitation of the Feshbach resonance at 10.926 eV as a function of H^- kinetic energy for several "garden-variety" laser lines of high intensity.

subsets of the larger diameter beam. Also one could monochromatize by photodetaching only those ions within a prescribed momentum bite by tuning the shifted laser beam to the frequency of the very narrow Feshbach resonance.

We believe these techniques are quite promising and powerful. There are also many variations that could be studied to find the optimum arrangement for a given application.[9] Therefore, at this point, it is important to design the space around the linear accelerator in such a way as to allow laser access to it. Equipment we have developed for use at LAMPF could be transferred over to experiments at the linac.

Further development of appropriate laser systems would also be called for.

3. Atomic Physics Research

In addition to the diagnostics and other applications described above, it appears that unique basic atomic physics could also be performed at the linac. The availability of beam is, of course, the great advantage that the Fermilab linac has over work at LAMPF. In fact, the prospects for a beam at LAMPF appear to be close to nil.

Of course, in the study of something as rich in phenomena as atomic physics, many new and unexpected ideas can arise, but we can only plan based on what we already know. Therefore we sketch below some of the kinds of physics one could do using the H^- beam at the Fermilab linac.

a) High Resolution Spectroscopy of H^-

Recently[4, 10] we have been able to study the highly correlated, doubly-excited states in H^- by first exciting them through the process

$$\gamma + H^- \rightarrow H^{-**} \rightarrow H^0(n) + e,$$

with subsequent motional field stripping of $H^0(n)$ in an appropriately-chosen magnetic field. A dissertation written on this work won the Louis Rosen prize for the best done at LAMPF in 1990.[11] The cases for which n = 4,5,6 and 7 were studied. See Figure 3. With better signal-to-noise, the levels studied could be pushed up to much higher n's so that the systematics could be established. We could achieve a much clearer signal by introducing a second laser beam, rather than the stripping field, to label the final H^0 state, through, for

---

[9] D.R. Swenson, E.P. MacKerrow, H.C. Bryant, "Non-invasive diagnostics for H^- ion beams using photodetachment by a focussed laser beam," 1993 Beam Instrumentaion Workshop, Santa Fe, NM (LA-UR-93-3600).

[10] P.G. Harris, H.C. Bryant, A.H. Mohagheghi, R.A. Reeder, C.Y. Tang, J.B. Donahue, C.R. Quick, Physics Review A 42, 6443-6465, (1990).

[11] P.G. Harris, Ph.D. Dissertation, May, 1990, UNM "Observation of High-Lying Resonances in the H^- Ion," (LA-11843-T).

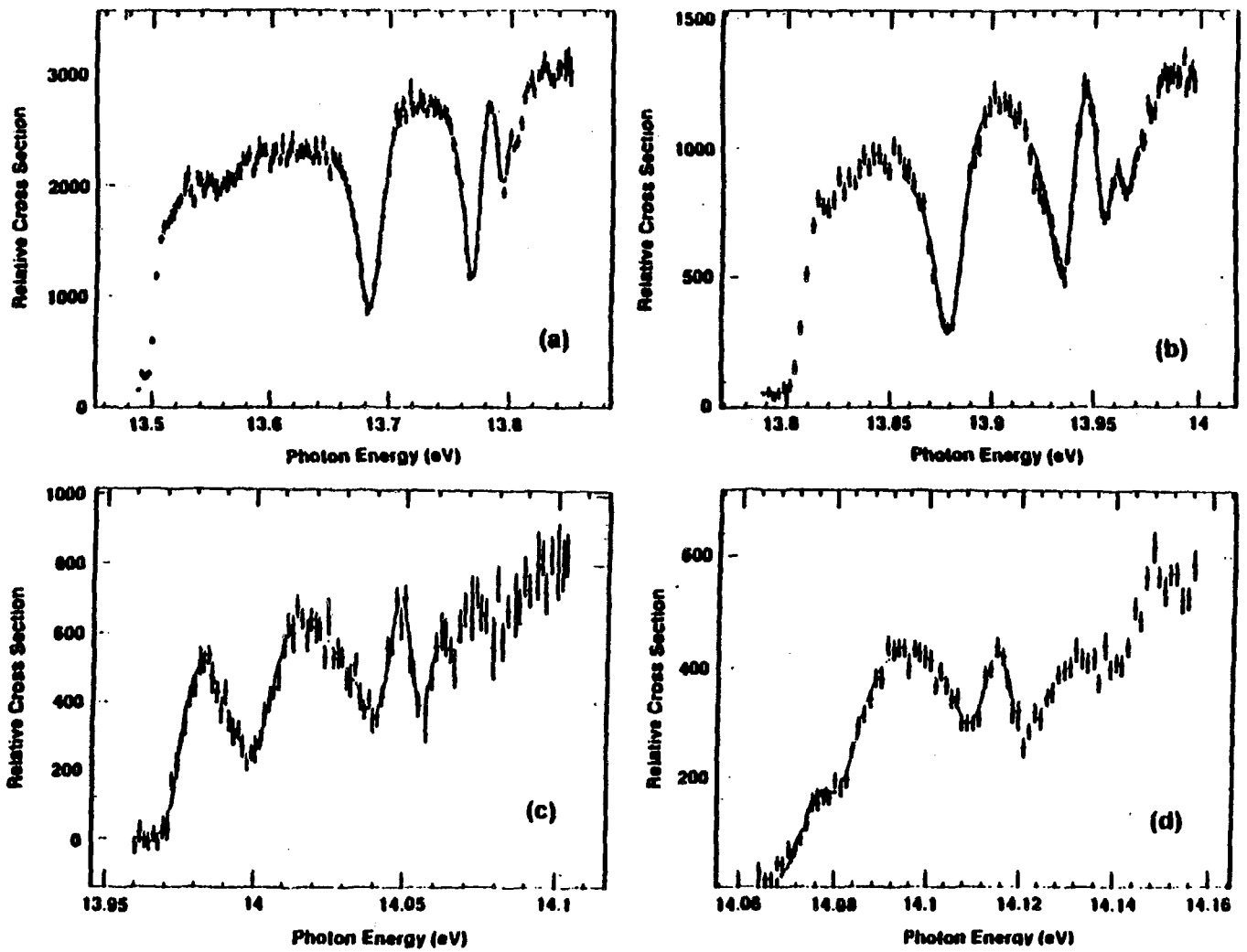

Fig. 3. High-lying resonances in the ^1P continuum of H^-. The energies of these resonances can be fitted to a remarkably simple formula reminiscent of that of Balmer for neutral hydrogen. The motional electric field is adjusted to strip $H^-(n)$ as follows: (a)$n \geq 4$, (b)$n \geq 5$, (c)$n \geq 6$, (d)$n \geq 7$.

example, its promotion to a higher n state, which could be unambiguously identified in an electron spectrometer e.g.

$$\gamma + H^0(n) \rightarrow H^0(12).$$

We demonstrated a "proof-of-principle" for this technique[12] in a short experimental run at LAMPF in August 1990.[13] And we obtained interesting data[14] on the n=2 channel in a run October 3-11, 1990. In the fall of 1993 a run was attempted at LAMPF using a specially-constructed magnet with a linear gradient to separate the final hydrogen states. Although the technique showed great promise, no new results were obtained, largely because of laser difficulties which could not be surmounted in the short time available for running.

By the application of external fields to the interaction region or by multiphoton excitation, a thorough picture of the resonance structure of H^- could be mapped out.

b) Multiphoton Studies

Currently our experimental program includes the study of multiphoton detachment of H^- using a CO_2 laser beam. Preliminary results are already available,[15 16 17] and work is continuing. With the CO_2 beam, with a lab photon energy of 0.117 eV, at 400 MeV we should be able to study detachment with photon numbers ranging from 2 to 15. If excess photon detachment occurs of course the number of photons involved can be even higher.

Because of the fundamental simplicity of the atomic system involved, along with the interesting complication of 2 electrons, these measurements merit precision work, for which conditions such as laser intensity and focal spot are carefully controlled.

The strong dependence of multiphoton processes on intensity adds another d dimension to the spectroscopy of H^-. A complete experimental study should include

---

[12]Collaborators in this effort included E. MacKerrow, M. Halka, A.H. Mohagheghi, C.Y. Tang, C.R. Quick, J.B. Donahue, J. Tiee, S. Cohen, H.C. Bryant.

[13]M. Halka et al., Physical Review A 46, 6942 (1992).

[14]M. Halka et al., Physical Review A 48, 419 (1993).

[15]C.Y. Tang et al., Phys. Rev. A 39, 6068 (1989).

[16]C.Y. Tang et al., International Conference on Multiphoton Processes (Invited Paper) Paris, September 24-28 (1990). Published in Multiphoton Processes edited by G. Mainfray and P. Agostini. Service de Physique des Atomes et des Surfaces, Centre d'Etudes de Saclay, 91191 Gif-sur-Yvette Cedex. 1990. pp. 69-78.

[17]W.W. Smith et al., J. Opt. Soc. Am. B 8, 17-21 (1991).

observations of intensity and polarization dependences as well as measurements of the energies and angular distributions of the detached electrons.

c) Strong-field effects

Our studies of H^- in strong electric fields have yielded surprises[18] (increased lifetimes in some cases and the atomic analogue of interference fringes)and such work should continue. A near-luminal H^- ion moving through a modest laboratory magnetic field experiences enormous electric fields in its barycentric frame yet is essentially undeflected because of its high magnetic rigidity.

d) Passage through thin foils and channeling

A recent Ph.D. dissertation[19] in our group was written on the study of the excitation of $H^0(n)$ by the passage of H^- through carbon foils ranging in thickness from 20 $\mu g/cm^2$ to 300 $\mu g/cm^2$. In this case the foil delivers an intense perturbation to the H^- ion for times of the order of a femtosecond. Additional data taken in 1993 using a technique sensitive to Stark states are currently under analysis.[20]

Further studies are contemplated[21] using very thin oriented crystals of Si or sapphire (Al_2O_3) in which channeling may be expected to occur for intact atomic systems. Such work may have practical applications.

At Fermilab we would be able to explore the stripping process at 400 MeV. These measurements would be the first on our agenda.

e) Searches for a preferred frame

Tests of relativity based on the exquisitely well-known energy levels of atomic hydrogen can be contemplated for a high quality 400 MeV H^- beam. At LAMPF we have checked the Doppler[22] formula to the 36th power of β.

---

[18] H.C. Bryant et al., Phys. Rev. Letters 58, 2412 (1987). J.D. Stewart et al., Phys. Rev. A 38, 5628 (1988). P.G. Harris, et al., Phys. Rev. A. 41, 5968-5973 (1990).

[19] A.H. Mohagheghi, Ph.D. Dissertation, September 1990, UNM, "Interaction of Relativistic H^-Ions with Thin Foils," LA. See A.H. Mohagheghi et al., Physical Review A 43, 1345-1365 (1991).

[20] J. Donahue et al., "Measurement of H^0 Excited States Produced by Foil Stripping of 800-MeV H^- Ions," 1993 Particle Accelerator Conference.

[21] Károly Rózsa, a collaborator from the Hungarian Academy of Sciences, has been investigating the manufacture of oriented crystal foils of submicron thickness.

[22] D.W. MacArthur et al., Phys. Rev. Letters 56, 282 (1986).

4. Reconstructed Hydrogen Atoms?

It is perhaps worthwhile pointing out the possibility of the production of very high energy hydrogen atoms (and perhaps even H^-) by the method of laser stimulated radiative recombination of protons.[23] A feasibility study of the production rates in a GeV test beam should be done before further speculation, however.

6. Conclusion

If the H^- linac at Fermilab were made available for atomic studies, there are many fascinating measurements that could be performed. Studies of H^- ions traversing thin foils have practical implications for accelerator physics as well as considerable intrinsic interest. Laser photodetachment measurements could map out accurately doubly excited structures in H^- , and the response of both H^- and H^0 to strong electromagnetic fields that are presently inaccessible by conventional techniques. In addition, a relativistic H^o beam could be used as a unique probe of the isotropy of space-time.

Acknowledgements

This work was supported by the Division of Chemical Sciences, Office of Basic Energy Sciences, Office of Energy Research, U.S. Department of Energy. This paper is derived from an earlier published discussion.[24]

---

[23] T. Morgan, "Laser Stimulated Radiative Recombination of Protons," in Atomic and Molecular Physics, C. Cisneros, I. Alvarez and T.J. Morgan, Eds. World Scientific, Singapore 1991. p. 26.

[24] H.C. Bryant, "Atomic Physics at the SSC," op. cit. p. 253.

TRANPARENCIES

400-MeV Beam International Conference
Fermilab
October 24 - 27, 1993

Workshop to solicit design criteria, applications and experiments from physics and medical physics users of beams derived from Fermilab's 400 MeV Linac. The workshop sponsored and held by Fermilab.

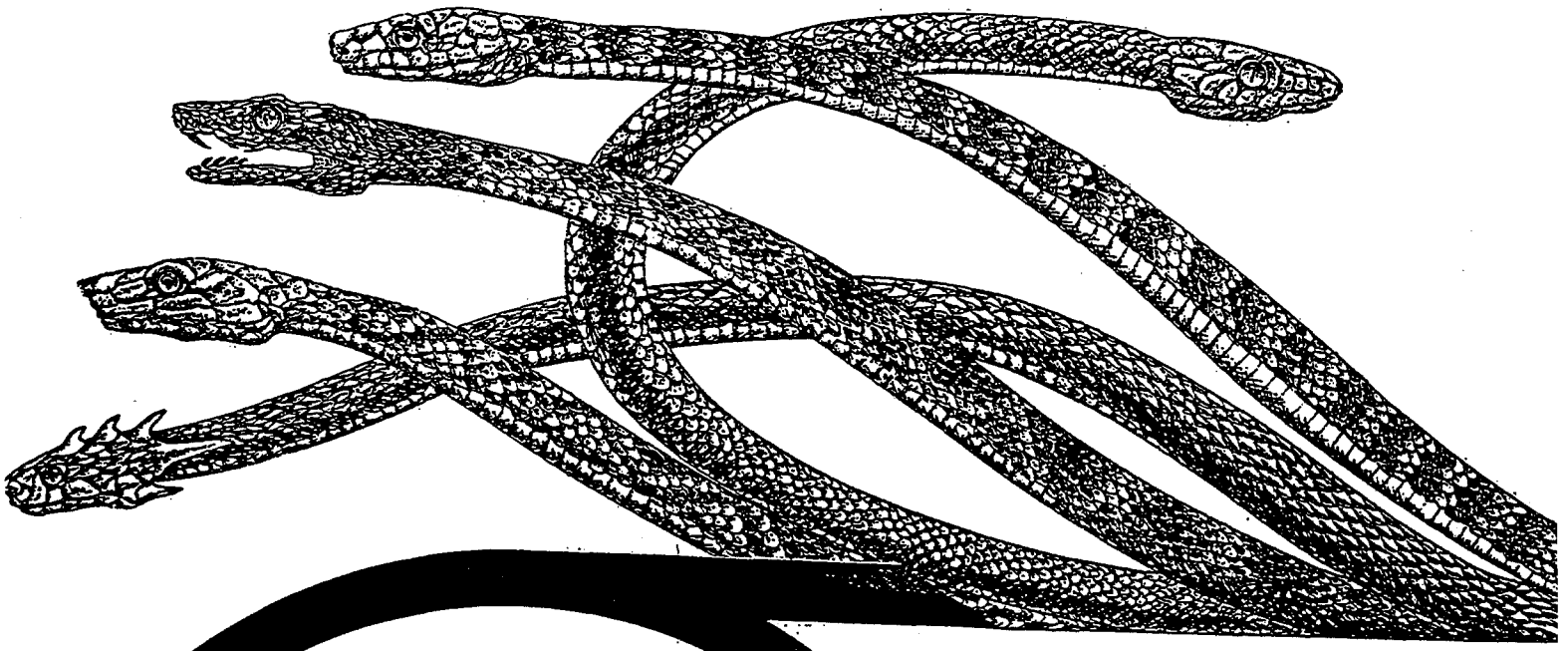

Organizing Committee:

Chuck Ankenbrandt (Fermilab)
Carol Johnstone (Fermilab)
Tom Kroc (Fermilab)
Arlene Lennox (Fermilab)
Howard Bryant (UNM
Stanley Cohen (LANL)
Dan Fitzgerald (LANL)
Eli Glatstein
(Southwest Medical Center)
Dan Miller
(Loma Linda Universtiy Medical Center)
Robert Wilson
(UT Medical Group)
Don Young
(PAC & Fermilab)

Operating Parameters of Proposed H^{-0+} Beams:

Energy:
min. 100 MeV
max. 400 MeV

Intensity:
min. few particles/pulse
max. 10^{13} particles/pulse

Pulse length:
min<1 μsec
max. 30 μsec

Transverse emittance
(unnormalized 90%):
min.<1 π mm-mrad
max. 7 π mm-mrad

Repetition rate:
15 Hz

FERMILAB 400 MEV WORKSHOP: CHARGE

Operating Characteristics

Energy:	400 MeV
Particle type:	H^-
Current:	50 mA
Pulse Length:	100 μsec
Repetition Rate:	15 Hz
Repetition Rate (pbar production):	0.417 Hz

Charge

Is there anything useful that can be done with the 35/36 cycles that are not required for support of the high energy physics program?

If so, what are they and what sorts of facilities would be required.

Let your imaginations roam and enjoy your stay.

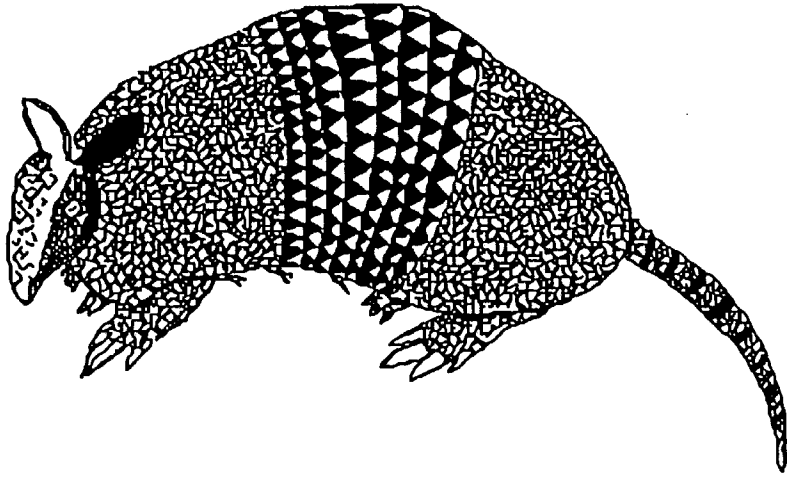

ARMADILLO

— **A**ccelerator for **R**adiobiology and **M**edical **A**pplications **D**eveloped for **I**dletime on the **L**ong **L**inac's **O**utput

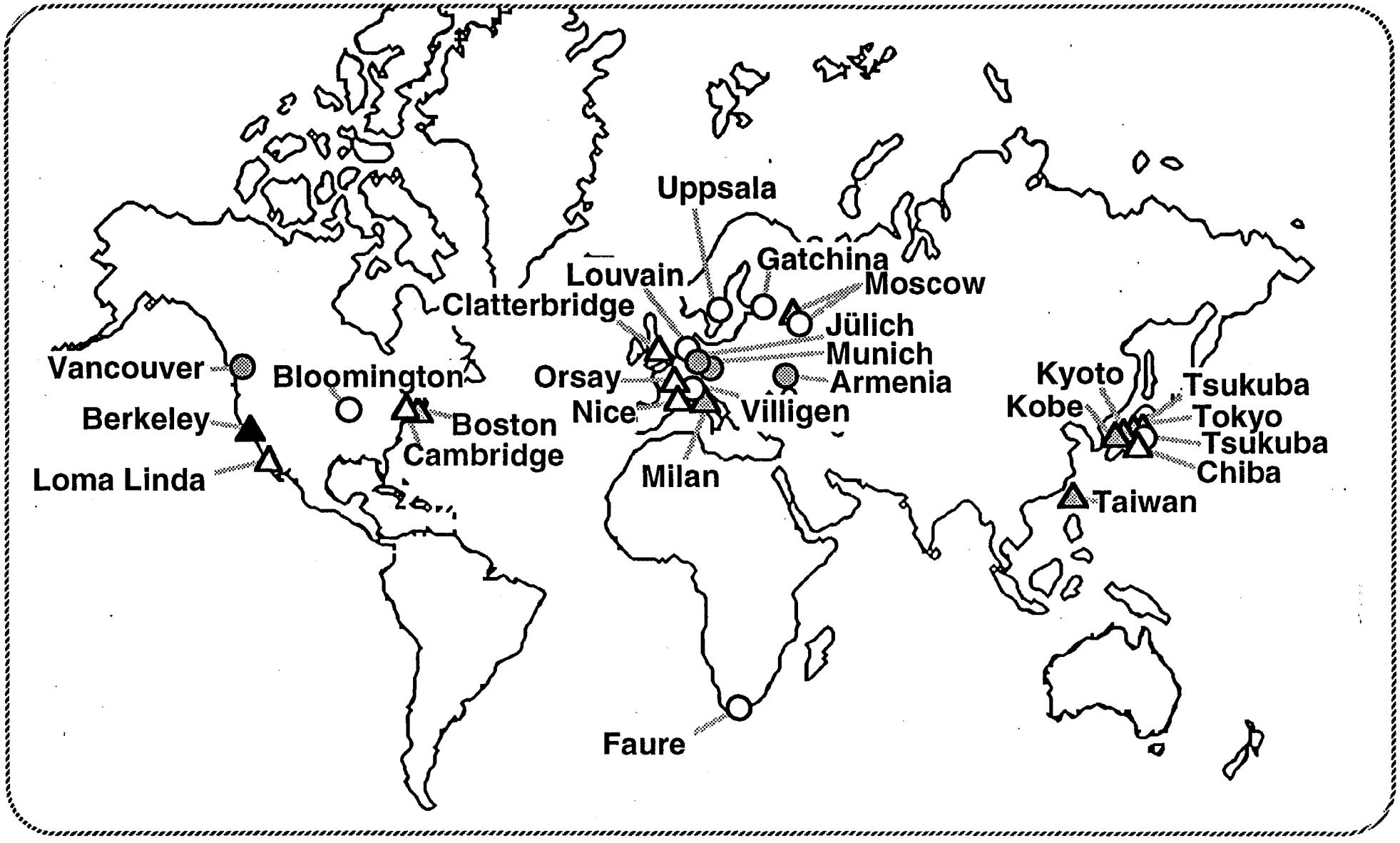

PROTON MEDICAL FACILITIES OF THE WORLD

○ shared (with physics) facilities

△ dedicated clinical facilities

□ operating, ▩ planned, ■ closed

Proton Medical Accelerators W. Chu 10/93

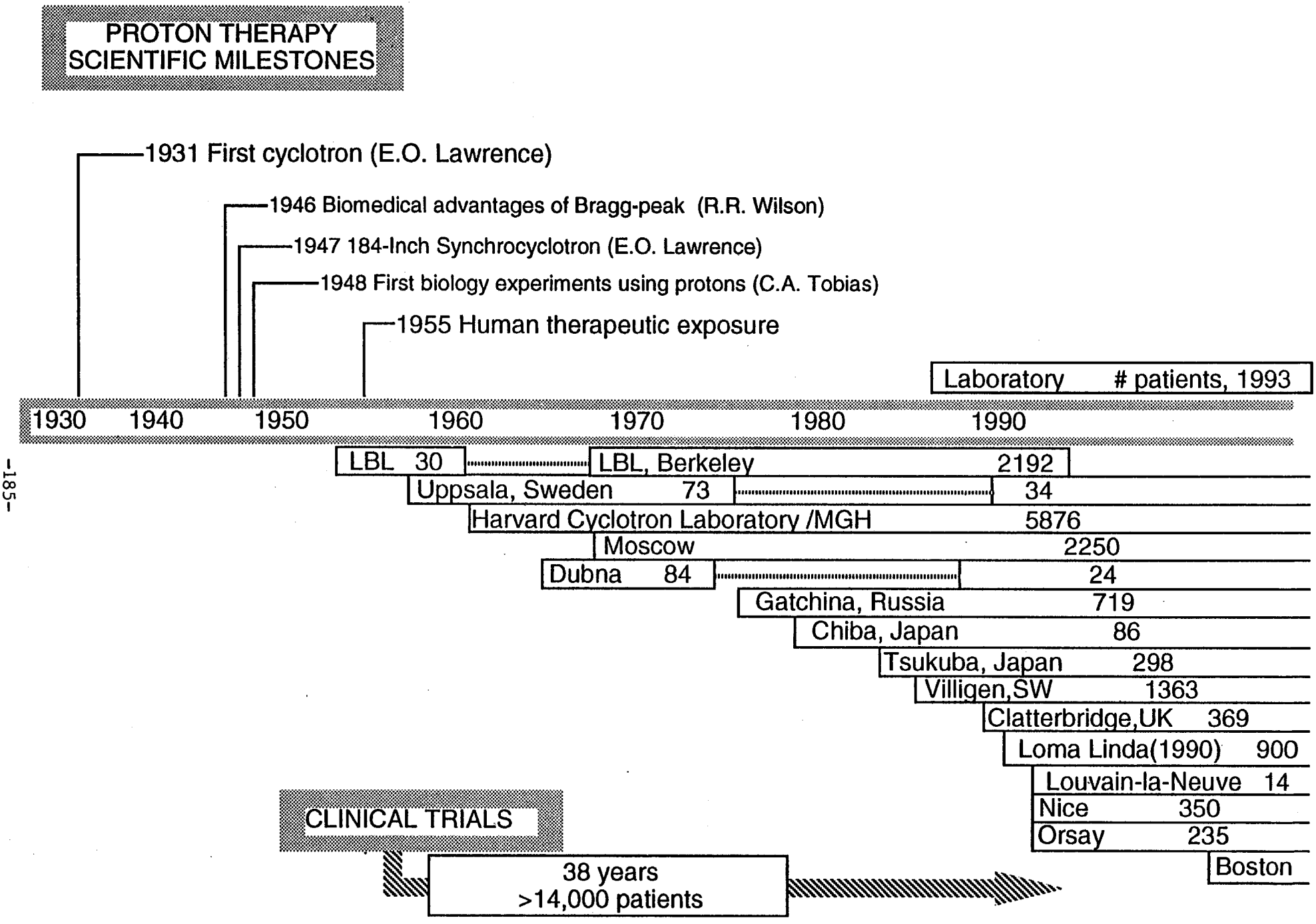
PROTON THERAPY
SCIENTIFIC MILESTONES
1931 First cyclotron (E.O. Lawrence)
1946 Biomedical advantages of Bragg-peak (R.R. Wilson)
1947 184-Inch Synchrocyclotron (E.O. Lawrence)
1948 First biology experiments using protons (C.A. Tobias)
1955 Human therapeutic exposure
Laboratory # patients, 1993
1930 1940 1950 1960 1970 1980 1990
LBL 30
LBL, Berkeley 2192
Uppsala, Sweden 73
34
Harvard Cyclotron Laboratory /MGH 5876
Moscow 2250
Dubna 84
24
Gatchina, Russia 719
Chiba, Japan 86
Tsukuba, Japan 298
Villigen,SW 1363
Clatterbridge,UK 369
Loma Linda(1990) 900
Louvain-la-Neuve 14
Nice 350
Orsay 235
Boston
CLINICAL TRIALS
38 years
>14,000 patients

Emittance

ε (m – rad) is invariant (unless the beam is collimated)

Therapy beam requirements:

proton beam — $z = 20$-cm range

$r = 10$-cm radius

multiple scattering — $\sigma_y \approx 0.43$ cm

comparable divergence is given by:

$$\varepsilon \approx r \cdot \theta \approx r \frac{\sigma_y}{z} \approx 10^{cm} \frac{0.43^{cm}}{20^{cm}} \approx 2.2 \times 10^{-3} \text{ m-rad}$$

Focal legion requirements:

proton beam — $z = 10$-cm range

$r = 0.5$-cm radius

multiple scattering — $\sigma_y \approx 0.23$ cm

comparable divergence is given by:

$$\varepsilon \approx r \cdot \theta \approx r \frac{\sigma_y}{z} \approx 0.5^{cm} \frac{0.23^{cm}}{10^{cm}} \approx 1.2 \times 10^{-4} \text{ m-rad}$$

Accelerator requirements:

$$\varepsilon \approx 10^{-5} \text{ m-rad} = 10 \text{ mm-mrad}$$

Practical limitations:

Multiple scattering in the beam path and in the target
angular confusion

Effective "source-to-target" distance

Published [Biological Nuclei](p, x) Data, Where [B N]=H, C, N, O

F. E. Bertrand and R. W. Peelle, "Complete hydrogen and helium particle spectra from 30- to 60-MeV proton beam bombardment of nuclei with A=12 to 209 and comparison with intranuclear cascade modes," **Phys. Rev. C8**, 1045-1064 (1973)

W. Bauhoff, Atomic Data and Nuclear Data Tables **35**, 429-447 (1986).

(Faure, South Africa)
J. V. Pilcher, A. A. Cowley, D. M. White, and J. J. Lawrie, "Protons of 200 MeV incident on ^{12}C. I. Coincident proton emission from the continuum," **Phys. Rev. C40**, 1937-1949 (1989).

A. A. Cowley, J. V. Pilcher, J. J. Lawrie, and D. M. White, "Protons of 200 MeV incident on ^{12}C. II. Quasifree proton knockout," **Phys. Rev. C40**, 1950-1958 (1989).

S. V. Förtsch, A. A. Cowley, J. V. Pilcher, D. W. White, J. J. Lawrie, J. V. Van Staden, and E. Friedland, "Continuum yields from ^{12}C(p, p') at incident proton energies of 90 and 200 MeV," **Nucl. Phys. A485**, 258-270 (1988).

(NIRS)
L. Sihver and T. Kanai, "Energy loss, range and fluence distributions, total reaction and projectile fragmentation cross sections in proton-nucleus and nucleus-nucleus interactions," National Institute of Radiological Sciences, Chiba, Japan, NIRS-M-87, HIMAC-002 (1992).

(LAMPF)
Y. Yang, L. Wang, J. Rapaport, G. D. Goodman, C. Foster, Y. Wang, W. Unkelbach, E. Sugarbaker, D. Marchlenski, S. de Lucia, B. Luther, J. L. Ullmann, A. G. Ling, B. K. Park, D. S. Sorenson, C. R. Howell, and W. Tornow, "Dipole and spin-dipole resonances in charge-exchange reactions on ^{12}C," **Phys. Rev. C48** (No. 3), 1158-1171 (September 1993).

Dose-Delivery Control System

- Failsafe
- Interruptible / recoverable

Beam Delivery System

- Scatterign
- Wobbler
- Raster scanner

Target Alignment Facility

- A computer-controllabl precision target alignment table, with 5 degrees of freedom in x, y, z, θ, and φ

- Multi-sample translator

Variations in the use of accelerated beams

	Particle physics experiments	Biomedical experiments
Set-up time	Long (months, sometimes years)	Short (minutes to hours at most)
Data taking time	Extended time between changing the accelerated beams	Short time between changing the accelerated beams (minutes to hours at most) Short but experiments are repeated on rigid schedules for fractionated irradiations
Time-sensitive	Not time-sensitive (Always there is next time and later time.)	Very time-sensitive (Often there is no next time or later time.)
Fail-safe	Desirable	Necessary

Biomedical Facility Requirements

- Multi-user facility

- Meets varied experimental requirements
  - Large targets, minute targets
  - Thick targets, thin targets
  - High dose, high dose rate
  - Low dose, chronic irradiation

- Ready when needed

- Reproducible
  - Dosimetry
  - Beam quality
  - Experimental set ups

- Reliable
  - Failsafe
  - Fail soft --- recover data

Biomedical User Facility

Experiment preparation rooms

Shielded irradiation rooms (multi-room operations)
- Switch beam lines
  - energies
  - beam-line setups

Beam delivery systems
- Control beam intensity, spill lengths
- Large fields (scatter, wobbler, and/or scanner)
- Micro-beams

Data collection systems
- Dosimetry
  - Dose distribution measurements
  - Beam quality measurements
  - Bragg peak localization
- Multi-sample irradiation
- Irradiation control systems

from a '92 Report

Duplicating the Biology Irradiation Facilities in Beam 40—Details and Costs

Bill Chu
Research Medicine and Radiation Biophysics Division
Amy Kronenberg
Cell and Molecular Biology Division

An estimate has been made to equip the existing Beam 40 irradiation enclosure with a biology irradiation system by duplicating some of the systems available in Cave 2. The items are grouped into the following categories:

- Control room—The operator must have visual access to all computer functions and monitors, and immediate access to the controls of critical devices to terminate irradiations in case of malfunctions. The estimate includes electronics racks and an operator's console.

- Dosimetry control computer system—Computers, peripheral devices, graphics display terminals. Also includes the software implementation and documentation costs. Two computers (VAX4000) are proposed here as one will be used for beam delivery operation while the other for development. This arrangement will provide most flexible and efficient operations.

- Irradiation room facilities—Includes laser localizers, x ray units to align animals, x ray film developer, automatic sample positioner for multi-sample experiments, overhead hoist, CCTV, and intercom system.

- Dosimetry system—optical rails, dosimetry control electronics, CAMAC and NIM crates and patch panels, wire chamber for beam tuning, ionization chambers for dose measurements, secondary emission monitor, associated power supplies and electronics, and fast beam chop system to terminate the irradiation. Also included is testing equipment such as a standard current source for calibrating recycling integrators, an electrometer for calibration verification, an oscilloscope, and a Geiger counter for monitoring items removed from radiation area.

- Beam-modifying devices—Degrader foil system to scatter the beam for broadening of the beam profile, and a variable water column to modulate the range of the beam

Costs for this project are detailed in Table 7, and summarized in Table 2. All work would be completed during FY 1992.

Biology experimental preparation rooms:

Basic Requirements for Upgrade to Cellular and Molecular Biology Laboratory Adjacent to Biomed Cave II Beamline Area

A general remodelling of the existing cell culture laboratory is required in order to provide a complete multi-user facility in which mammalian and human cells may be maintained under sterile culture conditions for prolonged periods of time under controlled atmospheric environments. In order to carry out combined exposures to hazardous chemicals (i.e., suspected carcinogens or radioprotective agents which may be toxic in larger quantities), there are certain upgrades that are required to meet current safety guidelines. Much of the present equipment in the cell culture laboratory is more than 15 years old and should be replaced. The following list of equipment are suggested as replacements and required improvements for the existing cell culture laboratory.

- Conventional Facilities—Remove existing walls sub-dividing room, construct a double-door to outside, alter existing heating/ventilating system.

- Biology Equipment—Provide cell counter, incubators, cell-freezer and dewars, waterbath, centrifuges, balances, pH meter, flammable-storage refrigerator, UV lighting fixtures and interlocks, and two laminar flow hoods, one for hazardous materials.

Costs for upgrading the existing laboratory adjacent to Biomed Cave II are detailed in Table 8 and summarized in Table 2. All work would be completed during FY 1992.

Basic Requirements for a New Cellular and Molecular Biology Laboratory and Animal Care Facility Adjacent to Beam 40 Area

To perform biology experiments, experimental preparation facilities must be located in the immediate vicinity of this irradiation room. Constructing a cell preparation room equipped with cell handling equipment, and a animal holding room which has two segregated areas to hold two different experiments are proposed.

It is proposed to build a new "Butler building," shown in Figure 8, which includes the animal holding room, the cell and molecular biology laboratory, and the Biomed Beam 40 control room. The following would be required to provide such a facility.

- Conventional Facilities—Butler building and concrete pad, utilities and sewer service, heating and ventilating systems (separate systems for animals and cells).

- Animal Facilities—Duplicate present animal holding area, including drains, shelves, sinks, and flammable-storage refrigerator.

- Biology Equipment—See section above.

- Laboratory Equipment—Provide chemical fume hood, sinks, workbenches, flammable-storage cabinet, water purification equipment, and autoclave.

Costs for completing this project are detailed in Table 9 and summarized in Table 2. All work would be completed during FY 1992.

Figure 8

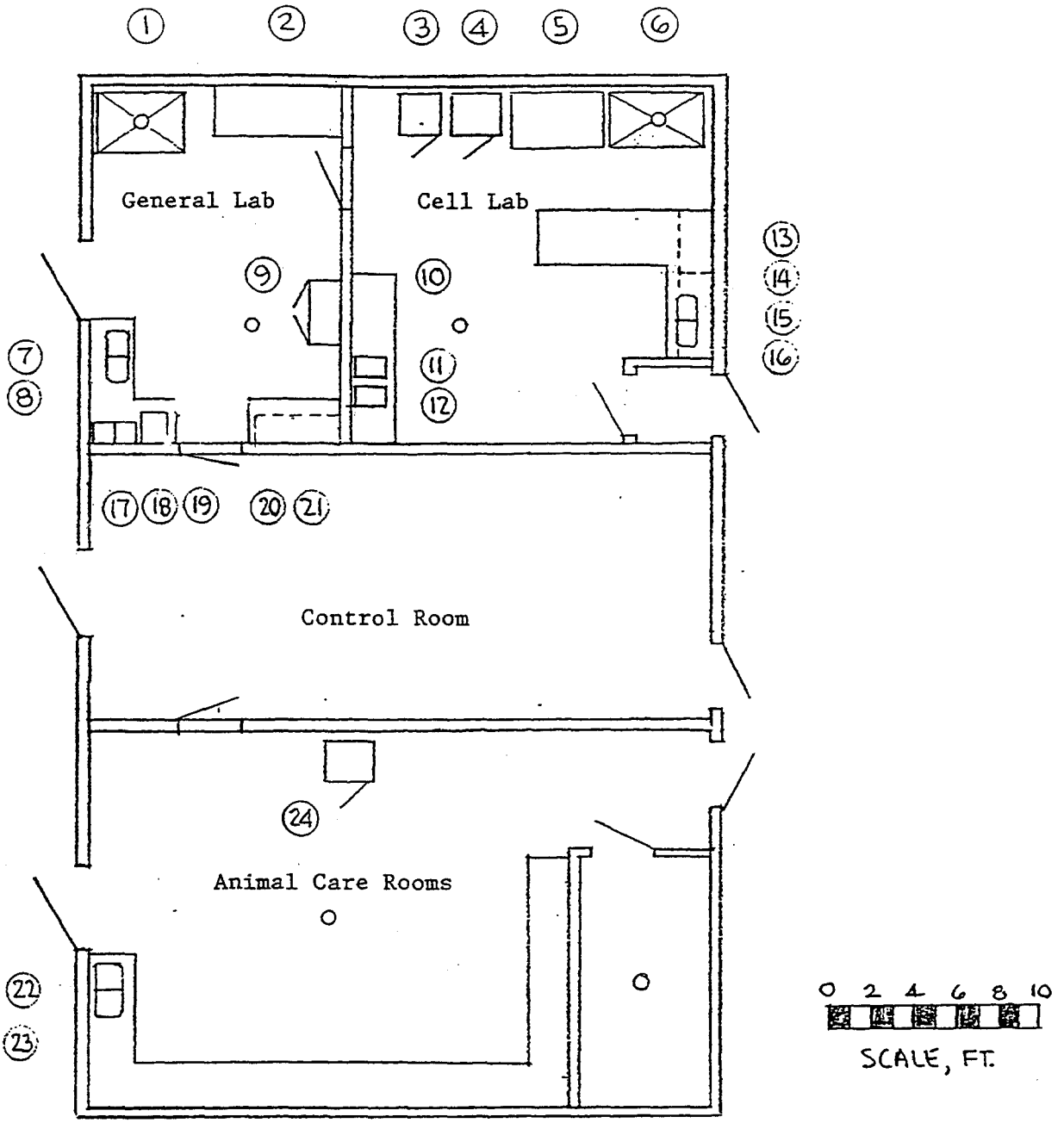

Equipment/Furniture List
(* indicates standard equipment which does not require any special installation.)

1 4' Chemical Fume Hood.
2 * 6' Workbench.
3 * CO2 Incubator.
4 * Flammable materials storage refrigerator.
5 Laminar Flow Hood.
6 Laminar Flow Hood, Vented.
7 * 2' Sinktop.
8 Double Sink.
9 * Flammable materials Storage Cabinet.
10 * 8' Workbench.
11 * Coulter Counter.
12 * Coulter Channelyzer.
13 * Two 4' workbenches, drawers under.
14 * 2' Sinktop.
15 Double Sink.
16 * Wall-hung Storage cabinets.
17 Milli-Que Purifier.
18 Milli-Pore Purifier.
19 * Sterilematic Autoclave.
20 * 2' Workshelf.
21 * Wall-hung Storage Cabinets.
22 * 2' Sinktop.
23 Double Sink.
24 * Flammable materials storage refrigerator.

Table 9

New Cellular and Molecular Biology Laboratory and Animal Care Facility Adjacent to Beam 40 Area

FY 1992

Salaries & Wages	Group	Rate/Yr	FTE	Sub-Total	
Maintanence Machinist	9111	$40	0.16	$6	
Laborers	9112	$33	0.80	$26	
Carpenters	9113	$41	0.78	$32	
Electricians	9114	$41	0.48	$20	
Plumbers	9115	$41	0.16	$7	
Painters	9116	$41	0.16	$7	
Sheet Metal	9121	$44	0.80	$35	
Air Conditioning	9122	$44	0.21	$9	
Engineering Supervision	9141	$67	0.85	$57	
Total Salaries			4.41	$199	
Payroll Burden		43.5%		$99	
Total Salaries & Payroll Burden					$298
Permanent Equipment					$269
Expendable S&E					
Under $5000					$116
Other Direct Costs					
Shop Burden					$29
Scientific Burden			5.3%		$23
Total Direct Cost					**$735**
Indirect (Overhead)			55.0%		**$256**
Total Direct and Indirect Costs					**$991**
DOE Added Factor			3.2%		**$32**
Total Costs for Fiscal Year 1992 (RY K$)					**$1,023**

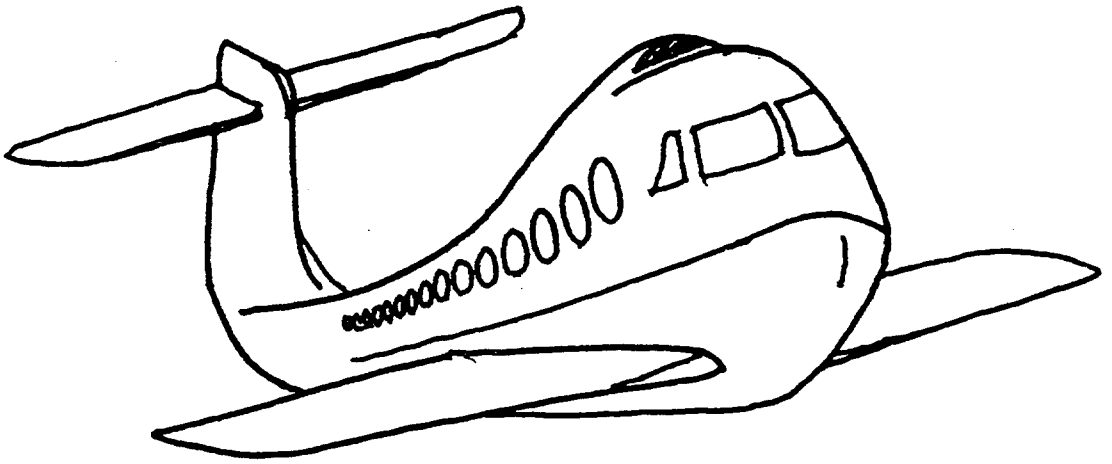

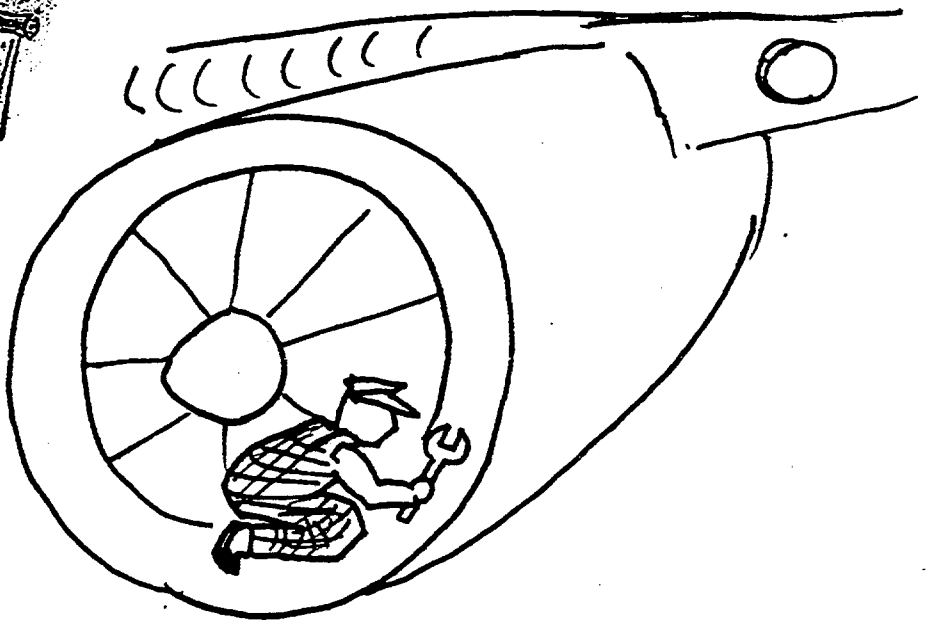

Physicists consider accelerators as machine, operations, and maintenance.....

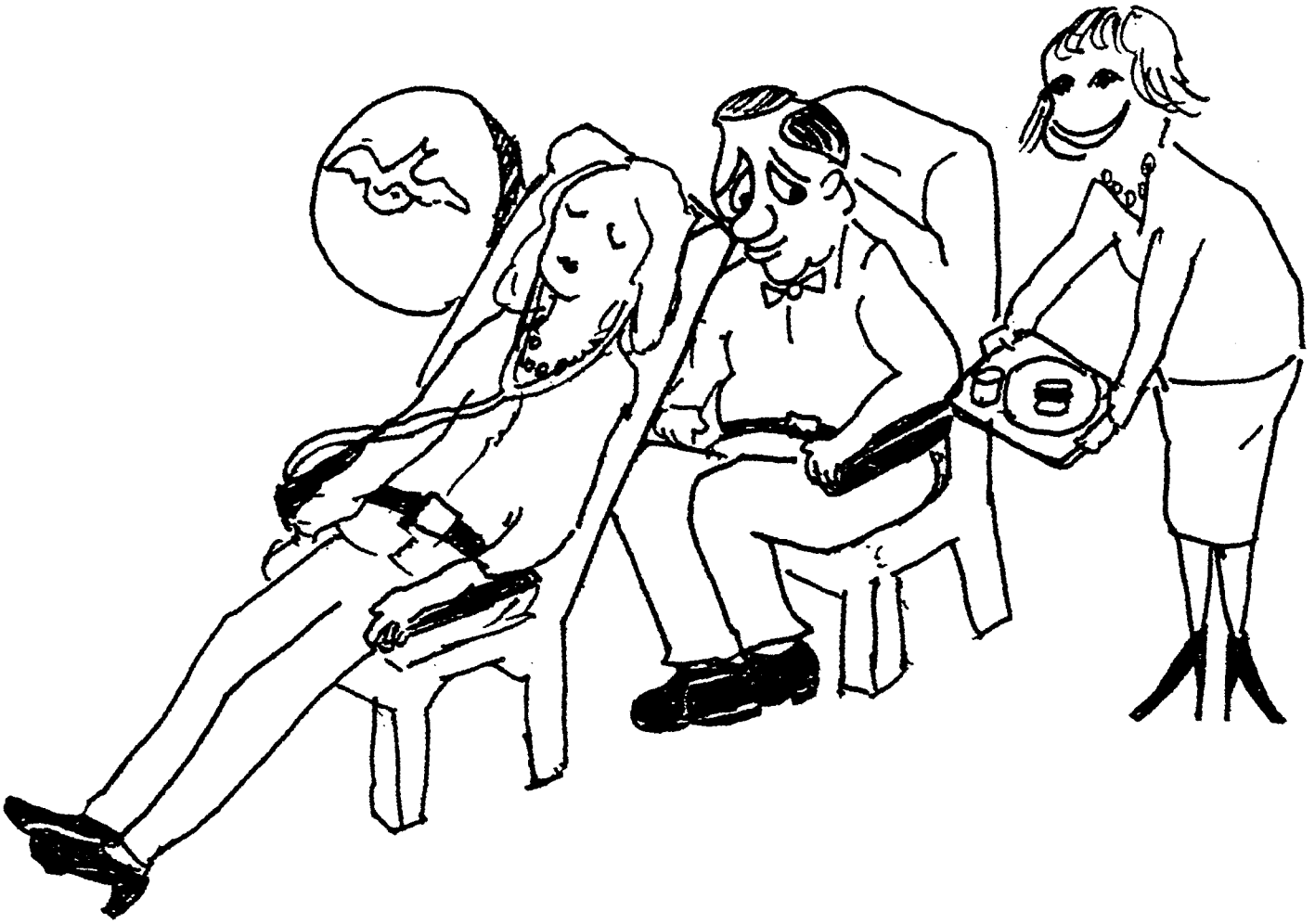

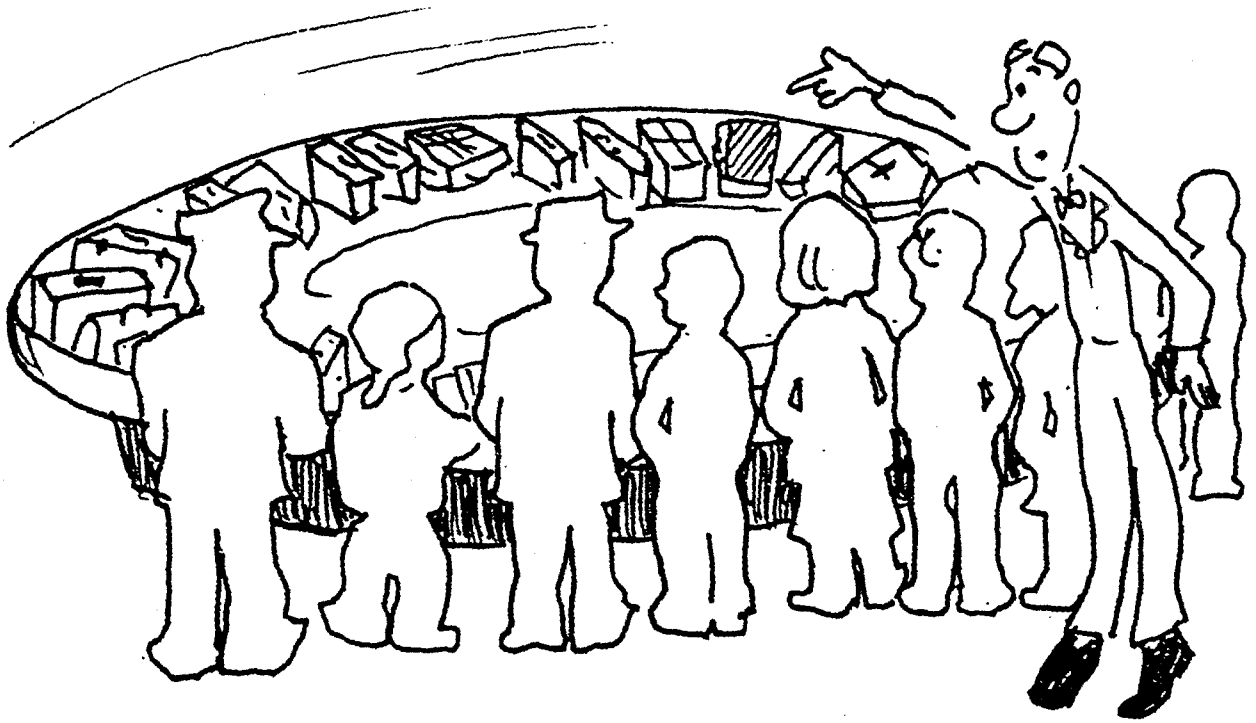

Biomedical users choose the accelerator facility based on its service and user facility

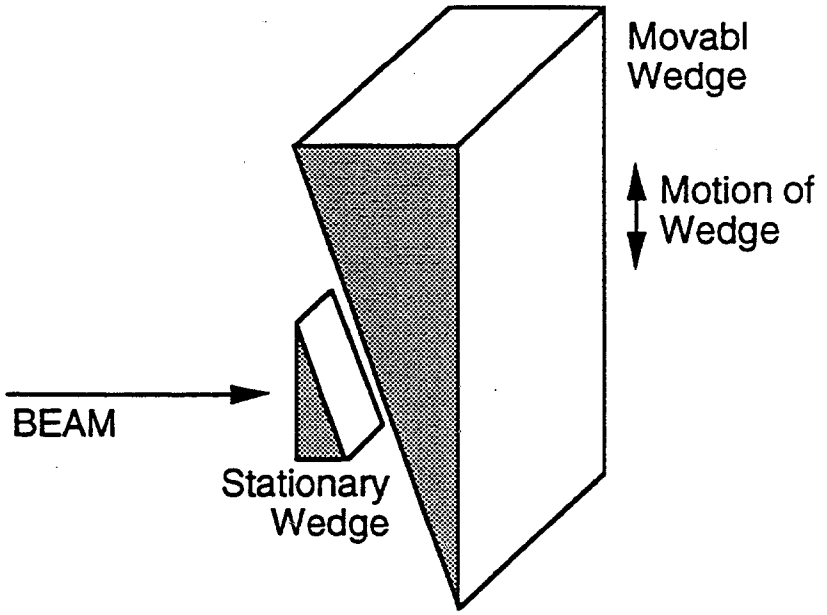

Fig. 18. Schematics of a double wedge system which is used to shift the range of the beam.

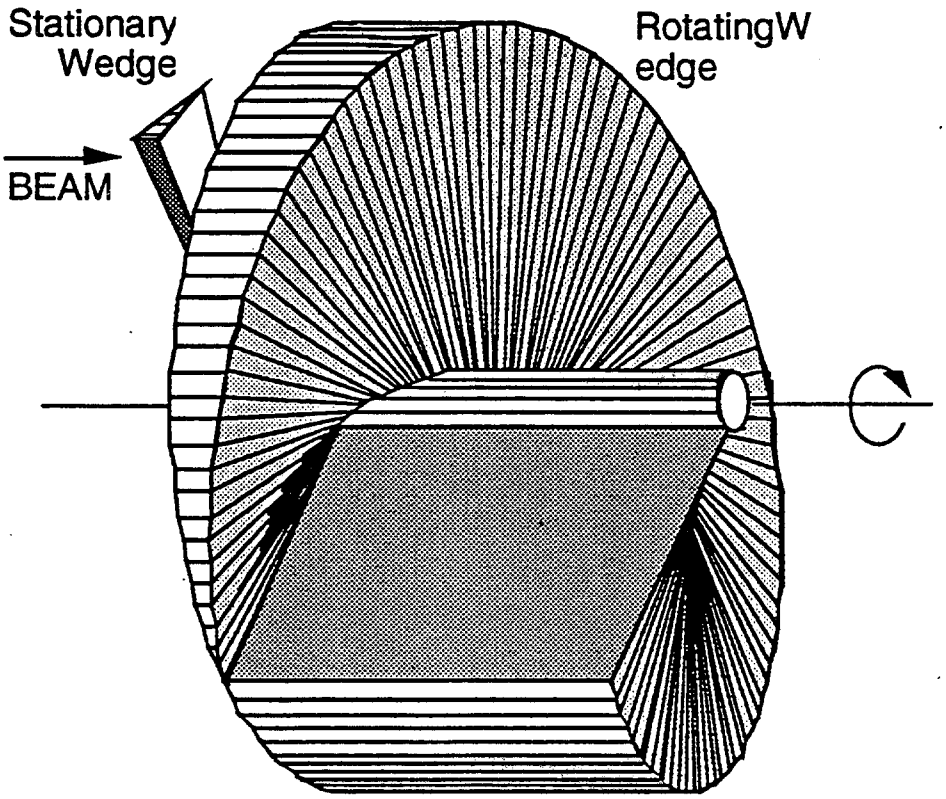

Fig. 19. Schematic drawing of a circular wedge used to reduce the size of the double wedge system. The thickness of the absorber is a function of angular displacement. The beam penetrates off-axis of the device.

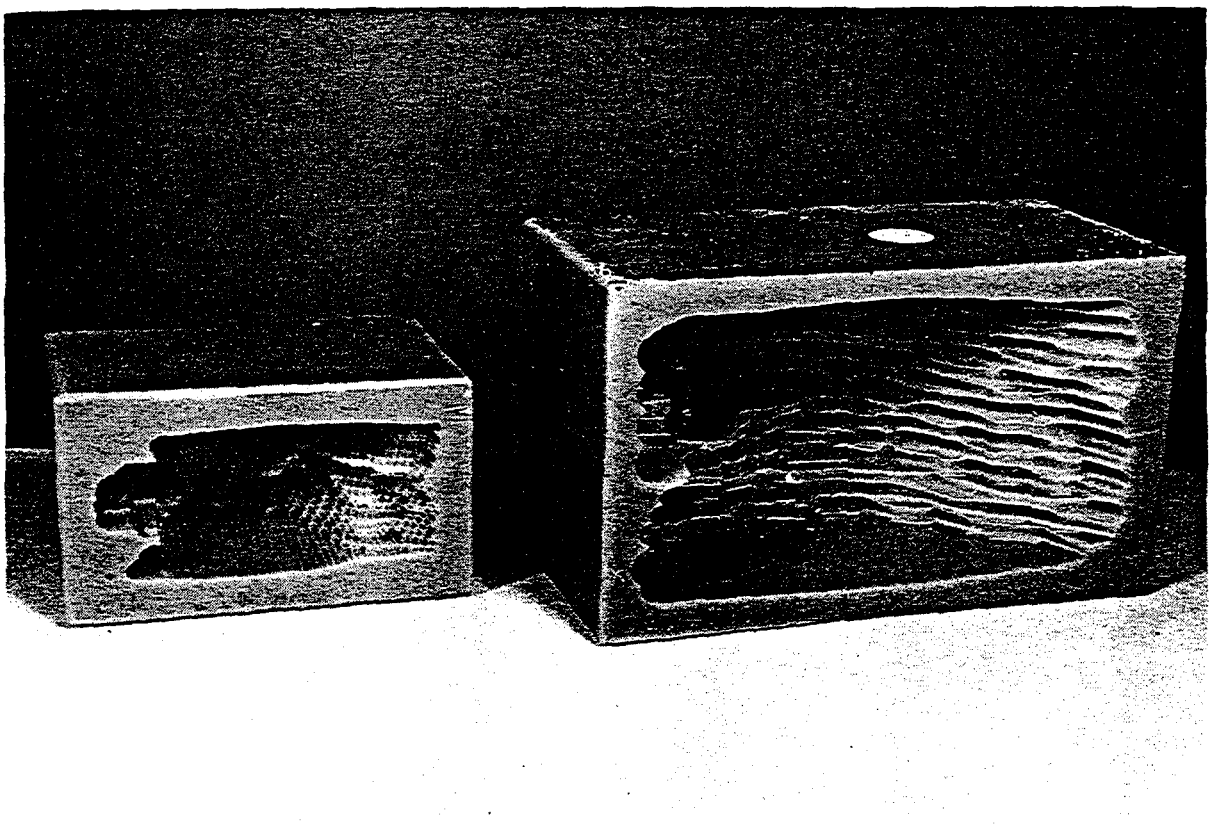

Fig. 23. Picture of compensators cut out of a hard wax block. (CBB 875-3748)

II.A.5.a. Off-line beam-range measurements

A measurement of the range of a beam can be made using a water column or binary filter along with two dose detectors, such as transmission ionization chambers. One detector placed upstream of the degrader measures the incoming beam. The second detector placed immediately downstream of the degrader measures the ionization of the exiting beam. The ratio of the two measurements as a function of the degrader thickness yields the relative ionization of the exiting beam. A Bragg ionization curve is measured if the beam is monoenergetic. The beam range can be deduced from the absorber thickness where the Bragg peak occurs. For a modulated beam, the range, usually in water, may be defined for clinical purposes as the depth of the distal line of 90% of the isoeffect contour. Alternatively, it may be defined operationally as the water depth of the position in the distal dose falloff where the relative ionization is 50% of that of the peak, *i.e.*, the peak position plus a portion of the width of the distal falloff due to the range straggling. If there are other absorbing material, including the air space, between the water column and the patient, their range-modifying characteristics must be included in the computation of the residual range in the patient.

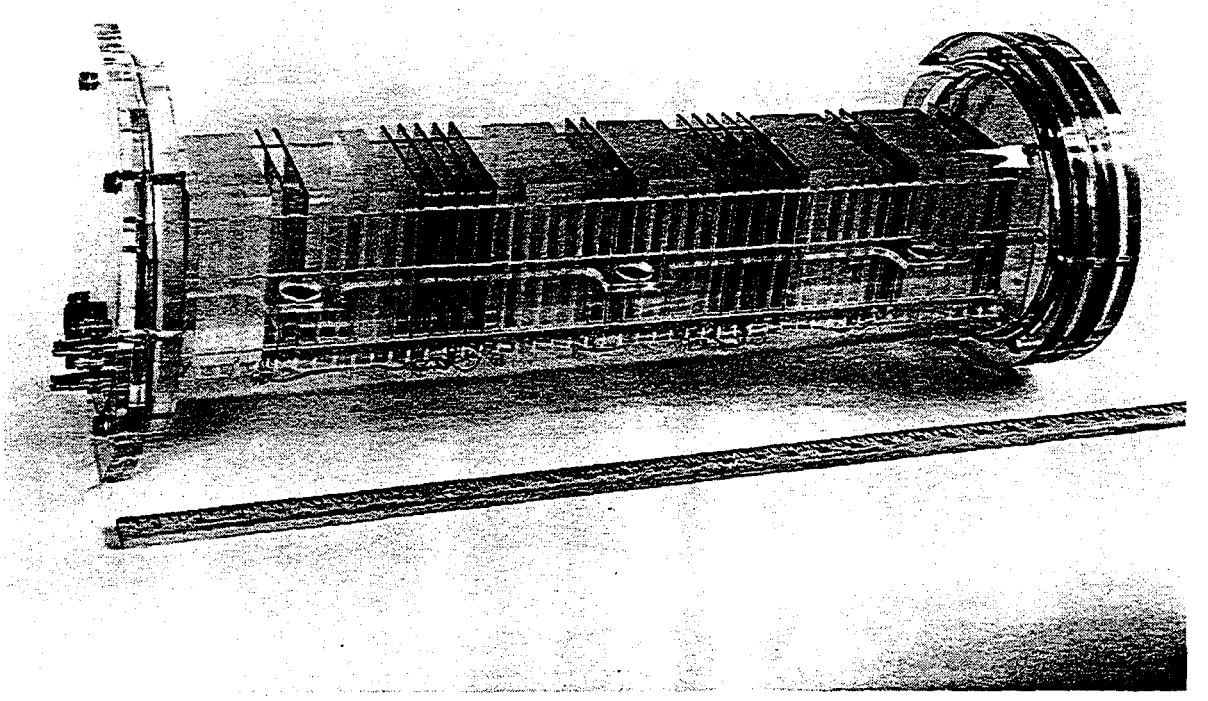

Fig. 24. The Bragg curve telescope measures a Bragg curve at several points using a series of ionization chambers, which are interspersed by pieces of material of known water-equivalent thickness. (CBB 874-5230)

An alternative method for obtaining the range is to measure a depth-dose distribution in a water phantom. Here a small detector, either an ionization chamber or a diode, is moved in a volume of water and its readings are normalized to the incoming beam. It is important that the size of the detector be small compared with the field so that the change in dose as a function of depth is not dominated by the effect of the beam divergence.

A plastic scintillator can also be used as a range detector. In a device developed at LLUMC, the beam is stopped in a scintillator block and the output of light as a function of depth is viewed by a CCD camera.[143] The light output is related to the energy loss of the beam, but is not exactly proportional to dose. Therefore, a calibration procedure is required to map the light output into a dose distribution. Its main advantage is that the entire range measurement can be done at once; however, the drawback is that such a device can be large, since the scintillation in the block must be optically imaged

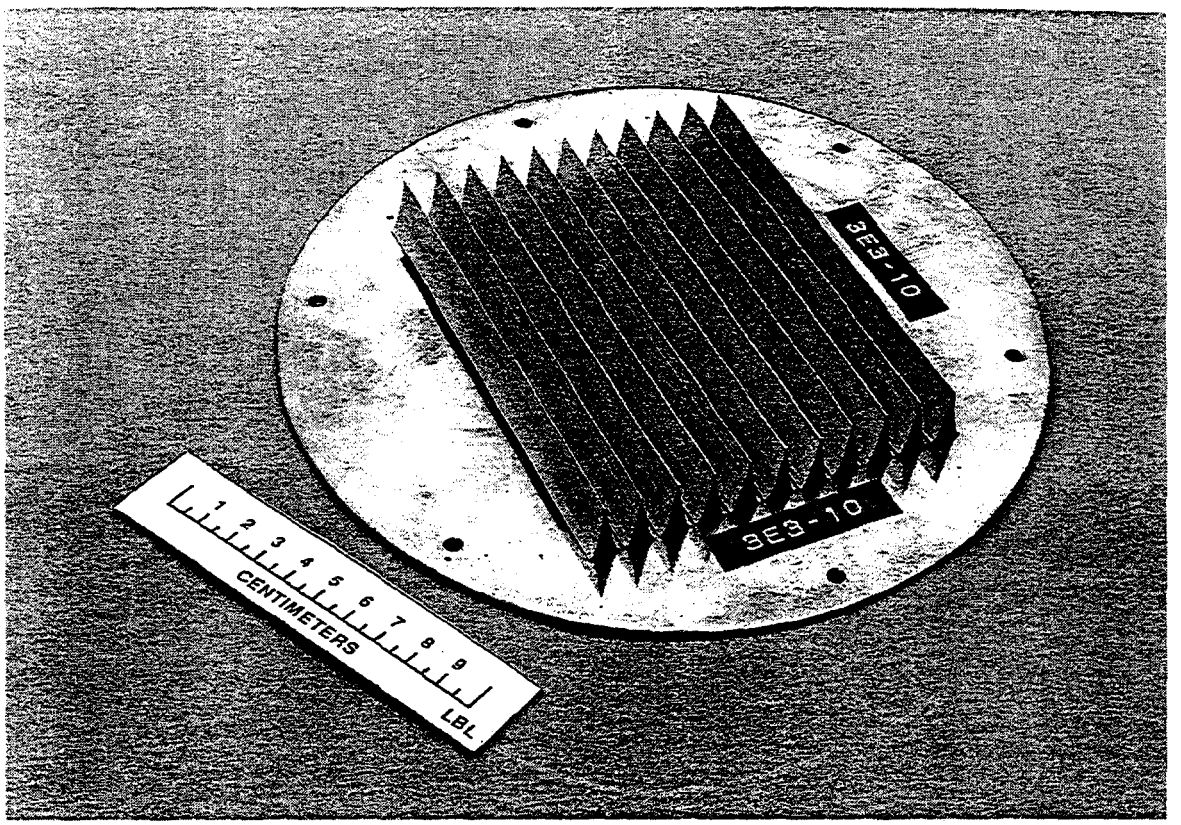

Fig. 31. A brass bar ridge filter for modulating the range of the Bragg curve is shown. This device is primarily used with the heavier ions where multiple scattering in the brass is less than for protons. Multiple scattering accounts for the lateral spreading of the different range particles over the target volume. (CBB 901-257)

$$\int_0^T F'(t)\,dt = 1 \tag{16}$$

where T is the maximum filter thickness. For $F'(t)$, a bi-exponential form is assumed, viz.,

$$F'(t) = A\left(Be^{-cT} + e^{-dT}\right) \tag{17}$$

The ridge shape is given by:

$$F(t) = -A\left(\frac{B}{c}e^{-cT} + \frac{1}{d}e^{-dT}\right) \tag{18}$$

For a neon-ion beam of an energy per nucleon of 585 MeV, the parameters used at LBL for the filter design were: B = 4, c = 0.4 (cm water equivalent)$^{-1}$, and d = 0.008 (cm water equivalent)$^{-1}$. A set of bar ridge filters of bi-exponential form for SOBP width of from 4 cm to 15 cm at a step size of

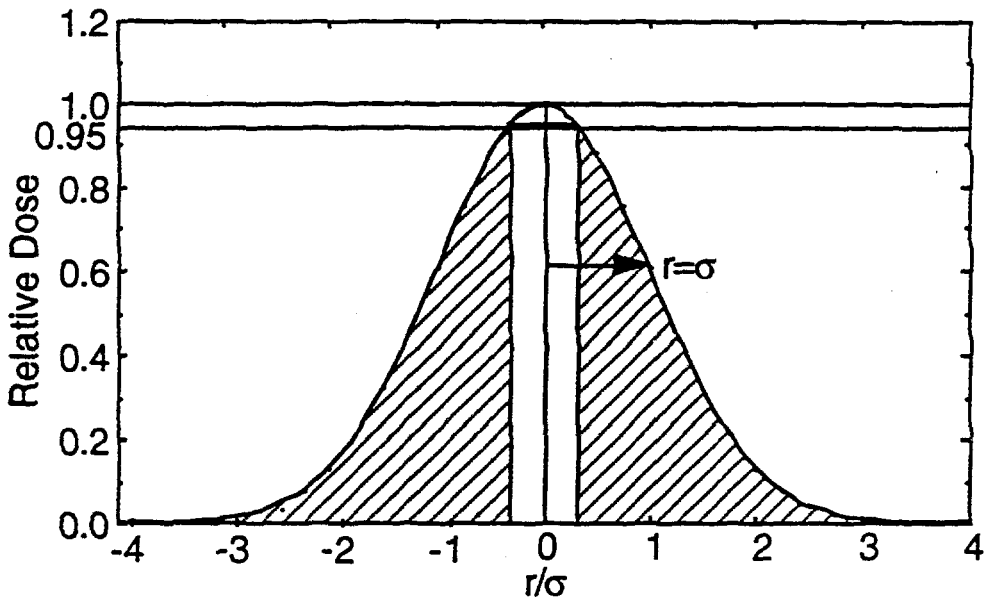

Fig. 34. A pencil beam passing through a thin scatterer results in a Gaussian-like dose distribution. A dose accuracy of ±2.5% is obtained if the beam outside of $r \geq 0.32\ \sigma$ is collimated out as shown in the hatched areas in the figure.

and also that, contrary to widely held views, Molière theory is valid for mixtures, compounds and thick targets (up to thickness of ≈97% of the mean proton range).[320]

A narrow pencil beam scattered by a thin scatterer produces an approximately 2-dimensional Gaussian dose distribution at isocenter.[321] Here a scatterer is called thin when the kinetic energy of the particle does not change significantly by traversing it. The dose distribution as a function of the radial distance, r, from the central axis is

$$D(r) = \frac{1}{\pi \bar{r}^2} e^{-\left(r^2/\bar{r}^2\right)}, \tag{21}$$

where $\bar{r}$ is the rms radius of multiple scattering, and is related to θ_0 above as

$$\bar{r} = T\left\langle \theta^2 \right\rangle^{1/2} = T\theta_0/\sqrt{2}, \tag{22}$$

where T is the drift-space distance from the scatterer to the isocenter. If the dose profile D is assumed to be strictly a Gaussian with a standard deviation σ, and the clinical requirements limit a dose variation to ±2.5%, only those particles near the central ray within the radius where the dose is ≈95% of the peak dose can be used. These particles provide a dose distribution of 97.5 ± 2.5% as

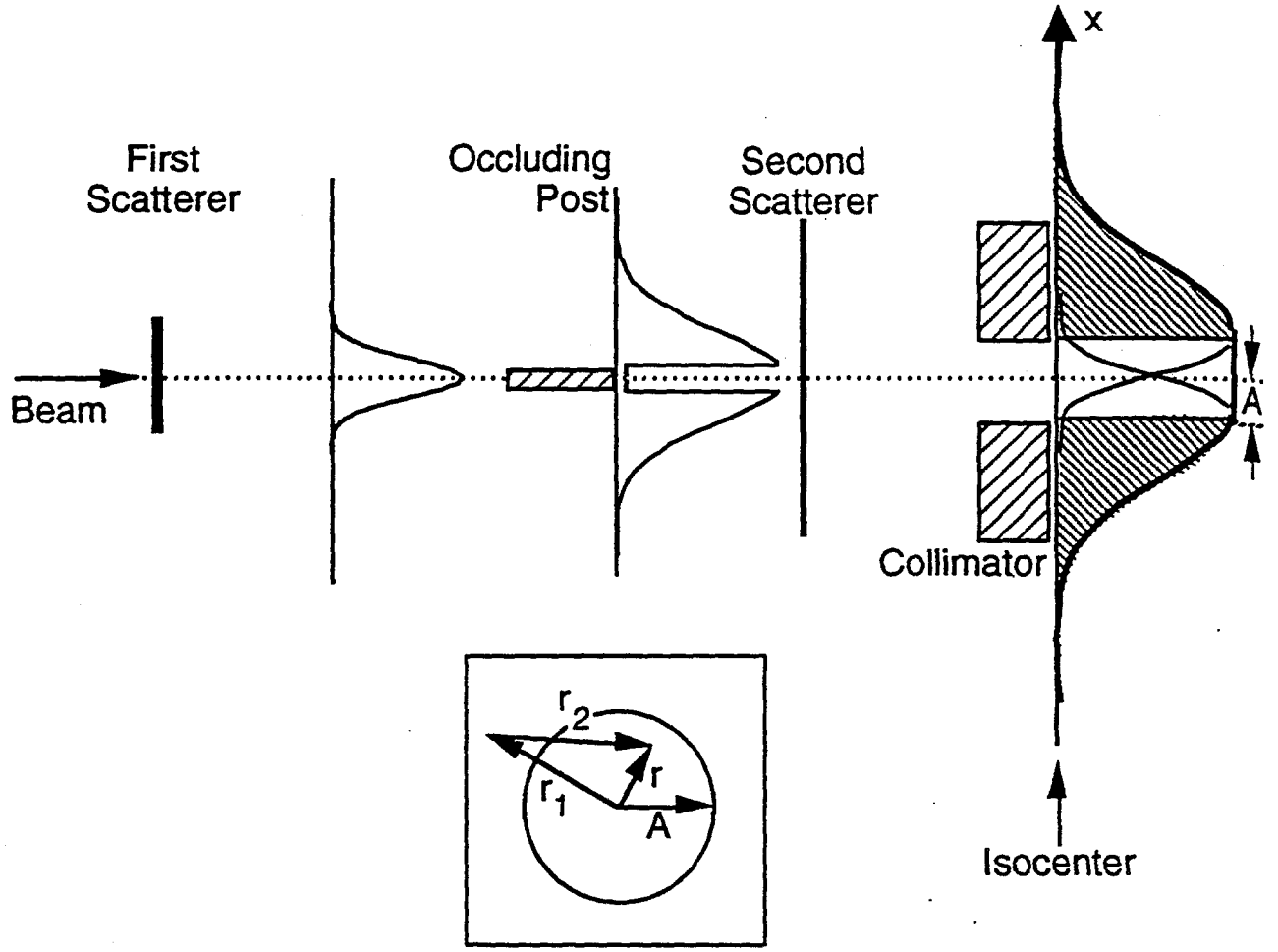

Fig. 35. Schematics of a double-scattering method using a central post occluder. The beam profiles downstream of the first scatterer, passed the occluding post, and at the isocenter are shown. The relationship between the size of the flat field at the isocenter (A), and the two scatterers is discussed in the text. In the lower figure, projected field at the isocenter is shown: the projected radius of the occluder is A, the beam enters at the center axis, the first scatterer scatters it by r_1 if there were no second scatterer, the second scatterer scatters it by r_2, and the net displacement is r.

For an occluding post, whose projected radius is A at the isocenter, the integration of Eq. (23) is for $\rho > A/R_2$. In one such system developed at HCL for the 180-MeV proton beam, the choice of two scatterers with $R_1 = 1.7A$ and $R_2 = 1.3A$ produced a flat proton field of a radius out to 1.5×A with a ±2.5% dose deviation.[322]

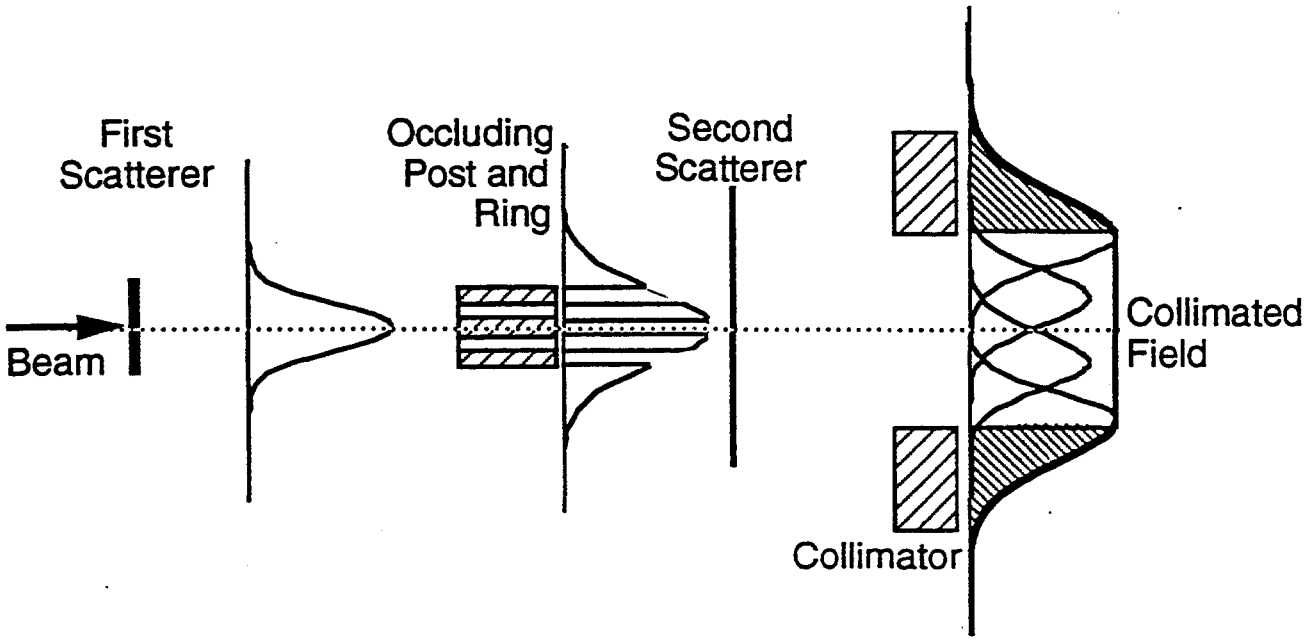

Fig. 36. Shown is the uniform field created using an annular ring plus a post occluder assembly.

For a broader beam, a simple annulus occluder can be used. The beam through the central opening and that outside the occluder will be transmitted. The dose profile in a plane through the central ray exhibits three peaks. When scattered by the second scatterer, the broadened three peaks fill the annular dose void and produce a large flat-dose area at the isocenter. For example, such a double-scattering system designed at HCL for 250 MeV proton beams, with a distance of 3 m from the first scatterer to the isocenter, produced ±2.5% flatness in a circular treatment area of ≈25 cm useful radius with ≈23 cm water-equivalent residual range.[323] PARMS at Tsukuba has also used a single annulus system to spread their 250-MeV vertical proton beam.[267]

A flat dose of even larger area can be obtained by using a set of annuli and/or post occluder system as shown in Fig. 36. Such a system was used at LBL to broaden a neon-ion beam of an energy per nucleon of 670 MeV to a flat field of a diameter of 20 cm. Successively larger-area dose fields could be obtained by increasing the number of annular rings of increasing radii. A practical limit is reached when the beam utilization efficiency drops too low to perform a treatment in a reasonable time, *i.e.*, several minutes.

In making large flat fields, a large portion of beam particles is stopped in the occluder as well as scattered into the collimators. Suppose the beam intensity profile at the isocenter in the absence of the occluder is $\Phi(r)$, where r is the radial distance from the central axis; $\Phi(r)$ is typically a Gaussian as shown in Fig. 37(a). Making a flat field of radius R, using the occluders is approximately

different materials of very different atomic numbers, for example, plastic and lead (see Sec. II.C.1.c below).[326, 327]

Another practical point to note is that the double scattering method requires thick scattering foils, which produces secondary particles for beam particles with Z>1, which lowers the peak-to-plateau ratio and raises the dose beyond the Bragg peak. These fragments also lower the RBE and raise the OER values, thereby lowering the biological advantage.[328] As discussed above, the beam utilization efficiency is low, typically 20%. The low efficiency implies that a large portion of radiation is absorbed in the occluder, as well as in collimators and scatterers, resulting in increased background radiation in the treatment room. This becomes a serious problem when a double-scattering system must be placed near the patient, such as in the case of mounting it on a rotating gantry. Shielding needed to block unwanted radiation may become unacceptably heavy.

II.C.1.c. Bi-material scattering

The different scattering characteristics of heavy charged particles for different atomic-mass scatterers may be exploited in the preparation of therapy beams. A high atomic-mass material scatters more with little range loss; whereas, a comparable low atomic-mass material scatters little while modulating the range more. A pencil beam is laterally spread out to a Gaussian-like beam spot and is made to impinge upon the second scatterer. In order to flatten the field, the rays near the

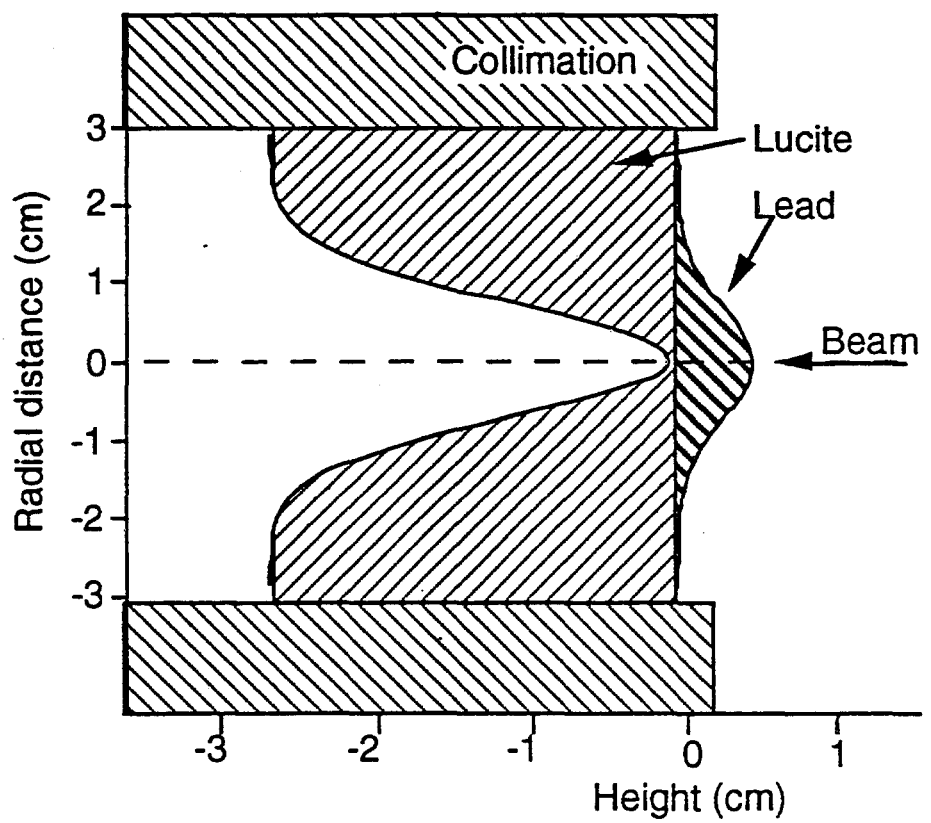

Fig. 39. Shown is a schematic representation of the cross-section of a bi-material filter for beam spreading. (Courtesy of Dr. B. Gottschalk, HCL.)

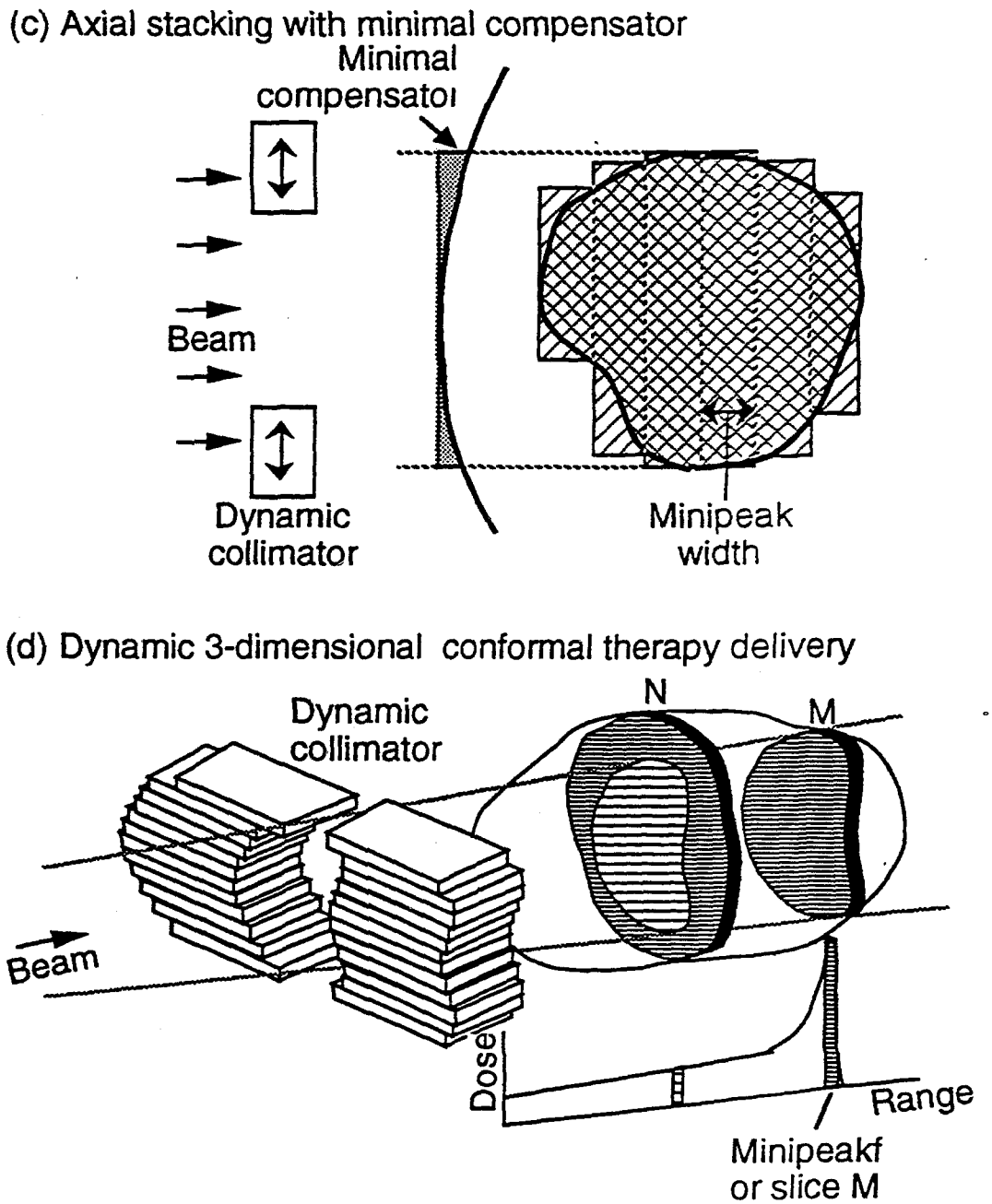

Fig. 49. (c) Axial stacking with a variable-speed raster scanning technique. (d) Schematic illustration of a 3-dimensional conformal therapy delivery.

non-physical quantity used as a descriptive clinical parameter and has a dimension of dose-volume. Improvements to the dose distributions offer improved tolerance to treatment and may allow an increase in the effective tumor dose with a resulting increase in the probability of tumor control. Lyman and Petti have performed treatment planning comparisons of the fixed versus variable Bragg-peak modulations in targets involving the prostate.[377] Based on the analysis of dose-volume

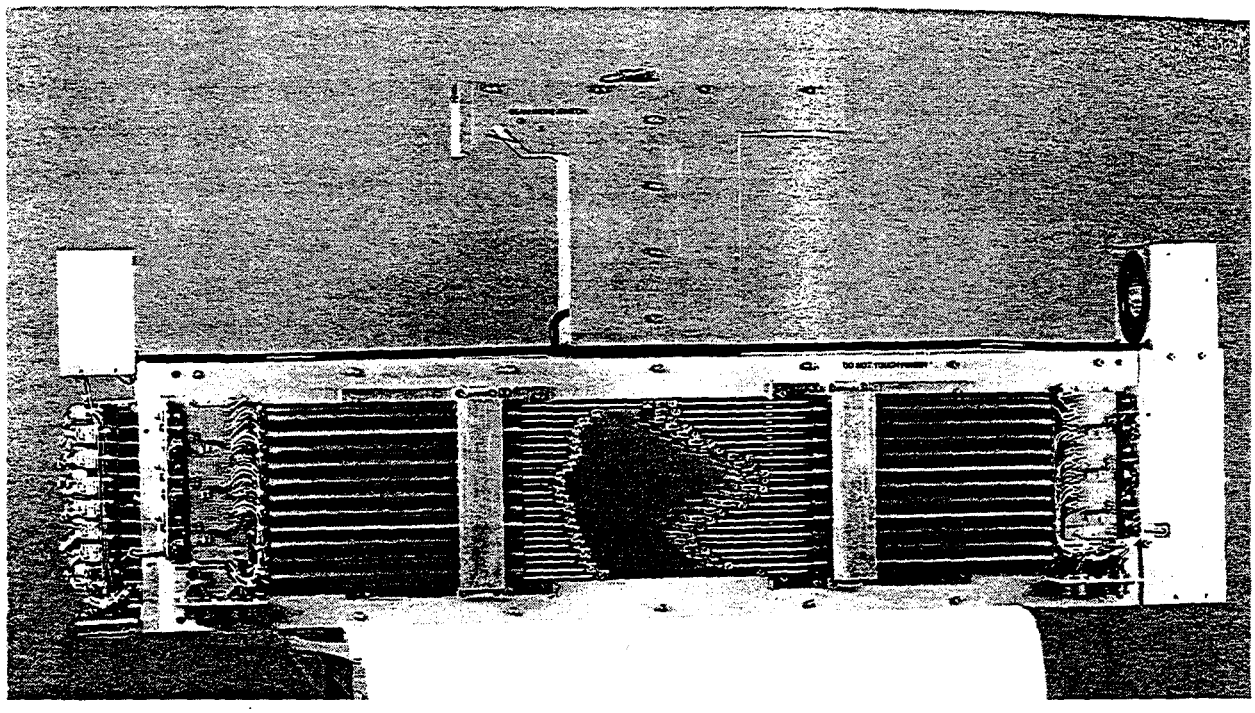

Fig. 55. A multileaf collimator are used with dynamic conformal radiotherapy to allow dynamic shaping of the radiation field to the tumor volume. (CBB 919-7469)

During a line scan, the slit is aligned with the scanning beam, and the radiation field is collimated to a rectangular shape of a specified length by the slit and the end blocks which are moved to the desired positions At the completion of a given line scan, the patient is moved to a position where the next line-scanned beam is aligned with the doses already delivered in preceding line scans. Repetition of this process produces an irregularly shaped radiation field in two dimensions. If the end blocks are made to rotate around pivots in such a way that their collimating edges align with the curved boundaries of the irregular port, the resulting irregular port shape conforms more closely to the target shape. This type of dynamic collimator has three controls: one for the patient motion and two for the linear motions of the end blocks. The pivoted version would require two additional controls for the angular displacements of the end blocks. The system can be adapted to two-dimensional scanning, in which the patient remains stationary and the line scans are moved across the patient.

An example of a variable aperture collimator is the multileaf collimator which defines irregular shapes by means of many movable absorber bars, called leaves or fingers. A multileaf collimator, whose leaves are manually moved, has been developed and used at NIRS.[394] Shown in Fig. 55 is

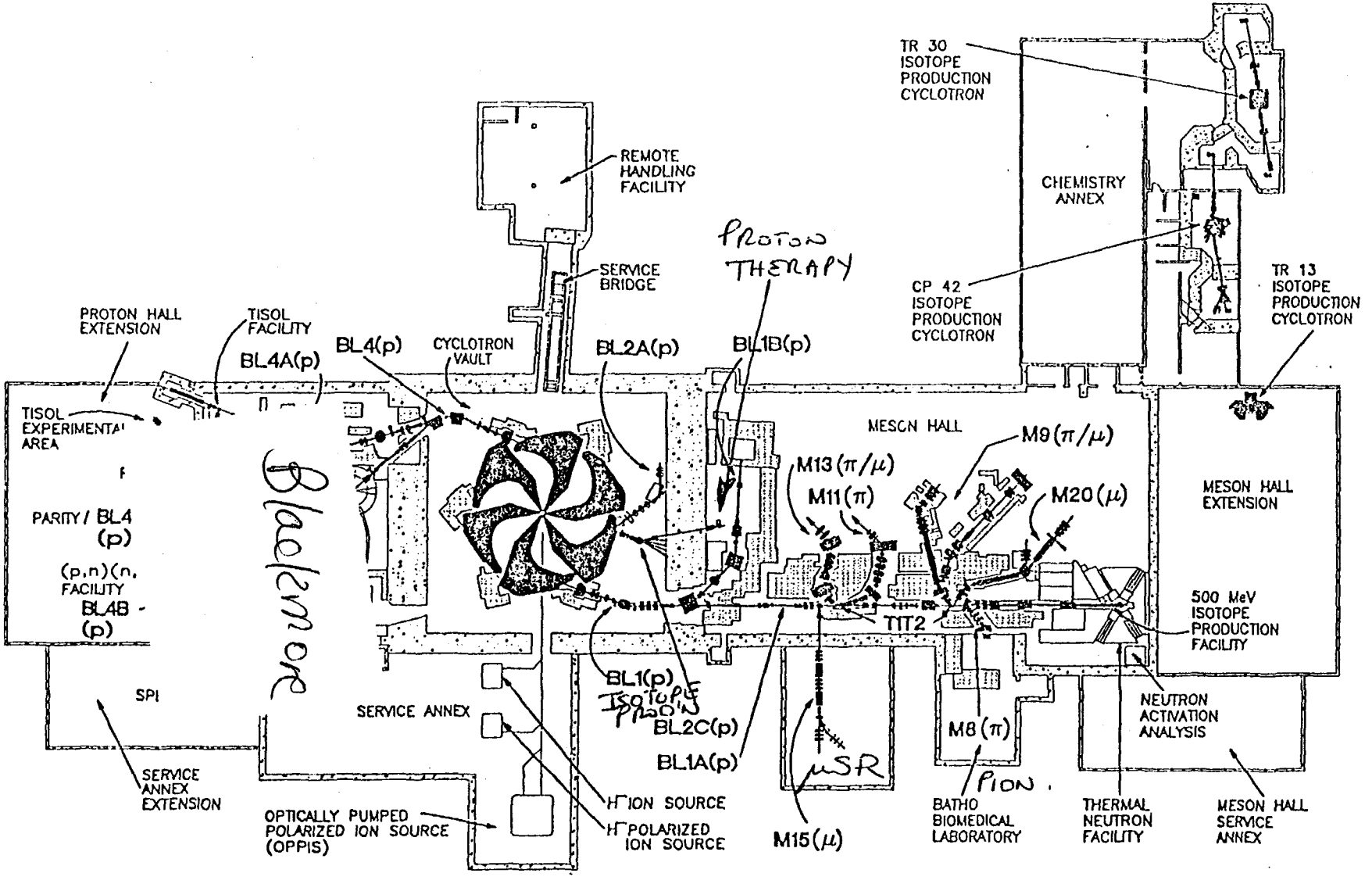

Fig. 2. Layout of the TRIUMF cyclotron(s) and beam lines

ESTIMATED USAGE OF SELECTED RADIOISOTOPES BY YEAR
(Curies)

Nuclide	$t_{\frac{1}{2}}$	Retail Consumption 1982	Retail Consumption 1987	Retail Consumption 1990
$^{99}Mo/^{99m}Tc$	66 h/6 h	100,000 (^{99}Mo)	120,000	150,000
^{111}In	68 h	150	160	185
^{123}I	13.2 h	75	1,250	3,100
^{127}Xe	36.4 d	100	100	100
^{133}Xe	5.2 d	25,000	25,000	45,000
^{201}Tl	73 h	500	2,500	6,000

Fig. 3. Useage of radioisotopes

Radioisotopes at TRIUMF

Commercial: Nordion International

^{201}Tl, ^{123}I, ^{67}Ga, ^{111}In, ^{57}Co

$^{82}Sr/^{82}Ru$ generator

PET: Neurodegenerative Disease Program

^{18}F (FDG, FDOPA), ^{11}C (Raclopride), ^{15}O, ^{13}N

Radioisotope/Radiopharmaceutical Development

^{188}Pt, ^{178}W, ^{97}Ru, ^{67}Cu, ^{127}Xe, $^{122}Xe/^{122}I$ generator

Target Preparation

^{22}Na, ^{44}Ti

Fig. 4. Radioisotopes produced at TRIUMF

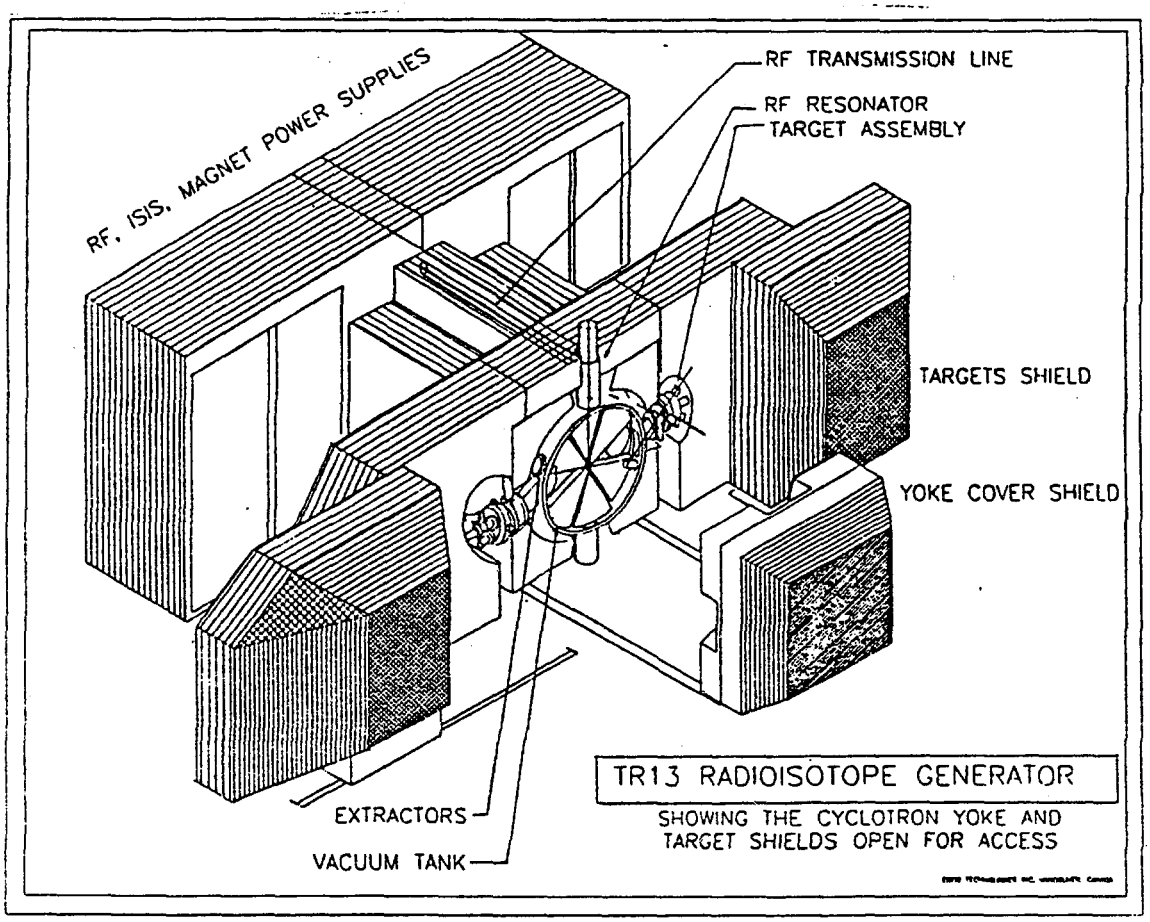

Fig. 5. Design of the TR13 - 13 MeV Cyclotron

TEST BEAMS at TRIUMF

Calibration, efficiencies, particle ID, high rate studies

- protons, neutrons to 500 MeV (1.10 GeV/c)
- pions, muons, electrons to 0.4 GeV/c (tagged)
- energy resolutions $\approx$ 1% or better
- secondary beam rates 10^2 to 10^8 particles/sec

Radiation Damage Studies

- protons to 10^9 rads/cm^2 per week
- proton fluxes between 10^5 to 10^{10} p/cm^2/sec
- uniform proton irradiations over areas of 10x10 cm^2
- some neutron irradiation capability
- proton and neutron energies in range of interest for space applications and TeV collider radiation damage

SOME APPLICATIONS USING TRIUMF BEAMS

Radiation Damage/Detector Studies

- TRIUMF - study of radiation damage to permanent magnet materials
- TRIUMF - study of radiation damage to magnet coil insulation
- Sandia - radiation hardened electronics
- Boeing - single upset rates in I.C.s
- U of Sask.- Calibration of SALAD detector with protons
- BNL/RHIC - CsI, PbF, BaF_2 crystals with 300 MeV/c e, π beams
- Tau/charm - CsI crystal tests
- BNL E787 - lead glass radiation damage
- SSC - diamond detector studies
- SDC/Santa Cruz - radiation damage in silicon microstrip detectors

Fig. 6. Radiation damage and detector R&D applications

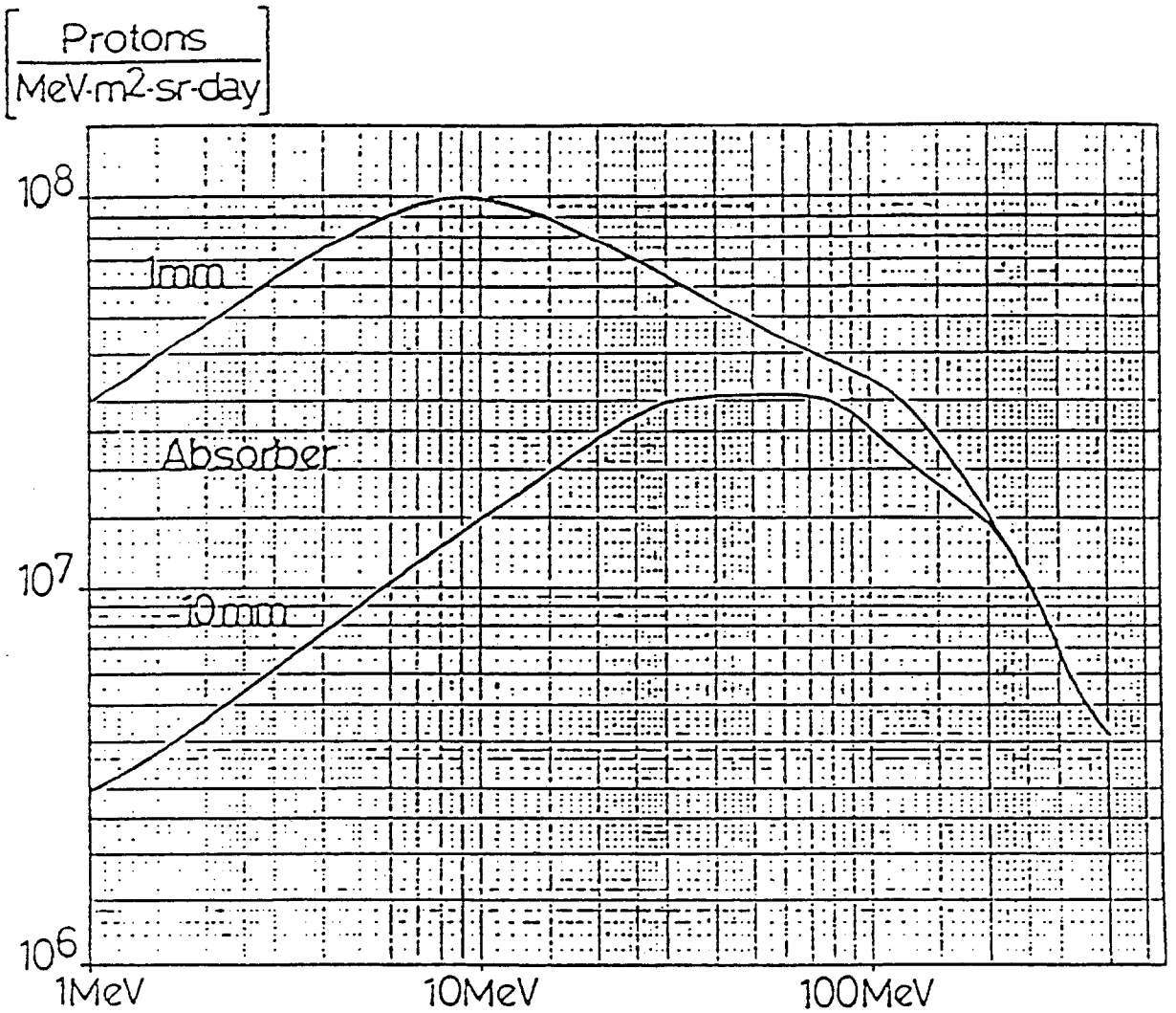

Fig. 7. Differential energy spectrum of trapped protons for 850 km 88.8° inclination.

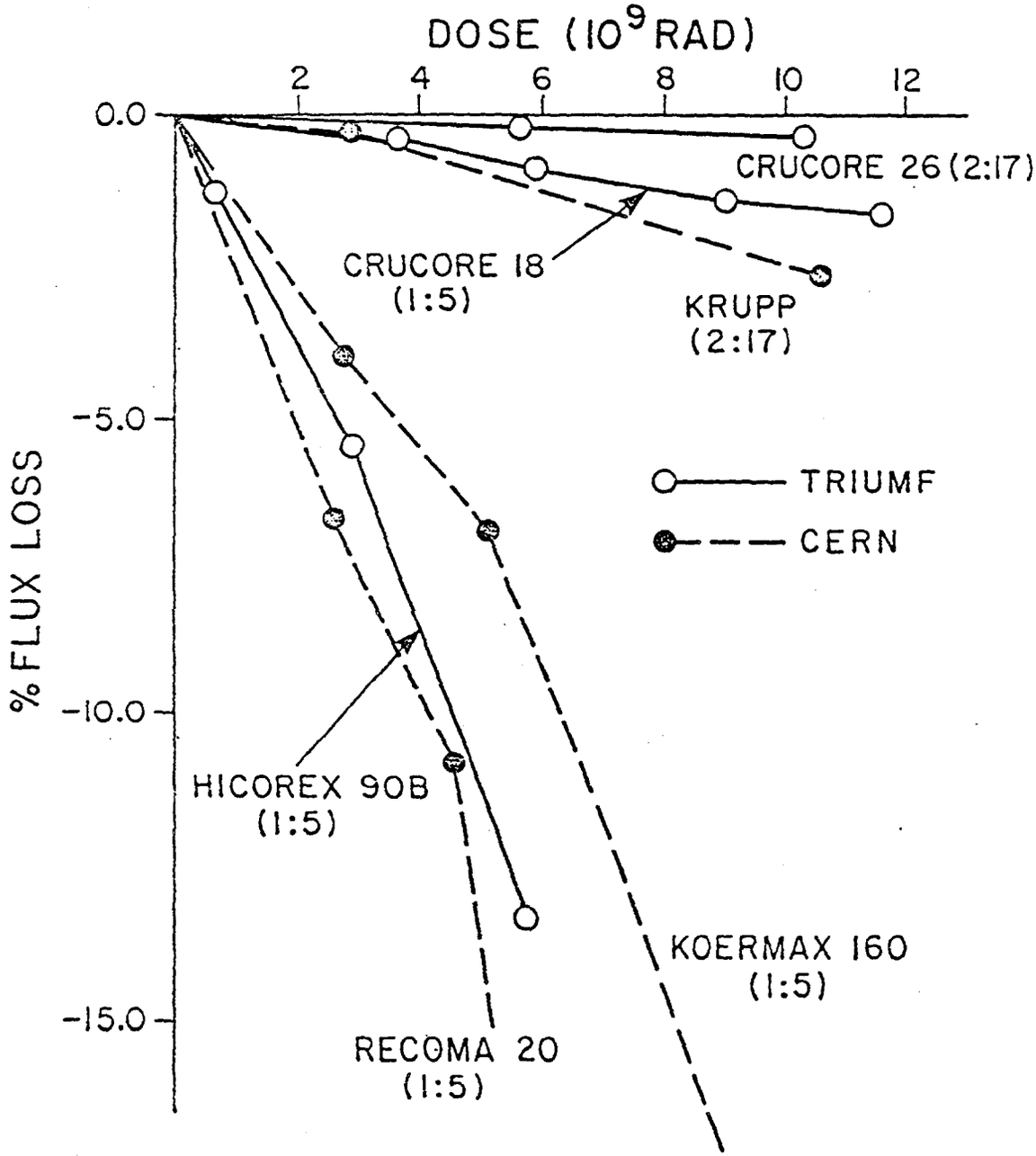

Fig. 8. Radiation damage of samarium-cobalt permanent magnet samples

Pion Therapy

Since 1982

$2 \times 10^8 \pi^-$/sec @ 180 MeV/c.

	1992
Total number of patients	306
no. of sites treated:	
Brain (Glioblastoma)	137
Pelvis (Prostate)	147
Leg	5
Groinskin	1
Nasopharynx	3
Chordoma	1
Schwanoma	1
Parotid	3
Meningioma	2
Temperal Bone Adeno CA	1
Melanoma Rt. Antrum	2
Adenoca L Middle Ear	1
Skin Nodule Trials	11
Total number of sites	315
Phase three - randomized trial patients	
Brain	
- Photons	32
- Pions	31
Total	63
Total no. required for trials	82
Prostate	
- Photons	54
- Pions	69
Total	123
Total no. required for trials	200

Fig. 9. Number of patients treated using pions at TRIUMF

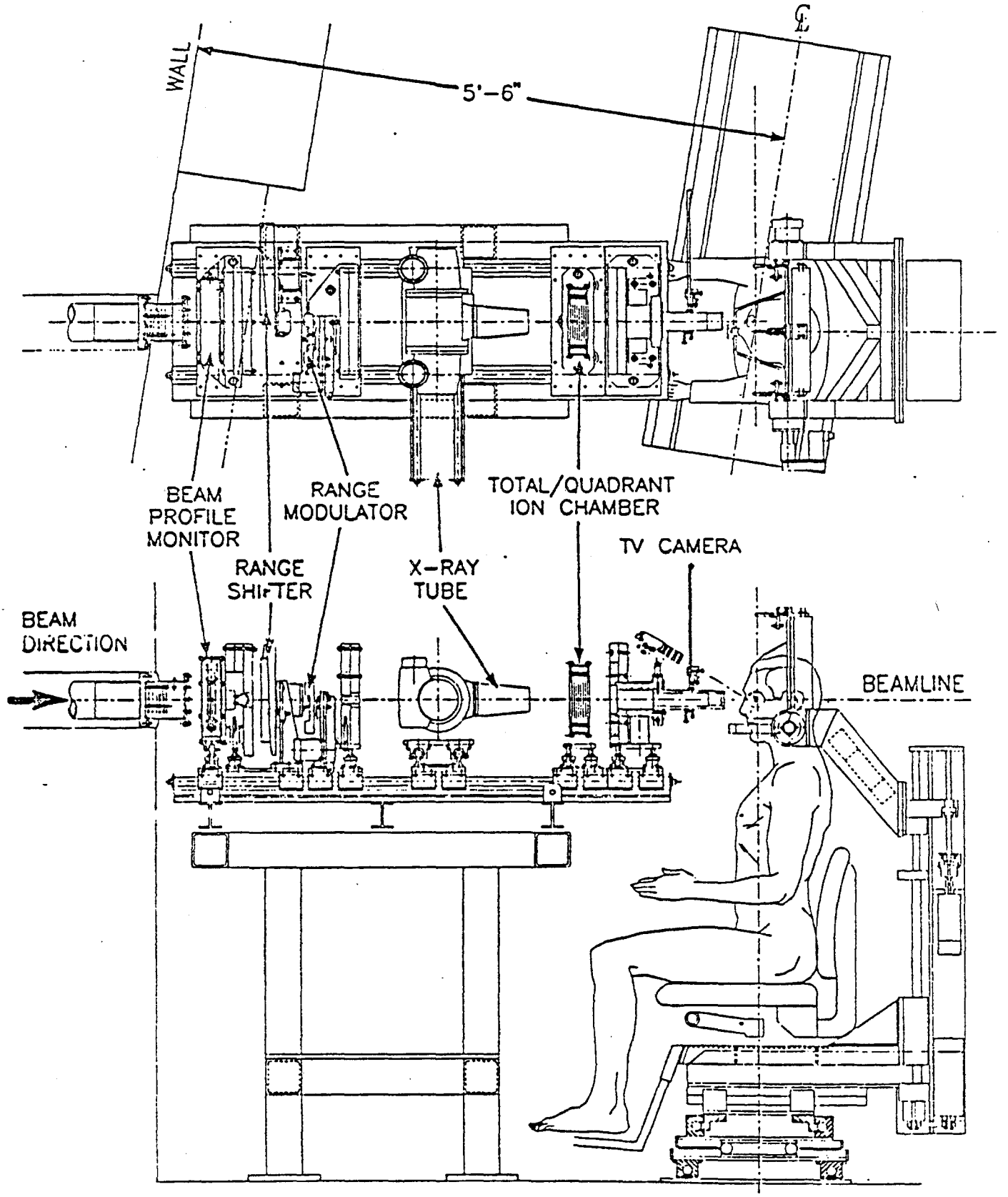

Fig. 10. Arrangement of eye therapy proton beam delivery system

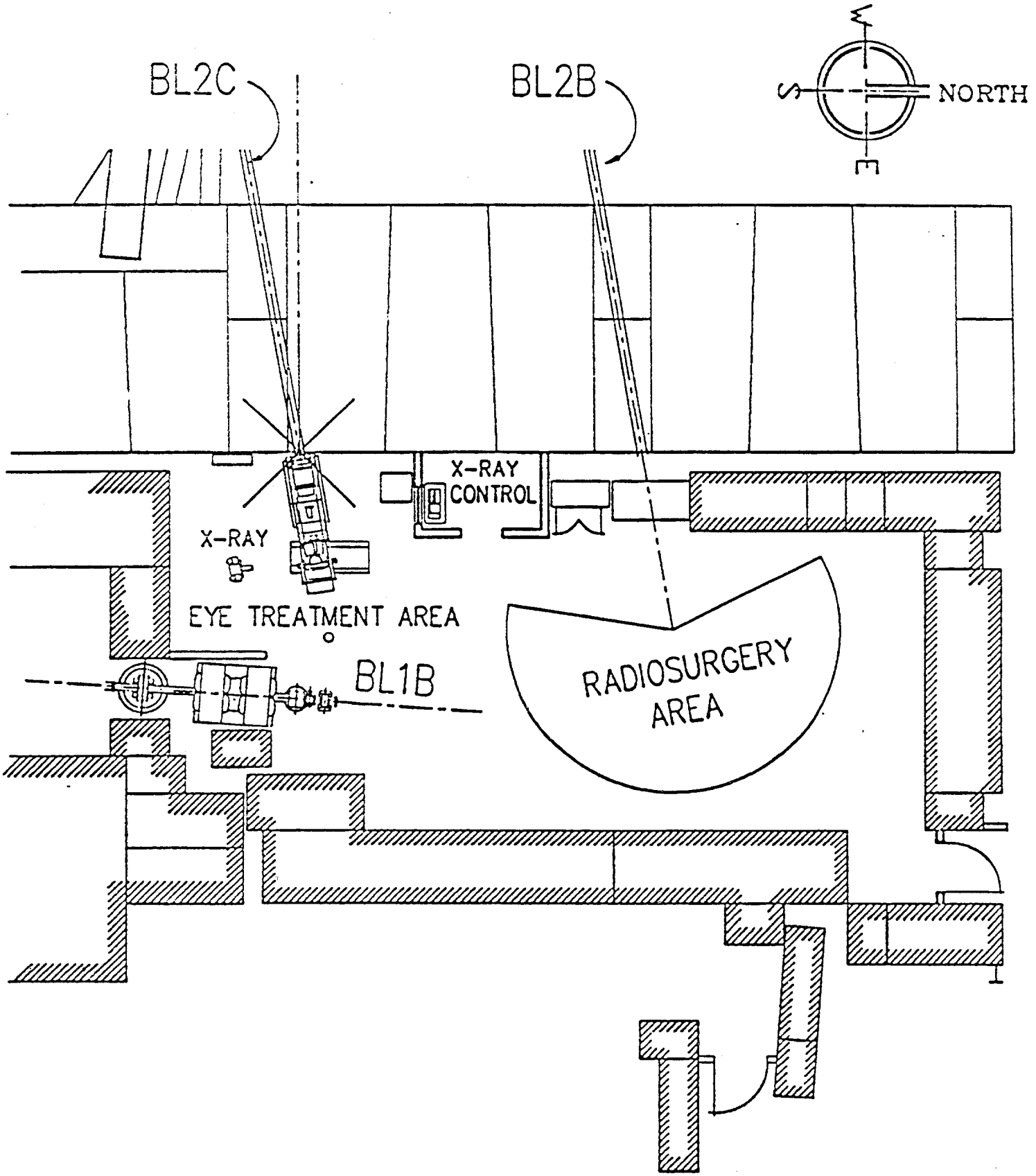

Fig. 11. Layout of the combined eye treatment and radiosurgery area.

PROTON RADIOGRAPHY

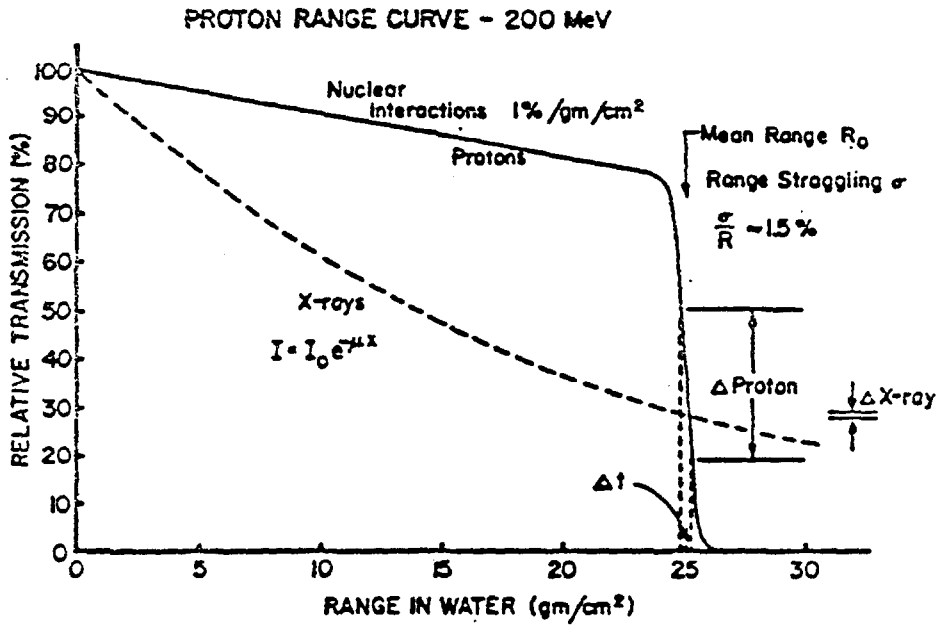

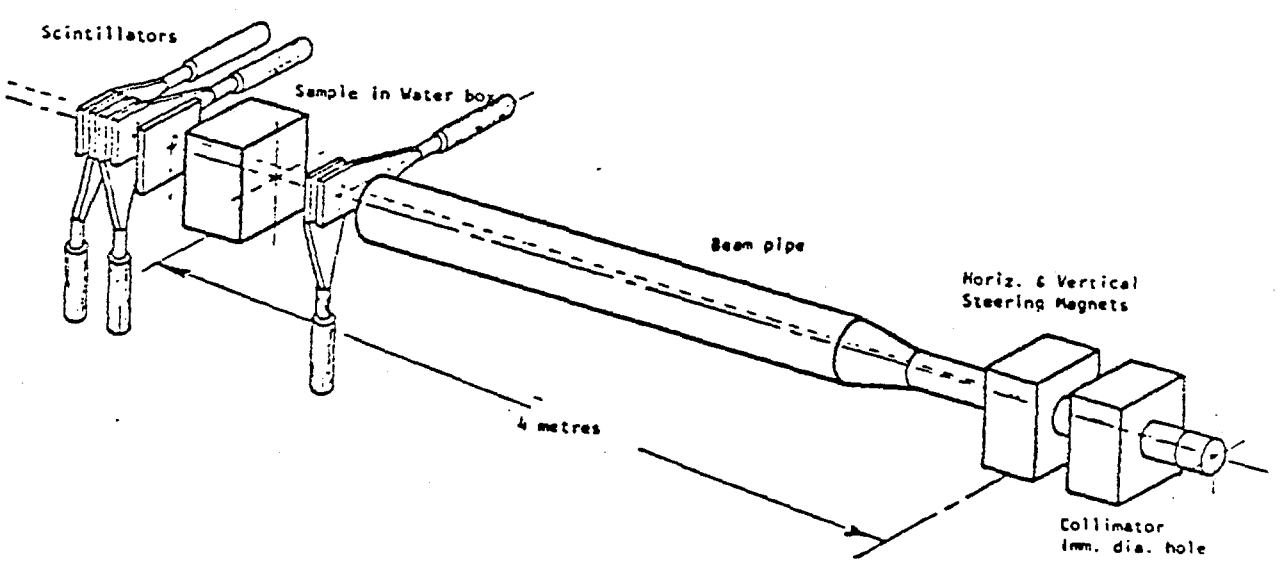

Fig. 12. Schematic arrangement for scanned beam proton radiography

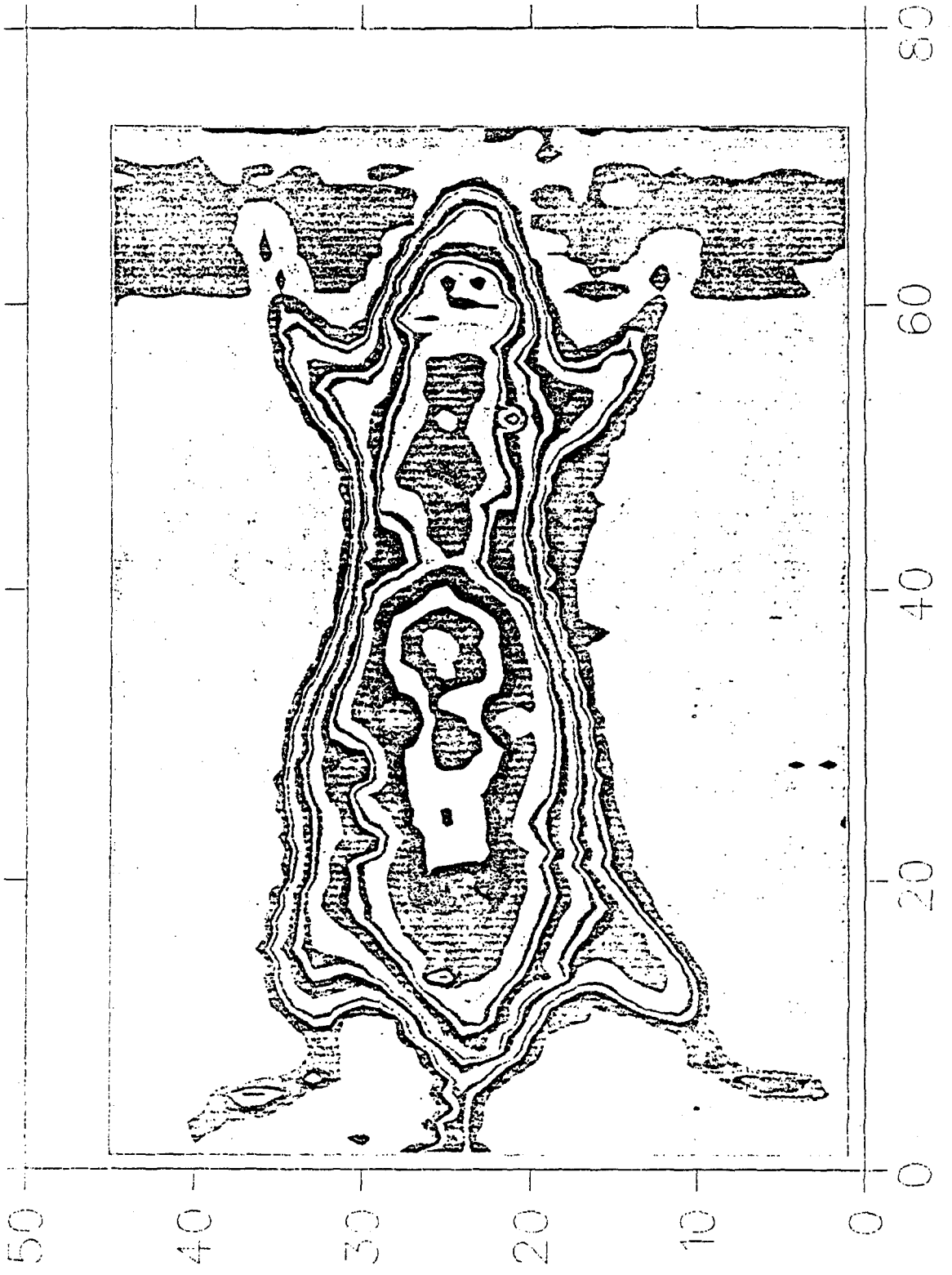

Fig. 13. Contour plot of mouse taken with 200 MeV protons.

(Prof. U. Amaldi)
Prof. G. Tosi

HADRONTHERAPY PROJECT

OF THE ISTITUTO NAZIONALE DI FISICA NUCLEARE (INFN)

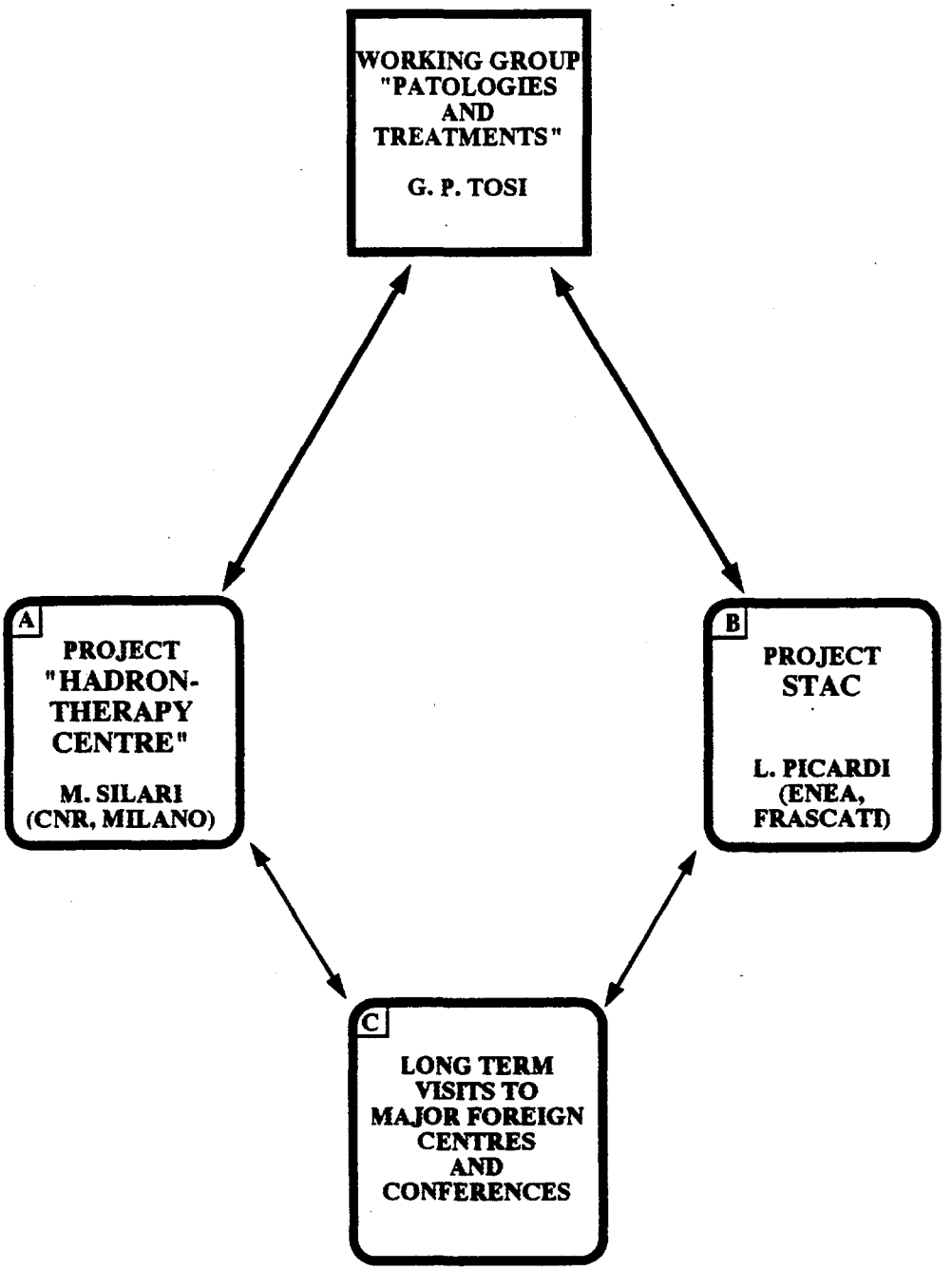

STAC = SYNCHROTRON TECHNOLOGICALLY ADVANCED and COMPACT

Category A: pathologies characterized by the proximity to highly critical structures:
- uveal melanomas;
- chordoma and chondrosarcoma of the base of the skull;
- paraspinal and spinal tumours;
- parasellar meningioma;
- craniopharyngioma;
- optic nerve glioma;
- acoustic nerve schwannoma;
- arterovenous malformations;
- hypophysis adenoma.

For these pathologies the use of proton beams is the only way to administer a radical dose without producing serious side effects.

Category B: pathologies characterized by a local evolution and by a low radiosensitivity:
- prostatic cancer
- retroperitoneal sarcoma;
- indifferentiated tumours of the thyroid gland;
- uterine cervix cancer (IIB bulky or IIIB)
- rectal cancer (advanced)
- salivary gland tumours.

For these pathologies traditional radiotherapy already obtains good results which can be however improved by the administration of higher doses.

Category C: pathologies for which the main indication for the use of protons is the boost on a restricted volume:
- head and neck cancer;
- low grade glioma;
- malignant thymoma;
- biliary tract tumours;
- lung tumours not microcitoma;
- oesophagus tumours;
- some pedriatic tumours (sarcomas, CNS).

The use of protons for the whole treatment of these pathologies is less interesting because the required irradiation volume is often characterized by a large safety margin including regions of potential diffusion where doses of about 50 Gy are considered adequate. The high probability of distant metastases or rapid unfavourable evolution requires a selection of the cases based on the initial response of the tumour to the irradiation.

Category D: locally advanced pathologies with unfavourable prognosis but which can allow a long survival with heavy symptomatology:
- pancreas cancer;
- local recurrence of rectal cancer;
- high grade glioma;
- isolated cerebral metastasis;
- paraorthic metastatic adenopaties;
- pelvic recurrences in previously irradiated areas;
- rinopharyngeal recurrences in previously irradiated areas.

The indication for the use of protons is to obtain a more complete and protracted palliation with fewer side effects in comparison to photon therapy. It is however possible that in some cases the administration of higher doses could give rise to episodic recoveries.

Estimate of the potential users for proton therapy

Category of pathologies	Group of users	N. of expected cases per year for proton RT
Category A	The whole national territory	450 - 680
Category B	North of Italy	960
Category C	Institutions of the "Progetto ADROTERAPIA" (Liguria, Toscana, Lombardia, Piemonte)	790
Category D	Institutions of the "Progetto ADROTERAPIA" (Liguria, Toscana, Lombardia, Piemonte)	200
Total		2400 - 2630

PROGETTO ADROTERAPIA
Goals

Hospital-based hadron-therapy "centre of excellence" whose main tasks will be:

- treatment of cancers and of other desases curable with radiation;
- development of new radiotherapeutic protocols and training of the medical staff of satellite hadron-therapy centres.

More than 1000 patients/year for proton therapy (70 - 250 MeV and $\geq 10^{10}$ p/s per treatment room).

After a few years upgrade of the H^- accelerator complex to accelerate light ions up to $^{16}O^{8+}$ to maximum energies of ~~430~~ 400 MeV/u.

5 treatment rooms:

- 1 equipped with two horizontal beam lines for eye and large field treatments;
- ~~3~~ 2 equipped with isocentric gantries; + 1 room with H and V beams
- 1 equipped with a horizontal beam line for future developments (light ions, ...);

and an experimental cave for calibrations, radiobiology, equipment test (scanning system, proton radiography, ...), etc. .

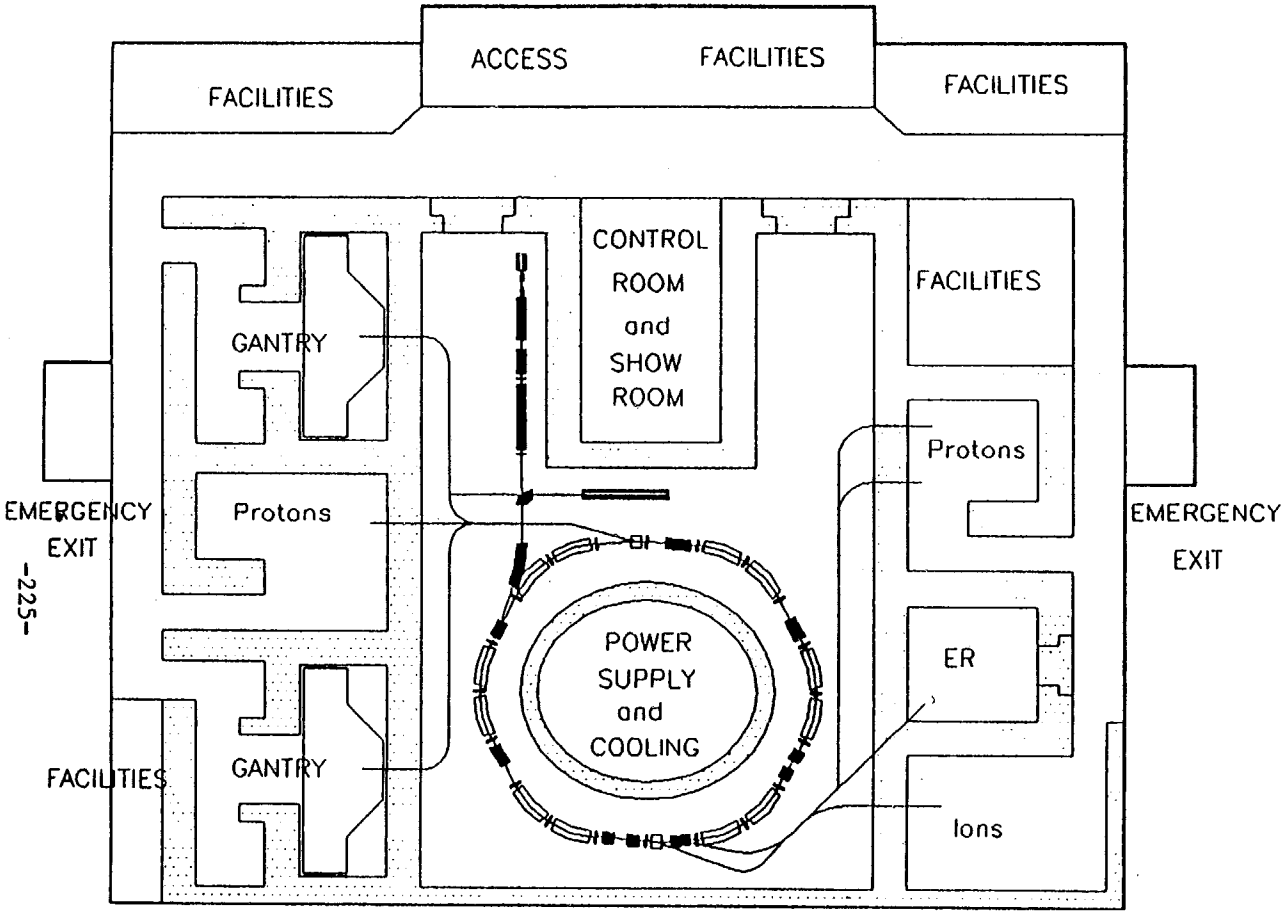

ER = Experiment with protons and ions

CENTRO PER ADROTERAPIA	PLANIMETRIA DEL BUNKER Primo piano interrato				
	Scala 1:400	Disegno n. 7	Note Versione con due piani interrati		
	Revisione	Data	Progettista	Disegnatore	Supervisore
	1	15 Luglio 1993	M. Honis	M. Honis	O. Campi
	2	8 Agosto 1993	M. Honis	M. Honis	O. Campi
	3				
	4				
	5				

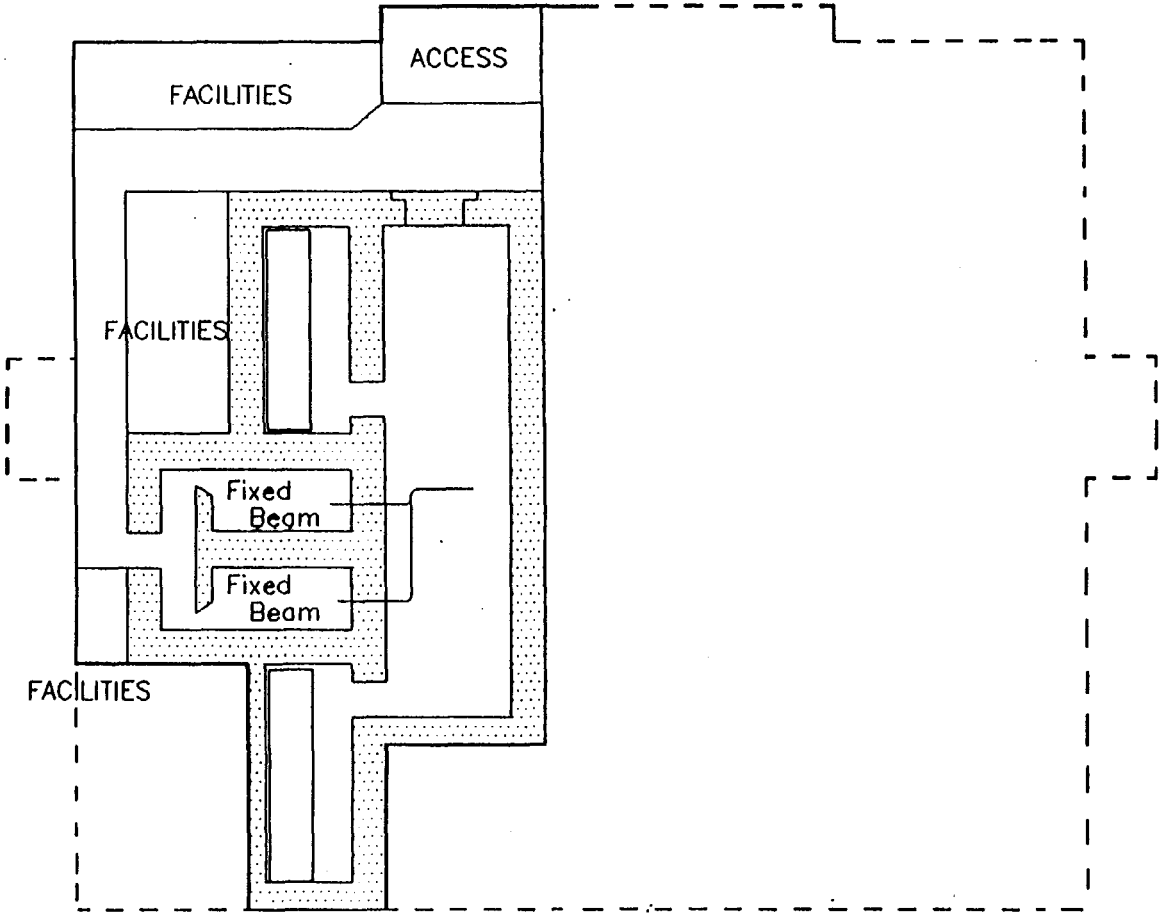

CENTRO PER ADROTERAPIA	PLANIMETRIA DEL BUNKER Secondo piano interrato				
	Scala 1:400	Disegno n. 7	Note Versione con due piani interrati		
	Revisione	Data	Progettista	Disegnatore	Supervisore
	1	15 Luglio 1993	M. Nonis	M. Nonis	D. Campi
	2	8 Agosto 1993	M. Nonis	M. Nonis	D. Campi
	3				
	4				
	5				

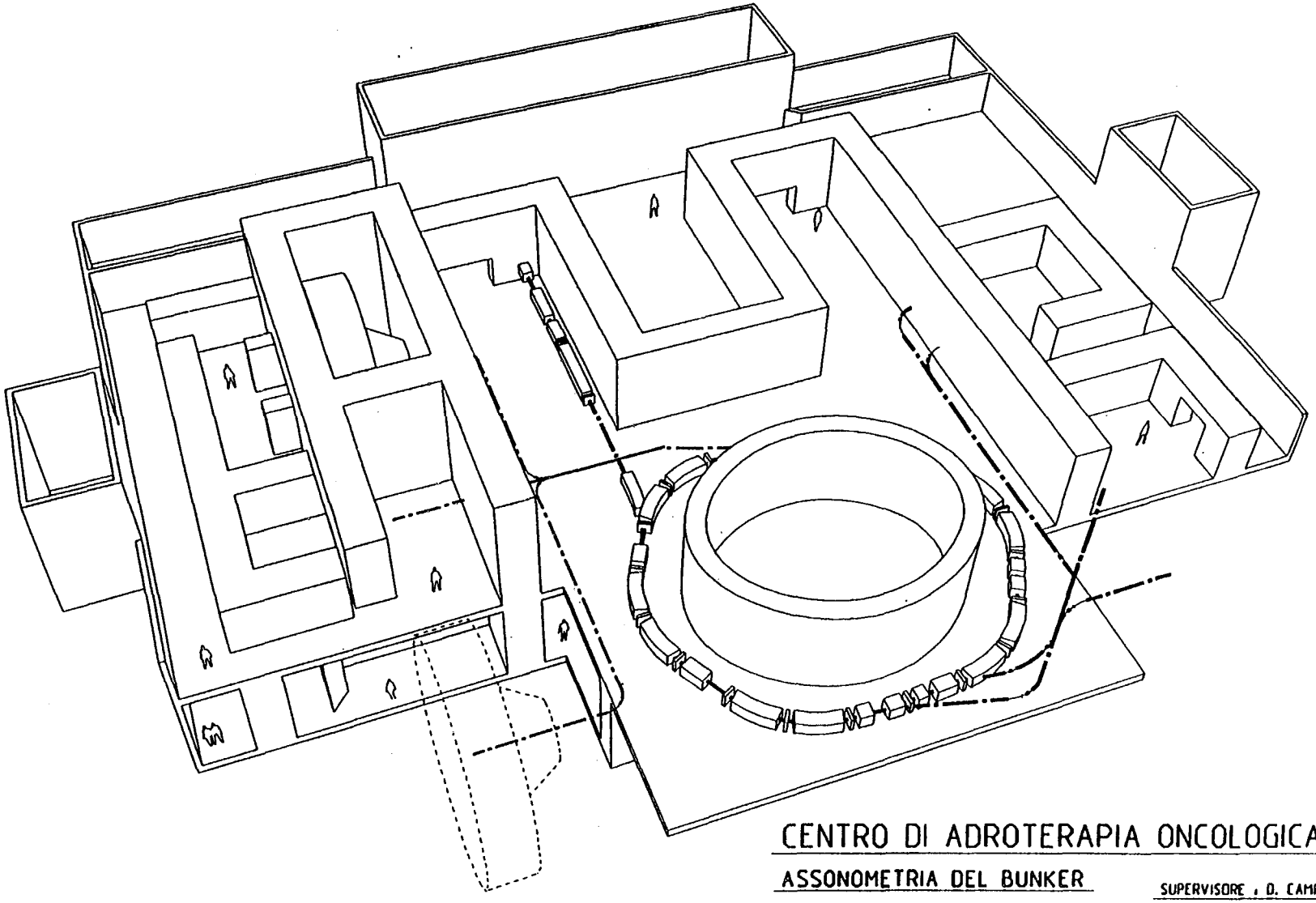

CENTRO DI ADROTERAPIA ONCOLOGICA

ASSONOMETRIA DEL BUNKER

SUPERVISORE : D. CAMPI

PROGETTISTI : M.NONIS, V. MAZZONE

CERN / ST 1 OTTOBRE 1993

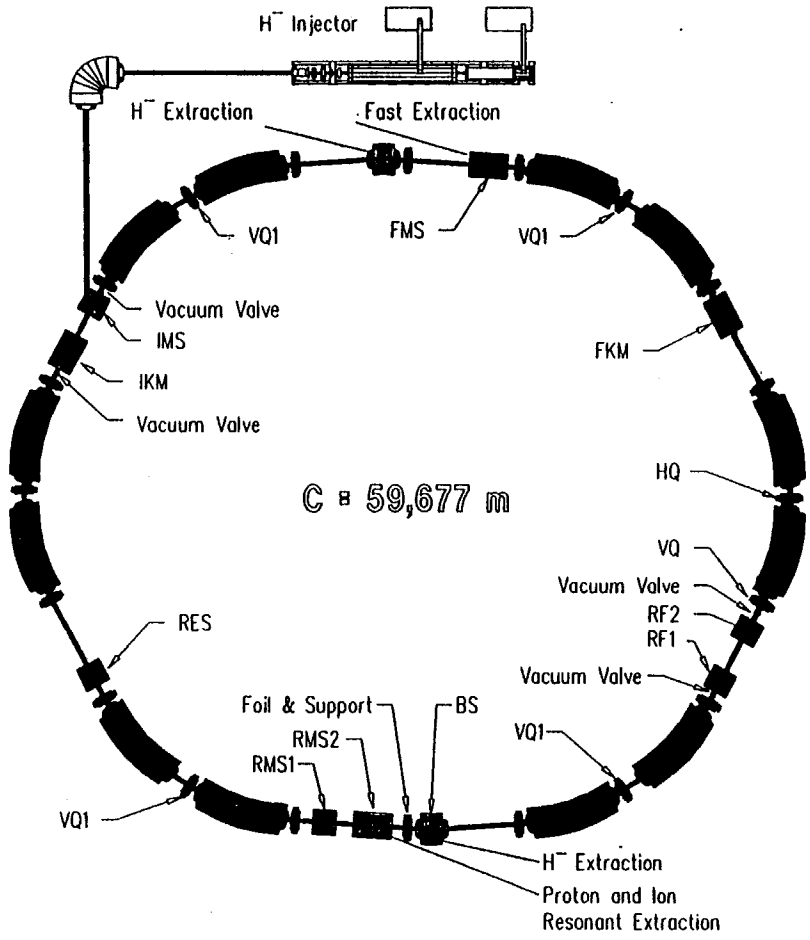

BL = Long Bending Magnet

BS = Short Bending Magnet

HQ = Horizontal Focusing Quadrupole

VQ = Vertical Focusing Quadrupole

IKM = Injection Kicker Magnet

IMS = Injection Magnetic Septum

FKM = Fast Extracion Magnet

FMS = Fast Extraction Magnetic Septum

RF1 RF2 = Accelerating Cavities

RES = Resonant Extraction Electrostatic Septum

RMS1 = Resonant Extraction Magnetic Septum

RMS2 = Resonant Extraction Magnetic Septum

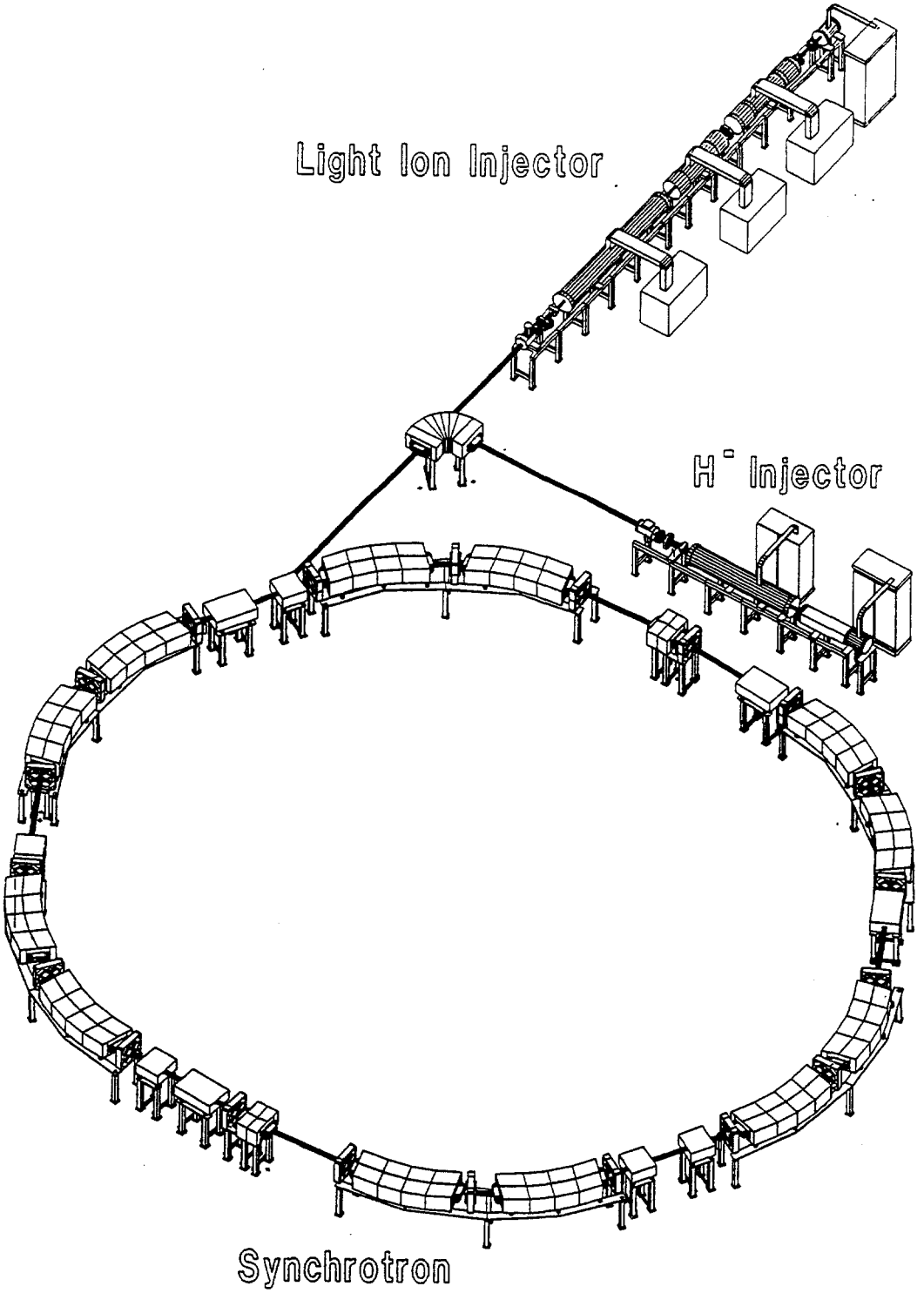
Light Ion Injector
H⁻ Injector
Synchrotron

Hadron therapy synchrotron parameters

Basic parameters:

	H^- / protons	$^{16}O^{+8}$
Charge-to-mass ratio (Z/A):	1	0.5
Injection scheme:	single turn	
Injection energy:	11 MeV	3 MeV/u
Extraction scheme:	stripping / resonant	resonant
Minimum extraction energy:	60 MeV	120 MeV/u
Maximum extraction energy:	250 / 300 MeV	400 MeV/u
Maximum magnetic rigidity [T·m]:	2.432 / 2.695	6.347
Required average current [pnA]:	11	0.36
Circumference [m]:	59.677	
Focussing scheme:	FODO	
Number of FODO cells:	10	

Beam optics parameters:

	horizontal plane	/ vertical plane
Betatron frequency:	2.31	2.40
Natural Chromaticity:	-1.13	-1.94
γ at transition energy:	2.111	
Maximum values of the β functions [m]:	10.9	10.7
Maximum value of the dispersion [m]:	5.14	0
Emittance at injection [π mm·mrad]:	20	20
Normalized emittance [π mm·mrad]:	3.07	1.61
$\Delta p/p$ at injection [%]:	± 0.22	
Beam maximum half-size [mm]:	26	15
Vacuum chamber minimum aperture [mm]:	96	46
Acceptance without dispersion [π mm·mrad]:	211	49
Acceptance with dispersion [π mm·mrad]:	124	49

Magnets:

	H^- / protons	$^{16}O^{+8}$

Dipoles: parallel-edge type

Bending radius [m]:	4.534	
Magnetic field at injection [T]:	0.106	0.110
Maximum magnetic field at extraction [T]:	0.537 / 0.595	1.40
Required physical aperture [mm^2]:	170 (H) x 60 (V)	

Long dipoles:	Number:	12
	Magnetic length [m]:	2.274
	Bending angle [mrad / °]:	502 / 28.7
Short dipoles:	Number:	2
	Magnetic length [m]:	0.600
	Bending angle [mrad / °]:	132 / 7.58

	H^- / protons	$^{16}O^{+8}$

Quadrupoles:

Magnetic length [m]:	0.15	
Required physical aperture [mm^2]:	110 x 110	

Type HQ[a] :	Number:	10	
	Maximum gradient [T/m]:	7.212 / 7.992	18.82
Type VQ[b] :	Number:	6	
	Maximum gradient [T/m]:	6.724 / 7.452	17.55
Type VQ1[b]:	Number:	4	
	Maximum gradient [T/m]:	5.476 / 6.068	14.29

[a] Horizontal focussing quadrupole.
[b] Vertical focussing quadrupole.

Straight sections:

Type O1:	Number:	6
	Length [m]:	2.774
Type O2:	Number:	2
	Length [m]:	1.924
Type O3:	Number:	22
	Length [m]:	0.250
Type O4:	Number:	4
	Length [m]:	0.550

	H^- / protons	$^{16}O^{+8}$
Timing:		
Repetition rate [Hz]:	2	1
Injected pulse length [μs]:	0.656	1.243
Acceleration time [s]:	0.15	0.4
Flat-top [s]:	0.25	0.3
Fall time [s]:	0.1	0.3
Magnetic field ramp [T/s]:	2.87 / 3.26	3.22

RF accelerating system:		
Frequency at injection [MHz]:	0.763	0.402
Maximum frequency at extraction [MHz]:	3.083 / 3.278	3.590
Effective accelerating voltage [kV]:	0.776 / 0.881	0.872
Peak accelerating voltage [kV]:	1.553 / 1.762	1.745
Stable phase [°]:	30	
Maximum frequency tuning rate [MHz/s]:	15.47 / 16.77	7.969

Required beam intensity on patient to obtain a dose rate of 5 Gy/min in a volume of 2 litres.

(particles per second)

p	He	C	N	O	Ne
$6x10^{10}$	$1.5x10^{10}$	$3x10^{9}$	$2.5x10^{9}$	$2x10^{9}$	$1.5x10^{9}$

Light ion injector

To achieve the required intensities with single-turn injection:

- high current low charge state production ($^{16}O^{+2}$ or $^{12}C^{+2}$);
- stripping to bare nuclei in two steps during acceleration.

==> Two separate linacs for H^- and light ion acceleration.

This means:

- greater reliability and simplicity of operation;
- greater flexibility in running parallel activities;
- fast switch between H^- and light ion acceleration modes;
- smaller impact on the costs of the initial project.

Preliminary configuration for the linac (reference ion: Oxygen):

- PIG, Chordis or ECR (optimized for low charge state production) ion source;
  peak current: 4.6 pmA $^{16}O^{+2}$ in pulses a few μs long, 1 Hz repetition rate;
  extraction potential: 20-30 kV (2.5 - 3.75 keV/u);

- low energy beam transfer line: two solenoids, no mass spectrometer for charge state selection;

- RFQ (2.5 --> 250 keV/u, $q/A \geq 1/8$), $f_{RFQ} \approx 100$ MHz, length ≈ 2.5 m;

- Alvarez DTL (0.25 MeV/u --> 0.85 MeV/u, $q/A \geq 1/8$), $f_{DTL1} = f_{RFQ}$, length ≈ 2 m;

- 1st stripping foil: stripping efficiency to $^{16}O^{6+} \approx 50$ %;

- Alvarez DTL (0.85 MeV/u --> 3 MeV/u, $q/A \geq 0.375$), $f_{DTL2} = 2f_{DTL1}$, length ≈ 4 m;

- 2nd stripping foil: stripping efficiency to $^{16}O^{8+} \approx 60$ %;

The same linac could be used for the acceleration of Carbon ions, the required peak current of $^{12}C^{+2}$ would be 4.3 pmA in pulses a few μs long and 1 Hz repetition rate.

Extraction system

H^- ===> stripping:

- simplicity;
- small emittance; ($\varepsilon_x \simeq \varepsilon_y$)
- several cheaper extraction ports (short beam lines);
- feedback on the extracted beam intensity.

light ions and protons ===> resonant

Fast extraction both for protons/H^- and light ions will be implemented to dump the beam in case of failure.

Vacuum ($\approx 10^{-10}$ torr)

- aluminium vacuum chamber + NEG;
- stainless steel vacuum chamber + ion pumps.

Fractional loss at 250 MeV as a function of the residual pressure.
The beam extraction time is 0.2 s

Composition of residual gas: 95% hydrogen, 5% oxygen

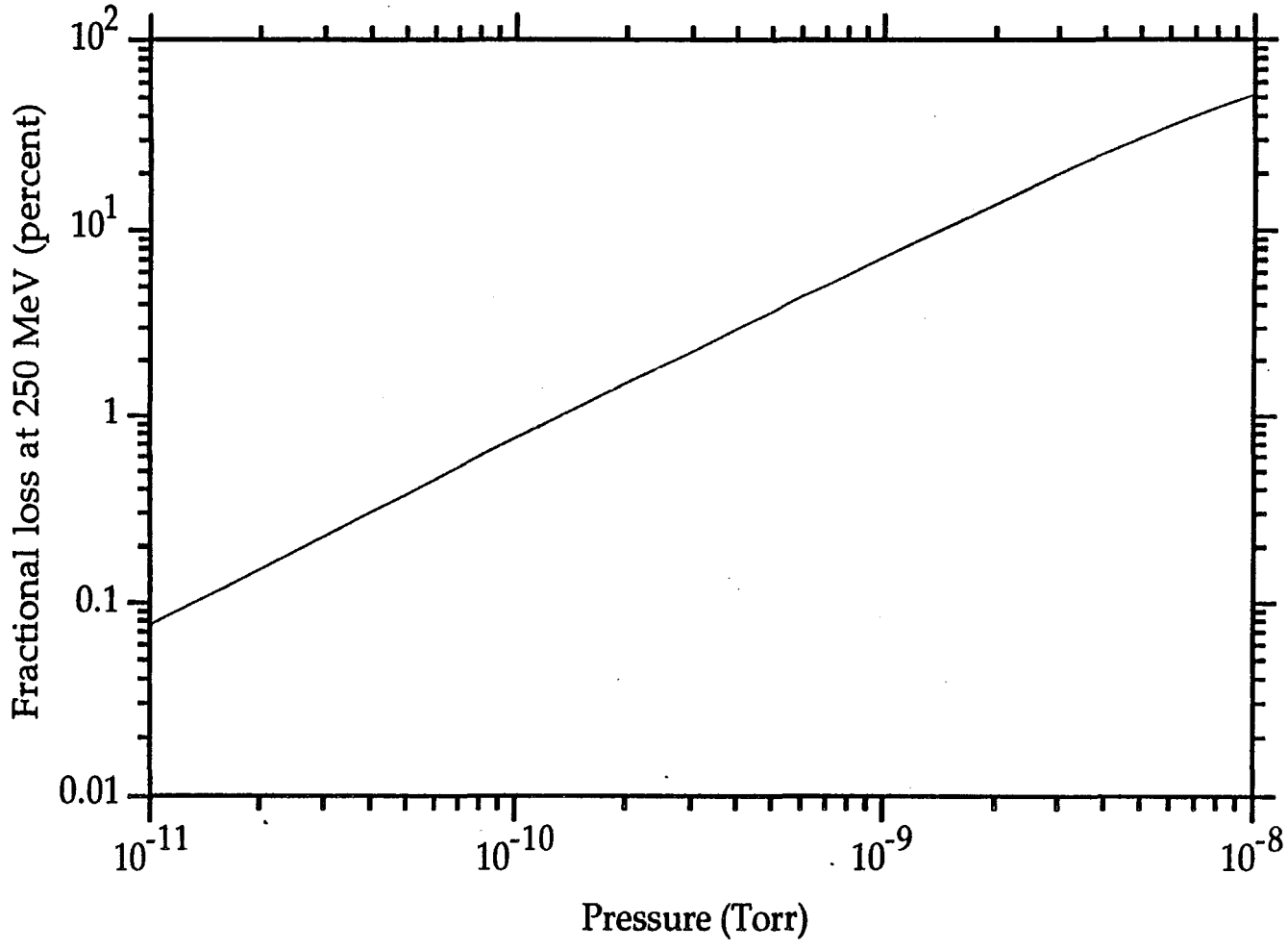

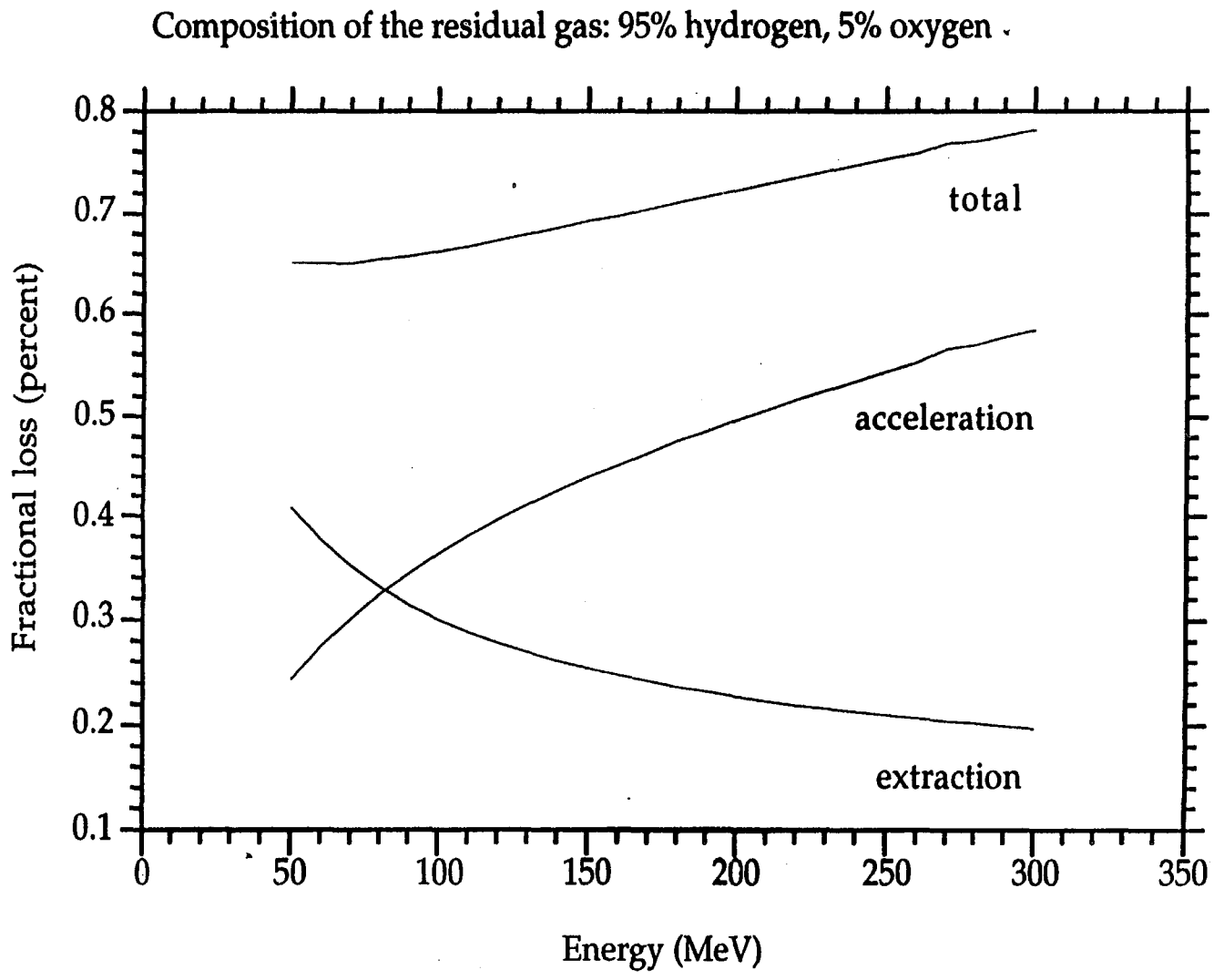

Fractional loss during acceleration, during extraction and total fractional loss vs. extraction energy, at a residual pressure of 1×10^{-10} torr. The beam extraction time is 0.2 s

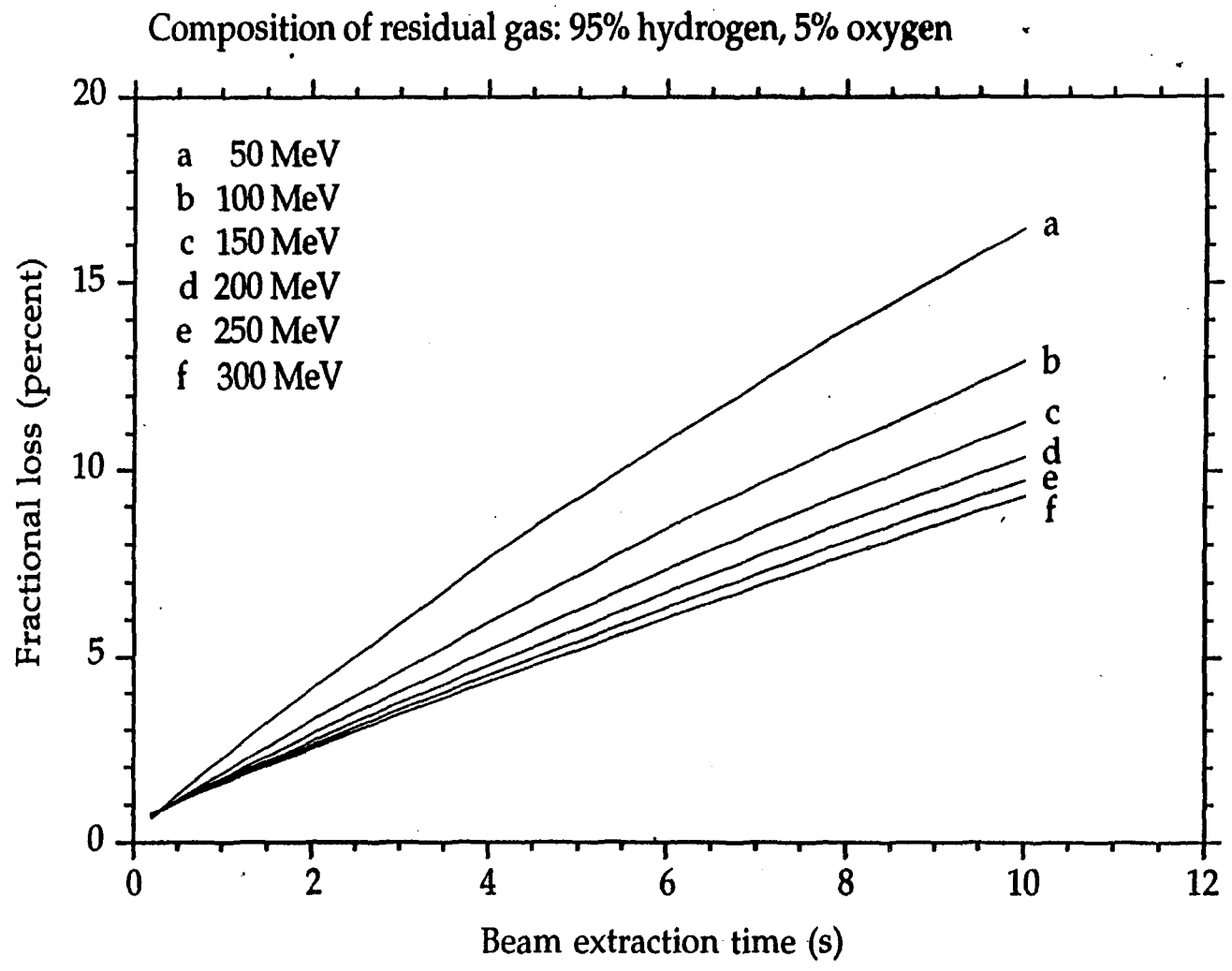

Fractional loss vs beam extraction time for different values of the extraction energy at a residual pressure of 1×10^{-10} Torr

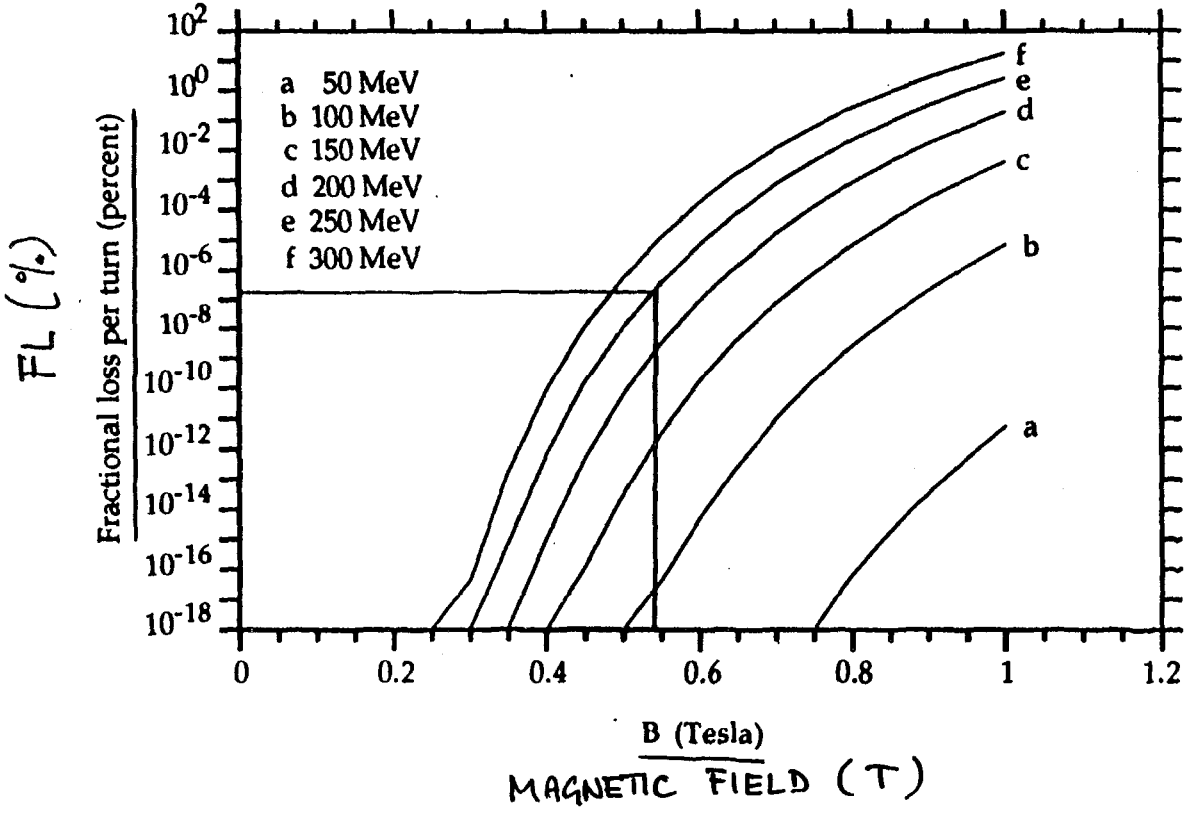

Fig. 11 Fractional loss per machine turn versus magnetic field.

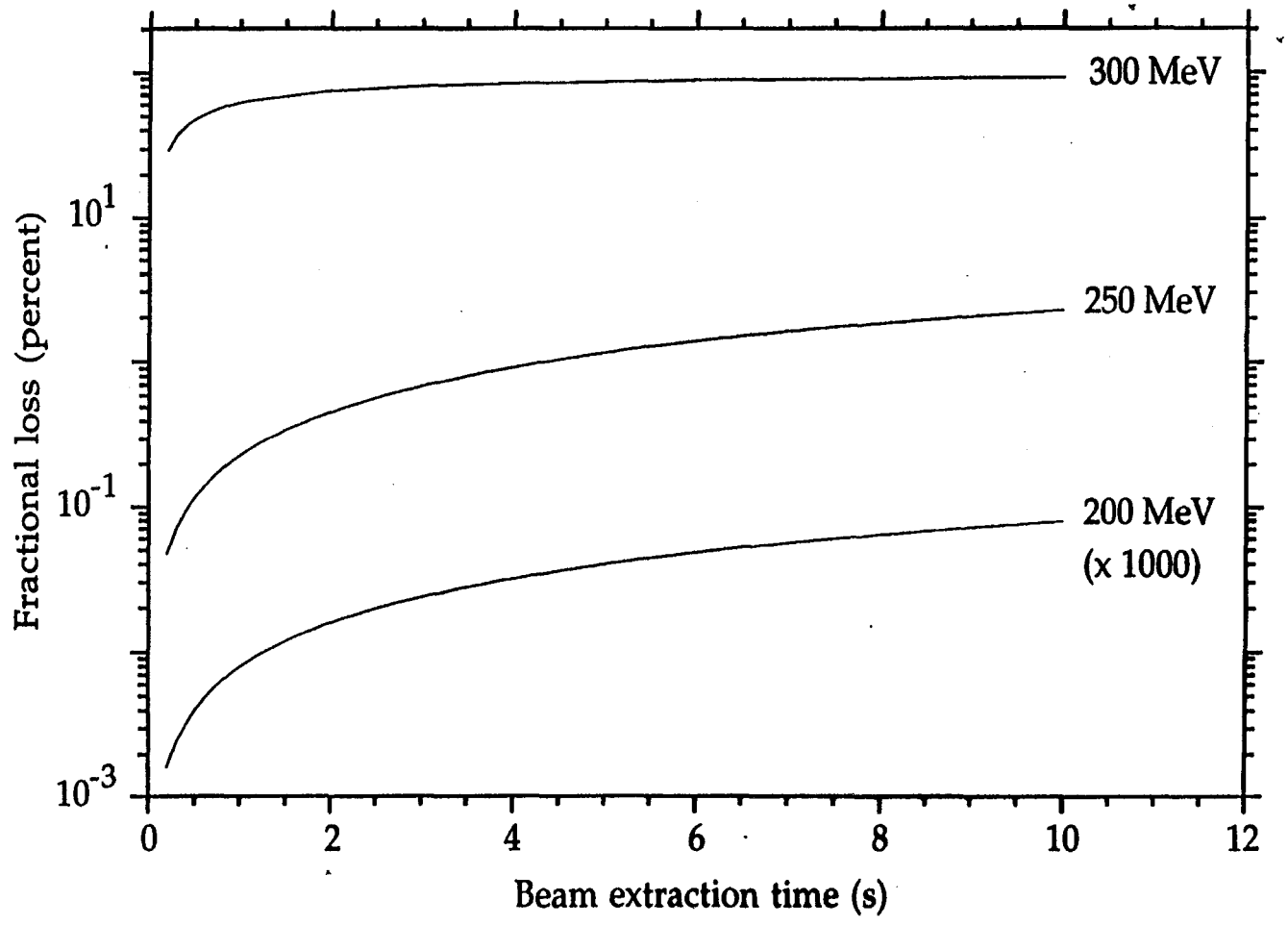

Fractional loss vs beam extraction time at three values of extraction energy

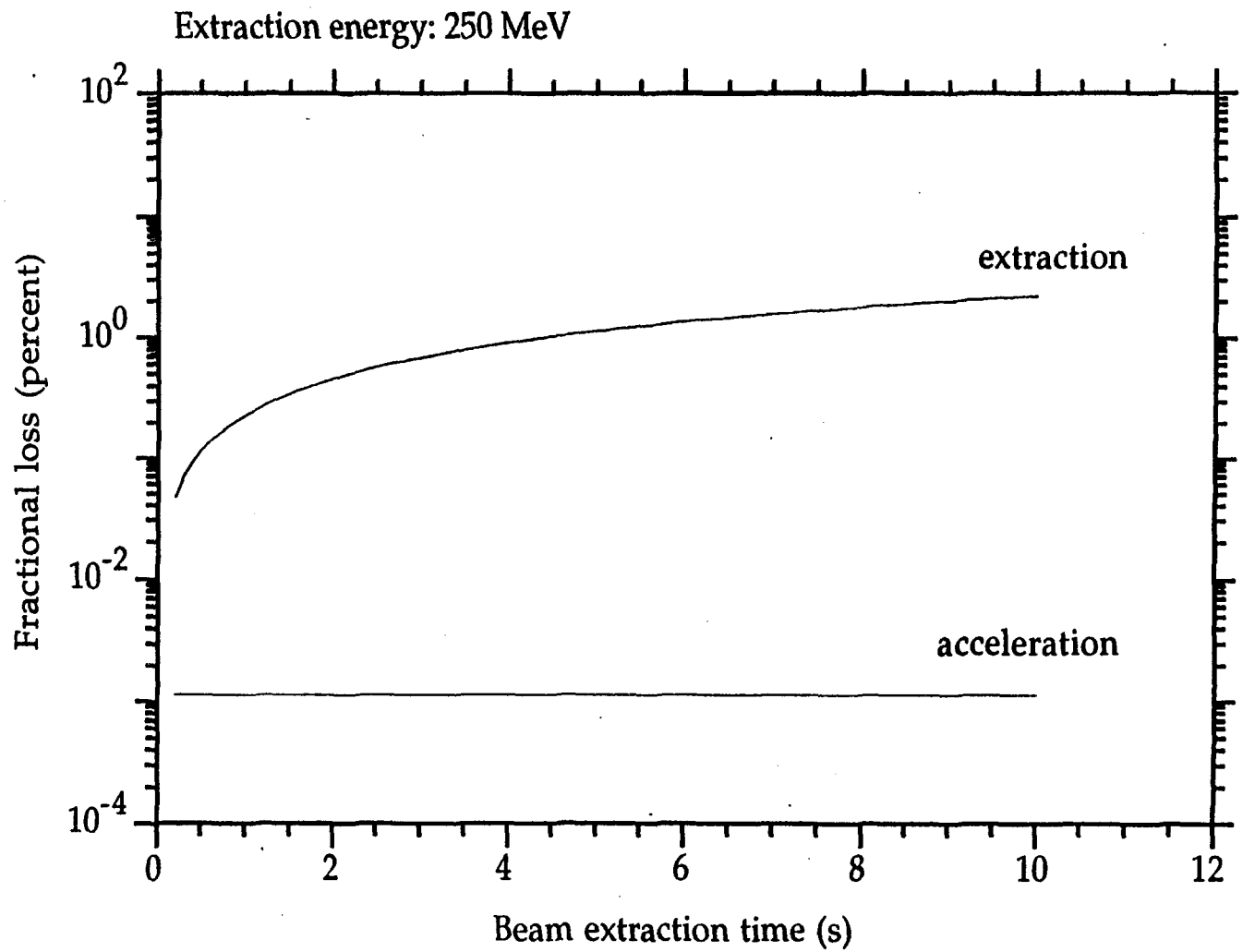

Fractional loss vs beam extraction time at 250 MeV. The losses during acceleration and extraction are shown separately.

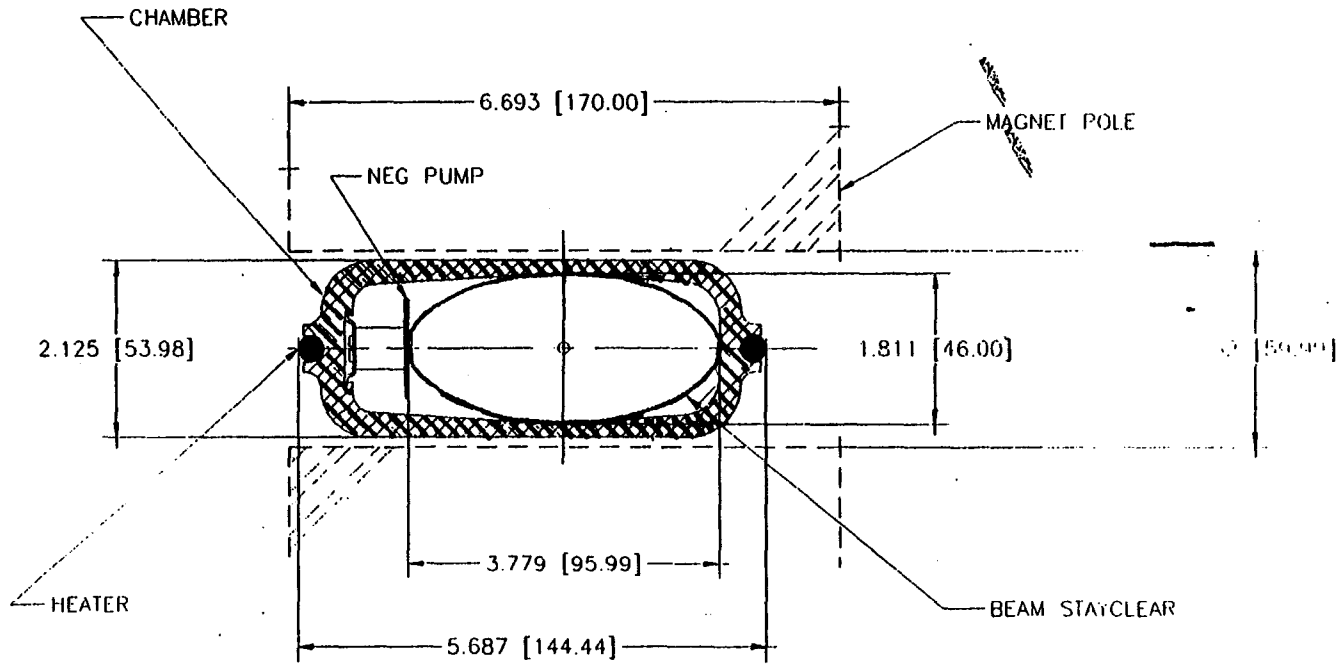
CHAMBER
6.693 [170.00]
MAGNET POLE
NEG PUMP
2.125 [53.98]
1.811 [46.00]
3.779 [95.99]
HEATER
BEAM STAYCLEAR
5.687 [144.44]

CONTROL SYSTEM STRUCTURE
HARDWARE

→ ALL COMMERCIAL AVAILABLE AND STANDARD COMPLIANCE COMPONENTS

→ HARDWARE ESTIMATED COST ≈ 30% OF TOTAL COST OF CONTROL SYSTEM

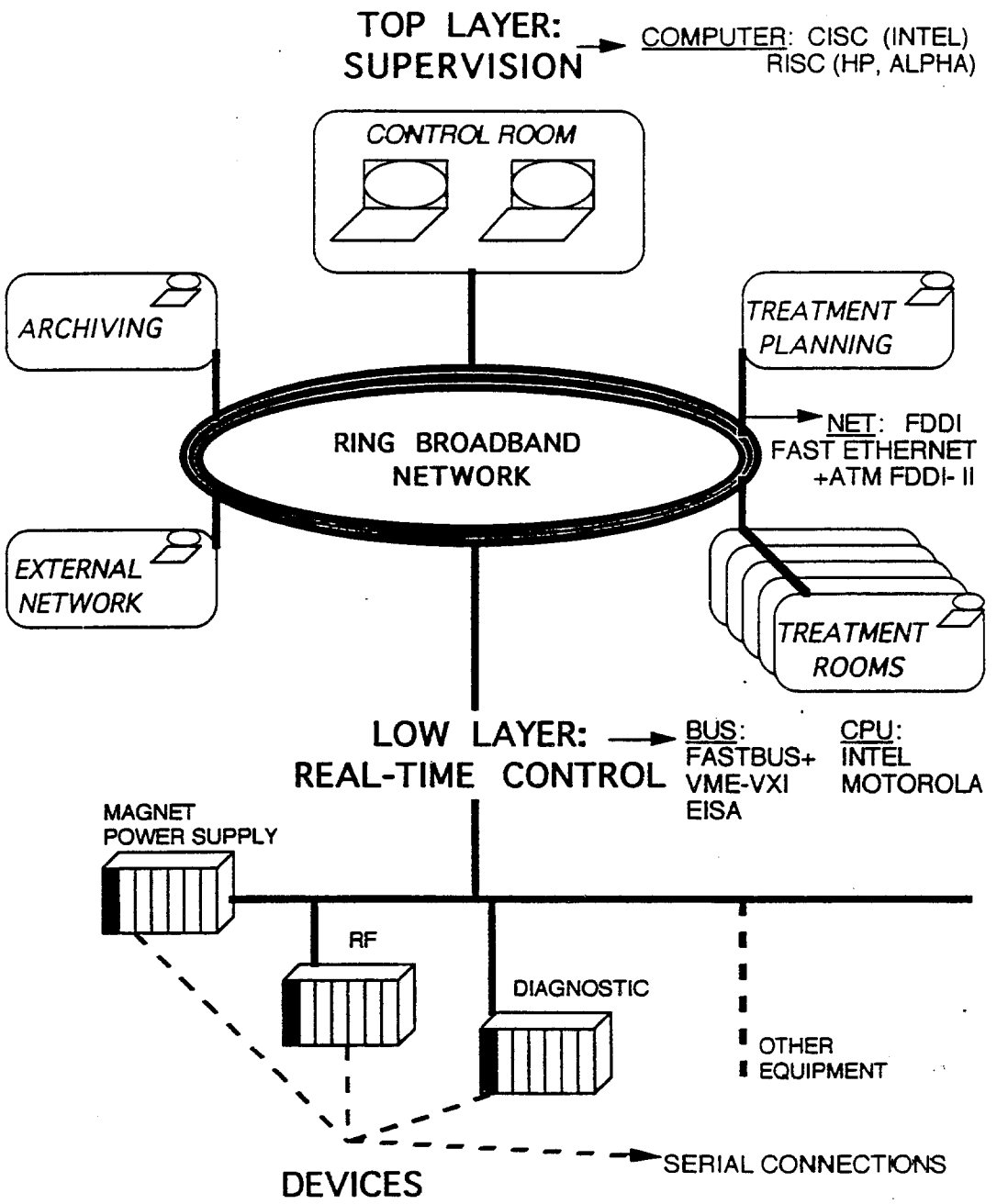

Beam diagnostics requirements

1 Closed orbit beam position monitoring

2 Beam current monitoring

3 Extraction current monitoring

4 Beam loss monitoring

5 Beam tune monitoring

6 Beam profile monitoring

3 Extraction current monitoring system (in the extracted beam line)

Multi-foil secondary emission monitor (SEM) - to be calibrated against an absolute monitor (e.g., a Faraday cup)

Fluorescent screen to observe beam position and profile

Measurements of the current of the electrons stripped from the H^- ions at extraction

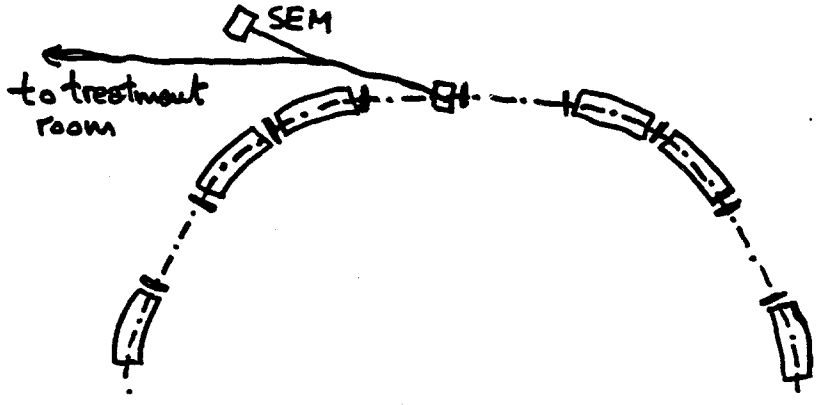

Energy

The information needed is the range in tissue and the relative energy variation (for step by step range modulation). The range measurement will be performed on the extracted beam.

Emittance of the extracted beam

Instrumentation for emittance measurements to be provided on one of the beam lines (during commissioning)

Interesting to compare emittance of H^- and proton beams

Feedback on the stability of the extracted beam

Two possibilities:

measure the current due to the electrons stripped from the H^- ions

use the signal from the ion chamber placed just before the patient

Possible use of fast bump magnets for feedback control

INP LAYOUT FOR A "PROTONTHERAPY CENTRE"

SILVESTROV et al.

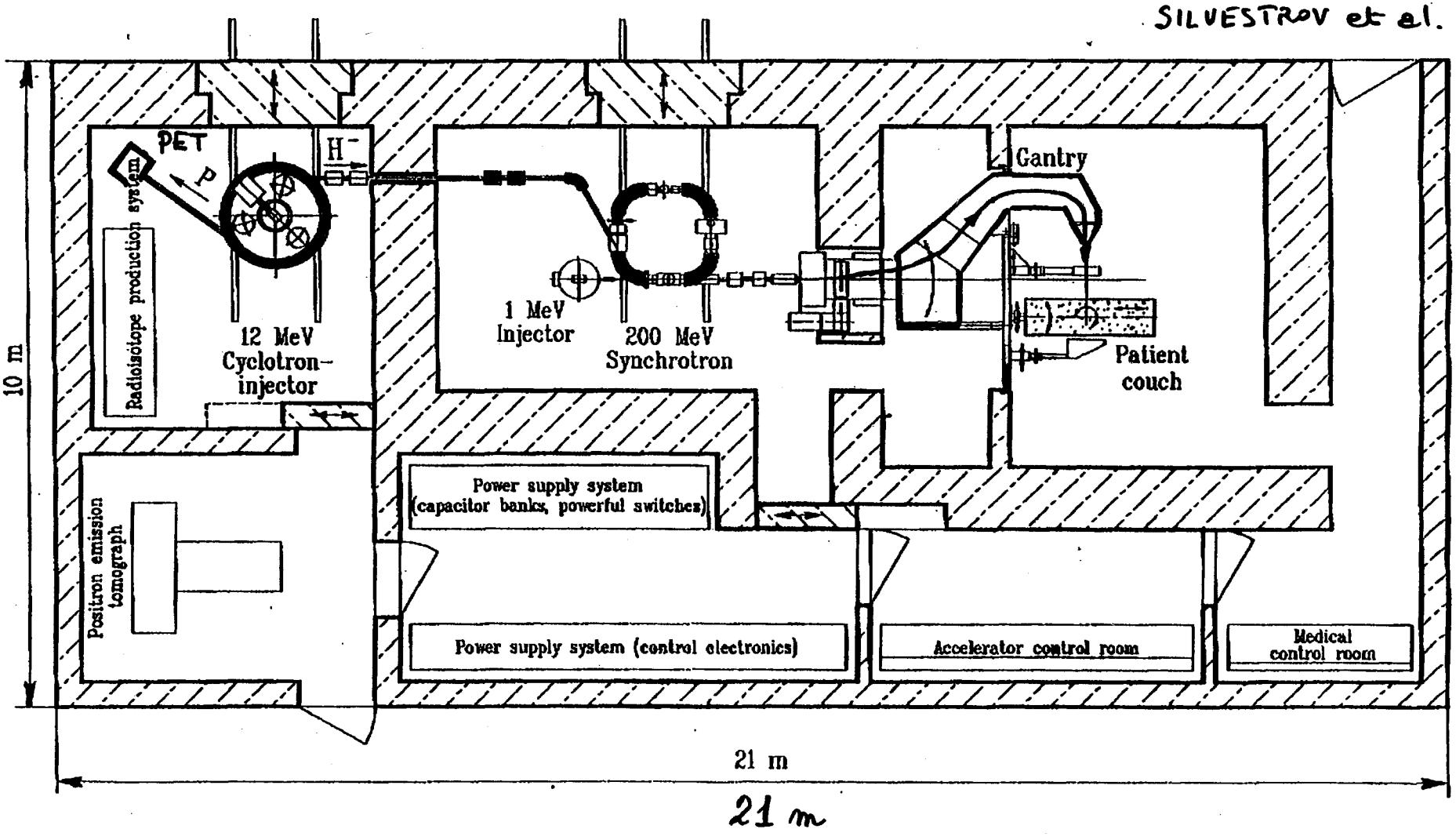

10 m

21 m

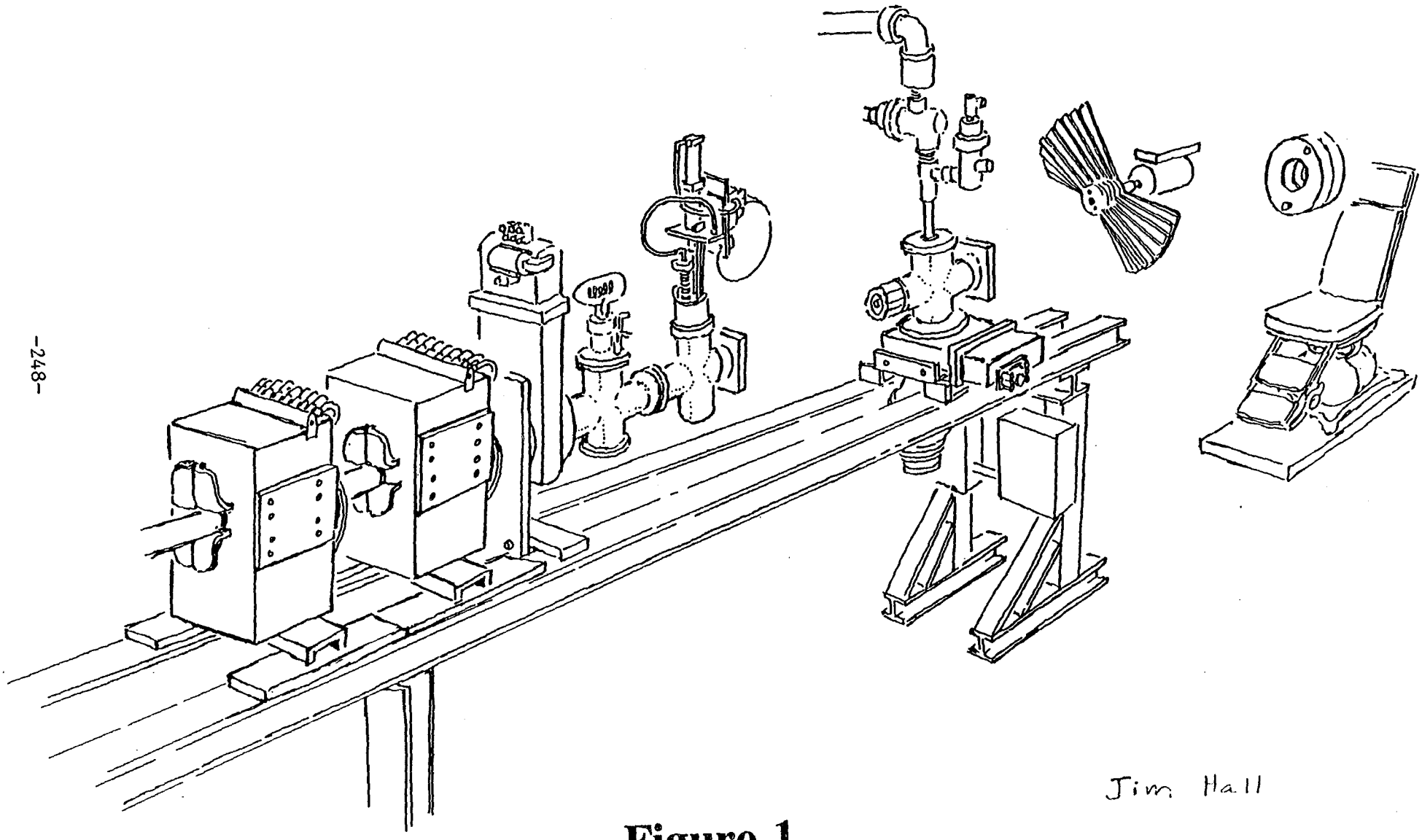

Figure 1

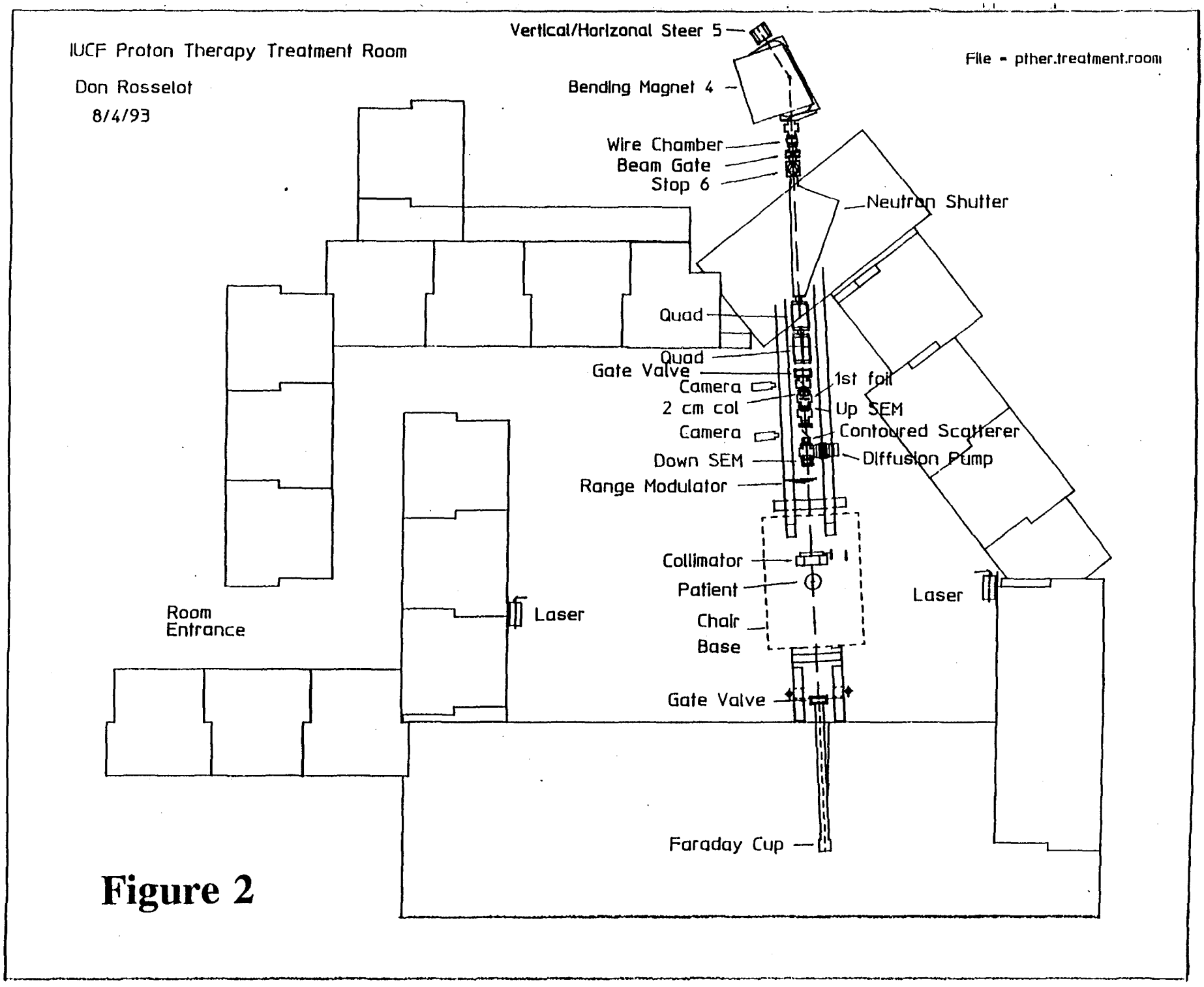
IUCF Proton Therapy Treatment Room
Don Rosselot
8/4/93
File - pther.treatment.room
Vertical/Horizonal Steer 5
Bending Magnet 4
Wire Chamber
Beam Gate
Stop 6
Neutron Shutter
Quad
Quad
Gate Valve
Camera
2 cm col
Camera
Down SEM
Range Modulator
1st foil
Up SEM
Contoured Scatterer
Diffusion Pump
Collimator
Patient
Chair
Base
Gate Valve
Faraday Cup
Laser
Laser
Room
Entrance

Figure 2

Figure 3

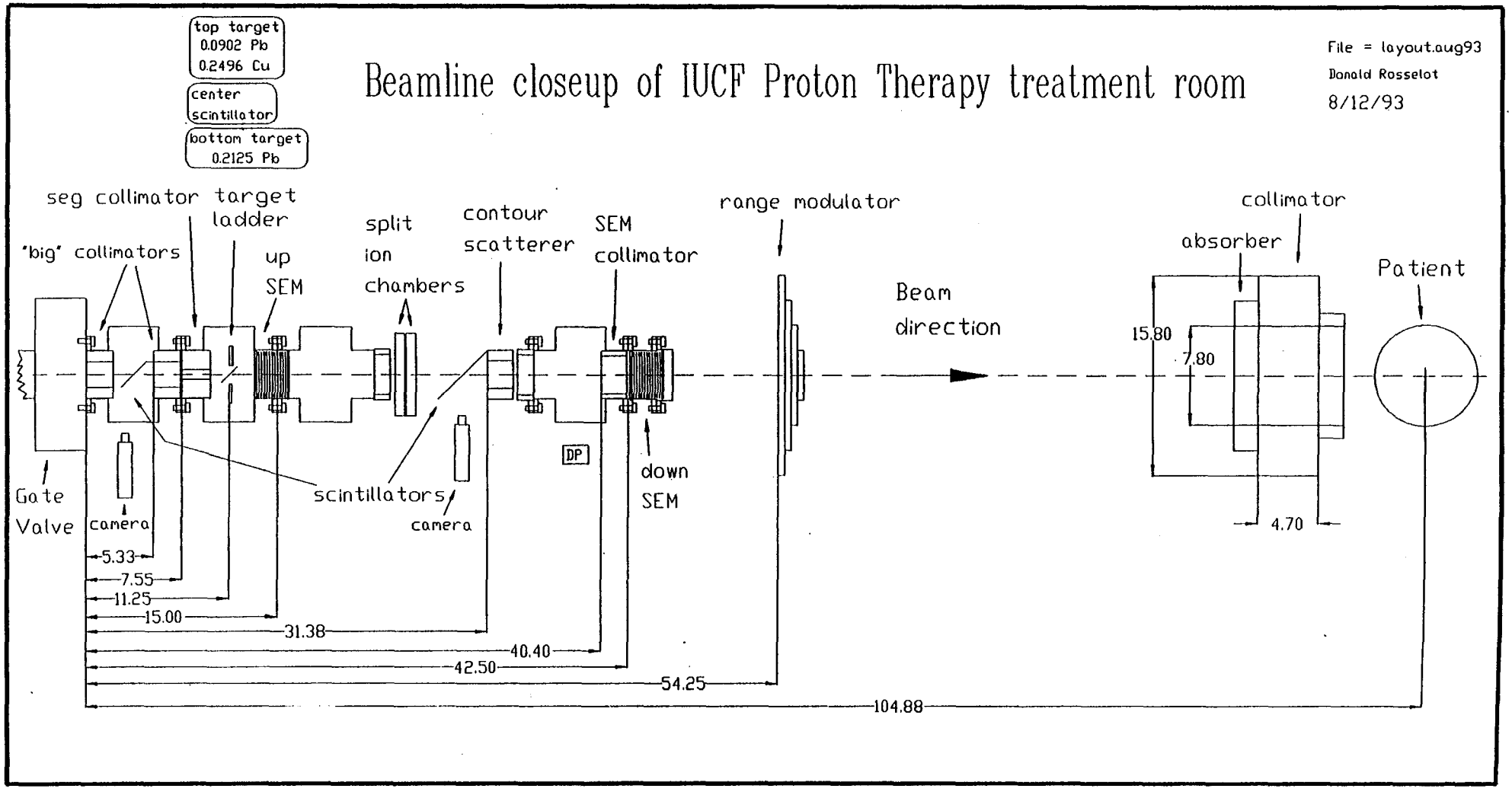
Beamline closeup of IUCF Proton Therapy treatment room
File = layout.aug93
Donald Rosselot
8/12/93
top target
0.0902 Pb
0.2496 Cu
center
scintillator
bottom target
0.2125 Pb
seg collimator
target
ladder
'big' collimators
up
SEM
split
ion
chambers
contour
scatterer
SEM
collimator
range modulator
Beam
direction
collimator
absorber
Patient
15.80
7.80
4.70
Gate
Valve
camera
scintillators
camera
DP
down
SEM
5.33
7.55
11.25
15.00
31.38
40.40
42.50
54.25
104.88

ransverse plane. Plot magnification= 1.00 Frame number 1
enter at X= 0.0 Y= -0.2 Z= 0.2 cm
0-OCT-1993 14:53:59
ignature _____

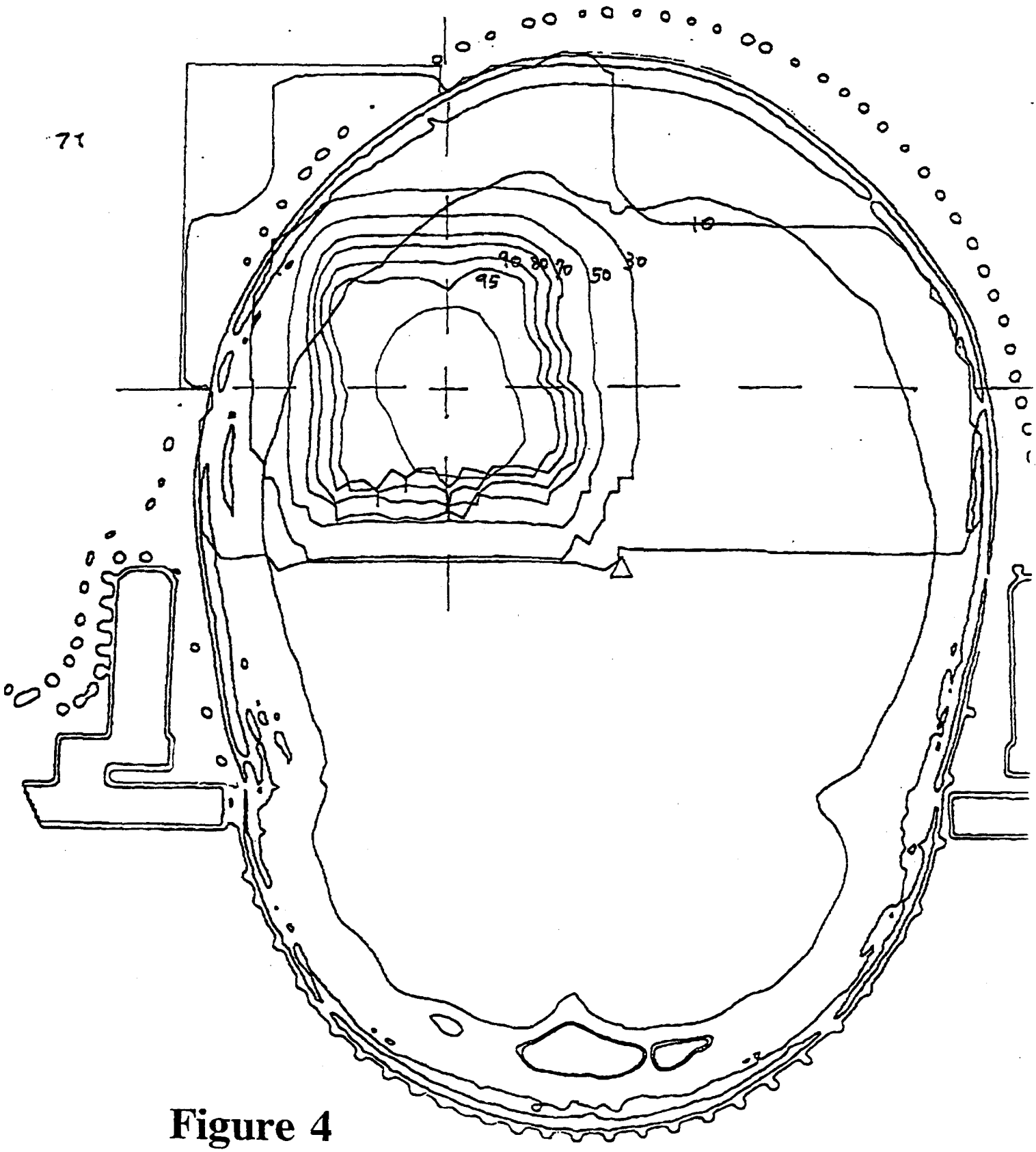

Figure 4

Figure 3 a

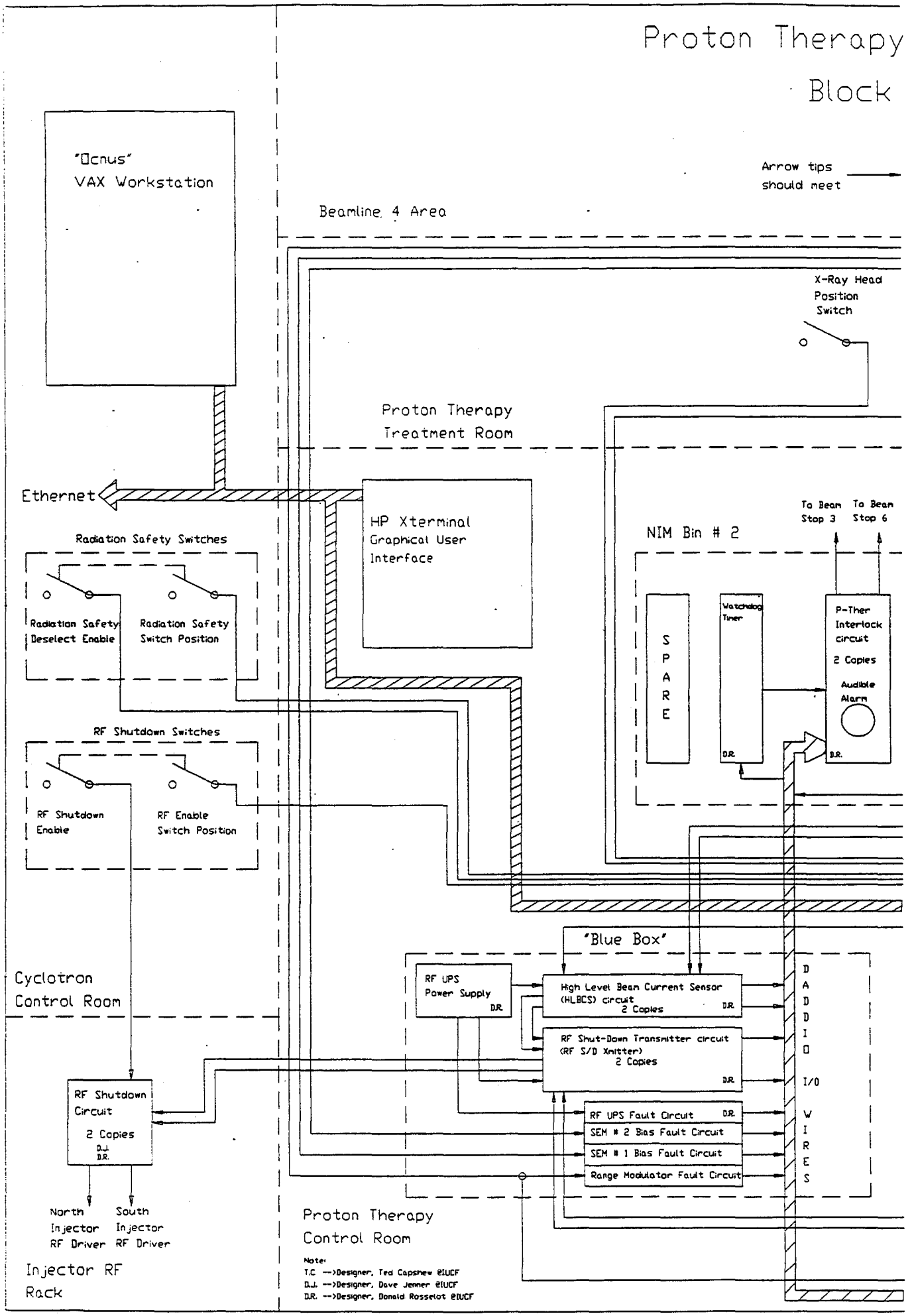
Proton Therapy Block
"Ocnus" VAX Workstation
Arrow tips should meet
Beamline 4 Area
X-Ray Head Position Switch
Proton Therapy Treatment Room
Ethernet
HP Xterminal Graphical User Interface
To Beam Stop 3
To Beam Stop 6
NIM Bin # 2
Radiation Safety Switches
Radiation Safety Deselect Enable
Radiation Safety Switch Position
SPARE
Watchdog Timer
D.R.
P-Ther Interlock circuit 2 Copies
Audible Alarm
D.R.
RF Shutdown Switches
RF Shutdown Enable
RF Enable Switch Position
"Blue Box"
RF UPS Power Supply
D.R.
High Level Beam Current Sensor (HLBCS) circuit 2 Copies
D.R.
RF Shut-Down Transmitter circuit (RF S/D Xmitter) 2 Copies
D.R.
RF UPS Fault Circuit
D.R.
SEM # 2 Bias Fault Circuit
SEM # 1 Bias Fault Circuit
Range Modulator Fault Circuit
DADDIO I/O WIRES
Cyclotron Control Room
RF Shutdown Circuit 2 Copies
D.J.
D.R.
North Injector RF Driver
South Injector RF Driver
Injector RF Rack
Proton Therapy Control Room
Note:
T.C. -->Designer, Ted Capshew @IUCF
D.J. -->Designer, Dave Jenner @IUCF
D.R. -->Designer, Donald Rosselot @IUCF

Figure 3 b

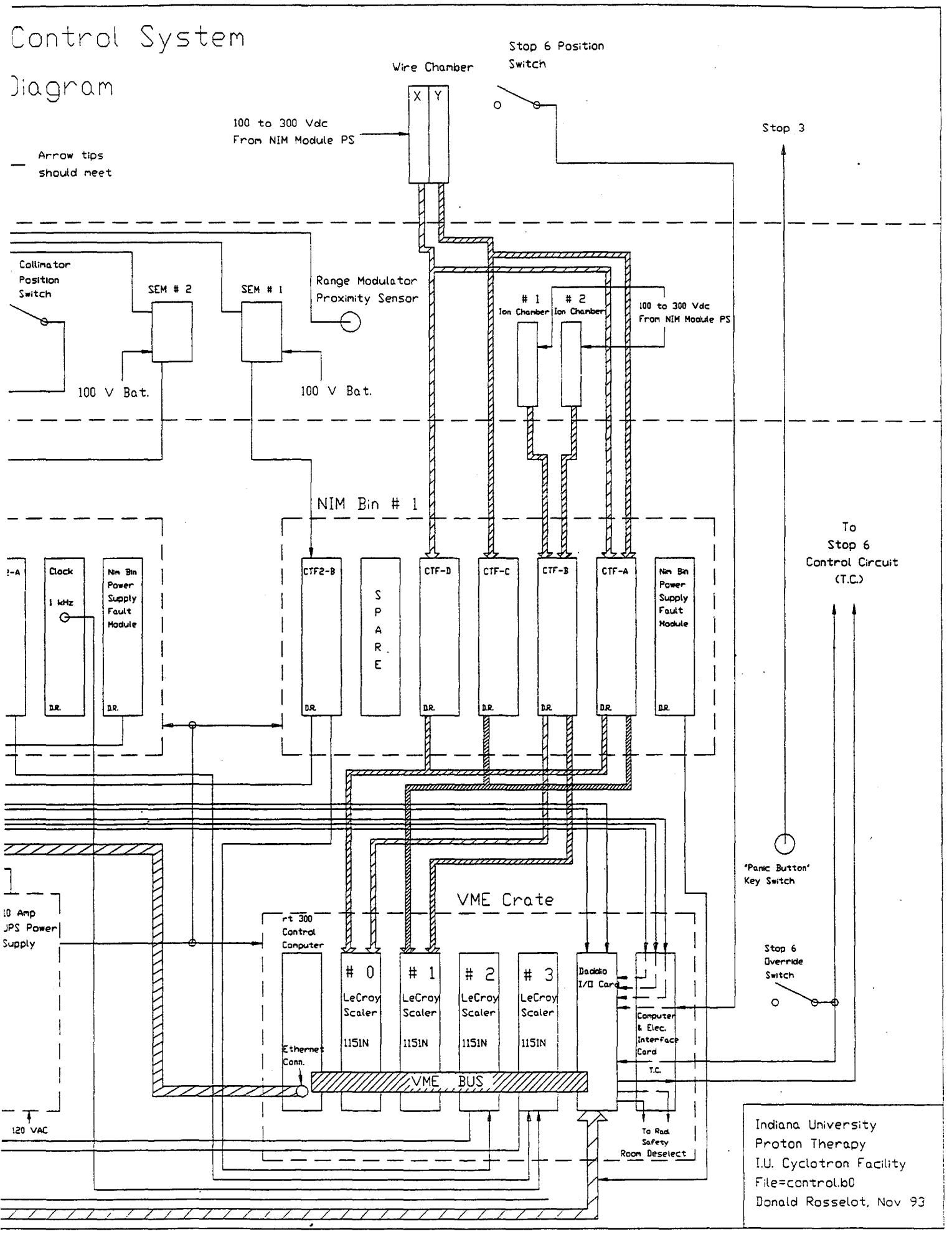
Control System
Diagram
Arrow tips
should meet
Wire Chamber
X
Y
Stop 6 Position
Switch
100 to 300 Vdc
From NIM Module PS
Stop 3
Collimator
Position
Switch
SEM # 2
SEM # 1
Range Modulator
Proximity Sensor
1
Ion Chamber
2
Ion Chamber
100 to 300 Vdc
From NIM Module PS
100 V Bat.
100 V Bat.
NIM Bin # 1
Clock
1 kHz
Nim Bin
Power
Supply
Fault
Module
D.R.
CTF2-B
SPARE
CTF-D
CTF-C
CTF-B
CTF-A
To
Stop 6
Control Circuit
(T.C.)
"Panic Button"
Key Switch
VME Crate
10 Amp
UPS Power
Supply
rt 300
Control
Computer
0
LeCroy
Scaler
1151N
1
LeCroy
Scaler
1151N
2
LeCroy
Scaler
1151N
3
LeCroy
Scaler
1151N
Daddio
I/O Card
Computer
& Elec.
Interface
Card
T.C.
Stop 6
Override
Switch
Ethernet
Conn.
VME BUS
120 VAC
To Rad
Safety
Room Deselect
Indiana University
Proton Therapy
I.U. Cyclotron Facility
File=control.b0
Donald Rosselot, Nov 93

SEM Assembly

Secondary Electron Emission Monitor

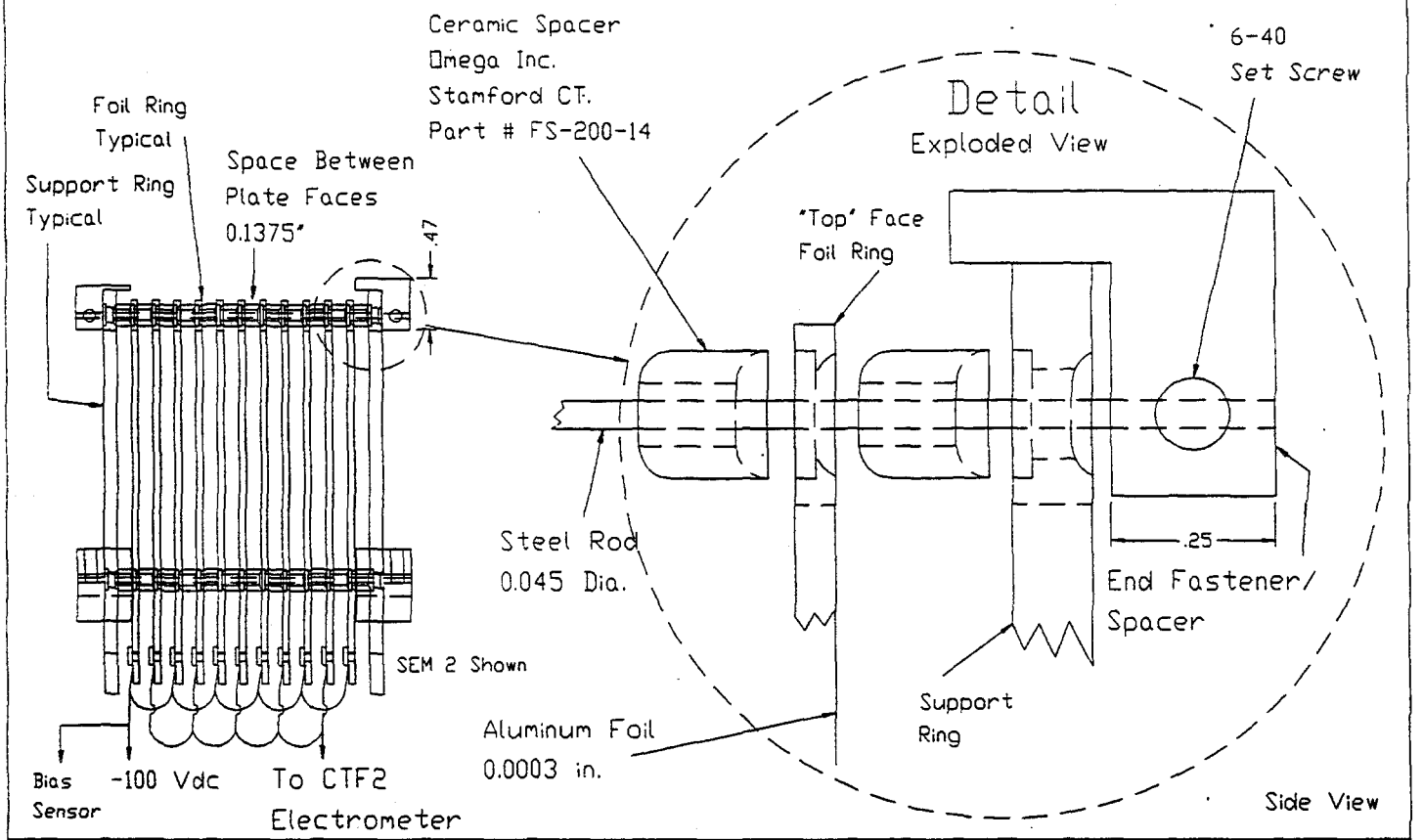

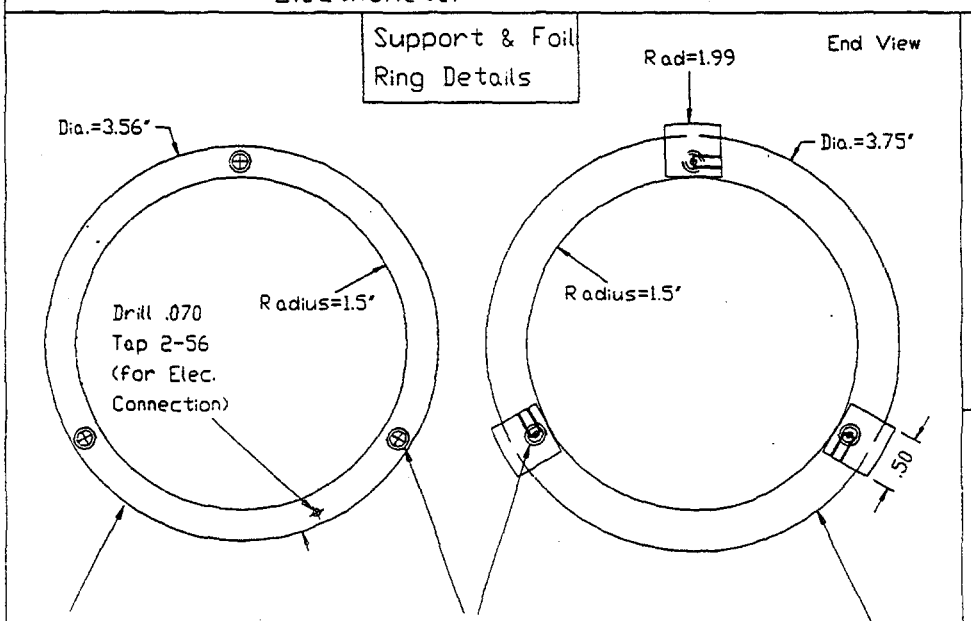

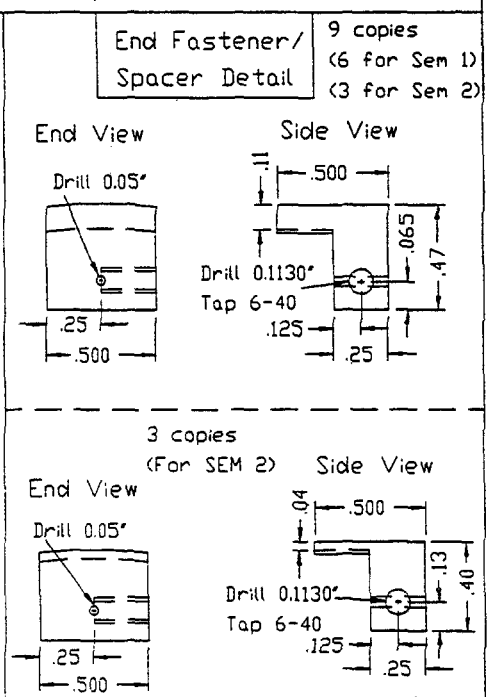

Note: All dimentions are in inches
Plot scale=0.54 for A size
Rot. ang.=90

Indiana University Proton Therapy
I.U. Cyclotron Facility
File=sem.m0
Don Rosselot Nov 93
Chkd by
Dwg. # pt000001.m0
Rev 0

Figure 6

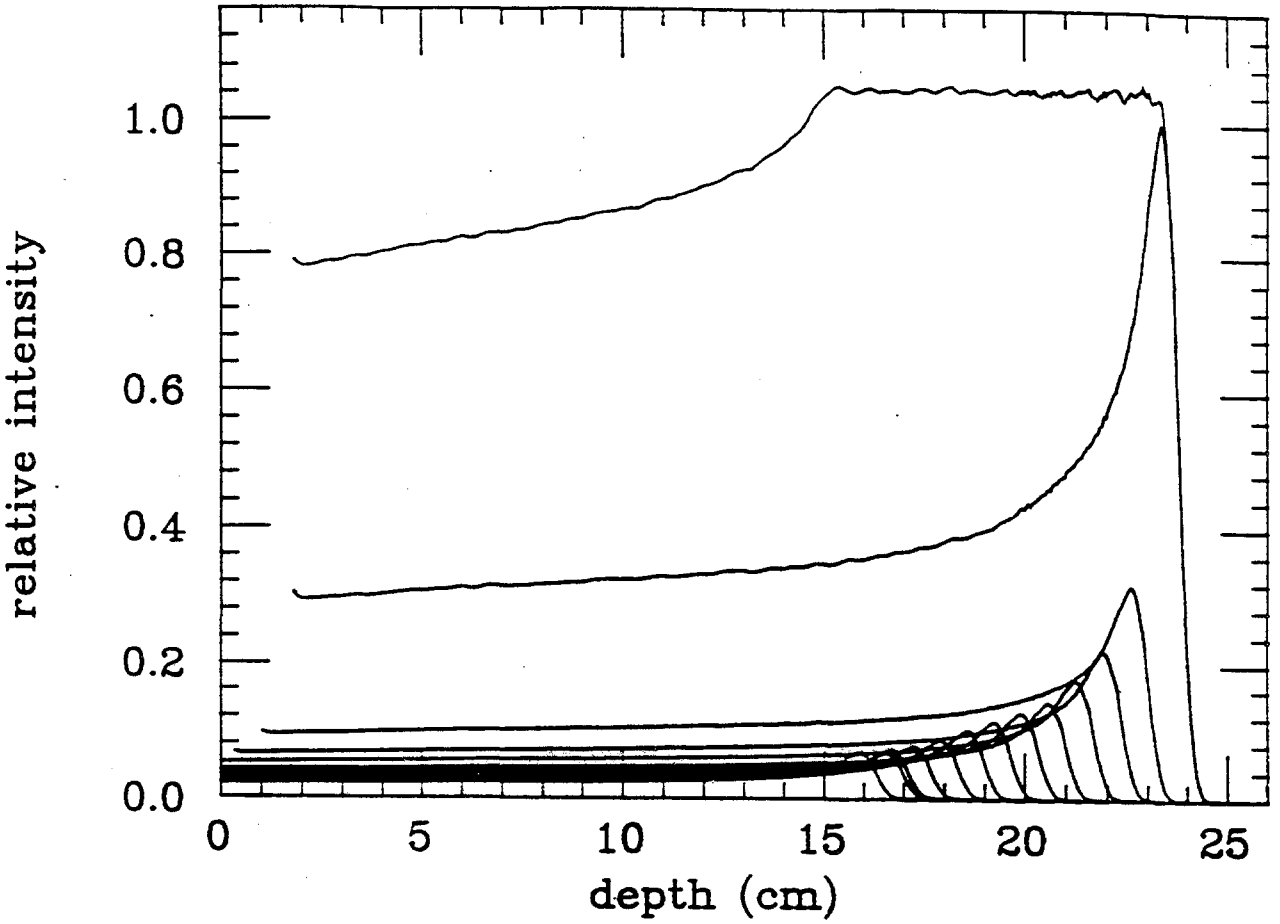

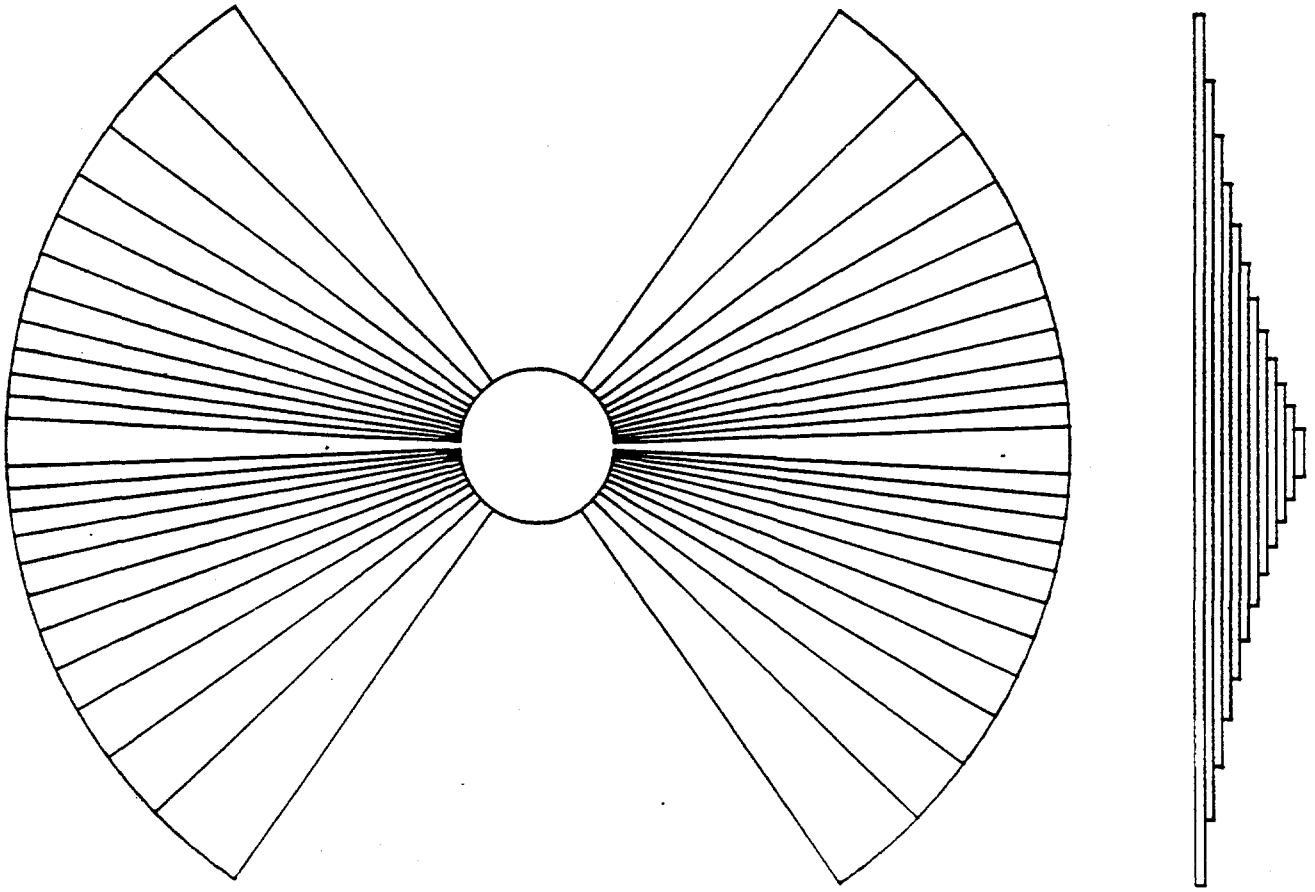

Figure 7

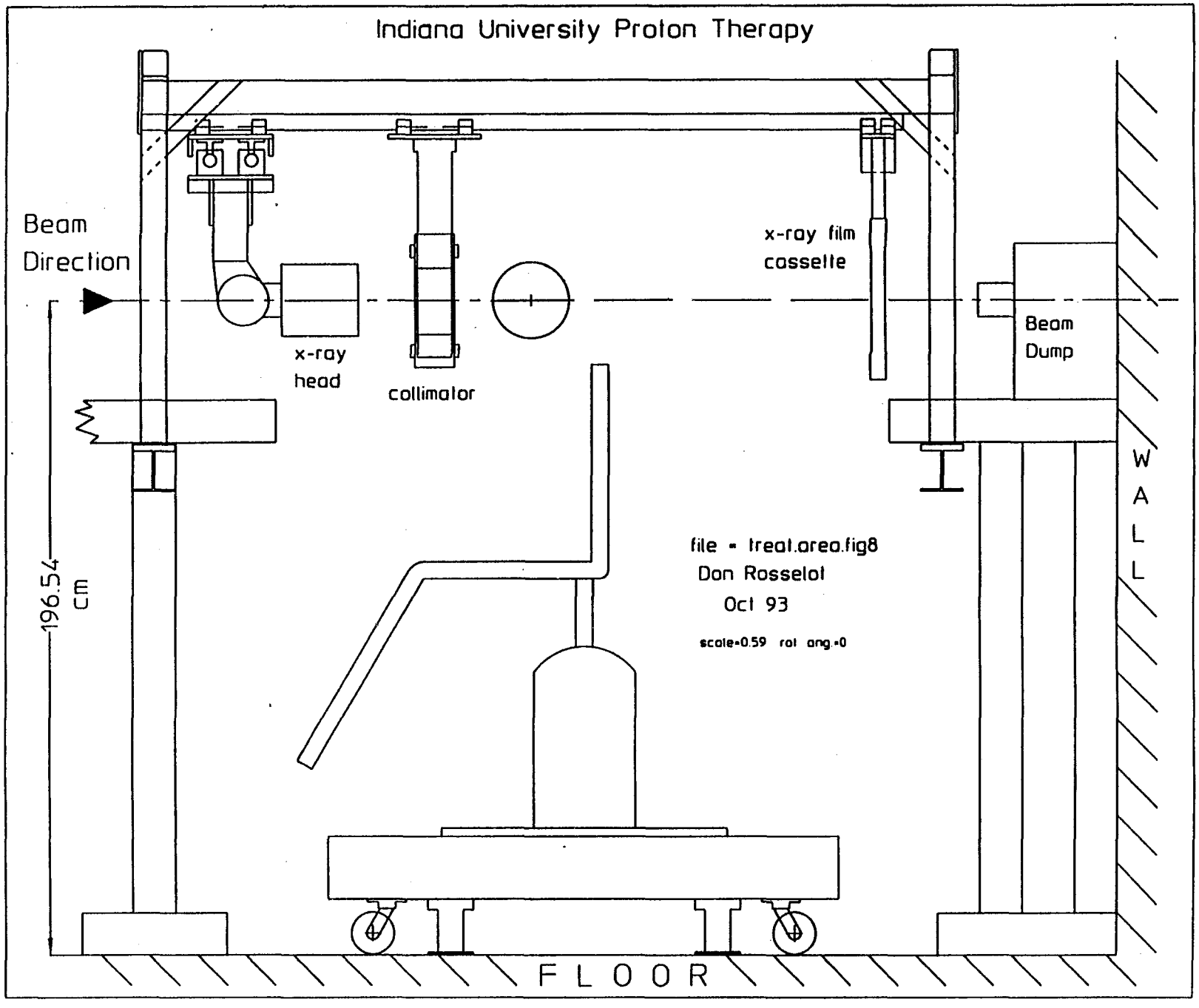
Indiana University Proton Therapy
Beam
Direction
x-ray
head
collimator
x-ray film
cassette
Beam
Dump
W
A
L
L
196.54
cm
file = treat.area.fig8
Don Rosselot
Oct 93
scale=0.59 rot ang.=0
F L O O R

Figure 8

Figure 9

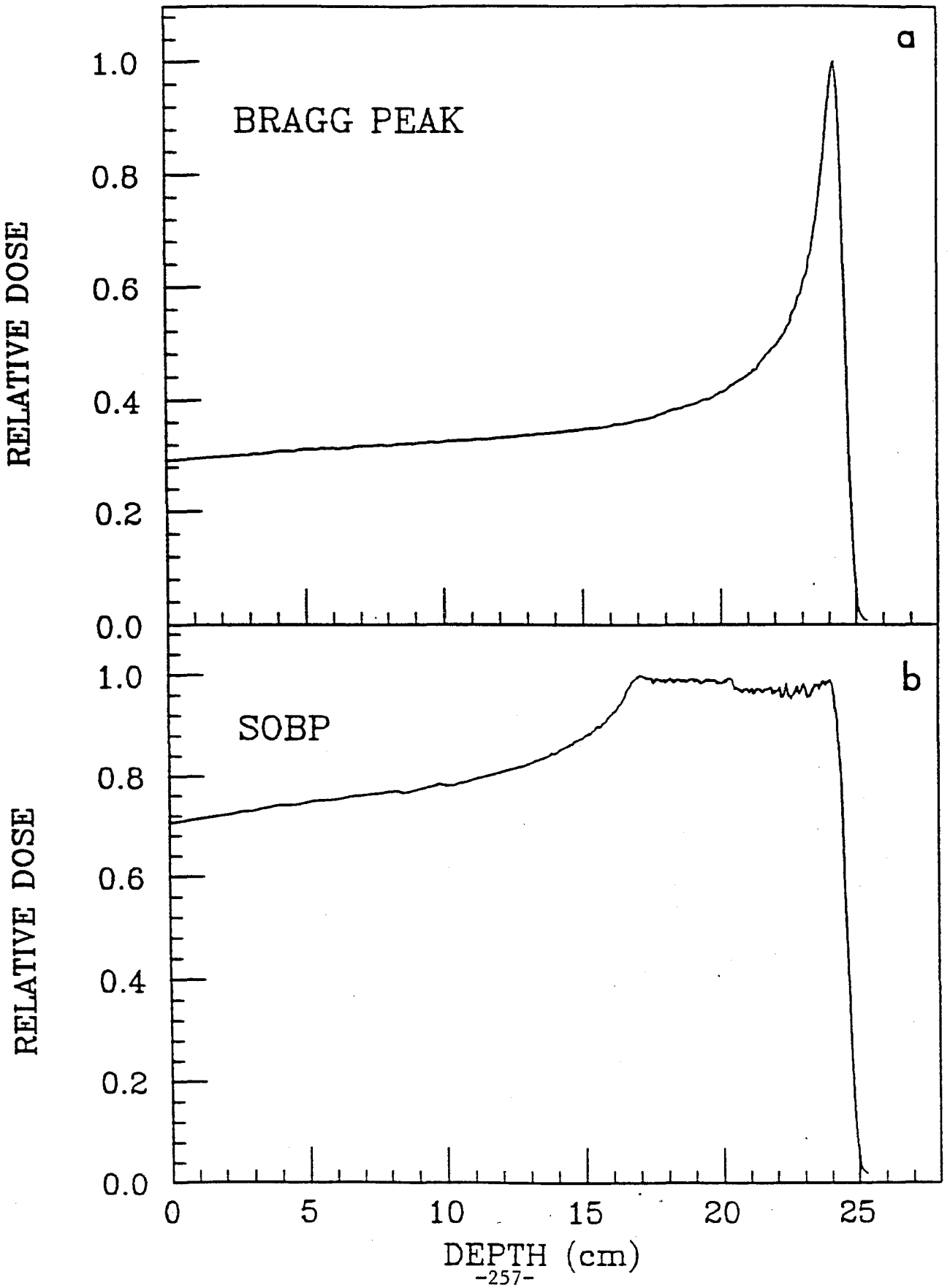
a
BRAGG PEAK
b
SOBP
RELATIVE DOSE
RELATIVE DOSE
1.0
0.8
0.6
0.4
0.2
0.0
1.0
0.8
0.6
0.4
0.2
0.0
0
5
10
15
20
25
DEPTH (cm)

J. FLANZ
MGH

TASKS FOR PROTON THERAPY DEVELOPMENT AT FNAL

Tasks	Done	Not Done	Can FNAL LINAC be used	Places Interested
SCANNING				
- Rapid Cycling vs. Slow Spill	?PSI			
- Raster Scan	?			LBL
- Conformal Scan				LBL, MGH LLUMC, ETC. . . .
Controls				
Software				
- Intensity Variation during Scan				e.g. LBL . . .
Beam Properties and Dose Distributio				
- Control Emittance and Energy Spr				MGH , etc. . . .
Comparte with monte carlo calcula				
and treatment planning algorithms				
different media including hybrid s				
Beam Line Optics/ Beam Cleaning				
- Techniques to minimize energy (distal falloff) from degraders,				
- Control of Penumbra				
Gantry Optics				
- Variable SAD and Focussing Conditions				
- e.g. spot size manipulations with optics; multipoles for flatter beam distribution				
3-D Dose Distribution Measurements, Verification				
Segmented Calorimetry				
Absolute Calibrations and Comparisons				
Measure E and I precisely at FNAL				
PET msmts for dose distributions				
build low cost detectors				
build sharable detectors				
Proton Tomography				
Alignment				

J. FLANZ
MGH

PROTON THERAPY AT FERMILAB

- Develope Systems for Treatment Centers or of General Interest to Proton Therapy:

  There is not enough time available at Clinical Therapy Centers for real development
  Exisiting or planned Proton Therapy facilities or places interested in proton research:
  LLUMC, MGH, Indiana, PSI, GSI, Italy, Nice, Paris, MSU, Uof M, U of Wisc. .....

  FNAL Spans any envisioned energy range

  There are "limited" resources for complicated detector developments at Therapy facilities - FNAL can build detectors to be "borrowed" by labs to help in particularly difficult calibrations... etc.

  Develope new systems:
  Beam Optics
  Beam Delivery Systems
  Detectors and detection methods
  New Techniques

- Develope an actual clinical therapy system

Proposed Test Facility

All devices on rail assembly for alignment with laser system for checkout.

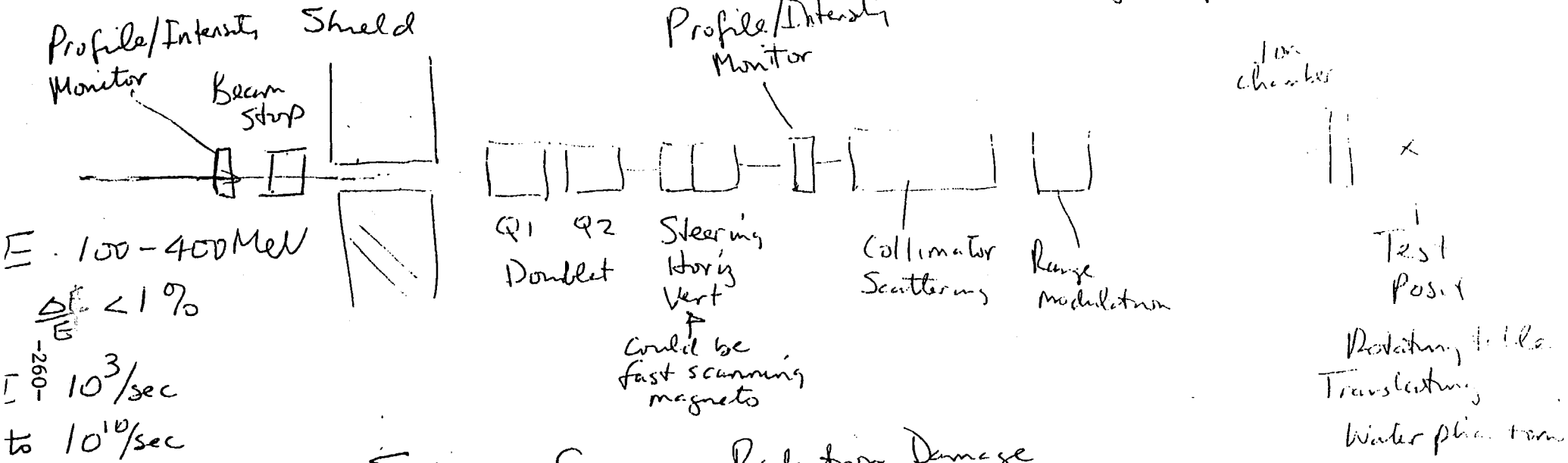

E . 100 – 400 MeV

$\frac{\Delta E}{E} < 1\%$

I ~ 10^3/sec to 10^{10}/sec

↓

Perhaps higher for some radiation damage studies to 10^6 Rads.

Setup for
- Radiation Damage
- Detector tests
- Proton therapy dosimetry
- Nozzle/Scattering/Modulation
- Biology studies.

1/ Beam uniform to < 5% over 15 cm x 15 cm at test position by scattering/collimation

2/ Frequent access - beam stop controlled by dosimetry instrumentation > 10-20/hour

1

Using short length pulse beam in proton therapy (ITEP experience).

Problems (parts):

1. Dosimetry and monitoring
2. Dose compliance, choosing intensity limit amd method of intensity control
3. Dose delivery systems

2

Terminology

Number of particles per pulse - N_p, particles/pulse
Pulse flux - F_p, particles/sec
Pulse fluence - Φ_p, particles/cm^2
Pulse Intensity - I_p, particles/cm^2 sec

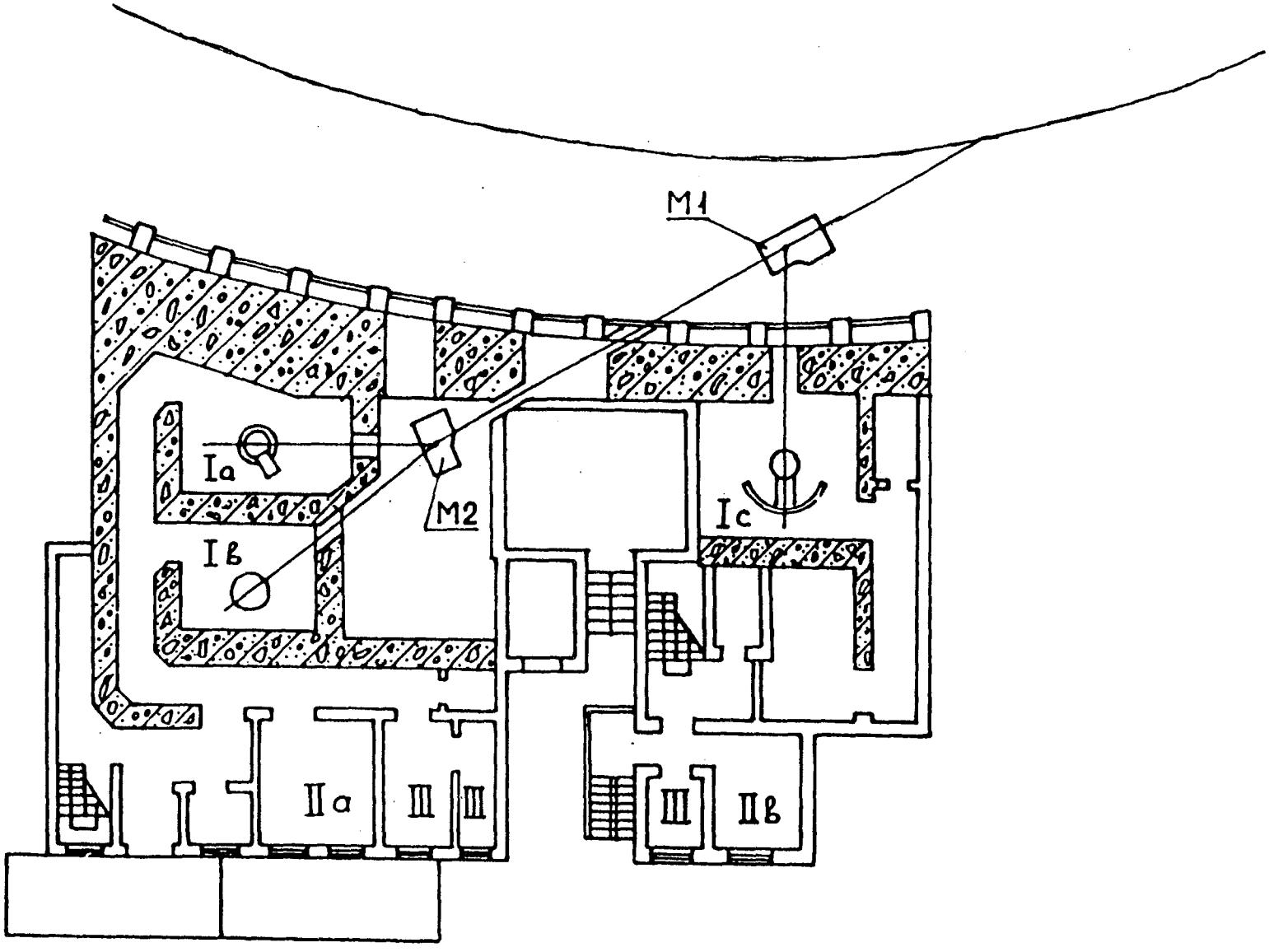
M1
M2
Ia
Ib
Ic
IIa
III
III
III
IIb

4 Main parameters of the internal beams

	ITEP	FNAL
Energy	70-200 Mev	100-400 Mev
N_p	10^9-$5*10^{10}$	10^{13}
Pulse length	100 nsec	30 μsec
Repetition rate	15 p/min	15 p/sec

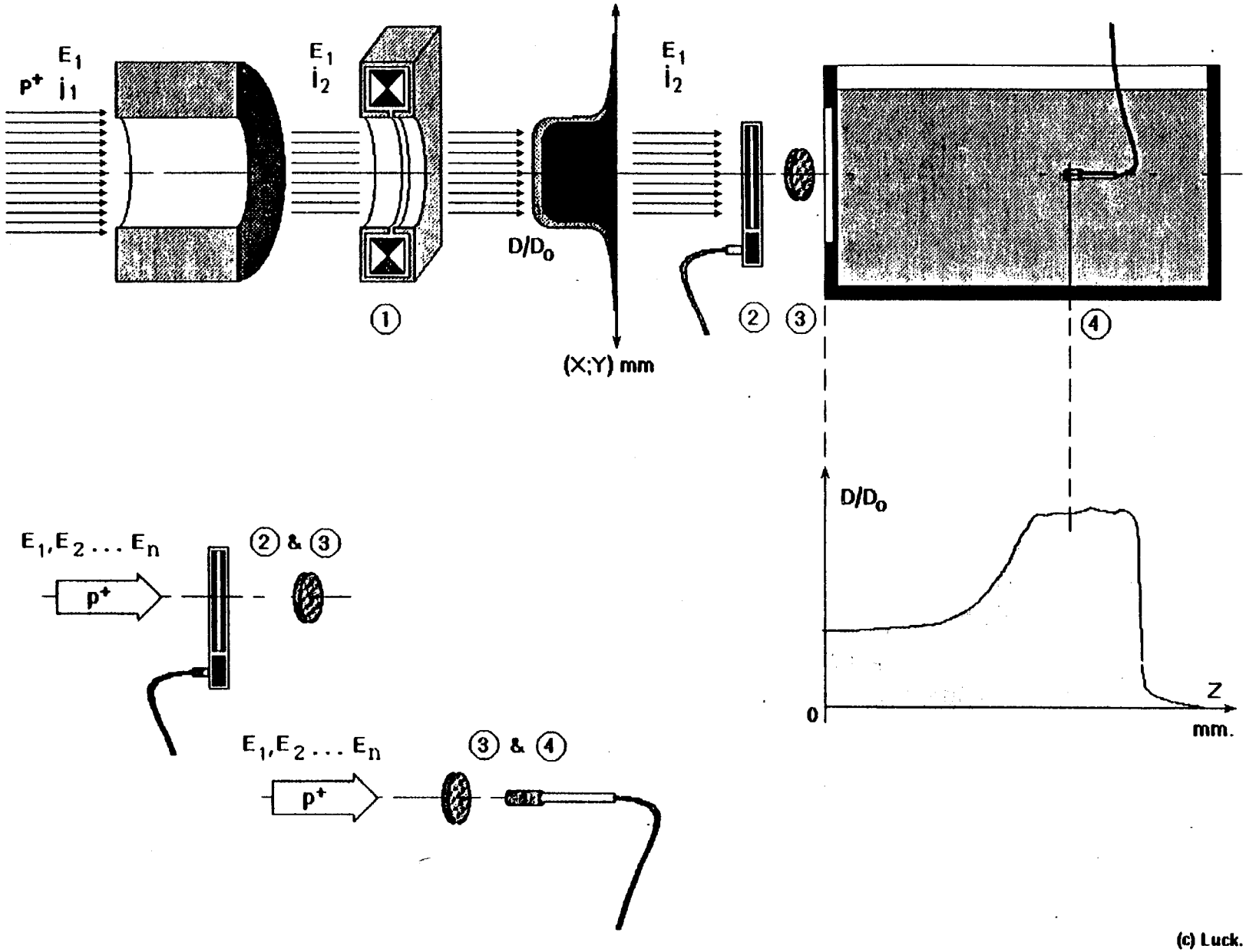

(c) Luck.

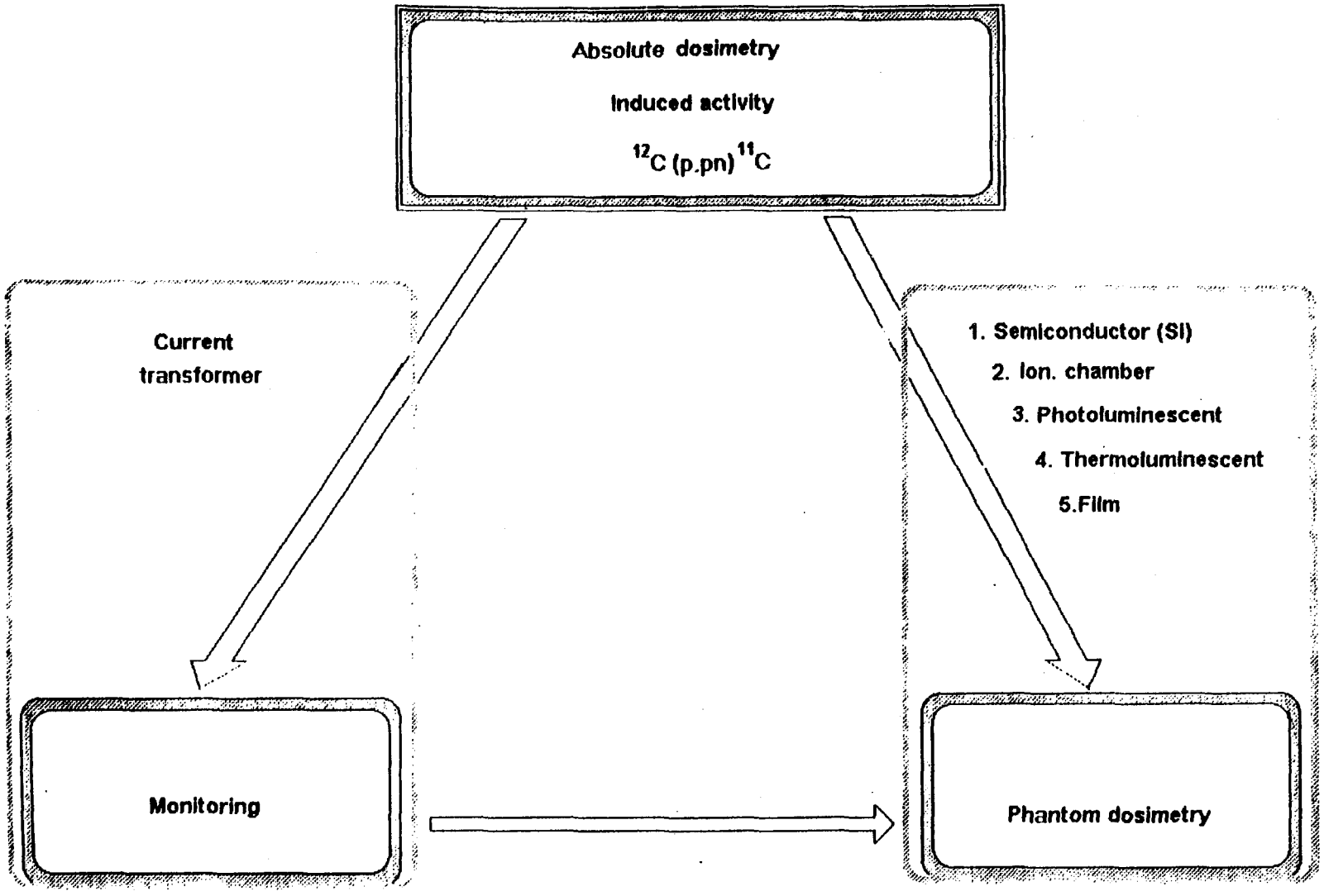
Absolute dosimetry
Induced activity
^{12}C (p.pn) ^{11}C
Current transformer
Monitoring
1. Semiconductor (Si)
2. Ion. chamber
3. Photoluminescent
4. Thermoluminescent
5.Film
Phantom dosimetry

(c) Luck.V.

[redacted]. Absolute dosimetry

Measurements of activity (β-γ coincidences) induced in polystyrene in reaction $^{12}C(p,pn)^{11}C$

[redacted] Beam monitor

Current transformer

[redacted] Phantom dosimetry
(dose distribution measurements)

a. Photographic (p → photographic film → microdensitometer) technique
b. Semiconductor dosimeter .4 Gy, 2 Gy
c. Thermoluminescent dosimetry (TLD)
d. Ionisation chamber
- ordinary g= 7 mm, V= 2 kV, T_V= 300 V/mm, $I_p \leq 10^9$-10^{10} p/cm^{2}sec
- non-ordinary g=1 mm, V=1.5 kV, T= 1.5 kV/mm, $I_p \leq 5*10^{15}$ p/cm^{2}sec

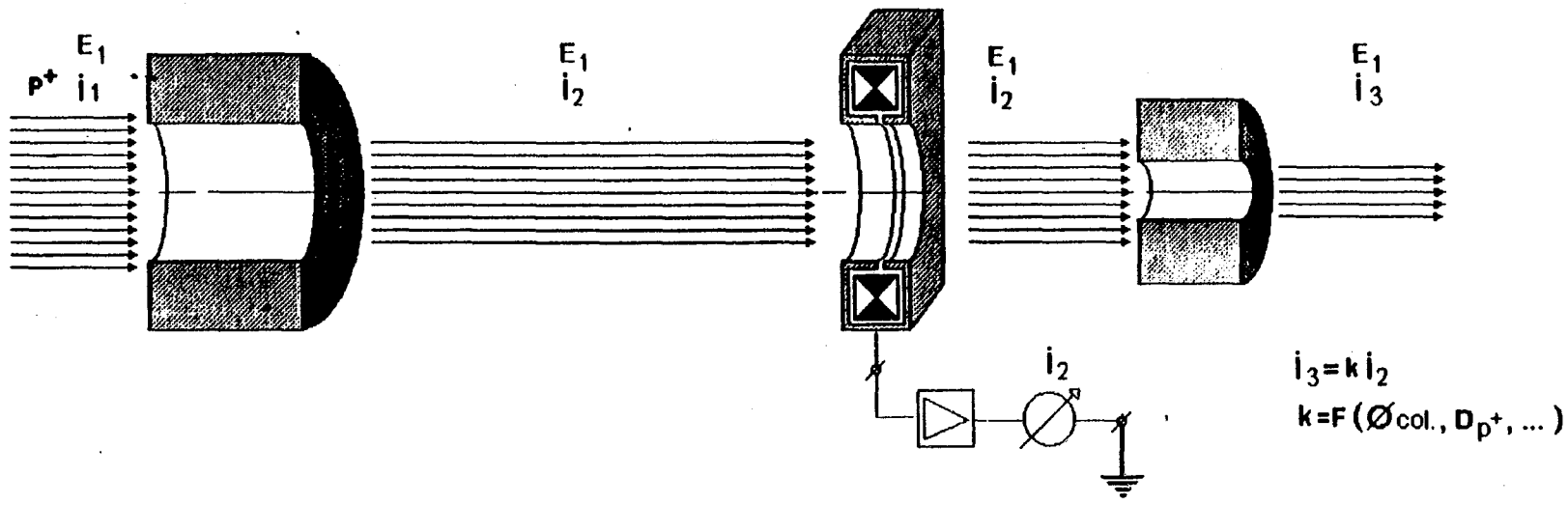
E1
p+ i1
E1
i2
E1
i2
E1
i3
i2
i3 = k i2
k = F (Ø col., Dp+, ...)

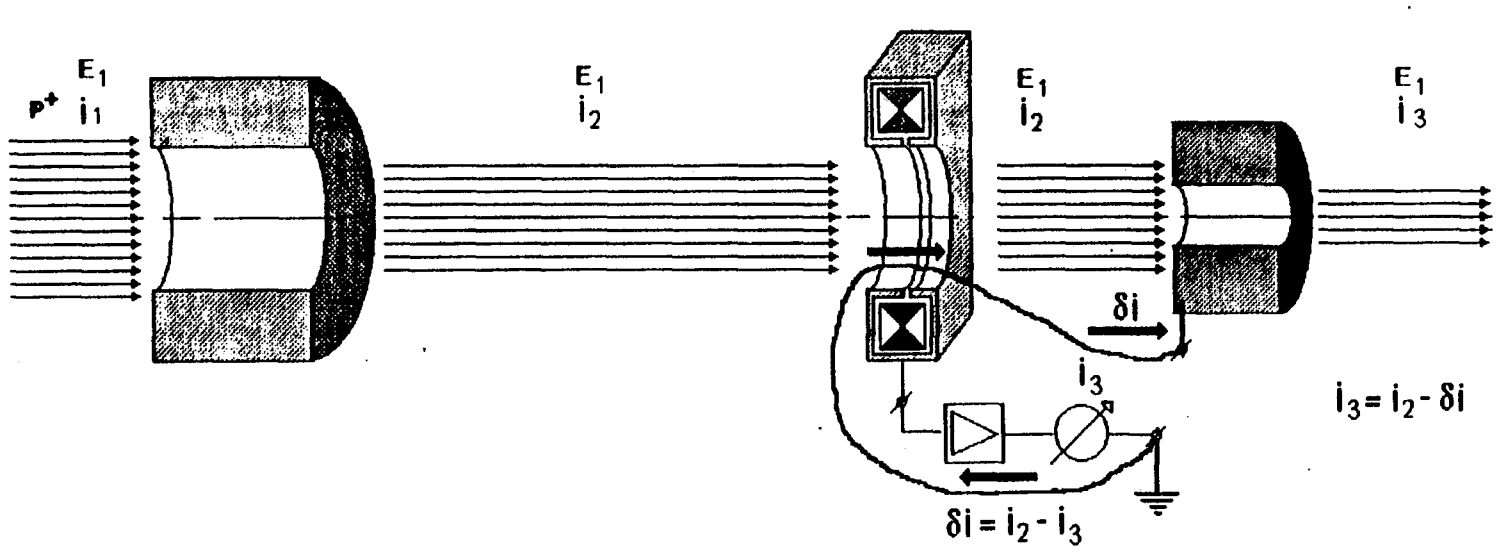
E1
p+ i1
E1
i2
E1
i2
E1
i3
δi
i3
i3 = i2 - δi
δi = i2 - i3

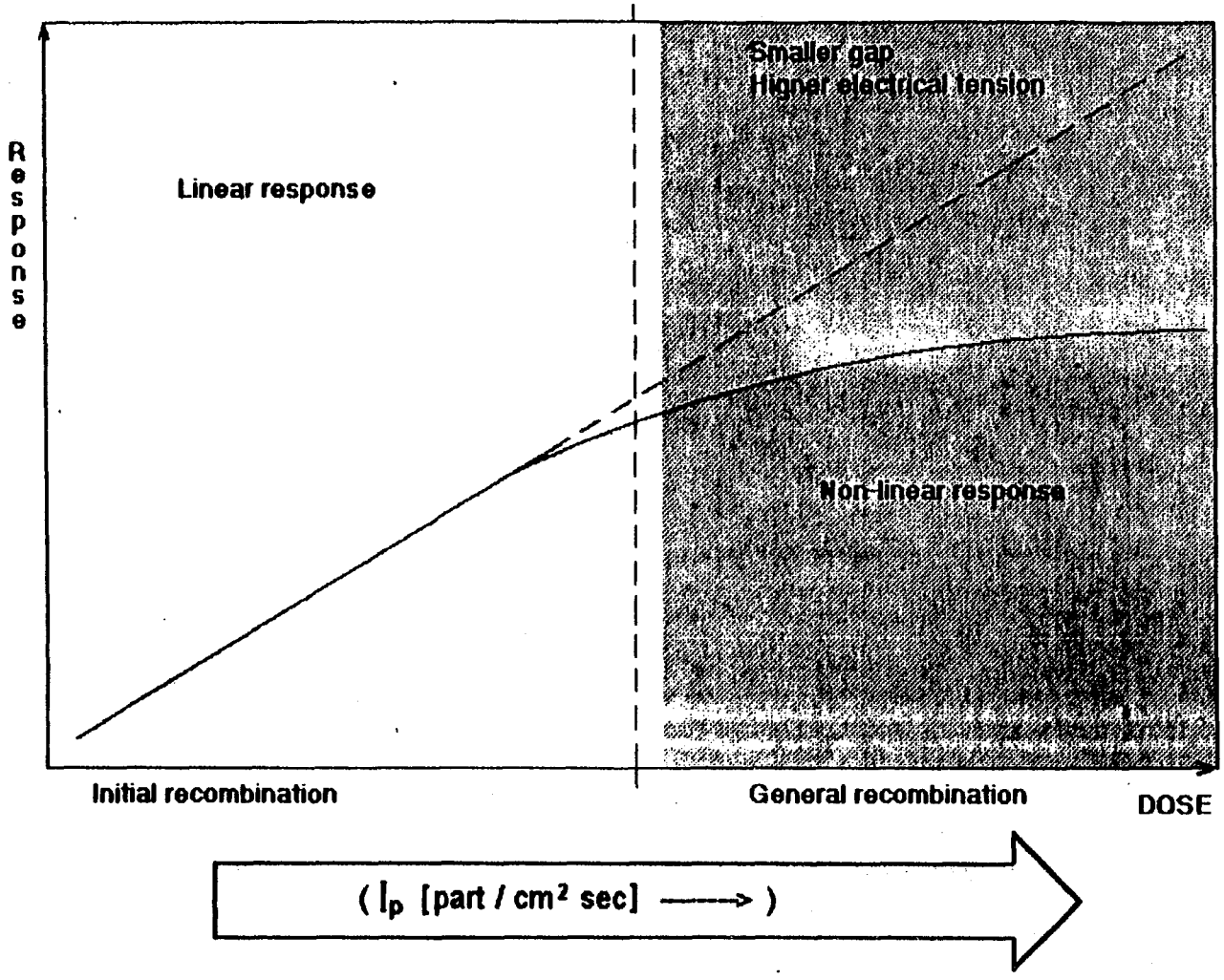
Response
Linear response
Smaller gap
Higher electrical tension
Non-linear response
Initial recombination
General recombination
DOSE
(I_p [part / cm² sec] ⟶)

(c) Luck.

10

Limit of pulse intensity for non-ordinary ICh < $5*10^{15}$ part/cm^2sec

ITEP synchrotron pulse intensity < 10^{16} part/cm^2sec

FL LINAC pulse intensity < $3*10^{16}$ part/cm^2sec (10^{13} part/pulse, 30 μsec, 4 cm target diameter)

Probably it is not too difficult to build ICh with transverse dimensions of 25-30 cm for I_p < 10^{13} part/cm^2sec

11 Conclusions:

1. It is possible to build a dosimetric system for all intensity ranges without an ionisation chamber, but it is not the best solution.
2. Even high-voltage strength ion chambers don't cover all ranges of ITEP and Fermilab pulse intensities and they can't be used as monitors at full intensities.
3. In order to use Ich it's desirable to have pulse intensity upper limit of 10^{13} part/cm^2sec.

12

Target volume - 15 litres ($25 \cdot 25 \cdot 25$ cm^3)

Dose - 2 Gy

Irradiation time - 100 sec

Total number of particles $\cong 5 \cdot 10^{12}$

Reserve - 2

Number of part. per pulse

$$N_p = \frac{5 \cdot 10^{12} \cdot 2}{100 \cdot 15} \cong 7 \cdot 10^9 \text{ part/pulse}$$

13

1. Probably there are no clinical cases requiring more than $7*10^9$ part/pulse at 15 Hz.

2. For all clinical and preclinical work, it is necessary to put this limit ($7*10^9$) to the number of particles in a pulse, the full pulse duration remaining 30 μs (for example, by decreasing the pulse flux of the source).

3. Pulse intensity of the beam incident to a large target or to a beam monitor, becomes

$$I_p = \frac{7*10^9}{25*25*30*10^{-6}} = 4*10^{11} \text{ part/cm}^2\text{sec}$$

4. Further decrease of the number of particles per pulse (down to 10^8-10^7 part/pulse) for irradiation of smaller targets, may be done in two ways (by decreasing the source pulse flux about 10 times and by shortening the pulse length).

5. The limit $I_p < 10^{13}$ must always be maintained.

As the result:

It becomes possible to use an ordinary simple large-aperture ionization chamber in all ranges of operation of pulse intensity for both purposes - as a research instrument in preclinical studies and as a dose monitor for treatment.

Since no less than few hundred pulses are required to deliver the dose, it becomes possible to provide compliance between prescribed and delivered doses in all cases.

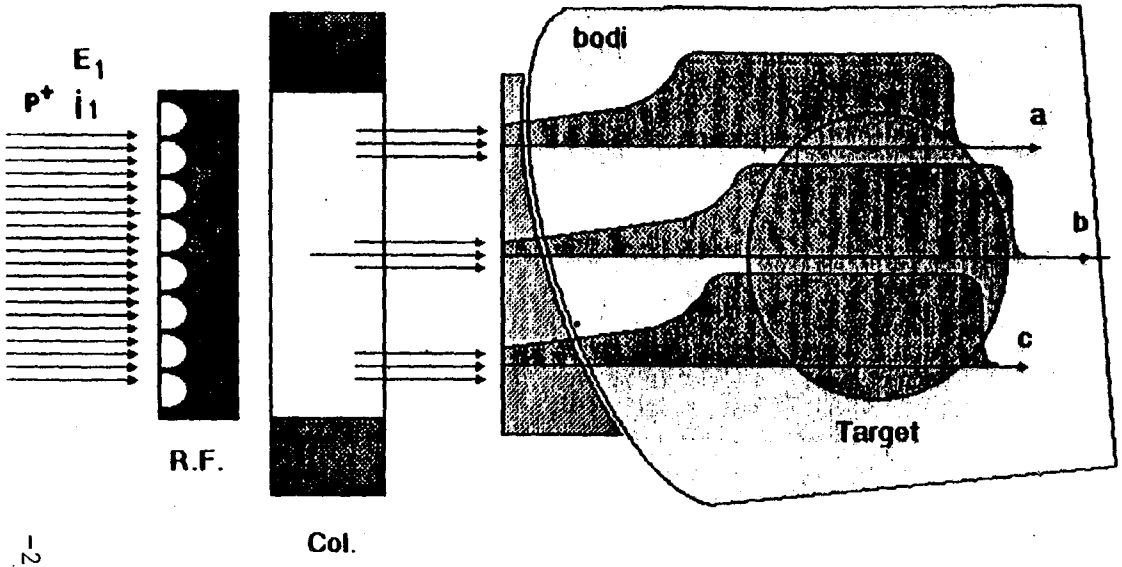
E1
P+ i1
R.F.
Col.
bodi
a
b
c
Target

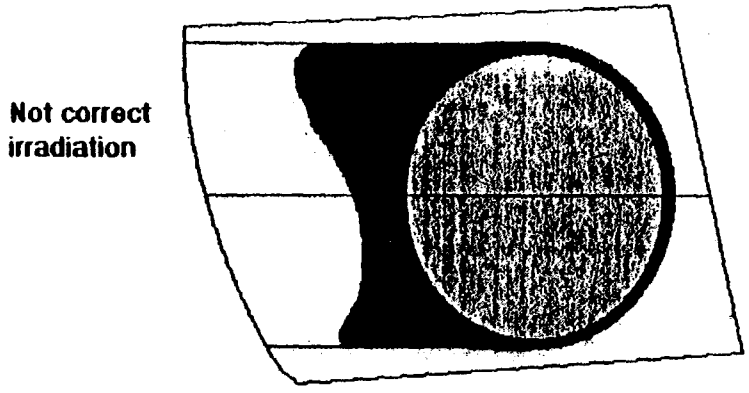
Not correct
irradiation

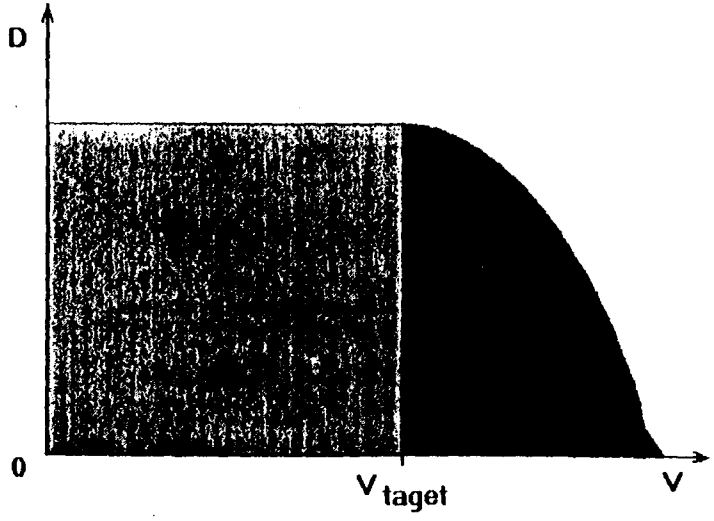
D
0
V taget
V

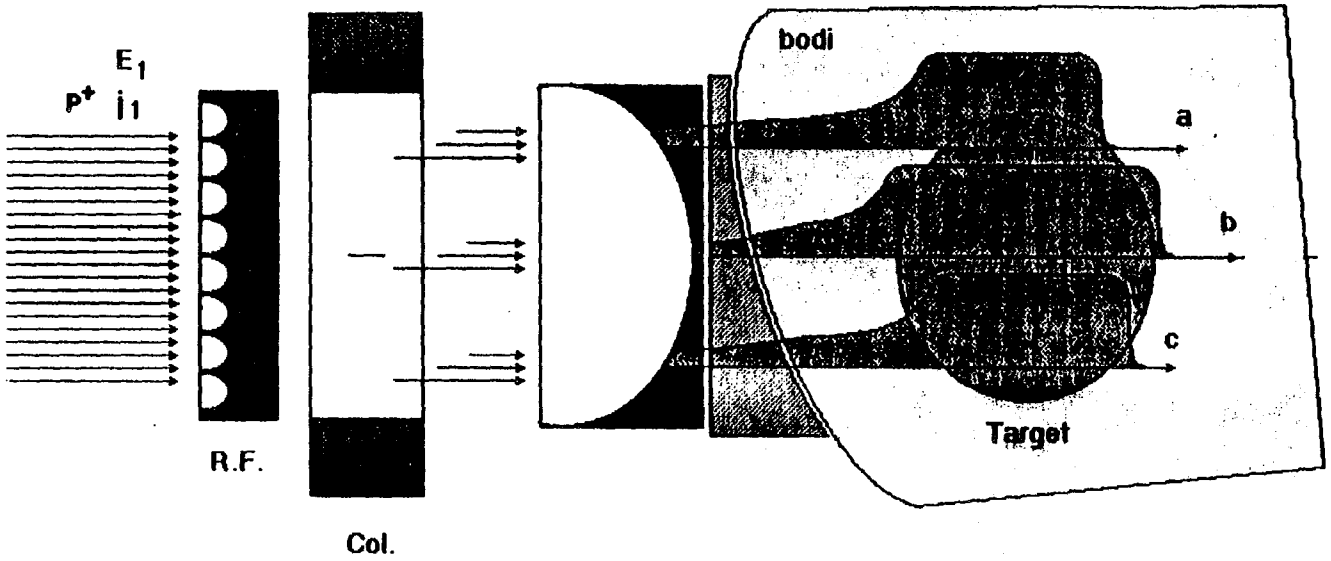

Correct irradiation

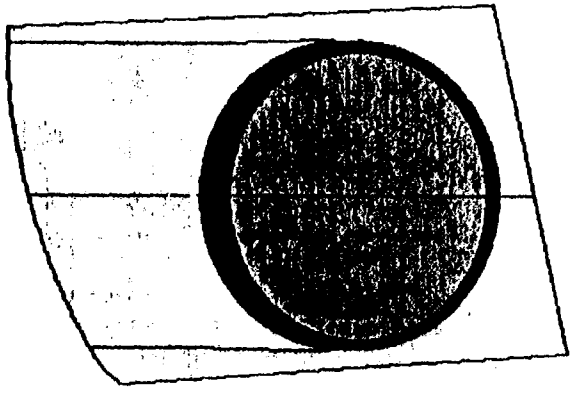

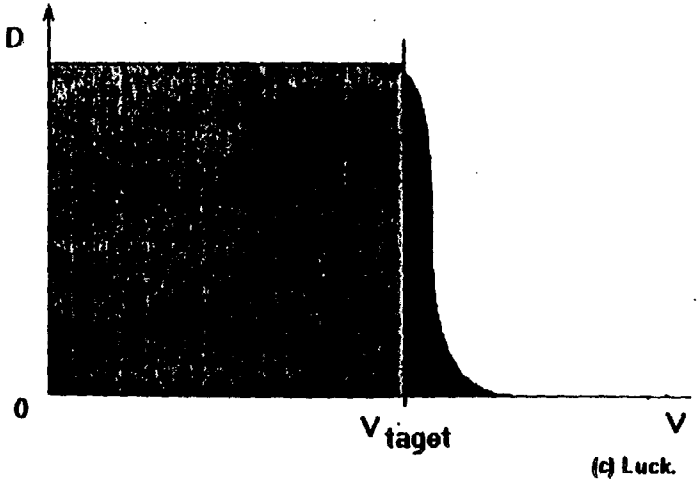

(c) Luck.

15

Conclusion

It is extremely desirable to look for the way to create dynamic dose delivery systems for the Fermilab linac.

15 Hz repetition rate, 30 μs pulse duration and, finally, the availability of the H^- beam open certain possibilities for it.

	CHARACTERISTICS	PRIORITY			
1.	SIZE	cyclotron	synch. H^+	synch. H^-	linac.
2.	WEIGHT	synch. H^-	synch. H^+	linac.	cyclotron
3.	OPERATION COSTS	synch. H^-	synch. H^+	cyclotron	linac.
4.	COST	synch. H^+	synch. H^-	linac.	cyclotron
5.	RELIABILITY	linac.	cyclotron	synch. H^+	synch. H^-
6.	RADIATION LEVEL	synch. H^-	synch. H^+	linac.	cyclotron
7.	PHASE SPACE OF EXTRACTED BEAM	synch. H^-	linac.	synch. H^+ linac.	cyclotron
8.	ENERGY SPREAD	synch. H^-	synch. H^+	linac.	cyclotron
9.	EXTRASTION ENERGY CHANGING	synch. H^-	synch. H^+	linac.	cyclotron
10.	BEAM INTENSITY CHANGING	synch. H^-	synch. H^+	linac.	cyclotron
11.	EXTRACTION DEVICE	linac.	synch. H^-	synch. H^+	cyclotron
12.	POSSIBILITY TO ACCELERATE LIGHT IONS WIHT SMALL CHANGE OF INSTALLATION	synch. H^-	-	-	-

NO PROBLEM WITH SPACE CHARGE LIMIT

SIMPL POWER SUPPLY SYSTEM

STABILITY OF EXTRACTED BEAM
DOES NOT DEPEND FROM
RIPPLE OF MAGNETIC FIELD

SIMPLE PF SYSTEM
SMALL FREQUENCY RANGE ~ 1,5

SMALL VACUUM CHAMBER APPERTURE

POSSIBLE TO USE AL VACUUM
CHAMBER WITH DISTRIBUTED
ION AND NEG PUMPS

HIGH DUTY FACTOR

Beam Intensity

1. **Beam intensity** (dN/dt): 10^{11}/second at 200 MeV, averaged over one cycle at end of gantry, including all losses in the transport system with the usual monitors required to be in the beam used during patient treatment, measured upstream of the vacuum exit window in the gantry.
2. **Spill Length:** 1.0 second minimum. Extended flat-tops are desirable with corresponding less current (dN/dt) acceptable corresponding to the same circulating current in the synchrotron as for the 1 second spill. Variable spill lengths down to 0.1 second are also acceptable if the synchrotron cycle rate can be correspondingly increased.
3. **Macroscopic (Spill to Total Cycle Time) Duty Factor:** Fraction of machine cycle in which beam is available: ≥50%
4. **Microscopic (r.f.) Duty Factor:** Full modulation by r.f. in the MHz range is acceptable.
5. **Undesired Beam Intensity Modulation:** Acceptable time structures in extracted beam are specified below for scanning and scattering modes.
6. **Beam Intensity Modulation Capability Within Pulse:** Minimum implementation: no modulation needed — variable velocity scanning used. Upgrade path: 100:1 dynamic range down from rate that produces maximum intensity, with bandwidth from d.c. to 5 kHz.
7. **Pulse-to-Pulse Selection of Beam Intensity:** 1000:1 variation of circulating beam intensity from pulse-to-pulse specified by data arriving no less than 0.1 second before injection with ±10% accuracy at the 10^8/second average intensity level, increasing in accuracy to ±2% at the 10^{11}/sec average intensity level.
8. **Beam ABORT Time:** ≤10 μseconds to completely shut off beam after a trigger signal is received.

The limits of the intensity excursion, or peak intensity, integrated within the specified window time for the instantaneous extracted beam rate are specified as follows:

Scanning Method Requirements

Window Time	Maximum Excursion
> 200 μsec	±20%
200 μsec – 100 μsec	Linearly rising to ±100% at 100 μsec
100 μsec–25 μsec	Linearly rising to excursions 5× average spill rate, or less than 5×10^6 particles, whichever is more at 25 μsec.
<25 μsec	No specification — will be controlled by the r.f. structure.

Scattering Method Requirements

Window Time	Maximum Excursion
1 millisecond	No more than 10^9 protons, or 0.1% of the total number of protons in the treatment, whichever is less.

Accelerator Performance Specifications

Energy

1. **Energy Range:** 70-250 MeV protons at the gantry exit measured with the beam monitors used during patient treatments, but before the vacuum exit window.[6]
2. **Time to Establish a New Extraction Energy:** Next pulse or one second.
3. **Energy Precision:** The energy will be within ±0.4 MeV of the requested energy over the entire range.
4. **Energy Variability:** The resolution of the energy-determining system will be no greater than ±0.4 MeV over the entire range.
5. **Energy Spread:** ≤±0.1% FWHM at exit of gantry at 100 MeV and up, measured with the beam monitors used during patient treatments, but before the vacuum window.
6. **Energy Variations of Extraction:** ≤±0.1%

Quality of Extracted Beam

1. **Transverse Emittance:** ≤0.5π cm-mrad, rms, unnormalized, at 200 MeV, at accelerator exit.
2. **Position and Angle Stability of extracted beam:** Extracted beam, measured at synchrotron exit, must not vary by more than ±1 mm or by ±1 mrad during the pulse, or between pulses at the same energy. See [Sec. 3].

Accelerator Beam Monitoring

1. **Monitoring of Beam Circulating in Synchrotron:** Primary beam monitor must operate down to 5×10^6 circulating protons with an accuracy no worse than ±10%, improving in accuracy to no worse than ±2% at 10^8 or more circulating protons.
2. **Time to recover from various shut-down conditions:** Time to start up or shut down from various conditions are specified in the table below.

Item	Startup/Shutdown Time
Facility startup from total shutdown	1 Day
Daily operation startup to point where dosimetry can be done	1 hour
Control system startup so start and check computer	30 minutes
Daily operation shutdown time to safe mode	15 minutes
Facility shutdown and secure time	4 hours

FACILITY FOR PROTON THERAPY OF CANCER

EJECTING MAGNET

INFLECTOR	RF SYSTEM	INJECTING MAGNET
DEFLECTOR		
DEFFECTING MAGNET	INJECTING CHANNEL	INJECTOR
EJECTING CHANNEL	REGISTRATION SYSTEM	LIFT-ROOM

LAY-OUT OF B-5 ACCELERATOR

1. ION SOURCE
2. BUNCHER
3. 2 GAPS LINEAR ACCELERATOR
4. INJECTING MAGNET
5. FRAME MAGNET
6. ENVELOP OF MAGNET
7. COIL
8. SUPPORT
9. MAGNET
10. INFLECTOR
11. DEFLECTOR
12. EJECTING MAGNET
13. VACUUM CHAMBER
14. RESONATOR

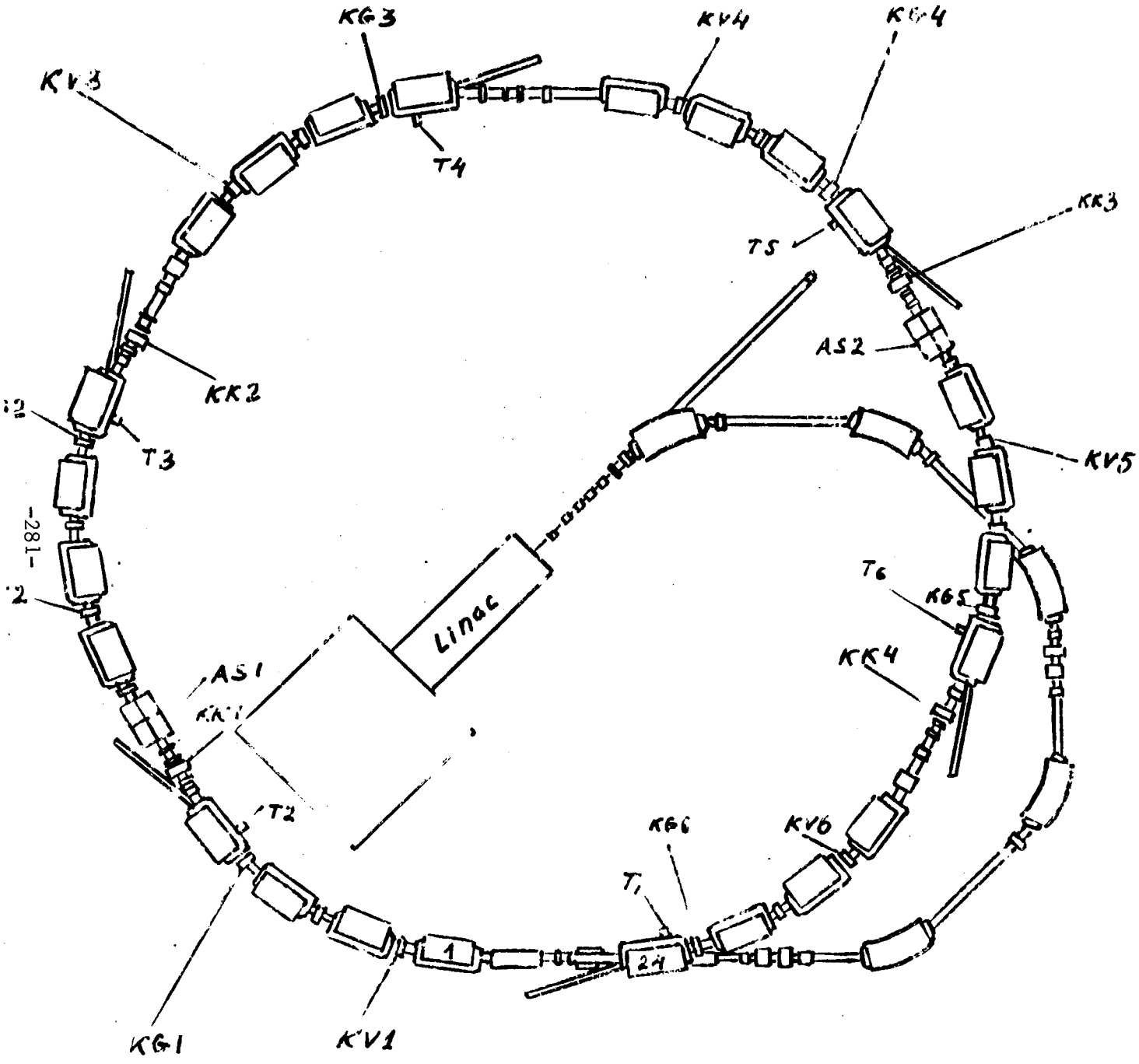

1-24 Magnets
T Targets
KK Quadrupole lenses
KV Vertical correctors
KG Horizontal correctors

Fig. 1. A schematic layout of the synchrotron.

Compact Accelerator for Proton Therapy

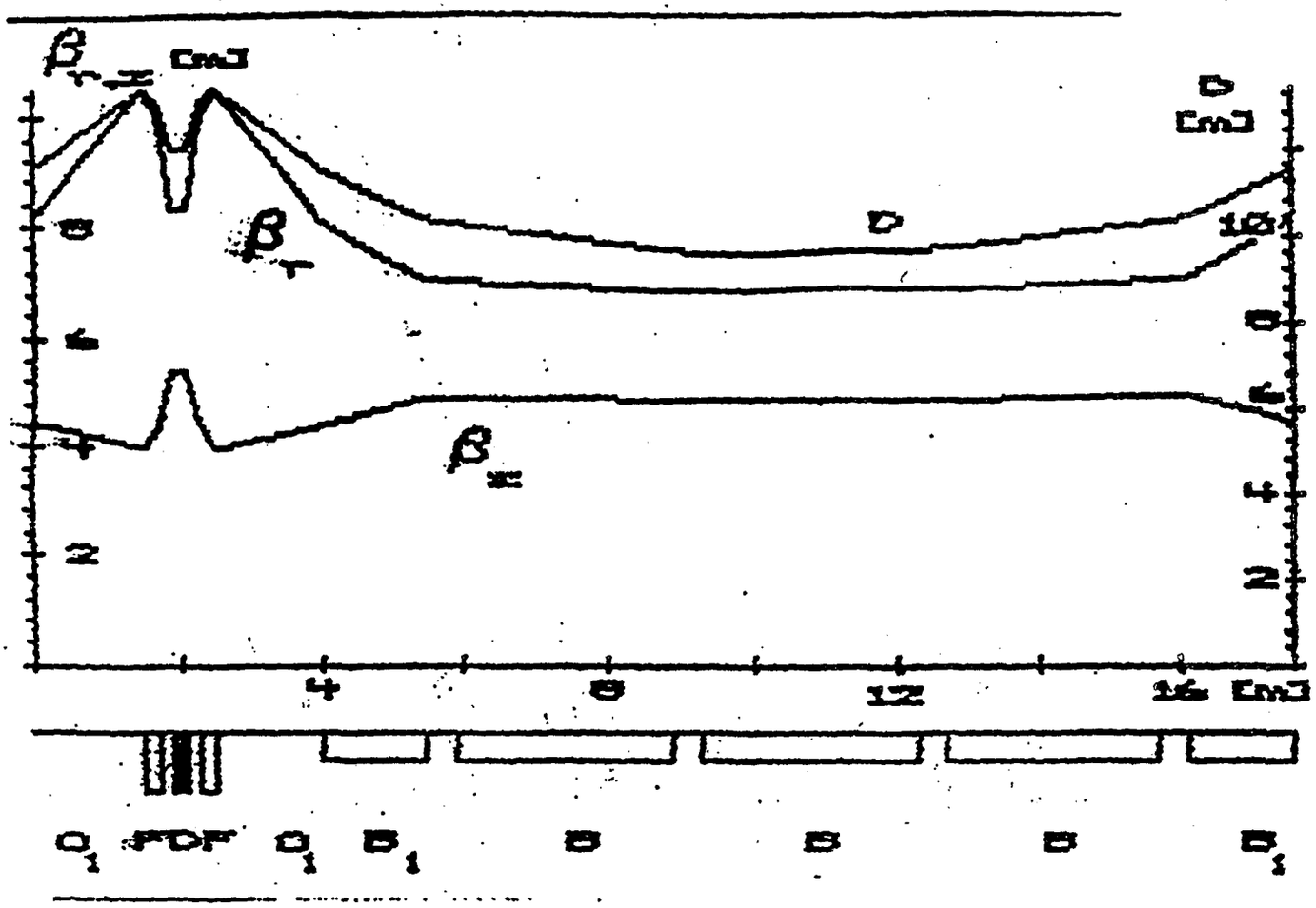

Transverse motion function for one superperiod.

Main synchrotron parameters

Intensity.....10^{11} p/s
Particle type.....H^-
Injection energy.....12 Mev
Ejection energy.....70÷250 MEV
Repetition rate.....5 Hz
Flat top duration.....30 ms
Orbit circumference.....35.2 m
Number of superperiods.....2
Superperiod structure:
$O_1FO_2DO_2FO_1B_1OBOBOBOB_1$, B_1,B - the edge vertical focusing magnets, F and D - focusing and defocusing quadrupoles, accordingly, O, O_1 and O_2 - straight sections
O_1 length.....1.5 m
O_2 length.....0.2 m
O length.....0.4 m
Total number bending magnets.....10
Field length of B.....3.0 m
Field length of B_1..... 1.5 m
Edge angles of B and B_1 (on entrance and exit)
Bending radius.....3.82
Injection field.....0.131 T
Maximum field.....0.636 T
Field gradient length of F and D.....0.2 m
Normalised gradient for F-lens.....2.5 m^{-2}
Normalised gradient for D-lens.....4.6 m^{-2}
Maximum field gradient in lenses..11.2 T/m
Horizontal tune, Q_r.....0.717
Vertical tune, Q_z.....1.235
Maximum value of β_r in magnets.....8.1 m
Maximum value of β_z in magnets.....5.0 m
Maximum of dispersion in magnets....11.5 m
Transition energy.....absent
Chromaticity $dQ/(dp/p)_{r,z}$....-0.16; 3.2736
Aperture in magnets R*Z.....120*35 mm^2
Half-aperture in lenses.....50mm
Vacuum.....$5\cdot10^{-10}$ Torr

Harmonic number.....2
Frequency change of RF.....2.71÷10.46 MHz
Acceleration time.....0.1 s
Acceleration voltage.....1.4 kV
Equilibrium phase

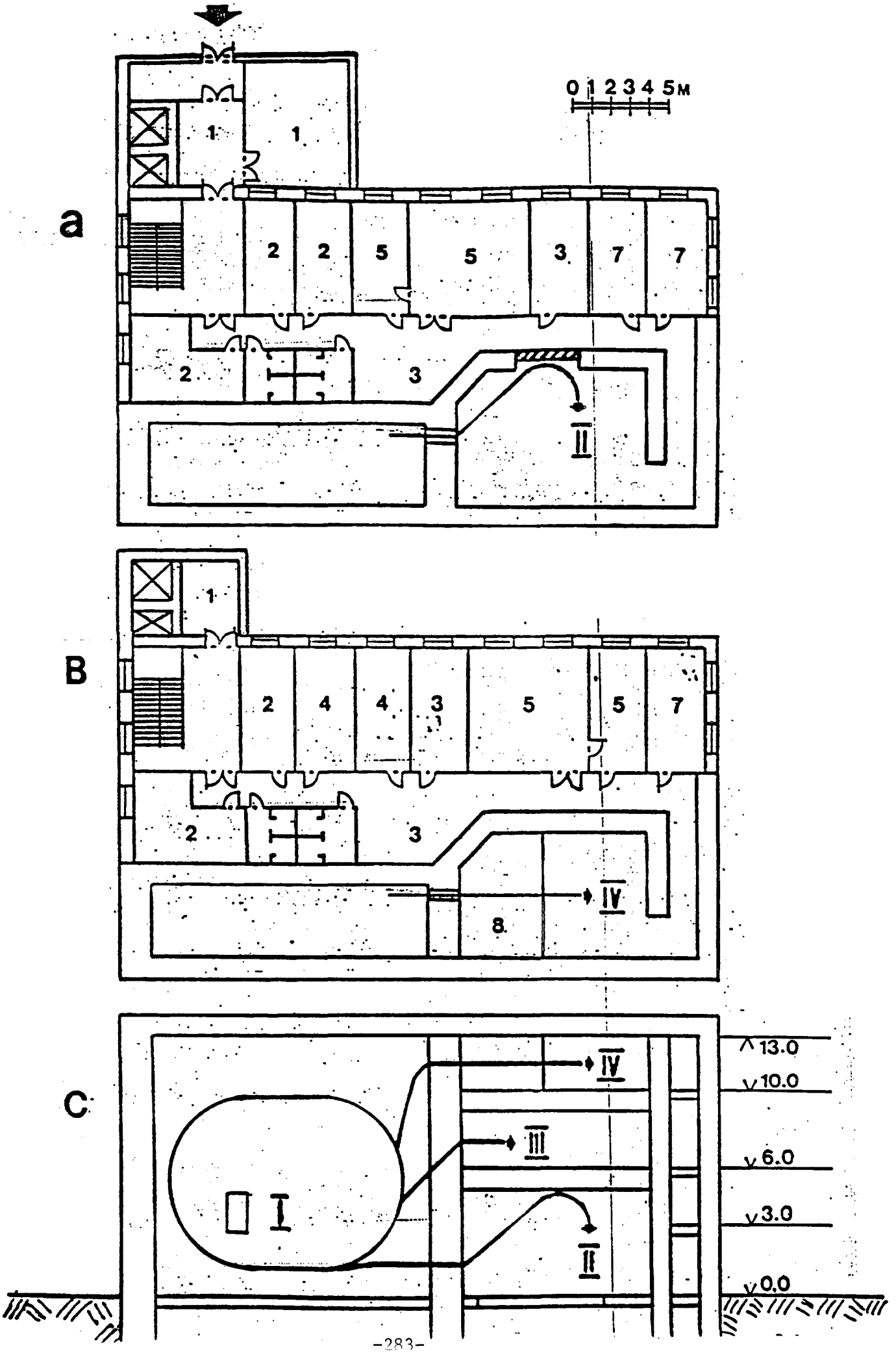
a
0 1 2 3 4 5м
1
1
2
2
5
5
3
7
7
2
3
II
B
1
2
4
4
3
5
5
7
2
3
IV
8
C
IV
III
I
II
13.0
10.0
6.0
3.0
0.0

H^- STRETCHER

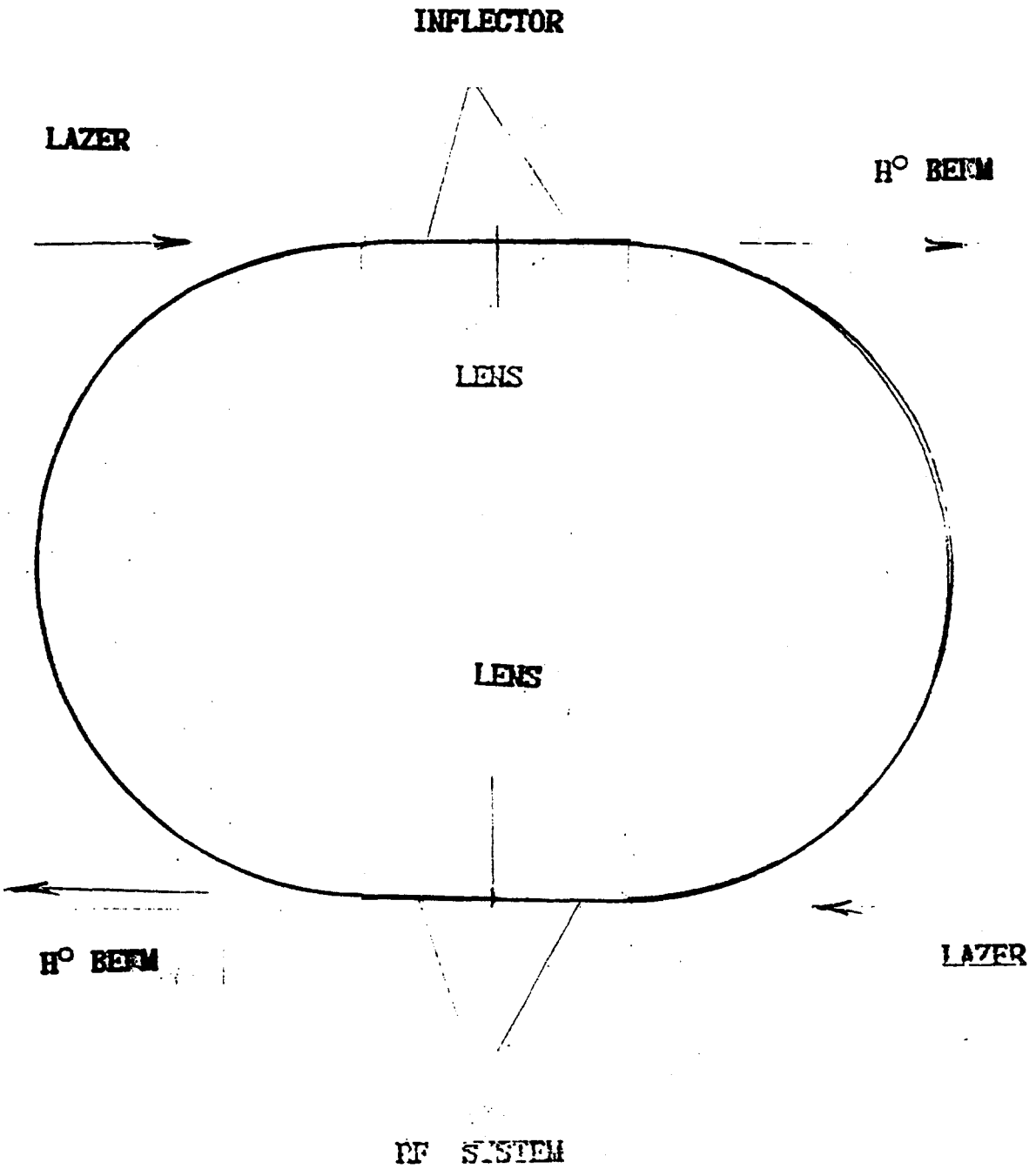

200 MEV

CIRCUMFERENCE ~ 30 m

Advantages of a laser extraction:

1. Stability of the external beam doesn't depend on magnetic field stability of the bending magnets and extraction devices.

2. It is possible to vary extracted beam intensity in a wide range.

3. It is not necessary to decrease accelerator intensity hundred times when low intensity external beam is to be used.

4. It is possible to change beam energy in a accelerator cycle.

5. Energy of the particles remaining in the accelerator can be slowed down thus decreasing activation level.

6. There is additional way to measure extracted beam intensity. The latter is proportional to the product of particle intensity in accelerator and laser beam intensity. These parameters can be measured in a simpler way than extracted beam intensity.

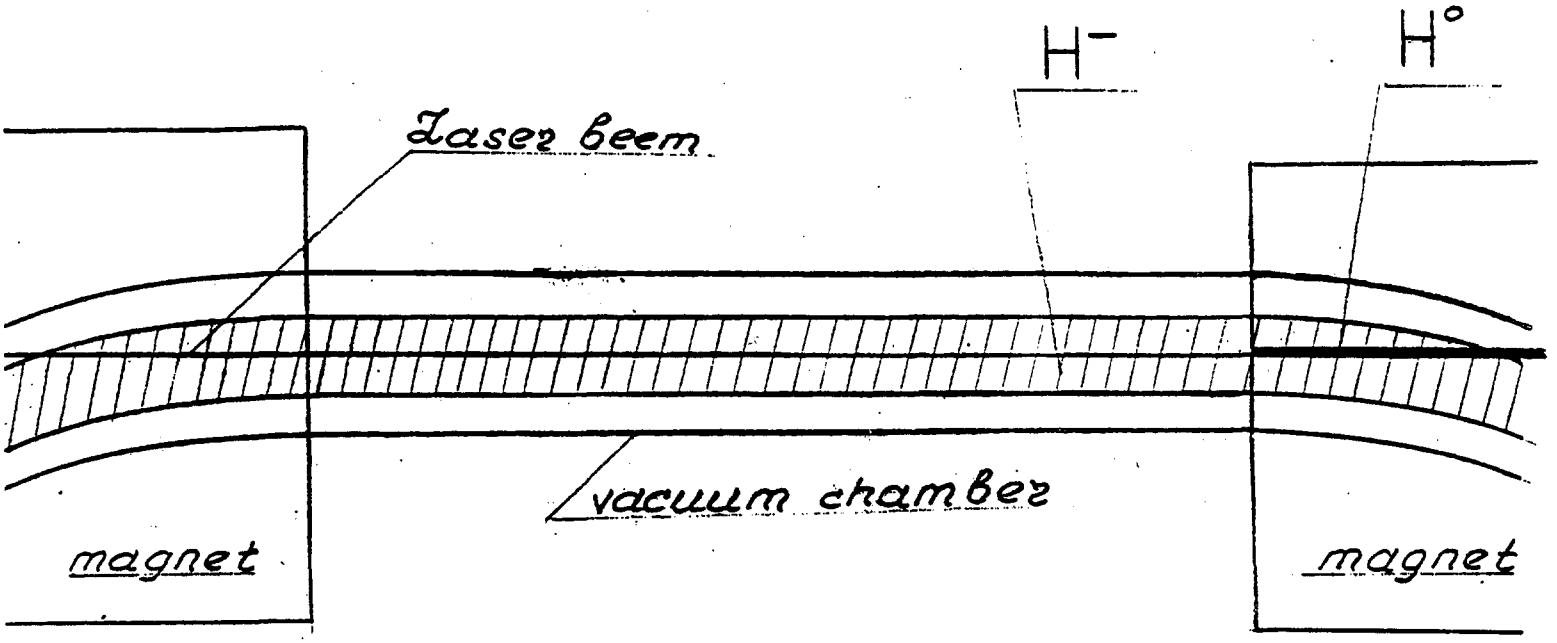
H⁻
H°
Laser beam
vacuum chamber
magnet
magnet

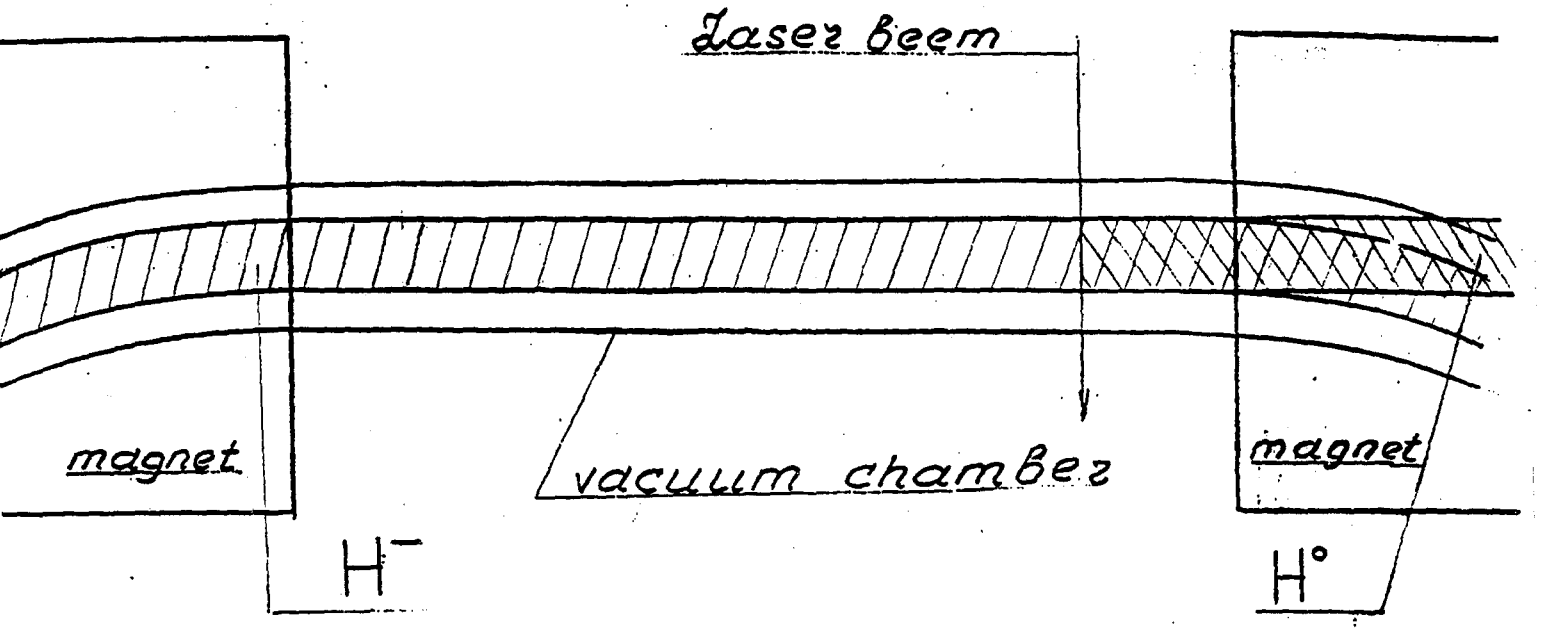
Laser beam
magnet
vacuum chamber
magnet
H⁻
H°

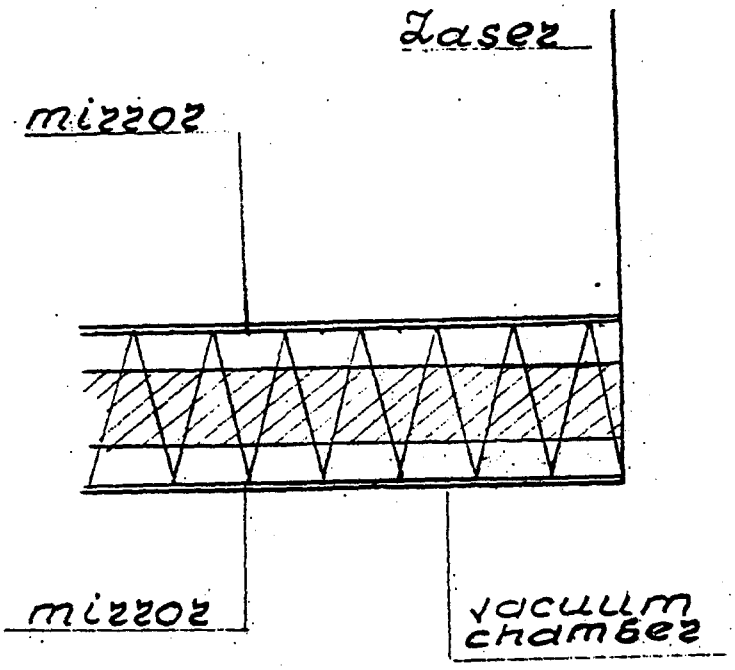
Laser
mirror
mirror
vacuum chamber

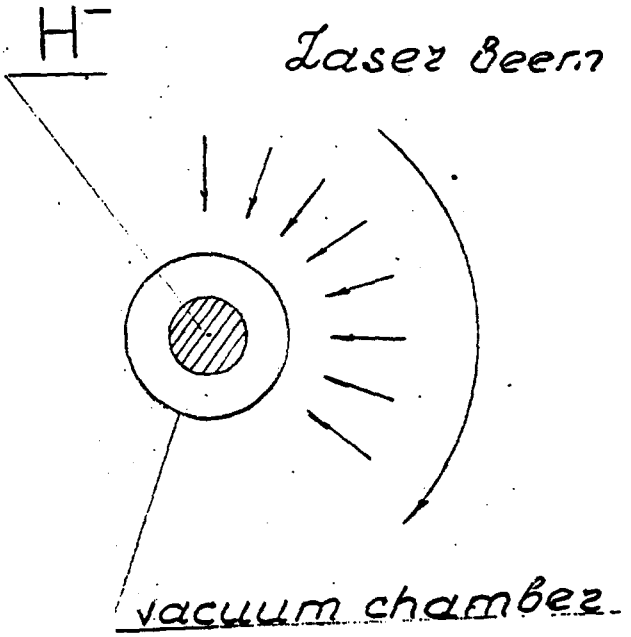
H⁻
Laser beam
vacuum chamber

Annexe III

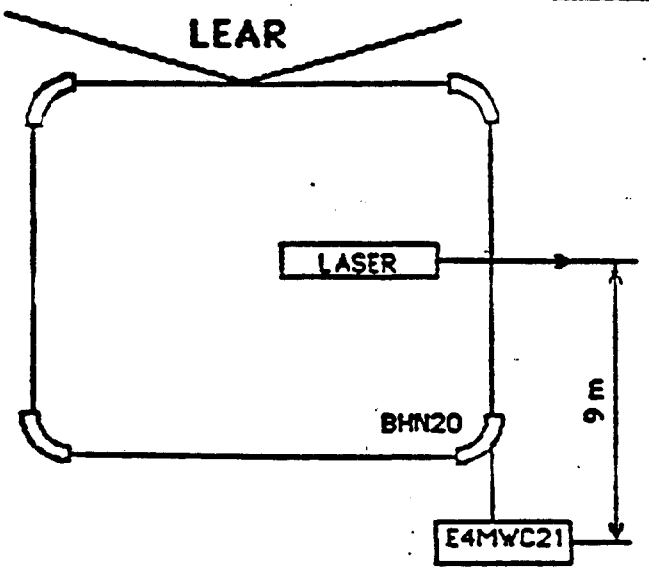

Laser : type YAG 580.10 QUANTEL
λ = 1.06 µm
E_0 = 120 - 230 mJ.

Fig. 3 : Schéma de l'installation du laser

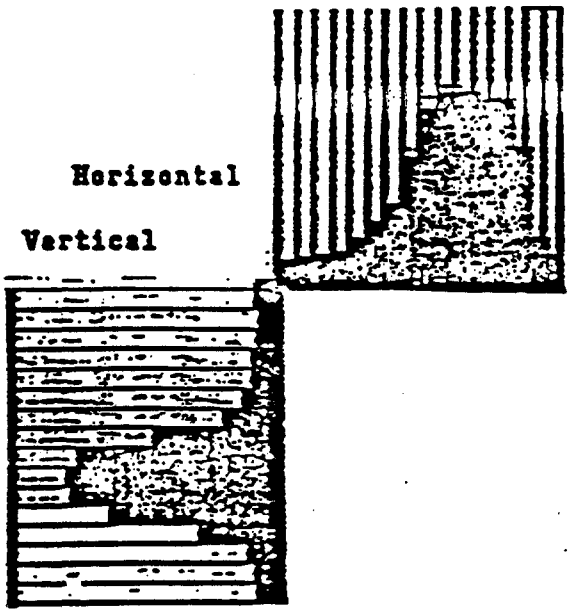

Fig. 4 : Chambre à fils MWC21
profils H et V obtenus
6mm/fil

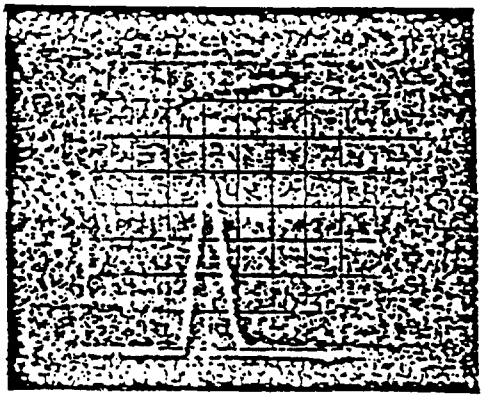

Fig. 5 : UWB22 : signal observé sur oscilloscope (20 ns/carreau 10mV/carreau) - 1.7 10^5 H^- circulant - 4.4 10^6 H_0

Transversal irradiation.

The continuous laser beam intersects in the transversal horizontal plane the circulating accelarated H^- beam at the drift space of synchrotron orbit. Assuming the laser beam as a "target" we can determine the number of the H^o as regards to the number of initial H^- particles:

$$N_o = N_- \, n \, \sigma \, l \qquad (1),$$

where N_o - flux of the H^o particles, N_- - flux of the H^- particles, n - γ-particles concentration in the "target", σ - cross section of recharging, l - "thickness" of the target. In this consideration l=d, where d - diameter of the laser beam.

The concentration n is:

$$n = \frac{4 \, W \, \lambda}{\pi \, d^2 \, h \, c^2} \qquad (2),$$

where W - power of laser, h - Planck's constant ($6.64 \; 10^{-34}$ Js), λ - wave length of laser.

From (1) and (2) it can obtain the number of H^o particles produced during time dt (that is reduction of the total number of H^- particles):

$$dN = - \frac{4 \, W \, \lambda \, K \, \sigma \, N(t)}{\pi \, d \, h \, c^2 \, T_{rev}} \, dt \qquad (3)$$

where T_{rev} - period of revolution of the particle in synchrotron, K - ratio of area of the "laser target" in tranversal phase space to the total tranversal phase volume of the circulating beam.

Assuming Gaussian distribution of the initial beam:

$$F(y,y') = \frac{1}{2 \pi \sigma_y \sigma_{y'}} \exp\left[- \frac{y^2}{2 \sigma_y^2} - \frac{y'^2}{2 \sigma_{y'}^2} \right]$$

, it can obtain (assuming: Twiss parameter $\alpha = 0$):

$$K = \int_{d/2}^{d/2} dy \int_{-\infty}^{+\infty} dy' \; F(y,y') = \mathrm{Erf}\left[\frac{d}{2 \sigma_y} \right] \qquad (4),$$

For $d \gg \sigma_y$ $\quad K \approx \frac{d}{\sqrt{\pi} \, \sigma_y}$, $\Delta y \approx 2.44 \, \sigma_y$, where Δy - vertical halfsize of the beam in the point of the interreaction.

Solution of equation (3) provides the number of H° particles to the time t:

$$N = N_t \, [1 - \exp(-t/\tau)] \qquad (5),$$

where N_t - total number of H^- particles to the begin of extraction

and τ is:

$$\tau = \frac{\pi^{3/2} \, h \, c^2 \, T_{rev} \, \sigma_y}{4 \, W \, \lambda \, \sigma} \qquad (6)$$

The parameters for (6) are:

T_{rev}= 0.46 mcsec, σ_y= 5.3 mm (T = 70 MeV)

$\lambda = 0.7 \; 10^{-6}$ m , $\sigma = 3 \; 10^{-21} m^2$.

For τ = 100 msec W = 1030 W. The phase volume of the extracted beam for d=1 mm is: Φ_x= 9 mm mrad, Φ_y = 0.2 mm mrad.

Longitudinal irradiation.

For this variant laser beam is directed along initial beam at the drift space in synchrotron. The axises of laser beam and H^- beam are coincidenced. Then l - length of laser beam and K is (for assumption Twiss parameters are constant for the drift space):

$$K = \mathrm{Erf}\left(\frac{d}{2\sigma_x}\right) \mathrm{Erf}\left(\frac{d}{2\sigma_y}\right) \approx \frac{d^2}{\pi} \qquad (7)$$

and τ is:

$$\tau = \frac{\pi^2 \, h \, c^2 \, T_{rev} \, \sigma_x \, \sigma_y}{4 \, W \, \lambda \, \sigma \, l} \qquad (8)$$

For l = 2 m , σ_x= 16.5 mm and τ = 100 msec W = 14.1 W. The phase volume of extracted beam is: Φ_x= 0.2 mm mrad, Φ_y= 0.2 mm mrad.

Recharging of impulse of H^- beam by laser impulse.

In the case of the transversal irradiation of H^- beam by laser beam he ratio of the number of H^o particles to the total number of particles in he impulse is (for K=1):

$$\frac{N^o}{N_{tot}} = \frac{4\,E\,\lambda\,\sigma}{\pi\,d\,t_i\,h\,c^2}\,, \qquad (9)$$

where E - impulse energy of laser, t_i - impulse duration.

or t_i = 30 mcsec , N^o/N_{tot}=1 and d=1mm E = 670 J.

n the case of the longitudinal irradiation formula (9) becomes:

$$\frac{N^o}{N_{tot}} = \frac{4\,E\,\lambda\,\sigma\,l}{\pi\,d^2\,t_i\,h\,c^2}\,, \qquad (10)$$

where l - H^- beam length.

or l = 1 m E = 0.67 J.

he practical recharging of H^- beam was carry out on LEAR.

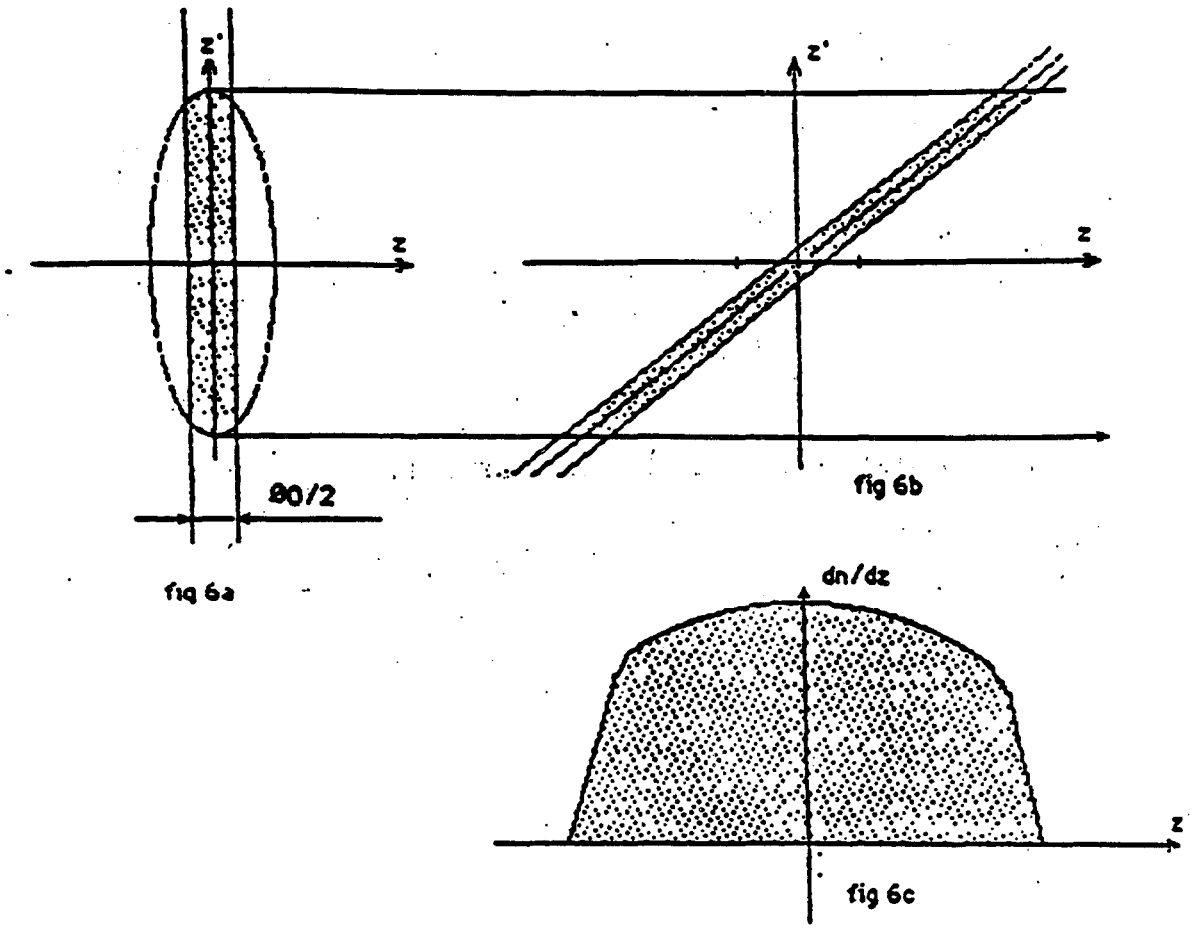

Fig. 6 : Epluchage par laser : a) la partie hachurée est la portion de l'espace de phase vertical vue par le laser, b) transport de la partie d'espace de phase correspond aux H⁻ épluchés au centre de la section 2 jus u'à la chambre MWC21, c) profil obtenu en MWC21 si la distribution dans l'espace de phase original est gaussienne.

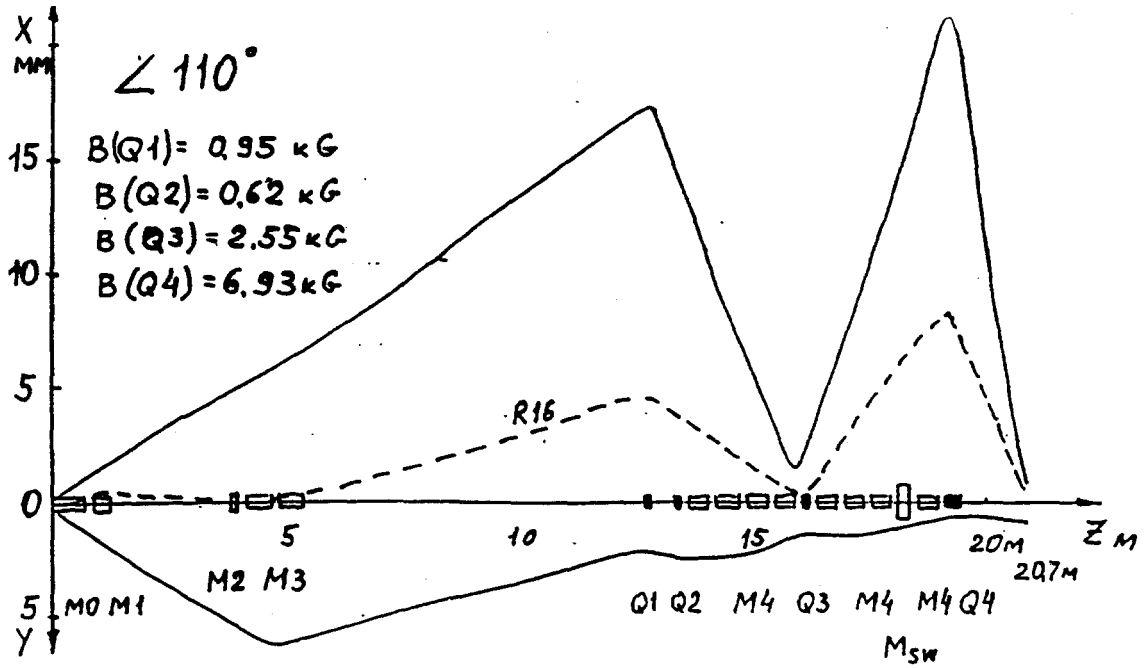
X
MM
∠ 110°
B(Q1)= 0.95 kG
B(Q2)= 0.62 kG
B(Q3)= 2.55 kG
B(Q4)= 6.93 kG
15
10
5
0
5
Y
R16
5
10
15
20M
20.7M
Z M
M0 M1
M2 M3
Q1 Q2
M4
Q3
M4
M4 Q4
Msw

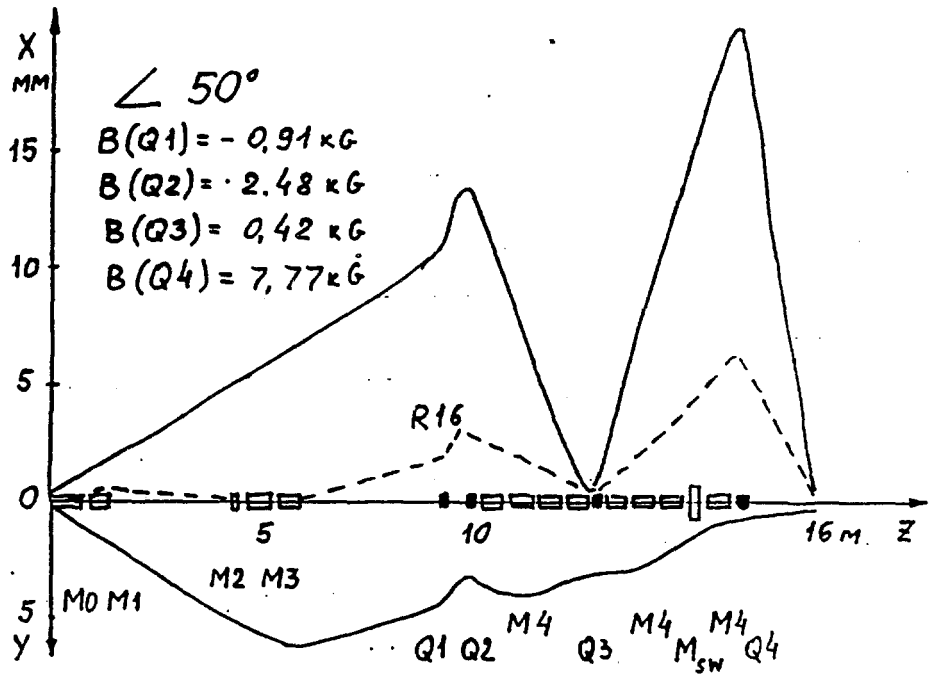
X
MM
∠ 50°
B(Q1)= - 0.91 kG
B(Q2)= 2.48 kG
B(Q3)= 0.42 kG
B(Q4)= 7.77 kG
15
10
5
0
5
Y
R16
5
10
16 M
Z
M0 M1
M2 M3
Q1 Q2
M4
Q3
M4
Msw
M4
Q4

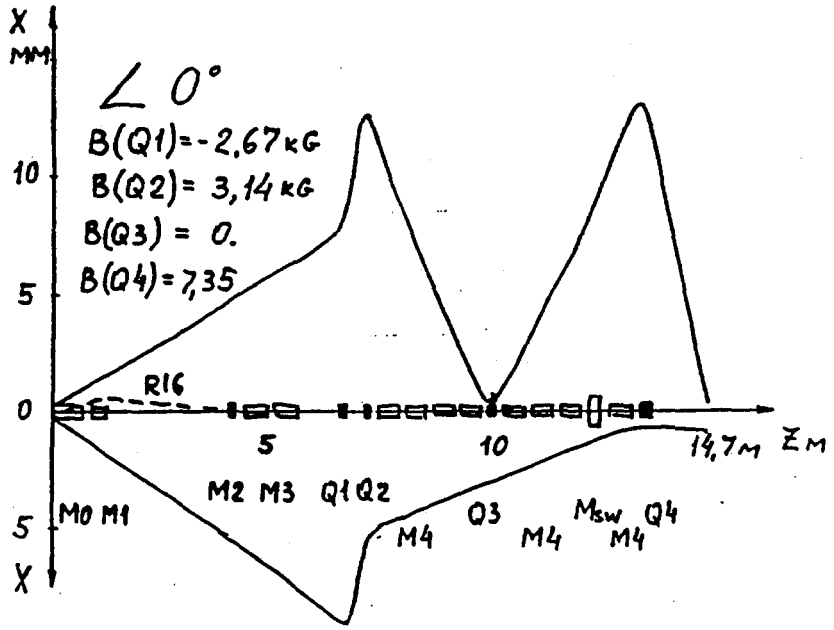
X
MM
∠ 0°
B(Q1)= -2.67 kG
B(Q2)= 3.14 kG
B(Q3) = 0.
B(Q4)= 7.35
10
5
0
5
X
R16
5
10
14.7M
Z M
M0 M1
M2 M3
Q1 Q2
M4
Q3
M4
Msw
M4
Q4

SHCEME OF FLAT VERTICAL GANTRY SYSTEM

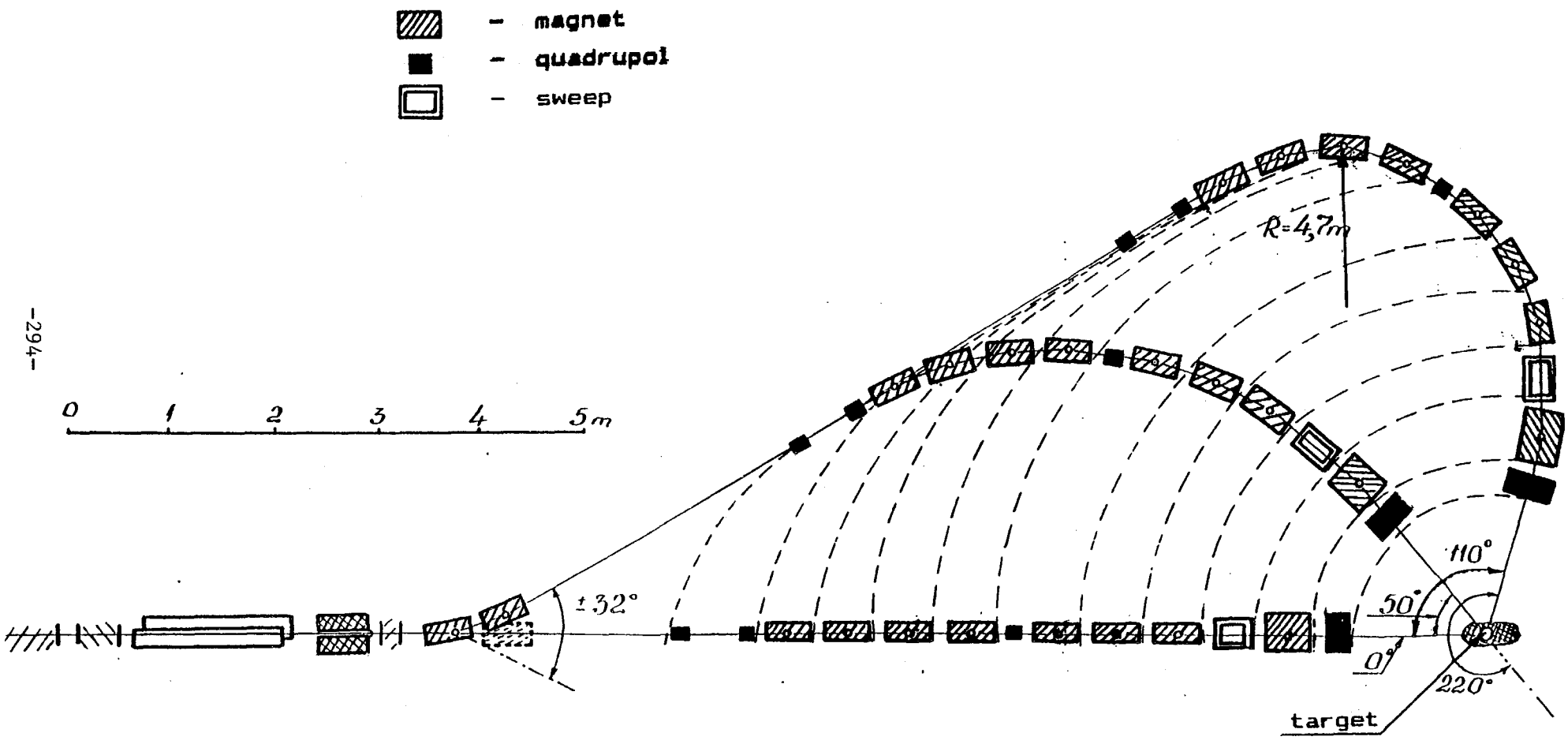

GANTRY MAGNET SHANNAL SHCEME

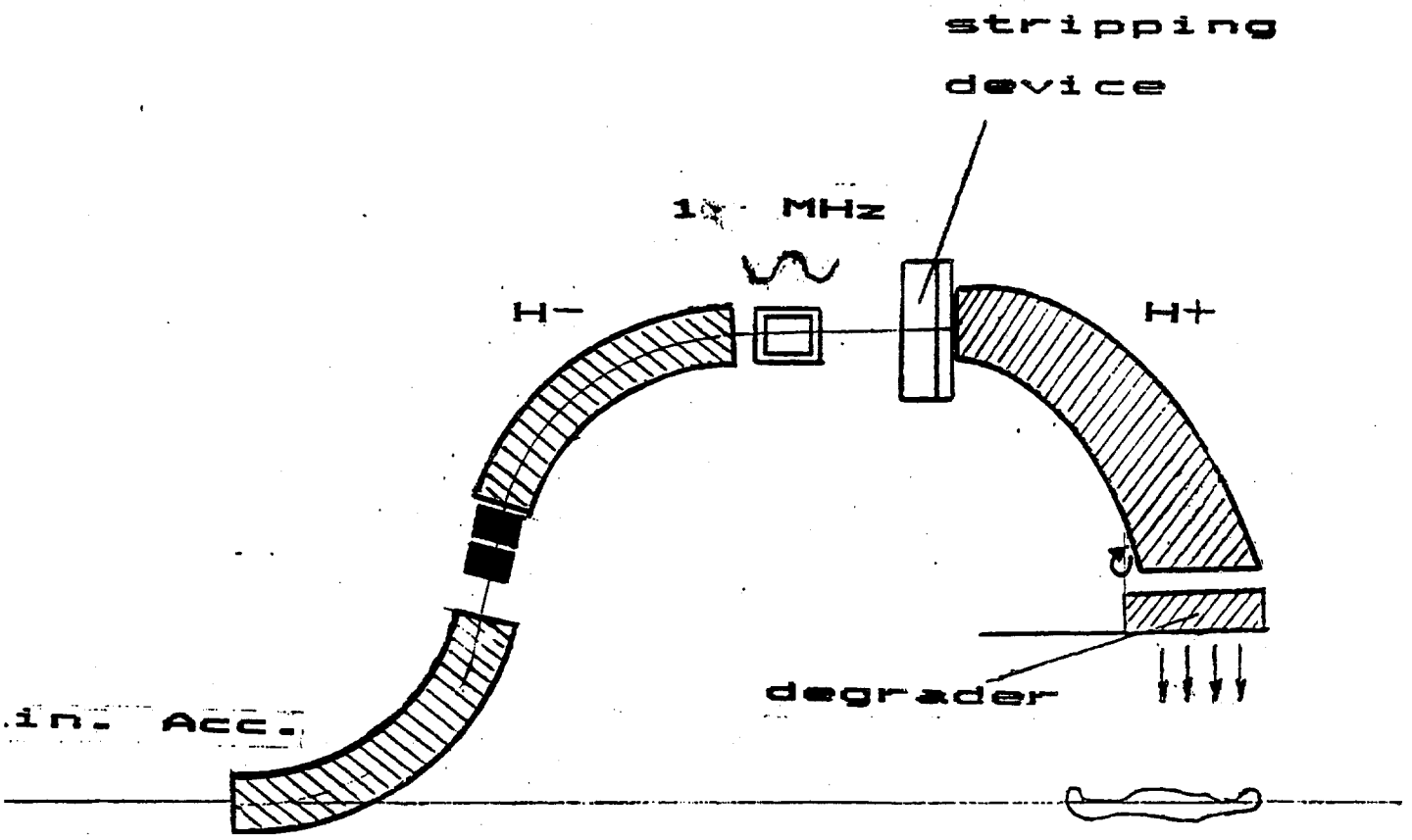

SCHEME OF IRRADIATION PERPENDICULAR SAGITAX AXE

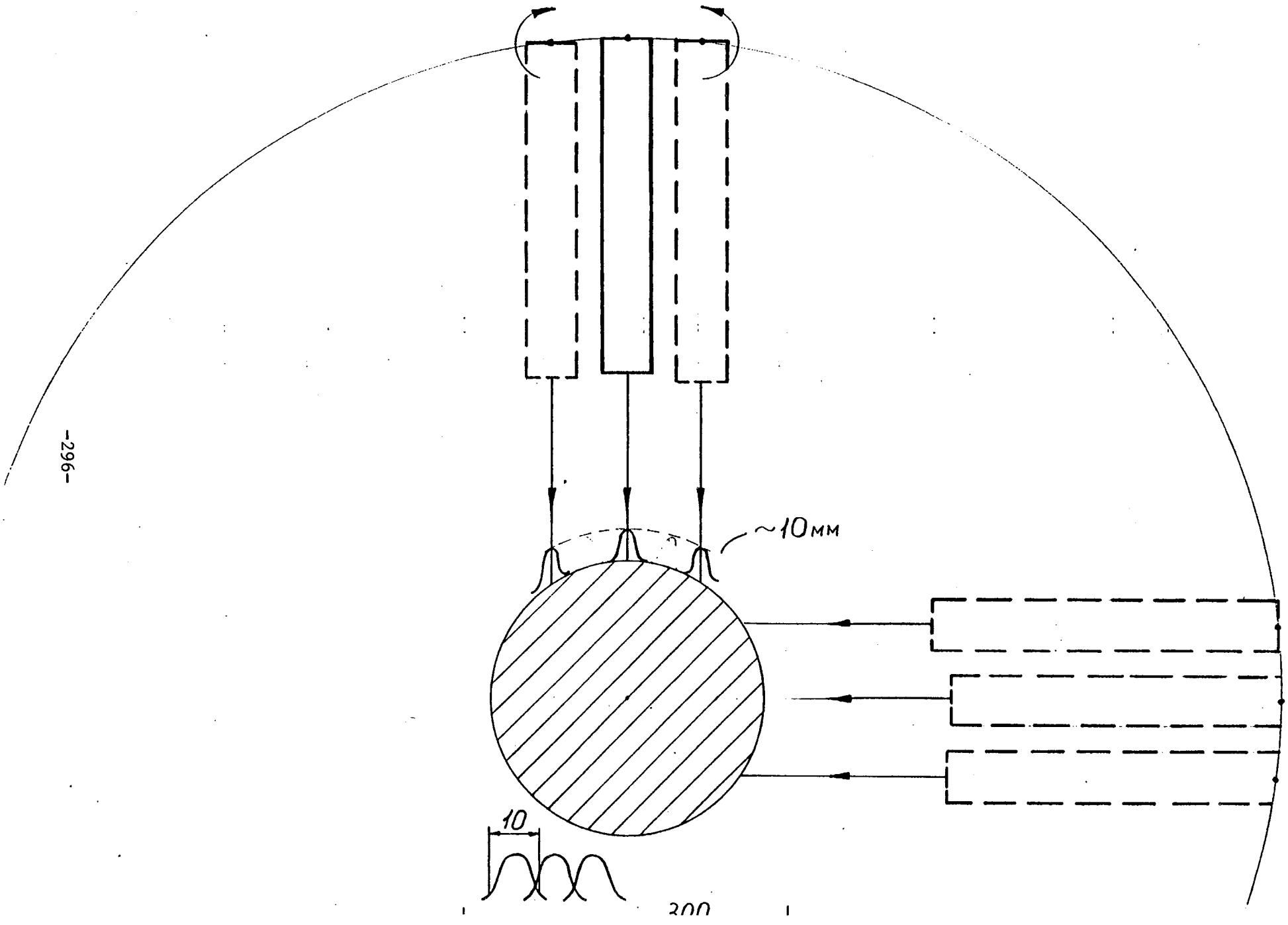

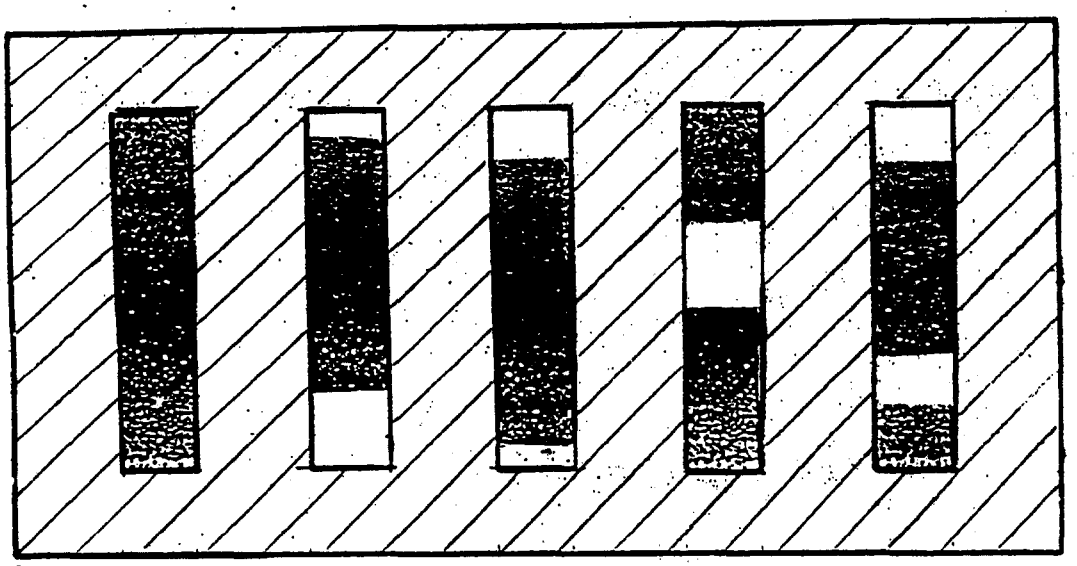

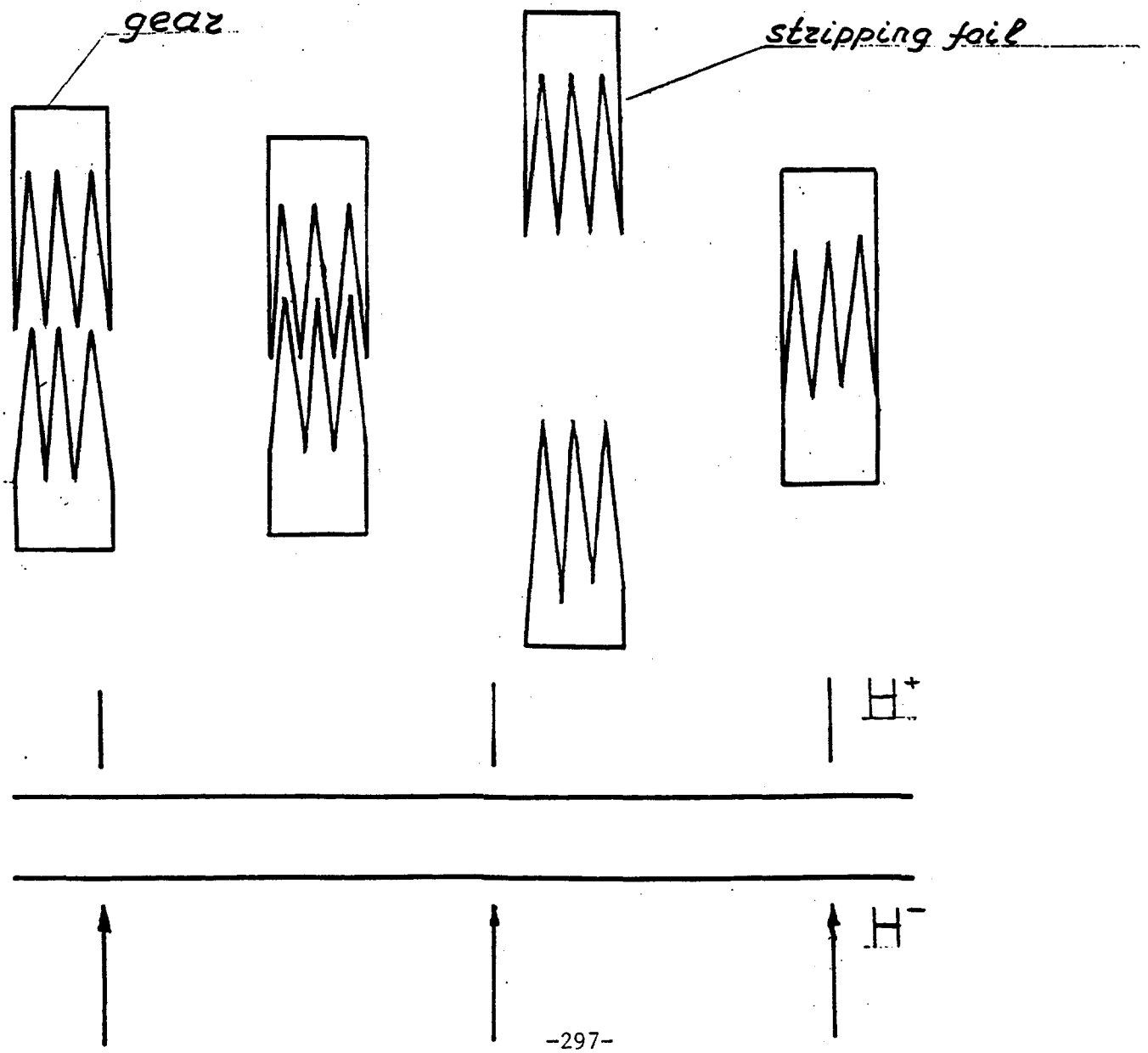
gear
stripping foil
H+
H−

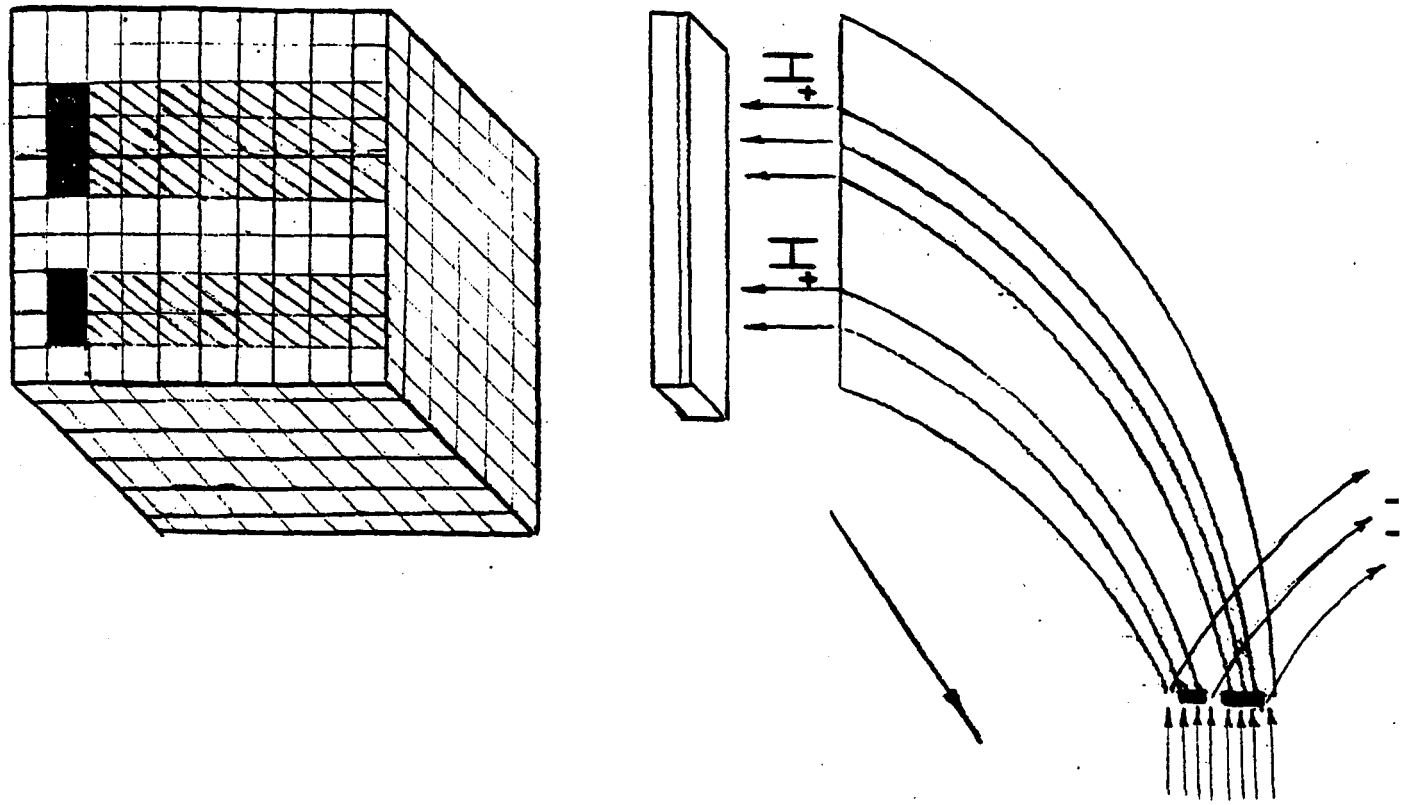

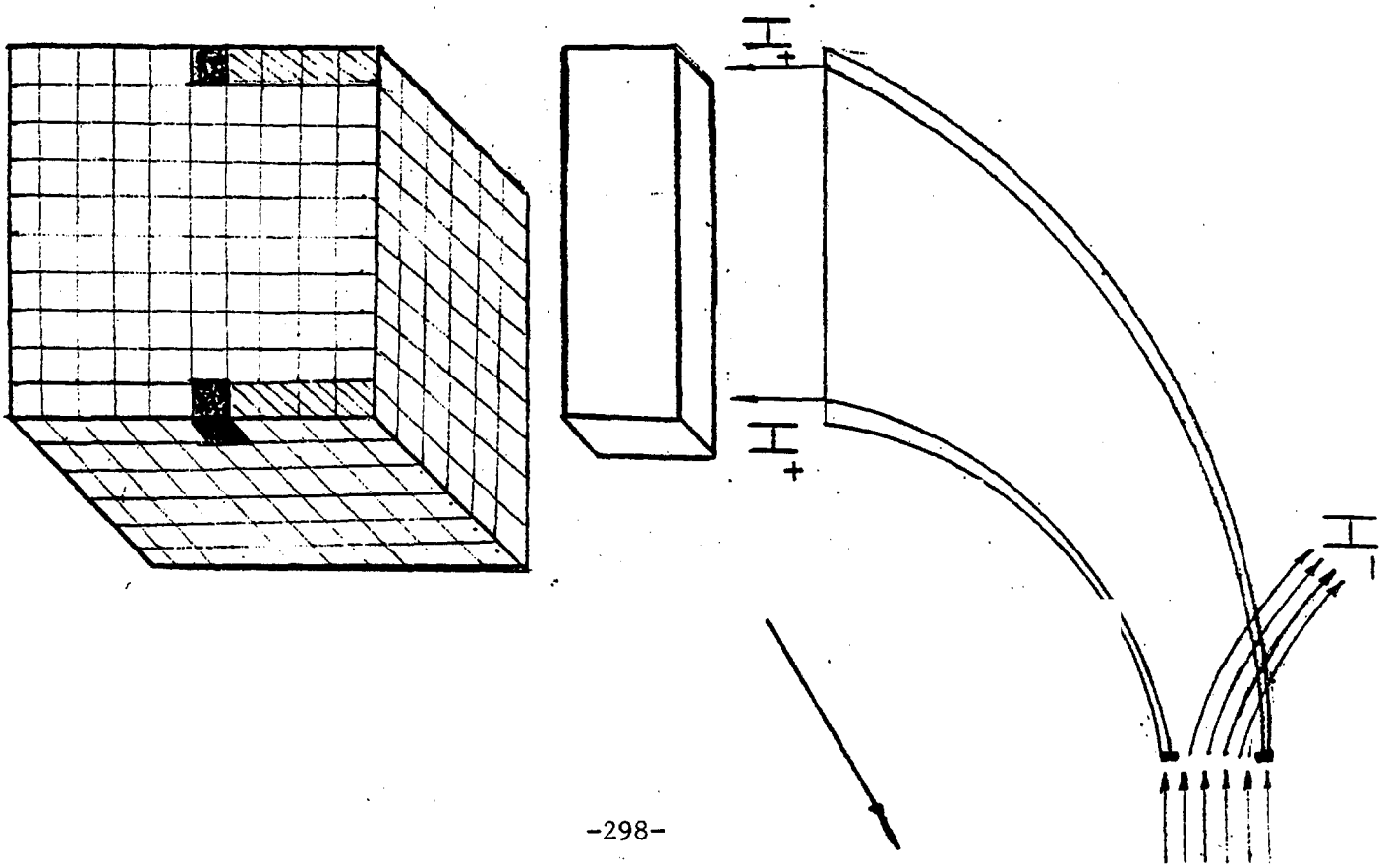

GANTRY MAGNET CHANNAL SHCEME

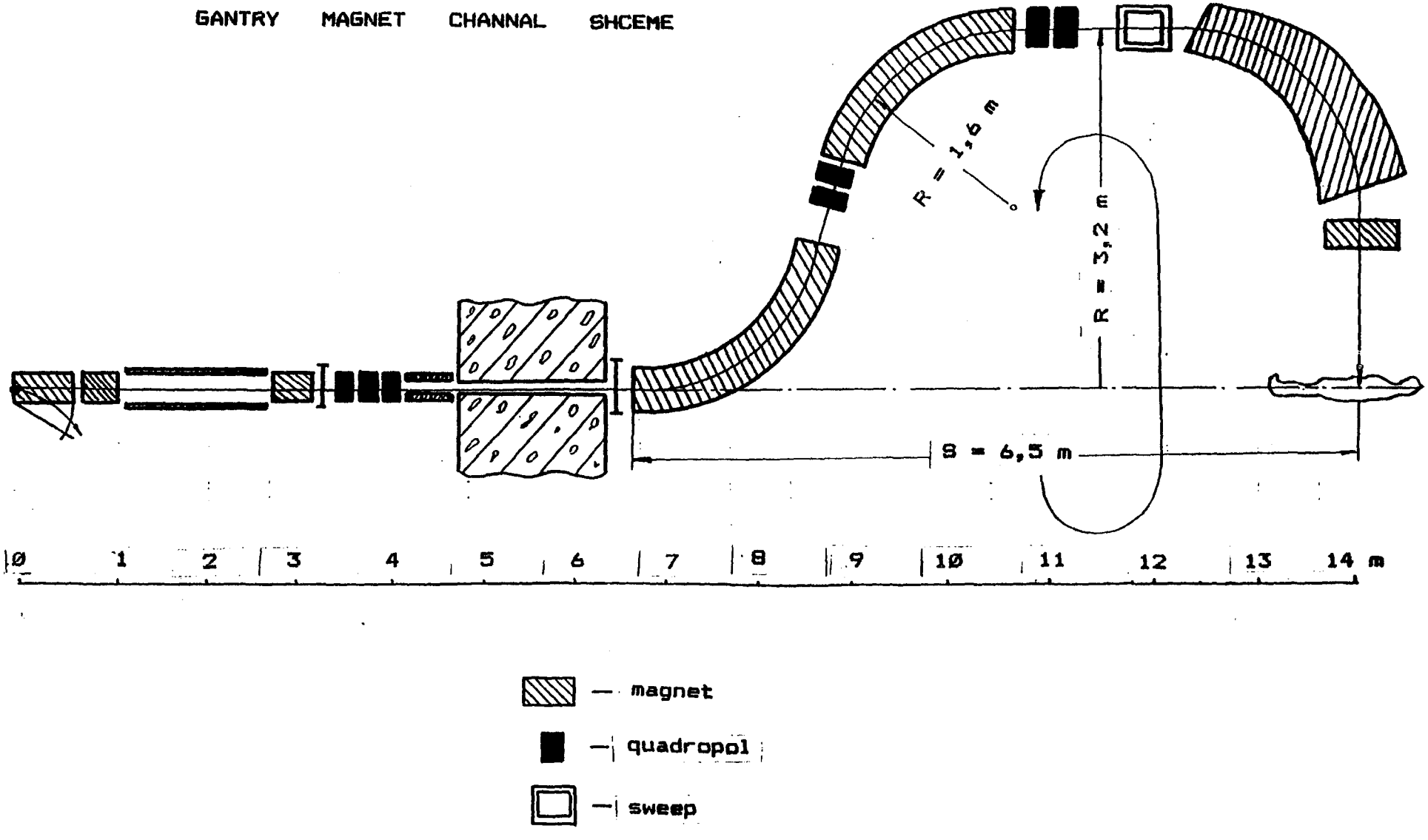

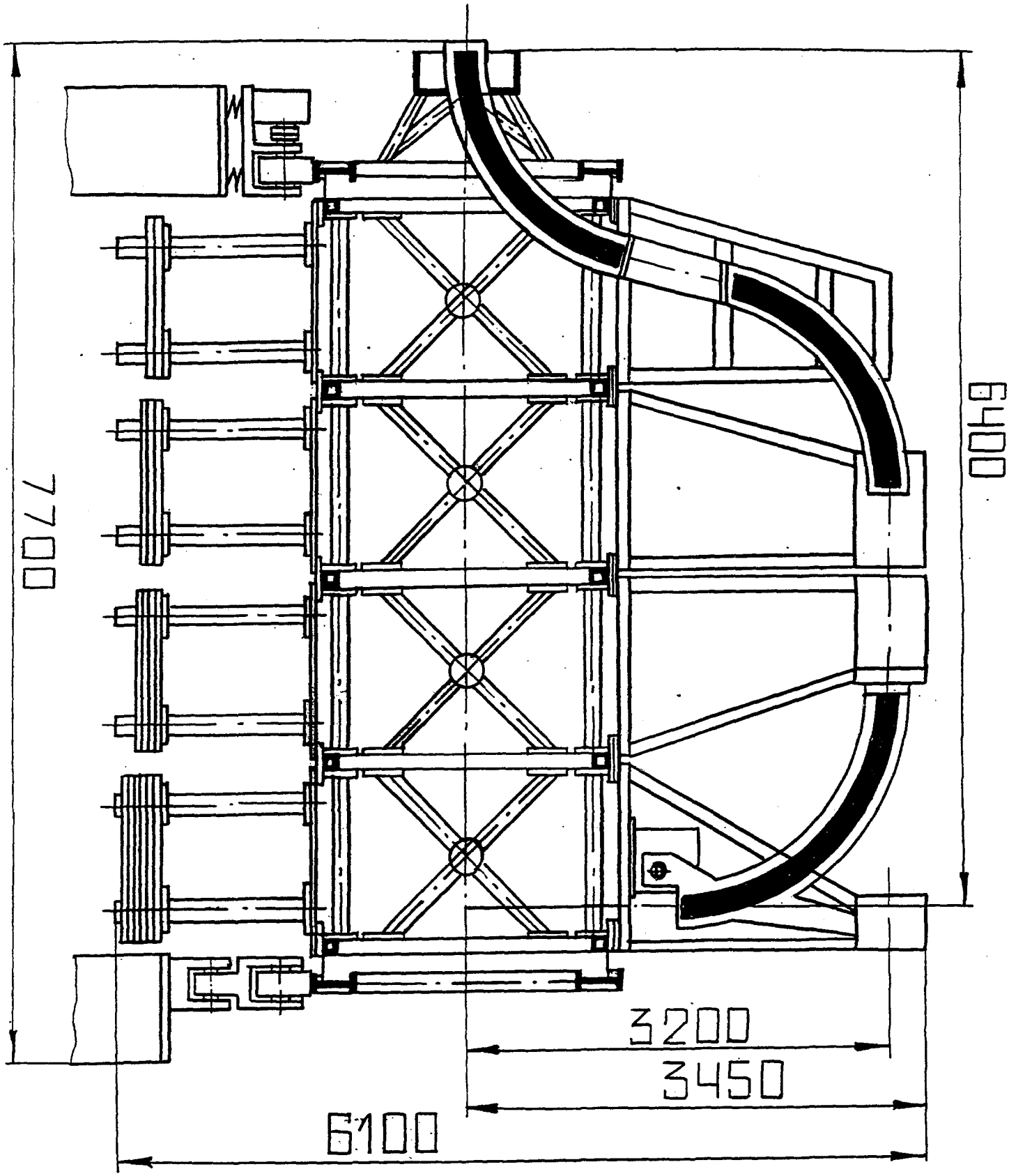
7700
6400
3200
3450
6100

SCHEME OF IRRADIATION ALONG SAGITAL AXE

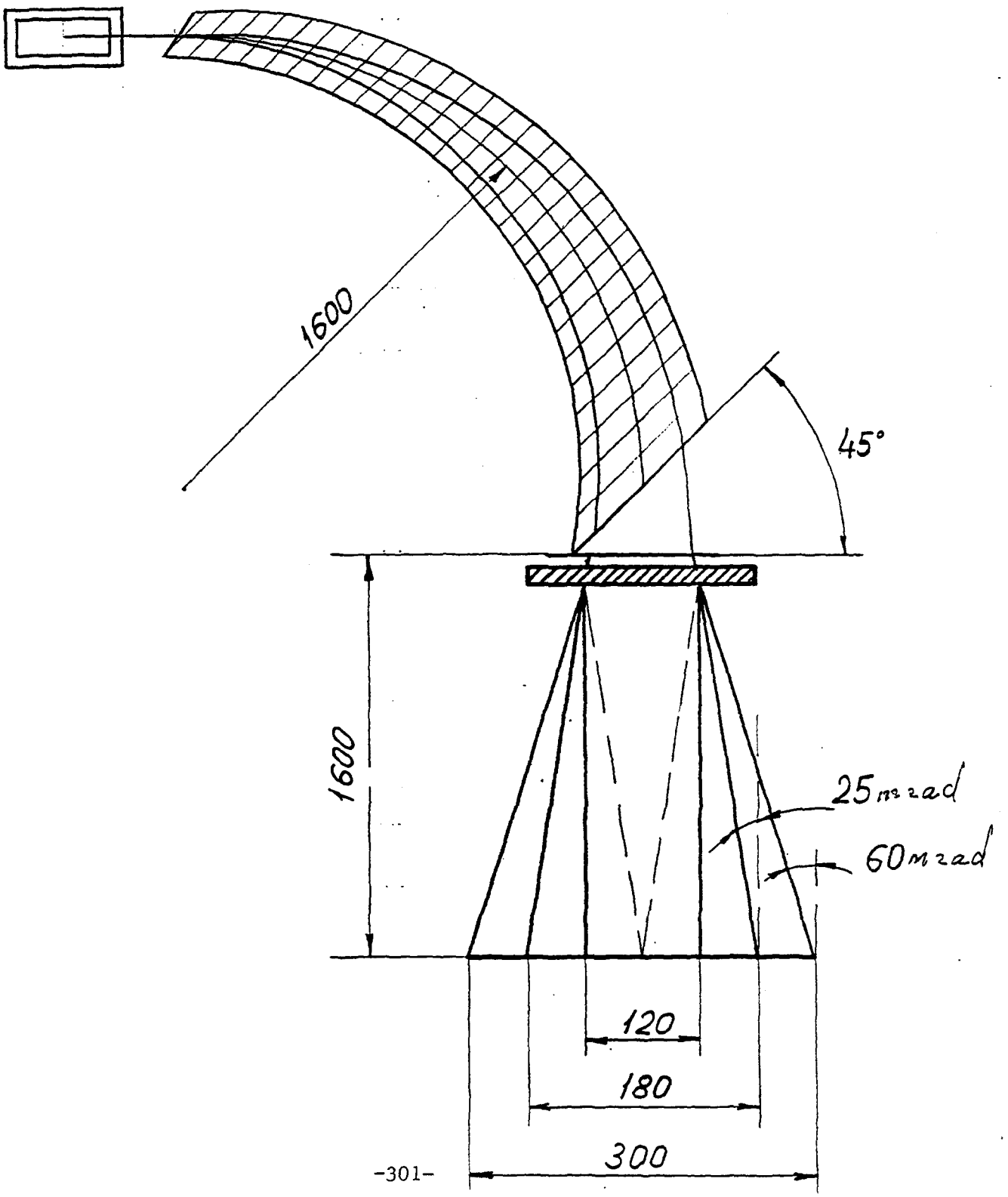

STUDY OF BEAM LOSS MECHANISMS AT PSR

(R. Macek, 10/25/93, Fermilab)

- Overview of PSR
- First-Turn losses and excited states of H^o
- Experiments on production of $H^o(n)$ in stripper foils
- Work that might be done at 400 MeV H^- beam facility

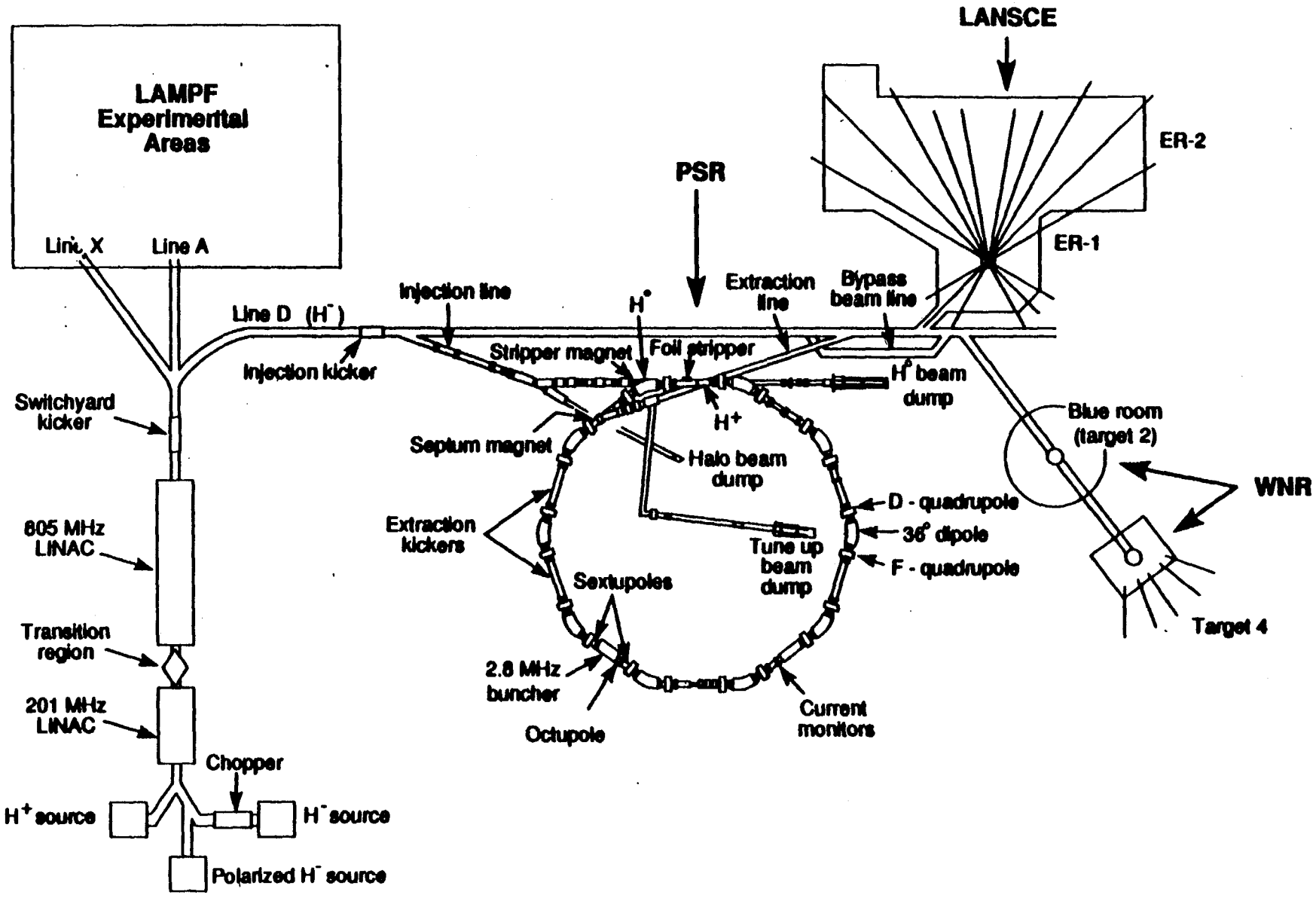
LAMPF
Experimental
Areas
Line X
Line A
Line D (H⁻)
Injection kicker
Injection line
Switchyard
kicker
805 MHz
LINAC
Transition
region
201 MHz
LINAC
Chopper
H⁺ source
H⁻ source
Polarized H⁻ source
PSR
H°
H⁺
Stripper magnet
Foil stripper
Septum magnet
Halo beam
dump
Extraction
kickers
Sextupoles
2.8 MHz
buncher
Octupole
Tune up
beam
dump
D - quadrupole
36° dipole
F - quadrupole
Current
monitors
Extraction
line
Bypass
beam line
H° beam
dump
LANSCE
ER-2
ER-1
Blue room
(target 2)
WNR
Target 4

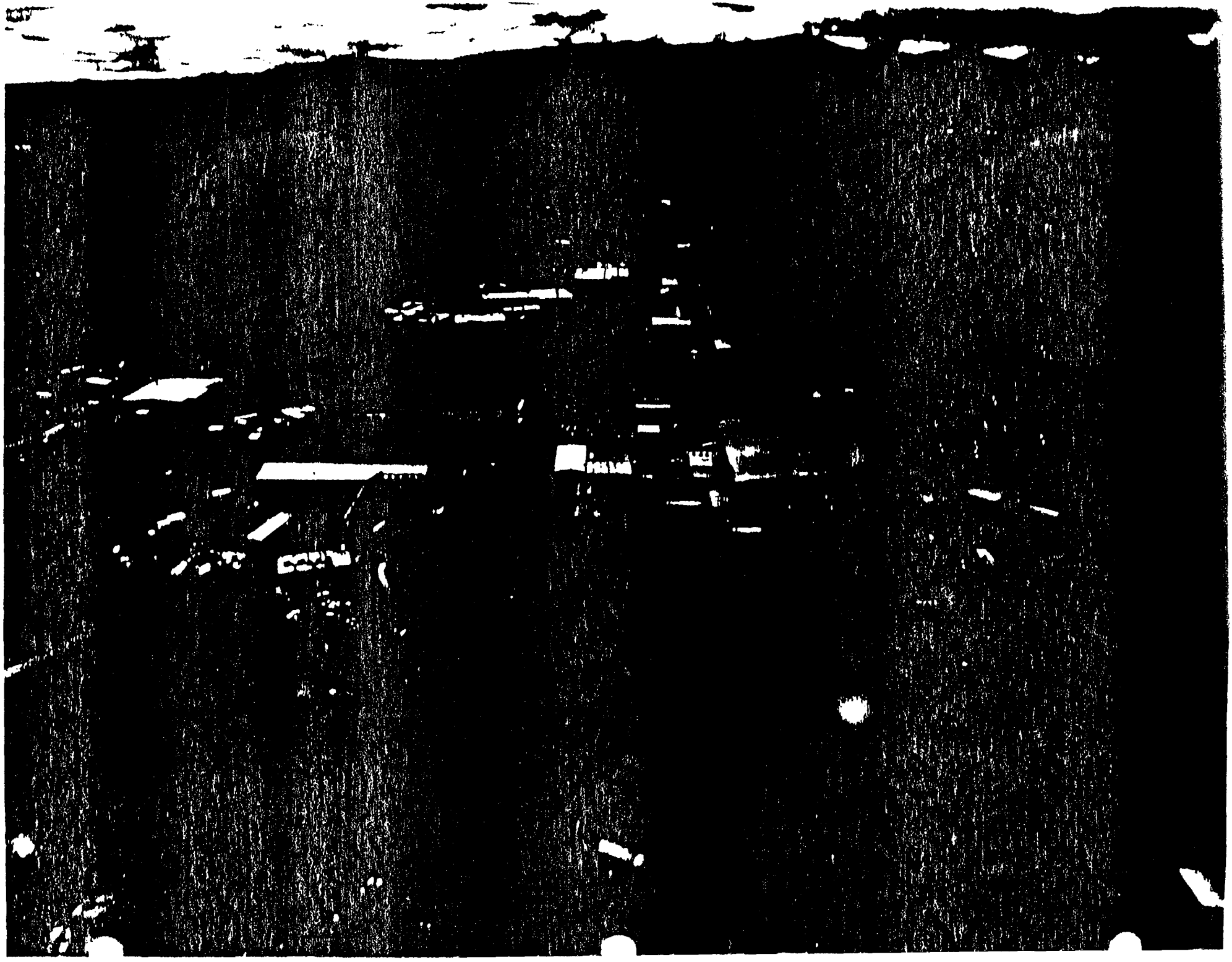

Some PSR Parameters

- $10 mA_{peak}$ injected beam current
- Accumulate ~ 1700 turns
- ~ 2.3×10^{13} protons/pulse
- 20 Hz Rep Rate
- ~ 75 μA ave current on target
- ~ 30 A peak circulating current
- ~ 1/4 μs pulse width (base) to target

INTENSITY LIMITATIONS WITH PRESENT PSR

- ***Average current*** limited to ~ 75 μA @ 20 Hz from beam losses in the ring and resulting radioactivation.
- ***Peak Intensity*** limited to 3 - 4 x 10^{13} from bunched beam instability
  - ~ 6 X 10^{12} ppp (coasting beam)
  - Instability believed to be e-p coupled oscillations

CLASSIFICATION OF BEAM LOSSES AT PSR

- Losses at Injection Foil (8 - 10 %)
  - Stripping inefficiency and beam that misses foil
- "First Turn" Losses (0.1 - 0.3 %)
  - Excited States of Ho that strip in downstream dipole
- Stored Beam Losses (0.3 - 0.5 %)
  - Primarily from scattering in the stripper foil
- Extraction Losses (~0.1%)
- Fast Losses - PSR Instability
  - Avoided in Present Operation

Loss Rate for 550 μs Accumulation
with Extraction Delayed 100 μs

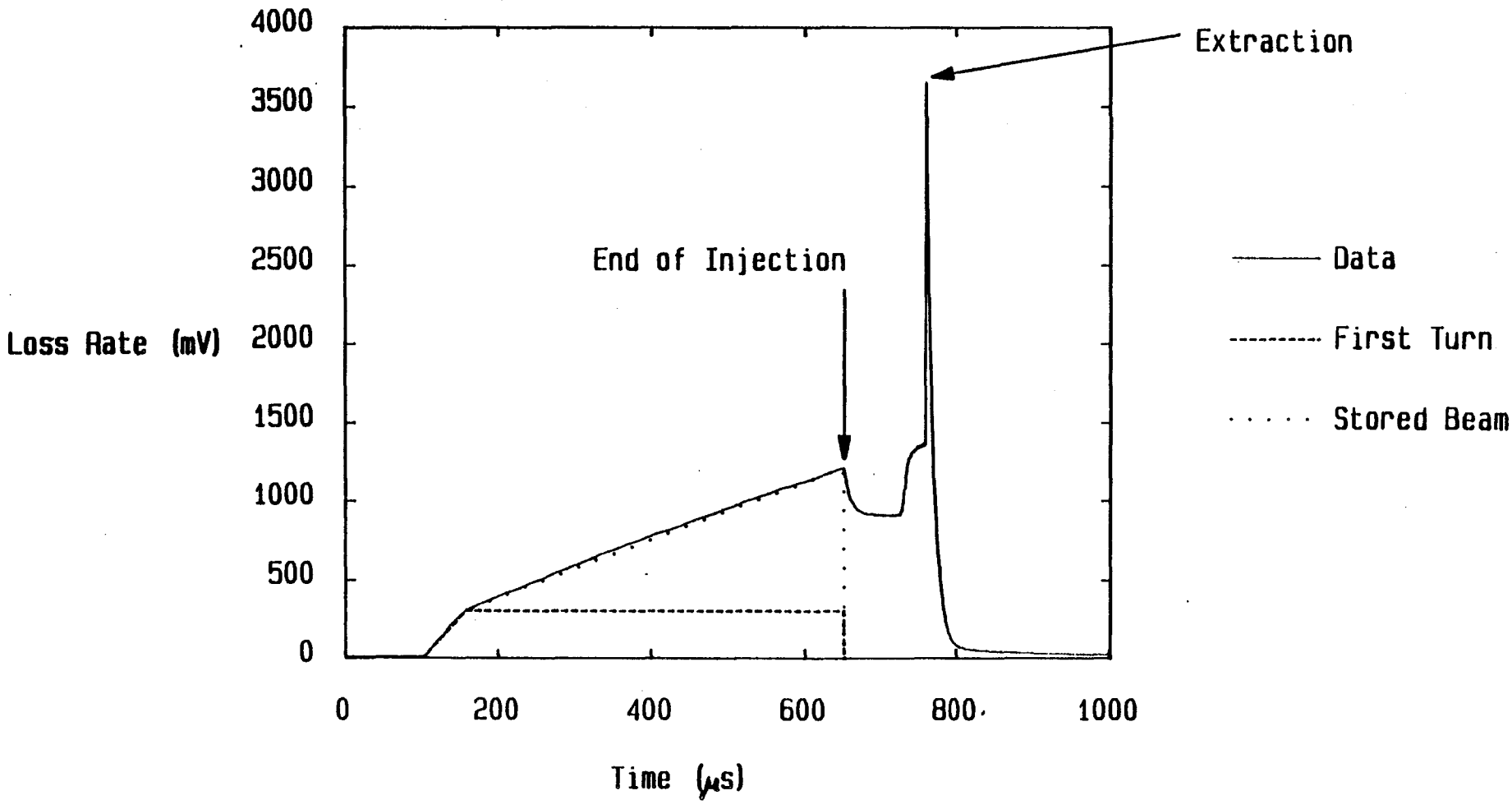

07LOSSDS.XLC

BEAM LOSS DISTRIBUTION

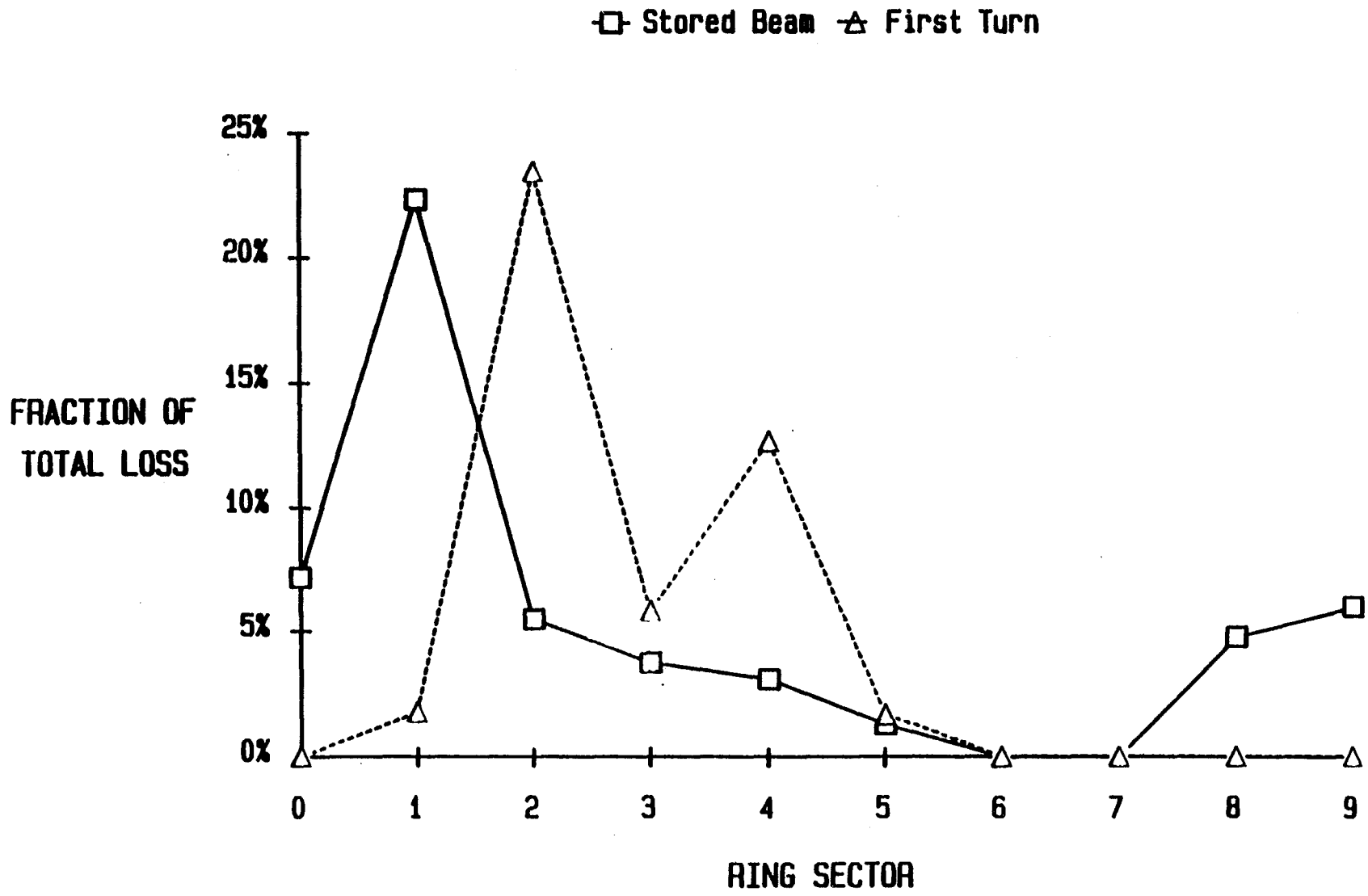

STORED BEAM LOSSES

- **Nuclear Scattering and Absorption.**

  $\sigma_N \simeq 0.33$ b

- **Large Angle Coulomb Scattering.**

  $\sigma_R = 0.68$ b $\quad 0 \geq 3mr$
  $\sigma_R = 1.53$ b $\quad 0 \geq 2mr$

- **Loss from sum of Nuclear and Coulomb Scattering.**

  $1 \cdot 10^{-5}$/foil traversal $\quad 0 \geq 3mr$
  $1.8 \cdot 10^{-5}$/foil traversal $\quad 0 \geq 2mr$

- **Observed**

  $\sim 2.2 \cdot 10^{-5}$/turn in 1987
  $\sim 0.5 \cdot 10^{-5}$/turn, September 1990

Offset Injection Scheme in Y-Y' Plane

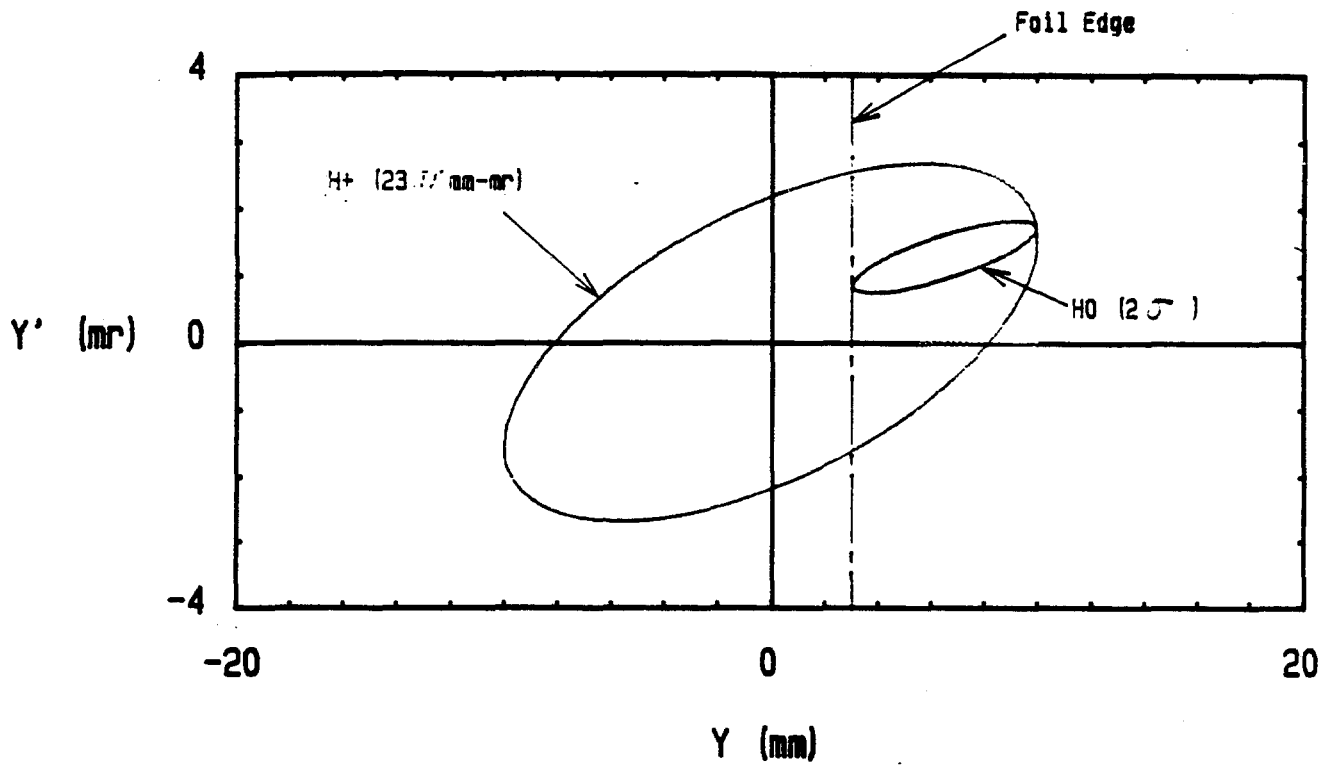

Present Injection Scheme in X-X' Plane

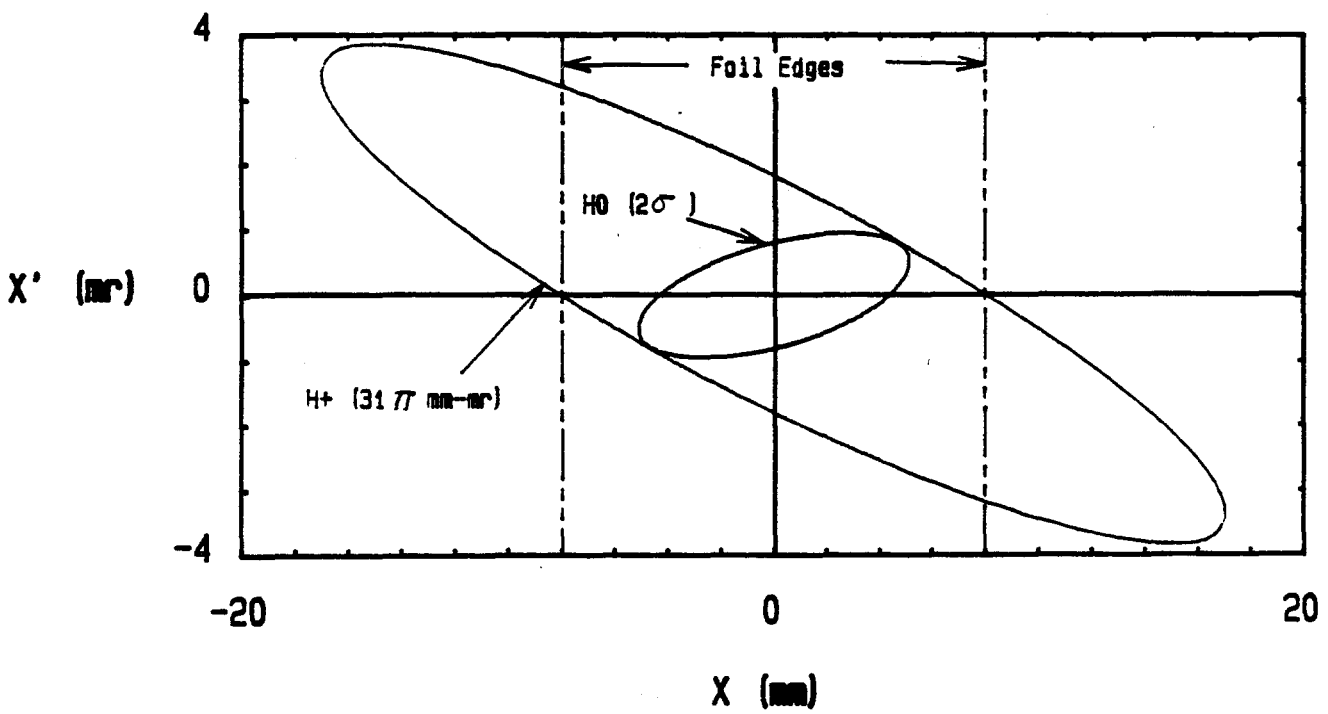

1991 STRIPPER FOIL FRAME

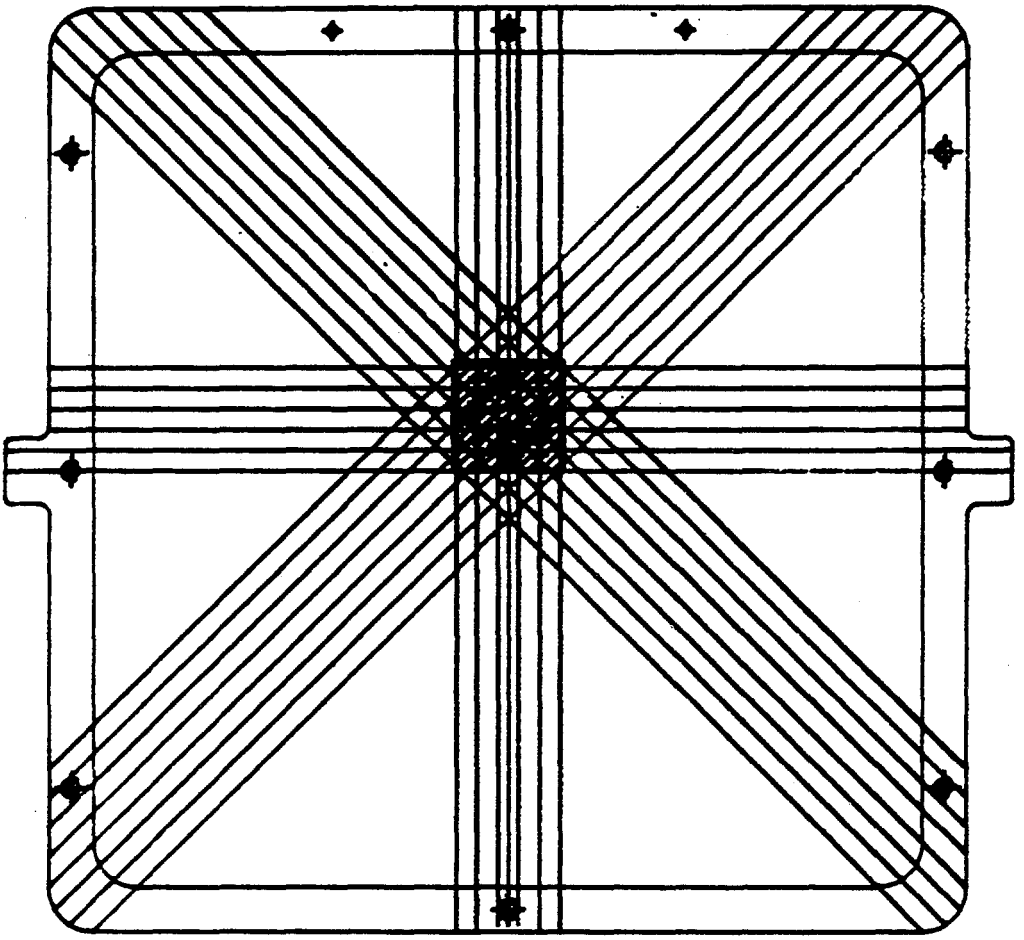

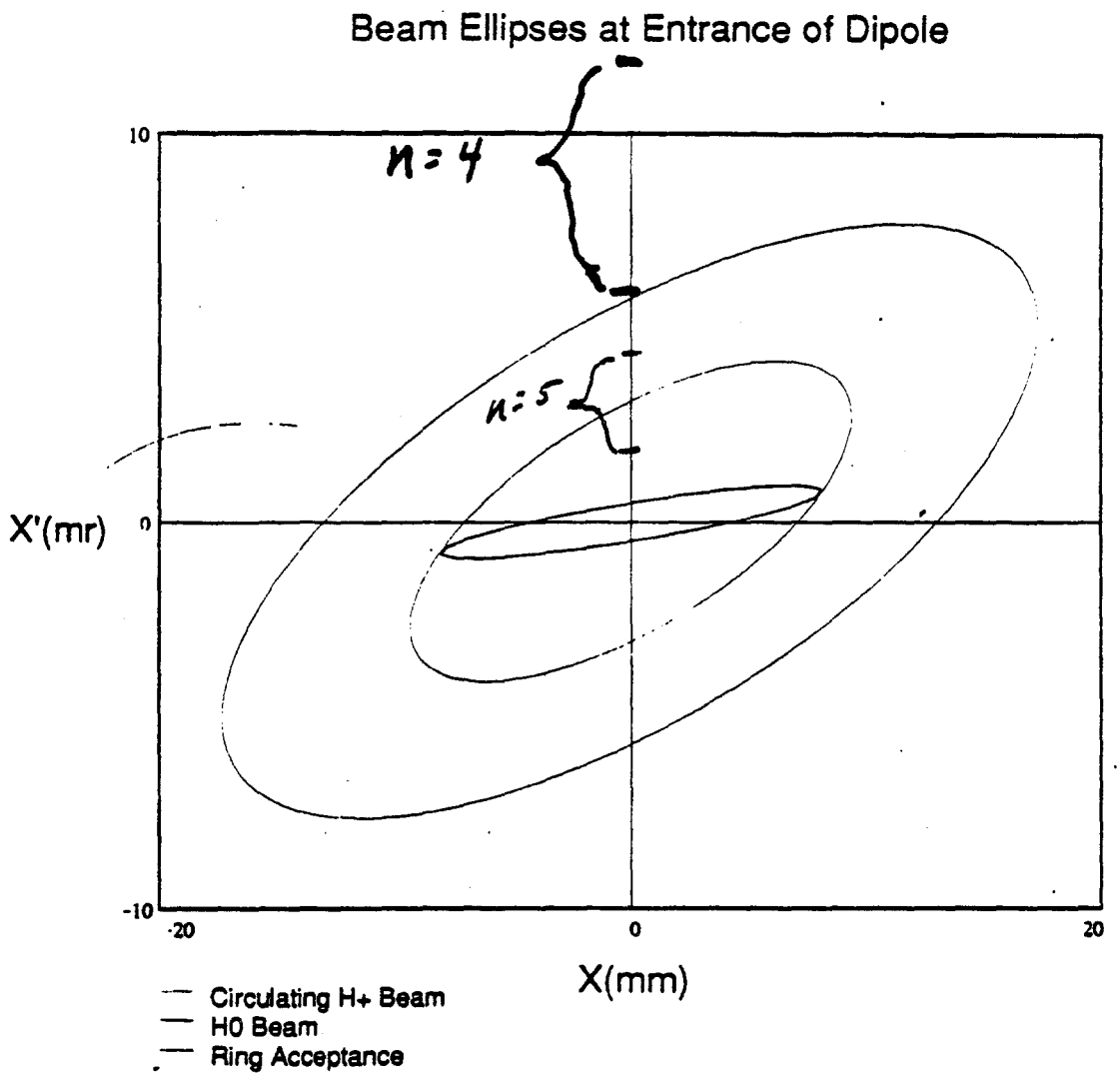

n	Δθ(mrad)	Loss location	Yield (200 μg/cm²) foil *
3	22-50	1st dipole + F quad	0.3% (.2% To Ma.
4	6.1-12	Next 2-3 F quads	0.2%
5	1.8-4.4	Halo +	0.15%

* ~1/2 of measured yield from H⁻ on 200 μg/cm² C-foil

Table 15. *Transition probabilities for hydrogen in 10^8 sec^{-1}.*

Initial	Final	$n=1$	2	3	4	5	Total	Lifetime in 10^{-6} sec
$2s$	np	—	—	—	—	—	0	∞
$2p$	ns	6.25	—	—	—	—	6.25	0.16
2	mean	4.69	—	—	—	—	4.69	0.21
$3s$	np	—	0.063	—	—	—	0.063	16
$3p$	ns	1.64	0.22	—	—	—	1.86	0.54
$3d$	np	—	0.64	—	—	—	0.64	1.56
3	mean	0.55	0.43	—	—	—	0.98	1.02
$4s$	np	—	0.025	0.018	—	—	0.043	23
$4p$	ns	0.68	0.095	0.030	—	—	0.81	1.24
	nd	—	—	0.003	—	—		
$4d$	np	—	0.204	0.070	—	—	0.274	3.65
$4f$	nd	—	—	0.137	—	—	0.137	7.3
4	mean	0.12_8	0.083	0.089	—	—	0.299	3.35
$5s$	np	—	0.012	0.008_5	0.006_5	—	0.027_7	36
$5p$	ns	0.34	0.049	0.016	0.007_5	—	0.415	2.40
	nd	—	—	0.001_5	0.002	—		
$5d$	np	—	0.094	0.034	0.014	—	0.142	7.0
	nf	—	—	—	0.000_5	—		
$5f$	nd	—	—	0.045	0.026	—	0.071	14.0
$5g$	nf	—	—	—	0.042_5	—	0.042_5	23.5
5	mean	0.040	0.025	0.022	0.027	—	0.114	8.8
$6s$	np	—	0.007_3	0.0051	0.0035	0.0017	0.0176	57
$6p$	ns	0.195	0.029	0.0096	0.0045	0.0021	0.243	4.1
	nd	—	—	0.0007	0.0009	0.0010		
$6d$	np	—	0.048	0.0187	0.0086	0.0040	0.080	12.6
	nf	—	—	—	0.0002	0.0004		
$6f$	nd	—	—	0.0210	0.0129	0.0072	0.04[illegible]2	24.3
	ng	—	—	—	—	0.0001		
$6g$	nf	—	—	—	0.0137	0.0110	0.02[illegible]	40.5
$6h$	ng	—	—	—	—	0.0164	0.0164	61
6	mean	0.0162	0.0092	0.0077	0.0077	0.0101	0.0510	19.6

FIRST-TURN LOSSES

- Field-stripping of excited states of H^0 in downstream dipole
- Stripping is accurately described by theory of Stark effect
- No quantitative theory for production of excited states in stripper foil
- Experiments to measure yields for relativistic H^- incident on thin foils
  - Yield ~ 1/2% each for n=3 and n=4 from 200 $\mu g/cm^2$ foil

EVIDENCE THAT FIRST-TURN LOSSES ARE FROM $H^o(n)$

- Location of Losses
- Variation with foil thickness
- Consistent with estimates for $H^o(n)$ production

Bergeman et al, PRL 53 #8, 775-8 1984

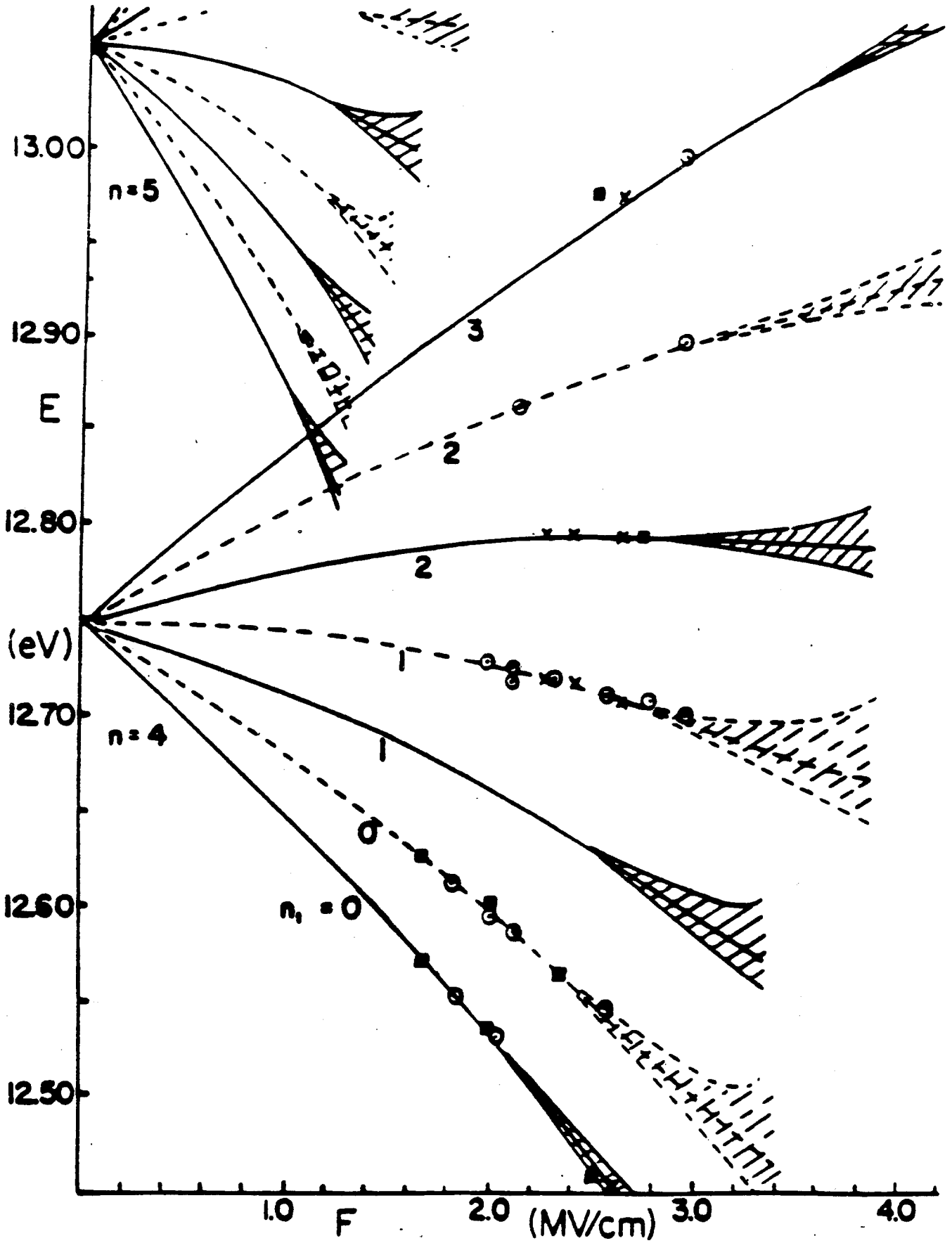

$$\tau * \Gamma = \hbar, \qquad (A2.11)$$

where Γ is the energy width of the given state. A semiempirical formula for Γ is derived by Damburg and Kolosov[55]

$$\Gamma = \frac{(4R)^{2n_2+m+1}}{n^3 n_2!(n_2+m)!}$$

$$\times exp(-\frac{2}{3}R - \frac{n^3 F}{4}(34n_2^2 + 34n_2 m + 46n_2 + 7m^2 + 23m + \frac{53}{3})), \qquad (A2.12)$$

where F is the electric field in atomic units, and R is a parameter given by

$$R = (-2E)^{3/2} F^{-1}, \qquad (A2.13)$$

$$E = -\frac{1}{2n^2} + \frac{3}{2}n(n_1 - n_2)F$$

$$-\frac{n^4}{16}[17n^2 - 3(n_1 - n_2)^2 - 9m^2 + 19]F^2$$

$$+\frac{3}{32}n^7(n_1 - n_2)[23n^2 - (n_1 - n_2)^2 + 11m^2 + 39]F^3$$

$$-\frac{n^{10}}{1024}[5487n^4 + 35182n^2 - 1134m^2(n_1 - n_2)^2$$

$$+1806n^2(n_1 - n_2)^2 - 3402n^2m^2 + 147(n_1 - n_2)^4 - 549m^4$$

$$+5754(n_1 - n_2)^2 - 8622m^2 + 16211]F^4$$

$$+\frac{3}{1024}n^{13}(n_1 - n_2)[10563n^4 + 90708n^2 + 220m^2(n_1 - n_2)^2$$

$$+98n^2(n_1 - n_2)^2 + 772n^2m^2 - 21(n_1 - n_2)^4 + 725m^4$$

$$+780(n_1 - n_2)^2 + 830m^2 + 59293]F^5. \qquad (A2.14)$$

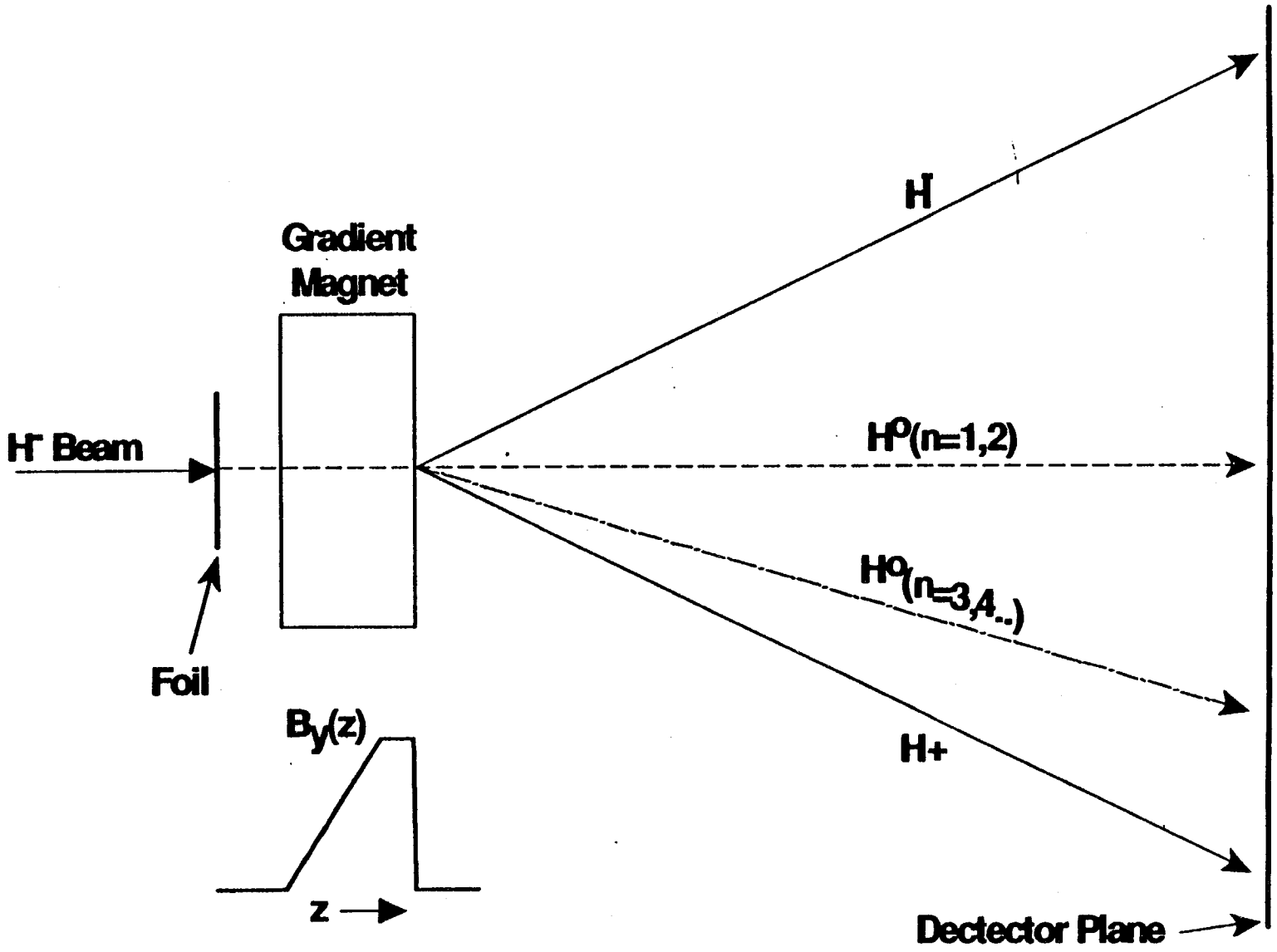
Gradient
Magnet
H⁻ Beam
Foil
By(z)
z
H⁻
H⁰(n=1,2)
H⁰(n=3,4..)
H+
Dectector Plane

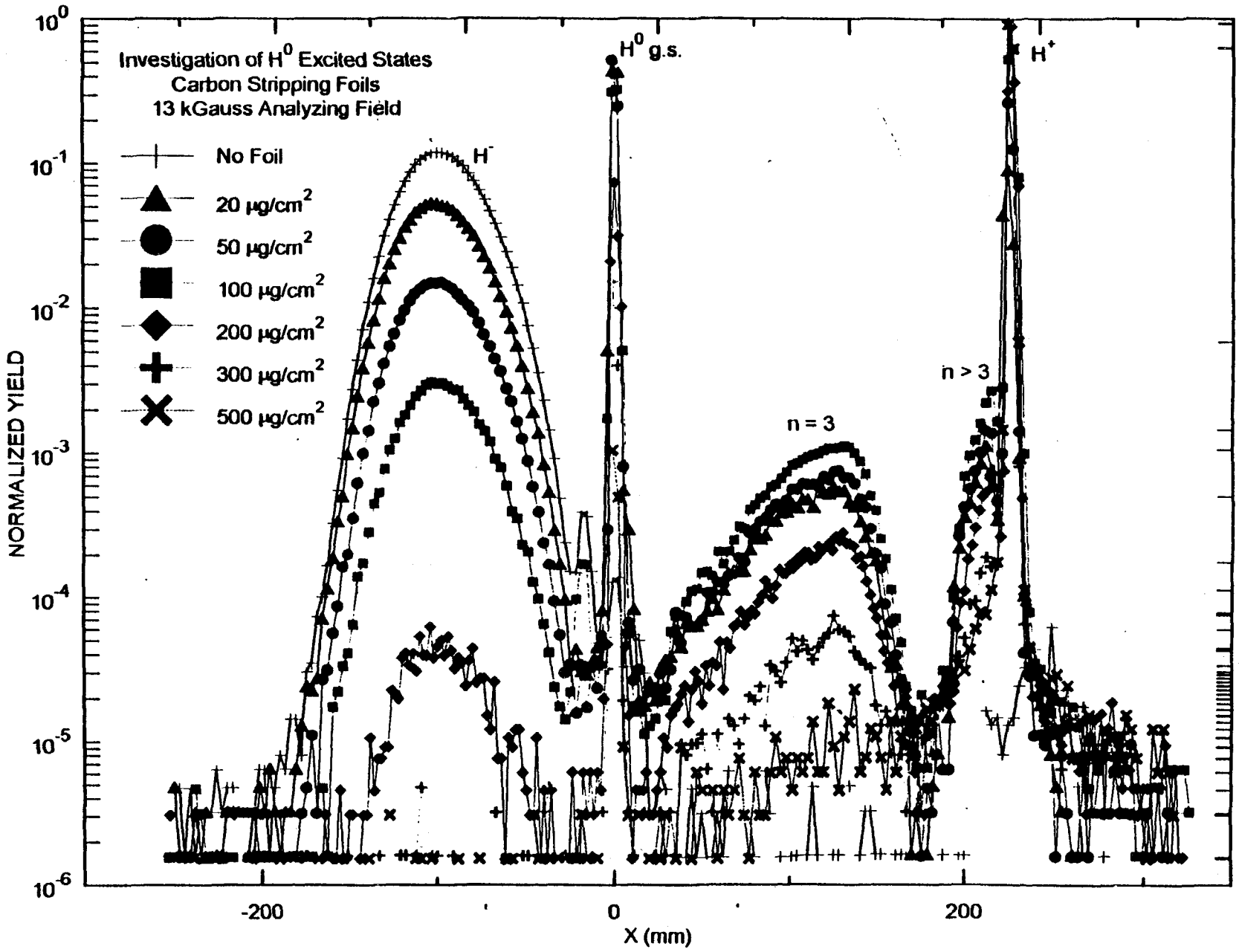
Investigation of H0 Excited States
Carbon Stripping Foils
13 kGauss Analyzing Field
No Foil
20 μg/cm2
50 μg/cm2
100 μg/cm2
200 μg/cm2
300 μg/cm2
500 μg/cm2
H-
H0 g.s.
n = 3
n > 3
H+
NORMALIZED YIELD
X (mm)
10^0
10^-1
10^-2
10^-3
10^-4
10^-5
10^-6
-200
0
200

Processes in Thin Foils

$$H^- + \text{Foil} \rightarrow H^-$$
$$\rightarrow H^\circ(n)$$
$$\rightarrow H^+$$

- Removal of H^- $\quad \sigma_{-1,0} + \sigma_{-1,1}$
- Production of $H^\circ(n)$ and H^+
- Removal of $H^\circ(n)$ $\quad \sigma_{0,1}$
- Foil is not a dilute gas!

Webber + Hajost IEEE Trans. Nuc Science Vol Nucs. No. 1979

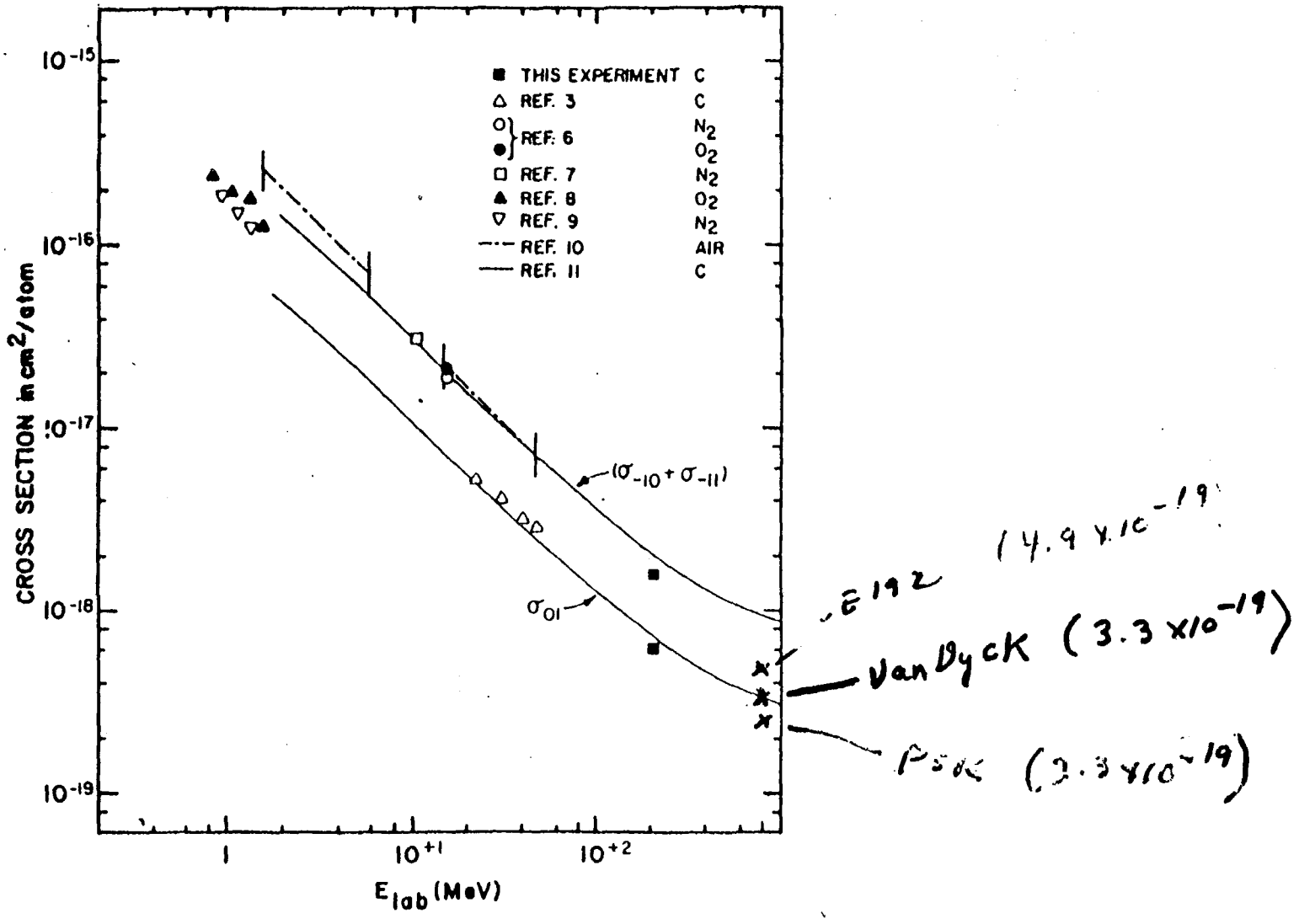

Fig. 4. Comparison of the results from this experiment with previous results and theoretical predictions.

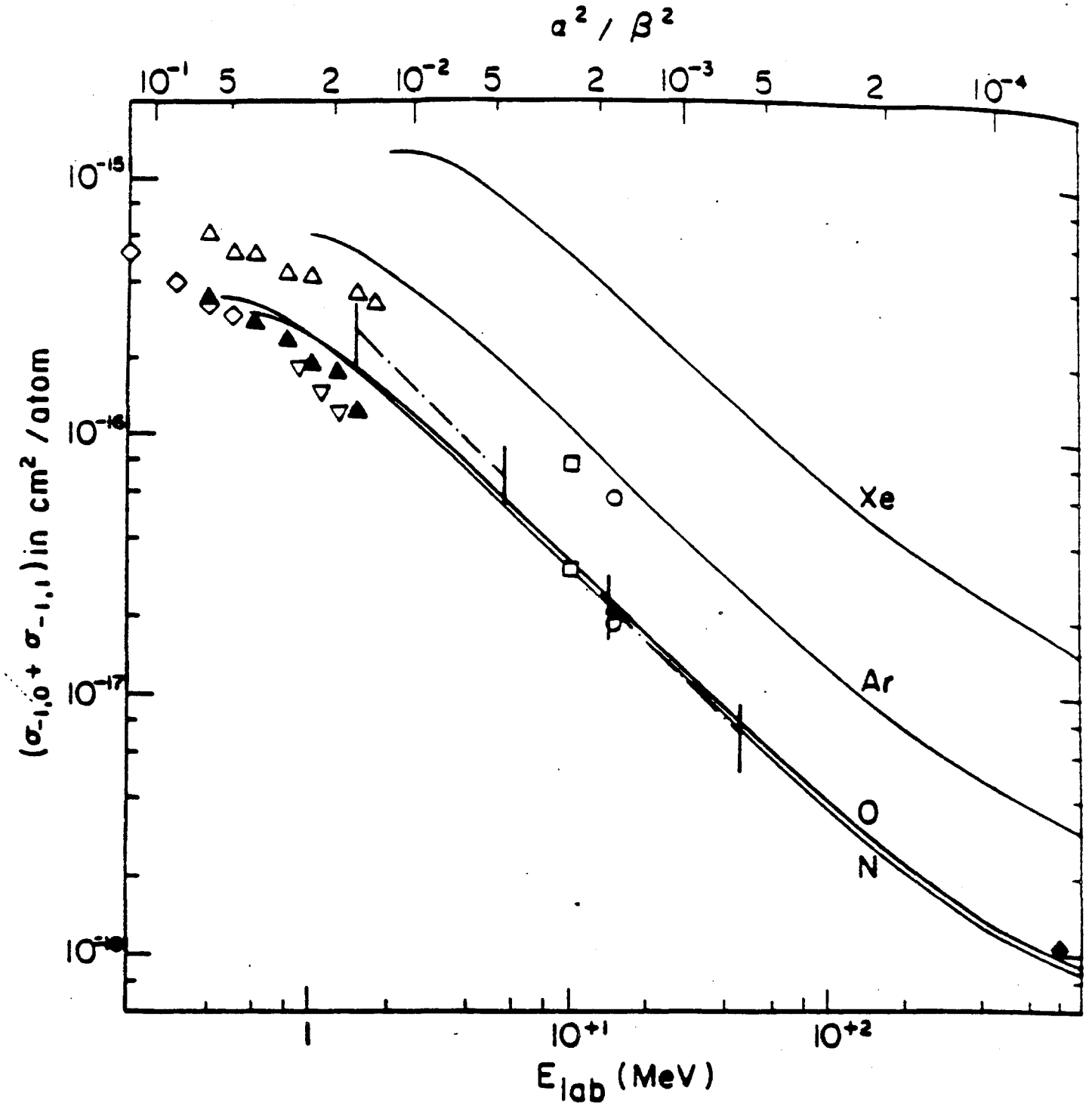

Gillespie Phy Rev A, Vol 16, No 3 Sept 1977

Mohaghaghi et al Phys Rev A, 43, R 1345 1991

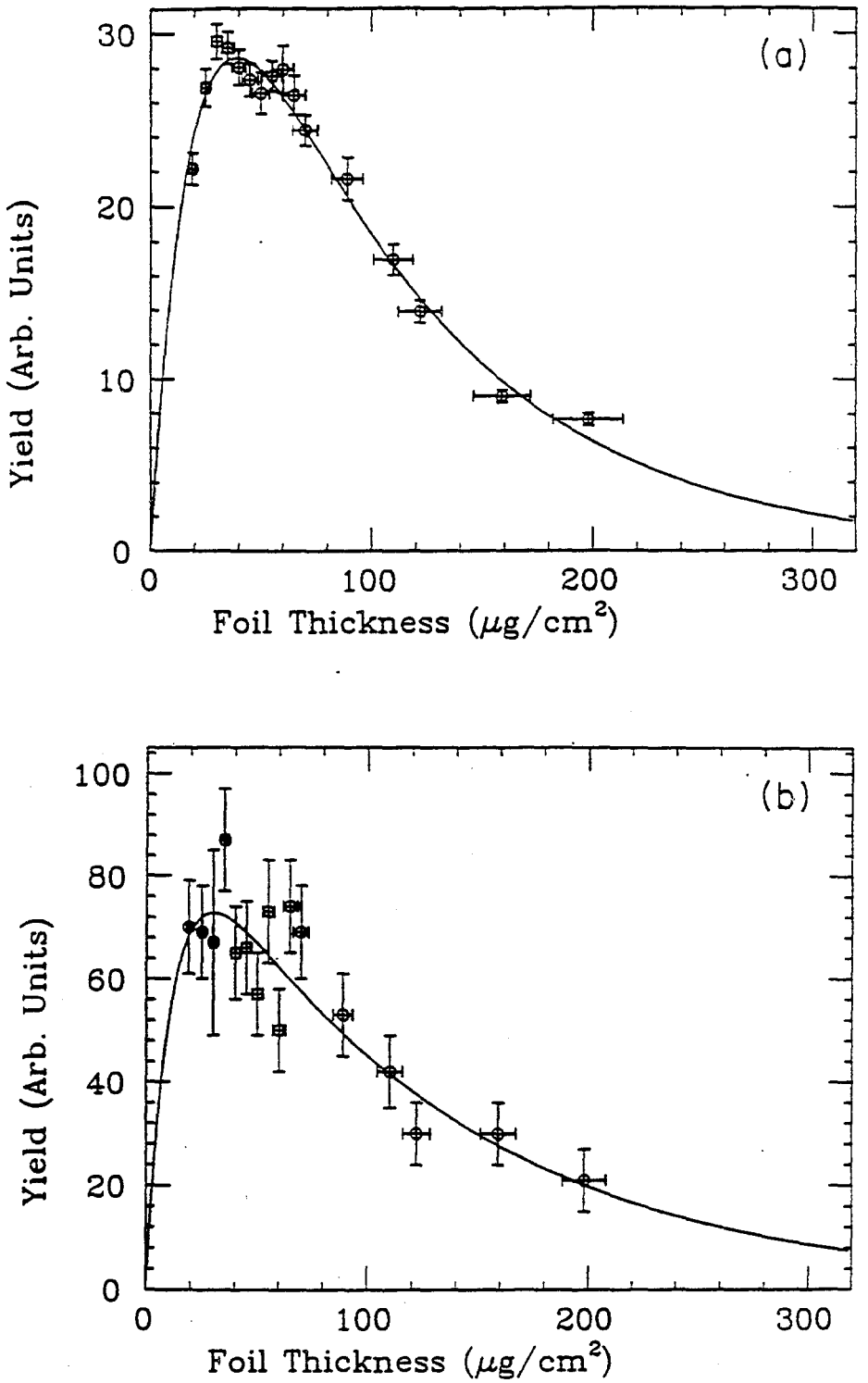

FIG. 19. Relative yield of (a) $n=1$ and (b) $n=2$ at 800 MeV as a function of carbon-foil thickness. The solid in each graph is the best fit to (5).

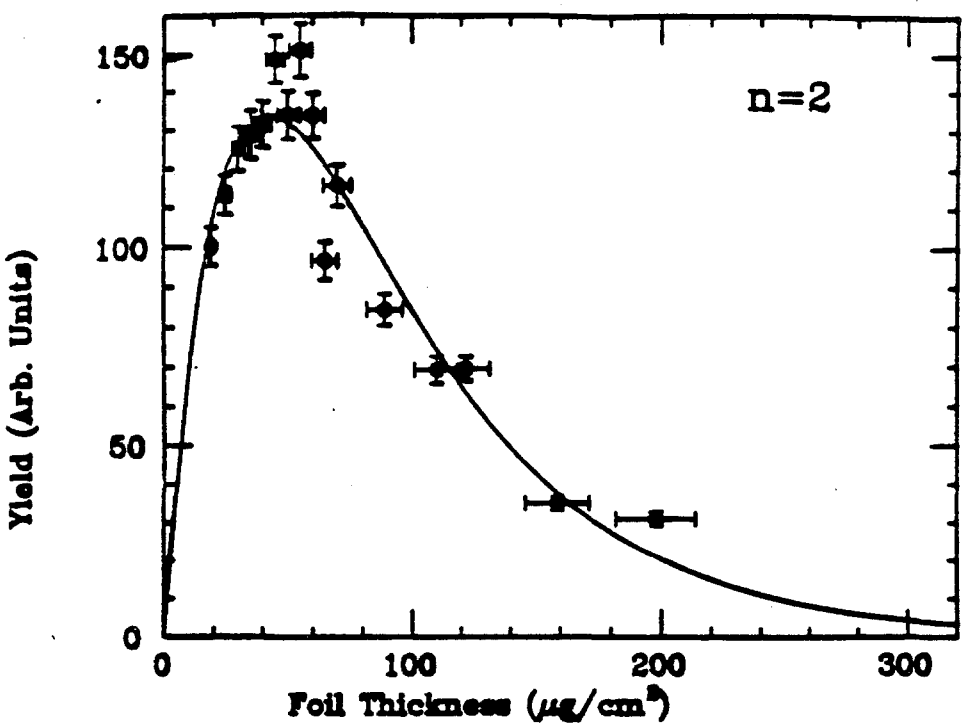

Figure 4.28 Relative yield of n = 2 at 800 MeV versus foil thickness. The solid line is the best fit to the simple rate equation.

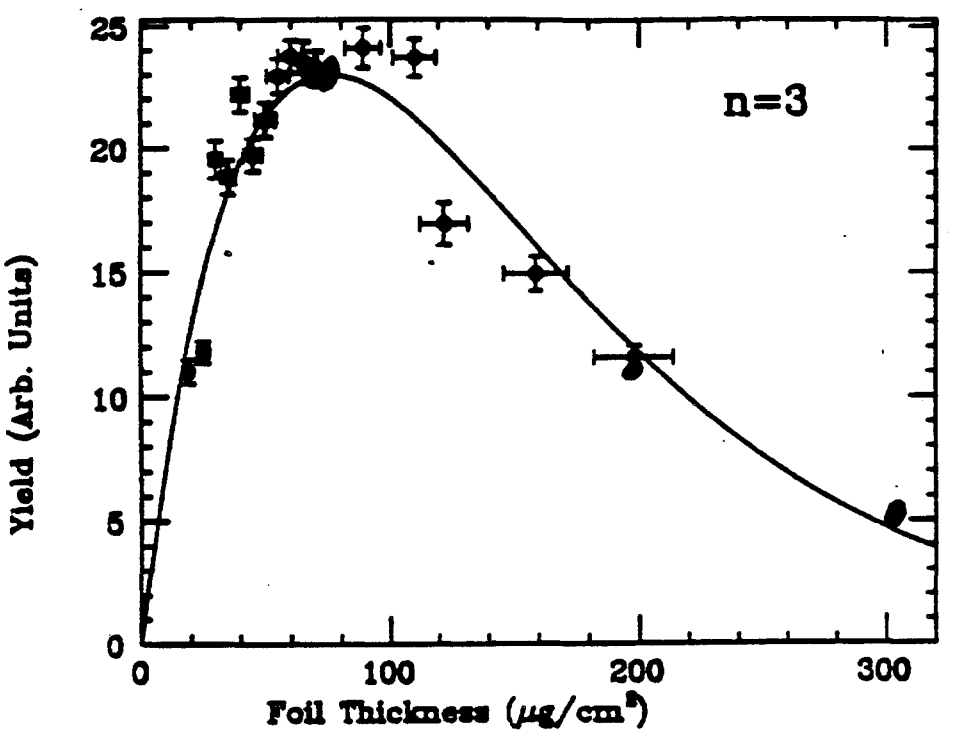

Figure 4.29 Relative yield of n = 3 at 800 MeV versus foil thickness. The solid line is the best fit to the simple rate equation.

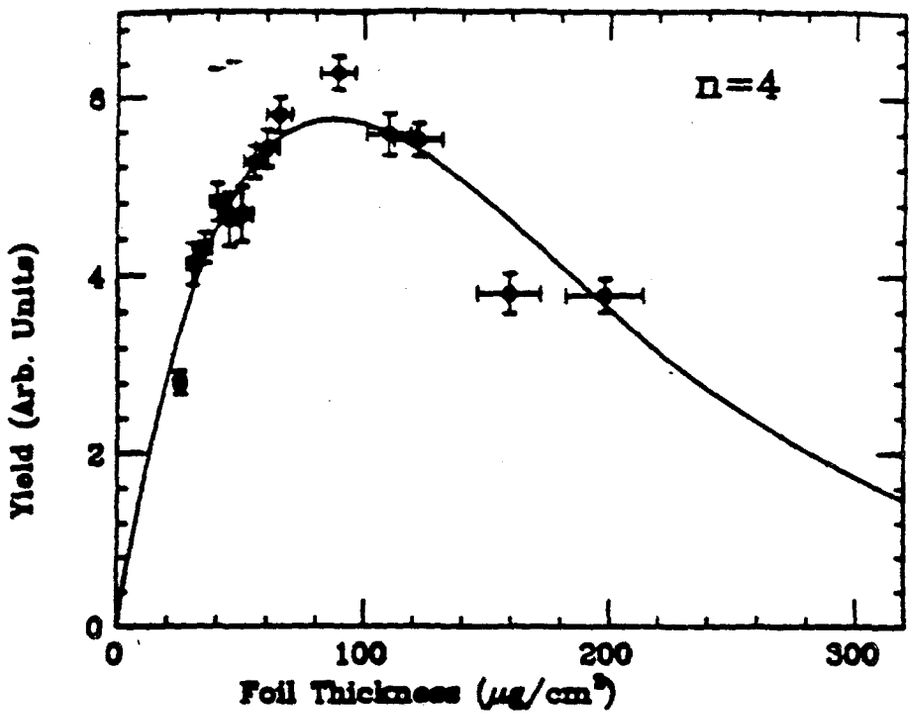

Figure 4.30 Relative yield of n = 4 at 800 MeV versus foil thickness. The solid line is the best fit to the simple rate equation.

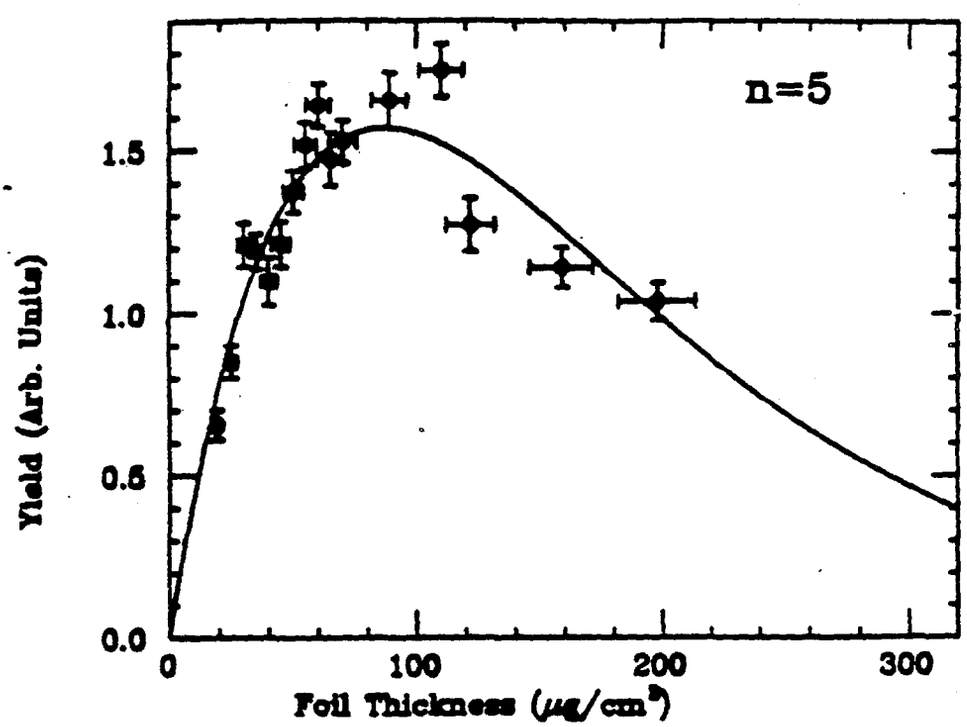

Figure 4.31 Relative yield of n = 5 at 800 MeV versus foil thickness. The solid line is the best fit to the simple rate equation.

Mohagheghi et al, PhysRev [illegible]

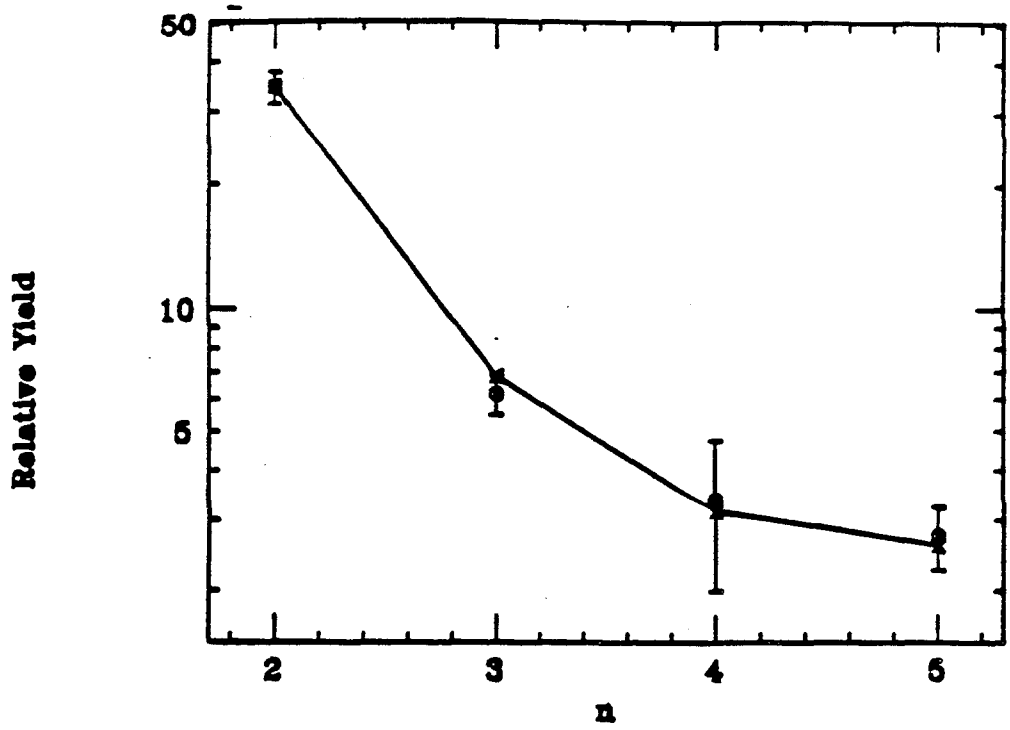

Figure 4.32 An example of the experimental (circles with error bars) and predicted (crosses) relative yields of n = 2, 3, 4, 5 for a 45 $\mu g/cm^2$ carbon foil.

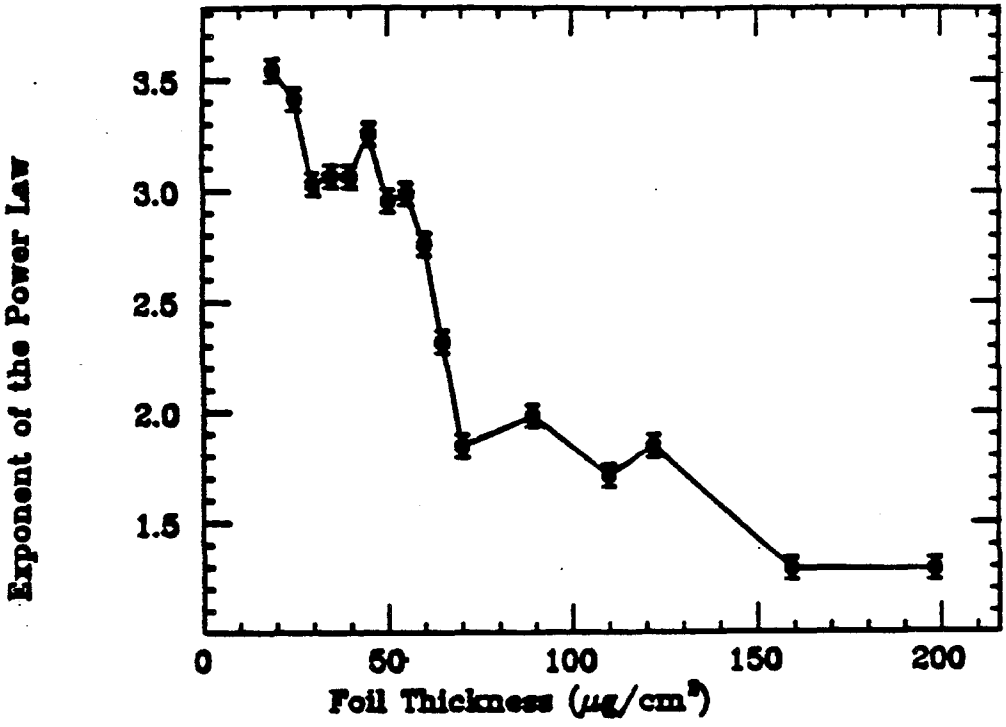

Figure 4.33 The fitted exponent of the power law n-distribution versus carbon foil thickness.

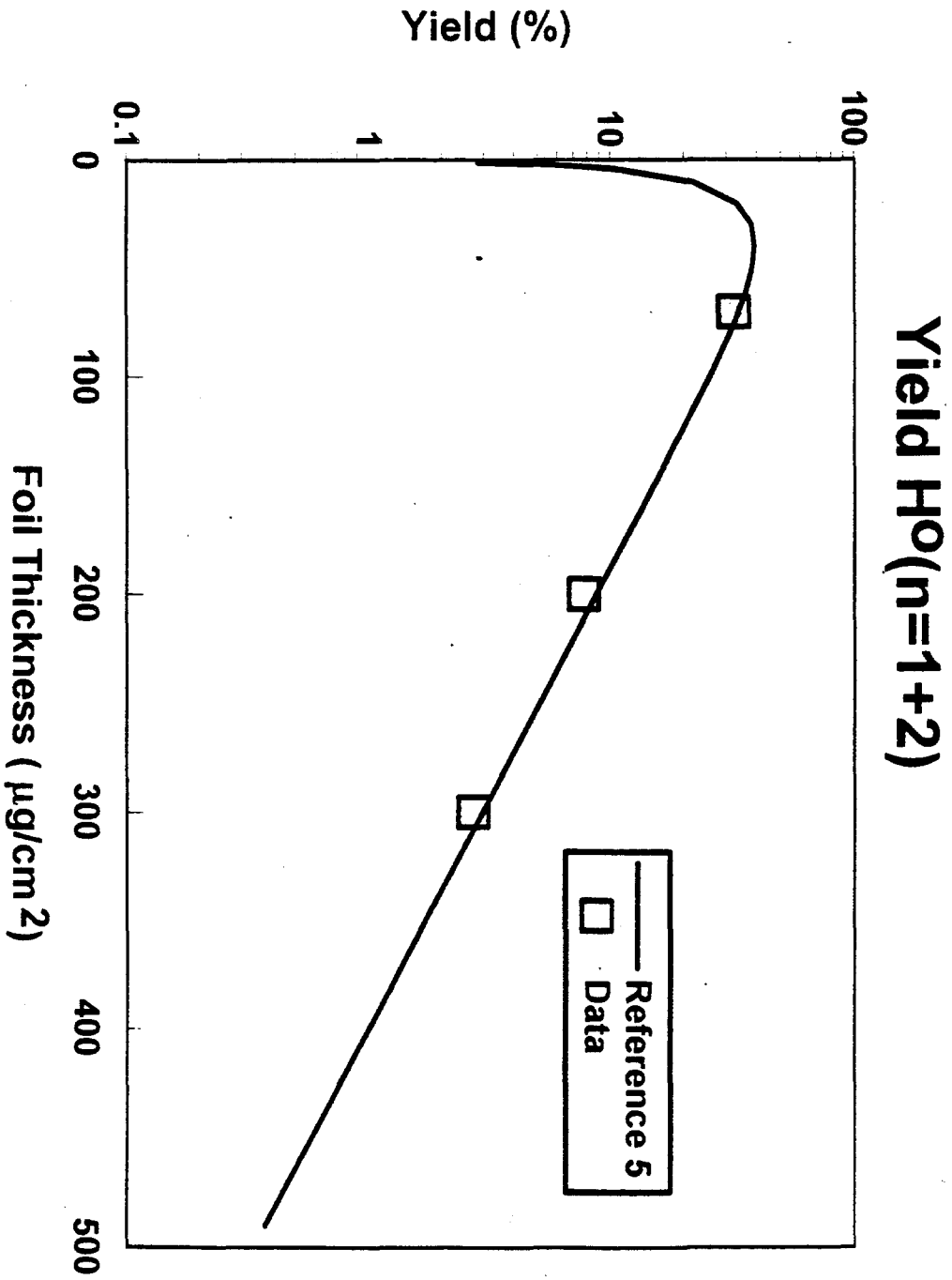
Yield H°(n=1+2)
Yield (%)
100
10
1
0.1
0
100
200
300
400
500
Foil Thickness (μg/cm 2)
Reference 5
Data

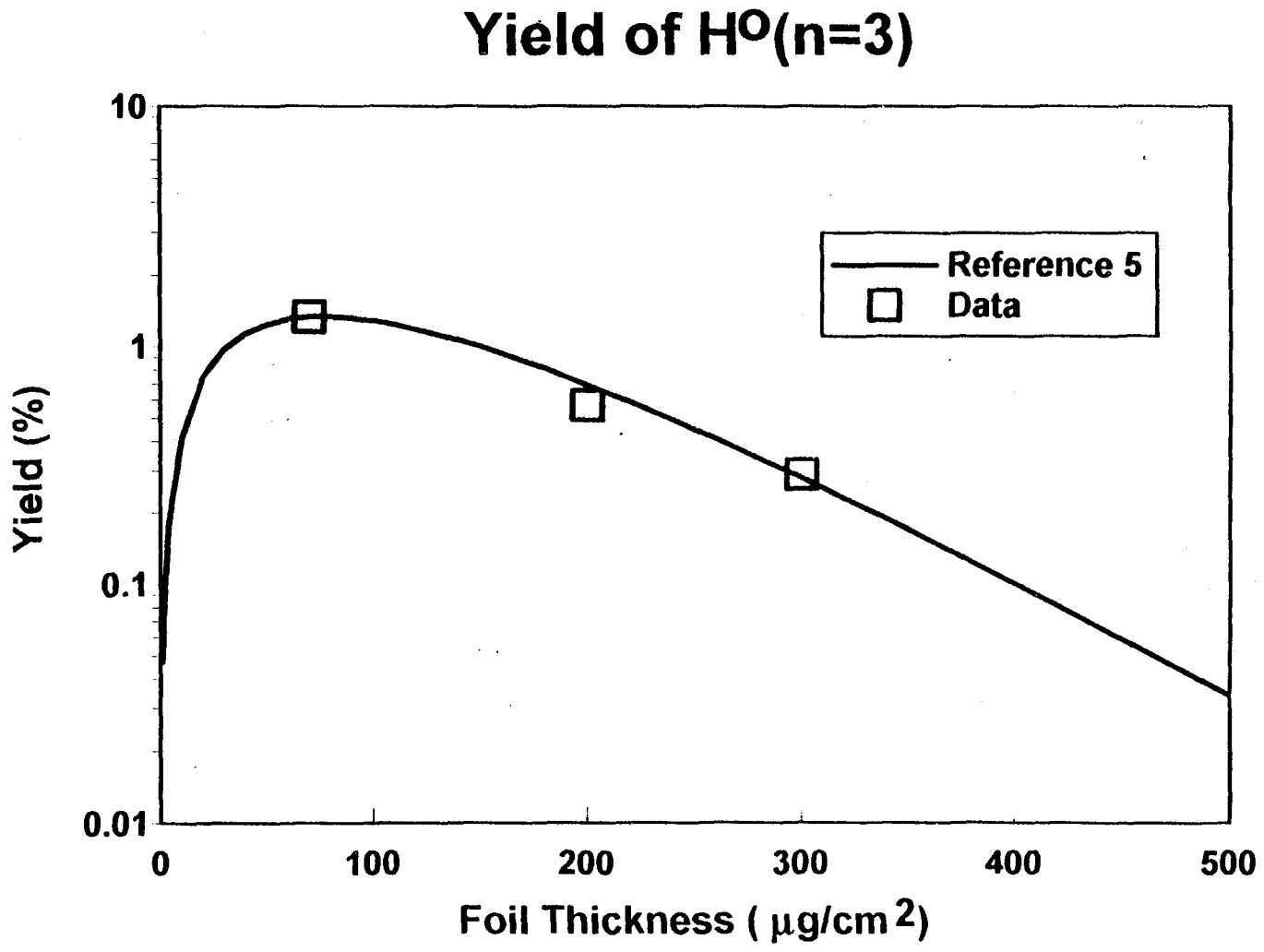
Yield of H°(n=3)
Reference 5
Data
Yield (%)
10
1
0.1
0.01
0
100
200
300
400
500
Foil Thickness (μg/cm 2)

Importance of Measuring Production of $H^0(n)$

Next Generation Spallation Neutron Source

Proposal	E_{inj}	$\bar{I}$
LANSCE II	800 MeV	1.3 – 6.3 mA
LANSCE IIB	1.2 – 2 GeV	2.5 – 4 mA
ESS	800 MeV	6.3 mA
IPNS upgrade	400 MeV	0.5 mA

Hands on maintenance of Ring $\Rightarrow$
point losses $<$ 10 – 100 nA

$\Rightarrow$ point losses $< 10^{-8} - 2 \times 10^{-6}$
not $\sim 10^{-3}$

factor of 10 – 500 lower than PSR!

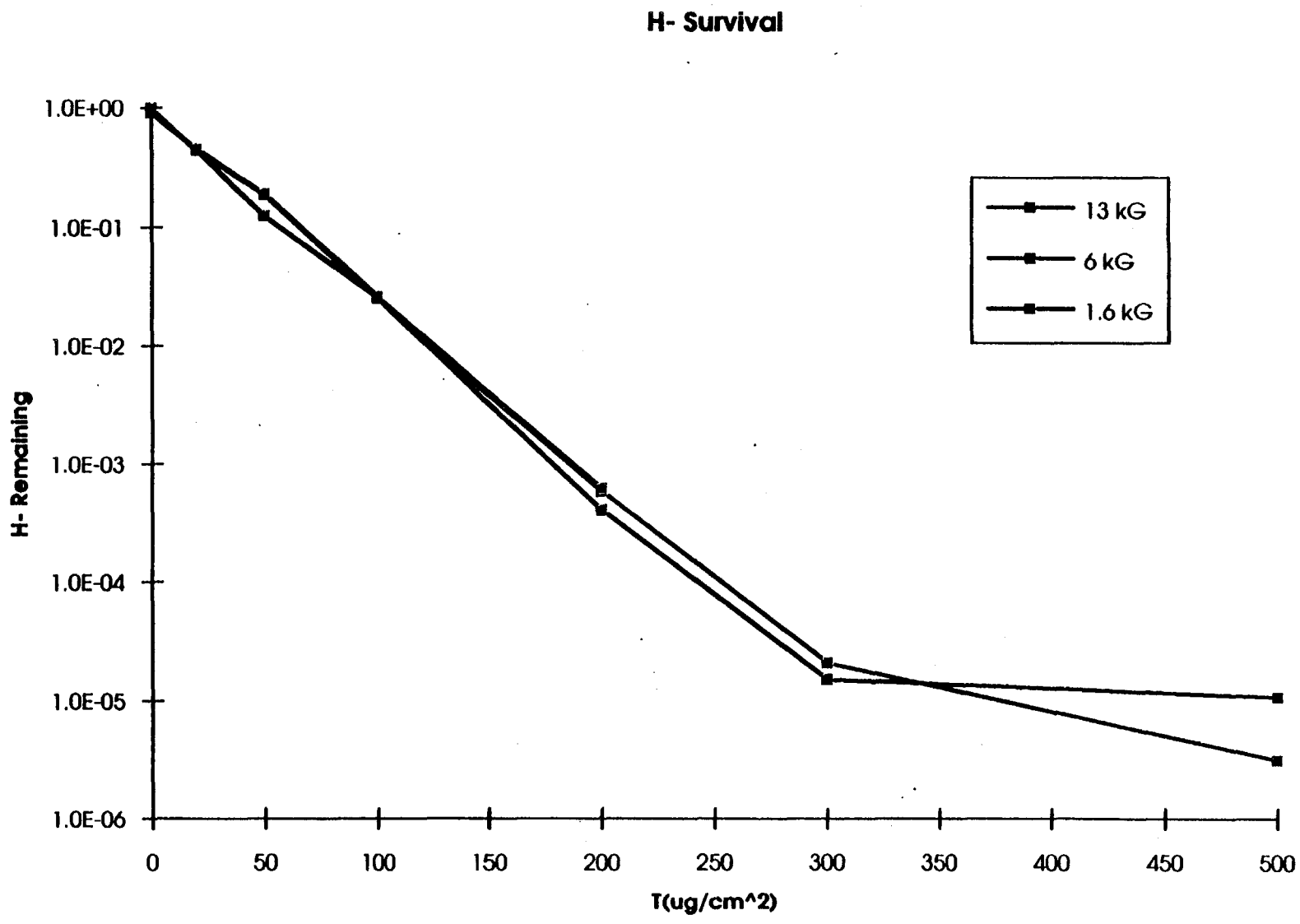
H- Survival
1.0E+00
1.0E-01
1.0E-02
1.0E-03
1.0E-04
1.0E-05
1.0E-06
H- Remaining
0
50
100
150
200
250
300
350
400
450
500
T(ug/cm^2)
13 kG
6 kG
1.6 kG

FOILYLD.XLS Chart 2

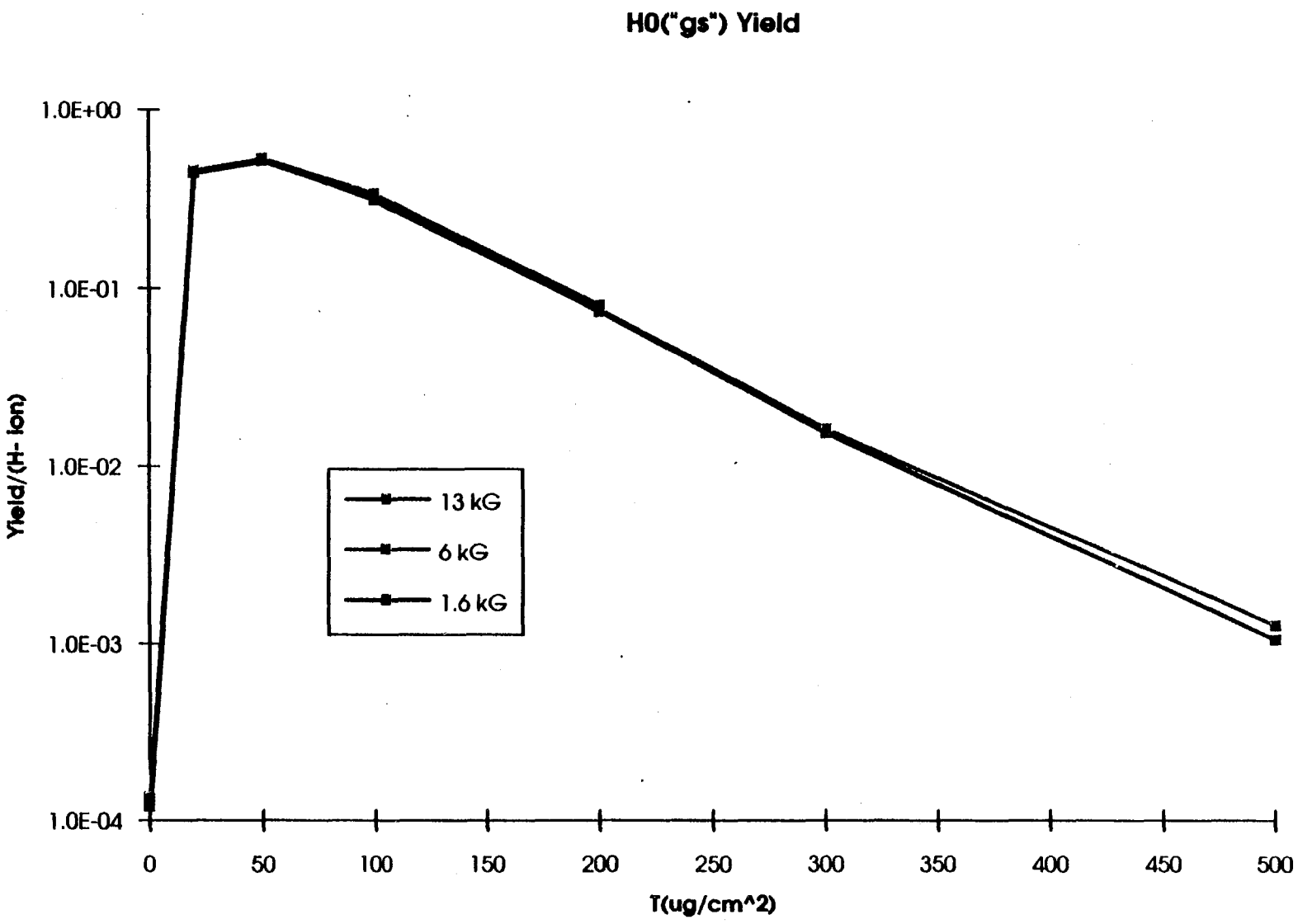

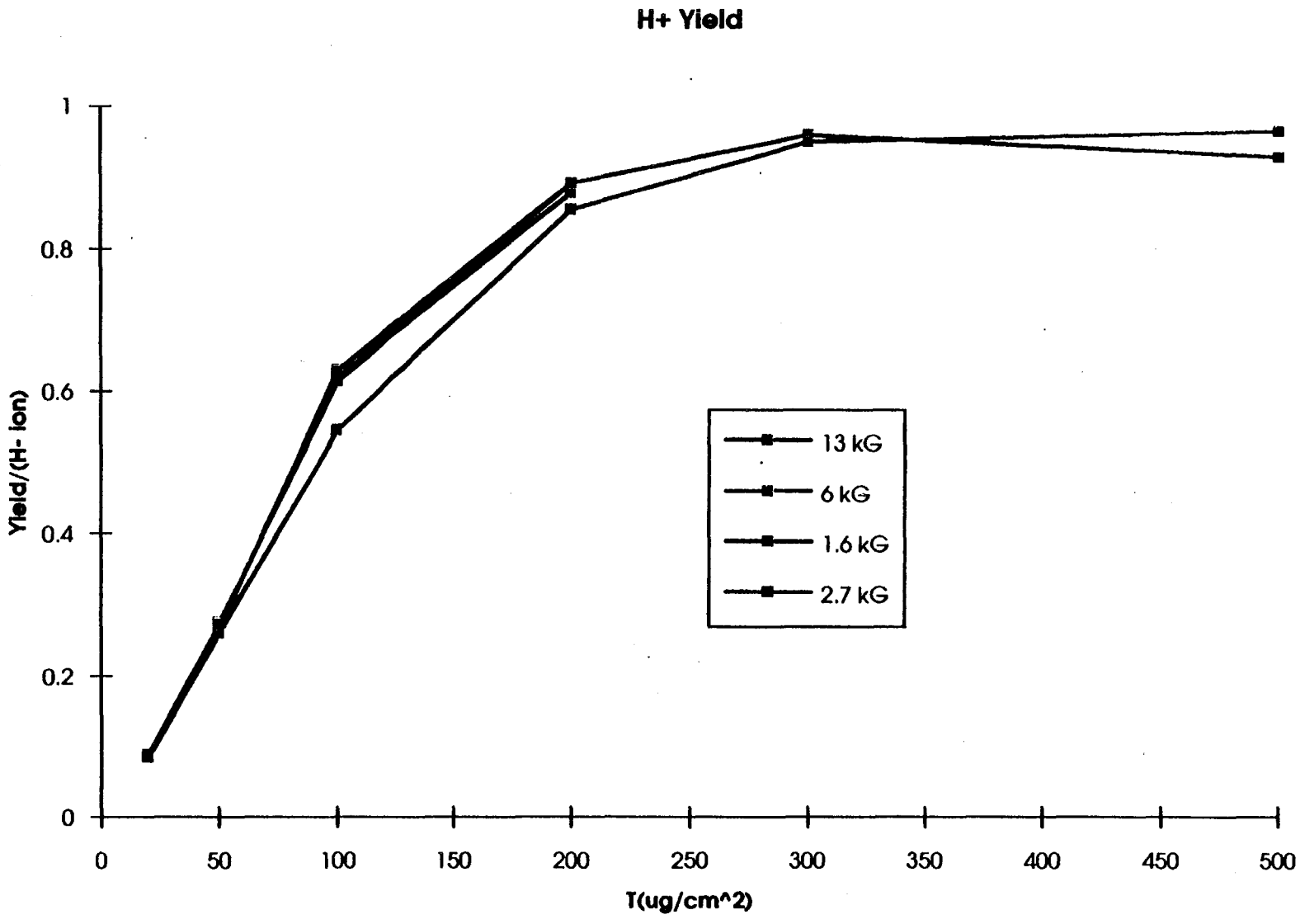
H+ Yield
Yield/(H- ion)
1
0.8
0.6
0.4
0.2
0
0
50
100
150
200
250
300
350
400
450
500
T(ug/cm^2)
13 kG
6 kG
1.6 kG
2.7 kG

C200NDIS.XLS Chart 1

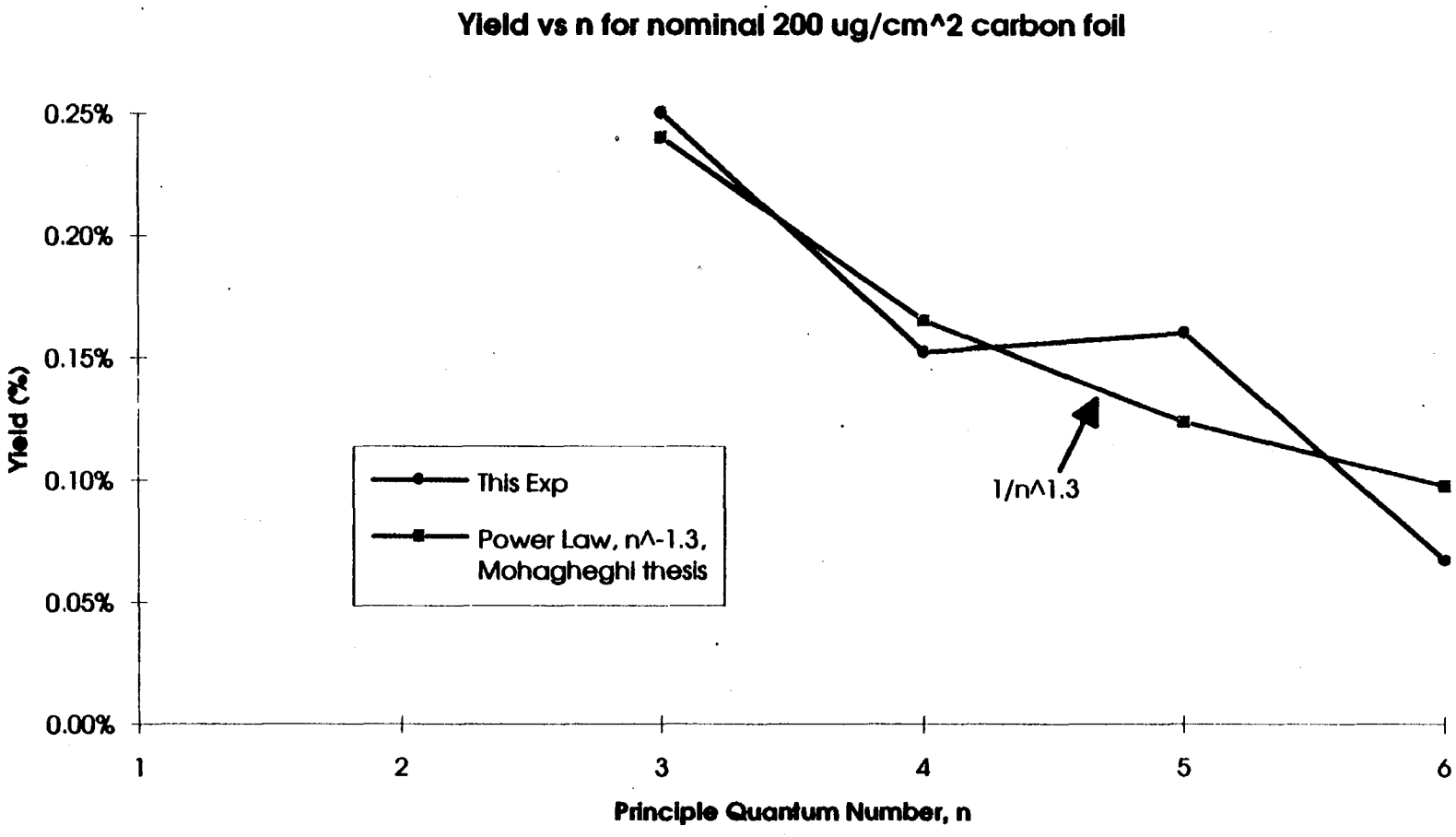

MINIMIZING HALOS AND LOSSES FROM $H^o(n)$

- Low field to separate H^+ and $H^o(n)$
  - $Y_n \alpha 1/n^p$
- Thicker foil
  - $Y_n \alpha e^{-T/\lambda n}$
  - Trade off with stored beam losses, $L_{stored} \alpha T$
- Ideal field for separating H^+ and $H^o(n)$

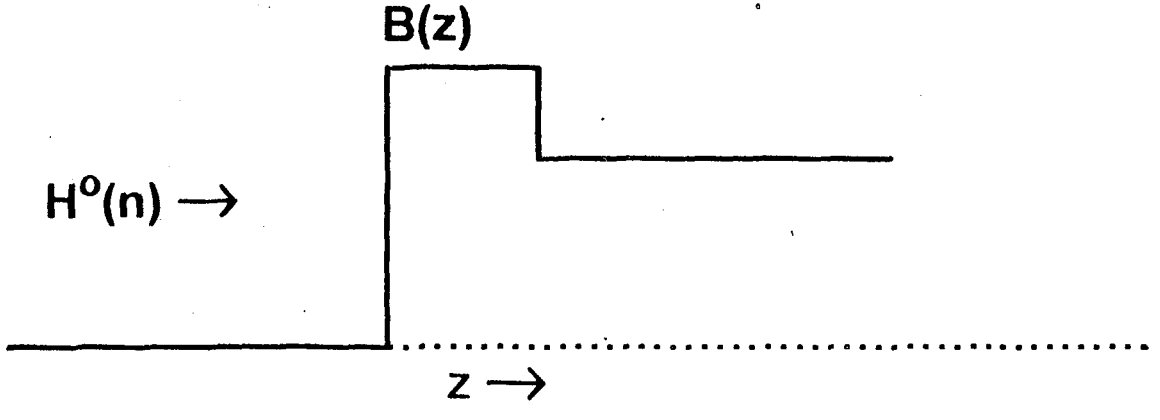

- Foil in magnetic field

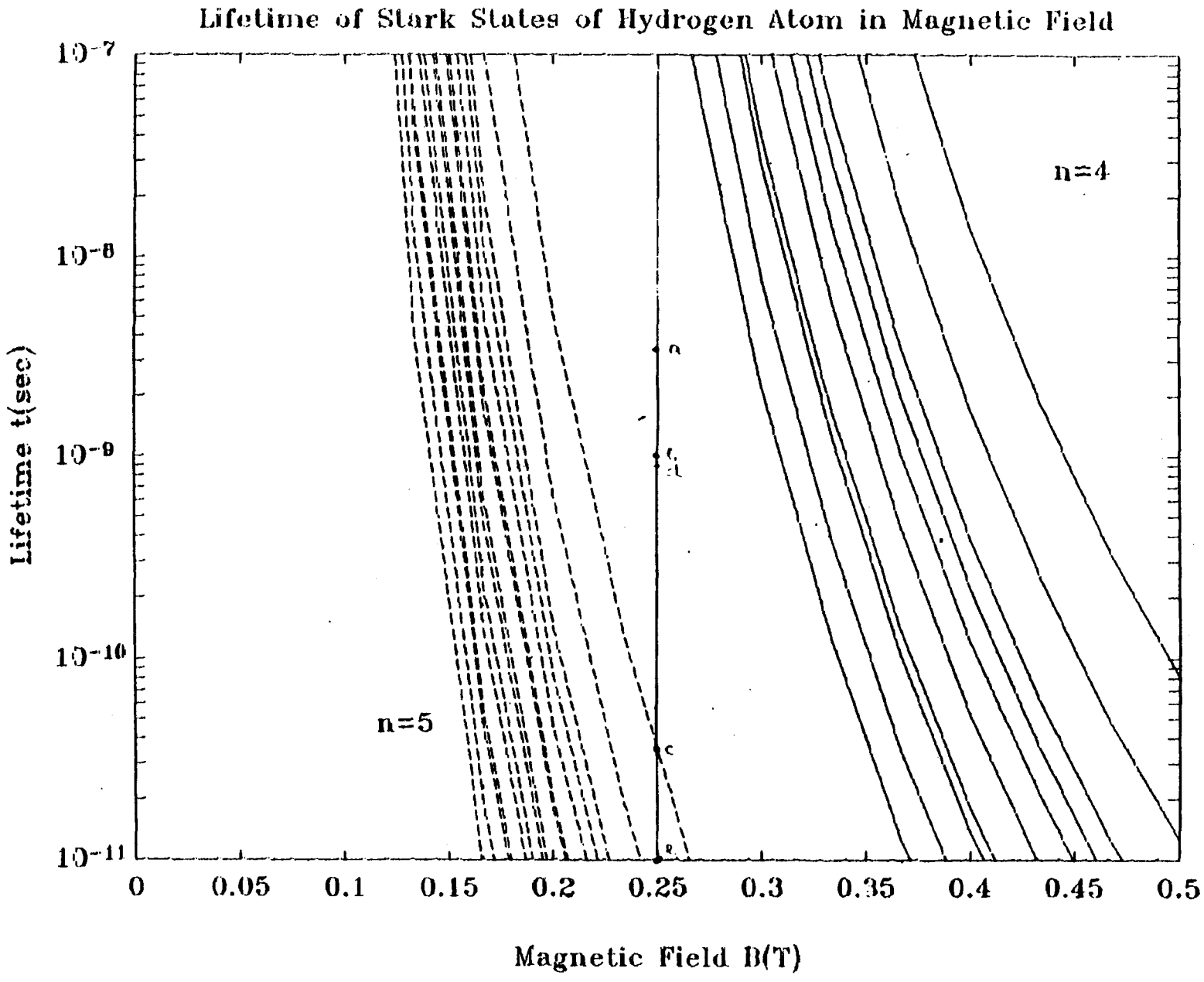
Lifetime of Stark States of Hydrogen Atom in Magnetic Field
Lifetime t(sec)
Magnetic Field B(T)
n=4
n=5
10^-7
10^-8
10^-9
10^-10
10^-11
0
0.05
0.1
0.15
0.2
0.25
0.3
0.35
0.4
0.45
0.5

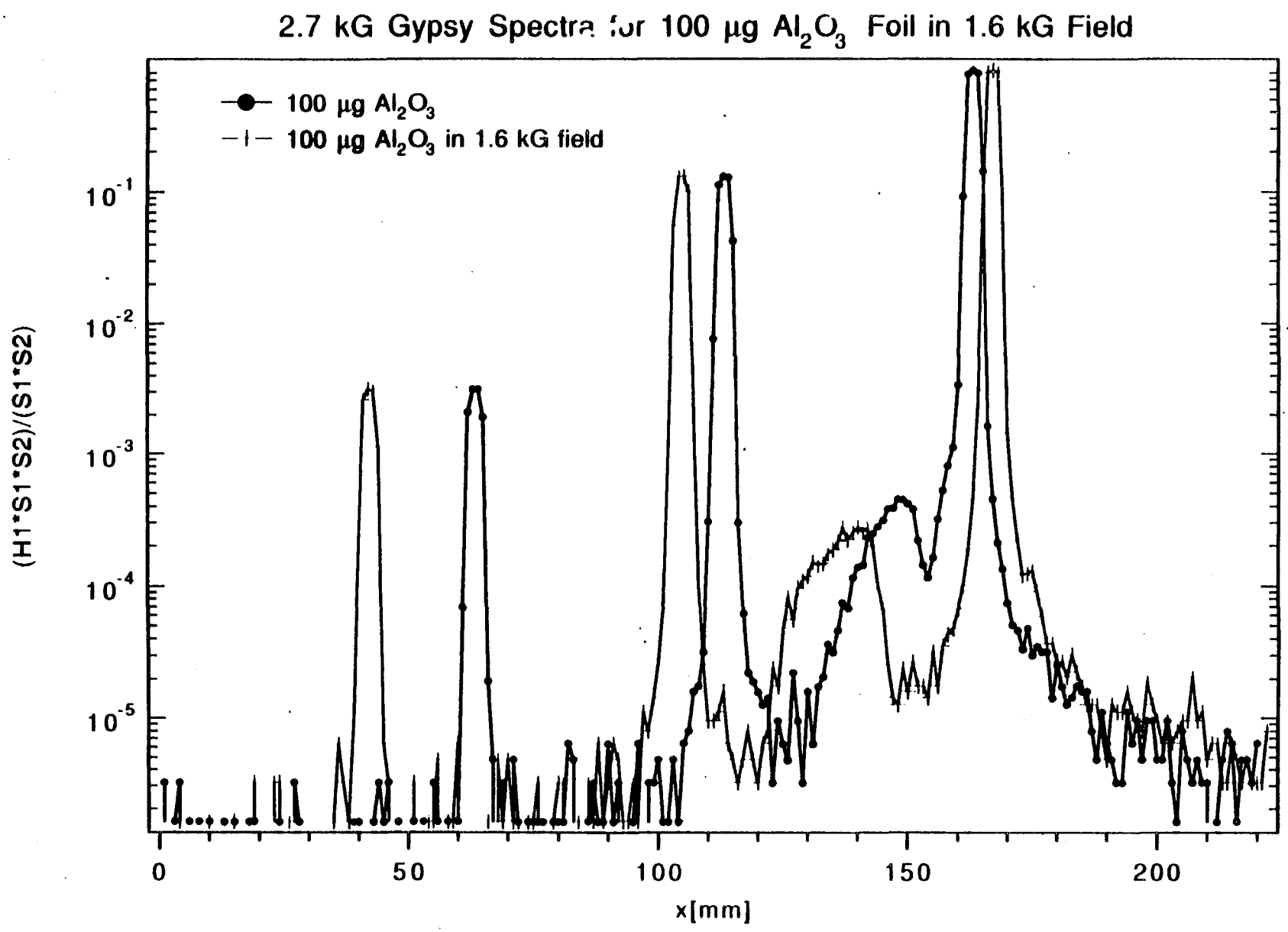
2.7 kG Gypsy Spectra for 100 µg Al_2O_3 Foil in 1.6 kG Field
100 µg Al_2O_3
100 µg Al_2O_3 in 1.6 kG field
(H1*S1*S2)/(S1*S2)
10^{-1}
10^{-2}
10^{-3}
10^{-4}
10^{-5}
0
50
100
150
200
x[mm]

FACTORS INFLUENCING PRODUCTION OF $H^o(n)$

- Incident H^-, H^o energy
- Foil thickness
- Z of foil
- Foil Angle ?
- Structure of foil material ?
- Magnetic Field in foil ?

Figure 4.21 Relative yield of n=2 at 226 as a function of the tilt angle of a 24 $\mu g/cm^2$ Formvar foil.

Figure 4.22 Relative yield of n=3 at 226 as a function of the tilt angle of a 24 $\mu g/cm^2$ Formvar foil.

FUTURE WORK

- Yield measurements at 400 MeV (B ⊥ p)
- Tests of prototype injection assemblies
  - Foil in magnetic field
- Comprehensive study of candidate stripper foil materials
- Measure yields for H^o incident

BEAM LINE REQUIREMENTS

- Well collimated, pure H^- beam
  - Collimate with strippers, sweep magnet after last stripper
- Duty Factor $\gtrsim 0.1\%$
- Good vacuum, $P < 10^{-7}$ Torr
- ~ 10 meters of beam line space for apparatus

CONCLUSION

Important aspects of charge exchange injection for high intensity machines can be studied at the proposed 400 MeV external H^- beam line at Fermilab

Some Ideas for the Application of the 400 MeV Linac to High Energy Physics

P. Colestock
Fermilab

Other related papers ....

Gerry Jackson
Accelerator Physics and Technology Applications

David Boehnlein
Health Physics Applications

HEP Applications

- Detector development
  - μ beams
- Shielding studies – D. Boehnlein
- Accelerator Physics
  - diagnostic development – G. Jackson
  - space charge physics
  - wakefield measurements
  - collimation studies
  - kicker measurements

Shielding studies

- Need to know neutron cross-sections in the range > 14 MeV

- Testing of specific shielding in accelerator structures

- Benchmarking of codes

Instruments that can be tested in a 100-400 MeV Muon Beam

Ring imaging Cerenkov counters
(E > 170 MeV)
- liquid and solid radiators

Time-of-flight detectors

Muon detectors
- scintillators
- gas counters
- resistive plate chambers

Tracking
- scintillating fibers
- Si detectors
- gas counters

(D. Anderson)

Diagnostic development

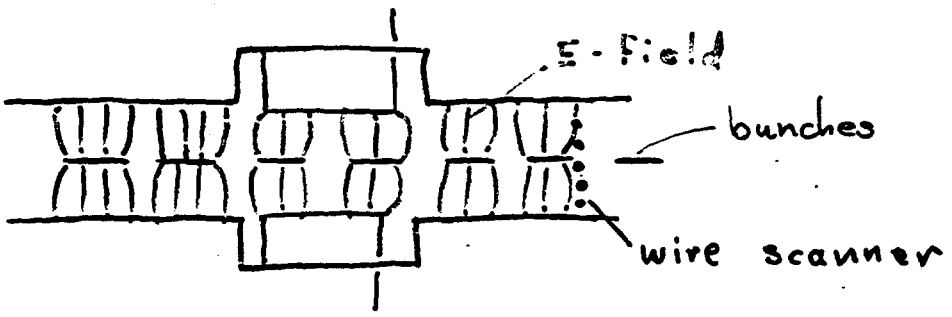

- used to calibrate & test beam pickups
- limited by low β
- low emittance
- steady state

Other devices to be tested ....

- profile monitors
- laser-based diagnostics

Laser-Driven Bunch-Length Detector

E. McCrory
October, 1993

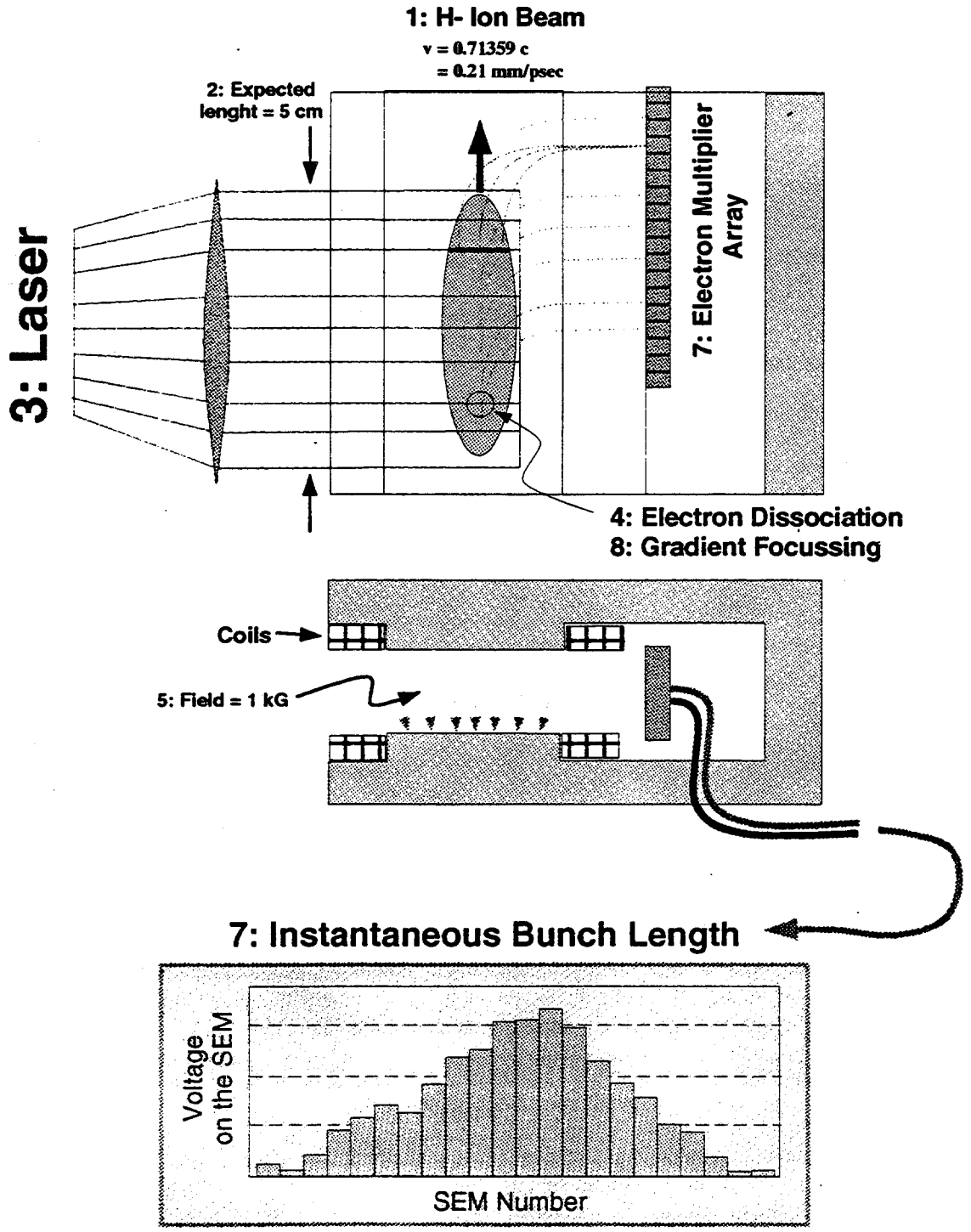

Beam Loading

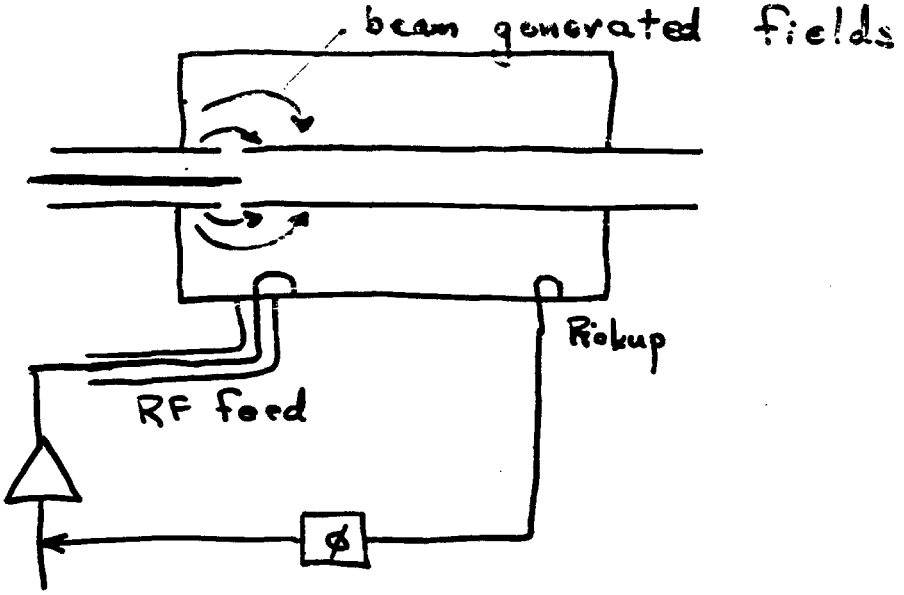

- test of beam-loading compensation

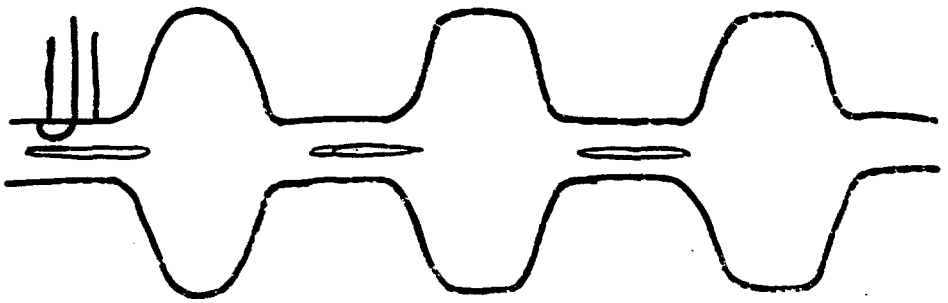

- test of multiple cavity filling
- investigate higher-order modes
- need to consider scaling

Space Charge Measurements

$$F_{sc} = \frac{e^2 N r}{2\pi \epsilon_0 a^2 \gamma^2}$$

(for a round beam of radius a)

- measure emittance dilution
- investigate diffusion rates
- extend to flat beams (TESLA or Asymmetric Collider)

Need some clever trick to follow particles ....

Laser Tagging !

What is a wakefield ?

The forces on a charge moving through a conducting structure are expressed in terms of wake functions.

$$F_r = e Q_m \, m r^{m-1} \cos m\theta \; W_m(s)$$
$$F_z = -e Q_m \, r^m \cos m\theta \; W_m'(s)$$

In the frequency domain, the wake functions are expressed in terms of the impedance.

$$Z_{\parallel} = \frac{L}{c} \int_{-\infty}^{\infty} e^{i\frac{\omega s'}{c}} W_0'(s') \, ds'$$

$$Z_{\perp} = \frac{L}{ic} \int_{-\infty}^{\infty} e^{i\frac{\omega s'}{c}} W_m(s') \, ds'$$

$$\boxed{\begin{aligned} \nabla_{\perp} F_z &= \frac{\partial \bar{F}_{\perp}}{\partial s} \\ Z_m^{\parallel} &= \frac{\omega}{c} Z_m^{\perp} \end{aligned}}$$

Wakefields can be measured in either the time or frequency domain.

Wakefield Measurement Methods

Current approaches: wires or beads

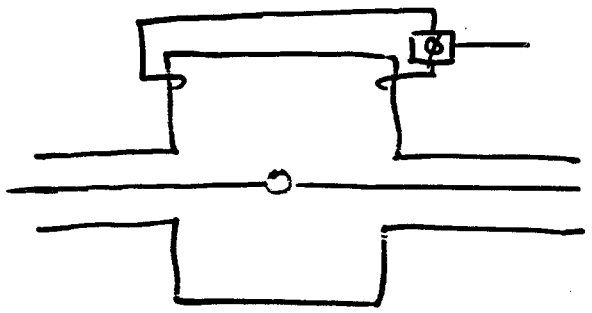

issues:
- high-Q needed
- E vs. B measurement

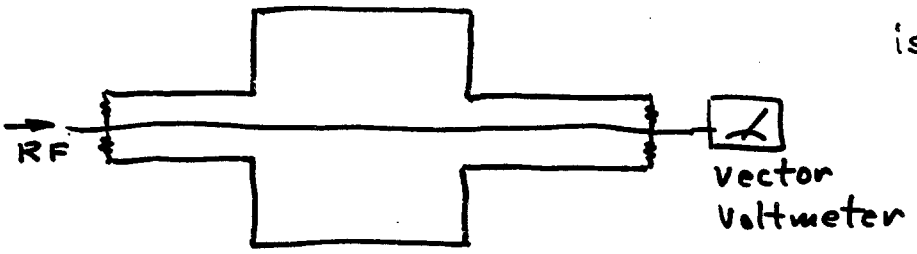

issues:
- transition matching
- decoupling of distributed systems

Also,

how does one handle $f > f_c$?

how does one get spatial resolution ?

how can small impedances be measured ?

Beam-based wakefield measurements

Frequency domain

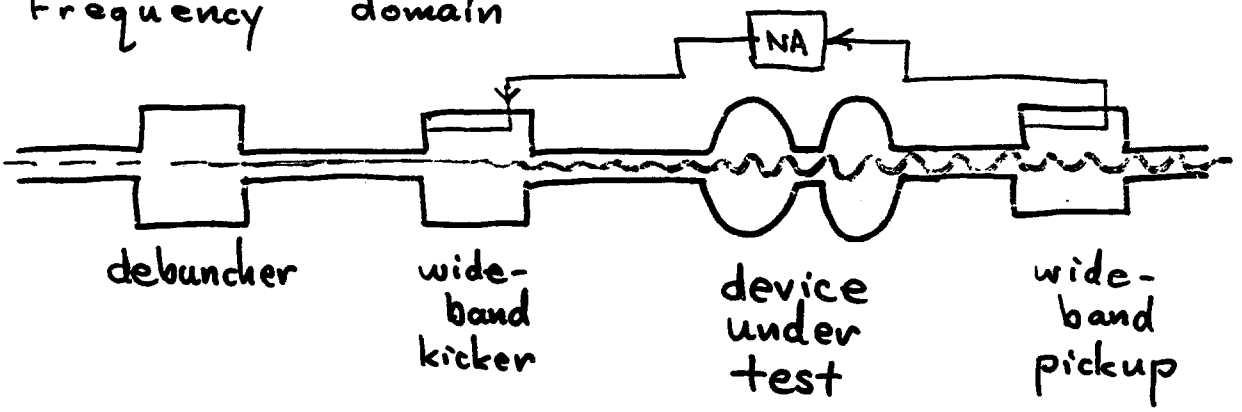

(G. Jackson)

Time domain

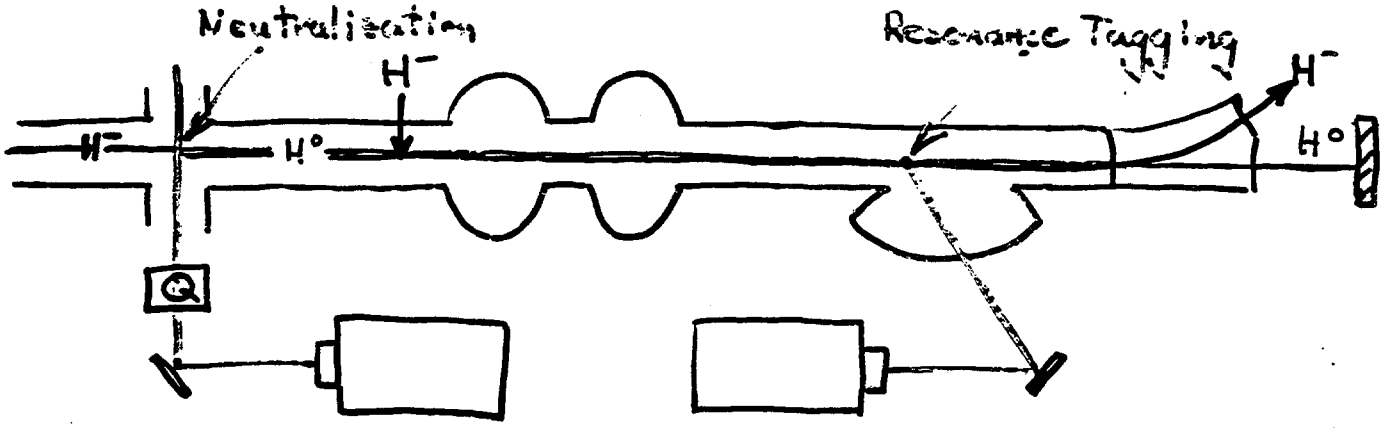

- Q-switched laser produces 10-100 psec edge
- resonance tagging permits very high energy resolution

Collimation Studies

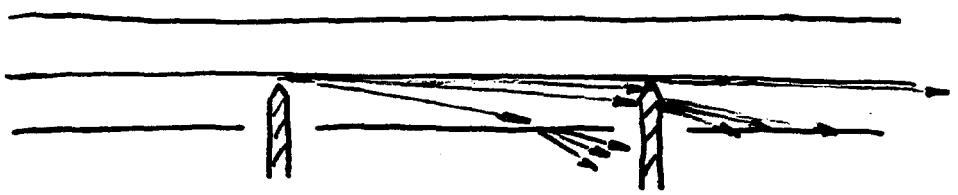

- benchmark codes
- investigate development of halo
- investigate energy deposition

Kicker Calibration

There are no convenient methods available to accurately measure fast-rising magnetic fields over large spatial scales $l \gtrsim \lambda$.

A beam-based method is the ideal way

- fast response
- integrated measurement
- no perturbing probes

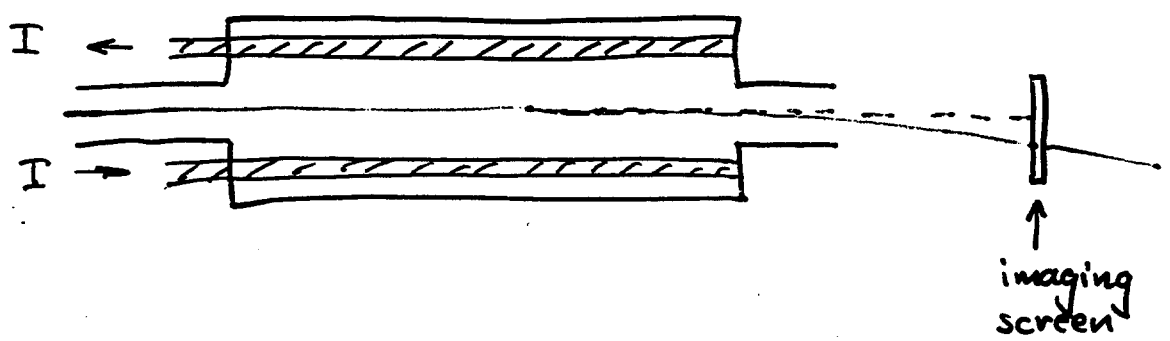

Summary

Advantages

Steady - state

Easy access

Compelling needs from HEP

Facility is cheap

Disadvantages

Low β

Nothing is free

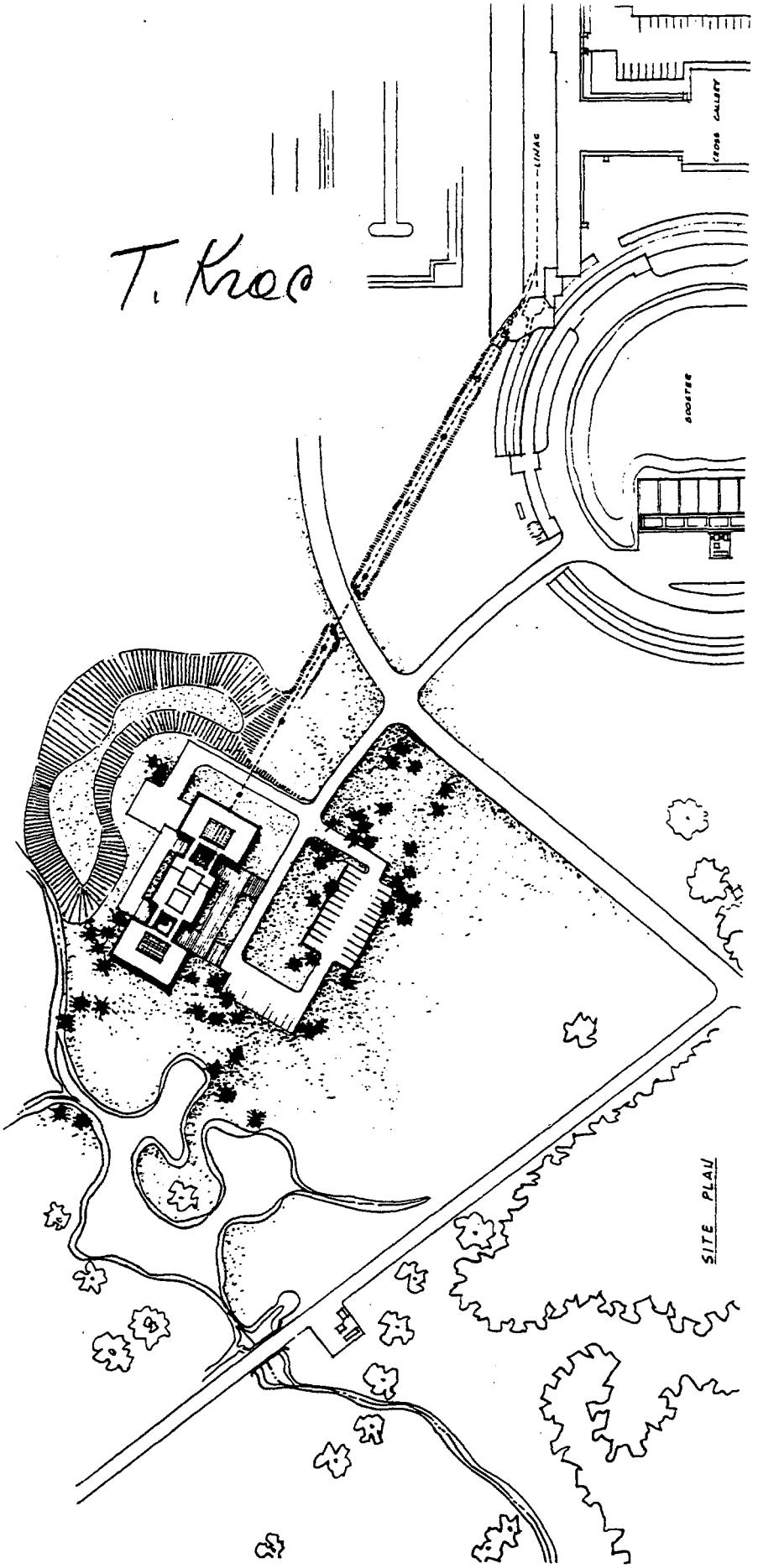

Wilsons Proposed Proton Therapy Facility

Pulse Width -

from one 200 MHz micropulse to 40 μs macropulse

Current -

5 - 35 mA

Intensity -

1×10^8 to 1×10^{13} particles per pulse

Momentum Spread -

.015% with 30' lever arms and 1 mm slits

Transverse Emittance -

7π, smaller with collimators

Energy -

116, 152, 190, 230, 271, 314, 357, 401 MeV

Repetition Rate -

single pulse to 15 Hz

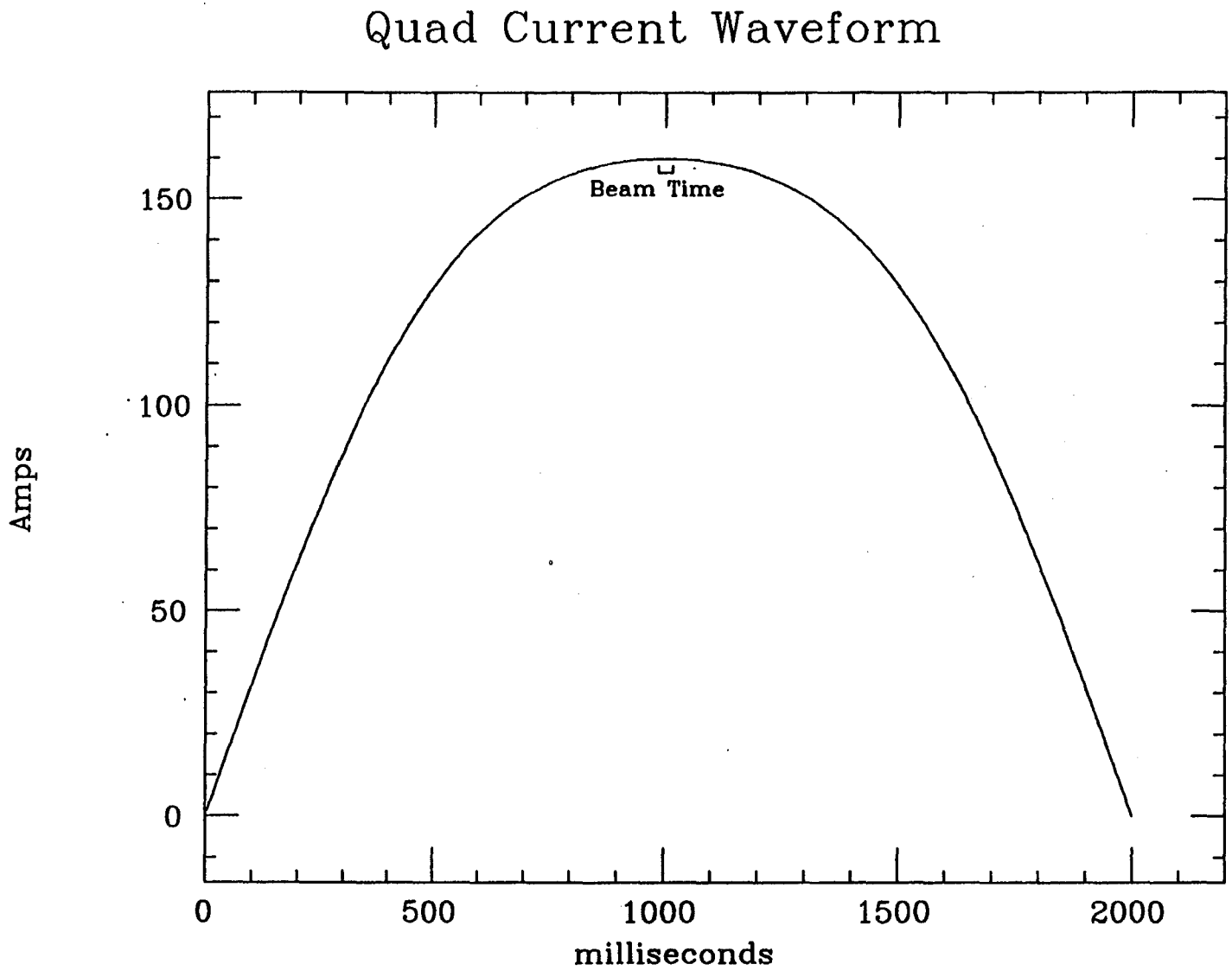
Quad Current Waveform
Beam Time
Amps
150
100
50
0
0
500
1000
1500
2000
milliseconds

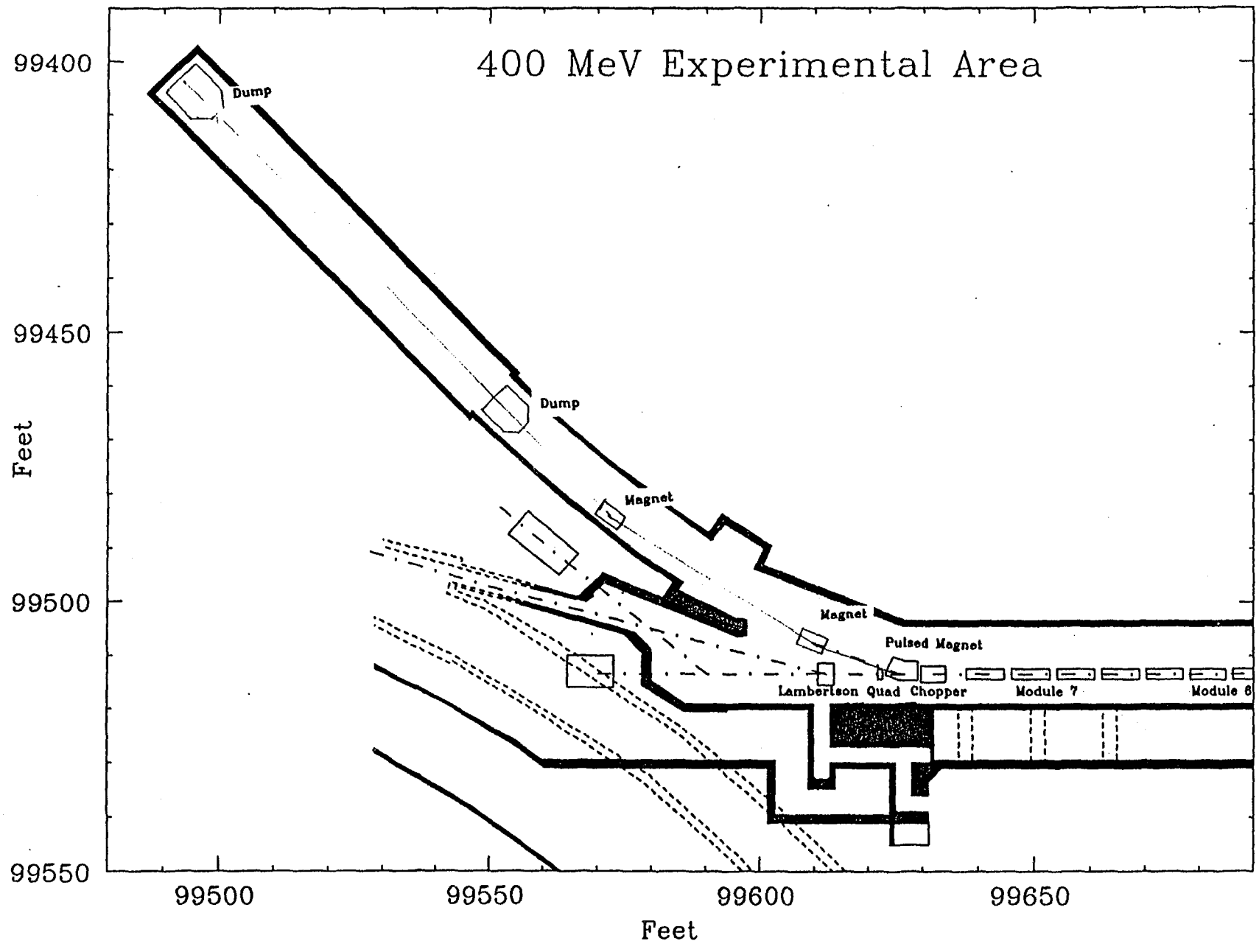
400 MeV Experimental Area
Dump
Dump
Magnet
Magnet
Pulsed Magnet
Lambertson
Quad
Chopper
Module 7
Module 6
99400
99450
99500
99550
Feet
99500
99550
99600
99650
Feet

Figure 1

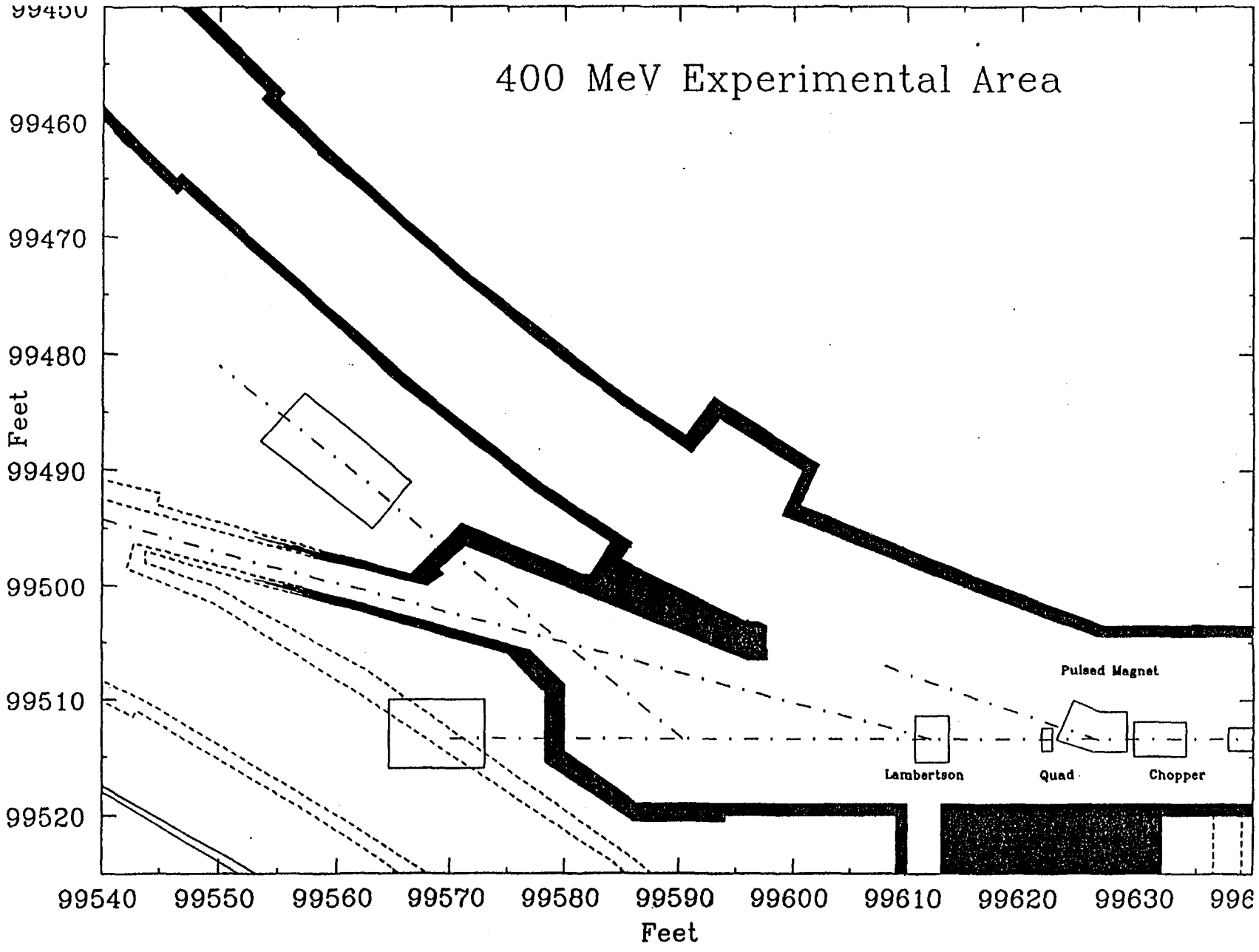
400 MeV Experimental Area
Pulsed Magnet
Lambertson
Quad
Chopper
Feet
99450
99460
99470
99480
99490
99500
99510
99520
99540
99550
99560
99570
99580
99590
99600
99610
99620
99630
Feet

Figure 2

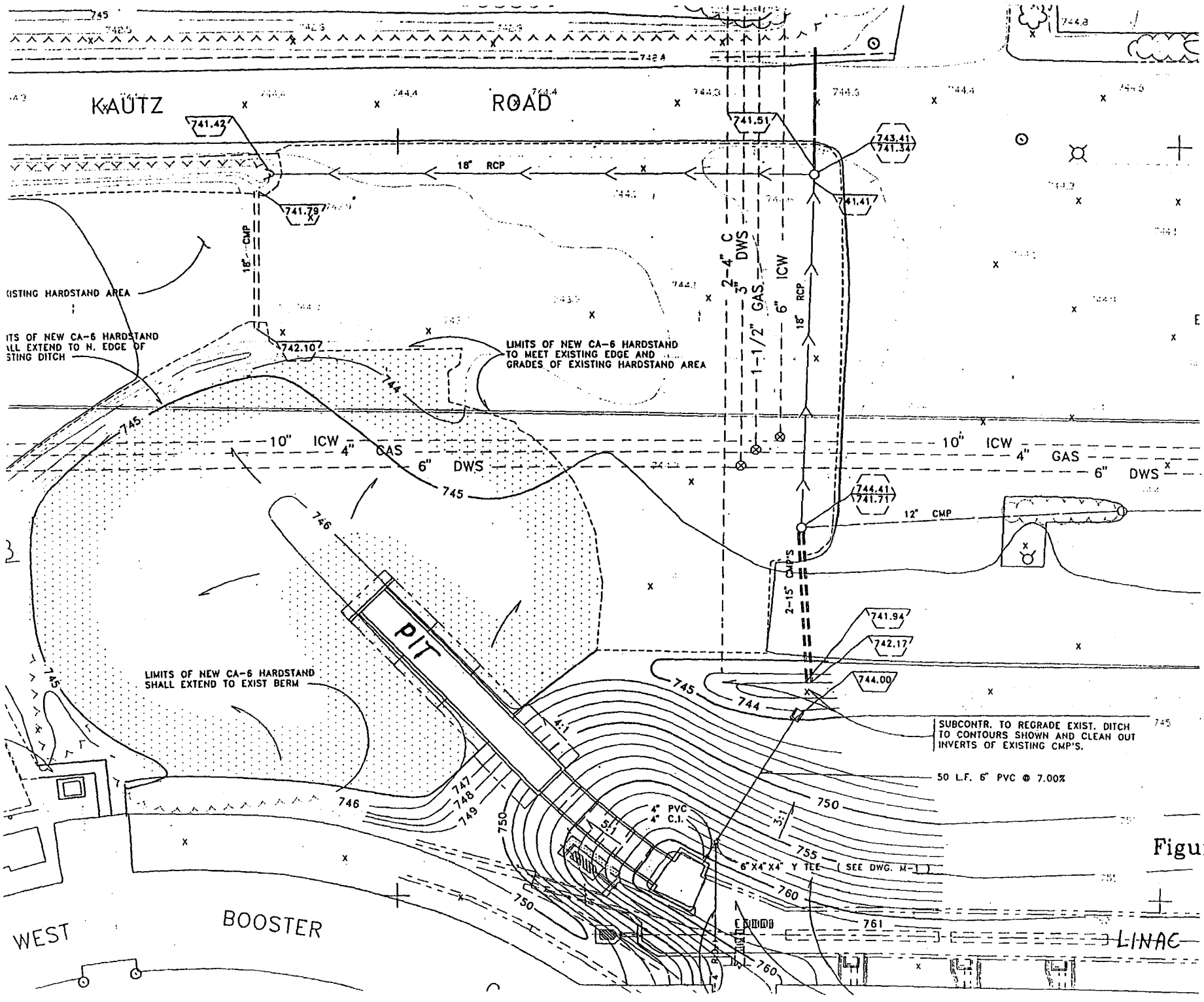
KAUTZ ROAD
741.42
741.51
743.41
741.34
741.41
741.79
18" RCP
18" CMP
742.10
744
745
746
747
748
749
750
755
760
761
10" ICW
4" GAS
6" DWS
2-4" C
3" GAS
1-1/2"
6" ICW
18" RCP
744.41
741.71
12" CMP
2-15" CMP'S
741.94
742.17
744.00
LIMITS OF NEW CA-6 HARDSTAND TO MEET EXISTING EDGE AND GRADES OF EXISTING HARDSTAND AREA
LIMITS OF NEW CA-6 HARDSTAND SHALL EXTEND TO EXIST BERM
PIT
4:1
3:1
4" PVC
4" C.I.
6"X4"X4" Y TEE (SEE DWG. M-1)
SUBCONTR. TO REGRADE EXIST. DITCH TO CONTOURS SHOWN AND CLEAN OUT INVERTS OF EXISTING CMP'S.
50 L.F. 6" PVC @ 7.00%
WEST BOOSTER
LINAC

Figure 3

400 MeV Beam for Less Than Half a Million, (Who Could Ask for More)

Milorad Popovic, Tom Owens and Tanya Bynum, Oct. 25, 1993

1) GOALS-

a) not to be seen by HEP,
b) to have 115 to 400+ MeV H beam,
c) for less then 0.5 M$

2) GOALS WILL BE ACCOMPLISHED- using;

a) 400MeV area
b) existing magnet gesign

3) EQUIPMENT NEEDED and COST-

a) two dipole magnts	121 k$
b) two power supplies	16 k$
c) two quads	36 k$
d) two power supplies	10 k$
c) pipes and ????	316 k$
TOTAL (tax inc.)	499 k$

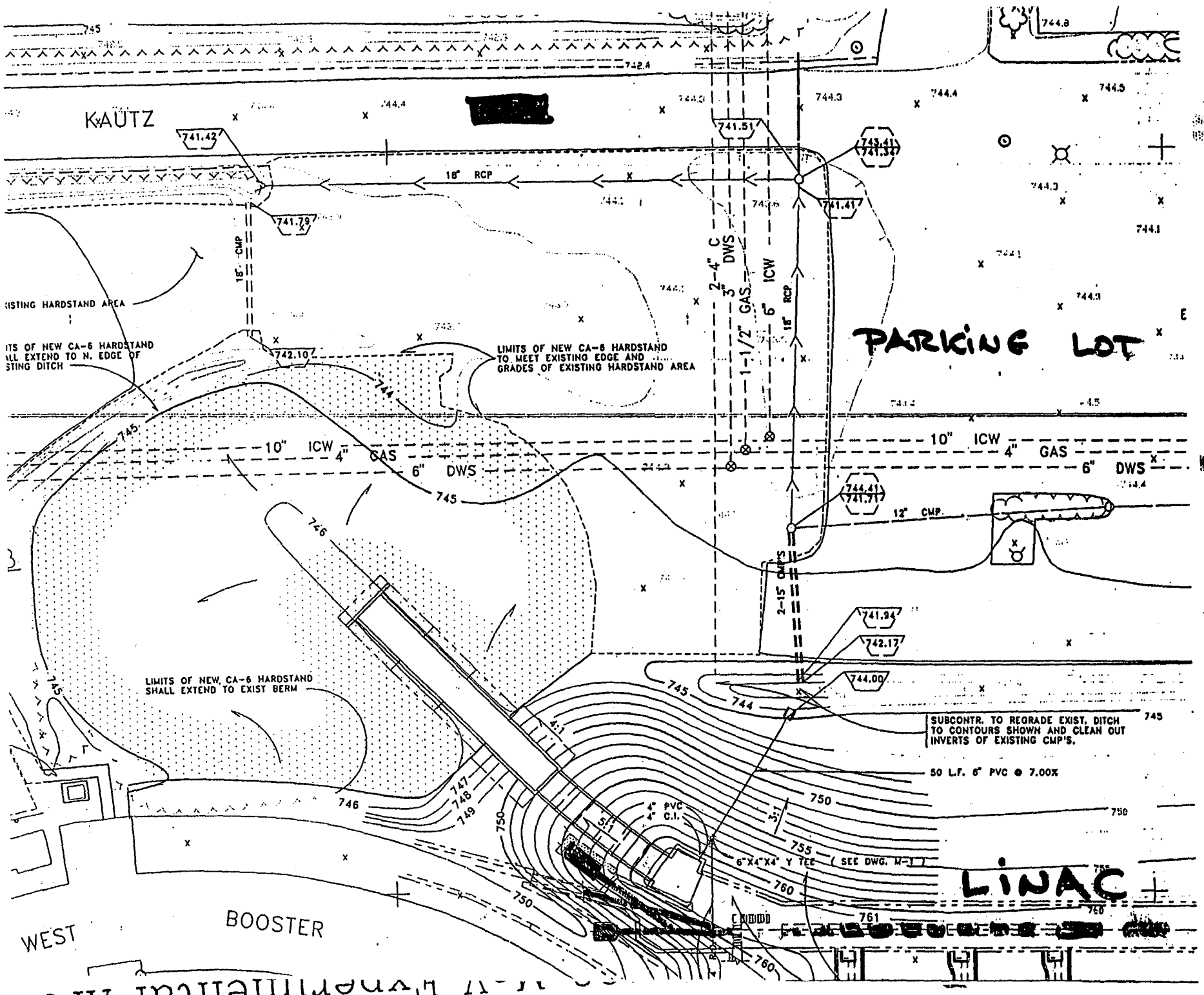
KAUTZ
[redacted]
741.42
741.79
741.51
741.41
741.34
741.41
741.94
742.17
744.00
741.71
742.10
18" RCP
15" CMP
15" RCP
2-4" C
3" DWS
1-1/2" GAS
6" ICW
10" ICW
4" GAS
6" DWS
12" CMP
2-15" CMP'S
EXISTING HARDSTAND AREA
LIMITS OF NEW CA-6 HARDSTAND SHALL EXTEND TO N. EDGE OF EXISTING DITCH
LIMITS OF NEW CA-6 HARDSTAND TO MEET EXISTING EDGE AND GRADES OF EXISTING HARDSTAND AREA
LIMITS OF NEW CA-6 HARDSTAND SHALL EXTEND TO EXIST BERM
PARKING LOT
LINAC
WEST BOOSTER
SUBCONTR. TO REGRADE EXIST. DITCH TO CONTOURS SHOWN AND CLEAN OUT INVERTS OF EXISTING CMP'S.
50 L.F. 6" PVC @ 7.00%
4" PVC
4" C.I.
6"X4"X4" Y TEE
(SEE DWG. M-1)
4:1
3:1
745
744
746
747
748
749
750
755
760
761

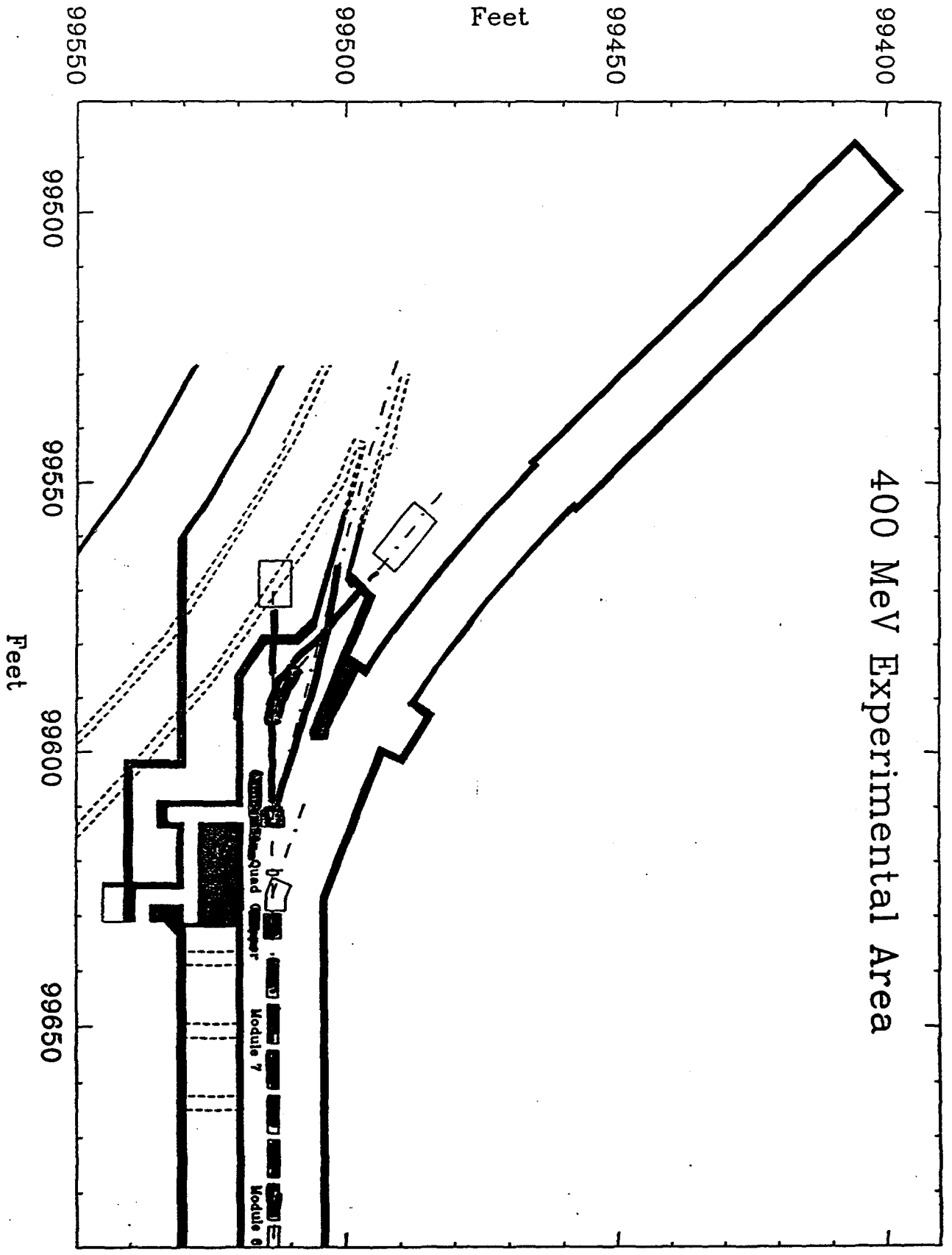
400 MeV Experimental Area
Feet
99400
99450
99500
99550
Feet
99500
99550
99600
99650
Quad
Module 7

400 MeV Experimental Area

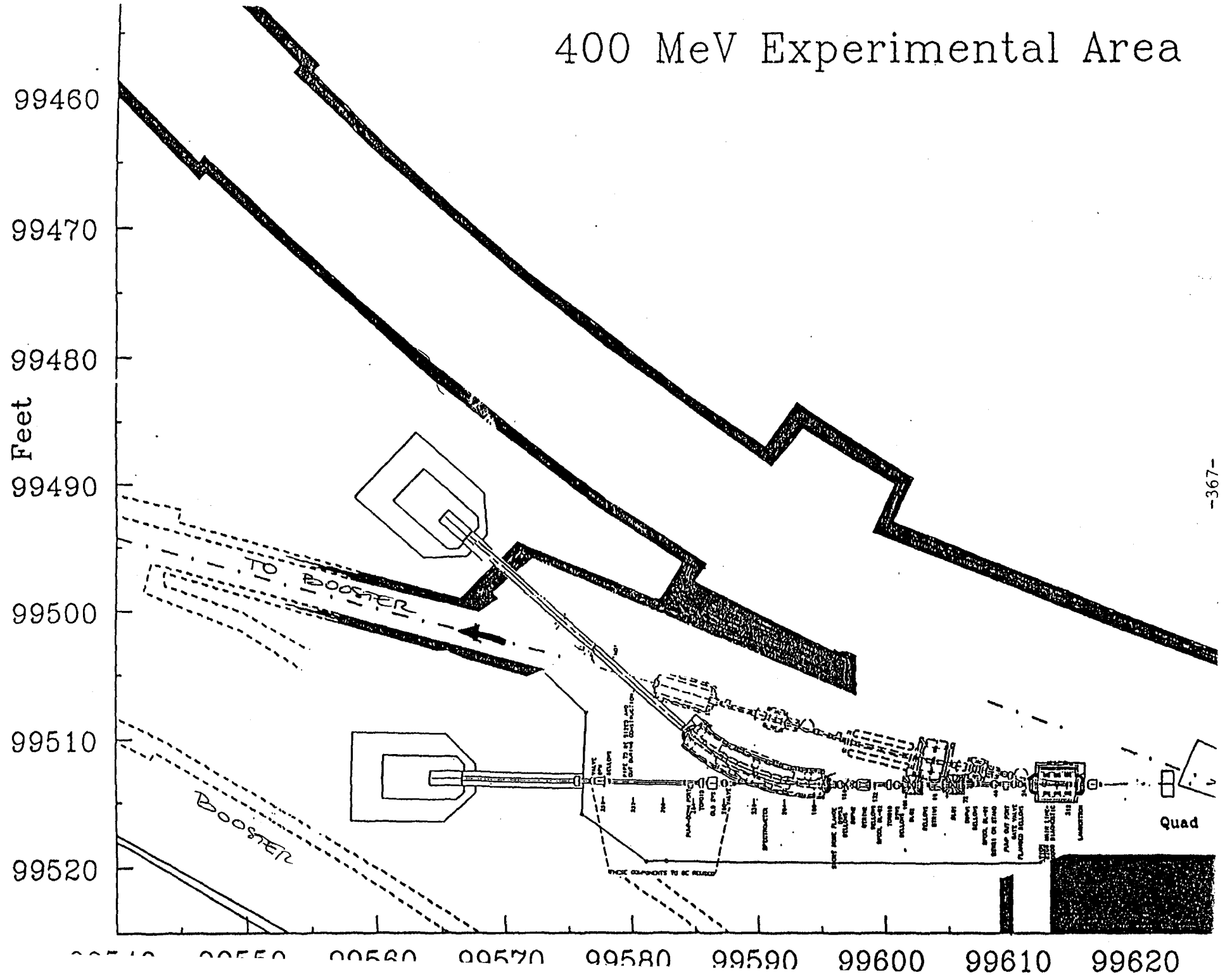

400 MeV Experimental Area

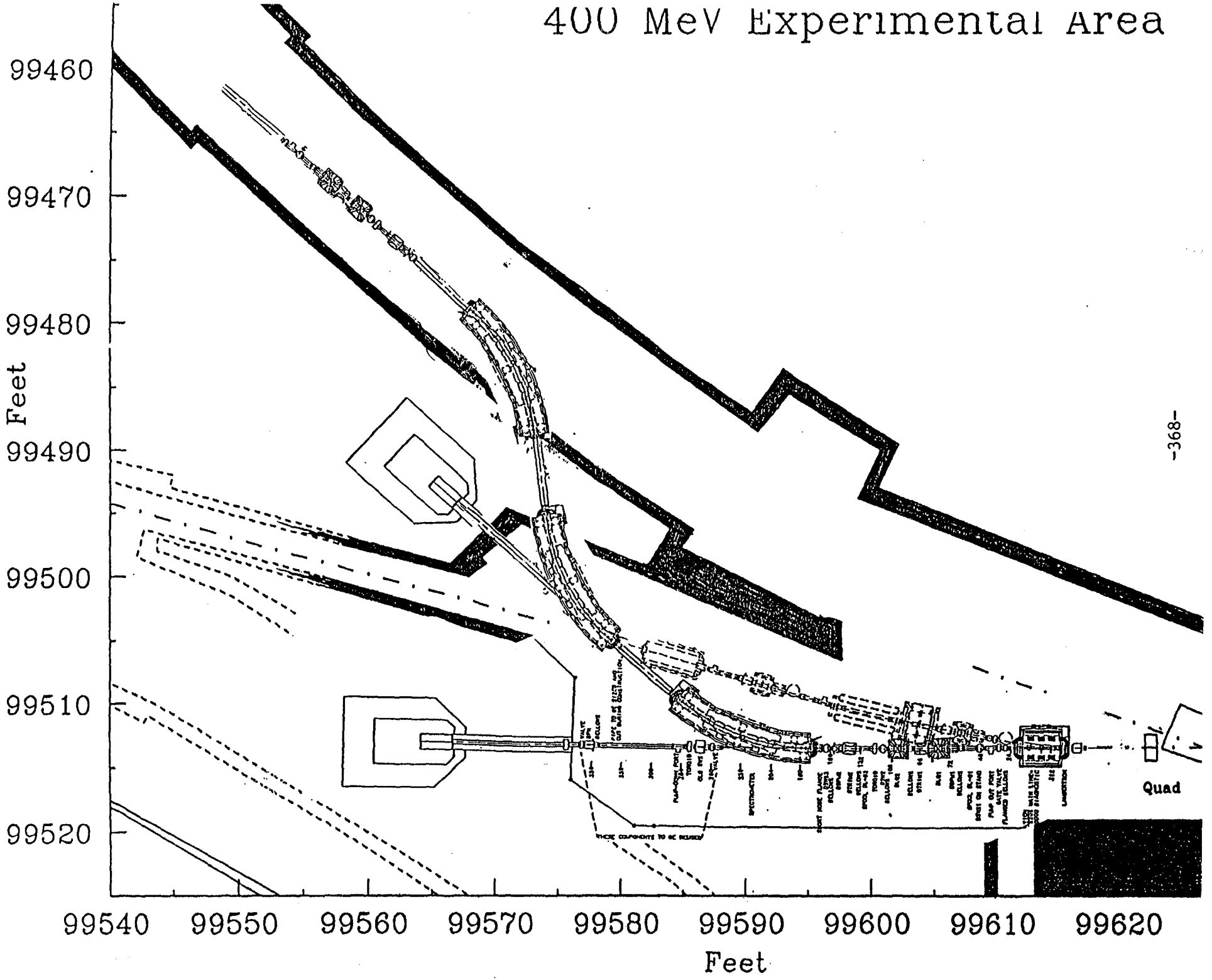

Console Location 3, 25-OCT-1993 09:00
PA:B5 BOO CAMAC TIMERS

```
B5   CHOP TIMES                          SET      D/A   A/D  Eng-U ♦COPIES♦
-<SNP>+ *SB♦ Mult   X=TIME     Y=B:CHG0  ,M IBEAMM,B CHG0   ,M BLB6
COMMAND BL-- Eng-U  I= 0       I= 0      , 0      ,-1       , 0
-< 1>+  EV14 AUTO   F= .04     F= 4      , 4      , 1       , .1
tmcr**  200 MEV   ap4    long3   long13 gamma-t   brf   by evnt
-B:CTCB13     Chop Time Begin - $13        2003     2003   uSEC .
-B:CTCE13     Chop Time End - $13          2005     2005   uSEC .
-B:FTCB13     Chop Time Fine Begin $13     2        2      10nS
-B:FTCE13     Chop Time Fine End   $13     3        3      10nS

-B:CTCB14     Chop Time Begin - $14        2003     2003   uSEC .
-B:CTCE14     Chop Time End - $14          2016     2016   uSEC .
-B:FTCB14     Chop Time Fine Begin $14     2        2      10nS
-B:FTCE14     Chop Time Fine End   $14     3        3      10nS

-B:CTCB15     Chop Time Begin - $15        2003     2003   uSEC .
-B:CTCE15     Chop Time End - $15          2012     2012   uSEC .
-B:FTCB15     Chop Time Fine Begin $15     2        2      10nS
-B:FTCE15     Chop Time Fine End   $15     9        9      10nS

-B:CTCB16     Chop Time Begin - $16        2003     2003   uSEC .
-B:CTCE16     Chop Time End - $16          2005     2005   uSEC .
-B:FTCB16     Chop Time Fine Begin $16     2        2      10nS
-B:FTCE16     Chop Time Fine End   $16     2        2      10nS

-B:CTCB17     Chop Time Begin - $17        2003     2003   uSEC .
-B:CTCE17     Chop Time End - $17          2005     2005   uSEC .
-B:FTCB17     Chop Time Fine Begin $17     2        2      10nS
-B:FTCE17     Chop Time Fine End   $17     3        3      10nS
```

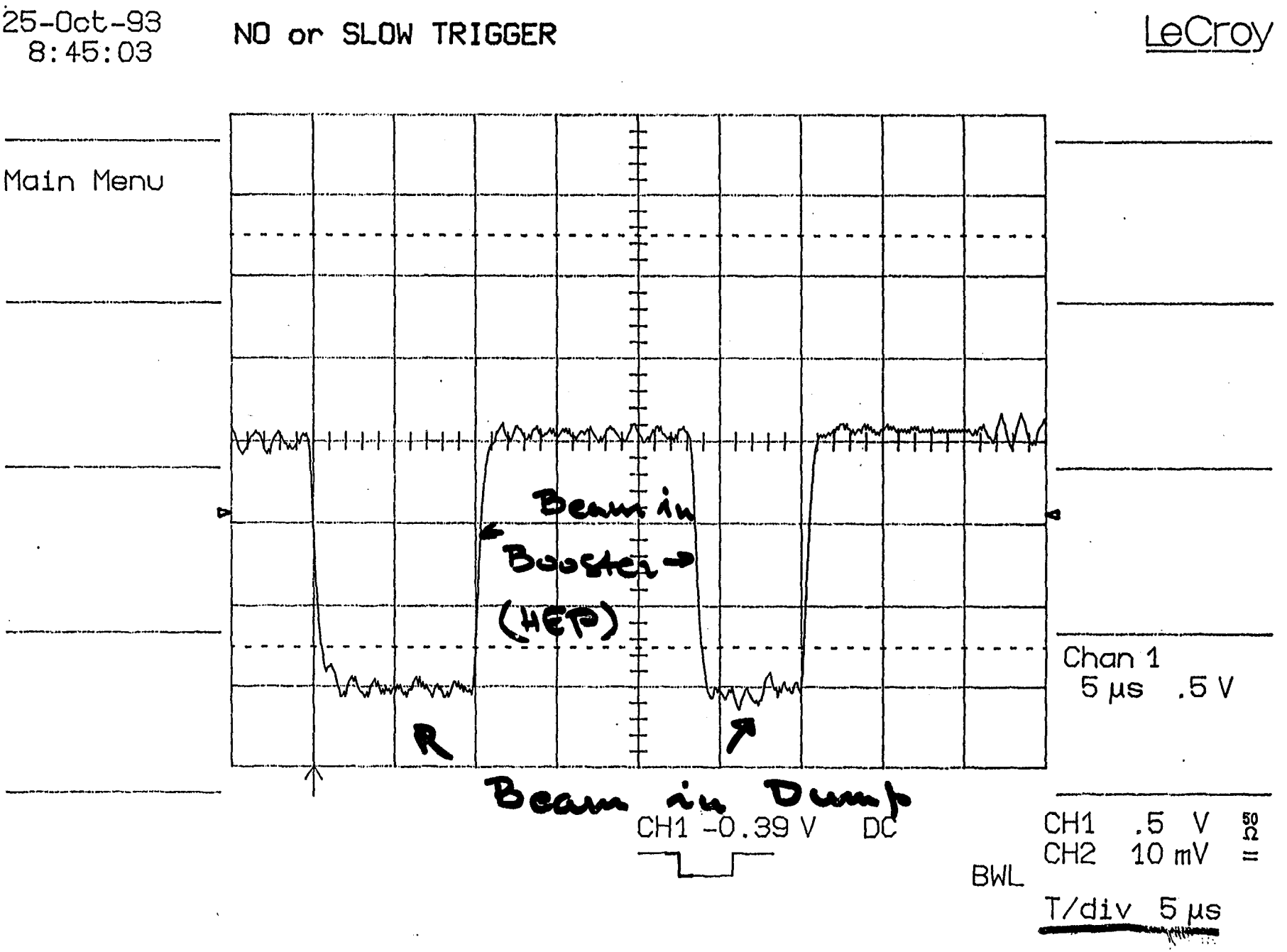
25-Oct-93
8:45:03
NO or SLOW TRIGGER
LeCroy
Main Menu
Beam in
Booster
(HEP)
R
Beam in Dump
Chan 1
5 µs .5 V
CH1 -0.39 V DC
CH1 .5 V
CH2 10 mV
BWL
T/div 5 µs

25-Oct-93
10:48:17

LeCroy

DT LINAC TANK #3

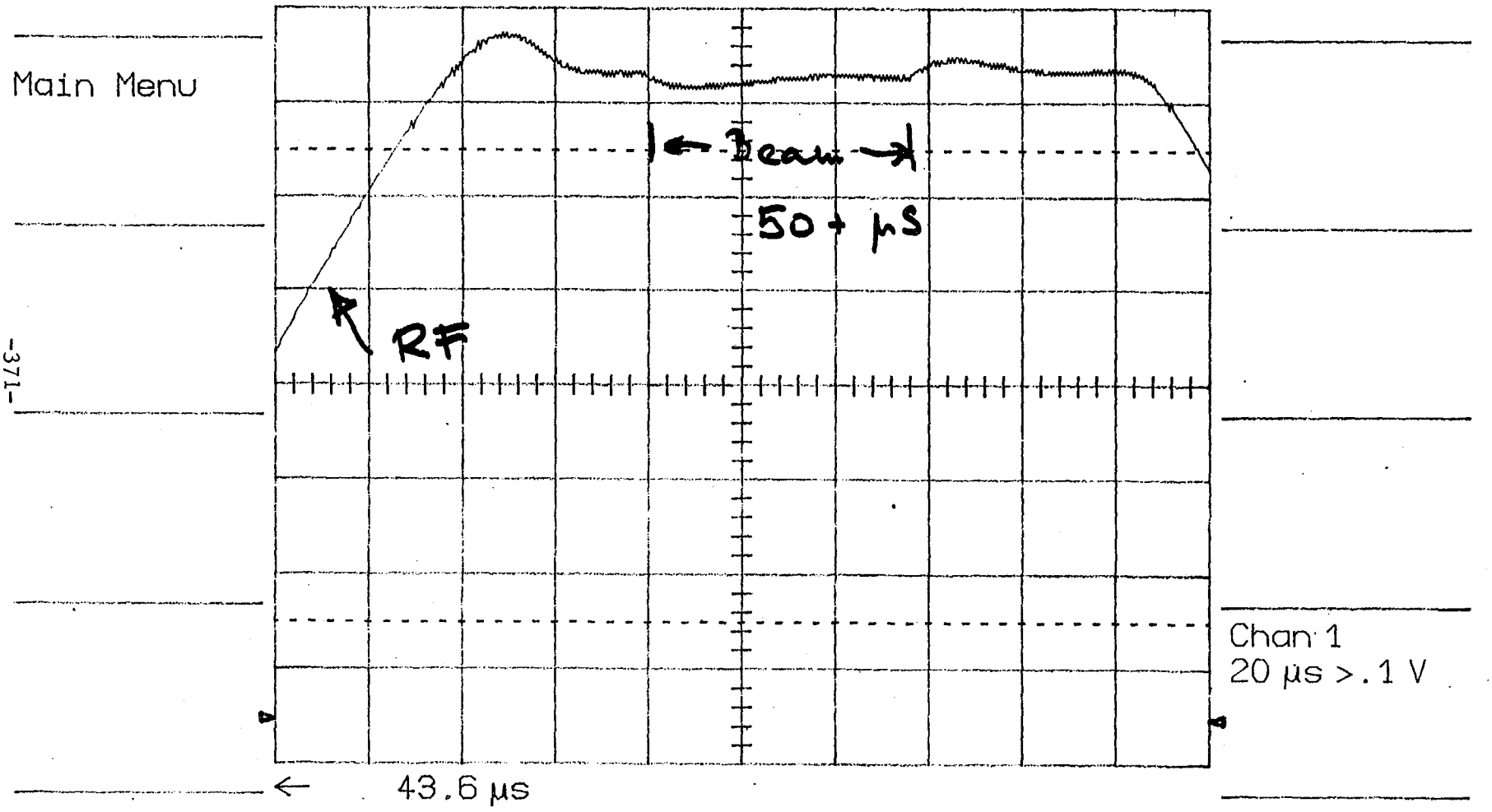

CH1 132 mV DC

BWL

CH1 >.1 V =
CH2 10 mV =

T/div 20 µs

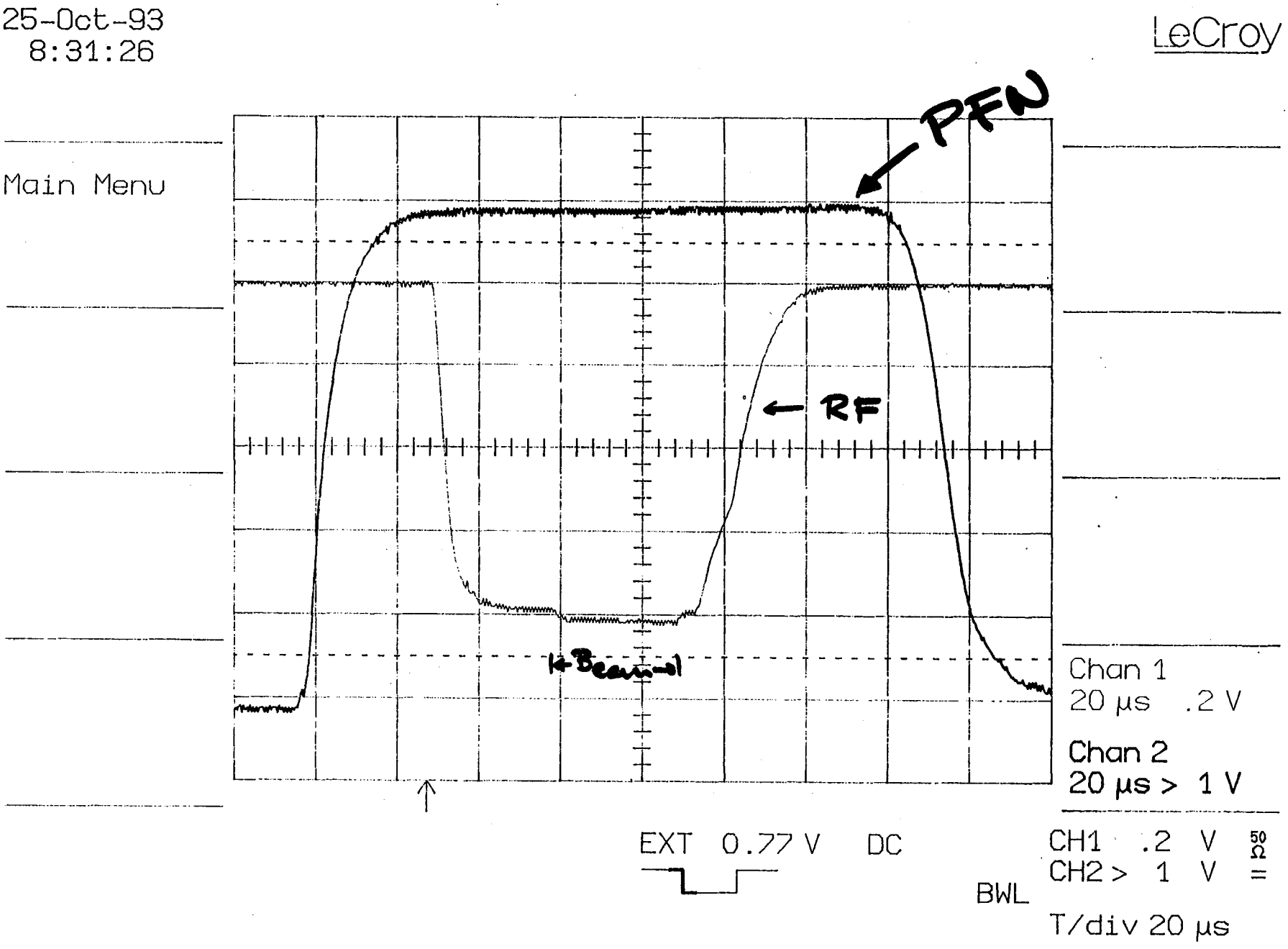
25-Oct-93
8:31:26
LeCroy
Main Menu
PFN
RF
Beam-1
Chan 1
20 µs .2 V
Chan 2
20 µs > 1 V
EXT 0.77 V DC
CH1 .2 V 50 Ω
CH2 > 1 V =
BWL
T/div 20 µs

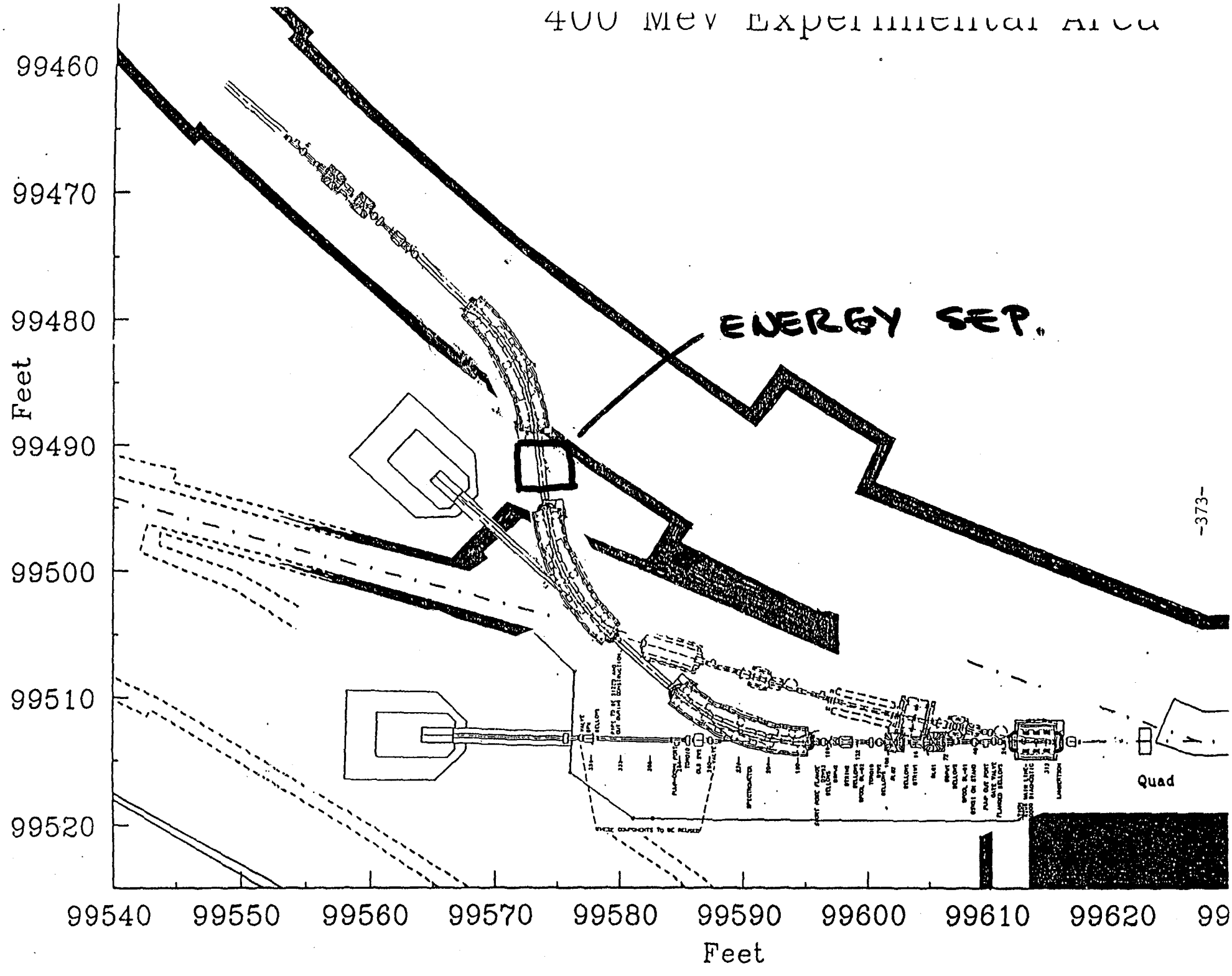
400 MeV Experimental Area
ENERGY SEP.
Quad
99460
99470
99480
99490
99500
99510
99520
Feet
99540
99550
99560
99570
99580
99590
99600
99610
99620
99
Feet

GxPA 1: None

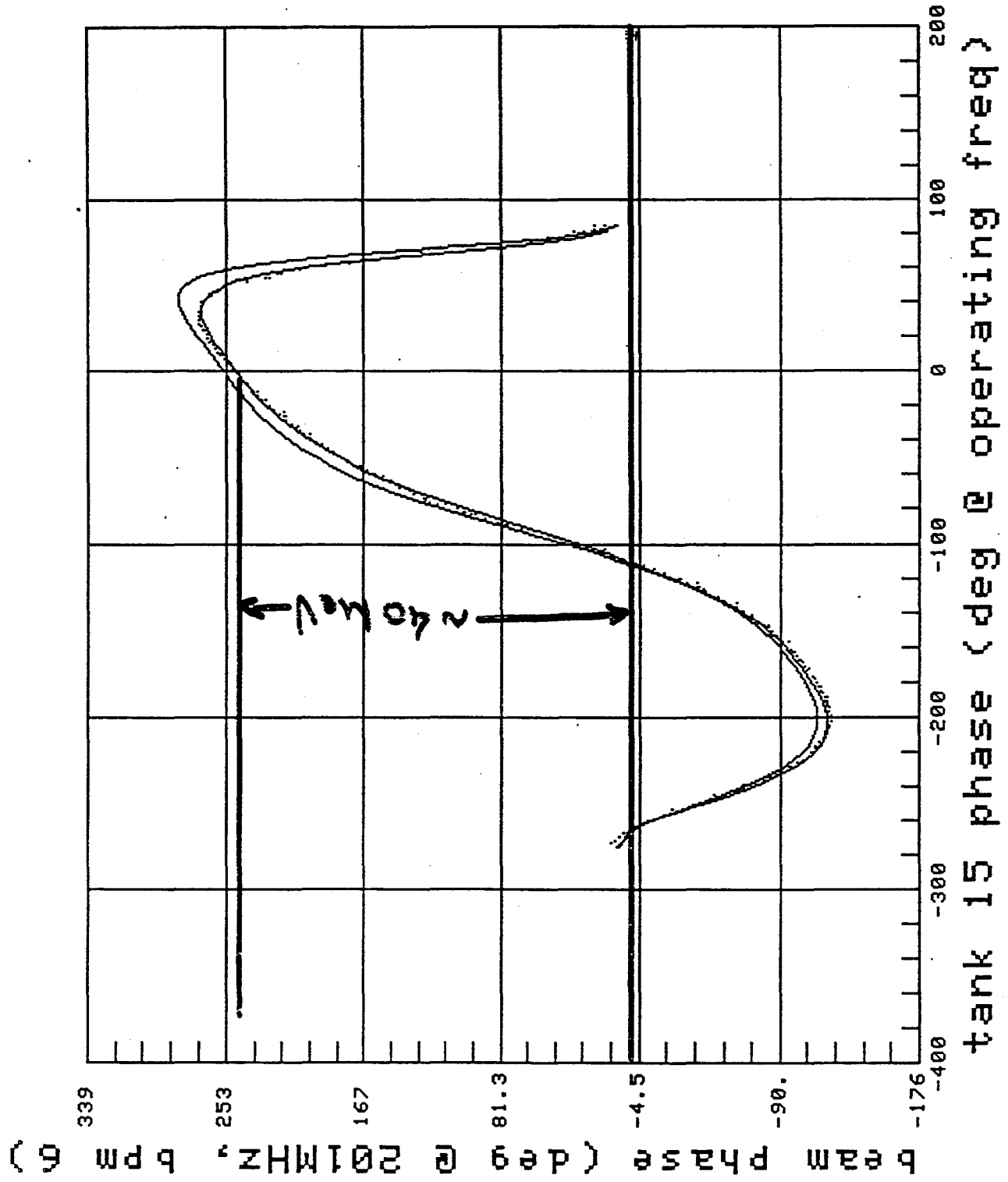
beam phase (deg @ 201MHz, bpm 6)
339
253
167
81.3
-4.5
-90.
-176
tank 15 phase (deg @ operating freq)
-400
-300
-200
-100
0
100
200
~40 μsec

Fermilab 400 MeV Beamline Workshop

Health Physics Applications for a 400 MeV Proton Beamline

David Boehnlein

October 25, 1993

Health Physics Applications for a 400 MeV Proton Beamline

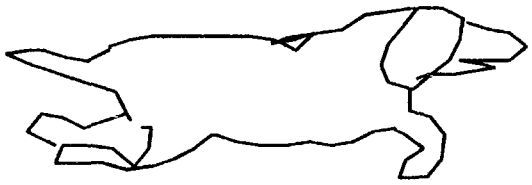

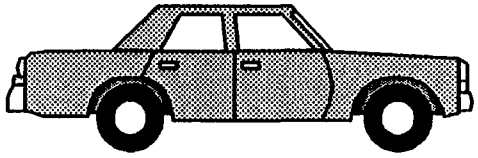

Potential Applications

- Dosimetry
- Materials activation
- Shielding studies
- Software benchmarking
- Instrumentation

Dosimetry Applications

- High energy neutron dosimetry
- Muon dosimetry
- Intercomparison studies
- Analysis of beam-on exposure

Gaithersburg Workshop

- High energy neutron dosimetry
- Sponsored by DOE in Gaithersburg, MD November 1992
- "High energy" is 20 MeV
- DOELAP accreditation is for 1 KeV to 2 MeV
  - Moderated Cf 252
  - Unmoderated Cf 252

Neutron Measurements at Fermilab

- J. Cossairt, A. Elwyn, W. Freeman, W. Salisbury, P. Yurista
- Multisphere technique used for measurements
  - 7 sphere sizes + bare detector
  - LiI(Eu) "phoswich" or LiF TLD
  - Neutrons detected through thermal capture reaction
- Spectra measured at 14 sites outside of shielding

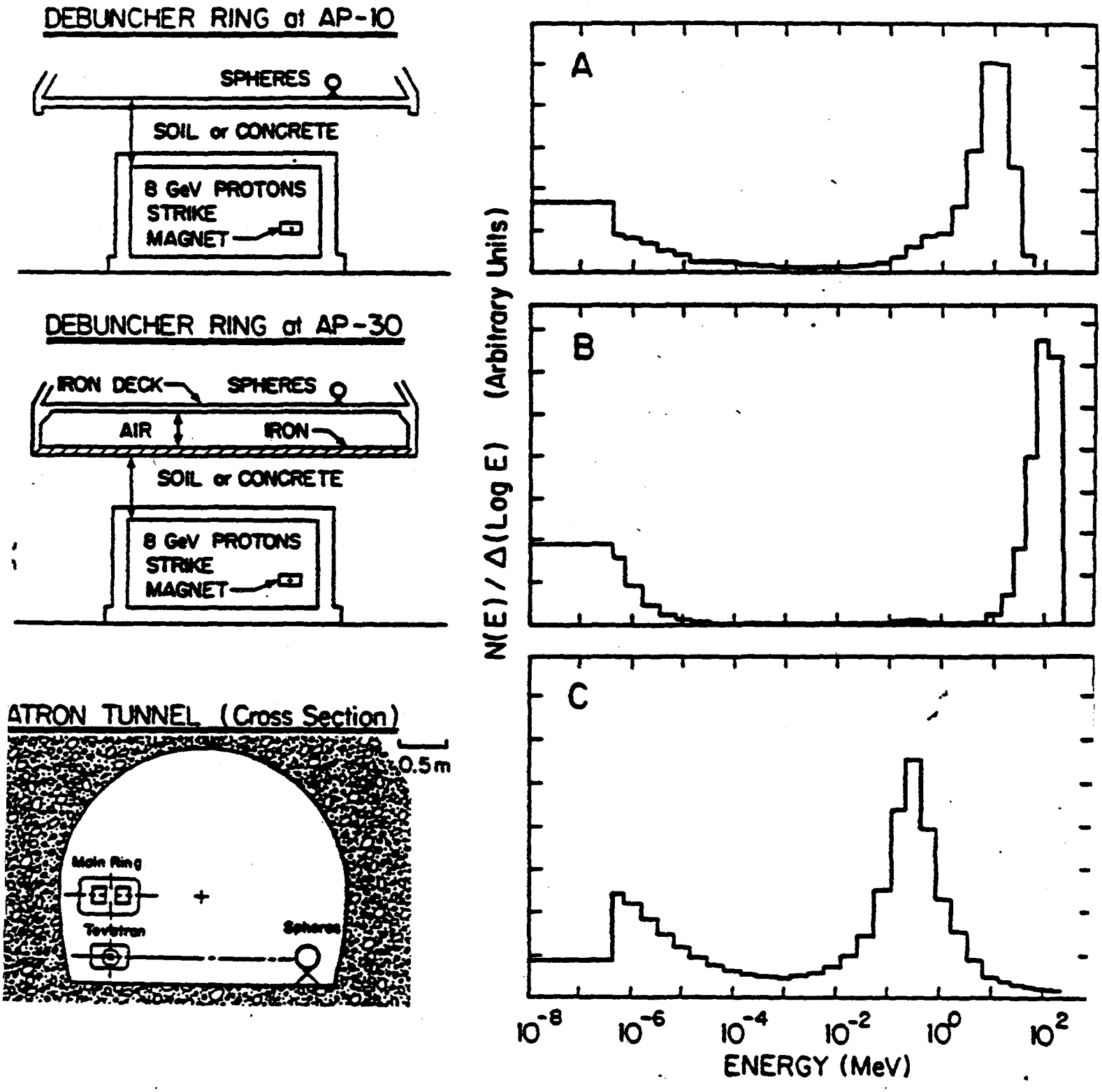

Figure 1. Shielding geometries (left) and corresponding unfolded neutron energy spectra (right) for situations A, B, and C. The abscissa is in arbitrary units of fluence per logarithmic energy interval.

Conclusions

- Neutrons with energy below 0.1 MeV
  - 77% of fluence
  - 23% of dose equivalent
- Neutrons with energy above 0.1 MeV
  - 23% of fluence
  - 77% of dose equivalent
- Neutrons with energy above 2 MeV
  - 13% of fluence
  - 50% of dose equivalent

Workshop Conclusions

- Measurements are imprecise and inaccurate above 2 MeV
- Better dosimeters and area monitors are needed
- Response of dosimeters as a function of energy is poorly known
- There are no calibration standards for high energy neutron detectors
- There is no serious R&D effort underway
- RECOMMENDATION: A committed neutron source

Muon Dosimetry

- Muon studies at CERN
  - dE/dx calculated (Stevenson 83)
  - Dose equivalent not well determined
  - Intercomparison studies (Hofert 87)
  - Calibration considered very important
- Muon studies at Fermilab
  - Dosimeter response in a mixed field (Cossairt,Elwyn 87)
  - Film, ion chambers
  - TLD, bubble detectors have not been tested

Health Physics Applications for a 400 MeV Proton Beamline

Table 1. Results of muon and neutron fluence measurements using plastic scintillators and the multisphere technique normalized to 10^{12} protons on target

Type	Fluence		Absorbed Dose		Dose Equivalent		QF
	$m^{-2} x 10^7$	Fraction	μGy	Fraction	μSv	Fraction	
Neutrons	9.12 ± 0.38	0.62	0.19 ± 0.06	0.08 ± 0.03	1.16 ± 0.31	0.34 ± 0.26	6.24 ± 0.18
Muons[a)]	5.62	0.38	2.25	0.92	2.25	0.66	1

[a)] Fluence based on singles counting rates. For fluence based upon coincidence rates, multiply by 0.75.

Data from (Cossairt,Elwyn 87)

- Quality factor = 1 from Stevenson 83
- Quality factor measured for field with recombination chamber

Health Physics Applications for a 400 MeV Proton Beamline

Table 2. Comparison of dosimeters with absorbed dose measurements using a tissue equivalent ion chamber, and the results of Table 1. The error determinations are explained in the text

Instrument Type[a]	Absorbed Dose (μGy) Total	Muon	Neutron	Normalized Absorbed Dose[b] Muon	Neutron
TEST ONE					
Ion Chamber	696	638±17[c]	56±17[c]	1.00	1.00
Pocket Dosimeters (8)		734±16		1.16±0.05	----
Film Badges (3)		600±100	100±38	0.94±0.16	1.72±0.90
TEST TWO					
Ion Chamber	704	644±18[c]	56±18[c]	1.00	1.00
Pocket Dosimeters (8)		748±20		1.15±0.05	----
Film Badges (5)		600±100	75±13	0.93±0.16	1.27±0.50

[a] Number in parenthesis is number of instruments used

[b] Normalized to ion-chamber values

[c] Obtained from total absorbed dose by use of the fractions indicated in Table 1.

Intercomparison Studies

- Oak Ridge studies
  - HPRR used for PDIS 1-12
  - Accelerators used for PDIS 13-16
  - Energies up to 15 MeV
  - Doses from 0.6 to 10 mSv
  - Under ideal conditions 51% of measurements were within 50% of reference values
- Battelle PNL study currently underway
  - Neutron irradiations from Be(p,n)B using 28 MeV and 50.0 MeV protons at Univer
  - No studies at higher energies are now contemplated

Beam-On Exposure

- Study dose deposition in tissue
- Study dependence on field composition, energy and geometry
- Use layered phantom with implanted TLDs or foils
- Study activation of tissue-equivalent material

Materials Activation

- Studies conducted at Fermilab (Cupps,Vaziri,Elwyn 92)
  - Studies are incomplete
  - Studies are not well controlled
  - Material histories not well known
- Characterization of low-level radioactive waste (Bonano 92)
  - Required by federal and state regulations
  - Much approximation is involved

Materials Activation

- Environmental studies
  - Ground water activation
  - Soil activation
- Radiation damage studies
  - Materials
  - Equipment

Shielding Studies

- Dose rate measurements
  - Vary geometries
  - Vary materials
- Measurements of "cone shape" in longitudinal and azimuthal dimensions

Health Physics Applications for a 400 MeV Proton Beamline

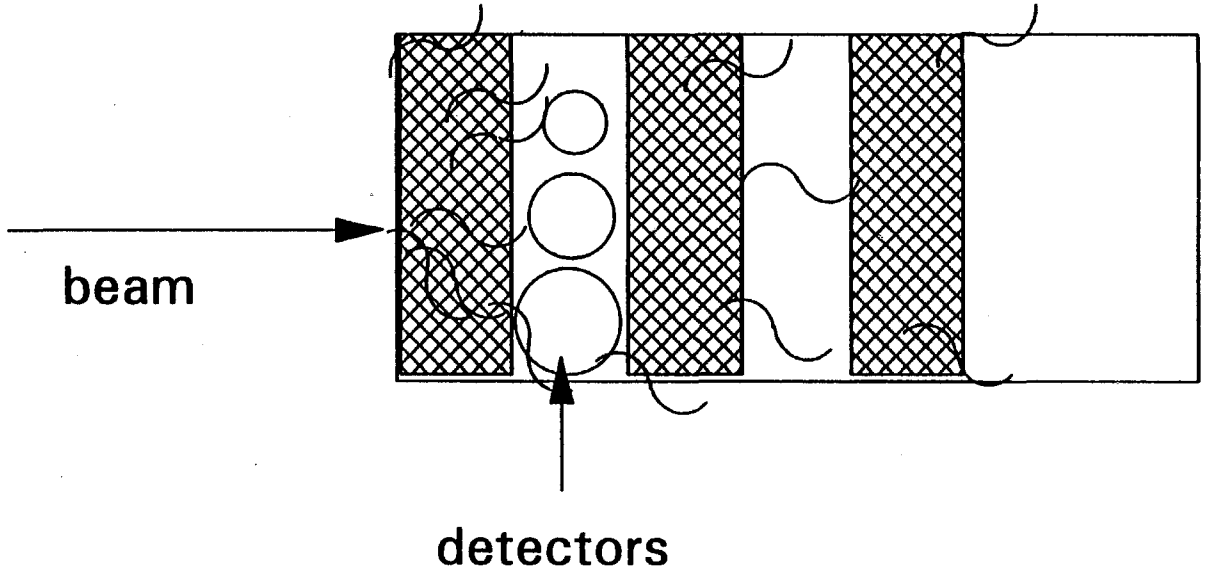

conceptual plan view

Software Benchmarking

- Shielding effectiveness is calculated using Monte Carlo Programs
  - Used generally for high energies
  - Low end cutoff at 50 MeV
- Some codes follow particles to lower energies
  - FLUKA
  - LAHET
- LAHET benchmarked using 113 MeV and 256 MeV protons **(Prael 89)**

Instrumentation

- Chipmunks used at Fermilab and Brookhaven
- Instruments are calibrated with sources (PuBe, AmBe)
- Response is not well known above a few MeV

Neutron Energy Response of the Chipmunk (1055) Chamber In Box (steel) to Unshielded Sources, using a ZP1301 GM Detector to Subtract Photon Dose 5/2/90, FK

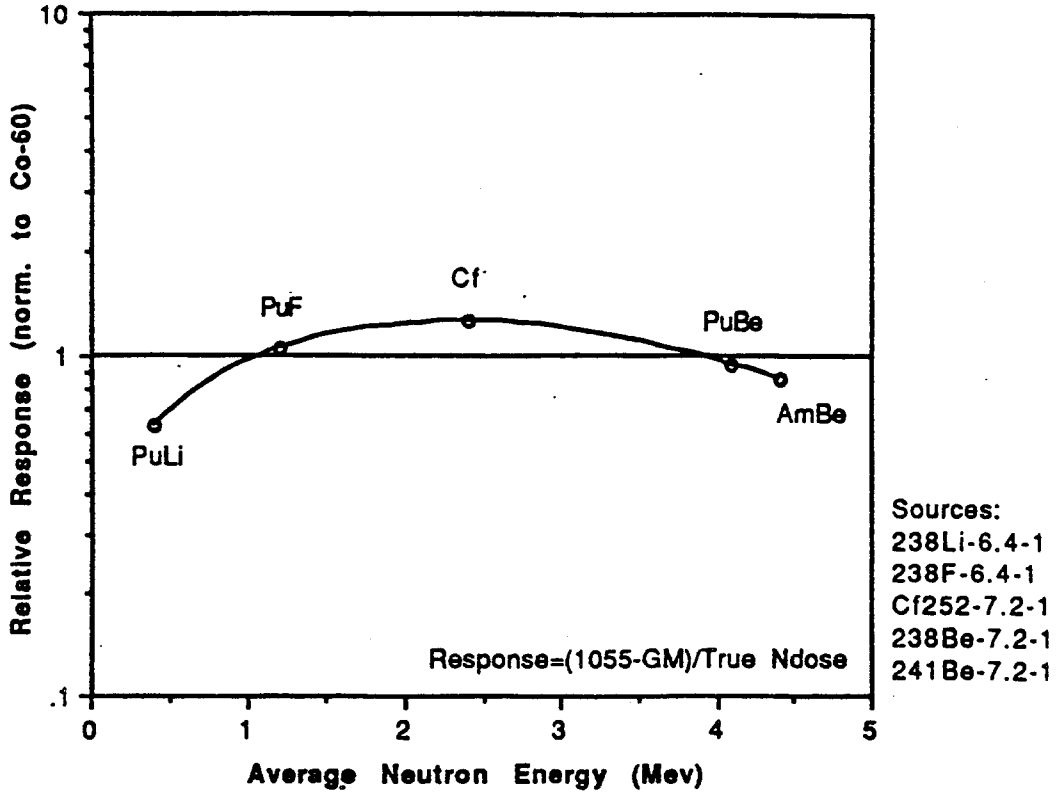

Figure 7

Neutron Energy Response of the Chipmunk (1055) Chamber In Box (steel), 5/2/90, FK

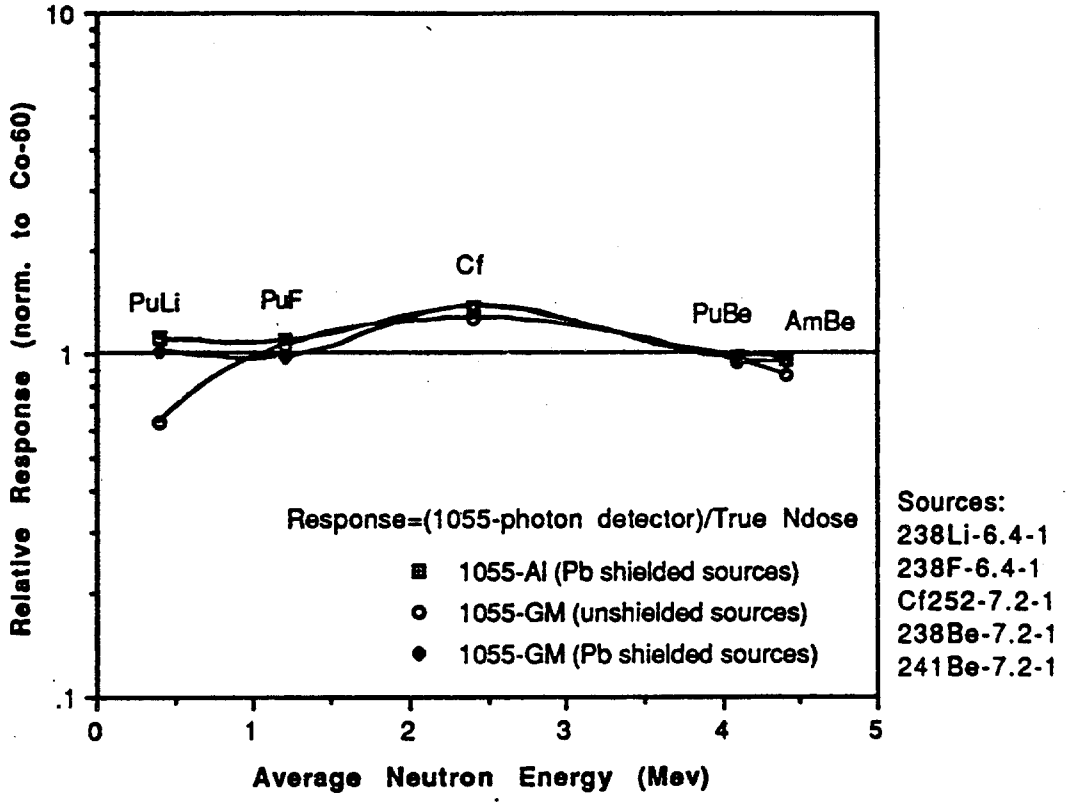

Figure 8

A.J. Lennox
10/27/93

Beam Requirements

Accelerator Physics and Dosimetry
- 70- 300 MeV
- 1-10 nA
- Ability to debunch
- Control emittance and energy spread

Biology
- as low as 10-50 eV
- as low as 1 proton per pulse
- adjustable on demand

Physical Requirements

Rails for installing nozzle components
Basic nozzle providing 10x10 cm^2 field
Beam flat to 10%
Positioning mechanism for phantoms
Laser alignment system
Local control room
Cell lab
Animal lab

A.J. Lennox
10/27/93

Nozzle and Gantry Design

Cyclotron vs Synchrotron issues

Range straggling and distall falloff
vs scanning and modulation
vs optics and modulator materials

Dosimetry

Absolute calibration - provide a standard beam

Develop 3-D detector for dose distributions
Complex but fast - (expensive)
Labor intensive - slow - low cost

Test treatment planning codes

Pulsed vs slow spill instrumentation

Proton Radiography (requires scanning)

"CAT" scans
Port films

Radiobiology

Cells or animals
RBE - cell survival - DNA damage

Radiation Damage Studies

400-MeV Beam Workshop

C. Schmidt
10/27/93

HEP/Accelerators

Fermilab Linac:

- 400-MeV beam, 30-35 mA at 15 Hz, ~0.1% duty factor (30-60 μsec pulse length) with 100-200 psec micropulses (1-2 x E 9 protons) at 200 MhZ (5 nsec separation).
- Operating for two month. Met our objective and doing good, becoming excellent.
- Operate ~10% for HEP and ~10% for NTF. 80% beam idle for possible other uses.

Other Uses:

- Instrumentation and Diagnostics Development. G. Jackson and P. Colestock

  Beam detector R&D, Impedance measurements, Ion dynamics exp.,kicker R&D, Advanced accelerator studies, etc.

- Radiation Health Physics Applications. D. Boehnlein

  Dosimetry, Materials activation, Shielding studies, Software benchmarking, and Instrumentation

- Atomic Physics. S. Cohen, D. Fitzgerald, H. Bryant, U. Fano

- Medical Physics and Uses.

Implementation:

- **Extract beam near Linac exit by kicker (T. Kroc)**
- **Use beam to momentum dump (M. Popovic)**
- **Beam sent into linac access way for experimental use.**
- **Present conditions with some shielding would allow only low intensity beams and limited use.**
- **High intensity beams and multi-purpose facility would require extensive improvement.**

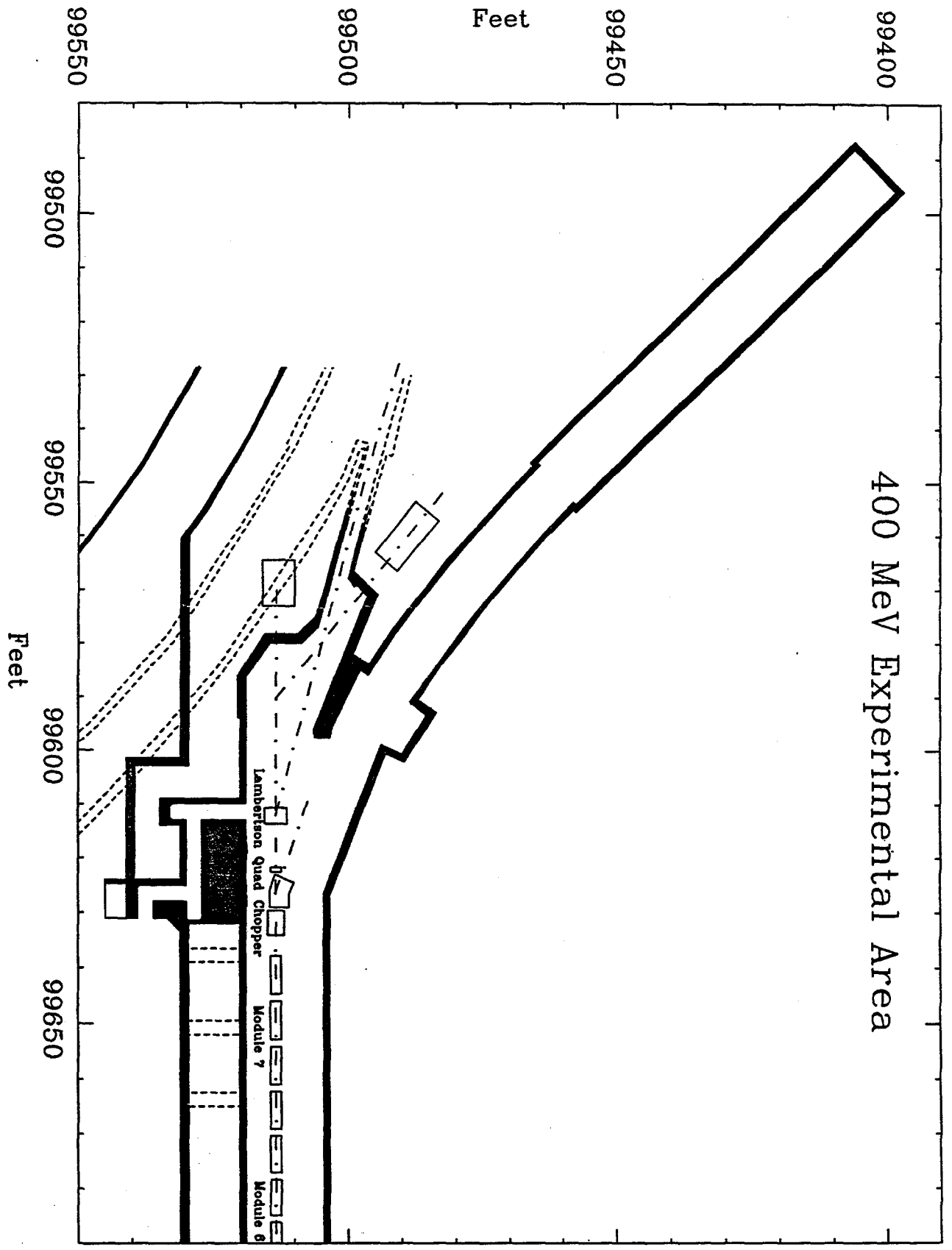
400 MeV Experimental Area
Feet
99400
99450
99500
99550
Feet
99500
99550
99600
99650
Lamberson Quad Chopper
Module 7
Module 6

Attendees for 400 MeV Beam Workshop

Larry Allen
Fermilab
MS 307
P.O. Box 500
Batavia, IL 60510

Chuck Ankenbrandt
Fermilab
MS 306
P.O. Box 500
Batavia, IL 60510

Granluigui Arduini
Consiglio Nazionale delle Ricerche
Instituto Tecnologie
Biomediche Avanzate
Via Ampere 56
20131 Milano Italy

Chandra Bhat
Fermilab
M.S. 323
P.O. Box 500
Batavia, IL 60510

Dr. Ewart Blackmore
TRIUMF
4004 Wesbrook Mall
Vancouver, BC
Canada V6T 2A3

Dave Boehnlein
Fermilab
M.S. 119
P.O. Box 500
Batavia, IL 60510

Alex Bogacz
Fermilab
M.S. 345
P.O. Box 500
Batavia, IL 60510

Howard Bryant
University of New Mexico
Department of Physics and
Astronomy
800 Yale Blvd., NE
Albuquerque, New Mexico 87131-
1156

Richard Carrigan
DOE/Fermilab
ER223/GTN
U.S. Department of Energy
Washington, DC 20545

William Chu
Lawrence Berkeley Laboratory
Berkeley, California 94720

Dr. Lionel Cohen
NTF @ Fermilab
1540 N. State Parkway
Chicago, IL 60610

Stan Cohen
Los Alamos National Laboratory
C238
P.O. Box 1663
Los Alamos, New Mexico 87545

Frank Cole
PAC

Patrick Colestock
Fermilab
M.S. 345
P.O. Box 500
Batavia, IL 60510

Joe Deasy
University of Wisconsin

Phillip Debenham
DOE
Division of High Energy Physics
ER-224
Washington, DC 20585

Ugo Fano
University of Chicago
5640 S. Ellis Avenue
Chicago, IL 60637

Jacob Flanz
Massachusetts General
Boston, MS 02114

David Finley
Fermilab
M.S. 306
P.O. Box 500
Batavia, IL 60510

Dan Fitzgerald
Los Alamos National Laboratory
MS H838
P.O. Box 1663
Los Alamos, New Mexico 87545

Sadayoshi Fukumoto
National Laboratory for High Energy Physics
Oho, Tsukuva
Ibaraki-ken
305 Japan

Eli Glatstein
South West Medical Center
5323 Harry Hines Blvd.
Dallas, TExas 75235-8590

Kathy Harkay
Argonne National Laboratory
9700 S. Cass Avenue
ASD, Bldg 360
Argonne, IL 60439

Stephen Holmes
Fermilab
M.S. 306
P.O. Box 500
Batavia, IL 60510

Zhang, Huashun
Fermilab
M.S. 307
P.O. Box 500
Batavia, IL 60510

Gerry Jackson
Fermilab
M.S. 341
P.O. Box 500
Batavia, IL 60510

Carol Johnstone
Fermilab
M.S. 341
P.O. Box 500
Batavia, IL 60510

Kevin Junck
Fermilab
M.S. 307
P.O. Box 500
Batavia, IL 60510

Vladimir Khoroshkov
Institute for Theoretical & Experimental Physics
B. Cheremushkinskaya 25
Moscow, Russia 117259

Tom Kroc
Fermilab
M.S. 307
P.O. Box 500
Batavia, IL 60510

Arlene Lennox
Fermilab
M.S. 301
P.O. Box 500
Batavia, IL 60510

Dale Litzenberg
University of Michigan
Department of Physics
500 East University St.
Ann Arbor, MI 48109

Robert Macek
Los Alamos National Laboratory
MP Division
MS H848
Los Alamos, New Mexico 87545

John Marriner
Fermilab
M.S. 341
P.O. Box 500
Batavia, IL 60510

Ron Martin

Elliott McCrory
Fermilab
M.S. 307
P.O. Box 500
Batavia, IL 60510

David McGinnis
Fermilab
M.S. 341
P.O. Box 500
Batavia, IL 60510

Harold Miller
Fermilab
M.S. 306
P.O. Box 500
Batavia, IL 60510

Fred Mills
Argonne National Laboratory
Bldg 360
9700 S. Cass Avenue
Argonne, IL 60439

Mike Notarus
Professional Management Services

Konstantin Onosovsky
Institute for Theoretical &
Experimental Physcics
B. Cheremushkinskays 25
Moscow, Russia 117259

Milorad Popovic
Fermilab
M.S. 307
P.O. Box 500
Batavia, IL 60510

Alan Riddiford
Fermilab
M.S. 341
P.O. Box 500
Batavia, IL 60510

Don Rosselot
Indiana University

Chuck Schmidt
Fermilab
M.S. 307
P.O. Box 500
Batavia, IL 60510

Donna Siergiej
University of New Mexico
@ Fermilab
P.O. Box 500, M.S. 341
Batavia, IL 60510

Marco Silari
Consiglio Nazionale delle Ricerche
Instituto Tecnologie
Biomediche Avanzate
Via Ampere 56
20131 Milano, Italy

James Slater
Loma Linda University Medical
Center
Department of Radiation Medicine
11234 Anderson Street, MCB 121
Loma Linda, CA 92354

Ray Tomlin
Fermilab
M.S. 341
P.O. Box 500
Batavia, IL 60510

David Wildman
Fermilab
M.S. 306
P.O. Box 500
Batavia, IL 60510

Donald Young
PAC
4513 Cornell
Downers Grove, IL 60532